UNIVERSITY OF CALIFORNIA SAN DIEGO
3 1822 02331 4693

QE
1
U595

UNIVERSITY OF CALIFORNIA, SAN DIEGO
3 1822 02331 4693

MULTIPART ITEM

consists of: Text volume and 2 plates in back pocket.

University of California, San Diego
Please Note: This item is subject to recall.
Date Due

CI 39a (4/91) *UCSD Lib.*

354

Shorter Contributions to General Geology 1959

GEOLOGICAL SURVEY PROFESSIONAL PAPER 354

UNITED STATES GOVERNMENT PRINTING OFFICE, WASHINGTON : 1961

SHORTER CONTRIBUTIONS TO GENERAL GEOLOGY, 1959—U.S.G.S. Professional Paper

UNITED STATES DEPARTMENT OF THE INTERIOR

STEWART L. UDALL, *Secretary*

GEOLOGICAL SURVEY

Thomas B. Nolan, *Director*

CONTENTS

[The letters in parentheses preceding the titles designate separately published chapters]

	Page
(A) Intrenched meanders of the North Fork of the Shenandoah River, Virginia, by John T. Hack and Robert S. Young	1
(B) Interpretation of the composition of trioctahedral micas, by Margaret D. Foster	11
(C) Giant waves in Lituya Bay, Alaska, by Don J. Miller	51
(D) Early Cretaceous (Albian) Ammonites from the Chitina Valley and Talkeetna Mountains, Alaska, by Ralph W. Imlay	87
(E) Interpretation of the composition of lithium micas, by Margaret D. Foster	115
(F) Zones and zonal variations in welded ash flows, by Robert L. Smith	149
(G) Deposition of uranium in salt-pan basins, by Kenneth G. Bell	161
(H) Foraminifera from Onotoa Atoll, Gilbert Islands, by Ruth Todd	171
(I) Occurrence and significance of marine animal remains in American coal balls, by Sergius H. Mamay and Ellis L. Yochelson	193
(J) *Lituyapecten* (new subgenus of *Patinopecten*) from Alaska and California, by F. Stearns MacNeil	225
(K) Stratigraphic Occurrence of *Lituyapecten* in Alaska, by Don J. Miller	241

U. S. GOVERNMENT PRINTING OFFICE : 1961 O - 579101

Intrenched Meanders of the North Fork of the Shenandoah River, Virginia

By JOHN T. HACK *and* ROBERT S. YOUNG

SHORTER CONTRIBUTIONS TO GENERAL GEOLOGY

GEOLOGICAL SURVEY PROFESSIONAL PAPER 354-A

A study of the channel of a river intrenched in hard rocks and an analysis of factors that cause it to meander

UNITED STATES GOVERNMENT PRINTING OFFICE, WASHINGTON : 1959

UNITED STATES DEPARTMENT OF THE INTERIOR

FRED A. SEATON, *Secretary*

GEOLOGICAL SURVEY

Thomas B. Nolan, *Director*

For sale by the Superintendent of Documents, U.S. Government Printing Office
Washington 25, D.C. - Price 20 cents (paper cover)

CONTENTS

	Page
Abstract	1
Introduction	1
Geology of the river basin	2
River channel	4
Longitudinal profile	4
Channel cross section	4
Bed material	4
Discharge	6
River channel—Continued	
Summary of channel characteristics	6
Controls of meander formation	6
Intrenchment hypothesis	7
Meandering streams in rocks other than the Martinsburg shale	9
Conclusion	9
References	10

ILLUSTRATIONS

	Page
PLATE 1. Outcrops of Martinsburg shale. *A*, Outcrop near Woodstock showing typical beds of fine sandstone and siltstone alternating with shale; *B*, Outcrop near Edinburg showing typical prismatic cleavage cutting a spheroid	Facing 6
FIGURE 1. Map of the meandering reach of the North Fork of the Shenandoah River	2
2. Simplified geologic map of the drainage basin of the North Fork, Shenandoah River	3
3. Longitudinal profile of the North Fork of the Shenandoah River	4
4. Graph on logarithmic scales comparing the dimensions of the channel of the North Fork at different places along the stream	5
5. Profiles of valley floor	8

TABLES

	Page
TABLE 1. Summary of data on size of fragments on the streambed, North Fork, Shenandoah River	4
2. Mean annual discharge at gaging stations on the North Fork of the Shenandoah River	6

522989—59

SHORTER CONTRIBUTIONS TO GENERAL GEOLOGY

INTRENCHED MEANDERS OF THE NORTH FORK OF THE SHENANDOAH RIVER, VIRGINIA

By John T. Hack and Robert S. Young[1]

ABSTRACT

The North Fork of the Shenandoah River traverses rocks of different lithology in areas of greatly different topography. The spectacular meanders in which the river travels 3.2 times as far as the direct down valley distance coincide with the outcrop area of a belt of Martinsburg shale. Along the entire river the channel is adjusted to carry bed material of approximately uniform size, and passes through the meandering reach without significant change in channel cross section. The profile of the stream follows a simple logarithmic curve from source to mouth. The upland on either side of the stream, however, slopes downstream at a grade much steeper in the area of the meanders than in the nonmeandering area upstream. It is concluded that the meanders are caused by strong planar and prismatic structures in the Martinsburg shale that favor northwest-southeast differential erosion. The topography of the adjacent upland is graded to the present river. There is no reason to believe that the river has been intrenched from an erosion surface on which the relief was less than that of the present upland or that changes in base level have influenced the meander development.

INTRODUCTION

The North Fork of the Shenandoah River, Va., is a classic example of a meandering stream intrenched in hard rocks. Photographs of these meanders have appeared in several textbooks of geology and geomorphology (Thompson, 1947, p. 175; Monnett and Brown, 1950, p. 110; Thornbury, 1954, p. 146). The meanders are prominently displayed in an illustration in a paper by Rich (1939) describing a section across the Appalachians. Butts (1940, p. 508) offers an interpretation of the origin of the meander belt, and Fisher (1955) describes the physical character of the meanders.

A similar meander belt on Conodoguinet Creek, near Harrisburg, Pa., has received at least an equal amount of attention as an example of an intrenched stream and has been studied by Strahler (1946).

Most authors who mention either of these meandering streams imply that they are inherited from a surface of low relief and were intrenched into the valley floor during rejuvenation, as a consequence of uplift or change in base level. As pointed out by Thornbury, however (1954, p. 145), geomorphologists are not agreed that all intrenched meanders have been formed in this way. For example, Cole (1930) has shown that meanders may form in hard rocks by erosion along joint planes. Gregory and Moore (1931, p. 136) believe that many of the meanders that are spectacular features of the Colorado Plateau region were formed by lateral corrasion of the hard rock strata.

The writers believe that the meandering reach of the North Fork of the Shenandoah River is simply a river segment with a smooth and regular profile, adjusted for the transportation of a certain load. The enclosing rocks have special characteristics favoring erosion in a preferred direction, and the adjusted channel slope is maintained in spite of the increase in sinuosity. No change in base level is necessarily involved in the formation of the meanders.

The meandering reach of the North Fork is shown in figure 1, a map prepared from the Strasburg and Edinburg quadrangles of the U.S. Geological Survey. The reach begins at Edinburg and ends at Strasburg, 14 miles downvalley. The sinuosity (the distance measured along the stream, divided by the distance measured along the valley) attains the remarkably high value of 3.2. The narrow valley bottom is 100 to 150 feet below the general level of the adjacent shale hills. Measured along the channel, the river has an average gradient of 5.5 feet per mile, whereas the valley floor, measured across the hilltops between the bends, has a gradient of 17 feet per mile. As shown on the geologic map, figure 2, the meander belt is localized within the outcrop area of the Martinsburg shale (Ordovician). This formation, as described on page 6, is lithologically unique in the region and its close relation to the meanders led the writers to undertake this study. The relation is not confined to the North Fork; similar meanders occur in other areas of Martinsburg shale, as on the Middle River, Augusta County, Va., and on Conococheague Creek, Washington County, Md. In these areas the meandering reaches correspond closely to the limits of the same formation.

The writers' work on the Shenandoah River grew out of bedrock geologic mapping by R. S. Young in the

[1] University of Virginia, formerly of the Virginia Division of Geology (now the Virginia Division of Mineral Resources).

FIGURE 1.—Map of the meandering reach of the North Fork of the Shenandoah River. Redrawn from the Strasburg, Va., quadrangle of the U.S. Geological Survey (1947).

Edinburg-Woodstock area in 1951–52, and studies of streams by J. T. Hack in the Shenandoah Valley in 1952–57. Measurements of the stream channel were made in 1957. The writers are grateful to colleagues in the Virginia Division of Geology and the U.S. Geological Survey for their suggestions and critical review.

GEOLOGY OF THE RIVER BASIN

The valley of the North Fork may be divided into three parts, each having distinctive geology, as shown on the map of the river basin, figure 2. The headwater area above Cootes Store is in folded sandstone and shale of Silurian and Devonian age. The interstream divides are steep sandstone ridges rising 1,500 to 2,000 feet above the shale valleys. Along the main streams the valleys are broad and flat floored. The channels are flanked by broad flood plains and gravel terraces. Rock is not exposed in the channels, and the beds and banks are composed of rounded cobbles in imbricate arrangement, derived from the flanking

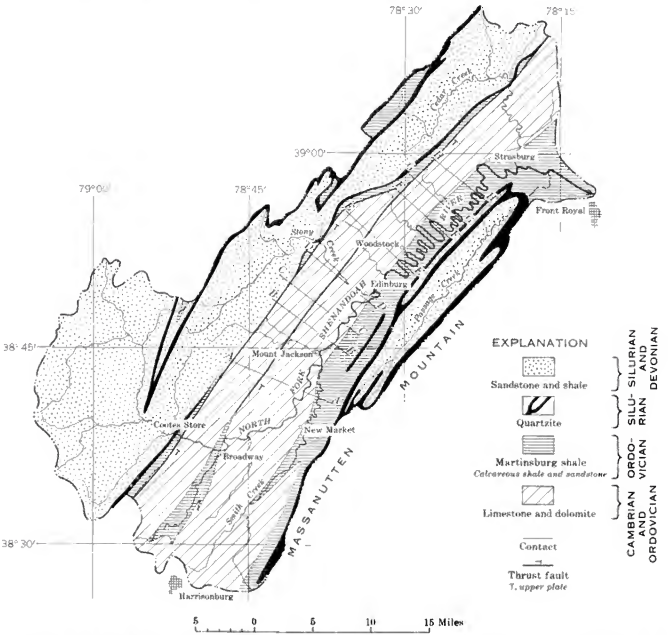

FIGURE 2.—Simplified geologic map of the drainage basin of the North Fork, Shenandoah River, showing relation of the meanders to the Martinsburg shale, and location of profiles (fig. 5).

sandstone ridges. In the segment of the river from Cootes Store to Edinburg the river crosses the main Shenandoah Valley, a rolling country with an average relief of about 200 feet, that is underlain by Cambrian and Ordovician carbonate rocks. The river is bordered by terraces, narrower than those upstream but nevertheless considerably wider than the channel. In a few places terraces are a mile wide. The width of the flood plain and terraces diminishes, however, in a downstream direction. Banks and bed are composed primarily of cobbles of sandstone transported from upstream. Above Broadway the river crosses the strike of the rocks at right angles. Below Broadway it parallels the strike following closely a belt of limestone at the top of the Cambrian. As far as Mount Jackson it remains on the northwest side of prominent and resistant cherty beds in the Beekmantown dolomite (Ordovician). Just above Edinburg the river crosses the cherty beds and enters a belt of Martinsburg shale.

Below Broadway, outcrops of limestone occur in the bed in many places. From Mount Jackson to Edinburg limestone outcrops are more numerous, and the

streambed contains angular cobbles and boulders of limestone of local origin equal in number to the sandstone cobbles transported from upstream.

The third distinctive segment of the river is the meandering reach extending from Edinburg to beyond Strasburg. In this segment the river flows on the Martinsburg shale, a tightly folded belt of weak siltstone, fine sandstone, shale, and subordinate calcareous shale, that has a prominent fracture cleavage and joint system oriented northwestward. The river is flanked on the southeast by the steep shale slopes of Massanutten Mountain, a complex syncline. The side of this mountain that borders the North Fork has a core of hard quartzite, of Silurian age, exposed at the crest. The quartzite breaks up in boulders forming talus slides and block fields that extend down the hollows in the mountainside to the meander bends of the river. In contrast to the upstream reaches, the riverbed in the meandering segment is mostly exposed bedrock. Gravel and cobbles occupy less than one third the area of the bed. The channel is bordered by a narrow flood plain and in some places by gravel terraces. In three places the terraces occupy abandoned meander loops 20 to 40 feet above river level.

RIVER CHANNEL

LONGITUDINAL PROFILE

It is of first importance to consider whether the profile is smoothly graded or whether there is a break in grade, an irregularity, or other change that marks the beginning of the meandering segment. Examination of the profile, measured along its channel, shows that it is uniform. The profile follows fairly closely a simple logarithmic curve, as shown in figure 3, though there are departures from it. It is a property of such a profile that the channel slope (S) at any point on the stream is inversely proportional to the stream length (L) (the distance from the source to the same point.) The ratio of the slopes at any two points (S_1 and S_2) is equal to the reciprocal of the ratio of the lengths of these points (L_1 and L_2):

$$\frac{S_1}{S_2} = \frac{L_2}{L_1}$$

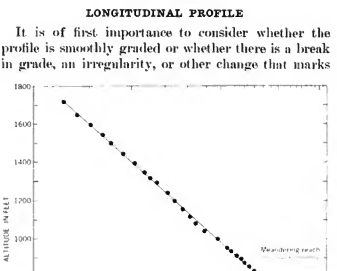

FIGURE 3.—Longitudinal profile of the North Fork of the Shenandoah River. The distance from the source is measured along the longest or principal stream of the drainage basin which heads on the Virginia-West Virginia boundary at lat 38°40′ N. The horizontal scale is logarithmic.

CHANNEL CROSS SECTION

Channel cross section is a significant factor affecting the adjustment of the stream to its load. If there were changes in the nature of the equilibrium conditions in the channel the cross section might be expected to change. The results of measurements made by traverses with tape and hand level across the channel from flood plain to flood plain are shown in figure 4. The variations within a reach are much greater than the variations between the meandering and nonmeandering reaches. Therefore no significant difference can be shown.

BED MATERIAL

Rock fragments resting on the bed of the North Fork are coarse throughout and consist of pebbles, cobbles, and boulders. The bed material was sampled at several localities, including two in the lower or meandering segment, two in the middle or limestone segment, and three in the upper segment above Cootes Store. Size was estimated by measuring the intermediate diameters of more than 50 fragments on the streambed selected at regular intervals along a tape stretched across the streambed. The size statistics at these localities are given in table 1.

TABLE 1.—*Summary of data on size of fragments on the streambed, North Fork, Shenandoah River*

[Results of analyses made in the field by the Wolman method (Wolman, 1954; Black, 1957)]

Locality						
Segment	Miles from source of river	Number of fragments in sample	Phi mean size	Phi standard deviation	Geometric mean (mm)	Percent sandstone in sample
Upper segment	7.8	50	−6.26	1.45	76	100
	15.4	50	−6.64	1.35	100	100
	18.8	52	−6.182	.93	64	100
Middle segment (limestone)	46.2	76	5.90	1.40	59	68
	48.2	103	−6.00	1.25	64	86
Lower segment (Martinsburg shale)	79.5	119	−5.45	1.74	44	37
	92.7	66	−6.59	1.37	95	25

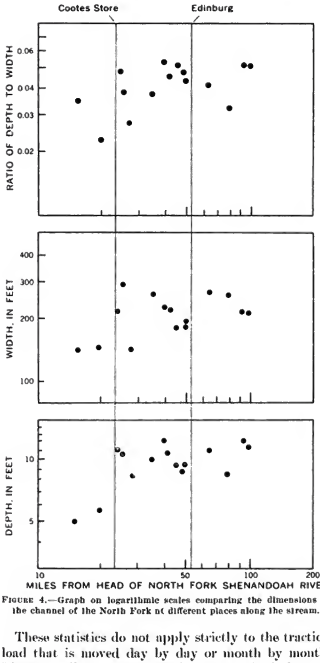

FIGURE 4.—Graph on logarithmic scales comparing the dimensions of the channel of the North Fork at different places along the stream.

These statistics do not apply strictly to the traction load that is moved day by day or month by month. They describe material that is now on the bed, some of which has been moved from upstream, and some of which is residual and represents a lag concentrate of fragments torn off the bedrock locally but that is not yet broken into sizes small enough to have been moved in the last flood. It was shown by studies in other streams in the Shenandoah Valley (Hack, 1957, p. 76–87), however, that siliceous rocks like sandstone and chert are moved great distances downstream from their source, whereas rocks like limestone and shale are soft and are not carried far downstream before they are broken into sizes too small to remain as a lag concentrate on the bed. Inasmuch as the bed samples of the North Fork all contain sandstone from upstream, in addition to locally derived rocks, and the sandstone is on the average coarser than the local rocks, it is inferred that the river is competent to move material of the size that is on the bed.

The sampling indicated no significant change in size of bed material along the stream, as shown by an analysis of variance of the phi mean sizes. The bed material is equally as coarse or coarser near the mouth, in the meandering reach at mile 92.7, as it is near the source, at mile 7.8. The lack of change of particle size along the stream is related to the regular form of the longitudinal profile. Studies in a wide selection of streams in the Shenandoah Valley and in nearby Maryland and Virginia (Hack, 1957) show that the range in the size of fragments on the streambeds is from mean sizes more than 600 millimeters to mean sizes less than 10 millimeters. These size variations are related to differences in discharge, channel slope, and to other hydrologic variables as well as to the material itself, and it was shown that streams with the competence to move the material of the same size along their entire course, have longitudinal profiles like that shown in figure 3, of the North Fork. In such profiles the fall is proportional to the logarithm of the length, and the channel slope is inversely proportional to the length.

The problem is illuminated by consideration of the relative proportions of the materials on the bed. It is noteworthy that in the upper segment the bed material is all sandstone. This is an area of high relief in which many tributaries enter the stream from ridges composed predominantly of sandstone of Silurian and Devonian age. Although the river itself is flowing in a shale valley, the bedrock is so soft, relative to the sandstone introduced by the tributaries, that the bedrock is broken up and carried away in small fragments, and the proportion that remains on the bed is too small relative to the sandstone to appear in the sample. In the middle segment (Cootes Store to Edinburg), where limestone is the dominant bedrock, sandstone on the bed diminishes in relation to limestone. This is because the part of the drainage basin underlain by sandstone diminishes as the basin enlarges in the limestone region. In the lower segment, underlain by Martinsburg shale, the proportion of sandstone diminishes still further, and fragments of Martinsburg shale, although much softer, make up three-fourths of the total material in transit on the bed.

Although not shown in table 1, wherever sandstone bed material is mixed with shale and limestone fragments, the sandstone component is the coarsest. The mean size of all the bed material sampled averages 68

millimeters. The mean of all sandstone fragments is 78 millimeters, and the mean of all limestone and shale fragments is 59 millimeters. Since sandstone is the most resistant material it determines the size of the other components of the bed material. Fragments of locally derived rock that are much smaller are quickly transported downstream, whereas larger fragments accumulate at their source until they are broken into sizes small enough to be moved by traction. The size of the sandstone fragments must be a function of several factors including inherent properties of the rock, such as its toughness, and the spacing of joints, and of external factors such as the distance from the source and rate of transport. If the sandstone were all derived from the headwater area above Cootes Store the size of fragments on the bed probably would diminish downstream as it does in the Middle River (Hack, 1957, fig. 38). In the North Fork, however, the load of large sandstone fragments transported only short distances is renewed downstream by tributaries like Smith Creek and by rock discharged into the stream from the slopes of Massanutten Mountain.

DISCHARGE

The North Fork shows a regular increase in discharge as the drainage area becomes larger. Data on the average discharge are available at three gaging stations along the river as shown in table 2.

TABLE 2.—*Mean annual discharge at gaging stations on the North Fork of the Shenandoah River*

[Commonwealth of Virginia, Division of Water Resources, 1952]

Location of gage	Drainage area (square miles)	Length of record (years)	Average annual discharge (cfs)
Cootes Store	215	25	184
Mount Jackson	509	7	351
Strasburg	772	25	568

SUMMARY OF CHANNEL CHARACTERISTICS

The North Fork of the Shenandoah River has a smooth longitudinal profile so regular that it follows closely a simple logarithmic curve throughout its length. Measurement of the bed material indicates that the channel slope and cross section are adjusted with the available discharge so as to transport bed material of the same size. This size is determined in part by the physical properties of sandstone beds of Silurian and Devonian age, the most resistant rocks of the drainage basin. The adjustment of various factors seems to be precise with regard to the bed material and longitudinal profile. This adjustment is maintained throughout the entire river course in spite of great changes in bedrock conditions and in the sinuosity of the river.

CONTROLS OF MEANDER FORMATION

The close correlation of the meanders with the outcrop area of the Martinsburg shale (fig. 2) shows that the meanders are related in origin to this formation. Furthermore, other rivers in the Shenandoah Valley have elongate meanders in the same rock formation. The straight reaches of the North Fork within the meander belt all trend uniformly northwestward, although as reported by Fisher (1955) the river has some short rectilinear reaches less than 1,000 feet long at the bends that trend N. 40° E.

The Martinsburg shale consists of thin laminae alternately of fine-grained sandstone, siltstone, and shale. Calcareous beds occur at some horizons, particularly near the base of the formation. A typical lithologic unit is exposed in a roadcut shown in plate 1. A section 25 feet thick at this locality contains 8 fine-grained sandstone beds averaging 2.3 feet in thickness and 7 siltstone and shale beds averaging 1.0 feet in thickness. The sandstone beds are notably more resistant to erosion than the shale. In the river channel the fine sandstone beds stand up as slablike corrugations, separated by grooves of shale, in places 2 feet deep. The corrugations are prominent and striking features of the riverbed for long distances, and at low-water periods form straight lines crossing the water surface northeastward at right angles to the channel banks.

The prominent slabs or laminations are cut by a strong joint system in which the most sharply defined planes are alined northwest-southeast. There is also a prominent fracture cleavage. The siltstone beds, in particular, are broken into crude match-shaped prisms whose long axes are oriented northwestward parallel to the principal joint planes. The prismatic cleavage is independent of the bedding. This structure is illustrated in plate 1. Spheroids are common in the Martinsburg, especially in the more massive siltstone beds. These bear no apparent relation to the fracture cleavage, which cuts through them.

Another characteristic of the Martinsburg shale that may favor meander development is its relatively low resistance to erosion. The shale is commonly found in the lowest parts of the valleys and is nowhere a ridge maker.

Examination of the meanders (fig. 1) shows that, unlike alluvial meanders, they consist of long straight reaches connected by 180° bends. The amplitude of the meanders is irregular and in places is more than twice the value of the wavelength. Alluvial meanders, on the other hand, are more symmetrical. The curves, or arcs, that form the bends generally exceed 180° of

A. OUTCROP NEAR WOODSTOCK

Showing typical beds of fine sandstone and siltstone alternating with shale

B. OUTCROP NEAR EDINBURG

Showing typical prismatic cleavage cutting a spheroid. The small talus apron at right is composed of siltstone prisms

OUTCROPS OF MARTINSBURG SHALE

are, and the amplitude is regular and may be nearly equal to but rarely larger than the wavelength. In alluvial meanders, crossovers (where the current crosses from one side of the stream to the other) generally occur at the same point on the bends. In the North Fork, crossovers occur not only on the bends but also in the straight reaches. This phenomenon is a consequence of the extraordinary amplitude of the meanders.

The North Fork meanders bear at least one similarity to alluvial meanders, however. Their wavelength is regular and is a function of the discharge or width of the stream. Opequon Creek, for example, and the Middle River, which are smaller streams in the Shenandoah Valley, have meanders of the same type but the wavelengths are smaller. Leopold and Wolman (1957, p. 58) have shown that there is a regular relation between the wavelength of the bends in a stream and the channel width and discharge. Streams with a channel width of 250 feet, like the North Fork, have an average meander wavelength of about 3,000 feet. The wavelength of the North Fork meanders is 4,000 feet which is in agreement with Leopold and Wolman's data, considering the range in variation.

In summary it has been shown that the North Fork has throughout its length just the slope and cross section required with the gradually increasing discharge to transport the more resistant rock fragments eroded in the drainage basin. The extraordinary elongate meanders are formed in the least resistant rock of the drainage basin and follow closely planes of structural weakness in that rock. In the upstream reaches the riverbed is mostly covered by cobbles and boulders, whereas in the meandering reaches the bed is mostly on exposed bedrock. The river travels a much greater distance within the meandering reaches for a given downvalley distance than it does in the nonmeandering reaches, and a larger proportion of the valley floor is occupied by stream channel.

The explanation for the meanders, then, is that in the Martinsburg shale the river channel was cut along lines of structural weakness in the rock while the slope and cross section necessary to transport cobbles and boulders derived from upstream or from tributaries was maintained. The lesser amount of sandstone and other transported cobbles on the bed suggests that in the meandering reaches, greater energy has been expended in the excavation of rock by elongation of the channel and less by the transportation of rock fragments. Instead of a bed composed largely of cobbles the river has a bed mostly of shale arranged in projecting laminae that resemble a washboard. These projections may supply a frictional resistance to streamflow similar to the resistance supplied upstream by gravel and cobbles and thus maintain the equilibrium of grade and cross section. Spacing of the meanders, as shown by a comparison with typical alluvial meanders, is a function of hydrologic factors rather than factors related to the bedrock.

INTRENCHMENT HYPOTHESIS

The argument in the preceding pages disposes of the hypothesis of meander origin suggested by Charles Butts (1940, p. 508), which supposes that the meanders are inherited from alluvial meanders formed on a peneplain and that they have been preserved but modified in shape as the river was rejuvenated during a postulated Pleistocene regional uplift. The meanders are coincident with the outcrop area of the Martinsburg shale, and are related in origin to structural properties of that formation rather than to an alluvial deposit that has been removed.

It has been noted by many geologists, however, that the North Fork is bordered by steep valley walls, and the stream has often been referred to as intrenched, or entrenched (for example Thornbury, 1954, p. 146, fig. 6.2). The word "intrenched" itself implies that the river has cut down through bedrock in a narrow valley but that at one time it flowed across a more open plain such as a peneplain or at least an open valley less narrow than the present one. If this were the case presumably the meanders developed during intrenchment.

The topography adjacent to the river is now considered to determine whether the intrenchment hypothesis is necessary in explaining the valley. Figure 5 shows a series of transverse profiles across the Shenandoah Valley from Massanutten Mountain to the sandstone ridges on the northwest. Profiles *A–A′* to *D–D′* cross the valley in the limestone area above the meandering reaches of the river, whereas profiles *E–E′* to *H–H′* cross the meanders. The topography as illustrated by these profiles is hilly and irregular. It is not feasible on the basis of this topography to reconstruct a hypothetical peneplain or erosion surface of low relief. The hilltops are too irregular in altitude and in relative height above the streams. Furthermore, study of the geology of the area shows that the height of the hills is closely related to their lithologic composition. The high hills in the western part of profile *A–A′*, for example, are underlain by limestone containing thick beds of chert. If the area ever were a peneplain its surface must have been above the present topography.

The narrow, bedrock valley of the North Fork typified by the cross section *H–H′* (fig. 5) is adequately explained without recourse to the idea of peneplanation or a surface of low relief. The topography along the North Fork is an equilibrium or graded topography

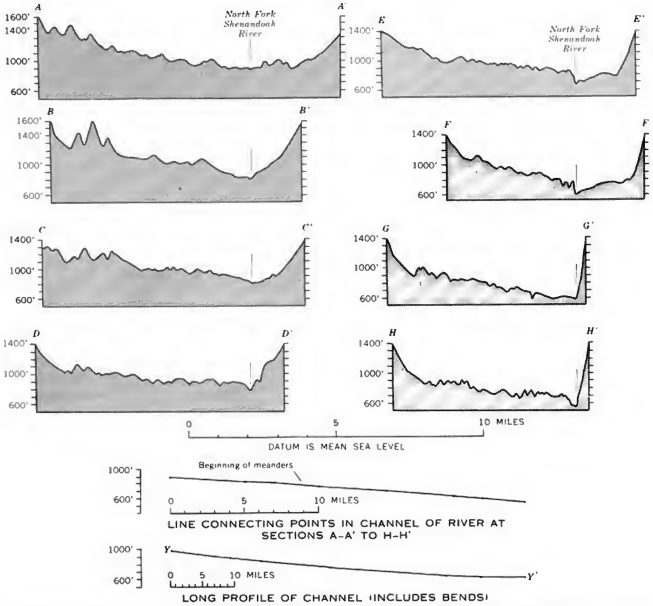

FIGURE 5.—Profiles with greatly exaggerated vertical scale showing the relief of the floor of the Shenandoah Valley in the outcrop area of Cambrian and Ordovician limestone and shale. The location of the profiles is shown on figure 2.

like that described by Hack and Goodlett (in press, 1960) in an area nearby, or by Strahler (1950) in the Verdugo Hills, California. As shown by many recent geomorphological works, principally that of Horton (1945), drainage networks are characteristically regular in pattern and the density of drainage of streams of the same order tends to be nearly constant in areas of the same climate and geology. As a consequence the interstream divides form a system of ridges rising above the streams about the same height. A large trunk stream in such a network of valleys and ridges appears to be intrenched because it is bordered mostly by the steep slopes of interstream areas. These slopes are graded for the transportation of soil and rock fragments by the process of creep, and hence are convex upward. The streams that intersect the trunk streams are mostly first-order streams and they intersect at a high angle. The appearance of intrenchment is enhanced if the topography is underlain by a nonresistant rock on which the profiles of the interstream areas are convex upward and therefore appear rounded or flattish.

Such a topography may be said to be composed of slopes that are everywhere in a state of continuous

adjustment so that the materials weathered and eroded from the surface are transported through a network of channels into larger and larger trunk streams. Depending on the rate of erosion and the total relief, the average slopes of such a topography may be very steep or very gentle.

The longitudinal profile of the North Fork shown at the bottom of figure 5 by the line Y–Y′, is drawn along the channel and includes the bends of the meanders. It is a smooth curve, gently concave upward and is of simple form because adjusted to transport material of the same size with a gradually increasing discharge. The profile above it (that has a larger horizontal scale) connects points in the river channel along a nearly straight line. It does not include the meander bends and therefore represents the profile, as the crow flies, drawn along the lowest points of the valley bottom. This curve is steeper in the meandering reaches than in the reaches upstream. The adjacent network of tributary channels and intervening hills are graded to the main trunk channel, and therefore the entire topographic surface adjacent to the North Fork has a downvalley or northeastward component of slope that is steeper in the meandering region than in the part upstream.

If the topography adjacent to the North Fork can be satisfactorily explained as a graded topography or a topography in which the erosional slopes are in equilibrium, then the meanders exist simply because they are in the Martinsburg shale, and we can expect that any river of comparable size with the gradient necessary to transport cobbles and boulders will also meander in the Martinsburg. An exception to this generalization would be a stream so heavily loaded with waste of material derived from upstream that the bed and banks would be blanketed by this material thereby insulating the river from the shale.

It becomes pointless to speculate on the geologic history of the North Fork and the manner in which it has cut down into the Martinsburg. The river may have eroded its way downward in the northwest limb of the Massanutten syncline thousands of feet, and may have developed and maintained a meandering course in the Martinsburg shale in the distant geologic past.

MEANDERING STREAMS IN ROCKS OTHER THAN THE MARTINSBURG SHALE

Meandering streams of the Shenandoah type are common in the central Appalachians, and they are not all confined to the Martinsburg shale. Meandering reaches are spectacular in the Middle River, Augusta County, Va., in Cambrian limestone. The Potomac River has well-developed meanders that are apparently structurally controlled in rocks of Devonian age. Meanders almost as striking as those in the Martinsburg shale occur in southwestern Virginia in metamorphic rocks on both sides of the Blue Ridge escarpment. The New River, Reed Island Creek, Dan River, and Blackwater River, for example, display meanders with extreme amplitudes. The meanders of the Dan, like the meanders of the North Fork, are confined in strongly laminated rocks, although the rocks are metamorphic with alternating thin layers of quartz mica schist and amphibolite schist.

CONCLUSION

The meanders of the North Fork have been explained within a framework of ideas in which rejuvenation and a former surface of low relief are not factors. In the writers' hypothesis the meanders are an essential part of a graded, erosional topographic system. The arrangement of the rocks in space and the action of hydrologic factors on them is the basis for our explanation of the topography and pattern of drainage, rather than a change in regimen or slope resulting from an uplift.

The elevation of the mouth of the North Fork is determined largely independently of conditions in its own drainage basin, for it empties into a much larger stream, the South Fork, which determines the local base level. The elevations of the headwaters of the North Fork are also to some extent determined independently for they are related to the physical and chemical resistance of the rocks under the drainage divides. Between these two independently fixed points the profile of the stream is determined by a combination of factors, some local—related to the rocks along the channel—others related to duties imposed from upstream such as quantity of water and size and amount of bed material. The meanders result from the interaction of these factors with those of local origin related to peculiar structural properties of the enclosing rock.

Leopold and Wolman (1957), dealing primarily with streams flowing in alluvial channels, have demonstrated a close relation between hydrologic factors, including channel slope, discharge, and load, that apparently determine whether or not a stream will meander. It seems from our data and analysis that the meanders of the North Fork, even though in bedrock, exist in harmony with the same kinds of factors. Probably streams that meander in bedrock are actively eroding streams that have a relatively small load for the slope and discharge and that erode weak rocks with strong linear and planar structures.

REFERENCES

Butts, Charles, 1940, Geology of the Appalachian Valley in Virginia: Virginia Geol. Survey Bull., v. 52, 568 p.

Cole, W. S., 1930, The interpretation of intrenched meanders: Jour. Geology, v. 38, p. 423–436.

Commonwealth of Virginia, Division of Water Resources, 1952, Surface water supply of Virginia, Potomac, Rappahannock, and York River Basins, 1942–50: Commonwealth of Virginia, Dept. of Conserv. and Devel. Bull. 12, 372 p.

Fisher, C. C., 1955, Elongate meanders of the North Fork of the Shenandoah River [abs.]: Geol. Soc. American Bull., v. 66, p. 1687.

Gregory, H. E., and Moore, R. C., 1931, The Kaiparowits region; a geographic and geologic reconnaissance of parts of Utah and Arizona: U.S. Geol. Survey Prof. Paper 164, 157 p.

Hack, J. T., 1957, Studies of longitudinal stream profiles in Virginia and Maryland: U.S. Geol. Survey Prof. Paper 294–B, p. 45–97.

Hack, J. T., and Goodlett, J. C., (1960), Geomorphology and forest ecology of a mountain region in the central Appalachians: U.S. Geol. Survey Prof. Paper 347, in press.

Horton, R. E., 1945, Erosional development of streams and their drainage basins; hydrophysical approach to quantitative morphology: Geol. Soc. American Bull., v. 56, p. 275–370.

Leopold, L. B., and Wolman, M. G., 1957, River channel patterns: braided meandering and straight: U.S. Geol. Survey Prof. Paper 282–B, p. 39–84.

Monnett, V. E., and Brown, H. E., 1950, The principles of physical geology: Boston, Ginn & Co., 450 p.

Rich, John L., 1939, A bird's eye cross section of the Central Appalachian Mountains and Plateau, Washington to Cincinnati; Geog. Rev., v. 29, p. 561–586.

Strahler, A. N., 1946, Elongate intrenched meanders of Conodoguinet Creek, Pa.: Am. Jour. Sci., v. 244, p. 31–40.

———, 1950, Equilibrium theory of erosional slopes approached by frequency distribution analysis: Am. Jour. Sci., v. 248, p. 673–696 and 800–814.

Thompson, H. D., 1947, Fundamentals of earth science: New York, John Wiley & Sons, 618 p.

Thornbury, W. D., 1954, Principles of geomorphology: New York, John Wiley & Sons, 618 p.

U.S. Geological Survey, 1947, Strasburg quadrangle, Virginia, scale 1:62,500, shaded relief.

Wolman, M. G., 1954, A method of sampling coarse riverbed material: Am. Geophys. Union Trans., v. 35, p. 951–956.

○

Interpretation of the Composition of Trioctahedral Micas

By MARGARET D. FOSTER

SHORTER CONTRIBUTIONS TO GENERAL GEOLOGY

GEOLOGICAL SURVEY PROFESSIONAL PAPER 354-B

A study of the compositional and layer charge relations of phlogopites, biotites, siderophyllites and lepidomelanes

UNITED STATES GOVERNMENT PRINTING OFFICE, WASHINGTON : 1960

UNITED STATES DEPARTMENT OF THE INTERIOR

FRED A. SEATON, *Secretary*

GEOLOGICAL SURVEY

Thomas B. Nolan, *Director*

For sale by the Superintendent of Documenst, U.S. Government Printing Office
Washington 25, D.C. - Price 35 cents (paper cover)

CONTENTS

	Page
Abstract	11
Introduction	12
Layer charge relations of the trioctahedral micas, theoretical	12
Accommodation of trivalent cations in natural trioctahedral micas	13
Calculation of formulas	13
Excluded analyses and formulas	15
Accommodation of extra positive octahedral charges in micas studied	16
R^{+2}-R^{+3} relation in trioctahedral micas	22
Mg-Fe^{+2} relation in trioctahedral micas	23
Magnesium replacement system	24
Phlogopites	26
Eastonite	26
Biotites	27
Annite	29
Siderophyllites and lepidomelanes	30
Chemical composition and geologic occurrence	32
Discussion of relation between mica composition and occurrence	37
Summary and conclusions	38
References cited	39
Index	49

ILLUSTRATIONS

	Page
FIGURE 6. Relation between additional positive octahedral charges and negative charges available to neutralize them	17
7. Relation between additional positive octahedral charges and negative tetrahedral charges in excess of 1.00	18
8. Relation between octahedral occupancy and the number of additional octahedral positive charges due to trivalent and quadrivalent cations in trioctahedral micas	20
9. Relation between R^{+3} cations displaced and proxying R^{+3} (and R^{+4}) octahedral cations	23
10. Distribution of trioctahedral micas with respect to the number of additional positive octahedral charges carried by trivalent and quadrivalent octahedral cations	24
11. Relation between Mg, Fe^{+2}(Mn^{+2}), and R^{+3}(Al, Fe^{+3}, and Ti) in trioctahedral micas	25
12. Relation between chemical composition and geologic occurrence of trioctahedral micas	33
13. Relation between the composition and the geologic occurrence of biotites	38

TABLES

	Page
TABLE 1. Calculation of structural formula	13
2. Average octahedral and tetrahedral cation content of formulas for phlogopites, Mg-dominant biotites, and Fe^{+2} dominant biotites in order of number of additional positive octahedral charges	19
3. Selected data on phlogopites from Holzner (1936, table 2) with added data for octahedral and total charge	22
4. Selected data on biotites from Holzner (1936, table 3) with added data for octahedral and total charge	22
5. Range in octahedral composition of phlogopites (in order of decreasing Mg content in terms of octahedral positions)	26
6. Range in octahedral composition of biotites (in order of decreasing Mg content in terms of octahedral positions occupied)	28
7. Average octahedral composition of biotites in order of decreasing Mg content	29
8. Formulas of representative siderophyllites	30
9. Formulas of representative lepidomelanes	31
10. Formulas of micas intermediate in composition between siderophyllites and lepidomelanes	32
11. Analyses and data for writing formulas of trioctahedral micas used in correlation study (in order of decreasing MgO content)	41
12. Analyses and data for writing formulas of trioctahedral micas not used in correlation study (in order of decreasing MgO content)	46

SHORTER CONTRIBUTIONS TO GENERAL GEOLOGY

INTERPRETATION OF THE COMPOSITION OF TRIOCTAHEDRAL MICAS

By Margaret D. Foster

ABSTRACT

Structural formulas calculated for more than 200 published analyses of phlogopites, biotites, siderophyllites, and lepidomelanes indicate that the additional positive charges carried by trivalent cations proxying for bivalent Mg in the octahedral group of trioctahedral micas are accommodated in two different ways, (1) by a positive charge on the octahedral layer, which is neutralized by an equivalent increase in the negative tetrahedral charge (increased replacement of Si by Al), and all the octahedral sites are occupied, or (2) are neutralized by negative charges associated with unoccupied octahedral sites.

In almost all the structural formulas the octahedral group had a positive charge and octahedral occupancy was less than 3.00, indicating some degree of accommodation by both methods. The degree to which accommodation is made by (1) or (2) varies greatly. In general, however, there is a greater accommodation by (2) than by (1) the greater the octahedral trivalent cation content. As a result, there is also a general decrease in octahedral occupancy with increase in octahedral trivalent cation content. In most biotites, siderophyllites, and lepidomelanes octahedral occupancy is significantly less than 3.00 sites—hence they are not truly trioctahedral, nor are they octaphyllites. The few formulas in which trivalent cations occupy more than one octahedral site suggests that this is the essential limit of replacement of R^{+2} by R^{+3} in these micas. It is also strong evidence against the existence of a complete series between phlogopite and muscovite.

Coincident with replacement of Mg by R^{+3}, there is also replacement of Mg by Fe^{+3}, ion for ion. With few exceptions the calculated formulas show both types of octahedral replacement. But the two types, although coincident, are independent; there is no relation between the amount of R^{+3} present and the amount of Fe^{+3} present. Neither type of replacement forms a separate series, as a series of Fe^{+3} only replacing Mg, of which Winchell's annite is the theoretical end member. No representative of this end member was found among the more than 200 analyses collected. On the evidence of the analyses and their calculated formulas, an octrahedral occupancy of more than 2.20 positions by Fe^{+3} is not to be expected.

The only trioctahedral micas in which more than 90 percent of the octahedral positions are occupied by one species of cation are some phlogopites. From pure phlogopite as the prototype, the composition of all other trioctahedral micas may be derived by replacement of Mg by, most commonly, Fe^{+3} and R^{+3} (Al and Fe^{+3}). In phlogopites the proxying of such cations for Mg is minor, and Mg occupies more than 70 percent of the occupied positions. Progressively greater proxying of these other cations for Mg leads successively to Mg biotites, in which Mg is still the dominant octahedral cation but in which Fe^{+3} is present in significant amounts, Fe^{+3} biotites, in which Fe^{+3} is the dominant octahedral cation, with Mg present in subordinate but significant amounts, and siderophyllites and lepidomelanes, in which Mg is essentially absent, with Fe^{+3} the greatly dominant bivalent octahedral cation and with significant amounts of aluminum and (or) ferric iron. These relations are expressed in the following formulas, which show the range in composition of the different groups:

Phlogopite

$$\underbrace{[(R^{+3}_{<0.30}Fe^{+3}_{<0.30}Mg_{3.00-2.00})}_{3.00-2.55}\overset{<+0.30}{}\overset{(-1.00)-(-1.30)}{(Si_{3.00-2.70}Al_{1.00-1.30})O_{10}(OH)_2]^{-1.00\pm0.10}K(Na,Ca/2)^{+1.00\pm0.10}_{1.00\pm0.10}}$$

Mg biotite
Fe^{+3} biotite

$$\underbrace{[(R^{+3}_{0.25-1.00}Fe^{+3}_{0.60-1.73}Mg_{(1.75-0.50)})}_{2.00-2.55}\overset{<+0.50}{}\overset{(-1.00)-(-1.50)}{(Si_{3.00-2.50}Al_{1.00-1.50})O_{10}(OH)_2]^{-1.00\pm0.10}K(Na,Ca/2)^{+1.00\pm0.10}_{1.00\pm0.10}}$$

Siderophyllites
and
lepidomelanes

$$\underbrace{[(R^{+3}_{0.50-1.00}Fe^{+3}_{2.25-1.85}Mg_{<0.15}Li_{0.15})}_{2.00-2.55}\overset{<+0.50}{}\overset{(-1.00)-(1.50)}{(Si_{3.00-2.50}Al_{1.00-1.50})O_{10}(OH)_2]^{-1.00\pm0.10}K(Na,Ca/2)^{+1.00\pm0.10}_{1.00\pm0.10}}$$

Thus the trioctahedral micas can be considered members of a complete system, at one end of which is phlogopite, with essentially complete octahedral occupancy by Mg, and at the other end of which is siderophyllite and lepidomelane, with essentially zero octahedral occupancy by Mg.

There is not a clear distinction in the composition of biotites from different kinds of rocks. Biotites from different igneous rocks, granites, diorites, granodiorites, nepheline syenites may be very similar in composition; on the other hand, biotites from the same kind of rock may differ greatly in composition. Micas at the extreme ends of the trioctahedral replacement system, phlogopites and siderophyllites-lepidomelanes, which have extremely high or extremely low Mg content, occur in more extreme types of rocks, peridotites and other ultramafic rocks, metamorphosed limestone, and contact zones of metamorphism on the one hand, and pegmatites and greisen on the other.

INTRODUCTION

This study of the compositional and layer charge relations of the trioctahedral micas is an extension of a similar study (Foster, 1956) of the composition and layer charge relations of the dioctahedral potassium micas. In that study it was shown that these micas may be classified and correlated on the basis of the relation between the charges on their tetrahedral and octahedral layers. It is the purpose of this paper to present a similar interpretation of the composition and layer charge relations of the trioctahedral micas.

LAYER CHARGE RELATIONS OF THE TRIOCTAHEDRAL MICAS, THEORETICAL

Ideally, the layer charge relations of the trioctahedral micas are the same as those of muscovite, as expressed in their theoretical or ideal formulas,

$$[(\overset{0.00}{\mathrm{Mg,Fe^{+2}}})_{3.00}(\overset{-1.00}{\mathrm{Si_{3.00}Al_{1.00}}})\mathrm{O_{10}(OH)_2}]^{-1.00}\mathrm{K}^{+1.00}_{1.00},$$

$$[\mathrm{Al}_{2.00}(\overset{0.00}{\mathrm{Si_{3.00}}}\overset{-1.00}{\mathrm{Al_{1.00}}})\mathrm{O_{10}(OH)_2}]^{-1.00}\mathrm{K}^{+1.00}_{1.00}.$$

In both of these formulas the octahedral group is neutral; all the inherent unit layer charge is on the tetrahedral group, owing to occupation of one-fourth of the tetrahedral cationic sites by Al.

Few natural micas, however, have the exact composition specified by these theoretical or ideal formulas. In the dioctahedral micas bivalent cations occupy some of the octahedral positions ideally presumed to be occupied by Al, and in the trioctahedral micas some of the octahedral positions, ideally presumed to be occupied by bivalent ions like Mg or Fe^{+2}, are occupied by trivalent ions like Al or Fe^{+3}. Proxying of a bivalent for a trivalent octahedral cation, ion for ion, in the dioctahedral micas induces a negative charge on the octahedral layer equivalent to the number of bivalent octahedral cations. Constancy of charge and K content is preserved by an equivalent decrease in the negative tetrahedral charge, that is, equivalent decrease in tetrahedral Al content and increase in Si content. These changes can be expressed by the equation, $+n\mathrm{R}^{+2}+n\mathrm{Si}=-2n\mathrm{R}^{+3}$. Replacement of one-half of the trivalent octahedral cations by bivalent cations produces the tetrasilicic end member of the trisilicic-tetrasilicic series,

$$[(\overset{-1.00}{\mathrm{R}^{+3}_{1.00}}\overset{0.00}{\mathrm{R}^{+2}_{1.00}})\mathrm{Si_{4.00}O_{10}(OH)_2}]^{-1.00}\mathrm{K}^{+1.00}_{1.00}$$

in which all the inherent unit layer charge is on the octahedral layer.

By analogy, proxying of a trivalent cation for a bivalent ion, ion for ion, in the octahedral group of a trioctahedral mica should induce a positive charge on the octahedral layer, which, for constancy of inherent layer charge and K content, would require an equivalent increase in the negative tetrahedral charge and, consequently, equivalently increased proxying of Al for Si. This charge relation is assumed in Winchell and Winchell's (1951, p. 373) formulas (recast in the notation used in this paper) for eastonite,

$$[(\mathrm{Al}_{0.3}\overset{+0.5}{\mathrm{Mg}_{2.3}})(\overset{-1.5}{\mathrm{Si}_{2.3}\mathrm{Al}_{1.3}})\mathrm{O_{10}(OH)_2}]^{-1.00}\mathrm{K}^{+1.00}_{1.00}$$

and siderophyllite,

$$[(\mathrm{Al}_{0.3}\overset{+0.5}{\mathrm{Fe}^{+2}_{2.3}})(\overset{-1.5}{\mathrm{Si}_{2.3}\mathrm{Al}_{1.3}})\mathrm{O_{10}(OH)_2}]^{-1.00}\mathrm{K}^{+1.00}_{1.00}$$

In these formulas it is also assumed that all 3 octahedral positions are occupied, as they would be if the proxying of trivalent for bivalent cations were 1 to 1.

Holzner (1936, p. 435) noticed, however, that in formulas calculated from biotite analyses, the number of occupied octahedral positions is between 2.89 and 2.49; in none of his formulas were 3.00 positions occupied. To explain this low octahedral occupancy he postulated that biotite is intermediate between phlogopite and muscovite in composition and that the crystal structure is built up of the 2 mica types, most biotites approximating the composition of 2 of phlogopite to 1 of muscovite, which yields a formula for biotite of:

$$[\underbrace{(\mathrm{Al}_{0.67}\overset{0.00}{\mathrm{Mg}_{2.00}})}_{2.67}(\overset{-1.00}{\mathrm{Si_{3.00}Al_{1.00}}})\mathrm{O_{10}(OH)_2}]^{-1.00}\mathrm{K}^{+1.00}_{1.00}$$

In this formula the tetrahedral group has the same composition and charge as it has in the ideal formulas for phlogopite and muscovite, and the octahedral layer is neutral, as in the theoretical or ideal formulas. The 0.67 additional positive charges carried by the 0.67 trivalent ions are neutralized by the 0.67 negative charges associated with the 0.33 unoccupied octahedral positions.

Thus in Winchell's formulas for eastonite and siderophyllite and in the formula suggested by Holzner for biotite, trivalent octahedral ions are accommodated in two quite different ways. In one the proxying of trivalent for bivalent octahedral ions is 1:1; all the octahedral cationic positions are occupied; and the additional positive charges carried by the trivalent octahedral ions form a positive charge on the octahedral layer and are neutralized by an equivalent increase in the negative tetrahedral charge owing to greater proxying of Al for Si. These relations are expressed in the equation

$$(+2n\mathrm{R}^{+3})=(-n\mathrm{R}^{+2})+(-n\mathrm{Si}^{+4}) \qquad \text{(A)}$$

In the other way of accommodating trivalent octahedral cations, 2 trivalent cations proxy for 3 bivalent cations. There is, consequently, no increase in the number of positive charges present, nor is there any change in the layer charge relations, between the octahedral and tetrahedral groups, but there is a decrease in the number of octahedral positions occupied equivalent to one-half of the number of trivalent octahedral cations. These relations are expressed in the equation

$$(+2nR^{+3})=(-3nR^{+2})+(-n\ \text{Oct. Pos.}) \qquad \text{(B)}$$

In the first type of accommodation for trivalent octahedral ions, the formula is characterized by full octahedral occupancy, a positive octahedral charge, and a negative tetrahedral charge greater than 1.00 by the number of trivalent octahedral cations; in the second type of accommodation the formula is characterized by deficient octahedral occupancy, a neutral octahedral layer, and a negative tetrahedral charge very close to 1.00.

ACCOMMODATION OF TRIVALENT CATIONS IN NATURAL TRIOCTAHEDRAL MICAS

CALCULATION OF FORMULAS

For a study of the general characteristics of natural trioctahedral micas and, particularly, their accommodation of trivalent octahedral cations, structural formulas were calculated from more than 200 analyses of phlogopites, biotites, siderophyllites, and lepidomelanes. The formulas were calculated by the method devised by Marshall (1949, p. 58) and modified by the author (Foster, 1951, p. 728). The calculations involved are illustrated by example in table 1. The gram-equivalents of cationic constituents in the structure are obtained by dividing the percent of each constituent present by a factor obtained by dividing the molecular weight of that constituent by the number of cationic valencies in its molecular formula. Thus for Fe_2O_3 the factor to be used is the molecular weight of Fe_2O_3, 159.70, divided by 6, which is 26.617; for FeO it is 71.85 divided by 2, or 35.925.

TABLE 1.—*Calculation of structural formula*

[For 49, table 11]

Percent	*Gram-equivalents of cationic constituents*	*Cationic valencies per unit cell*	*Cations per unit cell*		*Charge*
SiO_2 36.32	÷ (60.04÷4) = 2.419	÷ 0.1109 = 21.912	÷ 4 = 5.453	tetrahedral group	−2.547
			2.547		
			8.000		
Al_2O_3 14.66	÷ (101.96÷6) = 0.863	÷ 0.1109 = 7.781	÷ 3 = 2.594 → 0.047		
TiO_2 3.42	÷ (79.90÷4) = .171	÷ .1109 = 1.542	÷ 4 = .385	octahedral group	+0.630
Fe_2O_3 4.80	÷ (159.70÷6) = .180	÷ .1109 = 1.623	÷ 3 = .541		
FeO 14.74	÷ (71.85÷2) = .410	÷ .1109 = 3.697	÷ 2 = 1.848		
MgO 12.38	÷ (40.32÷2) = .614	÷ .1109 = 5.537	÷ 2 = 2.768		
MnO 0.34	÷ (70.93÷2) = .010	÷ .1109 = .090	÷ 2 = .045		
	Sum (−Si and Al)	12.489	5.634 (octahedral occupancy)		1.917 (composite layer charge)
	Octahedral Al cations × 3 →	.141			
		+12.630			
		−12.000			
		+ 0.630 (octahedral charge)			
CaO Trace					
Na_2O 0.90	÷ (61.98÷2) = 0.029	÷ 0.1109 = 0.261	÷ 1 = 0.261		
K_2O 8.63	÷ (94.20÷2) = .183	÷ .1109 = 1.650	÷ 1 = 1.650		
	4.879	1.911	1.911 (interlayer cationic charge)		
	4.879÷44 = 0.1109				
H_2O 2.72	-----	------	------		-------

Structural formula (half-cell)

$$\frac{[(Al_{0.05}Ti_{0.19}Fe^{+3}_{0.27}Fe^{+2}_{0.02}Mg_{1.38}Mn^{+2}_{0.02})(Si_{2.72}Al_{1.27})O_{10}(OH)_2]^{-1.00}(K_{0.83}Na_{0.13})^{+0.95}_{0.85}}{2.80}$$

+0.27 −1.27

The second step in the calculation is to convert gram-equivalents of the cationic constituents to cationic valencies in the unit cell. As the number of cationic valencies must be the same as the number of anionic valencies present, the number of cationic valencies present is usually based on the number of anionic valencies furnished by the H_2O+ and F reported in the analysis. However, in many of the analyses insufficient data were given for this; in some F was not reported, in others plus and minus waters were not reported, only total water, and in still others the H_2O+ and F together were much too low. The formulas were, therefore, all calculated on the basis of the cationic and anionic valence content of the idealized unit cell, 44. The sum of the gram-equivalents of the cationic constituents was, therefore, divided by 44 to obtain the factor for converting them to cationic valencies per unit cell. After dividing the gram-equivalents of each cationic constituent by this factor, the number of valencies per unit cell thus obtained of each cation is then divided by its valence to obtain the number of cations per unit cell.

The aluminum cations are divided between the tetrahedral and octahedral groups; enough Al is allocated to the tetrahedral group to bring the total, with silicon, to 8.00, and the remainder is assigned to the octahedral group. The sum of the cations in the octahedral group should, theoretically, be 6.00, but in most of the calculated formulas for trioctahedral micas it is less than 6.00.

Throughout this paper the discussion is based on the half-cell formula. To write the half-cell formula, the values for the cations and charges per unit cell are merely halved, as in the formula at the bottom of table 1. Attention is called to the order in which the groups and cations within each group in the formula are written. First the octahedral group (enclosed in parentheses) is noted, with the cations in that group written in order of decreasing valence, except for Ti, which is written after Al. Then the tetrahedral group (also enclosed in parentheses) is noted, with Si, the principle cation, written first. Above each group its charge is noted. After these two groups, which indicate the cationic composition, the anionic composition, $O_{10}(OH)_2$, is written; and the whole is bracketed, as indicating the composition of the composite layers. After the upper part of the closing bracket, the total negative charge on the composite layer unit is written. This is followed by a notation of interlayer cation content, with the positive charge carried by these cations being written at the top of the closing parenthesis, and the number of positions occupied by these cations at the bottom. The interlayer cations are written last, rather than first, the more conventional position, because the amount and charge of the interlayer cations is dependent on and must neutralize the charge on the composite layers.

Theoretically 32 of the 44 anionic or negative charges are allocated to the tetrahedral group and 12 to the octahedral group. Thus if the tetrahedral group is entirely made up of Si cations, which are quadrivalent, the number of positive charges present is exactly equal to the number of negative charges, $4\times8=32$, and the tetrahedral layer is neutral. But if the tetrahedral group contains some Al, which is trivalent, there are not enough positive charges to neutralize all the negative charges present and the tetrahedral layer has a negative charge. Thus in the example given in table 1, the tetrahedral group contains 5.453 Si cations and 2.547 Al cations, which carry 29.453 positive charges, and the tetrahedral layer has a negative charge of 2.547, exactly equal to the number of Al cations in that layer. If all the 6 octahedral positions in the unit cell of a mica are occupied by bivalent cations, as by Mg in phlogopite, the 12 positive charges they carry exactly equal the 12 negative charges allocated to that layer, and the layer is neutral; but if some of the positions are occupied by trivalent ions, the octahedral layer may have a positive charge, even though all the octahedral positions are not occupied, as in the example given in table 1. The number of positive octahedral charges present is calculated by multiplying the number of cations of each constituent by its valence and by adding these together. More simply, the same result can be obtained by taking the sum of the gram-equivalents per total of 44 of all the octahedral cations except Al cations and adding to this the number of octahedral Al cations (from the column headed cations per unit cell) multiplied by 3, as is shown in table 1. If this number, as in the example given, exceeds 12.000, the octahedral layer has a positive charge equal to the excess; if it is less than 12.000, the octahedral layer has a negative charge.

The algebraic sum of the tetrahedral and octahedral charges is the inherent charge on the unit layers and should closely agree with the charge on the interlayer cations, as it does in the example given. The negative inherent charge on the unit layers and the positive charge on the interlayer cations should be close to 2.00 (1.00 in the half-cell formula) for trioctahedral micas like the phlogopites and biotites. In evaluating the half-cell formulas used in this study, a variation of plus or minus 0.1 (0.2 in the unit cell) was permitted in these values. Formulas, in which either the negative inherent charge on the unit layers or the positive interlayer cation charge, or both, were greater or less than 1.00 by more than 0.1, were not used in the study. This was done in order to exclude from the study the formulas that may represent hydrous micas,

in which the interlayer cations are generally lower than in true micas, or, possible contamination of trisilicic trioctahedral micas with other materials.

The role of titanium in micas is ambiguous. Apparently no studies have been made to determine whether or not the titanium reported is actually in the mica structure. In some micas discrete crystals of rutile can be discerned, but what proportion of the total titanium content these represent is not known. In other micas discrete crystals of rutile are not discernible, and the color of the micas suggests that the titanium is in the layer structure. For some analyses used in this study, formulas were calculated as if all the titanium were in the layer structure and as if none of the titanium were in the layer structure. These calculations showed that for the amount of titanium usually reported, the inclusion or exclusion of titanium in calculating the formula has only a slight effect on the number of positions occupied by other octahedral cations. In accordance with general usage, therefore, titanium was included in the octahedral group in calculating the formulas herein used. The analyses (and data from which their calculated formulas may be written) that were used in the study are given in table 11; the excluded analyses (and data from which their calculated formulas may be written) are given in table 12.

EXCLUDED ANALYSES AND FORMULAS

Exclusion of certain analyses and formulas from the study does not necessarily indicate that they represent poor specimens or poor analyses. Many of the formulas in which the negative inherent unit layer charge and the positive interlayer cation charge is less than 0.90 represent very high magnesium trioctahedral micas, that is, phlogopites. In addition to their low inherent unit layer charge and low interlayer cation charge these formulas are, in general, characterized by a positive octahedral layer charge greater than the number of extra positive charges carried by their trivalent octahedral cations, and by a high octahedral occupancy, many of the formulas having an octahedral occupancy greater than 3.00. These characteristics indicate the allocation of too many cations to the octahedral layer, and too few to interlayer cation positions. Reallocation of some octahedral cations in these formulas to interlayer positions would produce more rational formulas.

For many years it was customary in calculating formulas from analyses of montmorillonite, which has the same structure as the micas, to allocate all the Mg to the octahedral group. The result was that in most formulas for montmorillonite the number of occupied octahedral positions was greater than 2.00, up to 2.24, and Ross and Hendricks (1945, p. 44) concluded that in montmorillonite more than 2.00 octahedral positions were characteristically occupied. However, the writer (Foster, 1951, p. 725) determined the exchangeable cations in a number of montmorillonites and found that they all contained some exchangeable Mg, and that when only nonexchangeable Mg was allocated to the octahedral layer, the number of octahedral positions occupied was 2.00±0.02 in the same specimens that apparently had as many as 2.12 octahedral positions occupied when all the Mg was allocated to the octahedral group.

These facts indicate that Mg can occupy interlayer positions and suggest that in the highly magnesium micas mentioned some of the magnesium should be considered as occupying interlayer positions. For example, if all the MgO, 24.60 percent, analysis D15, table 12, is allocated to the octahedral group in the usual way, the positive octahedral layer charge is 0.44, whereas only 0.32 additional positive charges are carried by the trivalent octahedral cations present; an excessive number of octahedral positions are occupied, 3.06; the inherent unit layer charge is only −0.82; and the interlayer cation charge in only +0.83. If, however, 0.75 percent of the MgO is allocated to the interlayer cations the positive octahedral layer charge is 0.28, 0.04 less than the number of positive charges carried by the trivalent octahedral cations present, 2.98 octahedral positions are occupied, the inherent unit layer charge is −0.98, and the interlayer cations charge is 0.99. A comparison of the two formulas,

$$\underbrace{[(Al_{0.16}Ti_{0.06}\overset{+0.44}{Fe^{+3}_{0.04}}Fe^{+2}_{0.19}Mg_{2.41})}_{3.06}\overset{-1.26}{(Si_{3.74}Al_{1.26})O_{10}(OH)_2}]^{-0.82}$$

$$(K,Na,Ba/2)_{0.83}^{+0.83}$$

$$\underbrace{[(Al_{0.16}Ti_{0.06}\overset{+0.28}{Fe^{+3}_{0.04}}Fe^{+2}_{0.19}Mg_{2.53})}_{2.98}\overset{-1.26}{(Si_{3.74}Al_{1.26})O_{10}(OH)_2}]^{-0.98}$$

$$(K,Na,Ba/2,Mg/2)_{0.99}^{+0.99}$$

shows that the only change in layer occupancy is in the number of octahedral positions occupied by Mg; the number of positions occupied by all the other cations, in both the octahedral and tetrahedral layers, is the same in both formulas. Therefore, if Mg does occupy interlayer positions in micas, analyses like this group which contain considerable Mg and in which the negative inherent layer charge and the positive interlayer cation charge are low, may not be faulty, or represent poor materials, but may simply represent trioctahedral micas in which some of the Mg occupies interlayer positions.

Another group of formulas was excluded from the study because their negative inherent unit layer charge and their positive interlayer ion charge was greater than 1.10. In formulas calculated from analyses in which lithium was not determined the high unit layer and interlayer charges may be due to the failure to separate lithium from sodium. Failure to separate lithium from sodium has a double effect on the formula calculation, as it is reported as sodium and is calculated as an interlayer cation rather than as an octahedral cation. Thus, in the formula the interlayer cations and their charge are high, the octahedral cations and the positive octahedral charge are low; and, consequently, the negative inherent unit layer charge is high. This double effect is shown in the formulas below for D58, table 12,

$$[\underbrace{(Al_{0.00}Ti_{0.04}Fe^{+3}_{1.09}Fe^{+2}_{1.13}Mg_{0.17}Mn^{+2}_{0.14})}_{2.57}(Si_{2.46}Al^{-1.54}_{1.34}Fe^{+3}_{0.20})O_{10}(OH)_2]^{-1.23}(K,Na,Ca/2)^{+1.34}_{1.23}$$

$$[\underbrace{(Al_{0.00}Ti_{0.04}Fe^{+3}_{1.09}Fe^{+2}_{1.13}Mg_{0.17}Mn^{+2}_{0.14}Li_{0.34})}_{2.87}(Si_{2.45}Al^{-1.55}_{1.34}Fe^{+3}_{0.20})O_{10}(OH)_2]^{-0.99}(K,\ Na,\ Ca/2)^{+0.98}_{0.97}$$

In the first formula, which is calculated from the analysis as reported, the negative inherent layer charge and the positive interlayer cationic charge are very high, but the octahedral occupancy is quite low. The second formula is a recalculation from the same analysis on the assumption that the Na_2O reported contained 1 percent of Li_2O. The formula content of other cations present is very little changed, but the octahedral occupancy is raised from 2.57 to 2.87, and the negative unit layer charge and the positive interlayer cation charge are reduced to 0.99 and 0.98, respectively. Thirteen of the eighteen formulas that were not used because of high unit layer charge and high interlayer cation charge were of the type most likely to contain lithium, high in Fe^{+2} and very low in Mg. Thus, although high unit layer and interlayer cation charges may be due to faulty analysis, particularly in determination of the alkalies, it is also possible that a calculated formula may show such high charges because of the analyst's failure to separate sodium and lithium. Failure to separate and determine Rb and Cs may also contribute to an apparently high alkali content.

In calculating the formulas for several analyses published as analyses of phlogopites or biotites, it was found necessary to allocate all the Al_2O_3, all the Fe_2O_3, and some of the TiO_2 to the tetrahedral layer to complete the filling of that layer, and in one phlogopite analysis it was necessary to assign all the Al_2O_3, Fe_2O_3, TiO_2, and FeO to the tetrahedral layer, leaving only MgO and a little Li_2O in the octahedral layer—even so, the octahedral occupancy was high, 3.08 positions. All such analyses and formulas were excluded from the study as not representing the general chemical composition of trioctahedral micas, the subject of this study, whether or not the analyses themselves may be faulty or may represent contaminated materials.

Two other small groups of analyses with their derived formulas that were excluded from the study were not representative of the kind of micas under consideration. In one group the K content was very low, occupying fewer than 0.75 positions, with relatively high Ca and (or) Na content; in the other group the octahedral trivalent occupancy was very high, greater than 1.50, and total octahedral occupancy was very low, less than 2.50 positions. In several of the latter group the trivalent octahedral cations made up more than 65 percent of the octahedral cations. In one analysis, D61, table 12, which has 19.49 percent of Fe_2O_3, and 14.10 percent of FeO, Clarke (1903, p. 77) suspected alteration. A later analysis showed 24.22 percent of Fe_2O_3 and 13.11 percent of FeO. Another analysis reports 27.19 percent of Fe_2O_3 with only 0.64 per cent of FeO. In the formula for this analysis bivalent cations occupy less than 30 percent of the occupied octahedral positions, all the rest are occupied by trivalent cations. In analyses that yield formulas with unusually high octahedral Al content, contamination with muscovite may be suspected. For example, the material represented by one analysis was obtained from arborescent aggregates of biotites with muscovite occurring in the terminals of the aggregates.

ACCOMMODATION OF EXTRA POSITIVE OCTAHEDRAL CHARGES IN MICAS STUDIED

In a few of the formulas included in the study, the proxying of trivalent for bivalent octahedral cations is in accordance with equation A, $(+2nR^{+3})=(-nR^{+2})+(-nSi^{+4})$, as in the following formula for a mica from Russia (26, table 11),

$$[\underbrace{(Al_{0.12}Ti_{0.06}Fe^{+3}_{0.08}Fe^{+2}_{0.46}Mg_{2.29})}_{3.01}(Si_{2.67}Al^{-1.33}_{1.23})O_{10}(OH)_2]^{-0.99}(K_{0.74},Na_{0.14}Ca/2_{0.06})^{+0.97}_{0.92}$$

In this formula the proxying of trivalent for bivalent ions is 1:1, 0.26 Al, Ti, and Fe^{+3} ions proxy for 0.25 R^{+3} ions, and all the octahedral positions are occupied. The additional positive charges carried by Al, Fe^{+3}, and Ti form a positive charge of 0.34 on the octahedral

layer, which is neutralized by an equivalent increase in the negative tetrahedral charge. On the other hand, a few formulas exhibit the type of accommodation for trivalent octahedral ions expressed by equation B, $(+2nR^{+3})=(-3nR^{+2})+(-n\text{Oct. Pos.})$, as does this formula for a biotite from L&ven Island (84 table 11),

$$\underset{2.79}{[(Al_{0.16}Ti_{0.04}Fe^{+3}_{0.32}Fe^{+2}_{1.26}Mg_{0.93}Mn^{+2}_{0.08})}^{+0.04}(Si_{1.93}Al_{1.07})O_{10}(OH)_2]^{-1.02}\overset{-1.07}{}$$

$$(K_{0.83}Na_{0.23})^{+1.06}_{1.06}$$

In this formula the proxying of trivalent for bivalent octahedral cations is approximately 2:3; 0.42 Al, Ti, and Fe^{+3} cations carrying 0.46 additional positive charges proxy for 0.63 R^{+2} cations, and 0.21 unoccupied octahedral positions furnish 0.42 negative charges to neutralize 0.42 of the additional positive charges. The octahedral layer is, therefore, almost neutral, having a positive charge of only 0.04; and the tetrahedral charge is 1.07, close to the 1.00 of the theoretical formula. However, most of the formulas calculated for this study are characterized by both a positive octahedral charge and a deficiency in octahedral occupation; this indicates a dual adjustment, as in this formula for a phlogopite from Uganda, 33, table 11,

$$\underset{2.85}{[(Al_{0.00}Ti_{0.13}Fe^{+3}_{0.22}Fe^{+2}_{0.31}Mg_{2.18}Mn_{0.02})}^{+.22}(Si_{2.71}Al_{1.29})O_{10}(OH)_2]^{-1.07}\overset{-1.29}{}$$

$$(K_{0.10}Na_{0.32}Ca/2_{0.23}Ba/2_{0.04})^{+1.04}_{0.98}$$

In this formula the trivalent and quadrivalent octahedral cations carry 0.52 positive charges in excess of the number of positive charges carried by the same number of bivalent cations. Of these additional charges, 0.30 are neutralized by 0.15 unoccupied octahedral positions and 0.22 form a positive charge on the octahedral layer, which is neutralized by an increase in the negative charge on the tetrahedral layers. The inherent layer charge is, consequently, very close to 1.00 (1.07), and is balanced by interlayer cations, K, Na, Ba, and Ca, carrying an equivalent positive charge.

As illustrated by this example, in dual accommodation for trivalent and quadrivalent octahedral cations in trioctahedral micas, the additional positive octahedral charges are neutralized by the negative tetrahedral charge in excess of 1.00, in accordance with equation A, and by the negative octahedral charges left available by unoccupied octahedral positions, in accordance with equation B. Theoretically, the sum of these negative charges should exactly equal the number of additional positive charges carried by the trivalent and quadrivalent octahedral actions. This relation in the trioctahedral micas studied is shown in figure 6, in which the number of additional positive charges carried

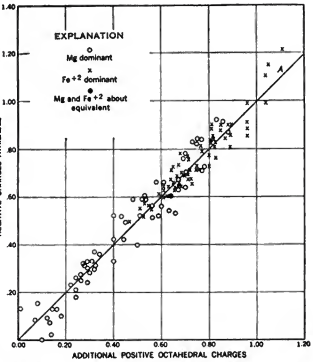

FIGURE 6.—Relation between additional positive octahedral charges and negative charges available to neutralize them.

by trivalent and quadrivalent octahedral cations in each formula is plotted against the number of negative charges available to neutralize them; that is, the sum of the tetrahedral charge in excess of −1.00 plus the number of unoccupied octahedral positions doubled. Points for formulas in which the number of additional positive octahedral charges is exactly equal to the sum of negative charges available fall on the line bisecting the figure. Location of a point above or below the line indicates that in the formula represented by the point the negative charges available are greater or less, respectively, than the number of additional positive octahedral charges, by the distance of the point from the line. The close clustering of the points along the line indicates that there is a fairly close agreement in the formulas between the number of additional positive octahedral charges and the number of negative charges available to neutralize them The points on or close to the line represent formulas in which the inherent unit layer negative charge and the interlayer cation positive charge is almost exactly 1.00. Those farthest from the line represent formulas in which the inherent unit layer negative charge and the interlayer cation positive charge is near 0.90 or 1.10. In the formulas in which the inherent unit layer negative charge and the interlayer cation charge is less than 1.00, the tetrahedral negative charge in excess of −1.00 is less than the octahedral positive charge; in formulas

in which the inherent layer negative charge and the interlayer cation positive charge is greater than 1.00, the tetrahedral negative charge in excess of -1.00 is greater than the octahedral positive charge. As pointed out in the discussion on the calculation of formulas (p. 13), these discrepancies may be due to analytical error, particularly in the determination of Ca, Na, and K, to failure to determine Li or CO_2, or to the use, in calculating the formulas, of the theoretical oxygen and hydroxide, fluorine values $(O_{10}(OH,F)_2)$ because of lack or obvious inaccuracy of data on these constituents in the analyses.

The degree of accommodation for additional positive octahedral charges by each of the two methods in the trioctahedral micas under study is shown (fig. 7) by plotting, for each formula, the additional positive octahedral charges against the number of negative tetrahedral charges in excess of 1.00. Points for formulas that exhibit accommodation for trivalent and quadrivalent octahedral cations exclusively in accordance with equation A fall on line A, those for formulas that exhibit accommodation for trivalent and quadrivalent octahedral cations exclusively in accordance with equation B fall on the ordinate, and those for formulas exhibiting both types of accommodation for trivalent octahedral cations fall between these two lines. The location of most of the points between these two lines makes it quite apparent that in most of these trioctahedral micas both types of accommodation for trivalent and quadrivalent octahedral cations are represented. In formulas represented by points near the middle of the area between lines A and B, accommodation has been made both ways about equally; in formulas represented by points closer to line A or to the ordinate of the graph, line B, that type of accommodation represented by line A or line B was made to a greater degree than by the other type.

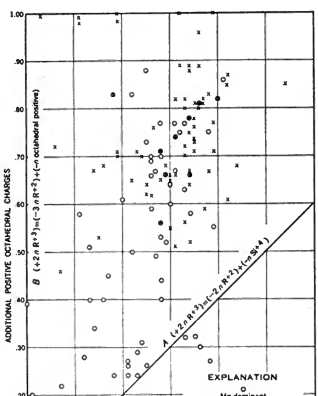

FIGURE 7.—Relation between additional positive octahedral charges and negative tetrahedral charges in excess of 1.00.

The average adjustment in trioctahedral micas for different amounts of additional positive octahedral charges due to trivalent cations is shown by the average formulas in table 2. To arrive at these average formulas the calculated formulas used in this study were grouped according to the number of additional positive charges carried by their trivalent (and quadrivalent) octahedral cations. If the formula contains no Ti, the number of additional octahedral positive charges is equivalent to the number of octahedral positions occupied by trivalent cations, usually Al and Fe^{+3}. But if the formula contains Ti, the number of positions occupied by Ti must be multiplied by 2, as Ti^{+4} carries 2 more charges than a bivalent cation, and this number is added to the number of octahedral positions occupied by trivalent cations. For example, in the formula for No. 33, table 11, trivalent cations occupy 0.22 octahedral positions and Ti occupies 0.15 octahedral positions. Thus the number of additional positive octahedral charges present is $0.22+(0.15\times2)=0.52$. From the formulas in each of these groups, separate average formulas were derived for the magnesium and for the bivalent iron-dominant micas when both are sufficiently represented in a group. However, sufficient numbers of formulas to permit derivation of average Fe^{+2}-dominant formulas are found only in the groups in which the number of additional positive charges is greater than 0.50. In only three Fe^{+2}-dominant formulas were the number of additional positive charges carried by trivalent and quadrivalent octahedral cations less than 0.50. On the other hand, Mg-dominant formulas are found in all the groups, and from these the general mode of adjustment of trioctahedral micas to the presence of trivalent and quadrivalent cations in the octahedral layer can be deduced.

TABLE 2.—*Average octahedral and tetrahedral cation content of formulas for phlogopites, Mg-dominant biotites, and Fe^{+2}-dominant biotites in order of number of additional positive octahedral charges*

Group	Number of additional positive octahedral charges	Number of formulas	Mg-dominant formulas	Number of formulas	Fe^{+2}-dominant formulas
A	0.00–0.10 / 0.05	6	$\overset{+0.05}{(Al_{0.00}Fe^{+3}_{0.05}Fe^{+2}_{0.05}Mg_{2.90})}\ \overset{-1.05}{(Si_{3.10}Al_{1.00})}$ / 3.00	None	
B	0.11–0.20 / 0.15	8	$\overset{+0.15}{(Al_{0.10}Fe^{+3}_{0.05}Fe^{+2}_{0.10}Mg_{2.75})}\ \overset{-1.15}{(Si_{3.85}Al_{1.15})}$ / 3.00	None	
C	0.21–0.30 / 0.25	14	$\overset{+0.25}{(Al_{0.15}Fe^{+3}_{0.10}Fe^{+2}_{0.20}Mg_{2.55})}\ \overset{-1.25}{(Si_{3.75}Al_{1.45})}$ / 3.00	None	
D	0.31–0.40 / 0.35	11	$\overset{+0.25}{(Al_{0.15}Ti_{0.05}Fe^{+3}_{0.10}Fe^{+2}_{0.20}Mg_{2.35})}\ \overset{-1.25}{(Si_{3.75}Al_{1.25})}$ / 2.95	1	
E	0.41–0.50 / 0.45	11	$\overset{+0.25}{(Al_{0.15}Ti_{0.05}Fe^{+3}_{0.05}Fe^{+2}_{0.20}Mg_{2.25})}\ \overset{-1.25}{(Si_{3.75}Al_{1.25})}$ / 2.90	2	
F	0.51–0.60 / 0.55	6	$\overset{+0.25}{(Al_{0.20}Ti_{0.10}Fe^{+3}_{0.15}Fe^{+2}_{0.20}Mg_{2.15})}\ \overset{-1.25}{(Si_{3.75}Al_{1.25})}$ / 2.85	6	$\overset{+0.25}{(Al_{0.15}Ti_{0.10}Fe^{+3}_{0.15}Fe^{+2}_{1.20}Mg_{0.95})}\ \overset{-1.25}{(Si_{3.75}Al_{1.25})}$ / 2.85
G	0.61–0.70 / 0.65	9	$\overset{+0.25}{(Al_{0.15}Ti_{0.10}Fe^{+3}_{0.20}Fe^{+2}_{0.20}Mg_{1.95})}\ \overset{-1.25}{(Si_{3.75}Al_{1.25})}$ / 2.80	14	$\overset{+0.25}{(Al_{0.15}Ti_{0.10}Fe^{+3}_{0.20}Fe^{+2}_{1.45}Mg_{0.95})}\ \overset{-1.25}{(Si_{3.75}Al_{1.25})}$ / 2.80
H	0.71–0.80 / 0.75	8	$\overset{+0.25}{(Al_{0.20}Ti_{0.10}Fe^{+3}_{0.25}Fe^{+2}_{0.25}Mg_{1.95})}\ \overset{-1.25}{(Si_{3.75}Al_{1.25})}$ / 2.75	17	$\overset{+0.25}{(Al_{0.20}Ti_{0.10}Fe^{+3}_{0.25}Fe^{+2}_{1.25}Mg_{0.95})}\ \overset{-1.25}{(Si_{3.75}Al_{1.25})}$ / 2.75
I	0.81–0.90 / 0.85	4	$\overset{+0.25}{(Al_{0.25}Ti_{0.10}Fe^{+3}_{0.20}Fe^{+2}_{0.20}Mg_{1.95})}\ \overset{-1.25}{(Si_{3.75}Al_{1.25})}$ / 2.70	12	$\overset{+0.25}{(Al_{0.25}Ti_{0.10}Fe^{+3}_{0.20}Fe^{+2}_{1.25}Mg_{0.75})}\ \overset{-1.25}{(Si_{3.75}Al_{1.25})}$ / 2.70

The average Mg-dominant formulas indicate, in general, that if the number of additional positive charges carried by trivalent and quadrivalent octahedral cations is less than 0.25, all the additional positive charges form a positive charge on the octahedral layer, the negative tetrahedral charge is greater than 1.00 by an amount equivalent to the positive octahedral charge, and all the octahedral cationic positions are occupied; that is, adjustment for the additional positive octahedral charges is predominantly in accordance with equation A. Thus the average formula for group A, in which the average number of additional octahedral positive

charges is 0.05, has a positive octahedral charge of 0.05, a negative tetrahedral charge of 1.05, and all the octahedral positions are occupied. Similarly in the average formulas for groups B and C, in which the average number of additional positive octahedral charges is 0.15 and 0.25, respectively, the positive charge on the octahedral layer is equivalent to the number of additional positive charges carried by R^{+3} octahedral cations, the negative tetrahedral charge is greater than 1.00 by an equivalent amount and all the octahedral positions are occupied. In the average formula for group D, however, in which the number of additional positive charges carried by R^{+3} (and R^{+4}) octahedral cations averages 0.35, only 0.25 of these extra charges form a positive charge on the octahedral layer—the remaining 0.10 charges are neutralized by the 0.10 negative charges associated with the 0.05 unoccupied octahedral positions. In succeeding group formulas the increasingly greater number of additional positive charges is reflected not in greater positive charges on the octahedral layer and greater negative tetrahedral charges but in greater nonoccupancy of octahedral positions, that is, an increasingly greater proportion of the adjustment for trivalent and quadrivalent octahedral cations is made in accordance with equation B. Thus, in the average formulas for groups E, F, G, H, and I, the average positive octahedral charge is the same, 0.25, but the average number of octahedral positions occupied progressively decreases from 2.90, in formula E, to 2.70, in formula I.

These relations between positive octahedral charge (equation A) and octahedral occupancy (equation B) with increase in the number of additional positive octahedral charges suggest that the amount of positive charge on the octahedral layer that can be accommodated comfortably by the structure is somewhat limited, and that with a greater number of positive octahedral charges to be neutralized, neutralization by negative charges associated with unoccupied octahedral positions is generally more tolerable to the structure than neutralization by a greater negative tetrahedral charge and the necessarily greater proxying of Al for Si. Throughout the range there are, of course, some formulas that deviate greatly from the average in their mode of adjustment (fig. 7) but the average formulas illustrate the general way in which different amounts of additional positive charges carried by trivalent octahedral cations are accommodated in the trioctahedral micas.

The general decrease in octahedral occupancy with increase in the number of additional positive octahedral charges is shown graphically in figure 8. In this figure, for each formula, the number of occupied octahedral positions is plotted against the number of additional positive charges carried by trivalent (and quadrivalent) octahedral cations. If three octahedral positions were generally occupied in the trioctahedral micas and if

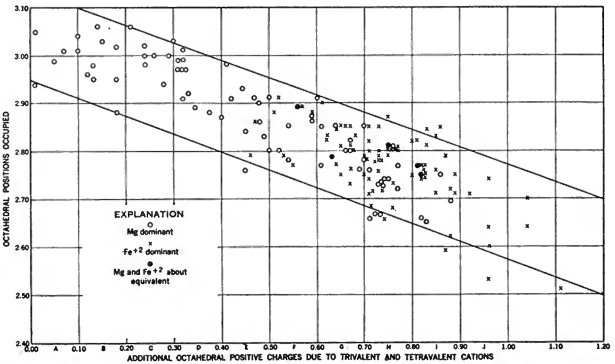

FIGURE 8.—Relation between octahedral occupancy and the number of additional octahedral positive charges due to trivalent and quadrivalent cations in trioctahedral micas.

accommodation for trivalent octahedral cations were generally made according to equation A, the points representing the extra R^{+3} charge-octahedral occupancy relation of the formulas would fall in a narrow horizontal band across the top of the figure. The general trend of the points diagonally downward from left to right indicates a general decrease in octahedral occupancy with increase in the number of additional octahedral positive charges due to some degree of adjustment for these additional charges in accordance with equation B. The width of the band indicates the variation in the degree to which adjustment for trivalent and quadrivalent octahedral cations is made in one way or the other. Formulas having quite different amounts of additional R^{+3} (and R^{+4}) positive octahedral charges may have the same octahedral occupancy, and vice versa, depending on the degree to which accommodation for additional R^{+3} (and R^{+4}) positive octahedral charges has been made in accordance with equation A or equation B. For example, the formulas for analysis 84, table 11,

$$[\underbrace{(Al_{0.10}Ti_{0.04}Fe^{+3}_{0.28}Fe^{+2}_{1.36}Mg_{0.85}Mn^{+2}_{0.06})}_{2.79}(Si_{2.93}Al_{1.07})O_{10}(OH)_2]^{-1.03}(K_{0.85},Na_{0.23})^{+1.08}_{1.08}$$

and for 109, table 11

$$[\underbrace{(Al_{0.06}Ti_{0.22}Fe^{+3}_{0.35}Fe^{+2}_{1.46}Mg_{0.66})}_{2.79}(Si_{2.58}Al_{1.42})O_{10}(OH)_2]^{-0.97}(K_{0.79},Na_{0.13},Ca/2_{0.02})^{+0.96}_{0.94}$$

differ greatly in the number of additional R^{+3} positive charges present, 0.46 and 0.87, respectively, and in positive octahedral charge but have the same octahedral occupancy. In the formula for 84 accommodation for R^{+3} (and R^{+4}) cations has been made almost entirely in accordance with equation B, 0.42 R^{+3} (and R^{+4}) ions proxying for 0.63 R^{+2} ions, whereas in the formula for 109 accommodation has been made almost equally by both methods. Of the 0.87 additional positive charges carried by the R^{+3} (and R^{+4}) octahedral cations present in the formula for 109, 0.45 form a positive charge on the octahedral layer and are neutralized by an approximately equivalent increase in the negative tetrahedral charge, and 0.42 are neutralized by the 0.42 negative charges associated with 0.21 unoccupied octahedral positions. The formulas for analyses 36,

$$[\underbrace{(Al_{0.21}Ti_{0.06}Fe^{+3}_{0.18}Cr^{+3}_{0.01}Fe^{+2}_{0.54}Mg_{1.73}Mn^{+2}_{0.02}Li_{0.03})}_{2.78}(Si_{2.87}Al_{1.13})O_{10}(OH)_2]^{-1.08}(K_{0.74},Na_{0.13},Ca/2_{0.12})^{+1.11}_{0.99}$$

and 96, table 11,

$$[\underbrace{(Al_{0.06}Ti_{0.09}Fe^{+3}_{0.25}Fe^{+2}_{1.54}Mg_{0.87}Mn^{+2}_{0.07})}_{2.91}(Si_{2.66}Al_{1.34})O_{10}(OH)_2]^{-1.00}(K_{0.89},Na_{0.13})^{+1.02}_{1.02}$$

have the same number of additional R^{+3} (and R^{+4}) charges, 0.51 and 0.52, respectively, but differ greatly in octahedral occupancy, in positive octahedral charge, and in negative tetrahedral charge. In the formula for 36, accommodation for R^{+3} and R^{+4} octahedral cations has been made predominantly in accordance with equation B, with 0.45 R^{+3} and(R^{+4}) cations proxying for 0.68 R^{+2} cations; in the formula for 96 about two-thirds of the accommodation for R^{+3} (and R^{+4}) octahedral cations is in accordance with equation A, and one-third in accordance with equation B.

Thus the vertical location of a point in figure 8 depends on the manner in which octahedral R^{+3} (and R^{+4}) cations have been accommodated in the structure. Points near the top of the diagonal band represent formulas of individuals in which the accommodation was predominantly in accordance with equation A; points near the bottom of the diagonal band represent formulas of individuals in which accommodation was predominantly in accordance with equation B. The width of the diagonal band indicates, therefore, the degree of variation in the manner in which the trioctahedral micas represented by the points have accommodated themselves to the presence of trivalent octahedral cations. However, despite such variations in manner of accommodation, it is quite obvious, from the average formulas in table 2, and from the downward trend of the band in figure 8, that there is, in the trioctahedral micas, a general decrease in octahedral occupancy with increase in octahedral trivalent cations. The trioctahedral micas are, in general, therefore, not strictly trioctahedral, nor are they strictly octaphyllites, as they contain fewer than eight cations per half cell.

Although Holzner (1936, p. 435) noted deficiency in octahedral occupancy in his biotite formulas and attempted to account for it by postulating that the biotite structure is made up of 2 layers of phlogopite to 1 of muscovite, he apparently failed to notice that in his formulas tetrahedral aluminum and consequently, tetrahedral charge, is, with but 2 exceptions (21 and 30, table 4) greater than 1.00, ranging from 1.01 to 1.40. On the other hand, the K(Na,Ca) values are, with but five exceptions, lower than the corresponding tetrahedral Al values. As the number of interlayer cations present is dependent on, and is usually equivalent to, the inherent layer charge, this discrepancy between Holzner's Al[4] (which represents the tetrahedral charge) and his K(Na,Ca) values

suggests that the octahedral layer in his formulas must carry a positive charge approximately equivalent to the difference between his Al[4] and K(Na,Ca) values. As Holzner included in his tables II and III the octahedral bivalent (Y″) and trivalent (Y‴) ion content, it is possible to calculate from them the octahedral charge and the inherent layer charge of his formulas. The results of these calculations are given in tables 3 and 4, together with Holzner's values for Y″, Y‴, Y″+Y‴ (equivalent to octahedral occupancy), Al[4] (equivalent to tetrahedral charge), and K(Na,Ca). All but five (2, table 3, and 13, 18, 21, and 23, table 4) have a positive octahedral charge, and the algebraic sum of these positive octahedral charges and the corresponding negative tetrahedral charges yields values for inherent layer charge consistent with the corresponding values for K(Na,Ca). Thus Holzner's formulas also exhibit the 2 types of adjustment for R^{+3} cations that were found in the formulas used in this study, 1 of which, adjustment in accordance with equation A, is not explained by his hypothesis, which is based entirely on accommodation in accordance with equation B.

TABLE 3.—*Selected data on phlogopites from Holzner (1936, table 8) with added data for octahedral and total charge*

No. of analysis	Y″	Y‴	Y″+Y‴	Octahedral charge	Al[4]=Tetrahedral charge	Total charge	K(Na, Ca)
1	3.081	.....	3.081	+0.062	−1.127	−1.065	1.077
2	2.906	0.020	2.926	−.128	−1.049	−1.177	1.180
3	2.931	.053	2.984	+.021	−1.134	−1.113	1.091
4	2.843	.082	2.925	+.068	−1.158	−1.090	1.077
5	2.915	.092	3.007	+.106	−1.086	−.980	.983
6	2.891	.122	3.013	+.148	−1.148	−1.000	.993
7	2.868	.197	3.065	+.207	−1.155	−.948	.950
8	2.895	.206	3.101	+.008	−1.223	−1.215	1.210
9	2.849	.223	3.072	+.287	−1.091	−.804	.794
10	2.677	.266	2.943	+.128	−1.217	−1.089	1.065
11	2.657	.270	2.927	+.124	−1.190	−1.066	1.064
12	2.755	.280	3.035	+.330	−1.233	−.973	.993
13	2.697	.287	2.984	+.235	−1.134	−.899	.878
14	2.675	.293	2.968	+.293	−1.177	−.884	.921
15	2.656	.337	2.993	+.323	−1.110	−.787	.783
16	2.608	.338	2.946	+.250	−1.170	−.940	.942
17	2.651	.350	3.001	+.352	−1.280	−.928	.938
18	2.549	.359	2.908	+.175	−1.180	−1.005	1.002
19	2.515	.458	2.973	+.404	−1.268	−.864	.882
20	2.420	.496	2.916	+.328	−1.332	−1.004	1.004

TABLE 4.—*Selected data on biotites from Holzner (1936, table 5) with added data for octahedral and total charge*

No. of analysis	Y″	Y‴	Y″+Y‴	Octahedral charge	Al[4]=Tetrahedral charge	K(Na, Ca)	Total charge
1	2.402	0.418	2.820	+0.086	−1.186	1.078	−1.128
2	2.356	.499	2.857	+.213	−1.222	1.016	−1.019
3	2.162	.554	2.716	+.296	−1.243	.922	−.947
4	2.307	.533	2.840	+.213	−1.169	.951	−.956
5	2.015	.791	2.806	+.403	−1.330	.881	−.927
6	2.169	.614	2.783	+.180	−1.251	.997	−1.071
7	2.190	.614	2.804	+.222	−1.254	.999	−1.032
8	2.040	.691	2.731	+.124	−1.147	.992	−1.023
9	2.308	.556	2.864	+.064	−1.114	.940	−1.030
10	2.315	.538	2.853	+.244	−1.242	.967	−.998
11	2.299	.595	2.894	+.362	−1.396	1.013	−1.013
12	2.161	.672	2.833	+.044	−1.053	1.016	−1.031
13	2.360	.413	2.773	−.041	−1.040	1.060	−1.081
14	2.040	.680	2.720	+.120	−1.185	1.035	−1.065
15	2.026	.653	2.679	+.151	−1.180	.968	−1.029
16	2.061	.644	2.705	+.054	−1.181	1.071	−1.127
17	1.966	.755	2.721	+.197	−1.110	.993	−1.013
18	2.080	.596	2.676	−.052	−1.042	1.023	−1.094
19	1.930	.798	2.728	+.054	−1.202	1.067	−1.055
20	2.029	.707	2.736	+.179	−1.221	.894	−1.042
21	2.135	.461	2.596	−.347	−.668	.974	−1.013
22	1.684	1.065	2.749	+.623	−1.277	.832	−.653
23	2.413	.355	2.768	−.019	−1.010	1.027	−1.029
24	2.049	.661	2.710	+.081	−1.137	1.059	−1.056
25	2.150	.607	2.757	+.121	−1.169	1.052	−1.048
26	2.027	.745	2.772	+.289	−1.136	.841	−.847
27	1.990	.706	2.692	+.098	−1.194	1.098	−1.098
28	2.228	.535	2.763	+.031	−1.117	1.118	−1.086
29	2.553	.302	2.855	+.030	−1.030	.991	−1.020
30	1.805	.842	2.647	+.136	−.958	.893	−.822
31	1.924	.821	2.745	+.311	−1.224	.952	−.913
32	1.877	.873	2.750	+.373	−1.187	.948	−.814
33	2.139	.582	2.721	+.024	−1.144	1.054	−1.120
34	1.950	.812	2.762	+.336	−1.260	.983	−.954
35	2.119	.678	2.797	+.372	−1.027	.959	−.825

R^{+3}-R^{+3} RELATION IN TRIOCTAHEDRAL MICAS

In the accommodation of trivalent octahedral cations according to equation A, $(+2nR^{+3})=(-nR^{+2})+(-nSi^{+4})$, the proxying of trivalent for bivalent octahedral ions is 1 to 1. In accommodation according to equation B, $(+2nR^{+3})=(-3nR^{+2})+(-nOct.Pos.)$, the proxying of trivalent for bivalent octahedral cations is 2 to 3 or 0.67 to 1. As both methods are exhibited to varying degrees in the natural trioctahedral micas studied, it follows that the proxying of trivalent for bivalent octahedral cations in these micas must vary between 1:1 and 0.67:1, depending on the relative degrees to which accommodation was made by one way or the other. This is illustrated in figure 9, in which the number of R^{+2} cations displaced is plotted against the number of proxying octahedral R^{+3} and R^{+4} cations. With few exceptions all the points fall along or between line A, which represents the proxying ratio of equation A, R^{+3}:R^{+2}=1:1, and line B, which represents the proxying ratio of equation B, R^{+3}:R^{+2}=0.67:1. Most of the points representing formulas having a trivalent octahedral cation content of less than 0.40 positions, as in most trioctahedral micas very high in Mg, that is, phlogopites, lie on or close to line A, whereas points representing formulas having a trivalent octahedral ion content of more than 0.40 positions lie closer to line B. These relations agree with the type of adjustment found for different amounts of additional trivalent octahedral positive charges in the average formulas (table 2). In trioctahedral micas in which the trivalent ion content is low, accommodation for their extra charges is predominantly in accordance with equation A, and the proxying ratio is 1 to 1. With increase in trivalent octahedral ion content an increasingly greater degree of accommodation is made according to equation B, and the proxying ratio approaches more nearly 0.67 to 1.0. As the trioctahedral micas generally exhibit both types of accommodation for octahedral trivalent cations, an equation representing the change in composition involved, as compared with the ideal, must be a combination of equations A and B. However, as the relative degree

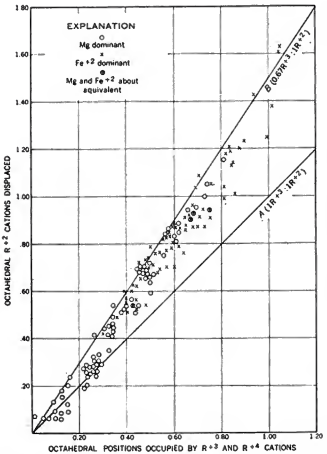

FIGURE 9.—Relation between R^{+3} cations displaced and proxying R^{+3} (and R^{+4}) octahedral cations.

to which the two types are used differs with each individual, the equation would, consequently, differ with each individual. The difficulties are further complicated by Ti which carries twice as many extra charges as octahedral positions occupied.

The scarcity of formulas having an octahedral R^{+3} ($+R^{+4}$) occupancy of more than 0.90 positions suggests that this R^{+3} ($+R^{+4}$) occupancy (about one-third of the occupied octahedral positions) is about the upper limit of the R^{+2} by R^{+3} ($+R^{+4}$) replacement in the trioctahedral micas. This is shown another way in figure 10, in which histograms represent the type and number of formulas in each additional positive octahedral charge group. Group H, in which the number of additional octahedral positive charges is between 0.71 and 0.80, includes the greatest number of formulas (25). From this high the number of formulas in each successive group drops to 16 in group I and to 2 in group J. This sharp drop in the number of formulas in each succeeding group from the high in group H, and the scarcity of formulas having an R^{+3} occupancy greater than 1.00, supports the suggestion that an R^{+3} ($+R^{+4}$) octahedral occupancy of one-third of the octahedral positions is the essential limit of replacement of octahedral R^{+2} (Mg) by R^{+3} (and R^{+4}) in the trioctahedral micas.

The small number of formulas having more than 1.00 positions occupied by R^{+3} and R^{+4} is also strong evidence against the existence of a complete series between phlogopite and muscovite and supports Deer (1937, p. 449) and Hutton (1947, p. 482) in their conclusions that it is not likely that the number of octahedral positions occupied varies between 2 and 3, as postulated by Pauling (1930, p. 128). Deer believed that any value between 2.5 and 3.0 is possible, but Hutton set the lower limit for octahedral occupancy at not less than 2.75. In six formulas used in the present study in which R^{+3} and R^{+4} occupied 1.00 ± 0.10 octahedral positions, total octahedral occupancy was between 2.45 and 2.75 positions, and averaged 2.60. In the two formulas having the lowest octahedral occupancy, 2.45 and 2.51 positions, accommodation for trivalent octahedral cations is almost entirely in accordance with equation B.

Mg-Fe^{+3} RELATION IN TRIOCTAHEDRAL MICAS

In addition to replacement of Mg by R^{+3} cations in the octahedral layer of trioctahedral micas, there is also replacement of Mg by Fe^{+2} cations. With but very few exceptions, all the formulas calculated from analyses of trioctahedral micas contain both Fe^{+2} and R^{+3} cations in the octahedral group. The exceptional analyses are of two kinds—almost pure phlogopites that contain only a very small amount of Fe^{+2} cations but no octahedral R^{+3} cations, or vice versa, and biotites in which Fe^{+2} was not determined but was included in total Fe as Fe_2O_3 in the analysis. Thus, coincident with replacement of Mg by R^{+3} cations, there is also replacement of Mg by Fe^{+2} cations. A very general relation between the amounts of Fe^{+2} and octahedral R^{+3} is suggested by the histograms in figure 10; (1) in formulas having very little octahedral R^{+3}, Mg is greatly predominant, (2) in formulas having moderate amounts of octahedral R^{+3}, Mg is still dominant but less so than in (1), and (3) in formulas having more than 0.60 octahedral positions occupied by R^{+3}, Fe^{+2} is the dominant octahedral cation in most of the formulas. However, the histograms also show the presence of some Mg-dominant biotites in the higher R^{+3} groups. This fact, and the great variability in the Fe^{+2}–octahedral R^{+3} ratio in the formulas indicate that no real relation exists, and that the two series, although concurrent, are independent. Also, the amount of octahedral R^{+3} present has no relation to the amount of Fe^{+2} present, and vice versa. On the other hand, the presence in all but a very few of the formulas of

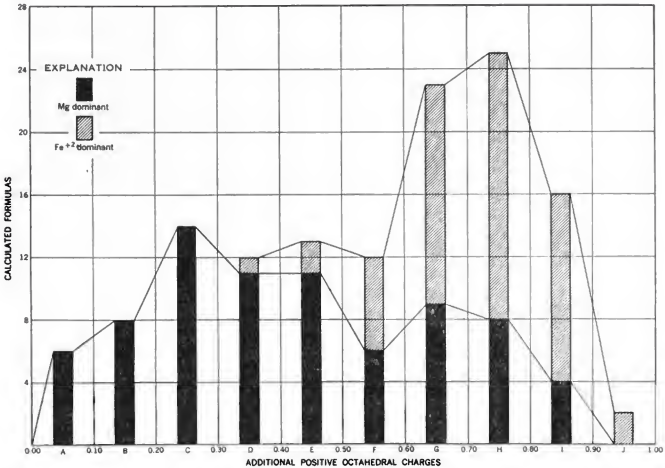

FIGURE 10.—Distribution of trioctahedral micas with respect to the number of additional positive octahedral charges carried by trivalent and quadrivalent octahedral cations.

both R^{+3} and Fe^{+2} in the octahedral group indicates that neither type of replacement forms a separate series. This statement includes Winchell's annite, the Fe^{+2} analog of phlogopite, and the theoretical end member of a Mg-Fe^{+2} replacement series. Such a mica was not found among the more than 200 analyses collected for this study.

Substitution of Fe^{+2} for Mg poses no problem of adjustment as does the substitution of R^{+3} for Mg. Both cations are bivalent, no excess nor deficiency of charge is involved, and substitution is ion for ion with no other change in the octahedral or tetrahedral layers.

On the evidence of the analyses and their derived formulas, an octahedral occupancy of more than 2.20 positions by Fe^{+2} is not to be expected. The highest Fe^{+2} in the formulas studied was 2.17, and only 4 formulas had an Fe^{+2} octahedral occupancy of more than 2.00.

MAGNESIUM REPLACEMENT SYSTEM

It has been shown that the only trioctahedral micas in which all, or almost all, the octahedral positions are occupied by one kind of cation are some phlogopites in which more than 90 percent of the octahedral positions are occupied by Mg. The Fe^{+2} analog of phlogopite, Winchell's annite, apparently does not exist in nature, or is very rare. With pure phlogopite as the prototype, all the other trioctahedral micas may be derived by the replacement of Mg by, most commonly, Fe^{+2} and R^{+3}. Thus, the trioctahedral micas may be considered as members of a system in which two principal types of replacement proceed concurrently but independently. The relation between Mg, (Fe^{+2} and Mn), and (Al, Fe^{+3}, and Ti) in this system is shown in figure 11, in which, for each formula, the percent of occupied octahedral positions occupied by Mg is plotted against the percent of occupied octahedral positions occupied by Fe^{+2} and R^{+3} on a triangular diagram. The points fall into 2 large groups and 1 small group. The first large group, at the top of the triangle, is made up of points representing trioctahedral micas in which Mg occupies more than 70 percent of the occupied octahedral positions; in the second large group are the points that represent trioctahedral micas in which Mg occupies

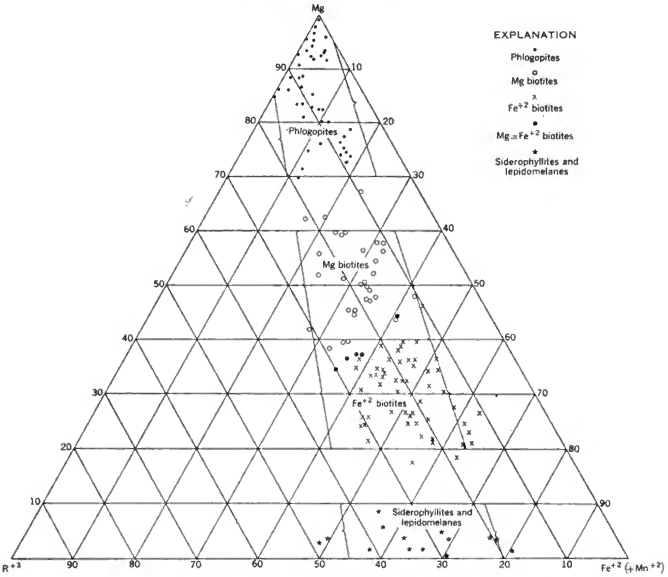

FIGURE 11.—Relation between Mg, Fe^{+2} (Mn^{+2}), and R^{+3} (Al, Fe^{+3}, and Ti) in trioctahedral micas.

between 63 and 20 percent of the occupied octahedral positions; in the small group, at the bottom of the triangle, are points representing trioctahedral micas in which Mg occupies fewer than 10 percent of the occupied octahedral positions.

Three-fourths of the analyses from which the formulas represented by points in the first group were derived were designated as analyses of phlogopite in the literature. A few were termed "biotites", with biotite being used in a general sense, simply meaning a trioctahedral mica. Consequently, the first group is considered as being made up of phlogopites and the first hiatus in the grouping of the points is considered as differentiating phlogopites from Mg biotites.

The second group of points represent biotites. Points representing Mg biotites occupy the upper half of this area, and, about halfway down the area, mingle with the points representing Fe^{+2} biotites, which occupy the lower half of the biotite area.

The third group of points represent Fe^{+2} dominant formulas having a very low Mg content, less than 0.15 octahedral positions, and high amounts of Al and (or) Fe^{+3}, that is, siderophyllites and lepidomelanes.

The trioctahedral micas may, therefore, be thought of as members of a system characterized by concurrent but independent replacement of Mg by Fe^{+2} and R^{+3} ions. At the beginning of the system, Mg occupies more than 98 percent of the octahedral positions; at its

end, Mg occupies fewer than 1 percent of the occupied positions. Thus phlogopite, $Mg_{3.00}(Si_{3.00}Al)O_{10}(OH)_2K$, is the prototype of the trioctahedral system, from which by displacement of Mg all other trioctahedral micas may be considered to be derived.

It is obvious that the character and composition of the members of a system like this cannot be adequately expressed by the kind of formulas usually given for these minerals. Such formulas suggest minerals of definite composition, not members of a system that are variable, within limits, in composition and that merge into one another. For members of such a system the formulas should indicate permissible limits of composition. The failure to define compositional limits has led in the past to considerable confusion in differentiating the various members of the system.

PHLOGOPITES

The name "phlogopite" refers to a trioctahedral mica in which almost all the octahedral positions are occupied by Mg. The formula usually given for phlogopite, $Mg_3(Si_3Al)O_{10}(OH)_2K$, specifies a complete occupancy of the octahedral group by Mg. Naturally-occurring phlogopites, however, contain other octahedral cations, most commonly Al, Fe^{+3}, and Fe^{+2}, and so do not conform perfectly to the ideal formula, although some, like the one below (1, table 11), approach the ideal very closely

$$[\underbrace{(Al_{0.01}Ti_{0.02}\overset{+0.04}{Fe^{+3}_{0.01}}Fe^{+2}_{0.01}Mg_{2.94})}_{2.99}\overset{-1.08}{(Si_{2.92}Al_{1.08})}O_{10}(OH)_2]^{-1.04}$$

$$K_{0.78},Na_{0.14},Ba/2_{0.06})^{+1.04}_{0.98}$$

This formula has the highest Mg occupancy of any of the formulas studied, Mg occupying 98 percent of the octahedral positions. Even in this formula, however, there are determinable amounts of Al, Ti, Fe^{+3}, and Fe^{+2}. Other formulas of phlogopites, arranged in order of decreasing Mg content, exhibit increasingly greater occupancy of octahedral positions by other cations, Fe^{+2}, Fe^{+3}, and (or) Al. However, all the formulas represented by points in the phlogopite area, figure 11, have more than 70 percent of their occupied octahedral positions occupied by Mg.

The average octahedral composition of phlogopites, based on the 42 formulas at hand, are shown in table 5. Only 4 of these formulas had a Fe^{+2} occupancy of more than 0.45 octahedral positions; in 2 of these Fe^{+2} occupied 0.50 positions, in the other 2, Fe^{+2} occupied 0.54 positions. The number of octahedral positions occupied by R^{+3} ions varies up to 0.54, with Al occupying between 0.00 and 0.35 positions, Ti

TABLE 5.—*Range in octahedral composition of phlogopites (in order of decreasing Mg content in terms of octahedral positions)*

Number of formulas	Mg	R^{+3} extra charge	Al	Fe^{+3}	Fe^{+2}	Octahedral positions
15	3.00-2.75	0.00-0.25	0.00-0.15	0.00-0.10	0.00-0.15	3.00-2.95
5	2.75-2.50	.25-.35	.10-.20	.05-.20	.00-.20	3.00-2.95
15	2.50-2.25	.20-.45	.00-.25	.00-.30	.15-.50	3.00-2.85
8	2.25-2.00	.25-.50	.00-.35	.05-.25	.30-.50	3.00-2.85

Formula indicating range in composition of phlogopites

$$\underbrace{(R^{+3}_{<0.50}\overset{<+0.30}{Fe^{+2}_{<0.50}}Mg_{3.00-2.00})}_{3.00-2.85}\overset{(-1.00)-(-1.30)}{(Si_{3.00-2.70}Al_{1.00-1.30})}$$

$$O_{10}(OH)_2K(Na,Ca/2)_{1.00\pm0.10}$$

between 0.00 and 0.10 positions, and Fe^{+3} between 0.00 and 0.30. However, in 30 of the 43 phlogopite formulas Al occupies 0.15 or fewer octahedral positions, and in 7 of these there is not only no octahedral Al, but also insufficient Al to complete the filling of the tetrahedral group, necessitating allocation of some Fe^{+3} to this group. Although Fe^{+3} occupies up to 0.30 positions, most of the phlogopite formulas had less than half that many positions occupied by Fe^{+3}. Titanium is generally very low, occupying an average of 0.10 positions.

From the ranges for Mg, Fe^{+2}, and R^{+3} in these formulas, general limits for these constituents in phlogopites may be formulated as shown at the bottom of table 5. The low of 2.00 octahedral positions occupied by Mg is equivalent to approximately 19 percent of MgO, and the high of 0.50 positions occupied by Fe^{+2} is equivalent to approximately 8.5 percent of FeO.

A number of phlogopite analyses were discarded because the formulas derived from them were low in interlayer ion content, that is, deficient in the amount of K, or other large cations present, and (or) were excessively high in octahedral occupancy. The implication of these features is discussed earlier in this paper.

EASTONITE

The name "eastonite" for pure dialuminum magnesium mica, $H_4K_2Mg_5Al_4Si_5O_{24}$, or $(Al_{0.5}Mg_{2.5})(Si_{2.5}Al_{1.5})O_{10}(OH)_2K$, in the notation used in this study, was derived from Easton, Pa., where, quoting Winchell (1925, p. 322, footnote 30) "Eyerman found a sample which approaches this composition very closely." Eyerman (1904, p. 46) published three analyses of biotite from Easton. One of these, analysis B, has only 6.30 percent K_2O, which is very low for a potassium mica. In the formulas derived from his analyses A and C, 16 and 15, table 11,

$$\underbrace{[(Al_{0.24}\overset{+0.14}{Fe^{+3}_{0.16}}Mg_{2.47})}_{2.87}(\overset{-1.16}{Si_{2.84}Al_{1.16}})O_{10}(OH)_2]^{-1.02}$$

$$(K_{0.34},Na_{0.06},Ca/2_{0.07})^{+1.04}_{0.97},$$

and

$$\underbrace{[(Al_{0.15}\overset{+0.30}{Fe^{+3}_{0.29}}Mg_{2.49})}_{2.93}(\overset{-1.28}{Si_{2.72}Al_{1.28}})O_{10}(OH)_2]^{-0.98}(K_{0.90},Ca/2_{0.03})^{+0.96}_{0.93},$$

Al occupies only 0.24 and 0.15 octahedral positions, respectively, not 0.50 as specified in Winchell's formula. These formulas can be said to approach the composition specified by Winchell's eastonite formula only if Al is interpreted broadly as meaning R^{+3} ions and to include Fe^{+3}. Furthermore, it is very doubtful whether the values given for Fe_2O_3 represent the actual Fe^{+3} content of the samples. No FeO is reported, and it is very probable that FeO was not determined and that the value given for Fe_2O_3 represents the total iron content of the sample, not Fe^{+3} only. In most samples of similar Mg and total iron content, in which both Fe_2O_3 and FeO were determined, FeO makes up one-half or more of the total iron content. It is very likely, therefore, that the Fe_2O_3 reported in these analyses includes FeO and that the actual trivalent ion content of these biotites is considerably less than shown in the formulas.

Aside from the Al and the total trivalent ion content, there are other points of disagreement between these formulas and Winchell's eastonite formula. In the eastonite formula it is presumed that all the octahedral positions are occupied, and, because tetrahedral Al, and consequently, tetrahedral charge, is 1.5, that all the extra charges (+0.50) carried by octahedral Al induce a positive charge on the octahedral layer. In the Easton formulas only 2.87 and 2.93 octahedral positions, respectively, are occupied, and only part of the additional charges carried by trivalent ions form a positive charge on the octahedral group, the rest being neutralized by negative charges associated with unoccupied positions. Consequently, the positive octahedral charge, the negative tetrahedral charge, and octahedral occupancy of the Easton formulas are all less than in the eastonite formula. X-ray study of the Easton, Pa., samples show them to be mixtures of serpentine and phlogopite. (Hatton S. Yoder, oral communication, 1957.)

Because in trioctahedral micas the extra charges carried by trivalent octahedral cations are accommodated in two different ways, in accordance with equation A or equation B, because decrease in Mg content is accompanied by increase in Fe^{+2} and R^{+3}, and because increase in R^{+3} is made up of increase in Fe^{+3} as well as increase in octahedral Al, none of the Mg dominant formulas studied closely approach Winchell's eastonite formula, in which accommodation for extra trivalent charges is assumed to be made only in accordance with equation A, and in which replacement of Mg is by Al only. All the formulas with a Mg content comparable to that in the eastonite formula contain Fe^{+3} and Fe^{+2} and have some unoccupied octahedral positions.

Among the analyses of trioctahedral micas collected for this study, only one had been called that of an eastonite (Simpson, 1932, p. 63), (D27, table 12). This analysis yielded the following formula,

$$\underbrace{[(Al_{0.20}Ti_{0.02}\overset{+0.42}{Fe^{+3}_{0.24}}Fe^{+2}_{0.93}Mg_{1.56}Mn^{+2}_{0.02})}_{2.97}(\overset{-1.29}{Si_{2.71}Al_{1.29}})O_{10}(OH)_2]^{-0.87}$$

$$(K_{0.82},Na_{0.07})^{+0.89}_{0.89}$$

In this formula Mg occupies only three-fifths and Al occupies only two-fifths of the number of octahedral positions designated in the eastonite formula, and the octahedral and tetrahedral charges are both considerably lower than in the eastonite formula. Only if Mg and Al in the eastonite formula are interpreted broadly as representing R^{+2} and R^{+3} ions generally, does the formula for Simpson's eastonite,

$$\underbrace{[(Al,\ Ti,\ Fe^{+3})_{0.46}(Fe^{+2},\ Mg,\ Mn^{+2})_{2.51}}_{2.97}(\overset{-1.29}{Si_{2.71}Al_{1.29}})O_{10}(OH)_2]^{-0.87}$$

$$(K,\ Na)^{+0.89}_{0.89}$$

approach Winchell's formula for eastonite. However, Winchell's formula represents the hypothetical dialuminum magnesium mica which was used by him as one of the components of biotite and as an analog of siderophyllite. A broader interpretation, as above, would tend to engender confusion with biotites proper.

In view of the confusion a broader interpretation would tend to engender, the apparent lack of natural representatives and the fact that the name had been previously given by Hamilton (1899, p.19) to a vermiculite occurring in the same locality as an alteration product of biotite, it is recommended that the name "eastonite" be discarded as referring to a natural trioctahedral mica and retained only as a hypothetical end-member.

BIOTITES

The term "biotite," although also used as a group name for the trioctahedral micas, is here specifically applied to trioctahedral micas that contain significant amounts of both Mg and Fe^{+2}. Biotites in which Mg is the dominant octahedral cation are termed Mg biotites; those in which Fe^{+2} is the dominant octahedral cation are termed Fe^{+2} biotites. Occurring midway in the Mg Fe^{+2}-R^{+3} system (fig. 11) between a Mg octahedral percentage of 50 and 20, the biotites occupy the

greatest area and constitute the greatest number of samples. Magnesium biotites dominate the upper part of the biotite area, with points representing formulas having the highest Mg content occupying the uppermost part of the area. With decreasing Mg content and increasing Fe^{+2} content Mg is gradually superseded by Fe^{+2} as the dominant octahedral cation, and Fe^{+2} biotites dominate the lower part of the biotite area. In the transition zone, points representing Mg biotites, Fe^{+2} biotites, and biotites having about equivalent amounts of Mg and Fe^{+2} intermingle.

The highest Mg content in any of the biotite formulas studied is 1.77 octahedral positions, the lowest is 0.48 octahedral positions. The highest Fe^{+2} content in any biotite formula is 1.78 octahedral positions; the lowest is 0.47. Thus Mg and Fe^{+2} in these biotite formulas have the same range, 1.75 to 0.50 octahedral positions (in rounded figures), but they are present in a reciprocal relation. This relation is illustrated in the following formulas, 36 and 116, table 11,

$$\frac{[(Al_{0.21}Ti_{0.06}Fe^{+3}_{0.18}Fe^{+2}_{0.54}Mg_{1.77}Mn^{+2}_{0.03}Li_{0.02})(Si_{3.37}Al_{1.13})O_{10}(OH)_2]^{-1.08}}{2.78}(K_{0.23},Na_{0.12},Ca/2_{0.17})^{+1.11}_{0.09}$$

$$\frac{[(Al_{0.09}Ti_{0.20}Fe^{+3}_{0.13}Fe^{+2}_{1.78}Mg_{0.59}Mn^{+2}_{0.03})(Si_{3.23}Al_{1.33})O_{10}(OH)_2]^{-0.99}}{2.82}(K_{0.36},Na_{0.06},Ca/2_{0.05})^{+1.02}_{0.08}$$

which belong, respectively, very near the high Mg-low Fe^{+2} and the low Mg-high Fe^{+2} ends of the Mg-Fe^{+2} range in biotites. In other biotite formulas, the Mg-Fe^{+2} relation varies between these extremes. However, because R^{+3} ions are present in different amounts, the relation between Mg and Fe^{+2} is quite variable. Formulas with similar Mg contents may have quite different Fe^{+2} contents and formulas with quite different Mg contents may have the same Fe^{+2} contents. Similarly, the relation between Mg and R^{+3} content is quite variable, as is also the relation between Mg and any of the ions making up R^{+3}. The relation between Mg and ($Fe^{2}+R^{+3}$) is however, quite regular.

Fe^{+3} generally occupies fewer than 0.35 octahedral positions in the biotite formulas. Only 6 formulas had a greater Fe^{+3} content, and of these 6 only 1 had a Fe^{+3} content greater than 0.45. There is no significant difference in the Fe^{+3} content of Mg dominant and Fe^{+2} dominant biotites. Indeed, the average Fe^{+3} content of these two types of biotites is essentially the same, 0.23 octahedral positions in Mg biotites, 0.25 octahedral positions in Fe^{+2} biotites.

With respect to Al content the biotite formulas fall into two groups; in about one-half the formulas there is little or no octahedral Al (fewer than 0.10 octahedral positions), in the other half, Al occupies between 0.20 and 0.55 octahedral positions. In about one-third of the low Al group, Al is so deficient that there is not only no octahedral Al, but there is not even sufficient Al present to complete the filling of the tetrahedral group; this requires the allocation of some Fe^{+3} to this group to complete it. Lack of sufficient Al to fill the tetrahedral group may be due simply to low Al content, or it may be due to low Si content, which would require proportionately more Al to complete the tetrahedral group. A comparison of the amounts of SiO_2 and Al_2O_3 reported in the analyses from which the formulas were derived shows, however, that low Al_2O_3 content, rather than low SiO_2 content, is the reason for the insufficiency of Al in formulas containing little or no octahedral Al. The SiO_2 content in analyses for the 2 groups is about the same, varying between 32 and 38 percent in analyses for both groups, with an average SiO_2 content of 35.5 percent for the low Al group, and an average of 34.8 percent for the higher Al group. The range in Al_2O_3 content in analyses of the low Al group, 11.0 to 16.3 percent, is, however, considerably lower than the range in Al_2O_3 content of the higher Al group, 15.7 and 21.3 percent, and the average Al_2O_3 content in analyses for the low Al group is almost 4 percent lower than the average Al_2O_3 content in analyses for the higher Al group, 14.6 percent as compared with 18.4 percent.

The compositional characteristics of each of the groups for different ranges of Mg content are summarized in table 6, and the average octahedral composition of each group for the same ranges of Mg content are given in table 7. For comparable Mg contents the low octahedral Al biotites are, in general, lower in R^{+3} but higher in Ti and Fe^{+3} content than the higher

TABLE 6.—*Range in octahedral composition of biotites*

[In order of decreasing Mg content in terms of octahedral positions occupied]

	Mg				
	1.75-1.50	1.50-1.25	1.25-1.00	1.00-0.75	0.75-0.50
Al<0.15					
Number of formulas	7	8	8	11	9
R^{+3}	0.35-0.70	0.60-0.75	0.50-0.80	0.45-0.80	0.55-0.85
Al	.00-.05	.00-.15	.00-.15	.00-.15	.00-.15
Ti	.20-.25	.10-.20	.20-.30	.05-.35	.10-.30
Fe^{+3}	.10-.45	.20-.35	.10-.45	.10-.35	.05-.45
Fe^{+2}	.60-.90	.80-.95	.90-1.35	1.25-1.55	1.45-1.75
($Fe^{+2}+R^{+3}$)	1.05-1.30	1.25-1.50	1.45-1.85	1.75-2.05	2.05-2.20
Al>0.15					
Number of formulas	6	4	6	12	11
R^{+3}	0.45-0.70	0.60-0.80	0.60-0.90	0.70-1.00	0.65-0.90
Al	.20-.55	.20-.40	.30-.50	.20-.40	.25-.50
Ti	.00-.15	.10-.20	.00-.15	.10-.30	.05-.20
Fe^{+3}	.00-.25	.10-.25	.00-.40	.05-.35	.05-.30
Fe^{+2}	.50-.95	.65-.95	.70-1.25	1.00-1.35	1.15-1.70
($Fe^{+2}+R^{+3}$)	1.00-1.35	1.30-1.55	1.50-1.80	1.70-2.00	1.90-2.20

TABLE 7.—*Average octahedral composition of biotites in order of decreasing* Mg *content*

[The figures preceding the parentheses enclosing the octahedral-group notation refer to the extra R^{+3} charge of the octahedral groups they precede]

Mg	Al <0.15	Al >0.15
1. 75–1. 50	$\overset{+0.25}{0.60}\underbrace{(Al_{0.00}Ti_{0.20}Fe^{+3}_{0.15}Fe^{+2}_{0.80}Mg_{1.70})}_{2.85}$	$\overset{+0.25}{0.55}\underbrace{(Al_{0.30}Ti_{0.05}Fe^{+3}_{0.15}Fe^{+2}_{0.70}Mg_{1.65})}_{2.85}$
1. 50–1. 25	$\overset{+0.25}{0.65}\underbrace{(Al_{0.05}Ti_{0.15}Fe^{+3}_{0.30}Fe^{+2}_{0.90}Mg_{1.40})}_{2.80}$	$\overset{+0.25}{0.75}\underbrace{(Al_{0.30}Ti_{0.15}Fe^{+3}_{0.15}Fe^{+2}_{0.85}Mg_{1.30})}_{2.75}$
1. 25–1. 00	$\overset{+0.30}{0.65}\underbrace{(Al_{0.05}Ti_{0.25}Fe^{+3}_{0.15}Fe^{+2}_{1.25}Mg_{1.10})}_{2.80}$	$\overset{+0.30}{0.80}\underbrace{(Al_{0.35}Ti_{0.10}Fe^{+3}_{0.25}Fe^{+2}_{0.95}Mg_{1.10})}_{2.75}$
1. 00–0. 75	$\overset{+0.25}{0.65}\underbrace{(Al_{0.05}Ti_{0.15}Fe^{+3}_{0.30}Fe^{+2}_{1.40}Mg_{0.90})}_{2.80}$	$\overset{+0.25}{0.85}\underbrace{(Al_{0.30}Ti_{0.20}Fe^{+3}_{0.15}Fe^{+2}_{1.20}Mg_{0.85})}_{2.70}$
0. 75–0. 50	$\overset{+0.25}{0.75}\underbrace{(Al_{0.05}Ti_{0.20}Fe^{+3}_{0.30}Fe^{+2}_{1.60}Mg_{0.60})}_{2.75}$	$\overset{+0.25}{0.85}\underbrace{(Al_{0.40}Ti_{0.10}Fe^{+3}_{0.25}Fe^{+2}_{1.35}Mg_{0.60})}_{2.70}$

octahedral Al biotites, although formulas with low octahedral Al are found throughout the entire R^{+3} range. Fe^{+2} is consistently higher, for comparable Mg contents, in low Al biotites than in higher Al biotites. Because of this difference in Fe^{+2} content with the same Mg content, the average formula for low Al biotites in the Mg range 1.25–1.00 has Fe^{+2} as the dominant octahedral cation, whereas the average formula for the higher Al biotites has Mg as the dominant octahedral cation. In an average of all formulas in this Mg range Mg and Fe^{+2} are present in approximately equivalent amounts,

$$[\underbrace{(Al_{0.20}Ti_{0.15}Fe^{+3}_{0.30}Fe^{+2}_{1.15}Mg_{1.10})}_{2.80}(Si_{2.70}Al_{1.30})O_{10}(OH)_2]^{-1.00}$$

$$K(Na, Ca/2)^{+1.00}_{1.00\pm.10}$$

Thus the Mg range of 1.25 to 1.00 octahedral positions is the transition zone between Mg and Fe^{+2} dominant biotites. All biotites having more than 1.25 octahedral positions occupied by Mg are Mg dominant; all biotites having fewer than 1.00 positions occupied by Mg are Fe^{+2} dominant. When the Mg content is between 1.25 and 1.00 octahedral positions, Mg is dominant in some biotites, Fe^{+2} is dominant in others, and Mg and Fe^{+2} are present in approximately equivalent amounts in still others.

On the basis of the ranges in content of Mg, Fe^{+2}, and R^{+3} shown in table 6, the ranges in content of these constituents to be expected in biotites may be formulated as

$$\underbrace{(R^{+2}_{0.25-1.00}Fe^{+2}_{0.50-1.75}Mg_{1.75-0.50})}_{2.90-2.65}\overset{<+0.50}{}\overset{(-1.00)-(-1.50)}{(Si_{3.00-2.50}Al_{1.00-1.50})}O_{10}(OH)_2$$

$$K(Na, Ca/2)_{1.00\pm0.10}.$$

ANNITE

Originally the name "annite" was applied by Dana (1868, p. 308) to a high Fe^{+2} biotite that occurs at Cape Ann, Mass., which was analyzed and described by Cooke (1867, p. 222). This material contained 12.07 percent Fe_2O_3. Subsequently Winchell (1925, p. 323) applied the name to a hypothetical Fe^{+2} analog of phlogopite, $Fe^{+2}_3(Si_3Al)O_{10}(OH)_2K$, which was used by him as 1 of the 4 components of biotite. Thus the name which Dana gave to a high trivalent iron mica was applied by Winchell to a hypothetical bivalent iron mica which was presumed to contain no trivalent iron.

One of the most significant features brought out by this study is the complete absence of Fe^{+2} dominant micas analogous to phlogopite. Only two formulas have as many as 2.00 octahedral positions occupied by Fe^{+2}, the lower limit for Mg in phlogopite, and in these, although Mg is very low, R^{+3} ions occupy about 0.50 octahedral positions.

Considering that the name "annite" had been used previously by Dana for a high Fe^{+3} biotite and the name and formula was used by Winchell for a hypothetical

ferrous trioctahedral mica, which does not, on the evidence of the formulas gathered, occur in nature, it is recommended that annite be discarded as referring to a natural trioctahedral mica, and retained only as a hypothetical end member.

SIDEROPHYLLITES AND LEPIDOMELANES

A group of Fe^{+2} dominant trioctahedral mica formulas in which Mg occupies less than 0.15 octahedral positions represents the end of the Mg replacement system. Points representing these formulas fall close to the base of the triangular diagram shown in figure 11, and are separated from the biotite area by narrow, very sparsely populated area. Some of these formulas are characterized by high Al content; others, by high Fe^{+3} content; and still others, by significant amounts of both Al and Fe^{+3}.

Siderophyllite, according to Winchell and Winchell (1951, p. 373) has the formula, $H_4K_2Fe_2Al_4Si_8O_{24}$, or, in the notation herein used, and assuming Fe to represent Fe^{+2}

$$(Al_{0.8}Fe^{+2}_{2.0})(Si_{2.50}Al_{1.50})O_{10}(OH)_4K_{1.00}$$

The full octahedral occupancy and the composition of the tetrahedral in this formula indicate that all the accommodation for extra positive charges (+0.50) carried by octahedral Al is assumed to have been made in accordance with equation A. Nockolds and Richey (1939, p. 38) suggested the formula, $H_4K_2Fe_2Al_4Si_8O_{24}$, or $(Al_{1.00}Fe^{+2}_{2.00})(Si_{3.00}Al_{1.00})O_{10}(OH)_2K$, for siderophyllite, as this formula was closer to the composition of a specimen studied by them (129; table 8). In this formula all the additional positive charges carried by octahedral aluminum (+1.00) are accommodated in accordance with equation B. The octahedral layer is neutral, and the tetrahedral layers have the same charge as in the classic formulas for phlogopite and muscovite. These two formulas, therefore, represent the two extremes in the accommodation of extra positive octahedral charges by the biotite structure. Octahedral Al in this formula occupies twice as many positions as in the Winchell formula and Fe^{+2} occupies only three-fifths as many positions.

In the formulas shown in table 8, octahedral Al varies between 0.47 and 0.99 positions. These relations suggest an isomorphous series in which Fe^{+2} is replaced by Al. Hypothetically, the beginning of the series would be a mineral similar to Winchell's annite, which would yield on increasing replacement of Fe^{+2} by Al, minerals whose compositions, except for lack of Li, approximate those of the siderophyllites shown in table 8:

$$\overset{0.00}{[Fe^{+2}_{2.00}}\overset{-1.00}{(Si_{2.50}Al_{1.50})}O_{10}(OH)_2]^{-1.00}\ K^{+1.00}_{1.00} \quad \text{Not represented.}$$

$$\downarrow$$

$$\underbrace{\overset{0.00}{[(Al_{0.50}Fe^{+2}_{2.25})}}_{2.75}\overset{-1.00}{(Si_{2.50}Al_{1.50})}O_{10}(OH)_2]^{-1.00}\ K^{+1.00}_{1.00} \quad \text{Approximates 132, table 8.}$$

$$\downarrow$$

$$\underbrace{\overset{0.00}{[(Al_{1.00}Fe^{+2}_{1.50})}}_{2.50}\overset{-1.00}{(Si_{2.50}Al_{1.50})}O_{10}(OH)_2]^{-1.00}\ K^{+1.00}_{1.00} \quad \text{Approximates 129, table 8.}$$

The first half of the series, up to an Al content of 0.50 octahedral positions, is not represented among the formulas studied. The second half is represented by formulas in table 8. Variations in octahedral occupancy, octahedral charges and tetrahedral charge are due to the varying degrees to which the structure has accommodated the extra positive charges carried by Al in accordance with equation A or equation B. In the formula for 132, table 8, 0.33 of the extra 0.47 charges carried by Al are balanced by the deficiency in the number of charges carried by Li, as one Li and one Al together carry the same number of charges as two bivalent cations. The 0.16 negative charges associated with 0.08 unoccupied octahedral positions are more than sufficient to neutralize the rest of the additional positive charges, and the octahedral layer has a slight negative charge. In the formula for 135, table 8, part of the additional positive octahedral charges are neutralized by negative charges associated with unoc-

TABLE 8.—*Formulas of representative siderophyllites*

Number in table 11	*Formula*
132	$\overset{-0.02}{[(Al_{0.47}Fe^{+2}_{2.02}Mg_{0.03}Mn^{+2}_{0.07}Li_{0.33})}_{2.92}\overset{-1.03}{(Si_{1.97}Al_{1.03})}O_{10}(OH)_2]^{-1.00}(K_{0.83}Na_{0.16}Rb_{0.01})^{+1.03}_{1.03}$
135	$\overset{+0.35}{[(Al_{0.72}Fe^{+3}_{0.06}Fe^{+2}_{1.88}Mg_{0.03}Mn^{+2}_{0.02}Li_{0.12})}_{2.82}\overset{-1.35}{(Si_{2.65}Al_{1.35})}O_{10}(OH)_2]^{-1.00}(K_{0.90}Na_{0.07}Ca/2_{0.01})^{+0.99}_{0.98}$
129	$\overset{-0.06}{[(Al_{0.99}Ti_{0.01}Fe^{+3}_{0.05}Fe^{+2}_{1.79}Mg_{0.08}Mn^{+2}_{0.02})}_{2.44}\overset{-1.03}{(Si_{1.97}Al_{1.03})}O_{10}(OH)_2]^{-1.00}(K_{0.86}Ca/2_{0.12})^{+1.10}_{0.98}$

cupied octahedral positions. In 129 all the extra positive R^{+3} charges are neutralized by negative charges associated with unoccupied octahedral positions, as in Nockolds and Richey's formula for siderophyllite. Because of these various degrees to which the extra positive charges carried by R^{+3} ions have been accommodated in accordance with equations A and B in these siderophyllite formulas, the formulas for the siderophyllite series are written to represent similar mixed accommodation of extra positive charges.

"Lepidomelane" is a term that has not been definitely defined and that has different meanings for different mineralogists. Dana (1892, p. 634) defines lepidomelane as a variety of biotite characterized by a large amount of ferric iron. Winchell and Winchell (1951, p. 376) states that "lepidomelane is any kind of biotite rich in iron." The state of valence of the iron is, apparently, unimportant, as this definition would include his annite. Kunitz (1924, p. 388) suggests that all the iron was originally in the ferrous state, and gives a formula in which all the iron is present in the ferrous state, $KH_2AlFe^{+2}_3(SiO_4)$. However, Hallimond (1926, p. 30) considers that there is no reason "* * * to believe that the natural melts are so deficient in oxygen as this assumption would imply, and it is much more probable that the average fresh biotite is substantially in the condition in which it crystallized." The formula given by Hey (1955, p. 193), $2[K_2(Fe^{+3}Fe^{+2}Mg)_{4-5}.(Si,Al,Fe^{+3})_8O_{20}(OH)_4]$, which includes both trivalent and bivalent iron, is qualified by the remark "* * * with high Fe^{+3} and low Mg (usually $Fe^{+2}>Mg$)." Hey includes Fe^{+3} in the tetrahedral group, as does also Grigoriev (1935, p. 79) in his formula for fluor (or hydroxyl) lepidomelane $FK(MgFe^{+2})_3[(Al,Fe^{+3})Si_3]O_{10}$, although Grigoriev includes only Fe^{+3} in the octahedral group. These examples illustrate the lack of agreement among mineralogists as to the meaning of the term "lepidomelane."

Among the Fe^{+2} dominant formulas studied was a group characterized by very low Mg content and analogous to the siderophyllite formulas but containing Fe^{+3} in place of Al. These formulas, of which typical examples are presented in table 9, bear the same relation to each other as do the siderophyllite formulas; that is, they represent part of an isomorphous series in which there is proxying of Fe^{+2} by Fe^{+3}, and their composition can be expressed by the same general formulas as given for the siderophyllite half series, by substituting Fe^{+3} for Al.

$$[\overset{0.00}{Fe^{+2}_{3.00}}(Si_{3.00}\overset{-1.00}{Al_{1.00}})O_{10}(OH)_2]^{-1.00}\ K^{+1.00}_{1.00} \text{ ------- Not represented.}$$

$$\downarrow$$

$$[\underbrace{(\overset{0.00}{Fe^{+3}_{0.50}}Fe^{+2}_{2.25})}_{2.75}(Si_{3.00}\overset{-1.00}{Al_{1.00}})O_{10}(OH)_2]^{-1.00}\ K^{+1.00}_{1.00} \text{ Approximates 124, table 9.}$$

$$\downarrow$$

$$[\underbrace{(\overset{0.00}{Fe^{+3}_{1.00}}Fe^{+2}_{1.50})}_{2.50}(Si_{3.00}\overset{-1.00}{Al_{1.00}})O_{10}(OH)_2]^{-1.00}\ K^{+1.00}_{1.00} \text{ Approximates 123, table 9.}$$

As in the siderophyllite series, only the latter half of the series is represented.

It is suggested here that the term "lepidomelane" be applied to minerals similar in composition to the formulas above and to those in table 9—minerals characterized by high Fe^{+2} and Fe^{+3} and by very low octahedral Al and Mg content, and analogous to siderophyllite (as herein defined) but containing Fe^{+3} in place of Al.

Another group of formulas characterized by high Fe^{+2} and very low Mg content contain significant amounts of both octahedral Al and Fe^{+3} (table 10). These formulas are intermediate in composition be-

TABLE 9.—*Formulas of representative lepidomelanes*

Number (table 11)	*Formula*
126	$[\underbrace{(\overset{+0.17}{Al_{0.00}Ti_{0.18}Fe^{+3}_{0.35}Fe^{+2}_{1.91}Mg_{0.09}Mn^{+2}_{0.20}}_{2.73})(Si_{2.77}\overset{-1.23}{Al_{1.02}Fe^{+3}_{0.21}})O_{10}(OH)_2]^{-1.06}(K_{0.83}Na_{0.16}Ca/2_{0.06})^{+1.11}_{1.05}$
125	$[\underbrace{(\overset{+0.22}{Al_{0.02}Ti_{0.24}Fe^{+3}_{0.47}Fe^{+2}_{1.73}Mg_{0.09}Mn^{+2}_{0.09}}_{2.63})(Si_{2.89}\overset{-1.11}{Al_{1.11}})O_{10}(OH)_2]^{-0.89}(K_{0.72}Na_{0.18})^{+0.89}_{0.89}$
124	$[\underbrace{(\overset{+0.39}{Al_{0.06}Ti_{0.02}Fe^{+3}_{0.51}Fe^{+2}_{2.17}Mg_{0.11}Mn^{+2}_{0.02}}_{2.89})(Si_{2.58}\overset{-1.42}{Al_{1.42}})O_{10}(OH)_2]^{-1.02}(K_{0.91}Na_{0.11})^{+1.02}_{1.02}$
123	$[\underbrace{(\overset{+0.39}{Al_{0.16}Ti_{0.05}Fe^{+3}_{0.79}Fe^{+2}_{1.37}Mg_{0.15}Mn^{+2}_{0.07}Li_{0.16}}_{2.75})(Si_{2.64}\overset{-1.36}{Al_{1.36}})O_{10}(OH)_2]^{-0.97}(K_{0.79}Ca/2_{0.08})^{+0.96}_{0.87}$

TABLE 10.—*Formulas of micas intermediate in composition between siderophyllites and lepidomelanes*

Number (tables 11 and 18)	*Formula*
130	$[\underbrace{(Al_{0.38}Fe^{+3}_{0.47}Fe^{+2}_{0.78}Mg_{0.04}Mn^{+3}_{0.03}Li_{0.30})}_{2.95}(Si_{2.68}Al_{1.32})O_{10}(OH)_2]^{-0.95}(K_{0.79}Na_{0.38}Ca/2_{0.54})^{+0.95}_{0.91}$ (+0.36, −1.31)
127	$[\underbrace{(Al_{0.31}Ti_{0.01}Fe^{+3}_{0.62}Fe^{+2}_{1.22}Mg_{0.58}Mn^{+2}_{0.02}Li_{0.13})}_{2.61}(Si_{2.68}Al_{1.32})O_{10}(OH)_2]^{-1.07}(K_{0.78}Na_{0.03}Ca/2_{0.56})^{+1.04}_{0.98}$ (+0.25, −1.32)
D63	$[\underbrace{(Al_{0.41}Fe^{+3}_{0.55}Fe^{+2}_{1.09}Mg_{0.37}Mn^{+3}_{0.04}Li_{0.15})}_{2.51}(Si_{2.98}Al_{1.02})O_{10}(OH)_2]^{-1.01}K^{+1.01}_{1.01}$ (+0.01, −1.02)

tween those given in tables 8 and 9. Other formulas, which could not be used because of their high alkali content (see discussion, p. 16), contain varying proportions of Al and Fe^{+3} and suggest the existence of an isomorphous series between siderophyllite and lepidomelane as they are herein defined. The interrelations possible between siderophyllites and lepidomelanes are expressed in the following diagram.

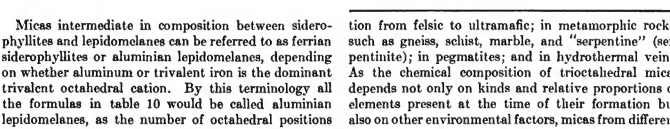

Micas intermediate in composition between siderophyllites and lepidomelanes can be referred to as ferrian siderophyllites or aluminian lepidomelanes, depending on whether aluminum or trivalent iron is the dominant trivalent octahedral cation. By this terminology all the formulas in table 10 would be called aluminian lepidomelanes, as the number of octahedral positions occupied by trivalent iron is greater than the number of positions occupied by aluminum in all of them.

Only one formula in tables 8, 9, and 10 contains tetrahedral trivalent iron, as specified in Hey's and Grigoriev's formulas for lepidomelane. The presence or absence of tetrahedral Fe^{+3} in a formula is indicative, not of high Fe^{+3}, but of insufficient Si or Al to fill the tetrahedral group, as Fe^{+3} is assigned to the tetrahedral group only when there is insufficient Si and Al to fill that group. Some of the phlogopite formulas calculated for this study contain tetrahedral Fe^{+3} because the Al content is very low and is not sufficient to complete the filling of the tetrahedral group, although the Fe^{+3} content is also very low. Thus tetrahedral Fe^{+3} is not a necessary characteristic of high Fe^{+3} biotites.

CHEMICAL COMPOSITION AND GEOLOGIC OCCURRENCE

The trioctahedral micas form under a great variety of conditions and occur in many kinds of rocks—in igneous rocks, both intrusive and extrusive, ranging in composition from felsic to ultramafic; in metamorphic rocks, such as gneiss, schist, marble, and "serpentine" (serpentinite); in pegmatites; and in hydrothermal veins. As the chemical composition of trioctahedral micas depends not only on kinds and relative proportions of elements present at the time of their formation but also on other environmental factors, micas from different kinds of rocks would be expected to differ in composition.

Information on geologic occurrence was available for about two-thirds of the analyses used in this study. Most of the analyses for which such information was available were those of biotites, siderophyllites, and lepidomelanes. Information on the phlogopites was sparse, and that available indicated quite diverse occurrences. The kinds of rocks from which there were enough micas to furnish an adequate conception of the composition of the micas in them were divided into the following groups: Granite, monzonite and quartz monzonite granodiorite, diorite and quartz diorite; nepheline syenite, gneiss and schist, and pegmatite. Micas that formed under apparently atypical conditions such as a biotite from a large zenolith (plagioclase) in biotite granite, or a biotite from a dark veinlet in granite, are not included in this discussion.

The relation between the chemical composition of the micas and their geologic occurrence is shown in figure 12. In this figure the Mg-(Fe^{+2},Mn)-(Al,Fe^{+3}),

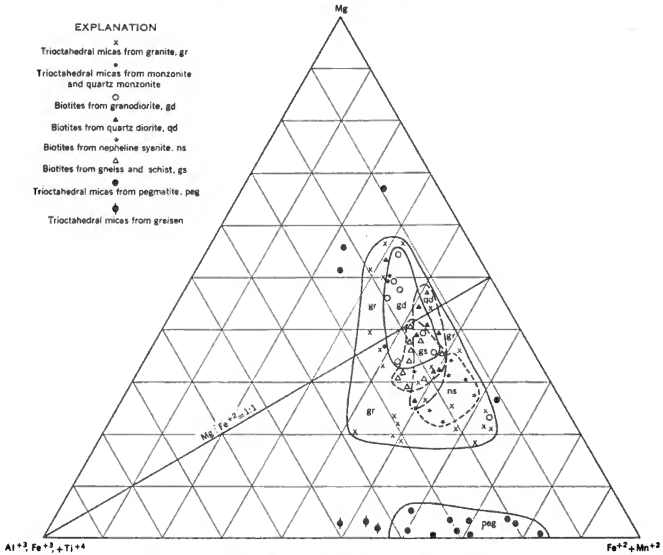

FIGURE 12.—Relation between chemical composition and geologic occurrence of trioctahedral micas.

Ti^{+4}) relation in the octahedral group of each mica is plotted on a triangular diagram, as in figure 11, and the area occupied by points representing micas from a given kind of rock is enclosed. The occupied areas indicate that the micas from the first six groups of rocks are all biotites; those from the seventh group, with a few exceptions, are siderophyllites or lepidomelanes.

Biotites from granite.—Biotites from granite comprise the largest group (23). Points representing these biotites occupy an area (gr) in figure 12 which embraces almost the entire biotite area as shown in figure 11. Thus biotites from granite vary widely in character, from those in which Mg is greatly predominant, as in these formulas calculated from analyses 41 and 42, table 11.

$$\frac{[(Al_{0.22}Ti_{0.17}Fe^{+3}_{0.02}Fe^{+2}_{0.81}Mg_{1.61}Mn^{+2}_{0.01})(Si_{2.46}Al_{1.34})O_{10}(OH)_2]^{-1.02}}{2.84}(K_{0.89},Na_{0.14},Ca/2_{0.02})^{+1.08}_{1.05}$$

$$\frac{[(Al_{0.01}Ti_{0.20}Fe^{+3}_{0.10}Fe^{+2}_{0.90}Mg_{1.60}Mn^{+2}_{0.01})(Si_{2.72}Al_{1.28})O_{10}(OH)_2]^{-1.07}}{2.84}(K_{0.91},Na_{0.14},Ca/2_{0.01})^{+1.08}_{1.07}$$

to those in which Fe^{+2} is similarly dominant, as in these formulas calculated from analyses 116 and 120, table 11.

$$\underbrace{[(Al_{0.09}Ti_{0.20}Fe^{+3}_{0.13}Fe^{+2}_{1.78}Mg_{0.59}Mn^{+2}_{0.03})}_{2.82}\overset{+0.26}{}(Si_{2.75}Al_{1.25})\overset{-1.25}{}O_{10}(OH)_2]^{-0.99}$$

$$(K_{0.86},Na_{0.06},Ca/2_{0.05})^{+1.03}_{0.98}$$

$$\underbrace{[(Al_{0.25}Ti_{0.14}Fe^{+3}_{0.14}Fe^{+2}_{1.69}Mg_{0.52}Mn^{+2}_{0.11})}_{2.85}\overset{+0.37}{}(Si_{2.66}Al_{1.34})\overset{-1.34}{}O_{10}(OH)_2]^{-0.97}$$

$$(K_{0.74},Na_{0.07},Ca/2_{0.07})^{+0.96}_{0.88}$$

In terms of percent composition, biotites from granite varied between 14.92 and 4.70 in MgO and between 12.69 and 26.80 in FeO.

In about one-half the biotites from granite, octahedral aluminum occupies fewer than 0.15 positions, as in 42 and 116, table 11 above. In some of these there is no octahedral aluminum, the aluminum present being insufficient to complete the filling of the tetrahedral group, and it was necessary to allocate some Fe^{+3} to that group. On the other hand, in other biotites from granite, octahedral aluminum is quite high, occupying 0.50 or more positions, as in this formula calculated from analysis 110, table 11,

$$\underbrace{(Al_{0.51}Ti_{0.07}Fe^{+3}_{0.23}Fe^{+2}_{1.22}Mg_{0.65}Mn^{+2}_{0.03}Li_{0.06})}_{2.77}\overset{+0.36}{}(Si_{2.63}Al_{1.37})\overset{-1.37}{}O_{10}(OH)_2]^{-1.01}$$

$$(K_{0.89},Na_{0.06},Ca/2_{0.03})^{+1.01}_{0.98}$$

In these biotites from granite, Al_2O_3 varies between 13.64 and 20.55 percent.

Fe_2O_3 content is also quite variable in these biotites—between 0.35 and 8.0 percent. These amounts of Fe_2O_3 are equivalent to 0.02 and 0.44 octahedral positions, respectively, occupied by Fe^{+3}. In the biotite in which Fe^{+3} occupies 0.44 octahedral positions, as well as in one other in which Fe^{+3} is fairly high and octahedral Al is fairly low, Fe^{+3} is the dominant trivalent octahedral cation. However, in most of the biotites from granite in which there is little or no octahedral aluminum, there is less Fe^{+3} than there is in those that have considerable octahedral aluminum. There is no apparent relation between FeO and Fe_2O_3, individuals of moderate FeO content may contain more Fe_2O_3 than others with twice as much FeO and vice versa.

The TiO_2 content of the granite biotites is quite uniform, varying between only 2.0 and 3.75 percent in 18 of the 22 analyses of biotites from granite.

In their accommodation of the additional charges carried by trivalent or quadrivalent octahedral cations the granite biotites apparently do not greatly tend to favor one method over the other, but exhibit a fairly equal degree of adjustment by both methods. Thus they are characterized by a moderate octahedral positive charge, +0.20 to +0.35, with an equivalent excess over 1.00 in tetrahedral negative charge, and by a moderate decrease (below 3.00) in octahedral occupancy, the number of octahedral positions occupied being generally between 2.85 and 2.70.

In summary, therefore, biotites from granite differ greatly in character and composition, varying from those in which Mg is the considerably predominant octahedral cation, through those in which Mg and Fe^{+2} are approximately equal, to those in which Fe^{+2} is considerably predominant. In any of these, octahedral Al may be very low or absent, moderate or high, and Fe^{+3} may be insignificant or an important constituent. Fuller data on the kinds of granite from which these biotites are derived might permit correlation between a particular type of granite and a particular type of biotite, but with the data at hand this is not possible.

Biotites from monzonite and quartz monzonite.—Only three of the biotites for which information as to geologic occurrence is available were from monzonite or quartz monzonite. Of these, the 2 from quartz monzonite (1 from Colorado and 1 from California) were very similar in composition, as shown by these formulas calculated from their analyses (48 and 50, respectively, table 11).

$$\underbrace{[(Al_{0.07}Ti_{0.15}Fe^{+3}_{0.27}Fe^{+2}_{0.87}Mg_{1.44}Mn^{+2}_{0.05})}_{2.85}\overset{+0.31}{}(Si_{2.70}Al_{1.30})\overset{-1.30}{}O_{10}(OH)_2]^{-0.99}$$

$$(K_{0.75}Na_{0.07},Ca/2_{0.08})^{+0.99}_{0.90}$$

$$\underbrace{[(Al_{0.04}Ti_{0.18}Fe^{+3}_{0.27}Fe^{+2}_{0.90}Mg_{1.40}Mn^{+2}_{0.03})}_{2.82}\overset{+0.31}{}(Si_{2.72}Al_{1.28})\overset{-1.28}{}O_{10}(OH)_2]^{-0.97}$$

$$(K_{0.89},Na_{0.05},Ca/2_{0.01})^{+0.97}_{0.96}$$

Both are Mg dominant biotites with very low octahedral Al and moderate Fe^{+3} content. Both have a moderate octahedral positive charge, with an equivalent increase in the negative tetrahedral charge; and in both the deficiency in octahedral occupancy is moderate, which indicates about equal adjustments by methods A and B for the additional positive charges carried by trivalent and quadrivalent octahedral cations. In the third member of the group, a mica from monzonite in Thuringia, Mg and Fe^{+2} occupy 1.01 and 1.02 octahedral positions, respectively. This biotite is also somewhat higher in Fe^{+3} content than the other two from quartz monzonite, but it is similar to them in octahedral and tetrahedral Al content and in TiO_2 and MnO content. In this biotite one-third of the adjustment for additional positive octahedral cations is by method A and two-thirds is by method B.

The points representing these three biotites fall on the left boundary of the area occupied by biotites from granodiorite (gd), figure 12.

Biotites from granodiorite.—The eight biotites from granodiorite occupy a large area (gd), in the upper part of the granite area (fig. 12). It also overlaps the line (Mg:Fe^{+2}=1:1) between the Mg and Fe^{+2} dominant biotites; thus both types of biotites are obtained from granodiorite. In these biotites, Mg and Fe^{+2} together generally occupy from approximately 2.30 to 2.45 octahedral positions, but the relative proportions of the two cations present varies greatly, as illustrated in the following formulas calculated from analyses 44, 67, and 111, table 11,

$$[\underbrace{(Al_{0.09}Ti_{0.31}Fe^{+3}_{0.17}Fe^{+2}_{0.91}Mg_{1.54}Mn^{+2}_{0.02})}_{2.87}(Si_{2.74}Al_{1.22}Fe^{+3}_{0.04})O_{10}(OH)_2]^{-0.39}$$
$$(K_{0.54},Na_{0.35})^{+0.89}_{0.96}$$

$$[\underbrace{(Al_{0.11}Ti_{0.18}Fe^{+3}_{0.17}Fe^{+2}_{1.20}Mg_{1.09}Mn^{+2}_{0.02})}_{2.77}(Si_{2.79}Al_{1.21})O_{10}(OH)_2]^{-1.07}$$
$$(K_{0.88},Na_{0.05},Ca/2_{0.35})^{+1.06}_{1.01}$$

$$[\underbrace{(Al_{0.15}Ti_{0.21}Fe^{+3}_{0.06}Fe^{+2}_{1.74}Mg_{0.46}Mn^{+2}_{0.02})}_{2.83}(Si_{2.74}Al_{1.26})O_{10}(OH)_2]^{-0.96}$$
$$(K_{0.80},Na_{0.22},Ca/2_{0.35})^{+0.99}_{0.96}$$

These formulas also serve to illustrate the characteristics of biotites from granodiorite: their generally low octahedral Al content, their fairly low Fe^{+3} content, and their moderately high TiO_2 content. In these biotites, as in those from granite and quartz monzonite, adjustment for the additional charges carried by these trivalent and quadrivalent octahedral cations is made almost equally by method A and method B, except for two, as in the second formula above, in which adjustment is predominately by method B.

Biotites from diorite and quartz diorite.—The points representing biotites from diorite and quartz diorite occupy an elongated area (qd) on the middle right side of the granite area in figure 12, most of the area being below the Mg:Fe^{+2}=1:1 line. This group also contains both Mg and Fe^{+2} dominant individuals, but 5 of the 7 in the group are Fe^{+2} dominant. However, in neither the Mg or Fe^{+2} dominant individuals is the dominance extreme, as is illustrated by these formulas of analyses (53 and 101, table 11) which represent the Mg and Fe^{+2} extremes of the group

$$[\underbrace{(Al_{0.38}Ti_{0.28}Fe^{+3}_{0.04}Fe^{+2}_{1.16}Mg_{1.34}Mn^{+2}_{0.01})}_{2.65}(Si_{2.74}Al_{1.26})O_{10}(OH)_2]^{-0.94}$$
$$(K_{0.88},Na_{0.05},Ca/2_{0.01})^{+0.93}_{0.93}$$

$$[\underbrace{(Al_{0.38}Ti_{0.15}Fe^{+3}_{0.20}Fe^{+2}_{1.26}Mg_{0.73}Mn^{+2}_{0.02})}_{2.83}(Si_{2.64}Al_{1.36})O_{10}(OH)_2]^{-1.02}$$
$$(K_{0.92},Na_{0.11},Ca/2_{0.02})^{+1.03}_{1.01}$$

The Mg dominant members of the group contain considerable Fe^{+3}, and the Fe^{+3} dominant members contain considerable Mg although Fe^{+2} may be more dominant in some Fe^{+2} dominant members than Mg is in any of the Mg dominant members. These two formulas also illustrate the extremes of octahedral aluminum content in members of the group. The Fe_2O_3 content of 5 of the 7 biotites in this group was less than 1 percent. The biotite represented by the formula for 101 above has the highest Fe_2O_3 content, 3.49 percent. Adjustment for the additional positive charges carried by trivalent octahedral cations in these biotites is, in general, fairly evenly distributed between method A and method B.

The one point representing biotite from diorite falls not in the quartz diorite area (qd) but near the top of the granite area. This biotite is more dominantly magnesian than other biotites from diorite and quartz diorite, but is not unlike them in other compositional characteristics.

Biotites from nepheline syenite.—The biotites from nepheline syenite are definitely more ferroan than the biotites heretofore considered. The almost round area (ns) in figure 12 enclosing points representing biotites in this group lies well below the Mg-Fe^{+2}=1:1 line, with the upper edge just touching the lower edge of the granodiorite area (gd). The formula calculated for analysis 109, table 11

$$[\underbrace{(Al_{0.86}Ti_{0.22}Fe^{+3}_{0.38}Fe^{+2}_{1.56}Mg_{0.42})}_{2.79}(Si_{2.58}Al_{1.42})O_{10}(OH)_2]^{-0.97}$$
$$(K_{0.79},Na_{0.13},Ca/2_{0.02})^{+0.95}_{0.94}$$

fairly well represents the general characteristics of the members of this group, which are quite uniform in composition. Octahedral Al is very low. In some members there is not enough to complete the filling of the tetrahedral group, and some Fe^{+3} must be allocated to this group for its completion. The Fe_2O_3 content is generally fairly high, varying between 4 and 10 percent in the analyses at hand. Mn is considerably higher than in the biotites heretofore studied, several of the nepheline syenite biotites having between 2 and 3 percent MnO. TiO_2 content is quite variable. Although in a few biotites in this group adjustment for additional positive octahedral charges is made equally by the two methods, in most the adjustment is dominantly by method B. Thus, many of the formulas for this group are characterized by a low positive octahedral charge, with fewer octahedral positions occupied than in the biotites heretofore considered.

Biotites from gneiss and schist.—Points representing biotites from gneiss and schist occupy an area in figure 12 which lies athwart the lower part of the granodiorite

(gd) area, the middle of the quartz diorite (qd) area, and the upper part of the nepheline syenite (ne) area. This location indicates that the biotites from gneiss and schist are somewhat higher in Fe^{+2} content than the biotites from granodiorite, but generally lower in Fe^{+2} content than biotites from nepheline syenite. The formula calculated for analysis 86, table 11, represents the general character of the biotites in this group:

$$[(\underbrace{Al_{0.78}Ti_{0.20}Fe^{+3}_{0.12}Fe^{+2}_{1.48}Mg_{0.84}Mn^{+2}_{0.02}}_{2.76})(Si_{2.64}Al_{1.36})O_{10}(OH)_2]^{-1.36}$$

$$(K_{0.89},Na_{0.16},Ca/2_{0.22})^{+1.09}_{1.07}$$

These biotites are all Fe^{+2} dominant, with moderate octahedral Al content and fairly low Fe^{+3} content. Adjuetment for additional positive octahedral cations is made about equally by methods A and B, with a moderate octahedral poeitive charge (0.30–.40), a moderate negative tetrahedral charge in excess of 1.00, and with an octahedral occupancy deficiency of about 0.2 poeition.

Biotites from pegmatite.—Of 14 analyses of micas from pegmatite, only 4 represented biotites; all the others represented Mg deficient trioctahedral micas, siderophyllites, lepidomelanes, and intermediatee of these. Three of the four biotites from pegmatite are highly Mg dominant and are lower in Fe^{+2} than any of the biotites from granite or granodiorite. Thus, the points representing them in figure 12 fall outside the upper boundary of the granite area. The fourth biotite from pegmatite is highly Fe^{+2} dominant. The point representing it falls just outside the granite area on the lower right side of figure 12.

Trioctahedral micas from pegmatite.—Ten of the fourteen analyses of micas from pegmatites are very low in Mg (<1.5 percent MgO) and high in Fe^{+2} content. They therefore represent the Mg deficient end of the Mg replacement system and occupy an area at the bottom of the triangular diagram shown in figure 12. Two of these analyees represent siderophyllites, with Al the greatly dominant trivalent octahedral cation, and with Fe^{+3} very low or absent; five represent lepidomelanes, with Fe^{+3} the greatly dominant trivalent octahedral cation, and with Al very low or absent. The other three analyses represent aluminian lepidomelanes, with significant amounts of both Fe^{+3} and octahedral Al, but with Fe^{+2} present in somewhat greater amounts than octahedral Al. The three micas from nepheline eyenite pegmatite are, however, quite similar in compoeition, like biotites from nepheline eyenite, and like them are characterized by iron. The Mg content in the micas from nepheline syenite pegmatite is, however, very much lower. All three of these micas (124, 125, and 126) are lepidomelanes, with octahedral Al very low or absent. In one the Al is so low that there is not sufficient to complete the filling of the tetrahedral group, making it necessary to assign some Fe^{+3} to that group.

Li is reported in 7 of the 10 analyses of Mg deficient trioctahedral micas from pegmatites, the amount reported varying from 0.08 to 1.01 percent Li_2O. No Li is reported in the three analyses from nepheline syenite pegmatite. This failure to report Li does not mean, necessarily, that Li is not present. Li, if present, but not determined, is reported as Na. As Li is considered an octahedral cation and calculated as such, failure to determine Li if present causes a double error in the formula calculation, too few octahedral cations and too many interlayer cations, the amount of error depending on the amount of Li present. In one of the formulas calculated from the three analyses in which Li is not reported, 126, table 11, the higher interlayer cation content, 1.11, euggests the possible presence of Li. In the other two formulas calculated from analyses in which Li is not reported, the interlayer cation content is not high, but this does not rule out the possible presence of small amounts of Li.

Other Mg-deficient trioctahedral micas.—Of the 3 other analyses of Mg deficient trioctahedral micas at hand, 2 are of micas from greisen, and 1 is of mica from offshoot veins of trap dike. One of the two micas from greisen is a siderophyllite, with less than 1 percent of Fe_2O_3, the other is about halfway between siderophyllite and lepidomelane. The latter is reported to contain 0.39 percent Li_2O. No Li is reported in the siderophyllite, but the high interlayer ion content is suggestive of its possible presence. The mica from offshoot veins from trap dike is an aluminian lepidomelane containing 0.59 percent Li_2O.

The Mg-deficient trioctahedral micas show a greater tendency toward one-sided adjustment for the extra charges carried by trivalent and quadrivalent octahedral cations than do the biotites. Of the 13 Mg deficient trioctahedral micas here considered, 8 showed preferential adjustment, 75 percent or more, by method B. In three the adjustment is entirely by method B, except for compensation due to Li.

Li, with its single positive charge, compensates for as many extra charges carried by trivalent octahedral cations as the number of octahedral positions it occupies. This may be illustrated by referring to the formula for D63, table 12,

$$[\underbrace{(Al_{0.48}Fe^{+3}_{0.68}Fe^{+2}_{1.09}Mg_{0.07}Mn^{+2}_{0.03}Li_{0.18})}_{2.51}^{-0.02}(Si_{2.98}Al_{1.02})^{-1.02}O_{10}(OH)_2]^{-1.04}K^{+1.01}_{1.01}$$

In this formula Al and Fe^{+3} carry 1.14 positive charges in excess of the number of positive charges that would be carried by the same number of bivalent cations. On the other hand, 0.18 Li carries only half as many positive charges as would be carried by the same number of bivalent cations. Thus the xLi cations compensate for x R^{+3} cations, the number of extra positive charges carried by the trivalent cations is reduced by the number of positions occupied by Li, and the layer structure must adjust for 0.96 extra charges, not 1.14. This adjustment is made entirely by method B, that is, unoccupancy of octahedral positions, with the anionic charges associated with these unoccupied positions available for the neutralization of the extra charges. Octahedral occupancy is only 2.51, the 0.49 unoccupied positions contributing 0.98 negative charges for the neutralization of the 0.96 extra positive charges, and the octahedral layer is left with a residual charge of −0.02.

DISCUSSION OF RELATION BETWEEN MICA COMPOSITION AND OCCURRENCE

This study of the relation between the composition and character of trioctahedral micas and their geologic occurrence indicates that igneous rocks such as granites, diorites, and nepheline syenites, and metamorphic rocks, such as gneiss and schist, yield trioctahedral micas in which both Mg and Fe^{+2} are present in significant amounts, that is, biotites, but do not yield trioctahedral micas, like phlogopites, with very high Mg content and low Fe^{+2} content, or micas like siderophyllites and lepidomelanes, with very low Mg content and high Fe^{+2} content. Heinrich (1946, p. 842, 844) found that phlogopites occur in peridotites and other ultramafic rocks and in metamorphosed limestones. The data that are available on phlogopites for the present study indicate that some phlogopites are from contact zones of metamorphism. All the siderophyllites and lepidomelanes are from pegmatites or greisen. Thus the extreme types of trioctahedral micas, those with extremely high or extremely low Mg content, are from extreme types of rocks.

There is not a clear distinction in the composition of biotites from different kinds of rocks. This is illustrated by these three formulas, calculated from analyses 49, 50, and 51, table 11:

$$[\underbrace{(Al_{0.02}Ti_{0.19}Fe^{+3}_{0.27}Fe^{+2}_{0.92}Mg_{1.38}Mn^{+2}_{0.02})}_{2.80}^{+0.27}(Si_{2.72}Al_{1.27})^{-1.27}O_{10}(OH)_2]^{-1.00}(K,Na)^{+0.96}_{0.96}$$

$$[\underbrace{(Al_{0.04}Ti_{0.18}Fe^{+3}_{0.27}Fe^{+2}_{0.90}Mg_{1.40}Mn^{+2}_{0.03})}_{2.82}^{+0.31}(Si_{2.72}Al_{1.28})^{-1.28}O_{10}(OH)_2]^{-0.97}(K,Na,Ca/2)^{-0.97}_{0.96}$$

$$[\underbrace{(Al_{0.00}Ti_{0.20}Fe^{+3}_{0.30}Fe^{+2}_{0.88}Mg_{1.39}Mn^{+2}_{0.01})}_{2.78}^{+0.26}(Si_{2.76}Al_{1.24})^{-1.24}O_{10}(OH)_2]^{-0.98}(K,Na,Ca/2)^{+0.95}_{0.93}.$$

These formulas are essentially identical, not only in the kinds and amounts of ions present, but in octahedral charge and occupancy, tetrahedral charge, and total charge. They are much more alike than many calculated formulas for biotites not only from the same kind of rock, but than some from the same rock at the same location. Yet 49 represents a biotite from granodiorite, 50 a biotite from monzonite, and 51 a biotite from granite. Thus biotites from different rocks may be very similar in composition and character. That they are not differentiated clearly in character is attested by the superimposing and overlapping of areas in figure 12. At 1 place at the middle right-hand side of the biotite area, the areas for 4 different rocks are superimposed.

Conversely, biotites from the same kind of rock may differ greatly in character and composition. This is particularly true of biotites from granites and to a lesser extent of biotites from granodiorite, diorite, and quartz diorite. The diversity in composition and character of biotites from granite is shown by the large area occupied by these biotites, which embraces practically the entire biotite area as shown in figure 11. This picture, however, is probably distorted to some extent by the loose usage of the term "granite" to cover monzonite, quartz monzonite, granodiorite, diorite, and quartz diorite.

The figures in Heinrich's study (1946, p. 836–848) of the relation between composition and geologic occurrence in the biotite-phlogopite series seem to indicate a more clear-cut differentiation between the composition of biotites and their parent rocks than was found in this study. However, he used a separate diagram for each of his rock groups. If the diagrams for his group 2 (granites, quartz monzonites, granodiorites), group 3 (tonalites, diorites), group 6 (syenites, nepheline syenites, but excluding nepheline syenite

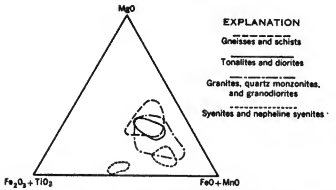

FIGURE 13.—Relation between the composition and the geologic occurrence of biotites. (After Heinrich, 1946, figs. 2, 3, 6, and 7 superimposed and reoriented.)

pegmatites), and group 7 (gneisses and schists), which include all the groups shown in figure 12 except pegmatites and greisen, are superimposed on each other, as in figure 13, it is found that the areas occupied by biotites from these different rocks overlap considerably. The tonalite-diorite area lies almost wholly within the granite, quartz monzonite, granodiorite area, and half of the gneiss-schist area overlies the same part of the same area. Thus at this 1 place the areas for 3 groups overlie each other. In figure 13 the triangular diagram of Heinrich has also been reoriented, so that MgO, FeO+MnO, and $Fe_2O_3+TiO_2$ occupy the same corners with respect to the viewer as do Mg, Fe^{+2}+Mn, and R^{+3}+Ti in figure 12. The occupied areas in the two figures occur in the same general part of triangular diagrams—a very good agreement in view of the different methods used in plotting the biotite compositions; Heinrich's biotites being plotted on the basis of percentage by analysis, in which octahedral Al and the great equivalent difference between Mg and Fe^{+2} is ignored, and the biotites in figure 12 being plotted on the basis of octahedral positions occupied, including octahedral Al.

However, correlations of this sort can show only the broader aspects of the relation between biotite composition and the parent rocks; details of the relation are possible only in more localized studies.

SUMMARY AND CONCLUSIONS

The composition of the trioctahedral micas can be interpreted as derived from phlogopite, $Mg_{3.00}(Si_{3.00}Al)O_{10}(OH)_2K_{1.00}$, by the proxying of other cations, particularly Fe^{+2}, Fe^{+3}, and Al, for Mg. Phlogopite, in its ideal form may, therefore, be considered the prototype of the trioctahedral micas, just as muscovite, in its ideal form, is the prototype of the dioctahedral micas. In natural phlogopites the proxying of other cations for Mg is minor, and Mg is greatly predominant, occupying more than 70 percent of the octahedral positions. Progressively greater proxying of other cations, particularly Fe^{+2}, for Mg leads successively to Mg biotites, in which Mg is still the dominant octahedral cation, but in which Fe^{+2} is present in significant amounts, Fe^{+2} biotites, in which Fe^{+2} is the dominant octahedral cation, with Mg present in subordinate but significant amounts, and siderophyllites and lepidomelanes, in which Mg is essentially absent, occupying less than 5 percent of the octahedral positions. Thus, in order of decreasing Mg content, the trioctahedral micas, phlogopites, biotites, siderophyllites, and lepidomelanes form a complete system, from full octahedral occupancy by Mg at one end to nil Mg occupancy at the other end. These relations are expressed in the following equations, which show the range in composition of three principal groups.

Phlogopite

$$[(\underbrace{R^{+3}_{<0.50}Fe^{+2}_{<0.50}Mg_{3.00-2.00}}_{3.00-2.85})(Si_{3.00-2.70}Al_{1.00-1.30})O_{10}(OH)_2]^{-1.00\pm0.10}K(Na,Ca/2)^{+1.00\pm.10}_{1.00\pm0.10}$$

$<+0.30$ $(-1.00)-(-1.30)$

↓

Mg biotite
Fe^{+2} biotite

$$[(\underbrace{R^{+3}_{0.25-1.00}Fe^{+2}_{0.50-1.75}Mg_{1.75-0.50}}_{2.90-2.65})(Si_{3.00-2.50}Al_{1.00-1.50})O_{10}(OH)_2]^{-1.00\pm0.10}K(Na,Ca/2)^{+1.00\pm0.10}_{1.00\pm0.10}$$

$<+0.50$ $(-1.00)-(-1.50)$

↓

Siderophyllites and lepidomelanes

$$[(\underbrace{R^{+3}_{0.50-1.00}Fe^{+2}_{2.25-1.50}Mg_{<0.15}Li_{0.15}}_{2.90-2.65})(Si_{3.00-2.50}Al_{1.00-1.50})O_{10}(OH)_2]^{-1.00\pm0.10}K(Na,Ca/2)^{+1.00\pm0.10}_{1.00\pm0.10}$$

$<+0.50$ $(-1.00)-(-1.50)$

Considered as derivatives of phlogopite as the prototype, all trioctahedral micas exhibit multiple proxying of other cations for Mg. The phlogopites are the only trioctahedral micas in which one kind of cation is greatly predominant in the octahedral group. Consequently, the low Mg end of the system is represented by siderophyllite and lepidomelane, not by annite, the Fe^{+2} analog of phlogopite.

The proxying of bivalent ions, like Fe^{+2} or Mn^{+2}, for Mg is ion for ion, and no layer charge adjustments are necessary, but the proxying of trivalent ions, like Al, or Fe^{+3}, for Mg, because of their greater valence, re-

quires layer charge adjustments. The two possible types of adjustment may be expressed by the following equations:

$$2nR^{+3}=nR^{+2}+n\mathrm{Si} \qquad (A)$$
$$2nR^{+3}=3nR^{+3}. \qquad (B)$$

In the (A) type of adjustment nR^{+3} ions proxy for nMg ions in the octahedral layer, and an additional nAl ion proxies for nSi ions in the tetrahedral layers. Formulas for trioctahedral micas that have accommodated trivalent octahedral cations in this way are characterized by a positive octahedral charge equivalent to the number of trivalent octahedral cations present, a negative tetrahedral charge greater than 1.00 by an amount equivalent to the positive octahedral charge, that is, to the number of trivalent octahedral cations, and by full octahedral occupancy. In the (B) type of adjustment $2nR^{+3}$ cations proxy for $3n$Mg ions. Formulas for trioctahedral micas that have accommodated trivalent octahedral cations in this way are characterized by a neutral octahedral layer, and a negative tetrahedral charge of 1.00 as in the ideal formula for phlogopite, but octahedral occupancy is deficient by an amount equivalent to one-half the number of trivalent octahedral cations. A few formulas for trioctahedral micas have the octahedral positive charge, the equivalently greater negative tetrahedral charge, and the full octahedral occupancy indicative of the (A) type of adjustment, and a few have the neutral octahedral group and deficient octahedral occupancy of the (B) type of adjustment, but most formulas for trioctahedral micas have characteristics of both types of adjustment—a positive octahedral charge, a negative tetrahedral charge greater than 1.00, and octahedral deficiency—indicating a combination of the two types of adjustment. The relative degree of adjustment by (A) or (B), and, consequently, the proxying ratio of trivalent for bivalent octahedral cations varies. However, the average proxying ratio in the 250 formulas included in this study is 0.73 Al for 1.00 Mg, a proxying ratio which is considerably closer to that of the (B) than to that of the (A) type of adjustment, indicating generally greater adjustment by (B) than by (A).

In general, the degree of adjustment by (B) increases with the octahedral R^{+3} content. This is reflected in a general decrease in the number of octahedral positions occupied with increase in octahedral R^{+3} content, with the average octahedral positive charge remaining about the same throughout the octahedral R^{+3} range. Thus most trioctahedral micas are not truly trioctahedral. Nor are they true octaphyllites, as the number of cations in the half cell is usually less than eight.

The trend of R^{+3} proxying is, therefore, toward muscovite or other dioctahedral mica. However, the distribution of the formulas studied over the R^{+3} range, and the scarcity of formulas having more 0.90 octahedral positions occupied by R^{+3}, strongly indicates that the normal extent of R^{+3} proxying for Mg is approximately one-third of the occupied octahedral positions and that there is not a continuous series between the trioctahedral and dioctahedral micas.

REFERENCES CITED

Clarke, F. W., 1903, Mineral analyses from the laboratories of the United States Geological Survey 1880 to 1903: U. S. Geol. Survey Bull. 220, p. 77.

Cooke, J. P., Jr., 1867, On cryophyllite, a new mineral species of the mica family, with some associated minerals in the granite of Rockport, Mass.: Am. Jour. Sci., 2d ser., v. 43, p. 217–230.

Dana, E. S., 1892, The system of mineralogy, 6th ed.: New York, John Wiley and Sons.

Dana, J. D., 1868, A system of mineralogy, 5th ed.: New York, John Wiley and Sons.

Deer, W. A., 1937, The composition and paragenesis of the biotites of the Carsphairn igneous complex: Mineralog. Mag., v. 24, p. 495–502.

Eyerman, John, 1904, Contributions to mineralogy: Am. Geologist, v. 34, p. 42–48.

Foster, M. D., 1951, The importance of the exchangeable magnesium and cation-exchange capacity in the study of montmorillonitic clays: Am. Mineralogist, v. 36, p. 717–730.

——— 1956, Correlation of dioctahedral potassium micas on the basis of their charge relations: U. S. Geol. Survey Bull. 1036–D, p. 57–67.

Grigoriev, D. P., 1935, Study of magnesium-iron micas: Soc. Russe minéralogie Mém., ser. 2, v. 64, p. 21–79. [Russian with English summary.]

Hallimond, A. F., 1926, On the chemical classification of the mica group II. The basic micas: Mineralog. Mag., v. 21, p. 25–33.

Hamilton, S. Harbert, 1899, Exploration of the Delaware Valley: The Mineral Collector, v. 6, p. 117–122.

Heinrich, E. W., 1946, Studies in the mica group; the biotite-phlogopite series: Am. Jour. Sci., v. 244, p. 836–848.

Hey, Max H., 1955, An index of mineral species and varieties, 2d rev. ed.: London, British Mus. (Nat. History), 728 p.

Holzner, Julius, 1936, Über den "anomalen" Kristallbau der Biotite: Zeitschr. Kristallographie, v. 95, p. 435–450.

Hutton, C. O., 1947, Contributions to the mineralogy of New Zealand, part 3: Royal Soc. New Zealand Trans., v. 76, p. 481–491.

Kunitz, W., 1924, Die Beziehungen zwischen der chemischen Zusammensetzung und der physikalisch-optischen Eigenschaften innerhalb der Glimmergruppe: Neues Jahrb. Mineralogie, Geologie u. Paläontologie, Beilage-Band 50, p. 365–413.

Marshall, C. E., 1949, The colloid chemistry of the silicate minerals: New York, Academic Press, 195 p.

Nockolds, S. R., 1947, The relation between chemical composition and paragenesis in the biotite micas of igneous rocks: Am. Jour. Sci., v. 245, p. 401–420.

Nockolds, S. R., and Richey, J. E., 1939, Replacement veins in the Mourne mountains granites, Northern Ireland: Am. Jour. Sci., v. 237, p. 27–47.

Pauling, Linus, 1930, The structure of mica and related minerals: Natl. Acad. Sci. Proc., v. 16, p. 123–129.

Ross, C. S., and Hendricks, S. B., 1945, Minerals of the montmorillonite group: U. S. Geol. Survey Prof. Paper 205–B, p. 23–79.

Simpson, E. S., 1932, Contributions to the mineralogy of Western Australia—Series VIII: Royal Soc. W. Australia Jour., v. 18, p. 61–74.

Winchell, A. N., 1925, Studies in the mica group: Am. Jour. Sci., 5th ser., v. 9, p. 309–327.

Winchell, A. N., and Winchell, H., 1951, Elements of optical mineralogy, part 2, Description of minerals, 4th ed.: New York, John Wiley and Sons, 551 p.

TABLE 11.—*Analyses and data for writing formulas of trioctahedral micas used in correlation study*

[In order of decreasing MgO content]

Analysis (See p. 44-45)	Percent																Octahedral positions occupied by—							Octahedral charge	Tetrahedral charge	Inherent layer charge	Interlayer cations	
	SiO_2	TiO_2	Al_2O_3	Fe_2O_3	FeO	MgO	MnO	CaO	Na_2O	K_2O	H_2O+	H_2O-	F	Total	O=F	Adjusted total	Al	Ti	Fe^{+3}	Fe^{+2}	Mn	Mg	Total				Charge	Positions
1	41.68	0.38	13.21	0.16	0.11	28.16			1.04	8.78	3.10		3.07	[1] 101.77	−1.29	100.48	0.01	0.02	0.01	0.01		2.94	2.99	+0.04	−1.08	−1.04	+1.04	0.98
2	40.96		13.14	.85	1.71	28.03		0.40	.96	10.25	2.06		3.15	101.50	−1.33	100.17	.00		.00	.10		2.92	3.02	+.04	[3] −1.13	−1.09	+1.11	1.08
3	40.64		14.11	2.28	.69	27.97			1.16	8.16	3.21		0.62	[2] 101.58	−.35	101.23	.00		.10	.04		2.90	3.04	+.18	[3] −1.17	−.99	+1.01	.95
4	43.00		13.27	1.71		27.70			.30	10.32	.38		5.67	102.35	−2.39	99.96	.04		.09			2.85	2.98	+.09	−1.03	−.94	+.95	.95
5	42.55		12.74	1.31	.49	27.62			.83	8.92	1.18		4.59	100.23	−1.93	98.30	.03		.07	.03		2.88	3.01	+.12	−1.02	−.90	+.91	.91
6	40.42	.34	14.76	.73	.81	27.58	0.03		.71	8.58	4.03	0.16	1.17	[4] 100.44	−.49	99.95	.06	.02	.04	.05		2.89	3.06	+.26	−1.16	−.90	+.92	.89
7	41.97		11.41	1.13	.68	27.42			1.27	9.98	4.06		3.67	101.09	−1.55	99.94	.00		.01	.02		2.91	2.94	−.07	[3] −1.01	−1.08	+1.08	1.08
7a	40.56	.10	14.63	1.14	.41	27.37	.08	.07	.20	10.73	4.68		.05	100.02	−.02	100.00	.06	.01	.06	.02		2.86	3.01	+.15	−1.15	−.99	+.99	.99
8	39.38		15.92	.71	.30	26.85		.28	.62	9.84	4.69	.38	.62	[5] 100.39	−.26	100.13	.12		.04	.06		2.83	3.04	+.24	−1.21	−.97	+.98	.98
9	40.81		17.03	1.67	.65	26.84			.66	9.58	2.42		2.78	102.44	−1.18	101.26	.16		.09	.04		2.74	3.02	+.28	−1.22	−.94	+.92	.92
9a	40.80	.05	13.16	1.84	2.16	26.72		.46	2.44	7.95	2.95		2.89	101.42	−1.22	100.20	.00		.06	.13		2.90	2.99	+.04	[3] −1.13	−1.09	+1.11	1.06
10	39.66	.56	17.00	.27	.20	26.49		nil	.60	9.97	2.33	.66	2.24	[6] 100.60	−.94	99.66	.17	.03	.01	.01		2.76	2.98	+.20	−1.23	−1.03	+1.02	1.01
11	39.68	1.14	14.28	.77	2.15	26.28	.05		.56	8.64	3.90	.23	1.16	[7] 99.94	−.70	99.24	.02	.06	.04	.13		2.79	3.04	+.26	−1.18	−.92	+.91	.89
12	42.19	.61	12.60	.33	2.91	25.61	.02	.06	.31	9.91	2.84	.33	2.66	[8] 100.51	−1.12	99.39	.04	.03	.02	.17		2.70	2.96	+.04	−1.01	−.97	+.94	.94
13	38.91	.22	16.53	2.01	1.46	25.45	.05	.19	.28	9.84	3.04	.67		98.65			.13	.01	.11	.09		2.66	3.00	+.26	−1.25	−.99	+.96	.94
14	36.96	.52	18.45	.70	1.37	25.23	.01	.21	.58	9.45		.82		[9] 99.91			.20	.03	.04	.08		2.69	3.04	+.38	−1.36	−.98	+1.00	.97
15	40.32		18.03	5.80		24.79		.46		10.50	.25			100.15			.15		.29			2.49	2.93	+.30	−1.28	−.98	+.97	.93
16	41.12		17.23	3.14		24.00		.89	.42	9.50	3.56			99.86			.24		.16			2.47	2.87	+.14	−1.16	−1.02	+1.03	.97
17	40.00		17.28	.72	4.88	23.91			1.47	8.57	1.37		1.57	99.77	−.66	99.11	.20		.04	.28		2.48	3.00	+.24	−1.21	−.97	+.98	.96
18	38.37	.54	17.01	.86	3.76	23.20	.07		.43	9.63		.16	2.23	[10] 100.83	−.93	99.90	.20	.03	.05	.22		2.48	2.98	+.27	−1.24	−.97	+.98	.98
19	40.95	.82	17.28	.43	2.38	22.95			.16	9.80	4.23	.48	.62	[11] 100.13	−.20	99.87	.30	.04	.02	.14		2.40	2.90	+.20	−1.18	−.93	+.90	.90
20	39.62	.35	16.02	2.21	5.37	22.86	.09	.05	1.55	8.87	.60	.04	.76	[12] 100.22	−.32	99.90	.10	.02	.12	.31	.01	2.39	2.94	+.14	−1.21	−1.07	+1.09	1.05
21	40.16	.45	12.65	5.52	4.39	22.68		.24	nil	9.62	3.00						.00	.02	.24	.26	.01	2.42	2.94	+.16	[3] −1.12	−.96	+.92	.90
22	42.56	2.09	12.18	2.73	.90	22.40		.20	.44	10.70	2.35		2.46	[13] 100.80	−1.03	99.77	.02	.11	.15	.05		2.36	[13] 2.73	−.11	−.98	−1.09	+1.11	1.07
23	36.81	1.00	17.00	2.32	7.70	22.00	.17	.61	1.00	8.78	1.65	.43		99.47			.05	.05	.12	.46	.01	2.34	3.03	+.33	−1.38	−1.05	+1.03	.98
24	37.53	1.61	14.74	4.93	3.02	21.83	.33	.15	.92	10.35	4.78		1.26	101.35	−.53	100.82	.00	.08	.24	.18	.02	2.36	2.88	+.16	[3] −1.28	−1.12	+1.11	1.10
25	43.02	.86	13.54	.39	5.18	21.85			.84	10.75	1.52		.30	[14] 99.91	−.13	99.78	.10	.04	.02	.30		2.26	[14] 2.87	−.10	−1.01	−1.11	+1.07	1.07
26	37.80	1.20	17.46	1.56	7.72	21.80	.05	.54	1.00	8.20	1.60	.27		99.30			.12	.06	.08	.46		2.29	3.01	+.34	−1.33	−.99	+.97	.92
27	40.63	1.15	13.04	1.12	7.62	21.47			.57	10.14	2.47		4.00	[13] 102.26	−1.68	100.58	.04	.06	.06	.46		2.30	2.92	+.06	−1.07	−1.01	+1.01	1.01
28	40.81		16.47	2.16	5.92	21.08			1.55	9.01	2.19			99.19			.23		.11	.35		2.20	2.89	+.12	−1.14	−1.02	+1.02	1.02
29	37.10	1.24	17.20	1.74	8.30	21.00	.13	1.09	.78	8.60	1.67	.35		99.20			.09	.07	.09	.50	.01	2.23	2.99	+.30	−1.35	−1.05	+1.06	.97
30	38.89		14.53	4.58	8.92	20.28			.40	10.08	.94		1.49	100.11	−.63	99.48	.02		.25	.54		2.17	2.98	+.23	−1.21	−.98	+.98	.98
31	39.82		19.25	2.62	5.73	20.00			.66	8.33	1.69			[16] 99.51			.36		.14	.33		2.08	2.91	+.32	−1.22	−.90	+.91	.87
32	38.06	.19	14.74	2.01	8.76	19.74	.19		.42	9.42		.12	2.21	[17] 100.03	−.93	99.10	.11	.01	.11	.54	.01	2.18	2.96	+.16	−1.18	−1.02	+1.00	.98
33	37.05	2.81	15.04	4.12	5.10	19.74	.28	.33	.23	9.55	4.15	.30	.40	[14] 100.36	−.17	100.19	.00	.16	.22	.31	.02	2.16	2.85	+.22	−1.29	−1.07	+1.04	.98
34	38.67	3.45	13.00	2.18	7.65	19.37		.12	.73	10.00	4.28			99.48			.00	.19	.07	.47		2.11	2.84	+.13	[3] −1.17	−1.04	+1.05	1.05
35	38.04	.39	15.77	2.62	11.13	18.35	.10	.91	.27	9.23	2.24	.20	.26	[15] 100.15	−.11	100.04	.11	.02	.14	.68	.01	1.98	[13] 2.94	+.17	−1.24	−1.07	+1.03	.96
35a	38.20		15.45	8.63	9.59	16.58		1.50	.18	9.17	1.94		1.16	102.39	−.48	101.91	.03		.46	.67		1.77	2.83	+.15	−1.27	−1.12	+1.09	.98
36	39.70	1.11	15.92	3.31	8.96	16.16	.24	1.60	.86	8.08	3.21		1.40	[20] 100.73	−.69	100.14	.21	.06	.18	.54	.02	1.73	[14] 2.78	+.05	−1.13	−1.08	+1.11	.99
37	40.65	0.33	19.88	Tr.	7.89	15.06	.12	.14	.83	9.46	2.90		2.57	[21] 101.08	−1.08	100.00	.56	.02		.47	.01	1.66	[11] 2.80	+.12	−1.11	−.99	+1.01	1.00
38	38.56	4.95	14.12	5.51	8.25	15.59	.20	1.06	.81	8.68	1.03		1.25	[22] 100.44	−.53	99.91	.00	.26	.18	.66	.01	1.64	2.76	+.18	[3] −1.28	−1.10	+1.08	.98
39	35.67	7.42	15.52	2.78	10.31	15.38		.58	1.07	8.77	2.39			99.89			.00	.40	.06	.63		1.66	2.76	+.36	[3] −1.41	−1.05	+1.05	1.01
40	35.68	1.29	19.60	1.87	11.45	15.06	.21	.97	1.04	8.12	2.92	.56	.47	[23] 100.00	−.20	99.80	.31	.07	.10	.70	.01	1.64	[23] 2.90	+.28	−1.39	−1.11	+1.09	1.00
41	35.85	3.16	18.24	.36	13.44	14.92	.17	.30	1.00	9.66	1.88		.41	100.38	−.17	100.21	.22	.17	.02	.81	.01	1.61	2.84	+.26	−1.34	−1.08	+1.08	1.05
42	37.12	3.74	15.30	1.72	14.68	14.65	.18	.15	.98	9.81	1.59		.43	100.36	−.18	100.18	.03	.20	.10	.90	.01	1.60	2.84	+.21	−1.28	−1.07	+1.08	1.07
43	37.71	1.64	19.29	2.24	9.72	14.22	.81	.00	1.33	9.33	4.29	.00		100.08			.39	.09	.12	.59	.02	1.54	2.75	+.19	−1.26	−1.07	+1.06	1.05
44	37.12	3.84	13.86	3.92	14.64	14.14	.35	Tr.	.63	8.84	1.54						.00	.21	.17	.91	.02	1.56	2.87	+.33	[3] −1.26	−.93	+.92	.92
45	38.22	2.96	14.71	3.83	13.44	13.45	.52	1.46	.50	7.90	1.89	.60		[24] 99.56			.08	.16	.21	.82	.03	1.47	2.77	+.16	−1.20	−1.06	+1.04	.92
46	37.88	2.06	19.23	4.09	10.47	13.19	.30	.00	1.40	9.85	1.56	.00		100.03			.33	.11	.22	.63	.02	1.41	2.72	+.21	−1.29	−1.09	+1.09	1.09
47	35.51	3.57	17.67	3.52	12.69	12.96	.30	.42	.67	9.42	2.74		1.05	100.43	−.44	99.99	.16	.20	.20	.78	.02	1.43	2.78	+.31	−1.38	−1.07	+1.05	.98
48	35.62	2.61	15.24	4.69	13.67	12.70	.74	.95	.50	7.72	4.36	.94		[24] 100.00			.07	.16	.27	.87	.05	1.44	2.85	+.34	−1.30	−.96	+.99	.90
49	36.32	3.42	14.66	4.80	14.74	12.38	.34	Tr.	.90	8.63	2.72						.02	.19	.27	.92	.02	1.38	2.80	+.27	−1.27	−1.00	+.96	.96
50	35.75	3.16	14.70	4.65	14.08	12.37	.45	.17	.32	9.19	3.54	1.03	.17	[26] 99.88	−.07	99.81	.04	.18	.27	.90	.03	1.40	2.82	+.31	−1.28	−.97	+.97	.96
51	35.79	3.51	13.70	5.22	13.72	12.13	.19	.05	.15	9.09	3.64	1.21	.76	[27] 99.60	−.37	99.22	.00	.20	.30	.88	.01	1.39	2.78	+.26	−1.24	−.98	+.98	.93
52	36.88	1.88	15.79	3.01	15.57	12.10	.11	.09	.18	9.47	3.70	.00		[28] 99.85			.24	.11	.17	.97	.01	1.35	2.85	+.33	−1.24	−.91	+.94	.94
53	36.40	4.68	14.60	.76	18.39	11.90	.20	.11	.30	8.97	2.90	.08		99.29			.04	.26	.04	1.15	.01	1.34	2.85	+.30	−1.26	−.96	+.92	.92
54	36.34	3.29	13.88	4.49	15.00	11.80	.52	.28	.67	8.80	3.00	.70		[25] 99.34			.02	.19	.26	.96	.03	1.34	2.80	+.26	−1.23	−.97	+.99	.96
55	36.60	3.30	14.98	1.00	19.23	11.15	.13	.18	.37	9.06	3.20	.20		[30] 99.53			.12	.19	.06	1.22	.01	1.26	2.86	+.28	−1.23	−.96	+.96	.94
56	36.22	3.02	16.39	3.92	14.41	11.11	.16		.37	8.97	4.00	.76	.08	[31] 100.19	−.03	100.16	.20	.17	.23	.91	.01	1.25	2.77	+.31	−1.26	−.95	+.96	.94
57	37.37	5.75	14.78	2.07	14.89	10.98		1.08	1.06	8.22	3.24			99.44			.07	.32	.12	.92		1.22	2.66	+.13	−1.22	−1.09	+1.11	1.02
58	35.12	2.77	18.65	.37	19.91	10.48	.27	.14	.48	9.42	2.08		.07	99.76	−.03	99.73	.27	.16	.02	1.25	.02	1.17	2.88	+.35	−1.37	−1.02	+.99	.98
59	34.96	3.99	15.29	2.90	18.30	10.42	.39	1.11	.41	7.99	3.07	.41	1.17	[32] 100.74	−.49	100.25	.03	.23	.17	1.16	.02	1.18	[33] 2.89	+.36	−1.34	−1.01	+1.02	.93
60	35.88	4.17	14.96	2.33	20.88	10.04	.18	.12	.36	9.20	.80		1.58	100.50	−.66	99.84	.03	.24	.13	1.31	.01	1.13	2.85	+.34	−1.30	−.96	+.96	.95
61	36.02	1.13	18.81	5.60	14.76	9.82	.80	.65	.38	9.32	2.57		.26	100.11	−.11	100.00	.32	.07	.31	.92	.05	1.08	2.75	+.27	−1.33	−1.06	+1.04	.99
62	37.39	2.48	20.17	2.05	14.32	9.80		.51	.87	8.56	3.03		1.67	[33] 100.90	−.70	100.20	.49	.14	.11	.88		1.07	2.69	+.26	−1.25	−.99	+1.00	.97
63	35.21	2.65	20.07	.68	16.88	9.78	.35	Tr.	.37	8.94	3.80	.53		99.26			.44	.15	.04	1.06	.02	1.10	2.81	+.40	−1.34	−.94	+.92	.92
64	37.67		18.79	6.48	15.28	9.72			1.92	8.93	2.33			101.12			.37		.36	.93		1.08	2.72	+.17	−1.25	−1.08	+1.11	1.11
65	35.64	1.12	18.62	5.54	14.60	9.72	.79	.90	.38	9.22	2.54	.48	.26	[34] 101.01	−.11	99.90	.22	.06	.31	.91	.05	1.09	2.74	+.23	−1.32	−1.09	+1.08	1.01
66	36.62	3.02	14.37	4.04	17.09	9.68	.40	1.48	.45	8.20	3.26	.90	.10	[35] 99.95	−.04	99.91	.09	.17	.23	1.09	.02	1.10	2.70	+.06	−1.19	−1.13	+1.13	1.00
67	36.17	3.15	15.23	3.00	18.83	9.61	.34	.63	.52	9.05	2.75	.20		[36] 99.65			.11	.18	.17	1.20	.02	1.09	2.77	+.18	−1.25	−1.07	+1.06	1.00
68	35.51	3.07	15.80	2.95	18.87	9.52	.35	.35	.26	9.40	3.13	.10		99.31			.14	.18	.17	1.21	.02	1.08	2.80	+.27	−1.28	−1.01	+1.01	.98

See footnotes at end of table, p. 43.

TABLE 11.—*Analyses and data for writing formulas of trioctahedral micas used in correlation study*—Continued

[In order of decreasing MgO content]

Analysis (see p. 44–45)	Percent																Octahedral positions occupied by—							Octahedral charge	Tetrahedral charge	Inherent layer charge	Interlayer cations	
	SiO₂	TiO₂	Al₂O₃	Fe₂O₃	FeO	MgO	MnO	CaO	Na₂O	K₂O	H₂O+	H₂O−	F	Total	O=F	Adjusted total	Al	Ti	Fe+3	Fe+2	Mn	Mg	Total				Charge	Positions
69	34.70	4.58	17.17	2.11	19.05	9.52	0.50		1.24	8.91	3.56		0.20	101.54	−0.08	101.46	0.13	0.26	0.12	1.20	0.03	1.06	2.80	+0.37	−1.39	−1.02	+1.03	1.03
70	35.67	3.32	14.56	3.03	23.23	9.24		1.13	.49	8.06	1.02	0.23	.16	[37] 100.22	−.07	100.15	.00	.19	.17	1.47		1.04	2.87	+.29	−1.30	−1.01	+1.03	.94
71	35.66		21.23	3.08	16.26	9.01	.28	.42	.68	8.41	2.74	.48		98.25			.57		.17	1.02	.02	1.02	2.80	+.24	−1.31	−.97	+.96	.94
72	36.25		18.25	6.36	17.09	9.01		.79		8.68	2.70			99.12			.35		.56	1.08		1.01	2.80	+.31	−1.27	−.96	+.96	.89
73	33.73	2.45	19.37	3.28	16.38	8.99	.29	.16	1.30	7.83	3.98	2.31		[38] 100.19			.35	.14	.19	1.05	.02	1.03	2.78	+.38	−1.40	−1.02	+.99	.98
74	34.97	5.64	15.30	2.81	21.23	8.83	.16	1.09	.27	7.17	3.03	.31		100.81			.00	.32	.16	1.34	.01	.99	2.82	+.44	−1.36	−.92	+.91	.82
75	34.32	3.47	16.22	7.13	15.85	8.82	.45	.36	1.82	7.58	4.15			100.17			.12	.14	.41	1.02	.03	1.01	2.73	+.27	−1.36	−1.09	+1.08	1.06
76	35.08	2.99	19.55	.69	18.11	8.80		Tr.	.40	9.53	3.72	.14		[39] 99.31			.42	.17	.04	1.16		1.00	2.78	+.36	−1.33	−.97	+.98	.98
77	35.04	3.65	15.68	1.84	20.31	8.75	.32	.62	.41	8.37	3.97	.53		99.41			.14	.21	.11	1.32	.02	1.01	2.61	+.29	−1.28	−.99	+.99	.94
78	35.06	3.29	16.53	.87	21.10	8.71	.48	.13	.26	9.46	3.10	.17		99.16			.20	.19	.05	1.36	.03	1.00	2.83	+.29	−1.30	−1.01	+.98	.97
79	36.82	4.82	16.34	1.85	18.02	8.62	.60	1.01	.47	8.82							.28	.16	.11	1.15	.03	.98	2.71	+.13	−1.19	−1.06	+1.09	1.01
80	35.91	2.89	14.36	3.72	19.64	8.59	.21	.98	.84	8.14	2.99	.82		99.09			.09	.17	.22	1.27	.01	.99	2.76	+.15	−1.22	−1.07	+1.09	1.01
81	36.97	2.64	17.51	2.26	14.81	8.45	.22	None	.45	8.50	2.48	.32	3.17	[40] 101.03	−1.34	99.69	.40	.15	.13	.94	.01	.96	[40] 2.79	+.21	−1.16	−.97	+1.00	1.00
82	34.77	2.84	19.05	.88	20.71	8.37	.10	.26	.24	8.49	3.44	.33	None	99.48			.36	.16	.05	1.32	.01	.95	2.85	+.43	−1.35	−.92	+.90	.88
83	34.64	3.48	16.30	3.22	19.94	8.23	.31	1.03	.80	7.90	2.88	.64	1.69	[41] 101.31	−.73	100.58	.14	.20	.18	1.28	.02	.94	[41] 2.84	+.32	−1.34	−1.02	+1.06	.98
84	37.88	.62	12.87	4.86	21.03	8.22	.88		1.53	8.65	3.50			100.04			.10	.04	.28	1.36	.06	.95	2.79	+.04	−1.07	−1.03	+1.08	1.08
85	35.06	2.78	15.79	5.51	17.83	8.17	.29		1.61	7.86	3.98			99.78			.12	.16	.38	1.14	.02	.93	2.75	+.32	−1.31	−.99	+1.00	1.00
86	34.24	3.41	18.19	2.14	18.26	8.17	.39	.23	1.05	9.08	3.19	1.60		99.85			.29	.20	.12	1.18	.03	.94	2.76	+.33	−1.36	−1.03	+1.09	1.07
87	34.90	3.53	17.64	.67	20.88	8.08	.63	.23	.34	9.08	3.10	.00		99.28			.31	.16	.05	1.35	.04	.93	2.83	+.32	−1.30	−.98	+.99	.97
88	34.03	2.74	16.46	2.01	21.54	8.06		.50	.34	8.88	3.29		.25	100.10	.10	100.00	.27	.16	.12	1.38		.92	2.85	+.41	−1.39	−.98	+1.00	.96
89	34.46	2.52	18.60	1.00	20.09	8.03	.51	None	.25	9.09	4.25	.74		99.44			.36	.16	.06	1.30	.03	.93	2.83	+.38	−1.33	−.95	+.94	.94
90	34.86	3.52	17.45	4.40	17.82	7.96		.30	.53	9.14	3.50	.45		99.93			.23	.20	.25	1.14		.90	2.72	+.32	−1.34	−1.02	+1.02	.99
91	34.73	3.20	18.00	.71	20.80	7.95	.80	.16	.34	9.24	3.30	.09		99.31			.30	.16	.04	1.34	.05	.91	2.82	+.34	−1.33	−.99	+.98	.97
92	35.36	4.07	19.73	.27	19.46	7.88	.16	Tr.	.44	8.99	3.00			99.34			.41	.23	.02	1.22	.01	.88	2.77	+.43	−1.34	−.91	+.93	.93
93	37.04	1.67	14.59	5.53	18.84	7.61	.92		1.23	8.52	3.60			99.84			.16	.10	.32	1.21	.06	.89	2.74	+.16	−1.16	−1.00	+1.02	1.02
94	34.13	2.62	19.73	2.07	18.97	7.76	.33	None	.21	9.15	4.30	.18		99.45			.41	.15	.12	1.22	.02	.89	2.81	+.45	−1.38	−.93	+.92	.92
95	37.42	5.52	15.78	3.00	15.79	7.70	.30	.58	.67	8.55	4.16		.45	[42] 100.00	.19	99.81	.21	.31	.17	.99	.02	.86	[42] 2.60	+.16	−1.19	−1.03	+1.02	.97
96	34.04	1.46	15.60	4.22	23.60	7.46	.99		.88	8.89	1.26		2.02	100.44	−.85	99.59	.09	.09	.25	1.54	.07	.87	2.91	+.34	−1.34	−1.00	+1.02	1.02
97	34.87	5.12	19.79	1.72	17.79	7.42	.02	.54	.67	8.18	2.89	.29	.42	99.72	−.18	99.54	.36	.29	.10	1.12		.83	2.70	+.44	−1.39	−.95	+.97	.92
98	35.87	2.77	16.85	3.37	20.15	7.20	.43	.95	.40	8.43	3.58	.18		[43] 100.53			.25	.16	.19	1.28	.03	.82	2.73	+.22	−1.27	−1.05	+1.03	.96
99	35.35	3.70	7.96	9.89	19.91	7.02	1.11	None	.50	9.00	3.66	1.39	.90	[44] 100.48	−.38	100.10	.00	.22	.23	1.35	.08	.85	2.73	+.13	[3] −1.14	−1.01	+1.01	1.01
100	33.42	3.14	12.22	9.41	21.83	6.84	.72		1.02	7.86	4.32			100.78			.00	.19	.35	1.45	.06	.80	2.84	+.41	[3] −1.35	−.94	+.95	.95
101	32.60	2.66	21.28	3.49	21.56	6.63	.39	.36	.77	9.23	1.83		.14	100.94	−.06	100.88	.35	.16	.20	1.36	.02	.76	2.83	+.61	−1.54	−1.03	+1.02	1.01
102	35.86	2.30	10.99	6.10	22.03	6.53	2.57	Tr.	1.02	8.56	2.41	.52	1.52	100.41	−.63	99.78	.00	.14	.25	1.46	.17	.77	2.79	+.11	[3] −1.16	−1.04	+1.03	1.03
103	33.40	3.51	13.59	2.04	25.82	6.41	1.10		.10	10.07	2.37		1.38	[45] 99.95	−.58	99.37	.00	.21	.09	1.73	.08	.77	2.88	+.27	[3] −1.31	−1.04	+1.05	1.05
104	34.39	3.28	19.54	.77	21.42	6.40	.45	.23	.36	9.09	3.30	.10		99.09			.40	.19	.04	1.37	.03	.73	2.76	+.34	−1.36	−1.02	+1.02	1.00
105	32.43	1.10	18.64	4.53	19.92	6.26	2.33	.41	.52	9.20	3.66	.45	.16	99.61	−.07	99.54	.29	.06	.27	1.31	.16	.74	2.83	+.34	−1.44	−1.10	+1.08	1.04
106	36.08	2.73	17.21	1.14	23.75	6.16	.36	1.74	None	7.27	1.28	.22		[46] 99.57			.31	.16	.07	1.52	.02	.70	2.78	+.26	−1.24	−.98	+.99	.85
107	33.86	2.74	14.93	8.02	26.02	6.03	.84	.39	.50	8.31	3.10	.43		100.17			.06	.16	.16	1.72	.06	.71	2.89	+.34	−1.33	−.99	+.95	.94
108	34.43	3.51	17.43	2.60	21.65	5.88	.44	1.22	.58	8.83	2.56	.11	1.12	[47] 100.44	−.47	99.97	.23	.20	.15	1.39	.03	.68	[47] 2.72	+.16	−1.36	−1.17	+1.16	1.08
109	33.07	3.84	16.32	5.97	22.46	5.85		.26	.87	7.92	3.87			100.43			.08	.22	.35	1.46		.68	2.79	+.45	−1.42	−.97	+.96	.94
110	33.93	1.39	20.55	3.91	18.79	5.61	.43	.35	.40	9.05	3.40	1.41	.90	[48] 100.31	−.38	99.93	.51	.07	.23	1.22	.03	.65	[48] 2.77	+.36	−1.37	−1.01	+1.01	.98
111	34.62	3.79	14.83	1.08	26.34	5.51	.58	.38	.17	8.97	3.08	.10		99.42			.12	.22	.06	1.74	.04	.65	2.83	+.28	−1.26	−.98	+.99	.98
112	32.24	1.97	15.54	8.53	21.94	5.32	2.08	.30	.46	8.13	3.35	.24	.13	100.23	−.05	100.16	.01	.12	.51	1.46	.14	.63	2.87	+.50	−1.45	−.95	+.96	.92
113	34.65	1.77	20.37	3.49	18.48	5.25	.48	.76	.53	8.31	4.52	1.00	.68	[49] 100.65	−.29	100.36	.52	.10	.20	1.19	.03	.60	[49] 2.74	+.30	−1.33	−1.03	+1.02	.95
114	34.32	8.64	14.84	1.86	26.17	5.16	.67	.33	.25	9.00	2.90	.08		99.22			.10	.22	.11	1.73	.04	.61	2.81	+.27	−1.28	−1.01	+1.00	.98
115	33.24	4.73	14.90	5.92	23.57	5.16	.95	.40	1.45	7.77	2.19			100.27			.00	.28	.29	1.53	.06	.60	2.76	+.37	[3] −1.42	−1.05	+1.06	1.02
116	34.60	3.33	14.28	2.10	26.80	4.98	.60	.60	.41	8.53	3.30	.16		99.58			.09	.20	.13	1.76	.03	.59	2.82	+.26	−1.26	−.99	+1.03	.98
117	33.48	2.94	13.64	8.00	23.54	4.97	1.02	.56	.53	7.80	2.63		.95	100.08	−.40	99.66	.00	.17	.41	1.56	.07	.59	2.80	+.35	[3] −1.34	−.99	+.98	.92
118	36.84	3.07	21.13	3.14	16.48	4.70	.36	1.22	1.36	7.79	2.01	.29	2.22	[50] 101.25	−.93	100.32	.60	.17	.16	1.03	.02	.52	2.52	+.16	−1.25	−1.09	+1.08	1.00
119	38.04	2.66	16.78	5.28	18.08	4.57	.46	.55	.64	7.79	3.12	.76	1.61	[51] 100.65	−.64	100.01	.39	.16	.30	1.15	.03	.52	[51] 2.65	+.18	−1.11	−.93	+.94	.89
120	33.68	2.28	17.16	2.42	25.60	4.46	1.66	.80	.48	7.37	3.60	.16		[52] 99.61			.25	.14	14	1.69	.11	.52	2.85	+.37	−1.34	−.97	+.95	.88
121	34.45	2.05	19.61	4.33	19.30	4.42	.54	.85	.43	8.15	3.84	1.38	.71	[53] 100.33	−.30	100.01	.47	.12	.25	1.25	.04	.51	[53] 2.71	+.31	−1.32	−1.01	+1.02	.94
122	34.72	3.76	11.09	8.12	28.96	2.44	.45	.79	.53	7.57	2.44	.75	.27	99.88	−.11	99.77	.00	.23	.24	1.96	.03	.29	2.76	+.20	[3] −1.19	−.99	+1.00	.93
123	32.32	.81	15.88	12.89	20.06	1.21	1.07	1.06	.04	7.53	3.32	2.34	.89	[54] 99.92	−.37	99.55	.16	.05	.79	1.37	.07	.16	[54] 2.76	+.39	−1.36	−.97	+.96	.87
124	31.64	.33	15.34	8.38	31.78	.90	.28		.67	8.70	1.93		.13	100.08	−.05	100.03	.06	.02	.61	2.17	.02	.11	2.89	+.39	−1.42	−1.03	+1.02	1.02
125	36.32	4.04	11.91	7.87	26.01	.76	1.34		1.15	7.06	2.76			99.22			.01	.24	.47	1.73	.09	.09	2.63	+.22	−1.11	−.89	+.89	.89
126	32.96	2.60	10.34	8.85	27.19	.73	2.79	.64	.98	7.75	4.36		None	99.42			.00	.16	.35	1.91	.20	.09	2.73	+.17	[3] −1.23	−1.06	+1.11	1.06
127	32.52	.21	19.07	10.08	17.83	.70	.21	.73	.21	8.53	3.17	3.21	2.36	[55] 99.22	−.99	98.23	.52	.01	.62	1.22	.02	.09	[55] 2.61	+.25	−1.32	−1.07	+1.06	.99
128	36.52	.76	14.99	7.73	22.41	.62	.74	.35	.44	7.68	3.62	2.20	1.97	[56] 100.53	−.83	99.70	.36	.05	.47	1.51	.05	.08	[56] 2.68	+.13	−1.06	−.93	+.92	.89
129	39.60	.21	22.80	.79	20.98	.46	.29	1.52	Tr.	8.96	2.93	.24	2.03	100.80	−.85	99.95	.99	.01	.05	1.32	.02	.05	2.44	−.06	−1.03	−1.09	+1.10	.95
130	31.96	.08	17.06	7.44	24.12	.29	.71	.48	.61	7.41	5.66	2.94	1.59	[57] 100.84	−.67	100.17	.39		.47	1.70	.05	.04	[57] 2.65	+.36	−1.31	−.95	+.95	.91
131	35.25	1.81	17.24	8.15	20.61	.28	.89	1.10	.27	7.21	2.99	2.78	1.67	[58] 100.43	−.70	99.73	.44	.09	.49	1.38	.06	.03	[58] 2.64	+.24	−1.19	−.95	+.96	.87
132	37.01	.02	15.89	Tr.	30.16	.22	1.01	.10	.58	9.02	1.92	None	3.88	[59] 101.37	[60] −1.68	99.69	.47			2.02	.07	.03	[59] 2.92	−.02	−1.03	−1.05	+1.03	1.03
133	36.91	.55	18.20	5.16	21.97	.20	.29	.23	.28	8.22	4.51		3.16	[61] 101.17	−1.32	99.85	.57	.03	.31	1.44	.02	.02	[61] 2.86	+.19	−1.10	−.91	+.90	.89
134	31.40	.53	15.66	11.72	23.73	.14	1.13	.87	.33	6.57	4.02	2.71	.43	[62] 99.32	−.18	99.14	.16	.03	.74	1.67	.08	.02	[62] 2.74	+.44	−1.36	−.92	+.91	.83
135	33.60	.06	22.36	1.44	28.54	.10	.33	.14	.46	8.90	1.66	.08	.89	[63] 98.91	−.37	98.54	.73		.08	1.88	.02	.01	[63] 2.82	+.35	−1.35	−1.00	+.99	.98

The following numbers are in terms of percentages.

[1] Includes 2.08 BaO.

[2] A little Fe^{+3} present in tetrahedral group.

[3] Includes 2.54 BaO.

[4] Includes 1.02 BaO, 0.05 Cl, and 0.06 S.

[5] Includes 0.30 CO_2, which is equivalent to all CaO and to 0.07 MgO reported.

[6] Includes 0.62 BaO.

[7] Includes 0.07 Cr_2O_3, 0.97 BaO, 0.05 Cl, and 0.07 S.

[8] Includes 0.13 P_2O_5.

[9] Includes 0.50 BaO, 0.08 Cl, 0.13 S, 0.13 P_2O_5, and 4.77 ignition loss.

[10] Includes 0.69 BaO, 0.04 Cl, 0.09 S, and 3.76 ignition loss.

[11] Includes 0.03 BaO.

[12] Includes 1.31 BaO, 0.07 Cr_2O_3, 0.08 P_2O_5, 0.14 Cl, and 0.02 S.

[13] Includes 0.73 Cr_2O_3 (equivalent to 0.04 octahedral formula positions), 1.00 BaO, and 0.06 P_2O_5.

[14] Includes 0.74 Cr_2O_3 (0.04 octahedral positions), 0.52 NiO (0.03 octahedral positions), 0.28 Li_2O (0.08 octahedral positions), and 0.12 BaO.

[15] Includes 0.04 BaO.

[16] Includes 1.41 BaO.

[17] Includes 0.79 BaO, 0.03 Cl, 0.16 S, 0.01 P_2O_5, and 3.24 ignition loss.

[18] Includes 1.26 BaO.

[19] Includes 0.09 CuO, 0.02 Cr_2O_3, 0.03 NiO, 0.01 V_2O_3, 0.01 SrO, 0.15 BaO, and 0.33 P_2O_5.

[20] Includes 0.08 Cr_2O_3 (0.01 octahedral positions), and 0.11 Li_2O (0.03 octahedral positions).

[21] Includes 0.28 Li_2O (0.08 octahedral positions), 0.37 Rb_2O, and trace Cs_2O.

[22] Includes 0.43 BaO.

[23] Includes 0.53 BaO, and 0.23 Li_2O (0.07 octahedral positions).

[24] Includes 0.08 P_2O_5.

[25] Includes 0.36 BaO.

[26] Includes 0.06 V_2O_3, 0.12 BaO, and 0.03 P_2O_5.

[27] Includes 0.13 BaO, 0.20 Cl, and 0.10 P_2O_5.

[28] Includes 0.07 CO_2, which is equivalent to the CaO (0.09) reported.

[29] Includes 0.07 P_2O_5.

[30] Includes 0.13 P_2O_5.

[31] Includes 0.06 V_2O_3, and 0.74 BaO.

[32] Includes 0.33 Li_2O (0.10 octahedral positions).

[33] Includes 0.02 Cr_2O_3.

[34] Includes 0.20 P_2O_5.

[35] Includes 0.33 BaO.

[36] Includes 0.21 P_2O_5.

[37] Includes 0.05 ZrO_2, and 0.03 Cr_2O_3.

[38] Includes 0.12 P_2O_5.

[39] Includes 0.30 P_2O_5.

[40] Includes 0.65 Li_2O (0.20 octahedral positions), 1.48 Rb_2O, and 1.14 Cs_2O.

[41] Includes 0.25 Li_2O (0.08 octahedral positions).

[42] Includes 0.12 Li_2O (0.04 octahedral positions).

[43] Includes 0.35 P_2O_5.

[44] Includes 0.09 BaO.

[45] Includes 0.07 BaO.

[46] Includes 1.65 ZrO_2.

[47] Includes 0.04 V_2O_3, and 0.14 Li_2O (0.04 octahedral positions).

[48] Includes 0.19 Li_2O (0.06 octahedral positions), and 0.04 V_2O_3.

[49] Includes 0.32 Li_2O (0.10 octahedral positions).

[50] Includes 0.24 TiO_2, 0.15 SO_3, 0.10 CO_2, and 0.15 Cl.

[51] Includes 0.37 Li_2O (0.11 octahedral positions), 0.04 BaO, and 0.04 V_2O_3.

[52] Includes 0.22 P_2O_5.

[53] Includes 0.21 Li_2O (0.07 octahedral positions, 0.02 BaO, and 0.04 V_2O_3.

[54] Includes 0.50 Li_2O (0.10 octahedral positions).

[55] Includes 0.39 Li_2O (0.13 octahedral positions).

[56] Includes 0.50 Li_2O (0.16 octahedral positions).

[57] Includes 0.59 Li_2O (0.20 octahedral positions).

[58] Includes 0.48 Li_2O (0.15 octahedral positions).

[59] Includes 1.01 Li_2O (0.33 octahedral positions), 0.19 Rb_2O, 0.12 Cs_2O, and 0.24 Cl.

[60] Includes 0 = Cl.

[61] Includes 1.48 Li_2O (0.47 octahedral positions).

[62] Includes 0.08 Li_2O (0.02 octahedral positions).

[63] Includes 0.32 Li_2O (0.10 octahedral positions).

Locality and reference for analyses in table 11

1. DeKalb, N.Y., Dana, E S., 1892, The system of mineralogy, 6th ed., New York, John Wiley and Sons, p. 633, No. 11.
2. Mansjö Mountain, Sweden, Eckermann, H. v., 1925, Tschermaks mineralog. petrog. Mitt., v. 38, p. 281, No. 2.
3. Edwards, N.Y., Dana, E. S., 1892, The system of mineralogy, 6th ed., New York, John Wiley and Sons, p. 633, No. 4.
4. Gouverneur, N.Y., Dana, E. S., 1892, The system of mineralogy, 6th ed., New York, John Wiley and Sons, p. 633, No. 7.
5. Pargas, Finland, Dana, E. S., 1892, The system of mineralogy, 6th ed., New York, John Wiley and Sons, p. 633, No. 5.
6. Slyudianka, Baikalia, U.S.S.R., Grigoriev, D. P., 1935, Soc. Russe minéralogie Mém., 2d ser., v. 64, p. 31, No. 1.
7. Pargas, Finland, Jakob, J., 1932, Zeitschr. Kristallographie, v. 82, p. 273, No. 71.
7a. Snake Creek, Salt Lake City, Utah, Orcel, J., 1925, Soc. Française mineralogie Bull., v. 48, p. 304. From phyllite.
8. Montville, N.J., Clarke, F. W., 1903, U.S. Geol. Survey Bull. 220, p. 76, D. C. Cattell, analyst. From serpentine.
9. Jefferson, Wrooman Lake, State not given, Kunitz, W., 1924, Neues Jahrb. Mineralogie, Geologie, u. Paläontologie, Beilage-Band 50, p. 412, table 2, No. 2.
9a. Mansjö Mountain, Sweden, Eckermann, H. v., 1925, Tschermaks mineralog. petrog. Mitt., v. 38, p. 281.
10. Burgess, Ontario, Clarke, F. W., and Schneider, E. A., 1890, Am. Jour. Sci., 3d ser., v. 40, p. 411. E. A. Schneider, analyst.
11. Slyudianka, Baikalia, U.S.S.R., Grigoriev, D. P., 1935, Soc. Russe minéralogie Mém., 2d ser., v. 64, p.31, No. 5.
12. Deal, Idaho, Hietanen, A., U.S. Geol. Survey Prof. Paper 344, in press.
13. U.S.S.R. (exact locality not given), Berkhin, S. I., 1954, Akad. Nauk SSSR Doklady, v. 95, p. 146, No. 260.
14. Slyudianka, Baikalia, U.S.S.R., Grigoriev, D. P., 1935, Soc. Russe. minéralogie Mém. 2d ser., v. 64, p. 31, No. 3.
15. Easton, Pa., Eyerman, J., 1901, Am. Geologist v. 34, p. 46, C.
16. Easton, Pa., Eyerman, J., 1901, Am. Geologist v. 34, p. 46, A.
17. Lake Baikal, U.S.S.R., Dana, E. S., 1892, The system of mineralogy, 6th ed., New York, John Wiley and Sons, p. 630, No. 1.
18. Slyudianka, Baikalia, U.S.S.R., Grigoriev, D. P., 1935, Soc Russe minéralogie Mém. 2d ser., v. 64, p. 31, No. 8.
19. Nancy Sound, New Zealand, Hutton, C. O., 1947, Royal Soc. New Zealand Trans., v. 76, p. 486. In marble associated with gneisses.
20. Southern Yakutia, U.S.S.R., Serdyuchenko, D. P., 1954, Akad. Nauk SSSR Doklady, v. 97, p. 152.
21. Northwest of Barkly West, Cape Province Africa, Nockolds, S. R., 1947, Am. Jour. Sci., v. 245, p. 413, No. 60. Associated with olivine and diopside augite.
22. Lucite Hills, Wyo., Hillebrand, W. F., 1903, U.S. Geol. Survey Bull. 220, p. 76, C.
23. U.S.S.R. (exact locality not given), Berkhin, S. I., 1954, Akad. Nauk SSSR Doklady, v. 95, p. 146, No. 1.
24. Alban Hills, near Rome, Italy, Washington, H. S., 1927, Am. Jour. Sci., 5th ser. v. 14, p. 189. Associated with nephilite-melilite rock.
25. Northern Caucasus, U.S.S.R., Serdyuchenko, D. P., 1951, Soc. Russe. minéralogie Mém., v. 80, p. 175. Associated with diopside, actinolite, and almandite.
26. U.S.S.R. (exact locality not given), Berkhin, S. I., 1954, Akad. Nauk SSSR Doklady, v. 95, p. 146, No. 3.
27. Rossie, N.Y., Dana, E. S., 1892, The system of mineralogy, 6th ed., New York, N.Y., John Wiley and Sons, p. 633, No. 12.
28. Greenwood Furnace, N.J., Dana, E. S., The system of mineralogy, 6th ed., New York, N.Y., John Wiley and Sons, p. 630, No. 2.
29. U.S.S.R. (exact locality not given), Berkhin, S. I., 1954, Akad. Nauk SSSR Doklady, v. 95, p. 146, No. 2.
30. Arendal, Norway, Dana, E. S., 1892, The system of mineralogy, 6th ed., New York, N.Y., John Wiley and Sons, p. 630, No. 10.
31. Sterzing, Tyrol, Dana, E. S., 1892, The system of mineralogy, 6th ed., New York, N.Y., John Wiley and Sons, p. 630, No. 14.
32. Slyudianka, Baikalia, U.S.S.R., Grigoriev, D.P., 1935, Soc. Russe minérologie Mém. 2d ser., v. 64, p. 31, No. 9.
33. Bufumbira, S. W. Uganda, Combe, A. D., and Holmes, A., 1948, Royal Soc. Edinburgh Trans. v. 61, p. 377.
34. Weinheim, Germany, Weyberg, Z., 1912, Neues, Jahrb. Min. B.B.I., p. 398, No. 6 a. Associated with augite and minette.
35. Malvern, England, Tha Hla, 1945, Mineralog. Mag. v. 27, p. 139. From granite pegmatite.
35a. Fillipstad, Sweden, Dana, E. S., 1892, The system of mineralogy, 6th ed., New York, N.Y., John Wiley and Sons, p. 630, No. 13.
36. Ridgway, Va., Stevens, R. E., 1945, U.S. Geol. Survey Bull. 950, p. 118.
37. Monte Somma, Tuscany, Pieruccini, R., 1950, Soc. Toscana Sci. Nat. Atti Mem., ser. A, vol. 57, p. 152. Associated with plagioclase and sanidine.
38. San Juan district, Colo., Larsen, E. S., Gonyer, F. A., and Irving, J., Am. Mineralogist, v. 22, p. 902. Associated with pyroxene.
39. Radautal, Germany, Kunitz, W., 1936, Neues Jahrb. Mineralogie, Geologie u. Paläontologie Beilage-Band 70 A, p. 401.
40. Northern Caucasus, U.S.S.R., Serdyuchenko, D. P., 1951, Soc. Russe Mineralogie Mém., v. 80, p. 176.
41. Kojatin, near Trebíč, Moravia, Czechoslovakia, Dudek, A., 1954, Československá Akad. Věd Rozpravy, v. 64, p. 31. From amphibole-biotite granite.
42. Kosov, near Jihlava, Moravia, Czechoslovakia, Dudek, A., 1954, Československá Akad. Věd, Rozpravy, v. 64, p. 33. From pyroxene-biotite granite.
43. Monti di Daro, Italy, Jakob, J., 1931, Zeitschr. Kristallographie, v. 79, p. 373, no. 58.
44. Morven-Strontian complex, northern Scotland, Nockolds, S. R., and Mitchell, R. L., 1947, Royal Soc. Edinburgh Trans., v. 61, p. 562, no. 5. Associated with tonalite-granodiorite.
45. Chocholowska Valley, Tatra Mountains, Zastawniak, F., 1951, Soc. Géol. Pologne Annales, v. 20, p. 128. In diorite.
46. Monti di Daro, Italy, Jakob, J., 1931, Zeitschr. Kristallographie, v. 79, p. 373, no. 57.
47. Zernovka, near Říčany, Bohemia, Czechoslovakia, Dudek, A., 1954. Československá Akad. Věd, Rozpravy, v. 64, p. 27. From biotite granite.
48. Bloods Station, Alpine County, Calif., Clarke, F. W., 1903, U.S. Geol. Survey Bull. 220, p. 75, E. Associated with quartz-monzonite.
49. Garabal Hill-Glen Fyne complex, Scotland, Nockolds, S. R., and Mitchell, R. L., 1947, Royal Soc. Edinburgh Trans., v. 61, p. 562, no. 14. From porphyritic granodiorite contaminated with sedimentary material.
50. Mt. Hoffman, Mariposa County, Calif., Clarke, F. W., 1903. U.S. Geol. Survey Bull. 220, p. 75, D. From quartz-monzonite.
51. Butte, Mont., Clarke, F. W., 1903, U.S. Geol. Survey Bull. 220, p. 75, G. From granite.
52. Bethel, Vt., unpub. analysis by Charles Milton, U.S. Geol. Survey, lab. no. D-953.
53. Ōbatake, Kāzo-Mura, Kuga-gōri, Yamaguti Pref. Japan, Tsuboi, S., 1938, Japanese Jour. Geology Geography, v. 15, p. 126, no. 24. In hypersthene-biotite-quartz diorite.
54. Senmaya, Rikutyū, Japan, Tsuboi, S., 1935, Japanese Jour. Geology Geography, v. 12, p. 112, no. 6. From hornblende-bearing biotite granodiorite.
55. Yokolake, Euasan district, Mino, Tsuboi, S., 1935, Japanese Jour. Geology Geography, v. 12, p. 110, no. 9. In gneissose granite.
56. Old Point, Charles Sound, New Zealand, Hutton, C. O., 1947, Royal Soc. New Zealand Trans. and Proc., v. 76, p. 482, no. 1. In pegmatitelike lenses in oligoclase-quartz-biotite gneiss.
57. River Tschul-sou-su, Altai, Mongolia, Timofeev, K., 1927, Neues, Jahrb. Mineralogie, Geologie u. Paläontologie, Ref. Bd. II, 81. From granodiorite.
58. Mrač, near Benešov, Bohemia, Czechoslovakia, Dudek, A., 1954, Československá Akad. Věd Rozpravy, v. 64, p. 36. From amphibole-biotite granodiorite.
59. Carsphairn complex, Southern Scotland, Deer, W. A., 1937, Mineralog. Mag., v. 24, p. 496, no. 3. From hornblende hybrid.
60. Ames Station, Belknap Mountains, N. H., Chapman, R. W., and Williams, C. R., 1935, Am. Mineralogist, v. 20, p. 512, no. 2. From monzodiorite.
61. El Capitan, Yosemite Valley, Calif., Iddings, J. P., 1911, Rock minerals, 2d ed., New York, John Wiley and Sons, p. 451.
62. Clove Valley, Dutchess County, N.Y., Barth F. W., 1936, Geol. Soc. America Bull., v. 47, p. 783, no. 2. From contact between sheared quartzitic schist and pegmatite.
63. Tenryūkyō, Simoina-gōri, Nagano Pref., Tsuboi, S., 1938, Japanese Jour. Geology Geography, v. 15, p. 128, no. 28. In cordierite-biotite hornfels.
64. Renchthal, Germany, Dana, J. D., 1892, The system of mineralogy, 6th ed., New York, John Wiley and Sons, p. 630, no. 16.
65. Yosemite Valley, Calif., Clarke, F. W., 1903, U.S. Geol. Survey Bull. 220, p 75, C. From granite.
66. North fork of Mokelumne River, above mouth of Bear River, Amador County, Calif., Clarke, F. W., 1903, U.S. Geol. Survey Bull. 220, p. 75, F. From pyroxene gneiss.
67. Isikawa-mati, Hukusima Pref., Tsuboi, S., 1938, Japanese Jour. Geology Geography, v. 15, p. 129, no. 31. In gneissose hornblende-biotite granodiorite.
68. Akasaka, Samekawa-mura, Higasisirakawa-gōri, Hukusima Pref., Tsuobi, S., 1938, Japanese Jour. Geology Geography, v. 15, p. 125, no. 19. In gneissose tonalite.
69. Freiburg, Germany, Becker, A., 1890, Zeitschr. Kristallographie, v. 17, p. 129. From gneiss.
70. Mora, Minnesota, Grout, F. F., 1924, Am. Mineralogist, v. 9, p. 160, no. 3. In granite.
71. U.S.S.R. (exact locality not given), Berkhin, S. I., 1954, Akad. Nauk SSSR Doklady, v. 95, p. 146, no. 106.
72. Monterey Bay, Calif., Galliher, E. W., 1935, Geol. Soc. America Bull., v. 46, p. 1359. From granite.
73. Minedera, near Tokyo, Japan, Kawano, Y., 1933, Imp. Acad. Tokyo Proc., v. 9, p. 610. In porphyritic biotite granite.
74. Glen Buchat, Aberdeenshire, Scotland, Walker, G. F., 1949, Mineralog. Mag., v. 28, p. 698, no. 1. From hypersthene gabbro.
75. Ehrenberg, Germany, Kunitz, W., 1929, Zeitschr. Kristallographie, v. 70, p. 512. From monzonite.
76. Hirasawa, Oda Mura, Tukuba-gōri, Ibaraki Pref., Tsuboi, S., 1938, Japanese Jour. Geology Geography, v. 15, p. 126, no. 21. Large zenolith enclosed in biotite granite.
77. Takato, Sinano, Japan, Tsuboi, S., 1935, Japanese Jour. Geology Geography, v. 12, p. 110, no. 8. From biotite granodiorite.
78. Tenryūkyō, Simoina-gōri, Nagano Pref., Tsuboi, S., 1938, Japan Jour. Geology Geography, v. 15, p. 126, no. 23. In biotite gneiss (injection gneiss).
79. Chestnut Ridge, Dutchess County, N.Y., Barth, F. W., 1936, Geol. Soc. America Bull., v. 47, p. 783, no. 1. From black phyllite.
80. Southwestern Finland, Hietanen, A., 1943, Acad. Sci. Fenn. Annales, ser. A. III. Geologica-Geographica., no. 6, p. 48. From diorite-trondhjemite.
81. Eight miles northwest of Custer, S. Dak., Wells, R. C., 1937, U.S. Geol. Survey Bull. 878, p. 99. From pegmatite.
82. Upington, Cape Province, South Africa, Mathias, M., 1952, Mineralog. Mag., v. 29, p. 939. From cordierite rock.
83. Carsphairn complex, southern Scotland, Deer, W. A., 1937, Mineralog. Mag., v. 24, p. 496. From granite of a complex intrusive.
84. Låven Island, Kunitz, W., 1929, Zeitschr. Kristallographie, v. 70, p. 512. From nepheline syenite.
85. Kamenz, Germany, Kunitz, W., 1929, Zeitschr. Kristallographie, v. 70, p. 512. From granodiorite.
86. Ornak, Tatra Mountains, Zastawniak, F., 1951, Rocznik Polsk. Towarz. Geol., v. 20 (1950), p. 129. From injection gneiss.
87. Mukuno, Kamano-mura, Ōsima-gōri, Yamaguti Pref., Tsuboi, S., 1938, Japanese Jour. Geology Geography. v. 15, p. 127, no. 25. In garnet-bearing schistose biotite-quartz diorite.
88. Mansjö Mountain, Sweden, Eckermann, H. v., 1925, Tschermaks mineralog. petrog. Mitt., v. 38, p. 277. From contact zone of pegmatite intrusive into eulysite and limestone.
89. Usugi, Takanuki district, Iwaki, Tsuboi, S., 1935, Japanese Jour. Geology Geography, v. 12, p. 112, no. 5. In garnet-bearing gneissose biotite granite (contaminated rock).
90. Altai, Mongolia, Timofeev, K., 1927, Neues Jahrb. Mineralogie, Geologie u. Paläontologie, Ref., v. 11, p. 81. From granodiorite.
91. Kamatu-mati, Ōsima-gōri, Yamaguti Pref., Tsuboi, S., Japanese Jour. Geology Geography, v. 15, p. 127, no. 26. In garnet-bearing biotite-quartz diorite.
92. Kaziyabara, Hidumi-mura, Kuga-gōri, Yamaguti Pref., Tsuboi, S., 1938, Japanese Jour. Geology Geography, v. 15, p. 127, no. 27. In biotite gneiss (injection gneiss).
93. Ruma Island, Los Archipelago, Kunitz, W., 1929, Zeitschr. Kristallographie, v. 70, p. 512. From nepheline syenite.
94. Takanuki district, Iwaki, Tsuboi, S., 1935, Japanese Jour. Geology Geography, v. 12, p. 112, no. 4. From injection biotite gneiss.
95. Stewart Island, New Zealand, Williams, G. J., 1934, Geol. Soc. London Quart. Jour., v. 90, p. 336. From granite.
96. Faraday Township, Hastings County, Ontario, Canada, Walker, T. L., and Parsons, A. L., 1926, Toronto Univ. Studies, Geol. ser., no. 22, p. 22. From nepheline syenite.
97. Belhelvie, Aberdeenshire, Scotland, Stewart, F. H., 1942, Mineralog. Mag., v. 26, p. 263. From SiO_2 poor hornfels.

Locality and reference for analyses in table 11—Continued

98. Usugi, Takanuki district, Iwaki, Tsuboi, S., 1933, Japanese Jour. Geology Geography, v. 12, p. 112. From gneissose biotite-granite.
99. Ristok, Kola Peninsula, U.S.S.R., Ivanov, B. V., 1937, Akad. Nauk SSSR Leningradskii Institut Geokhimii, Kristallografii i Mineralogii Trudy, no. 10, p. 43. From pegmatite and miaskite-nepheline syenite.
100. Brevik, Norway, Kunitz, W., 1924, Neues Jahrb. Mineralogie, Geologie u. Paläontologie, Beil.-Band 50, p. 413. Probably associated with aegirine, nepheline syenite pegmatite.
101. Prosecnice near Praha, Bohemia, Czechoslovakia, Dudek, A., 1954, Ceskoslovenská Akad. Věd Rozpravy, v. 64, p. 29. From biotite granodiorite.
102. Mariupol, Sea of Azov, U.S.S.R., Morozewicz, J., 1930, Tschermaks Mineralog. Petrog. Mitt., v. 40, p. 374. From marinpolite.
103. Dermone, Halland, Sweden, Wiman, E., 1930, Upsala Univ., Geol. Inst., Bull., 22, p. 56. From pegmatite containing microcline, quartz, and albite.
104. Hirasawa, Oda-mari, Tukibo-gori, Ibaraki Pref., Tsuboi, S., 1938, Japanese Jour. Geology Geography, v. 15, p. 125, no. 20. From biotite granite.
105. Fukushimazan district, central Korea, Inoue, T., 1950, Geol. Soc. Japan Jour., v. 56, p. 76. From nepheline syenite.
106. Rockville, Minnesota, Grout, F. F., 1924, Am. Mineralogist, v. 9, p. 161. From granite.
107. Sanaze-mura, Niii-Kamo-gori, Aiti Pref., Tsuboi, S., 1936, Japanese Jour. Geology Geography, v. 13, p. 335, no. 15. From biotite granite.
108. Widecombe, Dartmoor, England, Brammall, A., and Harwood, H. F., 1932, Geol. Soc. London Quart. Jour., v. 88, p. 234. From dark veinlet in granite.
109. Miask, Ural Mountains, U.S.S.R., Kunitz, W., 1924, Neues Jahrb. Mineralogie, Geologie u. Paläontologie Beil.-Band 50, p. 413. From nepheline syenite.
110. Sadile Tor, Dartmoor, England, Brammall, A., and Harwood, H. F., 1932, Geol. Soc. London Quart. Jour., v. 88, p. 231. From granite; associated with muscovite.
111. Hata, Tubo-mura, Kuga-gori, Yamaguti Pref., Tsuboi, S., 1938, Japanese Jour. Geology Geography, v. 15, p. 128, no. 29. From granodiorite.
112. Fukushimazan District, central Korea, Inoue, T., 1950, Geol. Soc. Japan Jour., v. 56, p. 76. From nepheline syenite.
113. Haytor quarry, Dartmoor, England, Brammall, A., and Harwood, H. F., 1923, Mineralog. Mag., v. 20, p. 23. From granite.
114. Tenryûkyo, Simoina-gori, Nagano Pref., Tsuboi, S., 1938, Japanese Jour. Geology Geography, v. 15, p. 126, no. 22. From porphyritic schistose hornblende-biotite granite.
115. Miask, Ural Mountains, U.S.S.R., Dana, E. S., 1892, The system of mineralogy, 6th ed., New York, John Wiley and Sons, p. 630, no. 22.
116. Tutiyane, Nada-mura, Kuga-gori, Kanagaui Pref., Tsuboi, S., 1936, Japanese Jour. Geology Geography, v. 13, p. 335, no. 14. From hornblende-bearing biotite granite.
117. Near Beech Hill, Percy quadrangle, N.H., Chapman, R. W., and Williams, C. R., 1935, Am. Mineralogist, v. 20, p. 512. From granite.
118. Unter-Wald-Miehelbach, Odenwald, Germany, Klemm, G., 1926, Vereins für Erdkunde und der Hessischen Geologischen Landesanstalt zu Darmstadt Notizblatt, 5th ser., No. 8, p. 106. Associated with muscovite, adamellite.
119. Swetter quarry, East Dartmoor, England, Brammall, A., and Harwood, H. F., 1932, Geol. Soc. London Quart. Jour., v. 88, p. 234. From granite.
120. Near Iwakura Railway Station, Opôri, Yamaguti Pref., Tsuboi, S., 1936, Japanese Jour. Geology Geography, v. 13, p. 334, no. 13. From biotite granite.
121. Prison quarry, Princeton, Dartmoor, England, Brammall, A., and Harwood, H. F., 1932, Geol. Soc. London Quart. Jour., v. 88, p. 231. From granite; associated with muscovite.
122. Laitila, Finland, Eskola, P., 1949, Comm. Geol. Finlande Bull., v. 23, p. 114. From fresh rapakivi ("moro").
123. Iisaka, Fukushima Pref., Shibata, H., 1952, Tokyo Bunrika Daigaku Sci. repts., v. 2, sec. C, no. 12, p. 162, no. 8. From graphic granite pegmatite.
124. French River, Sudbury district, Ontario, Canada, Walker, T. L., and Parsons, A. L., 1926, Toronto Univ. Studies, Geol. ser. no. 22, p. 8. From nepheline syenite pegmatite.
125. Wausau, Wisconsin, Weidman, S., 1907, Wisconsin Geol. and Nat. History Survey Bull. 16, p. 205. From quartz syenite pegmatite.
126. Mount Royal, Quebec, Canada, Finley, F. L., 1930, Canadian Jour. Research, v. 2, p. 236. Associated with aegirine, nepheline syenite pegmatite.
127. Ekisu Mine, Naegi district, Japan, Shibata, H., 1952, Tokyo Bunrika Daigaku Sci. Repts., v. 2, sec. C, no. 12, p. 162, no. 6. In greisen.
128. Hachiman, Naegi district, Japan, Shibata, H., 1952, Tokyo Bunrika Daigaku Sci. Repts., v. 2, sec. C, no. 12, p. 161, no. 2. In pegmatite.
129. Mourne Mountains, New Castle County, Ireland, Nockolds, S. R., and Richey, J. E., 1939, Am. Jour. Sci., v. 237, p. 58. In greisen veins cutting apiite veins in granite.
130. Hachiman, Naegi district, Japan, Shibata, H., 1952, Tokyo Bunrika Daigaku Sci. Repts., v. 2, sec. C, no. 12, p. 161, no. 3. In pegmatite.
131. Hachiman, Naegi district, Japan, Shibata, H., 1952, Tokyo Bunrika Daigaku Sci. Repts., v. 2, sec. C, no. 10, p. 114. In granite pegmatite.
132. Brooks Mountain, Alaska, Coates, R. R., and Fahey, J. J., 1944, Am. Mineralogist, v. 29, p. 373. From pegmatite sill intrusive into granite.
133. Volbynia, U.S.S.R., Buryanova, E. Z., 1940, Sov. Russe Minéralogie, Mem., v. 69, p. 552.
134. Iisaka, Fukushima Pref., Japan, Shibata, H., 1952, Tokyo Bunrika Daigaku Sci. Repts., v. 2, sec. C, no. 12, p. 162, no. 9. In greisen.
135. Yagenyama, Japan, Shibata, H., 1952, Tokyo Bunrika Daigaku Sci. Repts., v. 2, sec. C, no. 12, p. 162, no. 7. In greisen.

TABLE 12.—*Analyses and data for writing formulas of trioctahedral micas not used in correlation study*

[In order of decreasing MgO content]

Analysis (see p. 48)	Percent: SiO_2	TiO_2	Al_2O_3	Fe_2O_3	FeO	MgO	MnO	CaO	Na_2O	K_2O	H_2O+	H_2O-	F	Total	O=F	Adjusted total	Octahedral positions occupied by—: Al	Ti	Fe^{+3}	Fe^{+2}	Mn	Mg	Total	Octahedral charge	Tetrahedral charge	Inherent layer charge	Interlayer cations: Charge	Positions
D1	45.05	......	11.25	......	0.14	29.38	......	......	0.45	8.52	5.37		......	[1] 100.23	......	......	0.01	......	......	0.01	......	3.01	[1] 3.05	+0.09	−0.90	−0.81	+0.81	0.81
D2	39.41	0.29	13.44	2.27	.15	29.18	......	1.87	.58	7.59	2.33		1.55	[2] 100.35	−0.65	99.70	.00	0.00	0.00	.00	......	3.04	[3] 3.09	+.13	[3] −1.25	−1.12	+1.11	.91
D3	44.81	......	10.87	......	.31	28.90	......	......	.38	8.40	5.42	0.96	......	[4] 100.13	......	......	.01	......	......	.02	......	3.00	[4] 3.05	+.09	−.88	−.79	+.79	.79
D4	44.29	......	12.12	1.40	1.44	27.86	......	......	2.15	7.06	2.09		1.94	100.36	−.82	99.54	.01	......	.07	.08	......	2.84	3.00	+.08	−.97	−.89	+.90	.90
D5	35.64	2.83	15.13	2.65	1.55	27.62	......	Tr.	3.58	6.49	4.23	.81	......	100.53	......	......	.00	.08	.00	.09	......	2.92	3.09	+.34	[5] −1.40	−1.06	+1.08	1.08
D6	43.17	......	13.43	1.51	......	27.47	......	......	.39	8.73	.40		5.41	[6] 101.04	−2.28	98.76	.06	......	.08	......	......	2.82	[6] 3.10	+.20	−1.02	−.82	+.82	.82
D7	43.43	......	13.76	.16	1.35	27.20	......	......	1.30	8.06	.92		4.21	100.39	−1.77	98.62	.12	......	.01	.06	......	2.80	3.01	+.15	−1.00	−.85	+.88	.88
D8	41.38	.61	14.48	.40	1.40	26.71	0.01	.26	.50	8.53	.75	......	......	[7] 99.90	......	......	.10	.03	.02	.06	......	2.79	3.02	+.22	−1.10	−.88	+.88	.86
D9	40.47	2.44	14.66	2.42	.65	26.64	......	.50	.67	7.57	2.09		2.44	[8] 100.66	−1.02	99.64	.00	.13	.10	.04	......	2.73	[9] 3.03	+.39	[9] −1.21	−.82	+.83	.79
D10	40.15	......	15.79	2.53	4.12	26.15	Tr.	Tr.	.37	7.64	3.50		......	100.26	......	......	.07	......	.13	.24	......	2.70	3.14	+.48	−1.22	−.74	+.72	.72
D11	39.40	2.64	15.05	.76	2.40	25.44	0.07	Tr.	.03	8.57	4.50	.12	......	[10] 100.18	......	......	.03	.14	.04	.14	......	2.67	3.02	+.39	−1.22	−.83	+.83	.80
D12	39.12	......	17.44	2.03	1.88	25.37	......	.23	.57	8.71	3.18	.30	......	98.83	......	......	.18	......	.11	.11	......	2.65	3.05	+.39	−1.26	−.87	+.89	.87
D13	38.73	.86	16.76	.66	1.42	24.80	.06	......	2.04	10.34	3.91	.00	.86	100.44	−.36	100.08	.13	.04	.04	.08	......	2.61	2.90	+.05	−1.27	−1.22	+1.21	1.21
D14	41.70	......	16.86	2.23	2.74	24.70	......	......	.28	8.93	1.14		.96	99.53	−.40	99.13	.21	......	.12	.16	......	2.52	3.01	+.35	−1.15	−.80	+.82	.82
D15	38.68	1.12	16.83	.77	3.18	24.60	.05	......	......	8.70	4.85	.14	......	[10A] 99.72	......	......	.15	.06	.04	.19	......	2.51	3.06	+.44	−1.26	−.82	+.83	.81
D16	42.09	2.85	12.20	1.45	3.70	23.73	Tr.	Tr.	.61	8.91	1.81	......	2.39	[11] 100.72	−1.00	99.72	.00	.15	.02	.22	......	2.47	[11] 2.90	+.16	[3] −1.06	−.90	+.89	.88
D17	39.30	......	16.95	.48	7.86	21.89	.59	.82	.49	7.79	4.02		.89	101.08	−.39	100.69	.20	......	.03	.47	.04	2.31	3.05	+.33	−1.21	−.88	+.89	.83
D18	41.04	1.00	13.52	2.69	8.50	21.60	.25	Tr.	1.10	7.77	1.99	......	......	[12] 99.65	......	......	.01	.05	.14	.50	.02	2.25	[13] 3.02	+.24	−1.11	−.87	+.84	.84
D19	40.11	3.86	9.89	3.20	7.40	19.99	.11	None	2.61	9.05	2.46	1.08	.29	100.05	−.12	99.93	.00	.14	.00	.43	.01	2.16	2.76	−.20	[9] −1.02	−1.22	+1.20	1.20
D20	36.12	1.18	20.49	3.29	5.17	19.61	.17	.28	.78	8.14	.82	1.58	.60	[13] 98.66	−.26	98.40	.30	.06	.18	.31	.01	2.08	[13] 2.96	+.52	−1.42	−.90	+.90	.87
D21	39.29	.58	21.06	.30	5.81	19.13	.04	None	.33	8.60	4.69	.07	.08	99.98	−.03	99.95	.51	.03	.02	.34	......	2.01	2.91	+.41	−1.23	−.82	+.82	.82
D22	37.85	3.65	13.07	2.24	9.36	17.85	.24	.22	1.68	9.46	4.29		......	99.88	......	......	.00	.20	.05	.58	.02	1.96	2.81	+.07	[9] −1.21	−1.14	+1.16	1.14
D23	38.49	......	14.43	5.44	14.75	16.34	......	......	.53	8.12	.89		Tr.	98.99	......	......	.03	......	.30	.90	......	1.77	3.00	+.33	−1.19	−.86	+.83	.83
D23A	37.15	3.28	13.92	2.39	14.36	15.66	.34	Tr.	.57	7.85	2.38		......	97.91	......	......	.00	.18	.12	.89	.02	1.74	2.95	+.38	[9] −1.23	−.85	+.82	.82
D24	36.19	8.79	14.57	.67	11.38	14.96	......	......	.79	8.52	2.47		......	[13A] 99.40	......	......	.00	.42	.00	.70	......	1.63	2.75	+.34	[5] −1.29	−.95	+.97	.94
D25	38.20	1.72	18.57	1.73	13.23	14.93	None	1.85	3.01	4.88	1.60	.10	......	99.82	......	......	.27	.09	.09	.78	......	1.58	2.81	+.16	−1.29	−1.13	+1.14	1.00
D26	37.74	5.22	16.31	None	15.52	14.23	.06	.04	.44	8.88	1.17		.45	100.06	−.19	99.87	.11	.28	......	.94	......	1.53	2.86	+.39	−1.28	−.89	+.88	.88
D27	35.84	.36	16.68	4.14	14.69	13.87	.33	None	.48	8.48	4.24	.42	.96	100.53	−.40	100.13	.20	.02	.24	.93	.02	1.56	2.97	+.42	−1.29	−.87	+.89	.89
D28	38.69	12.56	9.45	3.09	10.63	13.80	.09	.83	1.69	7.96	.76		.71	100.26	−.30	99.96	.00	.41	.00	.64	.00	1.47	2.52	−.14	[9] −.97	−1.11	+1.09	1.02
D29	39.14	4.27	13.10	12.94	5.05	12.75	.14	1.64	.70	6.55	2.41	.58	1.11	100.38	−.46	99.92	.00	.23	.63	.30	.02	1.37	2.55	+.19	[9] −1.18	−.99	+.95	.83
D30	39.86	3.14	13.90	3.03	10.78	12.49	.07	2.44	2.38	7.76	......	......	......	[14] 99.78	......	......	.12	.17	.17	.66	......	1.37	2.49	−.39	−1.01	−1.40	+1.45	1.26
D31	37.77	2.12	15.96	6.63	14.43	12.26	......	......	.27	8.23	2.67		.44	100.78	−.19	99.59	.14	.12	.36	.88	......	1.34	2.74	+.42	−1.23	−.81	+.81	.81
D32	34.33	3.63	14.80	2.48	19.07	11.62	.35	1.56	.65	8.16	2.32	.18	2.38	[15] 101.89	−1.01	100.88	.00	.21	.07	1.21	.02	1.31	[11] 2.93	+.22	[3] −1.39	−1.17	+1.14	1.02
D33	36.47	2.59	19.70	1.44	15.37	11.44	.07	.17	.16	8.98	3.58	.15	.08	100.20	−.03	100.17	.40	.14	.08	.95	......	1.25	2.82	+.40	−1.32	−.92	+.89	.88
D34	39.01	......	15.44	9.37	13.67	11.30	......	......	.14	8.62	2.93		1.29	101.77	−.54	101.23	.22	......	.52	.84	......	1.19	2.77	+.28	−1.12	−.84	+.83	.83
D35	38.14	.23	16.92	7.37	11.25	9.84	.53	1.27	.20	7.60	[16] 6.65		......	100.00	......	......	.88	.01	.42	.71	.03	1.11	2.66	+.14	−1.12	−.98	+.96	+.86
D36	35.96	2.55	12.50	7.81	15.12	9.29	1.02	......	1.96	8.56	4.96		......	99.73	......	......	.00	.15	.40	.98	.07	1.06	2.68	+.06	[9] −1.20	−1.14	+1.14	1.14
D37	36.53	6.09	8.99	4.41	19.91	9.03	.75	......	.83	8.98	2.20	0.83	1.25	[17] 100.66	−0.53	100.13	.00	.30	.00	1.30	.05	1.05	2.70	.00	[3] −1.09	−1.09	+1.06	1.04
D38	35.78	......	16.39	14.55	11.02	8.67	1.08	......	.56	7.76	4.48		......	100.29	......	......	.17	......	.83	.70	.07	.98	2.75	+.50	−1.29	−.79	+.83	.83
D39	35.35	3.16	18.46	4.03	16.26	8.46	.61	.00	1.34	6.69	5.72		......	100.08	......	......	.34	.18	.23	1.03	.04	.96	2.78	+.49	−1.32	−.83	+.84	.84
D40	34.17	1.42	18.25	5.71	18.35	8.45	Tr.	1.07	1.07	8.56	2.70	.37	......	100.12	......	......	.23	.08	.33	1.17	......	.96	2.77	+.26	−1.40	−1.14	+1.16	1.08
D41	35.30	2.71	18.86	4.08	16.85	8.06	.44	.00	1.61	8.07	3.13	.00	......	100.04	......	......	.32	.15	.23	1.06	.03	.90	2.69	+.25	−1.35	−1.10	+1.10	1.10
D42	35.11	3.51	16.72	3.12	18.24	7.93	.56	.48	None	7.77	4.19		.29	[18] 98.65	−.12	98.53	.25	.20	.18	1.18	.04	.92	[13] 2.83	.43	−1.30	−.87	+.85	.84
D43	34.62	2.42	17.63	4.99	18.92	7.54	......	.38	3.09	7.75	2.65	.17	......	100.16	......	......	.20	.14	.28	1.20	......	.85	2.67	+.10	−1.38	−1.28	+1.27	1.24
D44	34.52	2.70	13.22	7.80	22.27	5.82	.41	......	.15	8.50	4.39		.34	[19] 100.56	−.14	100.42	.00	.16	.44	1.48	.03	.69	[10] 2.82	+.40	[9] −1.26	−.86	+.89	.89
D45	34.62	2.15	16.82	8.97	14.81	5.49	.47	.81	1.87	8.26	5.88		......	[20] 99.95	......	......	.25	.13	.53	.93	.03	.64	2.51	+.06	−1.30	−1.24	+1.26	1.18
D46	32.49	4.03	12.34	6.60	25.13	5.29	......	......	.88	9.50	2.42		1.61	100.34	−.68	99.66	.00	.24	.20	1.70	......	.64	2.80	+.24	[9] −1.37	−1.13	+1.13	1.13
D47	36.20	......	15.95	27.19	.64	5.00	1.50	.50	.16	8.65	......	......	......	[21] 99.69	......	......	.12	......	1.53	.04	.09	.56	2.34	+.33	−1.28	−.95	+.93	.90
D48	34.60	......	18.88	4.29	22.54	4.55	1.33	.47	.17	7.64	3.43	.63	......	98.51	......	......	.48	......	.25	1.48	.09	.53	2.83	+.39	−1.27	−.88	+.87	.83
D49	34.37	4.68	6.84	24.89	7.47	4.05	2.41	.78	2.13	9.03	2.27		......	98.92	......	......	.00	.28	.84	.50	.16	.48	2.26	−.08	[9] −1.28	−1.36	+1.37	1.30
D50	33.32	1.27	17.44	19.15	7.89	3.86	.34	.05	.42	7.19	5.19	3.99	.03	100.14	−.01	100.13	.27	.08	1.14	.52	.02	.46	2.49	+.55	−1.36	−.81	+.79	.79
D51	35.55	......	17.08	23.70	3.55	3.07	1.95	.61	.35	9.45	......	......	......	[22] 99.61	......	......	.24	......	1.36	.23	.13	.35	2.31	+.22	−1.29	−1.07	+1.08	1.02
D52	30.49	1.17	16.40	14.01	18.00	2.40	.69	1.10	4.88	5.65	3.79	.93	.61	100.12	−.26	99.86	.02	.07	.85	1.22	.05	.29	2.50	+.01	−1.54	−1.53	+1.53	1.44
D53	32.09	......	13.33	17.75	19.88	2.19	.31	1.15	1.50	6.30	4.68	.60	.30	100.08	−.13	99.95	.00	......	1.00	1.36	.02	.27	2.65	+.30	[9] −1.38	−1.08	+1.10	1.00
D54	33.22	1.36	20.25	20.86	6.52	2.08	.89	.82	1.32	7.74	2.34	1.24	1.50	[23] 100.32	−.63	99.69	.34	.08	1.19	.41	.06	.24	[23] 2.38	+.39	−1.47	−1.08	+1.08	1.01
D55	32.56	.28	25.32	11.83	12.06	2.03	.54	.94	1.01	7.51	3.48	2.15	.48	[24] 100.46	−.20	100.26	.75	.02	.68	.77	.03	.23	[24] 2.58	+.52	−1.52	−1.00	+1.03	.96
D56	34.67	......	30.09	2.42	16.14	1.98	.85	None	1.67	7.55	4.64		.28	100.29	−.12	100.17	1.18	......	.13	1.00	.05	.22	2.58	+.47	−1.44	−.97	+.95	.95
D57	32.32	.29	28.11	9.65	8.82	1.86	.52	1.06	.05	7.56	5.70	3.76	.37	[25] 100.23	−.16	100.07	1.03	.02	.56	.57	.03	.21	[25] 2.47	+.52	−1.51	−.99	+.99	.91
D58	29.21	.70	13.48	20.22	16.03	1.37	2.00	.10	1.99	8.29	4.27	2.26	......	99.92	......	......	.00	.04	1.09	1.13	.14	.17	2.57	+.31	[9] −1.54	−1.23	+1.24	1.23
D59	36.68	......	20.41	1.55	25.50	1.14	2.10	.81	1.09	9.20	1.01		......	[26] 99.86	......	......	.62	......	.09	1.62	.14	.13	[26] 2.71	+.02	−1.19	−1.17	+1.18	1.12
D60	32.97	2.42	11.88	16.48	20.72	1.08	3.64	......	.30	8.03	3.35		1.29	102.15	−.54	101.62	.00	.15	.78	1.40	.25	.13	2.71	+.50	[9] −1.36	−.86	+.87	.87
D61	32.09	......	18.52	19.49	14.10	1.01	1.42	......	1.55	8.12	4.62		......	100.92	......	......	.23	......	1.15	.92	.09	.12	2.51	+.40	−1.48	−1.08	+1.05	1.05
D62	32.14	1.38	12.74	18.96	14.50	.88	.99	1.22	.50	6.12	3.68	3.60	1.60	[27] 98.48	−.67	97.81	.00	.09	1.16	1.02	.07	.11	[27] 2.51	+.30	−1.30	−1.00	+.96	.85
D63	39.91	......	16.73	12.07	17.48	.62	......	......	......	10.66	1.50		......	[28] 100.16	......	......	.45	......	.68	1.00	......	.07	[28] 2.51	+.01	−1.02	−1.01	+1.01	1.01
D64	29.43	.12	13.64	20.98	21.61	.44	.33	.71	.12	6.74	3.12	3.02	.14	[29] 100.68	−.06	100.62	.00	.01	1.12	1.31	.02	.06	[29] 2.82	+.68	[9] −1.54	−.86	+.86	.90
D65	35.48	.70	21.73	2.14	19.60	.34	1.13	.06	2.42	9.28	4.72	1.72	.86	[30] 100.36	−.36	100.00	.93	.04	.13	1.30	.08	.04	2.52	−.18	−1.19	−1.37	+1.32	1.31
D66	37.58	1.42	15.43	4.69	25.00	.32	.20	1.15	1.67	7.34	n.d.	.52	2.01	[31] 97.00	−.90	96.70	.41	.08	.28	1.65	.01	.04	2.47	−.21	−1.03	−1.24	+1.19	1.10
D67	32.53	.88	17.90	4.45	30.93	.13	.49	.20	.10	7.19	3.57	......	1.21	[32] 100.35	−.51	99.84	.34	.05	.27	2.09	.03	.01	[32] 3.04	+.54	−1.37	−.83	+.79	.78
D68	32.03	3.42	11.92	8.00	30.41	.06	.21	.23	1.54	8.46	4.19		......	100.47	......	......	.00	.21	.35	2.11	.02	.01	2.70	+.15	[9] −1.35	−1.20	+1.19	1.17
D69	37.40	......	11.60	27.66	12.43	([33])	......	([33])	......	9.20	.60		......	99.15	......	......	.00	......	1.53	.80	......	......	2.33	+.19	−1.12	−.93	+.94	.92

The following numbers are in terms of percentage.

[1] Includes 0.07 Li_2O (0.02 octahedral positions).

[2] Includes 0.20 Li_2O (0.05 octahedral positions), 1.28 BaO, and 0.21 Cl.

[3] All the Al, Fe^{+3} and Ti and some Fe^{+2} are necessary to fill the tetrahedral group.

[4] Includes 0.08 Li_2O (0.02 octahedral positions).

[5] All the Al and Fe^{+3}, and some Ti are necessary to fill the tetrahedral group.

[6] Includes 0.13 Li_2O (0.14 octahedral positions).

[7] Includes 0.03 Cr_2O_3, 0.30 percent BaO, 0.05 percent Cl, 0.14 S, 0.12 P_2O_5, and 4.23 ignition loss.

[8] Includes 0.11 Li_2O (0.03 octahedral positions).

[9] Some tetrahedral Fe^{+3}.

[10] Includes 0.04 Cr_2O_3, 1.00 BaO, 0.07 Cl, and 0.09 S.

[10A] Includes 0.09 BaO, 0.06 Cl, and 0.05 S.

[11] Includes 0.79 Cr_2O_3 (0.04 octahedral positions), and 0.19 BaO.

[12] Includes 0.16 Li_2O (0.05 octahedral positions), and 0.03 NiO.

[13] Includes 0.34 NiO (0.02 octahedral positions) and 0.09 BaO.

[13A] Includes 1.06 BaO.

[14] Includes 3.88 ignition loss, and 0.05 P_2O_5.

[15] Includes 0.36 Li_2O (0.11 octahedral positions).

[16] H_2O by difference.

[17] Includes 0.27 CO_2, and 0.01 Cl, and 0.58 BaO.

[18] Includes 0.06 V_2O_5, 0.05 ZrO_2, 0.08 BaO, 0.18 Li_2O (0.06 octahedral positions), and 0.36 P_2O_5.

[19] Includes 0.30 NiO (0.02 octahedral positions), and 0.04 Li_2O.

[20] Includes 0.30 BaO.

[21] Includes 3.90 ignition loss.

[22] Includes 4.30 ignition loss.

[23] Includes 0.18 Li_2O (0.06 octahedral positions).

[24] Includes 0.28 Li_2O (0.09 octahedral positions).

[25] Includes 0.16 Li_2O (0.05 octahedral positions).

[26] Includes 0.37 Li_2O (0.11 octahedral positions).

[27] Includes 0.17 Li_2O (0.06 octahedral positions).

[28] Includes 0.60 Mn_2O_3 (0.03 octahedral positions), and 0.59 Li_2O (0.18 octahedral positions).

[29] Includes 0.26 Li_2O (0.10 octahedral positions).

[30] Includes 0.18 P_2O_5.

[31] Includes 0.27 Cl.

[32] Includes 0.77 Li_2O (0.25 octahedral positions).

[33] MgO+CaO=0.26. The formula values given are based on the assumption that the value given for combined CaO+MgO is predominantly CaO. Assuming this value to be predominantly MgO makes no change in the tetrahedral layer or in the number of positions occupied by Fe^{+3}, but changes the number of positions occupied by Fe^{+2} to 1.32, adds 0.03 positions occupied by Mg, changes the octahedral charge to +0.16, and the inherent layer charge to 0.96. This analysis represents the compositions of the type lepidomelane.

Locality and reference for analyses in table 18

D1. Edwards, St. Lawrence County, N.Y., Clarke, F. W., 1910, U.S. Geol. Survey Bull. 419, p. 289, A.

D2. Mansjö Mountains, Sweden, Eckermann, H. v., 1925, Tschermaks mineralog., petrog. Mitt., v. 38, p. 281. From contact zone of pegmatite intrusive into eulysite and limestone.

D3. Edwards, St. Lawrence County, N.Y., Penfield, S. L., and Sperry, E. S., 1888, Am. Jour. Sci., 3d ser., v. 36, p. 330.

D4. Pennsville, Pa., Dana, E. S., 1892, The system of mineralogy, 6th ed., New York, John Wiley and Sons, p. 633, no. 2.

D5. Monte Biacelo, Val Malenco, Italy, Paglianti, G., 1940, Soc. Ital. Sci. Nat. Milano, Atti., v. 79, p. 21. In limestone.

D6. Rossie, St. Lawrence County, N.Y., Dana, E. S., 1892, The system of mineralogy, 6th ed., New York, John Wiley and Sons, p. 633, no. 6.

D7. Parga, Finland, Dana, E. S., 1892, The system of mineralogy, 6th ed., New York, John Wiley and Sons, p. 633, no. 1.

D8. Baikalia, U.S.S.R., Grigoriev, D. P., 1935, Soc. Russe Minéralogie Mém., v. 64, ser. 2, p. 31, no. 2.

D9. Mansjö Mountains, Sweden, Eckermann, H. v., 1925, Tschermaks mineralog. petrog. Mitt., v. 38, p. 281. From contact zone of pegmatite intrusive into eulysite and limestone.

D10. Morawitza, Hungary, Dana, E. S., 1892, The system of mineralogy, 6th ed., New York, John Wiley and Sons, p. 630, no. 5. In magnetite.

D11. Bilaikhada, Lake Baikal, U.S.S.R., Grigoriev, D. P., 1935, Soc. Russe Minéralogie Mém. v. 64, ser. 2, p. 31, no. 6.

D12. U.S.S.R. (exact locality not given), Berkhin, S. I., 1954, Akad. Nauk SSSR Doklady, v. 95, p. 146, no. 48.

D13. Ambatondro, Madagascar, Jakob, J., and Parga-Pondal, I., 1932, Zeitschr. Kristallographie, v. 82, p. 273, no. 62.

D14. Monzoni, South Tyrol, Italy, Dana, E. S., 1892, The system of mineralogy, 6th ed., New York, John Wiley and Sons, p. 630, no. 4.

D15. Bilaikhada, Lake Baikal, U.S.S.R., Grigoriev, D. P., 1935, Soc. Russe. Minéralogie Mém. v. 64, p. 31, no. 7.

D16. Portuna, Murcia, Spain, Osann, A., 1906, Rosenbusch Festschrift, p. 271. Associated with olivine and augite, verite.

D17. Vesuvius, Italy, Berwerth, F., 1877, Mineralogische Mitteilungen, p. 112, no. 9.

D18. Bolshii Lahy, North Caucasus, U.S.S.R., Serdiukenko, D. P., 1951, Soc. Russe Minéralogie Mém., v. 80, ser. 2, p. 177. In granite-aplite vein cutting through serpentine.

D19. Mutsuresima, Japan, Kozu, S., and Tsurumi, S., 1931, Japanese Assoc. Mineralogists, Petrologists and Econ. Geologists Jour., v. 5, p. 150.

D20. Laurel Creek mine, Habun County, Ga., Clarke, F. W., 1912, U.S. Geol. Survey Bull. 416, p. 289, B. From corundum mine.

D21. Smith Ridge, Boehls Butte quadrangle, Idaho, Hietanen, A., 1956, Am. Mineralogist, v. 41, p. 7. From kyanite-andalusite-sillimanite-cordierite gneiss.

D22. Tatra Mountains, Czechoslovakia, Weyberg, Z., 1912, Neues Jahrb. Mineralogie, Geologie u. Paläontologie, pt. 1, p. 368. Probably associated with nunite, kernantite.

D23. Chebarkul, southern Urals, U.S.S.R., Dana, E. S., 1892, The system of mineralogy, 6th ed., New York, John Wiley and Sons, p. 630, no. 11.

D23A. Morven-Strontian complex, Scotland, Nockolds, S. H., and Mitchell, R. L., 1947, Royal Soc. Edinburgh Trans., v. 61, p. 562. From granodiorite.

D24. Odenwald, Germany, Kunitz, W., 1926, Neues Jahrb. Mineralogie, Geologie, u. Paläontologie, Beilage-band, v. 70, Abt. A., p. 401. Associated with nunite and augite.

D25. Hill of Strone, Ferfarshire, Scotland, Phillips, F. C., 1939, Mineralog. Mag., v. 22, p. 255, no. viii.

D26. Black Cascade, Tripyramid Mountain, N.H., Chapman, H. W., and Williams, C. R., 1935, Am. Mineralogist, v. 20, p. 512. From gabbro.

D27. Dowerin, Western Australia, Simpson, E. S., 1933-35, Royal Soc. Western Australia Jour., v. 18, p. 63. In pegmatite, associated with cummingtonite, actinolite, almandine, andesine feldspar, and chrysoberyl.

D28. Katzenbacket, Odenwald, Germany, Freudenberg, W., 1920, Badischen Geol. Landesanstalt, Mitt, v. 8, p. 321. From mica-nepheline porphyry.

D29. San Juan district, Colo., Larsen, E. S., Gonyer, F. A., and Irving, J., 1937, Am. Mineralogist, v. 22, p. 902. From quartz-latite monzonite.

D30. Round Lake, near Kingston, Ontario, Love, W. T., 1940, Royal Soc. Canada Trans., 3d ser., v. 34, sec. 4, p. 58. From gneiss.

D31. Persberg, Sweden, Dana, E. S., 1892, The system of mineralogy, 6th ed., New York, John Wiley and Sons, p. 630, no. 15.

D32. Cairnsmore, southern Scotland, Deer, W. A., 1937, Mineralog. Mag., v. 24, p. 496. From tonalite.

D33. Ross-shire, northwestern Scotland, Harker, R. I., 1954, Geol. Mag., v. 91, p. 452. From "cordierite"-biotite-plagioclase hornfels.

D34. Hitterö, Norway, Dana, E. S., 1892, The system of mineralogy, 6th ed., New York, John Wiley and Sons, p. 630, no. 17.

D35. Cornish, Argyllshire, Scotland, Phillips, F. C., 1930, Mineralog. Mag., v. 22, p. 254.

D36. Kellia, Impilahti, Finland, Mehmel, M., 1937, Chemie der Erde, v. 11, p. 307.

D37. Kukisvumchorr, Kola Peninsula, U.S.S.R., Ivanov, B. V., 1937, Akad. Nauk SSSR Lomonosovskii Institut Geokhimii, Kristallografii i Mineralogii Trudy, no. 10, p. 38.

D38. Baltimore, Md., Clarke, F. W., 1903, U.S. Geol. Survey Bull. 220, p. 77, E.

D39. Cima, Val del Molino, Tessin, Italy, Jakob, J., 1931, Zeitschr. Kristallographie, v. 79, p. 373, no. 59.

D40. Val Feder, Italy, Tomba, A.M., 1952, Accad. Naz. Lincei Atti., rend., Cl. Sci. fis. mat. nat., ser 8, v. 13, p. 80. Inclusions in staurolite in mica schist.

D41. Claro, Val del Molino, Tessin, Italy, Jakob, J., 1931, Zeitschr. Kristallographie, v. 79, p. 373, no. 60.

D42. Skiddaw, Cumberland, England, Hitchen, C. S., 1934, Geol. Soc., London, Quart. Jour. v. 90, p. 172. From granite.

D43. Tomnanova Valley, Tatra Mountains, Poland, Zastawniak, F., 1951, Rocznik Polsk. Towarz. Geol., v. 20 (1950), p. 128. In gneiss.

D44. Port Henry, New York, Clarke, F. W., 1903, U.S. Geol. Survey Bull. 220, p. 77, F.

D45. Kremsta, East Tatra Mountains, Czechoslovakia, Weyberg, Z., 1912, Neues Jahrb. Mineralogie, Geologie u. Paläontologie, pt. 1, p. 366. In granite.

D46. Lake Ilmen, Miask, U.S.S.R., Dana, E.S., 1892, The system of mineralogy, 6th ed., New York, John Wiley and Sons, p. 630, no. 12.

D47. Ballycrum, County Donegal, Ireland, Haughton, S., 1859, Geol. Soc. London Quart. Jour., v. 15, p. 131. In granite.

D48. U.S.S.R. (exact locality not given), Berkhin, S. I., 1954, Akad. Nauk. SSSR Doklady, v. 95, p. 146.

D49. Langesund Fiord, Norway, Dana, E. S., 1892, The system of mineralogy, 6th ed., New York, John Wiley and Sons, p. 634, no. 7.

D50. Ishikawa, Fukushima, Pref. Japan, Yoshiko, B., 1933, Imp. Acad. Tokyo Proc., v. 9, p. 321. In pegmatite dikes traversing granite.

D51. Ballyelin, County Carlow, Ireland, Haughton, S., 1859, Geol. Soc. London Quart. Jour., v. 15, p. 130. In granite.

D52. Baveno, Italy, Gallitelli, P., 1936, Periodico Mineralogia, Roma, v. 7, p. 64. In granite.

D53. Baveno, Italy, Gallitelli, P., 1936, Periodico Mineralogia Roma, v. 7, p. 64. In granite.

D54. Haka, Japan, Shibata, H., 1952, Tokyo Bunrika Daigaku Sci. Repts., v. 2, sec. C., no. 12, p. 163, no. 16.

D55. Makabe Town, Ibaraki, Pref. Japan, Shibata, H., 1952, Tokyo Bunrika Daigaku Sci. Repts., v. 2, sec. C., no. 12, p. 163, no. 16. From pegmatite.

D56. Merrow Ledge, Auburn, Maine, Clarke, F. W., 1903, U. S. Geol. Survey Bull. 220, p. 75, A. From quartz monzonite.

D57. Yamatsuo, Tsukuba, Japan, Shibata, H., 1952, Tokyo Bunrika Daigaku Sci. Repts., v. 2, sec. C., no. 10, p. 143, no. 15. From pegmatite.

D58. Heiko-gun, Kogen-do, central Korea, Inoue, T, 1950, Geol. Soc. Japan Jour., v. 56, p. 76.

D59. Pikes Peak, Colo., Lewis, H. C., 1876, Philadelphia Acad. Nat. Sci., Proc., v. 22, p. 264.

D60. Brevick, Norway, Dana, E. S., 1892, The system of mineralogy, 6th ed., New York, John Wiley and Sons, p. 634, no. 6.

D61. Litchfield, Maine, Clarke, F. W., 1903, U.S. Geol. Survey Bull. 220, p. 77, A.

D62. Iwaka, Fukushima, Pref. Japan, Shibata, H., 1952, Tokyo Bunrika Daigaku Sci. Repts., v. 2, sec. C., no. 10, p. 121. From granite pegmatite.

D63. Rockport, Mass., Cooke, J. P., Jr., 1867, Am. Jour. Sci, 2d ser., v. 43, p. 225.

D64. Hiaka, Fukushima, Pref. Japan, Shibata, H., 1952, Tokyo Bunrika Daigaku Sci. Repts., v. 2, sec. C., no. 10, p. 121. From granite pegmatite.

D65. Mungunhe, Province Beira, Portugal, Mário de Jesus, A., 1933, Portugal, Servicos Geol., Comun., v. 19, p. 128.

D66. Kuduru Town, Nigeria, Bain, A. D. N., 1933, Geol. Soc. London, Quart. Jour., v. 89, p. 227. From granite.

D67. Volhynia, U.S.S.R., Buryanova, E. Z., 1940, Soc. Russe Minéralogie Mem., v. 69, p. 332. From pegmatite in ravaskylite granite.

D68. Rockport, Mass., Clarke, F. W., 1903, U. S. Geol. Survey Bull. 220, p. 77, C. In feldspathic vein in granite.

D69. Wermland, Sweden, Dana, E. S., 1892, The system of mineralogy, 6th ed., New York, John Wiley and Sons, p. 634, no. 1.

INDEX

Page

Analyses and formulas, excluded from study 15-16, 46
used in study 15, 41-42
Anionic composition of micas 14
Annite, Dana's 29-30
Winchell's 24, 30, 31

Biotites, average formula 29
average octahedral composition 29
composition of, Holzner's hypotheses 12
Fe^{+2} dominant 27-29
from diorite 35
from gneiss and schist 35-36
from granite 33-34
from granodiorite 35
from monzonite 34
from nepheline syenite 35
from pegmatite 36
from quartz diorite 35
from quartz monzonite 34
Mg-dominant 23, 28-29, 31
range of composition 28
selected data on, from Holzner 22
Bivalent octahedral cations 16, 17, 22

Cape Ann, Mass 29
Cationic composition of micas 14
Cations, bivalent octahedral 16, 17, 22
trivalent, accommodation of 12
in natural trioctahedral micas 13, 22
Charge, calculation of 14
Charges, accommodation of extra positive octahedral 16-22
Clarke, F. W 16
Cooke, J. P., Jr 29

Dana, E. S 31
Dana, J. D 29
Deer, W. A 23
Dioctahedral micas 12

Eastonite, Simpson's formula 27
Winchell's formula 12, 27
Extra positive octahedral charges 16-22
Eyerman, John 26

Formulas, calculation of, from analyses of montmorillonite 15
Foster, M. D 12, 13, 15
Fe^{+2} biotites 25, 27, 28
Fe^{+3}, tetrahedral 32
Formula, notation 14
Formulas, calculation 13-15

Grigoriev, D. P 31, 32

Half-cell formula 14
Hallimond, A. F 31
Hamilton, S. Harbert 27
Heinrich, E. W 37
Hendricks, S. B 15
Hey, Max H 31, 32
Holzner, Julius 12, 21, 22
Hutton, C. O 23

Kunitz, W 31

Page

Lepidomelane, aluminian 32
Lepidomelanes, representative formulas 31
Lithium, effect of, in formula calculation 16
in siderophyllites and lepidomelanes 30

Magnesian biotites 25, 27
Magnesium, exchangeable in montmorillonites 15
interlayer positions 15
Magnesium replacement system 24-26
Marshall, C. E 13
Mg-deficient trioctahedral micas 36
Mg-dominant biotites 23, 25, 28
Micas, anionic composition 14
composition and occurrence 32-38
dialuminum magnesium 26, 27
dioctahedral potassium 12
intermediate between siderophyllites and lepidomelanes 32
Fe^{+2} dominant 18
layer charge relations, theoretical 12-13
octahedral group 12-15
Montmorillonite 15
Muscovite, ideal formula 12

Nockolds, S. R 30, 31

Octahedral group 12, 14, 15, 33
Octahedral occupancy 20

Pauling, Linus 23
Phlogopites, average formula 19
geologic occurrence 32, 37
interlayer Mg 15
range in composition 26
selected data from Holzner 22

Quadrivalent octahedral cations 17, 18, 19

Richey, J. E 30, 31
Ross, C. S 15

Siderophyllite, ferrian 32
Nockold's and Richey's formula 30
Winchell's formula 12, 30
Siderophyllite-lepidomelane series 32
Siderophyllites, representative formulas 30

Tetrahedral group 12, 13, 14, 28, 34
Titanium, role of, in micas 15
tetrahedral 32
Trioctahedral micas, accommodation of trivalent cation 13-22
analyses not used in study 15-16, 46
analyses used in study 15, 41-42
chemical composition 32-37
from pegmatite 36
geologic occurrence 32-37
layer Charge relations 12-13
Mg-deficient 36
Mg-Fe^{+2} relation 23-24
Trisilicic-tetrasilicic series 12
Trivalent octahedral cations 12, 15, 16, 17, 18, 19, 20, 21, 22, 34

Winchell, A. N 12, 26, 29, 30, 31
Winchell, H 12, 30, 31

Yoder, Hatton 27

Giant Waves in Lituya Bay Alaska

By DON J. MILLER

SHORTER CONTRIBUTIONS TO GENERAL GEOLOGY

GEOLOGICAL SURVEY PROFESSIONAL PAPER 354-C

A timely account of the nature and possible causes of certain giant waves, with eyewitness reports of their destructive capacity

UNITED STATES GOVERNMENT PRINTING OFFICE, WASHINGTON : 1960

UNITED STATES DEPARTMENT OF THE INTERIOR

FRED A. SEATON, *Secretary*

GEOLOGICAL SURVEY

Thomas B. Nolan, *Director*

For sale by the Superintendent of Documents, U.S. Government Printing Office
Washington 25, D.C.

CONTENTS

	Page
Abstract	51
Introduction	51
Acknowledgments	53
Description and history of Lituya Bay	53
Geographic setting	53
Geologic setting	55
Exploration and settlement	56
Giant waves	57
Evidence	57
Wave on July 9, 1958	57
Setting and sources of information	57
Eyewitness accounts	57
Account of Howard G. Ulrich	57
Account of William A. Swanson	58
Other observations on July 9	59
Observations of the writer on July 10	59
Effects of the wave	60
Destruction of vegetation	60
Other effects	62
Nature and cause of the wave	63
Comparable waves in other parts of the world	67
Waves on October 27, 1936	67
Setting and sources of information	67
Eyewitness accounts	67
Account of Fred H. Fredrickson	67
Accounts of Bernard V. Allen and James Huscroft	68
Giant waves—Continued	
Waves on October 27, 1936—Continued	
Effects of the waves	69
Nature and cause of the waves	70
Sudden draining of an ice-dammed body of water	71
Fault displacement	71
Rockslide, avalanche, or landslide	71
Submarine sliding	72
Movement of a tidal glacier front	72
Tsunami in the ocean	74
Other possible causes	74
Waves between 1854 and 1916	74
Eyewitness accounts	74
Other evidence	74
Dates	75
Effects of the waves	75
Nature and cause of the waves	75
Wave in 1853 or 1854	76
Eyewitness accounts	76
Other evidence	77
Date	77
Effects of the wave	77
Nature and cause of the wave	77
Possibility of future waves	79
Summary and conclusions	79
References cited	81
Index	85

ILLUSTRATIONS

		Page
PLATE 2. Map of Lituya Bay area	In pocket	
3. View of Lituya Bay, 1954 and August 1958	Facing	62
4. Gilbert Inlet and head of Lituya Bay, August 1958	Follows	62
5. *A*. South shore of Lituya Bay. *B*. Broken spruce tree at Harbor Point	Follows	62
6. *A*. View west on Cenotaph Island. *B*. North shore of Lituya Bay, August 1958	Facing	63
7. Spur southwest of Gilbert Inlet, August 1958	Facing	72
8. Zones of denudation by giant waves and section of spruce tree from above 1936 trimline	Follows	72
9. Destruction of forest by 1936 giant waves	Follows	72
10. Section of spruce tree from above 1853–54 trimline	Facing	73
FIGURE 14. Map of part of southeastern Alaska, showing location and regional geographic setting of Lituya Bay		52
15. Map of Lituya Bay showing setting and effects of 1958 giant wave		58
16. Detailed map of head of Lituya Bay		61
17. Map of Lituya Bay showing setting and effects of 1936 giant waves		68
18. Map of Lituya Bay showing trimlines of one or more giant waves that occurred between 1854 and 1916		76
19. Map of Lituya Bay showing setting and effects of giant wave that occurred in 1853 or 1854		78
20. Map of head of Lituya Bay, showing areas susceptible to sliding		80

TABLE

TABLE 1. Data on localized giant waves generated by falling or sliding of solid masses	66

SHORTER CONTRIBUTIONS TO GENERAL GEOLOGY

GIANT WAVES IN LITUYA BAY, ALASKA

By Don J. Miller

ABSTRACT

Lituya Bay, on the northeast shore of the Gulf of Alaska, is an ice-scoured tidal inlet with a maximum depth of 720 feet and a sill depth, at the narrow entrance, of only 33 feet. The northeastward-trending stem of the T-shaped bay, 7 miles long and as much as 2 miles wide, transects the narrow coastal lowland and foothills belt flanking the Fairweather Range of the St. Elias Mountains. The two arms at the head of the bay, Gilbert and Crillon Inlets, are part of a great trench along the Fairweather fault. Gentle slopes border the outer part of the bay, but the walls of the inner, fiordlike part rise steeply to altitudes of 2,200 feet to more than 6,000 feet.

Until recently, little notice was taken of the giant waves that have rushed out from the head of Lituya Bay, leaving sharp trimlines to mark the upper limit of total or near total destruction of the forest along the shores. The dates of occurrence of 4 known and 1 inferred giant waves, and the maximum altitudes of their trimlines are as follows: July 9, 1958—1,720 feet; October 27, 1936—490 feet; 1899(?)—about 200 feet; about 1874—80 feet; and 1853 or 1854—395 feet.

In 1958 about 40 million cubic yards of rock, loosened either by displacement on the Fairweather fault or by the accompanying shaking, plunged into Gilbert Inlet from a maximum altitude of about 3,000 feet on the steep northeast wall. This rockslide caused water to surge over the opposite wall of the inlet to a maximum altitude of 1,740 feet, and generated a gravity wave that moved out the bay to the mouth at a speed probably between 97 and 130 miles per hour. Two of three fishing boats in the outer part of the bay were sunk, and two persons were killed. The interpretation that water was primarily responsible for destruction of the forest over a total area of 4 square miles, extending to a maximum altitude of 1,720 feet and as much as 3,600 feet in from the high-tide shoreline, is supported by eyewitness accounts of the survivors, by the writer's field investigation, and by R. L. Wiegel's study of a model of Lituya Bay and his calculations from existing theory and data on wave hydraulics.

The giant waves in 1936 were generated in Crillon Inlet. They were described by eyewitnesses at a point about midway along the bay as 3 waves of increasing height, in close succession and traveling about 22 miles per hour. Of the possible causes considered here, movement of a tidal glacier front or submarine sliding seems most likely but can be neither disproved nor conclusively supported from the information at hand.

The configuration of trimlines formed by giant waves in late 1853 or early 1854 (dated by tree ring count) and about 1874, suggests sliding from the south wall of Lituya Bay at Mudslide Creek as a likely cause. A slide, fault displacement, or some other disturbance in Crillon Inlet may have caused another giant wave during one of the great earthquakes in September 1899.

The frequent occurrence of giant waves in Lituya Bay, as compared to other similar bays, is attributed to the combined effect of recently glaciated steep slopes, highly fractured rocks and deep water in an active fault zone, heavy rainfall, and frequent freezing and thawing. These waves are likely to occur again, and should be taken into account in any future use of Lituya Bay. Other giant waves have been caused by sliding of part of a mountain into Shimabara Bay in Japan; repeatedly by falling or sliding of rock masses into Loen Lake, Tafjord, and Langfjord in Norway; by avalanching of a hanging glacier into Disenchantment Bay in Alaska; and repeatedly by landslides into Franklin D. Roosevelt Lake in Washington.

INTRODUCTION

Lituya Bay is an ice-scoured, nearly landlocked tidal inlet on the northeast shore of the Gulf of Alaska (fig. 14). Most descriptions of Lituya Bay, including that of its discoverer La Perouse (1798), have dwelt at length on the hazards of the strong tidal current in the narrow entrance, but until recently, little notice was taken of an even more remarkable and potentially more dangerous hydraulic oddity of the bay—its propensity for developing enormous waves. At least four times during a little more than a century giant waves have rushed out from the head of the bay, destroying the forest on the shores and leaving trimlines similar to those formed by glaciers. The latest and largest of these waves washed out trees to a maximum altitude of 1,720 feet, more than 8 times the maximum recorded height of a tsunami breaking on an ocean shore (Leet, 1948, p. 179).

The writer became interested in the giant waves while studying the Tertiary rocks in Lituya Bay and adjoining area in 1952 and 1953, as a part of the U.S. Geological Survey's program of petroleum investigations in the Gulf of Alaska region. The two trimlines then recognized were mapped and their approximate ages determined, inquiries were made of residents and former residents of the region, and a search was begun for references to the origin of the trimlines in Lituya Bay and to comparable features in other places. In a

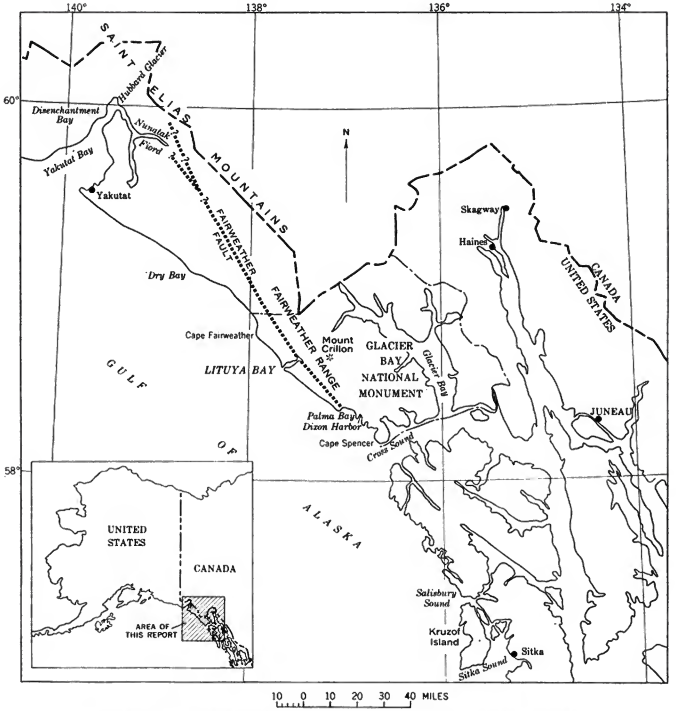

FIGURE 14.—Map of part of southeastern Alaska, showing location and regional geographic setting of Lituya Bay.

paper read at geological meetings in Seattle, Wash. and Anchorage, Alaska, and published in abstract (Miller, 1954) the trimlines in Lituya Bay were attributed to cataclysmic floods or waves of water moving out from the head of the bay at high velocity. The information then available did not give conclusive support to any of several possible mechanisms that were suggested for setting the water in motion.

The investigation of the cause of the floods or waves was laid aside, except for correspondence and the accumulation of additional references, until the spring of 1958 when assignment to a field mapping project based

in Juneau afforded opportunities to resume the search for local sources of information. On July 9 much new information was provided in a dramatic and wholly unexpected way when a major earthquake centering near Lituya Bay was followed almost immediately by a wave that denuded an area of about 4 square miles in Lituya Bay, destroyed 2 of 3 fishing boats anchored in the bay, and killed 2 people. The problem of the cause of the waves, until then mainly of scientific interest, became overnight a matter of general public interest.

The earthquake late in the evening of July 9[1] was strongly felt on the U.S. Geological Survey power barge, *Stephen R. Capps*, at anchor in Glacier Bay about 60 miles east of Lituya Bay. Rocks fell into the water from steep cliffs nearby, causing small waves that broke with a height of not more than 2 or 3 feet on the shores; no large waves were seen, however. Upon learning by radio on the following morning of the destruction in Lituya Bay, the writer chartered a small pontoon-equipped airplane, and spent about 1½ hours flying over the bay at low altitude. Observation and photography were hampered by low ceiling, rain, and fog, and no landings could be made in the debris-choked bay. Early in August, when the power barge was anchored in Dixon Harbor about 30 miles southeast of Lituya Bay, a helicopter was used for 1½ days of ground and aerial observations and photography of the bay. In late August and early September the writer again photographed and examined Lituya Bay on several flights with fixed-wing aircraft, and camped for 3 days in the bay.

On August 29, 1958, a photographic mission of the U.S. Coast and Geodetic Survey photographed the entire Lituya Bay area with a 9-lens aerial camera, and also made single-lens vertical photographs of the entrance.

ACKNOWLEDGMENTS

D. L. Rossman, George Plafker, R. C. Ellis, E. A. Hainze, and Todd Nelson all assisted in the field at times during the 1952–53 seasons. R. L. Velikanje, C. L. Sainsbury, R. E. Marsh, Mrs. Caroline Jensen, and L. H. Bayers in the Juneau office of the U.S. Geological Survey canvassed potential sources of information by interview and letter. R. F. Taylor, forester in charge of the Alaska Forest Research Center in Juneau, gave advice on tree ring studies made in the field in 1953 and arranged for preparation of tree sections; R. M. Godman of the same organization counted and interpreted the growth rings.

A. J. Mitchell, superintendent of the Sitka and Glacier Bay National Monuments, in 1958 aided in gathering local information on the waves, provided logistic support and encouragement to the investigation, and accompanied the writer on one flight to Lituya Bay. J. P. McKee, E. L. Henrickson, V. I. Mann and Edward Berdusco of the Fremont Mining Co. provided a valuable record of conditions in Lituya Bay immediately preceding the 1958 wave and also called attention to evidence for movement along the Fairweather fault near Lituya Bay. Part of the logistic support for the 1958 field investigation was provided by the Geological Survey's southeastern Alaska project barge and helicopter and by Seventeenth Coast Guard District airplane. Special thanks are due to pilot Kenneth Loken of Juneau for making it possible to inspect Lituya Bay shortly after the 1958 wave, despite adverse weather.

Don Tocher of the University of California Seismographic Station joined the writer in making a field investigation of the effects of the 1958 earthquake, and contributed valuable suggestions on the interpretation of the giant waves and on the preparation of this report. R. L. Wiegel of the Institute of Engineering Research, University of California, made a model study of the 1958 wave and generously contributed the resulting observations for quotation in this report. A. R. Tagg of the U.S. Geological Survey made the photogrammetric measurements of trimline altitudes. The writer is indebted to F. H. Fredrickson, Mr. and Mrs. W. A. Swanson, and H. G. Ulrich for their cooperation in providing eyewitness accounts of the waves. Photographs of Lituya Bay and information on the waves were furnished by W. O. Field, Jr., of the American Geographical Society, Bradford Washburn, of the Museum of Science, Boston, Mass., and Tom Smith, Trevor Davis and Robert De Armond of Juneau. Finally, many other persons not specifically mentioned here have contributed suggestions as to the cause of the waves, sources of information and methods of attacking the problem, and helpful criticism of the manuscript.

DESCRIPTION AND HISTORY OF LITUYA BAY

GEOGRAPHIC SETTING

Lituya Bay is a T-shaped inlet that cuts through the coastal lowland and foothills belt flanking the Fairweather Range of the St. Elias Mountains, on the south coast of Alaska (fig. 14, pl. 2).

The entrance of the bay, at lat 58°36′45″ N., long 137°39′40″ W., is 122 miles west of Juneau and 99 miles southeast of Yakutat. The main part of the bay, corresponding to the stem of the letter T, is 7 miles long and ranges from three-fourths of a mile to 2 miles in width except at the entrance, which has a width of only

[1] Morning of July 10, Greenwich civil time; Pacific standard time (120° W. meridian time) is used throughout this report.

1,000 feet at low tide. Cenotaph Island divides the central part of the bay into two channels, two-fifths and four-fifths of a mile in width. Gilbert and Crillon Inlets extend northwestward and southeastward, respectively, from the head of the bay to form the upper part of the T, which in 1958 was about 3 miles long. The name "Lituya," according to Emmons (1911, p. 294), is a compound word in the Tlingit language meaning "the lake within the point," in reference to the nearly landlocked nature of the bay.

Lituya Bay was aptly described by Dall (1883, p. 204) as "a Yosemite Valley, retaining its glaciers and with its floor submerged six or eight hundred feet." The bay fills and slightly overflows a depression only recently occupied by a piedmont glacier lobe and its tributary valley glaciers, of which the present Lituya, Cascade, and North Crillon Glaciers are remnants (pl. 2). The maximum stand of the Lituya Glacier system is clearly recorded by the arcuate end moraine that forms La Chaussee Spit and is continuous with lateral moraines and trimlines rising gradually to an average altitude of about 1,800 feet at the head of the bay (pl. 3 *A*.). The Solomon Railroad (pl. 2), a part of the end and lateral moraine north of the bay, rises abruptly like a railroad embankment to a sharp, even crest standing as much as 600 feet above the adjoining lowlands.

Lituya and North Crillon Glaciers, each about 12 miles long and 1 mile wide, originate in ice fields at altitudes of 4,000 feet and higher near the crest of the Fairweather Range. Both glaciers flow southwestward down the flank of the Fairweather Range and make nearly right-angle turns into the northwestward-trending trench between this range and the foothills. In the summer of 1958 about 1,600 feet or one-third of the total width of the front of North Crillon Glacier was tidal at the head of Crillon Inlet. The surface of this glacier near the front was mostly debris covered and relatively smooth. Just prior to the earthquake and wave in 1958 about 3,000 feet of the front of Lituya Glacier was tidal. The surface of this glacier near the front was rough, with little debris cover except along the southwest margin and at a narrow medial moraine near the northeast margin. At the end of August 1958 almost the entire front of Lituya Glacier was tidal, and deeply crevassed. Cascade Glacier is about 4 miles long and very steep. Its terminus in recent years has been low and largely debris covered. At the end of August 1958 only a small part of the glacier terminus reached the high-tide shoreline at the head of Lituya Bay.

The shores around the outer part of Lituya Bay are mainly bouldery beaches, the adjoining land rising away from the beach at rates ranging from 100 feet in a horizontal distance of 6,000 feet, near Fish Lake, to 540 feet in a horizontal distance of 1,200 feet at The Paps (pl. 2). Around the head of the bay the walls are steep and fiordlike, rising to altitudes between 2,200 and 3,400 feet in the foothills immediately to the north and south, and to more than 6,000 feet in the Fairweather Range less than 2 miles from the shore of Crillon Inlet. The submarine contours, based on soundings made in 1926 and 1940 (U.S. Coast and Geodetic Survey, 1942), show a pronounced U-shaped trench with steep walls and a broad, flat floor sloping gently downward from the head of the bay to a maximum depth of 720 feet just south of Cenotaph Island, and rising again toward the outer part of the bay. The minimum depth in the entrance is 33 feet at mean lower low water; hence the bay has a closure of at least 687 feet. The tide in the bay is diurnal, with a mean range of 7 feet and a maximum range of about 15 feet (U.S. Coast and Geodetic Survey, 1957). The tidal current in the narrow entrance attains a velocity of 12 knots (U.S. Coast and Geodetic Survey, 1952), or about 13.8 statute miles per hour.

Weather records for the 2 stations nearest Lituya Bay, at Cape Spencer 47 miles to the southeast and at Yakutat 99 miles to the northwest (U.S. Weather Bureau, 1958), indicate that the total annual precipitation ranges from 111 to 134 inches and the mean annual temperature ranges from 39° to 41° F. in this coastal area. Because of the heavy precipitation and mild climate at low altitude, the lower slopes (from the high-tide line to an altitude of 1,700 to 2,000 feet) where not overly steep or poorly drained, normally are covered by a dense growth of trees and brush. Reforestation of land newly exposed by the retreat of glaciers or the sea, or, as in Lituya Bay, denuded by waves, under present climatic conditions at this latitude takes place in the following succession: dense stands of alder (*Alnus*) and willow (*Salix*) grow within a few years, but are soon exceeded in height by cottonwood (*Populus trichocarpa*); Sitka spruce (*Picea sitchensis*) next dominates but gradually becomes mixed with hemlock (*Tsuga heterophylla and T. mertensiana*); and finally Alaska cedar (*Chamaecyparis nootkatensis*) appears. At the time of the 1958 wave, forests of five distinct ages were growing on or near the shores of Lituya Bay. These zones, as identified on plate 8*A*, are: mixed alder, willow, cottonwood, and spruce with a known maximum age of 22 years (shore to *h*); 2 bands of mixed spruce and cottonwood with maximum ages of about 84 years (*h–j*) and of 105 years (*j–k*); mixed spruce and hemlock with an estimated age of 400 years or more (*k–m*);

and mixed spruce, hemlock, and cedar probably more than 1,000 years old (above *m*).

GEOLOGIC SETTING

Lituya Bay lies near the southeast end of and transects a geologic province in which sedimentary rocks of Tertiary age are exposed or inferred to underlie lowland areas (Gryc, Miller, and Payne, 1951, p. 159–162). The two arms at the head of Lituya Bay are part of a great trench that extends for many miles to the northwest and southeast along the southwest front of the Fairweather Range and the southern part of the St. Elias Mountains (fig. 14). Mertie (1931, p. 123) first recognized this trench as the topographic expression of a major fault, named more recently the Fairweather fault (Miller, 1953). Field investigations by the writer and by D. L. Rossman (written communication, 1957) indicate that the Fairweather fault from the vicinity of Lituya Bay southeast to Palma Bay is vertical or dips steeply to the northeast. Along this fault the crystalline rocks exposed on the northeast side are inferred to have moved up relative to less altered and in part younger rocks exposed in the lowland and foothills belt on the southwest side. St. Amand (1957, p. 1357–1359) suggested, however, that the fault is of lateral or oblique habit, and cited as evidence some of the effects of the 1899 earthquakes in Yakutat Bay.

Instrumental and field observations point to movement along the Fairweather fault as the cause of the earthquake immediately preceding the 1958 wave in Lituya Bay. Tocher and Miller (1959) studied the surface breakage where the trace of the fault is exposed near Crillon Lake, 6 to 10 miles southeast of Lituya Bay. At one point the southwest side moved northwestward at least 21½ feet and up 3½ feet. Slides and other evidence of strong shaking observed elsewhere along known or inferred trace of the Fairweather fault from Palma Bay to the latitude of Nunatak Fiord near Yakutat Bay, indicated tearing along the fault probably for 115 miles or more. The instrumental epicenter of the earthquake, as determined by the U.S. Coast and Geodetic Survey (Brazee and Jordan, 1958, p. 36), is lat 58.6°N., long 137.1°W., a point in the Fairweather Range about 7½ miles east of the surface trace of the Fairweather fault and 13 miles southeast of the head of Lituya Bay. A later determination from a larger number of stations (William Stauder, written communication, paper given at Tucson meeting of Geol. Soc. America; oral communication, Apr. 29, 1959) places the epicenter farther southeast but nearer the assumed surface trace of the Fairweather fault.

Bedrock is exposed or lies beneath only a thin veneer of soil, glacial drift, or talus at water level around most of Cenotaph Island and from a point 4½ miles inside the entrance on the south shore around the head of Lituya Bay to a point 5½ miles inside the entrance on the north shore. The rocks are largely hard schist on the northeast shore of Gilbert and Crillon Inlets. Diorite and slightly metamorphosed volcanic rocks, slate, and graywacke are exposed on the southwest shore of Gilbert Inlet and the adjoining north shore of the bay, on the southwest shore of Crillon Inlet, and on the south shore of the bay as far as the mouth of Coal Creek. Bedded sedimentary and volcanic rocks of Tertiary age are exposed on Cenotaph Island and on the south shore west of Coal Creek. Around most of the outer part of the bay boulder till is exposed at the surface or lies under a thin soil.

Field observations in 1952 and 1953 indicated that the forest inside the moraine enclosing the outer part of Lituya Bay, but above the highest trimline, is distinctly younger than the forest growing along the coast outside of the moraine. Although no tree ring counts were made, the writer noticed that there was much less deadfall in the forest inside the moraine, and that the spruce and hemlock trees were smaller inside the moraine. Moreover, Alaska cedar trees as much as 3 feet in diameter were found growing up to the outer edge of the moraine, but not even small cedars were seen inside the moraine. This evidence of a post-Wisconsin advance of ice to the mouth of Lituya Bay is now corroborated by evidence newly exposed by the 1958 giant wave. An ice-sheared stump, rooted in a humus-rich soil just below the surficial till on the south shore near the entrance of the bay (fig. 15, loc. *A*), has a radiocarbon age of 6,060 ±200 years B. P. (Meyer Rubin, written communication, U.S. Geological Survey lab. no W–800 report, May 26, 1959).

The evidence indicates that ice stood at or near the mouth of Lituya Bay within the time required for growth of a climax forest in this region, possibly less than 1,000 years ago. However, the ice fronts were farther back when the La Perouse expedition visited Lituya Bay in 1786 than at the present time. The map made under the direction of La Perouse (1798, opposite p. 146; also Klotz, 1899) shows two tidal glaciers at the head of each inlet, which indicates that the ice fronts had retreated to positions beyond the points where the Lituya and North Crillon Glaciers enter the trench at the head of the bay. The combined length of Gilbert and Crillon Inlets then was about 9 miles. By 1894 both Lituya and North Crillon Glaciers had readvanced nearly to their present positions (Klotz, 1899). Prior to the 1958 wave low deltas of gravel had built out into Gilbert Inlet at the southwest and northeast margins of the Lituya Glacier front, and into Crillon Inlet

across about two-thirds of the width of the North Crillon Glacier front (fig. 15). These deltas formed after 1894, and they may be, or may have been, in part underlain by ice projecting from the glacier fronts below sea level.

EXPLORATION AND SETTLEMENT

Available records of the exploration and settlement of the northeastern Gulf of Alaska coast afford only a sketchy history of Lituya Bay beginning in 1786. Little information has been found for the period 1788–1874, during which time at least one destructive wave occurred and Indian settlements in the bay were abandoned, perhaps as a direct result of a wave. Records of visits to or settlement in the bay after 1874, including the accounts of geographic surveys and scientific investigations, contain few references to the occurrence of large waves.

The French explorer La Perouse (1798, p. 115–169) is generally credited with the discovery of Lituya Bay, which he named Port des François. In the course of a projected trip around the world La Perouse took his ships *La Boussole* and *L'Astrolabe* into Lituya Bay on July 2, 1786. During a stay of nearly a month the expedition mapped Lituya Bay on a scale of 1:50,000, traded with the Indians then living in and near the bay, and recorded observations on the native culture and the plant and animal life in the vicinity. Twenty-one men were drowned when three small boats engaged in a survey of the entrance were swept into the tidal bore and two were wrecked. In July 1788 Ismailof and Becharof entered Lituya Bay on the ship *Three Saints* to claim the land for Russia and to induce the natives to accept Russian rule (Shelikof, 1812, p. 108–112). The lack of any reference to waves within the bay in either of these early accounts, together with the mention of trees and native dwellings near the shore, are indirect evidence that no giant waves had occurred in Lituya Bay for some time prior to 1788.

For the remainder of the period of Russian rule and the early years of American rule, until 1874, the literature examined contains only brief mention of exploration in Lituya Bay: in connection with an expedition of the Russian ship *Orel* to obtain sea otter skins in 1796 (Bancroft, 1886, p. 356–357); the reported discovery and mining of gold placer deposits on the beaches in the vicinity of Lituya Bay by the Russian censuses of the Tlingit tribe give the population American whaling ships (Dall, 1883, p. 202). Russian censuses of the Tlingit tribe give the population of the Lituya clan or settlement as 200 in 1835, and 590 in 1861 (Petroff, 1884, p. 96, 99). Perhaps only a small part of the clan lived in Lituya Bay, for the French and Russian expeditions in 1786 and 1788 reported that the main village was northwest of the bay.

A U.S. Coast and Geodetic Survey party entered Lituya Bay in 1874 to make geodetic observations and to revise the La Perouse chart of the outer part of the bay (Dall, 1878, p. 158; 1883). No natives were then living in the bay and the village on the south shore seemed to have been abandoned for a long time. In 1894 a topographic map of the region adjoining Lituya Bay was made by a Canadian party of the International Boundary Survey (U.S. Congress, 1904; International Boundary Commission, 1952, p. 254); observations on the glaciers at the head of the bay were later published by Klotz (1899, p. 524–526, maps). The bay was visited by field parties of the U.S. Geological Survey for 3 days in 1906 (Wright, F. E., and Wright, C. W. *in* Reid, 1908, p. 53; *in* Buddington and Chapin, 1929, p. 269–270) and in 1917 (Mertie, 1931), and for 5 days in 1943 (Kennedy and Walton, 1946, p. 67–72). Surveys of the bay were resumed by the U.S. Coast and Geodetic Survey in 1926 and 1940, resulting in the current navigation chart on a scale of 1:20,000 (U.S. Coast and Geodetic Survey, 1942). In 1926, and during part of each summer from 1930 to 1934, expeditions engaged in mountain climbing or geographical and geological exploration were based in or near Lituya Bay (Carpe, 1931; Washburn, 1935, 1936; Goldthwait, 1936). Except for the brief mention of "evidence of flooding or washing to a height of at least 10 feet," which Dall (1883, p. 203) attributed to damming of the entrance by ice during the winter, none of the reports on the expeditions just described contain any reference to the giant waves in Lituya Bay.

Placer mining of the gold in the sands along the ocean beach adjacent to the mouth of Lituya Bay was begun by the Americans in 1890 (Boursin, 1893, p. 230) and continued intermittently at least until 1917 (Mertie, 1931, p. 133). Since Lituya Bay served as a port for this operation, during this period it was probably occupied or at least visited frequently. One man, James Huscroft, lived on Cenotaph Island in Lituya Bay almost continuously from 1917 to about 1940. Huscroft and another man were on the island, and two men were in a boat nearby, at the time of the 1936 waves. Their eyewitness accounts, the observations of Tom Smith and others who visited the bay only a few days later, and the observations of J. P. Williams nearly a year later, led to the earliest known published references to the unusual "waves or floods" of water in Lituya Bay (Alaska Daily Press, 1936; Williams, 1938).

Lituya Bay was incorporated in the Glacier Bay National Monument when the boundary was extended in 1939 to include the coastal area from Cape Spencer north to Cape Fairweather (fig. 14). No one has lived permanently either in or near the bay since Huscroft died, but in recent years the bay has come into increasing use as an overnight anchorage and refuge in bad weather for the trolling boats of the fishermen who ply the adjoining waters of the Gulf of Alaska during the summer and early fall.

THE GIANT WAVES

EVIDENCE

Two kinds of evidence testify to the occurrence of at least four giant waves in Lituya Bay: (a) direct observation of the waves, including the published, written, or oral accounts of eyewitnesses and possibly tidal gage records from elsewhere in the Gulf of Alaska; (b) effects that remain for later observation, mainly the destruction and transportation of vegetation, but also the erosion and transportation of unconsolidated deposits, destruction of marine life, and the destruction of works of man. The wave on July 9, 1958, and the waves on October 27, 1936, are documented beyond any doubt by both types of evidence. At least 1 and possibly 2 waves between 1854 and 1916 are indicated by trimlines shown on photographs taken from 1894 to 1929. These trimlines were largely destroyed by the 1936 wave, and were entirely gone after the 1958 wave. An oral report placing one of these waves in 1899 has not been substantiated. A wave in 1853 or 1854 is recorded in a trimline and a band of even-aged trees that was examined and mapped on the ground and dated by tree ring counts in 1952 and 1953. Possible references to the 1853–54 wave in Indian legends have not been confirmed.

WAVE ON JULY 9, 1958

SETTING AND SOURCES OF INFORMATION

Three trolling boats, each about 40 feet long and with two persons aboard, were anchored in the outer part of Lituya Bay at the time of the wave on July 9 (fig. 15; pl. 3*B*). The *Edrie* rode out the wave inside the bay; the *Badger* was carried across La Chaussee Spit and wrecked on the outside; the *Sunmore*, under way near the entrance, was swamped by the wave and went down with her occupants. The wave reportedly was first sighted within 3 minutes after the earthquake was first felt, or, using the instrumentally determined origin time for the earthquake of 06ʰ15ᵐ51ˢG.c.t., July 10 (Tocher and Miller, 1959), between 10:16 and 10:19 p. m. on July 9, local time. This is about sunset at this latitude and time of year; the weather was clear, with high scattered clouds, and the head of the bay was clearly visible from boat level at the outer part of the bay. The tide was ebbing and at about plus 5 feet (U. S. Coast and Geodetic Survey, 1957) or less than a foot above mean tide stage in the bay. The following eyewitness accounts are abstracted from articles published in newspapers and a magazine (Daily Alaska Empire, 1958a; Ulrich, 1958; Alaska Sportsman, 1958), from a personal interview with W. A. Swanson (oral communication, July 16, 1958) and correspondence with H. G. Ulrich (written communication, Oct. 24, 1958).

EYEWITNESS ACCOUNTS

ACCOUNT OF HOWARD G. ULRICH

Mr. Ulrich and his 7-year-old son, on the *Edrie*, entered Lituya Bay about 8:00 p.m. and anchored in about 5 fathoms of water in a small cove on the south shore (fig. 15). Ulrich was awakened by the violent rocking of the boat, noted the time, and went on deck to watch the effects of the earthquake—described as violent shaking and heaving, followed by avalanching—in the mountains at the head of the bay. An estimated 2½ minutes after the earthquake was first felt a deafening crash was heard at the head of the bay. According to Ulrich,

> The wave definitely started in Gilbert Inlet, just before the end of the quake. It was not a wave at first. It was like an explosion, or a glacier sluff. The wave came out of the lower part, and looked like the smallest part of the whole thing. The wave did not go up 1,800 feet, the water splashed there.

Ulrich continued to watch the progress of the wave until it reached his boat about 2½ to 3 minutes after it was first sighted. Being unable to get the anchor loose, he let out all of the chain (about 40 fathoms) and started the engine. Midway between the head of the bay and Cenotaph Island the wave appeared to be a straight wall of water possibly 100 feet high, extending from shore to shore. The wave was breaking as it came around the north side of the island, but on the south side it had a smooth, even crest. As it approached the *Edrie* the wave front appeared very steep, and 50 to 75 feet high. No lowering or other disturbance of the water around the boat, other than vibration due to the earthquake, was noticed before the wave arrived. The anchor chain snapped as the boat rose with the wave. The boat was carried toward and probably over the south shore, and then, in the backwash, toward the center of the bay. The wave crest seemed to be only 25 to 50 feet wide, and the back slope less steep than the front.

After the giant wave passed the water surface returned to about normal level, but was very turbulent,

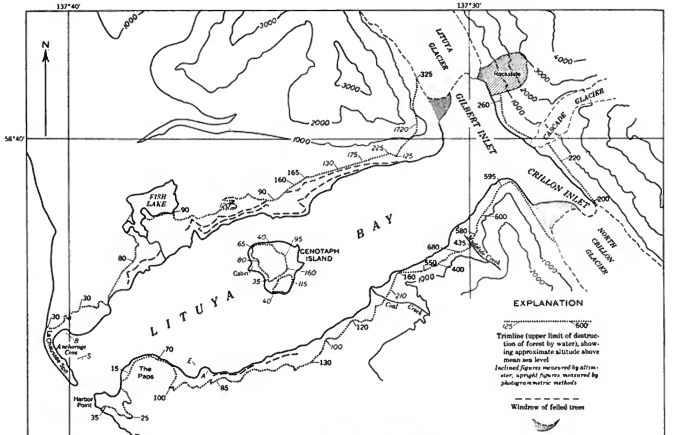

FIGURE 15. Map of Lituya Bay showing setting and effects of 1958 giant wave.

with much sloshing back and forth from shore to shore and with steep, sharp waves up to 20 feet high. These waves, however, did not show any definite movement either toward the head or the mouth of the bay. After 25 to 30 minutes the bay became calm, although floating logs covered the water near the shores and were moving out toward the center and the entrance. After the first giant wave passed Ulrich managed to keep the boat under control, and went out the entrance at 11:00 p.m. on what seemed to be a normal ebb flow.

ACCOUNT OF WILLIAM A. SWANSON

Mr. and Mrs. Swanson on the *Badger* entered Lituya Bay about 9:00 p.m., first going in as far as Cenotaph Island and then returning to Anchorage Cove on the north shore near the entrance, to anchor in about 4 fathoms of water near the *Sunmore* (fig. 15). Mr. Swanson was wakened by violent vibration of the boat, and noted the time on the clock in the pilot house. A little more than a minute after the shaking was first felt, but probably before the end of the earthquake, Swanson looked toward the head of the bay, past the north end of Cenotaph Island and saw what he thought to be the Lituya Glacier, which had "risen in the air and moved forward so it was in sight. * * * It seemed to be solid, but was jumping and shaking * * * Big cakes of ice were falling off the face of it and down into the water." After a little while "the glacier dropped back out of sight and there was a big wall of water going over the point" (the spur southwest of Gilbert Inlet). Swanson next noticed the wave climb up on the south shore near Mudslide Creek. As the wave passed Cenotaph Island it seemed to be about 50 feet high near the center of the bay and to slope up toward the sides. It passed the island about 2½ minutes after it was first sighted, and reached the *Badger* about 1½

minutes later. No lowering or other disturbance of the water around the boat was noticed before the wave arrived.

The *Badger*, still at anchor, was lifted up by the wave and carried across La Chaussee Spit, riding stern first just below the crest of the wave, like a surfboard. Swanson looked down on the trees growing on the spit, and believes that he was about 2 boat lengths (more than 80 feet) above their tops. The wave crest broke just outside the spit and the boat hit bottom and foundered some distance from the shore. Looking back 3 to 4 minutes after the boat hit bottom Swanson saw water pouring over the spit, carrying logs and other debris. He does not know whether this was a continuation of the wave that carried the boat over the spit or a second wave. Mr. and Mrs. Swanson abandoned their boat in a small skiff, and were picked up by another fishing boat about 2 hours later.

OTHER OBSERVATIONS ON JULY 9

So far as is known to the writer, no other persons were near enough to Lituya Bay to see the wave, and no photographs were taken. A party of eight mountain climbers was camped in tents on the shore of Anchorage Cove, at the base of La Chaussee Spit, until about 8:00 p.m. on July 9, when they left in an amphibious airplane only a little more than 2 hours before the wave washed over their campsite. They did not notice any unusual noises or disturbance of the water in the bay, nor any foreshocks of the earthquake up to the time they left (Paddy Sherman, written communication, Oct. 20, 1958). At least one foreshock of the earthquake was felt on the morning of July 9 on boats between Lituya Bay and Cape Spencer (William Swanson, oral communication, July 16, 1958), and on land as far away as Juneau (E. L. Keithahn, written communication, Apr. 3, 1959).

Minor anomalous waves which may have been a direct result of the giant wave in Lituya Bay were recorded on the U.S. Coast and Geodetic Survey tide gage at Sitka, on Sitka Sound, 137 miles southeast of the entrance of Lituya Bay. The waves began at 11:25 p.m., July 9, with a height of about 0.1 foot, and continued for many hours. The maximum wave height of about 0.3 foot occurred at about 2:40 a.m., July 10 (H. A. Karo, written communication, May 20, 1959). The first wave arrived at Sitka approximately 65 minutes after the giant wave washed over the entrance of Lituya Bay into the sea; the indicated average speed of about 126 miles per hour, assuming a nearly straight line route of travel through Salisbury Sound and the narrow waterways east of Kruzof Island, is comparable to the observed velocities of tsunamis. It is possible that the waves at Sitka were generated by fault displacement or some effect of the resulting earthquake at a point of origin other than Lituya Bay. Such waves were observed within a few minutes after the earthquake at Dixon Harbor 45 miles southeast of Lituya Bay (William Brammer, oral communication, July 10, 1958) and at Yakutat 99 miles northwest (Brazee and Jordan, 1958, p. 38), as well as on inland waters in Glacier Bay 60 miles to the east (observed by the writer).

OBSERVATIONS OF THE WRITER ON JULY 10

About 1½ hours were spent over Lituya Bay in a small airplane on the morning of July 10, beginning about 12 hours after the wave had passed through the bay. Observations made at this time on the more ephemeral phenomena associated with the earthquake and wave are described separately here because they bear particularly on the interpretation of the eyewitness accounts and on the nature and sequence of events in Lituya Bay on the day of the wave. The observations were recorded on a map, and by means of notes, still photographs, and movies. Kenneth Loken, pilot of the airplane, had flown over Lituya Bay on July 7 and was able to make an on-the-spot comparison of conditions before and after the July 9 earthquake and wave.

On the morning of July 10 Gilbert and Crillon Inlets and the upper part of the main trunk of Lituya Bay for a distance of 2½ miles from the head were covered by an almost solid sheet of floating ice blocks. Many of the blocks were much larger than are normally seen in the bay, with exposed dimensions, as estimated from oblique photographs, of as much as 50 by 100 feet. Nearly all of the larger blocks had flat upper surfaces and were heavily debris laden, and many had scattered, loose, large rounded boulders on their exposed surfaces. Only scattered small pieces of ice, in normal abundance, were floating in the outer part of the bay beyond Cenotaph Island. Only on the northeast shore of Gilbert and Crillon Inlets and on the large delta at the southeast end of Crillon Inlet was any great amount of ice left stranded on the beach above the high-tide line. The absence of stranded ice blocks on the spur southwest of Gilbert Inlet is especially significant as an indication that the glaciers were not involved in the generation of the initial splash or surge of water at the head of the bay.

The front of Lituya Glacier on July 10 was a nearly straight, vertical wall almost normal to the trend of the valley. Comparison of oblique photographs taken by the writer on July 10 and by Edward Berdusco on July 7 indicate that during the earthquake and wave as much as 1,300 feet of ice had been sheared off of the glacier

front, but that the southwest margin had changed very little (fig. 16). The delta on the northeast side of Gilbert Inlet had completely disappeared, and the delta on the southwest side was much smaller. It is possible that ice projected beyond the subaerial part of the glacier front, beneath the inner parts of these deltas and that these projections are the source of the large debris-laden blocks of ice floating in the bay on July 10. The glacier surface for several hundred feet from the front was severely crevassed, probably more so than normal; beyond this terminal zone, however, the glacier as far up as the partly subglacial lake near the sharp bend in Lituya Glacier (pl. 2) showed no evidence of any unusual movement. The level of the lake, according to Loken, may have lowered as much as 100 feet since he had seen it 2 days earlier.

The front of North Crillon Glacier and the adjoining large delta showed no indications of any significant forward movement of the glacier or of any other disturbance except effects of washing by the component of the wave that had moved southeastward into Crillon Inlet. The front and lower part of Cascade Glacier similarly showed no effects other than of washing by the wave, which had exposed a narrow tongue of nearly clear ice extending to the shoreline.

The most striking change at the head of Lituya Bay, aside from the new trimline, was the fresh scar on the northeast wall of Gilbert Inlet, marking the recent position of a large mass of rock that had plunged down the steep slope into the water (fig. 16; pl. 4*A*). Loose rock debris on the fresh scar was still moving at some places, and small masses of rock still were falling from the nearly vertical rock cliffs at the head of the scar. The fresh scar is not present on an oblique photograph taken by Edward Berdusco on July 7. This evidence, as well as Ulrich's account, indicates almost certainly that the rockslide was triggered by the earthquake on July 9. The rockslide is described in greater detail on page 65.

Floating logs and other vegetation formed a nearly continuous raft as much as 1,200 feet wide along the outer 3 miles of the north shore of the bay. Small rafts of logs and individual logs were evenly distributed throughout the rest of the bay, beyond the limits of the ice, and over a fan-shaped area of the sea as much as 5 miles from the entrance of the bay.

Water was still dripping from the wave-washed slopes around the shore of the bay as high as the new trimline on the morning of July 10. The volume of water in streams flowing from Fish Lake and other lakes reached by the wave on both the north and south shores was much larger than normal.

EFFECTS OF THE WAVE

DESTRUCTION OF VEGETATION

The trimline (upper limit of total or near total destruction by water of the forest and other vegetation) along the shores of Lituya Bay is plotted on figure 15 and is illustrated by several photographs (pls. 3*B*, 4*B*, 5*A*, 6*B*, 7 *A* and *B*). The altitude at the highest point on the trimline and at other critical points was measured by means of an altimeter that was set at mean sea level, carried up to the trimline, and read again at sea made within a period of 1 hour or less. The horizontal level. At most stations the series of three readings was position of the trimline was plotted by transferring its trace by inspection from the oblique photographs taken by the writer in 1958 to vertical photographs taken in 1948, and thence to the maj of the bay. Additional altitudes were determined photogrammetrically from the 1948 vertical photographs and from the 1958 U.S. Coast and Geodetic Survey single-lens vertical photographs covering the outer mile of the bay. Prints of some 9-lens photographs taken after the 1958 wave were obtained in February 1959. Since suitable photogrammetric equipment was not available, they could be used only to add details to the trimlines in areas of low relief around the outer part of the bay. A map of Lituya Bay on a scale of 1:10,000, with a 50-foot contour interval, has been compiled from the 9-lens photographs by the U.S. Coast and Geodetic Survey (H. A. Karo, written communication, Apr. 28, 1959).

The trimline formed by the 1958 wave extended to a maximum height of 1,720 feet above mean sea level, on the spur southwest of Gilbert Inlet, (pl. 4*B*). Its maximum horizontal distance was about 3,600 feet from the high-tide shoreline, in the vicinity of Fish Lake. Along a 1-mile segment midway between the head and entrance of the bay the band of destruction on the north and south shores averages 1,200 feet in width and extends to an average altitude of about 110 feet. The total area between the trimlines and the high-tide shorelines in the bay is about 4 square miles. This figure includes small lakes and small areas of steep slopes and beaches where little or no vegetation was growing, but it is a measure of the total area over which the wave was capable of felling a large proportion of the trees. The total area inundated by the wave is still larger, probably at least 5 square miles.

One of the most impressive aspects of the 1958 wave is the thoroughness of its destruction of the forest nearly extending to the upper limit of inundation; this can best be conveyed by photographs. In most places the trees were washed out and carried away, leaving bare ground (pl. 5*A*). In some places, mostly on steep slopes where the roots were anchored in bed-

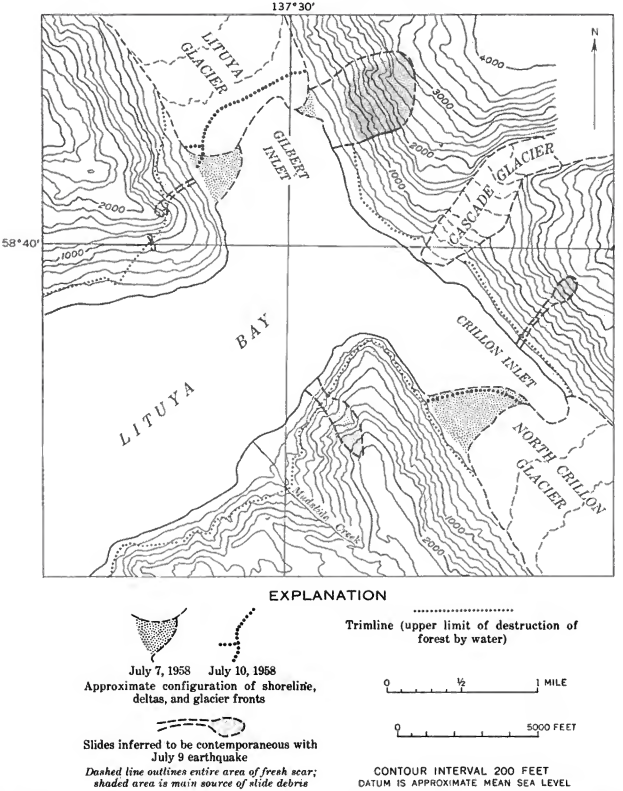

FIGURE 16.—Detailed map of head of Lituya Bay, showing slides, changes in the shoreline and glacier fronts, and trimlines resulting from the 1958 earthquake and giant wave.

rock, the trunks were twisted or broken off just above ground level. At Harbor Point a living spruce tree was broken off cleanly about 3 feet above the root system, where it measured 4 feet in minimum diameter (pl. 5*B*). At a few places, mainly at the edge of the trimline, trees were pushed over but not washed out (pl. 7*B*, lower left). Only along the outer mile of the bay were clumps of trees left standing within the trimline. The forest was left standing to the high-tide line at only two points, on the south shore 0.4 mile from the entrance and on the north shore 1.4 miles from the entrance (fig. 15). The wave's competency is shown also by the sharp trimline and by the narrow channels cut through the trees on Cenotaph Island (pl. 6*A*), into a small lake east of Fish Lake and into the lakes east of Harbor Point. On steeper slopes from Cenotaph Island toward the heard of the bay the water had washed into the forest generally not more than 10 to 20 feet vertically above and 30 to 100 feet horizontally beyond the trimline. On low slopes in the outer part of the bay, however, the water at some places flowed through the forest for much greater distances, probably as much as a quarter of a mile, beyond the trimline. Salt poisoning of some bushes and plants was indicated by the brown tone of the foliage just above the trimline; this was particularly noticeable on steep slopes at the head of the bay in late August. The larger trees showed no effects of the brief submergence in salty water, although the lower trunks of many trees bordering the trimlines were injured by impact with other trees felled or transported by the wave (pl. 6*A*).

Many of the trees felled by the 1958 wave were reduced to bare stems, with the limbs, roots, and even the bark removed (pl. 6*B*). Removal of the projecting limbs and roots was due to grinding action as the trees were rotated in the turbulent water. On many of the trees, however, the cambium layer was still smooth or even slippery and showed little evidence of abrasion, suggesting that water under high pressure or moving at high velocity stripped off the bark by a process analogous to that used for peeling logs in plywood and pulpmills.

Along much of the north shore of Lituya Bay and for short distances along the south shore and on Cenotaph Island part of the felled timber is concentrated in poorly defined to well-defined windrows at variable heights above the high-tide line. The more conspicuous of the windrows are shown on figure 15. The longest continuous line of debris can be traced for about 2 miles along the north shore.

OTHER EFFECTS

No attempt was made to measure accurately the amount of erosion accomplished by the 1958 wave, and probably at only a few points along the shore of the bay are measurements made or photographs taken before 1958 sufficiently detailed to allow more than a rough estimate. From the effect on the vegetation an average minimum thickness of a foot of soil almost certainly was removed over the entire area between the trimline and the shore. This alone represents a volume of more than 4 million cubic yards. Cut banks 1 to 3 feet high were seen along the trimline at some places in the bay. At the small rounded projection of the south shore, 1.7 miles east of Harbor Point (fig. 15 loc. *A*), the wave cut a nearly vertical cliff about 25 feet high into till and underlying stratified sand and gravel. Large areas of bedrock were newly exposed and left as bare and clean as though washed down with a hose on the spur west of Gilbert Inlet, along most of the steep south shore from Crillon Inlet to a point 1 mile west of Coal Creek, and around much of the shore of Cenotaph Island.

Marine plants attached to rocks and marine invertebrates attached to rocks or burrowed in mud or sand were largely destroyed by the wave, at least down to mean lower low water level. On Cenotaph Island and on the south shore of Lituya Bay near the entrance, where in 1952–53 barnacles and mussels almost completely covered the rocks in the intertidal zone, and many edible clams were dug, not one living shellfish was seen in August 1958. At these localities even the basal attachment plates of most of the barnacles had been removed from the rocks. The shells of clams, barnacles, and crabs were scattered along the shore above the high-tide line and a few were seen at or near the upper limit reached by the water on Cenotaph Island and at several other places in the outer half of the bay. Failure to find the remains of any fish or deep-water shells suggests that the wave had little immediate effect on the larger swimming vertebrates and did not bring up bottom-dwelling invertebrates from a depth of more than a few tens of feet. The writer had no opportunity to examine closely the forest adjoining the trimlines near the entrance of the bay, however, where the water flowed out through the trees and where stranded fish would most likely be found. Probably many bottom-dwelling invertebrates in deep water were killed in place by settling of sediment eroded and transported by the wave. Some fresh-water organisms probably were also killed by the invasion of salt water into Fish Lake and smaller lakes and ponds along the shores of the bay, but these bodies of water were not examined.

Few works of man existed in Lituya Bay at the time of the 1958 wave, but judging from the effects on the vegetation and the boats, the wave would have wreaked enormous destruction on ordinary buildings and on

A. VIEW OF LITUYA BAY, 1954

Trimlines of the 1936 giant waves (*g*) and the 1853–54 giant wave (*k*). Lateral moraines (*m*) and the end moraine in the right and left foreground record a recent advance of ice to the mouth of the bay. Mount Crillon, altitude 12,726 feet, is the highest peak on the skyline

B. VIEW IN AUGUST 1958

A giant wave generated on July 9, 1958, by a rockslide from the cliff (*r*) at the head of the bay destroyed the forest over the light areas to a maximum altitude of 1,720 feet at *d* and to a maximum distance of 3,600 feet in from the high-tide shoreline at Fish Lake (*F*). A fishing boat anchored in the cove at *b* was carried over the spit in the foreground; a boat under way near the entrance was sunk and a third boat, anchored at *e* rode out the wave

A. NORTHEAST WALL OF GILBERT INLET, AUGUST 1958

Shows scar of rockslide. Head of slide, at about 3,000 feet altitude, was just below snowfield in upper center. Front of Lituya Glacier at lower left corner

B. VIEW NORTHWEST AT HEAD OF LITUYA BAY, AUGUST 1958

Large rockslide plunged into Gilbert Inlet at lower right corner, shearing off part of the front of Lituya Glacier and causing water to surge over the spur opposite. The trimline slopes down to right, across scars of slides that occurred before the 1958 earthquake

A. View west from Coal Creek, on south shore of Lituya Bay, August 1958. Trimline at left margin is at an altitude of about 180 feet, and is 1,000 feet in from the high-tide shoreline

B. Stump of living spruce tree broken off by the 1958 giant wave at Harbor Point, mouth of Lituya Bay. Brim of hat is 12 inches in diameter

A. VIEW WEST ON CENOTAPH ISLAND

Shows channel cut through forest by the 1958 giant wave. Note injured tree standing at portal of channel, on right

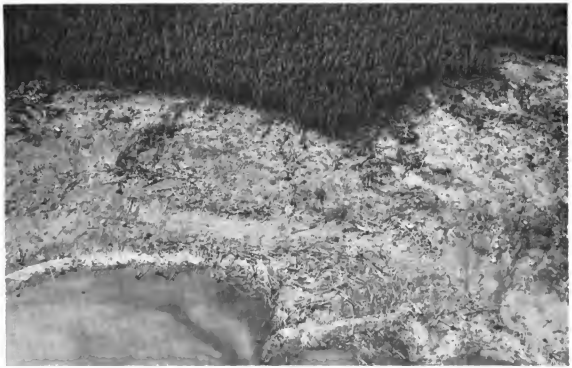

B. NORTH SHORE OF LITUYA BAY, AUGUST 1958

View is 2 miles from entrance. August 1958; forest as dense as that in the upper part of view formerly extended nearly to the shoreline. Width of zone of destruction by the 1958 giant wave is about 1,700 feet at right margin of photograph. Note trees with limbs and bark removed, in foreground

shore structures such as docks. At the foundation sites, no trace could be found of the well-constructed cabin on the west or lee side of Cenotaph Island, used by the writer as a base camp in 1952 and 1953, or of the lighthouse mounted on concrete piers at Harbor Point. A few cut pieces of wood and some metal utensils from the cabin on Cenotaph Island were found several hundred feet from the former site.

Equipment left by a mining company at an intended campsite near the south shore was washed away (Henrickson, 1959, p. 18). Monuments marking U.S. Coast and Geodetic Survey triangulation points at Harbor Point and several other stations along the north and south shores of the bay are believed to have been washed out or moved. Station "Ice," marked by a bronze disk set in a large boulder on the shore at the head of the bay was found by the writer and apparently had not moved. Markers set in bedrock on the north and south shores just west of the two arms at the head of the bay, and one marker set in a concrete post on La Chaussee Spit seem, from study of photographs, to have remained in place also.

With regard to the destructiveness of the wave, R. L. Wiegel (written communication, Mar. 31, 1959) commented as follows:

> The method by which the wave broke and uprooted trees is easily explained using existing theory and data on wave-induced forces (Wiegel and Beebe, 1956; Wiegel, Beebe, and Moon, 1957); Wiegel and Skjei, 1958). For example, taking a conservative estimate of wave height and water depth, the total moment about the bottom of a tree 50 feet high with an effective dense crown diameter of 20 feet and trunk diameter of 2 feet was computed to be of the order of 25 million foot-pounds, which is far in excess of the conservative 300,000 foot-pounds necessary to snap the tree or uproot it (Fons and Pong, 1957).
>
> The problem of peeling the bark off a tree is a little more difficult. It may be due to the high water particle velocities in the waves. A solitary wave 100 feet high moving in water 400 feet deep will have a horizontal component of water particle velocity in excess of 100 feet per second just under the wave crest. This, combined with the observation in the model that the wave crest along the edges of the bay moved at the same velocity as the wave in the center of the bay, indicates that a water particle velocity of this magnitude would have existed over a substantial portion of the forested slope. The shear stress on the bark due to this velocity and extreme hydraulic roughness of the bark might have been adequate to strip the bark from the trees, especially as cracks probably formed in the bark as the trees were being bent prior to breaking.
>
> The water particle velocities along the edges of Cenotaph Island would have been great also, and this might explain the stripping of barnacles from the rocks.
>
> The water particle velocities at the bottom of the main portion of the bay would have been much lower.

NATURE AND CAUSE OF THE WAVE

From the foregoing evidence the nature, sequence, and approximate time of events associated with the July 9, 1958, wave in Lituya Bay are interpreted as follows:

Beginning at about 10:16 p.m. the southwest side and probably most of the bottom of Gilbert and Crillon Inlets moved northwestward and possibly up relative to the northeast shore at the head of the bay, on the opposite side of the Fairweather fault. Observations of the surface breakage along the Fairweather fault 6 to 10 miles southeast of Crillon Inlet indicate that the displacement occurred in several pulses and that the total movement was about 21 feet horizontally and 3 feet vertically (Tocher and Miller, 1959). Intense shaking in Lituya Bay continued for at least 1 minute according to the account of William A. Swanson, and possibly as much as 4 minutes according to Howard G. Ulrich. Slides and avalanches started in the mountains at the head of the bay within a minute after the shaking was first felt. Not less than 1 minute nor more than 2½ minutes after the earthquake was first felt a large mass of rock slid from the northeast wall of Gilbert Inlet. The initial movement of this rock mass, with attendant clouds of rock dust and avalanching snow and ice, may account for the "moving glacier" observed by Swanson. The impact of the large rockslide on the surface of the water caused the "deafening crash" heard by Ulrich and caused a huge sheet of water to surge up over the spur on the opposite side of Gilbert Inlet. The sudden displacement of a large volume of water as the rock mass plunged into Gilbert Inlet set in motion a giant gravity wave with a steep front, traveling at high velocity and with its greatest force directed initially about due south. The gravity wave, probably supplemented by the surge of water over the spur southwest of Gilbert Inlet, struck first against the steep cliffs on the south side of the bay in the vicinity of Mudslide Creek; the maximum force of the wave was then reflected and refracted toward the north shore a little farther out the bay, and again back to the south shore near Coal Creek. Variations in the height and intensity of the gravity wave as it moved out the bay, as recorded in the trimlines, may have been caused also by the interaction of diagonally refracted waves, by seiche wave motion, and by reflection of waves from the narrow entrance. Estimates by Ulrich and Swanson of the time elapsed from the first sighting of the wave front until it reached their boats indicate that the crest of the gravity wave moved out the bay at an average speed between 97 and 130 miles per hour. After the giant wave passed, the water in the bay was set into turbulent wave motion and continued to surge from shore to shore for 25 minutes or more.

According to R. L. Wiegel (written communication, Mar. 31, 1959), the wave speed as calculated from the estimated time elapsed is in good agreement with the theoretical speed as calculated from the formula

$$C=\sqrt{g(d+H)}$$

where g is the acceleration due to gravity, d is the depth of water below sea level, and H is the height of the wave above sea level. He states:

> If the water depth averaged between 400 and 500 feet and the wave height averaged between 200 and 300 feet the wave would travel at a theoretical speed of about 100 miles per hour. If the water depth were taken as a conservative 400 feet and the wave height at a conservative 100 feet the theoretical wave speed would be about 56 miles per hour.

From evidence observed and photographed from an airplane on July 10, the writer with Kenneth Loken as pilot, concluded that water had risen to a height of about 1,800 feet on the spur southwest of Gilbert Inlet and caused destruction of the forset to the sharp trimline across this spur (Daily Alaska Empire, 1958b; Seismol. Soc. America Bull., 1958, p. 406). This conclusion was based on the following evidence: (a) The "washed" appearance of the bedrock below the trimline on the spur; (b) the sharp and even appearance of the trimline, and its similarity to and continuity with the trimline known to have been caused by water action farther out the bay; (c) at the highest point on the trimline, where the 1,800-foot altitude was estimated from the airplane altimeter, about 30 large trees were turned upslope and back into the forest. The roots of some of the upturned trees were bare and white, as though they had been washed out rather than merely pulled out of the soil (pl. 7*A*).

The initial report of wave damage to 1,800 feet above a water surface was widely doubted both on theoretical grounds and on the basis of aerial observations and study of photographs by others. This figure is more than 8 times the maximum height attributed to a 179) and nearly 8 times the maximum height reached by the largest of the slide-generated waves in Norway. Brazee and Jordan (1958), from study of aerial photographs and evaluation of reports of field observations, including those of the writer and Don Tocher, concluded that the spur southwest of Gilbert Inlet "has been denuded to a height of 1,800 feet either by avalanche, wave action or a combination of the two." Jordan later stated (written communication, Dec. 29, 1958) "More information is now available and it seems that landsliding is the major activity for any elevation above 300 feet or so," and this view is expressed also in an announcement of plans for a field investigation of Lituya Bay by the U.S. Coast and Geodetic Survey (Daily Alaska Empire, 1959). T. N. Davis, from aerial observations in Lituya Bay on July 12, 1958 first attributed the destruction of trees at high altitude on the spur southwest of Gilbert Inlet to "earthslide" (paper read at Alaska Science Conf., Sept. 2, 1958), but on reexamination of his photographs he found a few trees stripped of bark high on the slope and now believes that this damage to the trees is more likely due to action of high-velocity water than to slide action alone (written communication, Apr. 6, 1959).

After examining the area of the high trimline again from the air and on the ground later in the summer, it is still the writer's conclusion that water was primarily responsible for destruction of the forest cover. Examination on the ground confirmed that trees just above the highest point on the trimline, at 1,720 feet altitude as remeasured by a hand-carried altimeter, had been washed out and overturned by water. At this point on the crest of the spur the water rose about 20 feet higher than the highest overturned trees and flowed across the ridge and at least a quarter of a mile down the opposite side into the forest, leaving rocks and driftwood on the moss. It is true that rockslides either accompanied or closely followed the earthquake on the northeast side of the spur. Cracks trending parallel to the scar were seen in the forest on the crest of the spur, just above the trimline. Comparison of the 1958 oblique photographs taken after the earthquake with the 1948 vertical photographs show, however, that the 1958 slides occurred mainly in old landslide or rockslide scars, and that the volume of new sliding was small. Moreover, the trimline which the writer believes was formed by water, cuts across the tracks of these slides (pl. 4*B*). After the water had dashed over the spur there was minor sliding from the unstable scarp at the trimline. The conspicuous streaks of debris left by small slides on the otherwise washed, bare bedrock surface of the southwest face of the spur (pl. 7*B*) provide further convincing evidence against landsliding or avalanching as the primary cause of the destruction here. Also, along the margin of the trimline on the southwest face of the spur from the low point to an altitude of about 700 feet the trunks of many large trees knocked down but not washed out by the water are oriented parallel to the trimline, with their tops turned to the west (pl. 7*B*). These trees, if felled by avalanching or sliding, should be preferentially oriented parallel to the gradient of the surface.

Small slides occurred, presumably at the time of the earthquake, on the south side of Lituya Bay between Mudslide Creek and Crillon Inlet. The area affected by new slides is much smaller than is shown by Brazee and Jordan (1958, fig. 3). The trimline formed by

the wave continues across this area, between slide scars, at altitudes ranging from 500 to 600 feet (fig. 16).

The large mass of rock that plunged into Gilbert Inlet from the northeast wall during the 1958 earthquake is referred to as a rockslide in this report, although it is near the borderline between rockslide and rockfall as defined in two classifications of landslides (Sharpe, 1938, p. 76–78; Varnes *in* Eckel, 1958, p. 20–32 and pl. 1). This rockslide as stated on page 63 probably caused the 1958 giant wave at Lituya Bay. The rockslide occurred in an area of previously active sliding and gulleying to an altitude of about 3,000 feet on a slope averaging 40°. The rocks in this area, as mapped by D. L. Rossman (written communication, 1957), are mainly amphibole and biotite schists; bedding and schistosity strike about N. 50° W. and dip steeply northeastward, into the slope.

The new slide area on the northeast wall of Gilbert Inlet, as shown on figure 16, was plotted by transferring the outer limits of the new scar by inspection from oblique photographs taken after July 9, 1958, to the vertical photographs taken in 1948, and thence by photogrammetric methods to the map. The dimensions of the slide on the slope are reasonably accurate, but the thickness of the slide mass normal to the slope can be estimated only roughly from the data and photographs now available. The main mass of the slide, as outlined on figure 16, is a prism of rock that is roughly triangular in cross section, with dimensions of 2,400 feet and 3,000 feet along the slope, a maximum thickness of about 300 feet normal to the slope, and a center of gravity at about 2,000 feet altitude. From these dimensions and an assumed specific gravity of 2.7, the volume and weight of the rock mass are, respectively, 40 million cubic yards and 90 million tons. It is highly probable that this entire mass plunged into Gilbert Inlet as a unit at the time of the earthquake, although the only known fact is that it fell between about noon on July 7 and about 10 a.m. on July 10.

The writer went to Lituya Bay in 1958 with a strong belief that fault displacement was the most likely mechanism for generating the giant waves originating in the fault zone at the head of Lituya Bay. The magnitude of the slide on the northeast wall of Gilbert Inlet was not fully realized from the aerial inspection on July 10, and it was first considered to be only a minor factor in the generation of the 1958 wave. Tocher (written communication, Aug. 1, 1958), however, suggested avalanching of rock or ice from the northeast wall of Gilbert Inlet as a possible generating mechanism before he was informed that a rockslide had occurred there. Arguments advanced by Tocher, information obtained later in the field and from the literature on similar waves elsewhere in the world, and the model studies made by Wiegel all have contributed to the writer's present acceptance of the rockslide as the major, if not the sole cause of the 1958 giant wave. Among the arguments against fault displacement as an important contributing mechanism to the generation of this wave, the following seem most significant: (a) Eyewitness reports of a lapse of 1 to 2½ minutes between the onset of the earthquake and the first sighting of the wave at the head of the bay: (b) The predominantly horizontal movement along the Fairweather fault, as indicated by ground breakage a few miles southeast of Lituya Bay. If the fault trace lies near the northeast side of Gilbert and Crillon Inlets, nearly the entire area under water at the head of the bay moved relatively northwestward and possibly up; wave motion resulting from this displacement should be directed toward the northwest and southeast side of the bay and (or) toward the head of the bay. (c) Vertical displacement of the bottom of the bay along the Fairweather fault probably would generate waves as a line source. An eyewitness account and the configuration of the trimlines, however, indicate radial propagation from a point source in Gilbert Inlet.

The comments of R. L. Wiegel on the nature and cause of the wave follow (written communication, Mar. 31, 1959):

> It is a well documented fact that waves with large energy content are generated impulsively by such varying mechanisms as underwater seismic disturbances, islands exploding, atomic bombs, and large masses of water added suddenly to a body of water. The characteristics of waves generated by such mechanisms depend upon the disturbing force and the rate at which it is applied. The resulting waves may be oscillatory in character, nearly solitary in form, a complex multicrested non-linear wave existing entirely above the initial undisturbed water surface, or a bore (Prins, 1958a, 1958b).
>
> The size of the slide, the water depth, and the general dimensions of Lituya Bay indicated that a wave similar to a solitary wave should form, but with a complex "tail" to the wave. A rough model was constructed at the University of California, at a 1:1,000 scale. Motion pictures were taken of the model tests and measurements were made of the water surface time histories at two points. Observations of the effects of various types of slides in the model indicated that the prototype must have fallen almost as a unit, and very rapidly. If the slide occurred rapidly then a sheet of water washed up the slope opposite the landslide to an elevation of at least three times the water depth. At the same time a large wave, several hundred feet high, moved in a southerly direction, causing a peak rise to occur in the vicinity of Mudslide Creek. This same wave swung around into the main portion of Lituya Bay, due to refraction and diffraction. The movements of the main wave and the tail were complicated within the bay due to reflections and due to the effect of bottom hydrography. One further wave characteristic was noticed when large waves were obtained, and this was that the crest appeared to move at a nearly uniform velocity across the bay even though the water

TABLE 1.—*Data on localized giant waves generated by falling or sliding of solid masses*

Location, date, and time of occurrence	Generating mechanism	Nature of water body, velocity and height of waves	Effects of waves	References
Japan				
Shimabara Peninsula, Kyushu Island, May 21, 1792, about 8 p.m.	During period of intense earthquakes and volcanic activity about 700 million cu yds of rock and soil to a maximum altitude of 1,700 ft on the east flank of Mayo-yama slid 1¾ miles down a slope averaging 10°, and plunged into the sea along a front 3 miles wide.	Shimabara Bay, length about 80 miles, average width 10 miles, maximum depth 210 ft near the slide; opens into East China Sea at southwest end. At Shimabara 3 waves in rapid succession, the second and largest wave rising on land to a maximum height of about 33 ft.	Trees as much as 9 ft in diameter felled, buildings destroyed. More than 15,000 people were killed, most of them by the waves. Wave destruction extended about 50 miles along the shores of the bay.	Omori (1907); Ogawa (1924, p. 219–224, pls. 6, 7).
Norway				
Langfjord, Feb. 22, 1756.....	About 15.7 million cu yds of bedrock and soil to a maximum altitude of 1,312 ft on the fiord wall at Tjelle slid down a slope averaging 25° or more, and plunged into the fiord. Landslide may have been triggered by heavy rainfall.	Langfjord (fiord), length about 20 miles, average width 1.5 miles, maximum depth about 1,100 ft; opens into Norddalsfjord to west. Three waves observed, rising to a maximum height of 120 ft on shore opposite the slide.	Vegetation, soil, buildings, and boats destroyed, 32 people killed. Effects of the waves were noticed as much as 25 miles from slide.	Jørstad (1956).
Loen Lake, Jan. 15, 1903, about 11 p.m.	About 450,000 cu yds of bedrock and talus to a maximum height of 1,640 ft on Ravnefjell (Raven Mountain) fell and slid down a slope averaging 65°, and plunged into lake.	Loen Lake, length 7 miles, average width 0.6 mile, maximum depth 436 ft. Wave 10 ft high in middle of lake; rose to maximum height of 131 ft on shore opposite the slide and to 19 ft at the far end of the lake, 4.8 miles from the slide.	Vegetation, soil, buildings, and boats destroyed; iron steamboat 48 ft long was carried 830 ft and stranded 56 ft above lake level; 61 people killed.	Holmsen (1936, p. 173–177, figs. 2, 3); Bugge (1937, especially figs. 1, 8, and 10); Brigham (1906); Holtedahl (1953, p. 1044–1045).
Loen Lake, Sept. 13, 1936, 5 a.m.	About 1.3 million cu yds of bedrock to a maximum height of 2,625 ft on Ravnefjell felt at the same locality as the 1903 slide. Slide about 1,300 ft wide at lakeshore.	Loen Lake, see above. Wave appeared 3–6 ft high in center of lake; it rose to a maximum height of 230 ft on shore opposite the slide, and to 50 ft at the far end of the lake.	Vegetation, soil, buildings, boats and bridges destroyed, 72 people killed. Remains of stranded steamboat carried on up to 164 ft above lake level.	Holmsen (1936, p. 183–186, photograph opposite p. 176); Bugge (1937, figs. 8 and 10, p. 357); Holtedahl (1953, p. 1045–1046).
Loen Lake, Sept. 21, 1936, in evening.	Rockslide or rockfall from Ravnefjell.	Loen Lake, see above. Wave rose to maximum height of 49 ft on shore.	Boats used for rescue work were damaged.	Holmsen (1936, p. 186).
Loen Lake, Nov. 11, 1936, at night.	Rockslide or rockfall from Ravnefjell; volume as large as that on Sept. 13, 1936.	Loen Lake, see above. Wave rose to about the same height as on Sept. 13.	Nothing left to destroy.....	Holmsen (1936, p. 190), supplement, in German.
Tafjord, April 7, 1934, 2 a.m.	Overhanging rock mass of nearly 2 million cu yds volume fell from maximum altitude of 2,395 ft on fiord wall with an average slope of 45°, and plunged into the fiord along a front 750 ft wide. Rockfall triggered by melting of ice in fractures.	Tafjord (fiord), length about 5.6 miles, average width 0.7 mile, maximum depth 700 ft; opens into Norddalsfjord to west. Three waves of increasing height were observed at several places. Water rose to maximum height of 204 ft about 650 ft from the slide margin, to 122 ft on shore opposite the slide, and to 3 ft above normal high-tide line about 31 miles from the slide. Approximately measured velocities range from 13.4 to 26.8 miles per hour.	Vegetation, soil, buildings, and boats destroyed, 44 people killed along fiord within 2 miles of the slide; extensive damage to boats and docks as much as 31 miles from the slide.	Kahlisel and Kolderup (1937); Holmsen (1936, p. 177–183, figs. 4 and 5); Bugge (1937, especially figs. 4, 5 and 6); Holtedahl (1953, p. 1046).
Norddalsfjord, across from Stranda, 1938.	Landslide from Skafjell.	Norddalsfjord (fiord). Three waves reported.	Not described in reference.	Jørstad (1956, p. 330). Incidental mention only; no detailed description found.
United States				
Disenchantment Bay, Alaska, July 4, 1958.	Fallen Glacier, a hanging glacier about 3,500 ft long and 1,200 ft wide, avalanched from an altitude of 1,950 ft down a slope averaging about 16°, and plunged into bay along a front 0.5 mile wide.	Disenchantment Bay, length about 10 miles, average width 3 miles, maximum depth 942 ft; opens into Yakutat Bay to south and into Russell Fiord to east. Waves 15–20 ft high observed for half an hour on Russell Fiord 15 miles from the avalanche; water rose to maximum height of 115 ft about 2.5 miles from the avalanche.	Unconsolidated deposits eroded, bushes broken off or washed out; area uninhabited.	Tarr (1909, p. 67–68). According to Indian legend falling glaciers in this area generated similar waves at least twice before; reportedly 100 Indians were killed by a wave about 1845.
Reed Terrace area near Kettle Falls, Columbia River valley, Washington; from April 8, 1944, to Aug. 19, 1955.	Landslides in terrace scarps underlain by bedded unconsolidated deposits. Narrow segment of the scarp on a slope averaging about 23° suddenly gave way and slid into the lake. Debris came down from maximum height of 210 ft above water level.	Franklin D. Roosevelt Lake, average width 5,000 ft, maximum depth 160 ft at slide area. Waves were generated by at least 11 different slides; the largest wave rose to maximum height of 65 ft on opposite shore, and was observed 6 miles up the lake. Observed velocity of one series of waves was about 45 miles per hour.	Vegetation destroyed, unconsolidated deposits eroded; barges and boats broke loose from dock 6 miles from slide area.	F. O. Jones and W. L. Peterson (written communications, Mar. 16 and May 7, 1959); Jones in Eckel (1958, figs. 31, 32, p. 40–41).
Mouth of Hawk Creek near Lincoln, Columbia River valley, Washington, July 27, 1949.	Landslide in terrace scarp underlain by bedded unconsolidated deposits. A narrow segment of the scarp on a slope averaging about 31° suddenly gave way and slid into the lake. Debris came down from maximum height of 340 ft above lake level.	Franklin D. Roosevelt Lake, bay about 1,200 ft wide and 120 ft deep at slide area. Wave rose 65 ft on shore opposite the slide.	Trees knocked down.	F. O. Jones and W. L. Peterson (written communications, Mar. 16 and May 7, 1959).
East side of Columbia River valley north of Kettle Falls, Washington, Feb. 23, 1951.	Debris slide in bedded unconsolidated deposits and talus from maximum height of several hundred feet above lake level.	Franklin D. Roosevelt Lake.	Not described in references.	Jones in Eckel (1958, fig. 23 on p. 33); W. L. Peterson (written communication, May 7, 1959).

depths at the edge were considerably less than the water depth in the center of the channel. It is believed that this phenomenon is associated with the phenomenon studied by Perroud (1957).[3] The model study movies showed that the wave elevation was higher along the edges of the bay than in the center.

The action of the wave over the center of Cenotaph Island and at La Chaussee Spit are due to shoaling effects which have not been studied in detail for solitary, or similar, waves.

The energy in a solitary wave 100 feet high in water 400 feet deep with a channel width of 8,000 feet can be computed using an equation given by Ippen and Mitchell (1957). It is about 6×10^{13} foot-pounds. The potential energy of the landslide was about 3.5×10^{14} foot-pounds. Hence, only about 2 percent of the potential energy of the slide went into the main wave. This is of the same order of magnitude as obtained by model studies of a similar type of disturbance (Wiegel, 1955).

COMPARABLE WAVES IN OTHER PARTS OF THE WORLD

Waves similar to the 1958 giant wave in Lituya Bay have been generated by the sliding of part of a mountain into Shimabara Bay in Japan, by the sliding or falling of large masses of rock into a lake and several fiords in Norway, by the avalanching of a hanging glacier into a bay in Alaska, and by landslides into a lake in Washington. References and significant data on several such localized waves that have come to the writer's attention are summarized on table 1. An exhaustive search of the literature no doubt would reveal many other such occurrences in parts of the world where steep or unstable slopes are adjacent to bodies of water. Earthquakes acted as a triggering mechanism for the slide in Japan, but no earthquake was reported at the time of the 1905 wave in Alaska or at the time of any of the large waves in Norway and Washington. Some waves that accompanied earthquakes in uninhabited or sparsely inhabited areas and were attributed to tectonic movement, as for example the 1899 wave in Yakutat and Disenchantment Bays and Russell Fiord in Alaska (Tarr and Martin, 1912, p. 46–47) may have been generated instead by slides or avalanches triggered by the earthquakes. On the other hand one interpretation of the April 2, 1868 tsunami on the south coast of the Island of Hawaii as the result of a mudflow (Omori, 1907, p. 144) is not correct, according to G. A. Macdonald (written communication, Apr. 15, 1959).

WAVES ON OCTOBER 27, 1936

SETTING AND SOURCES OF INFORMATION

Four men were in Lituya Bay on October 27, 1936. James Huscroft and B. V. Allen were in a cabin on the west shore of Cenotaph Island (fig. 17) and Nick Larsen and F. H. Frederickson were on a 38-foot trolling boat *The Mine*. Larsen and Frederickson, who had entered Lituya Bay on October 26, anchored their boat first near the north shore south of Fish Lake and, after the first wave was sighted, moved to the west shore of the island near the cabin. According to the most detailed accounts, there were three giant waves in close succession, beginning at about 7:00 a.m., about an hour before sunrise. According to Frederickson the weather was clear but it was too dark to see much at the head of the bay; moreover, after *The Mine* was moved to the lee of Cenotaph Island, the head of the bay was hidden from all four observers. The tide at the time of the waves was flooding and about at mean tide stage (U.S. Coast and Geodetic Survey, 1935).

Two nearly identical articles based on an oral report by Allen (called to the writer's attention by Robert De Armond, oral communication, July 22, 1958) were published in newspapers soon after the waves occurred (Alaska Daily Press, 1936; Alaska Weekly, 1936). Information related by Huscroft about a year later was incorporated in an article on Lituya Bay by Williams (1938). De Armond also recalled seeing another account in a Ketchikan newspaper, based on the oral report by Larsen and Frederickson, but attempts to find this article have failed (L. H. Bayers, written communication, Apr. 7, 1959). The eyewitness account of F. H. Frederickson is abstracted from his recollections as related to the writer in a telephone conversation and a letter in September 1958.

EYEWITNESS ACCOUNTS

ACCOUNT OF FRED H. FREDRICKSON

During the night of October 26–27, 1936, *The Mine* was anchored near the north shore of Lituya Bay, a mile due west of the cabin on Cenotaph Island (fig. 17). About 2 hours before sunrise on October 27, at about 6:20 a.m. local time, a loud, steady roar was heard. It seemed to be coming from the mountains beyond the head of the bay, but, although the weather was clear, it was too dark to see much there. No shaking was felt on the boat. The roar continued until about 6:50 a.m., at which time a large wave was first seen in the narrow part of the bay, just west of the two arms at the head. The wave at this position appeared as a steep wall of water extending from shore to shore and possibly 100 feet high. On first sighting the wave the men raised the anchor and started the boat toward the Cenotaph Island; an estimated 10 minutes later, when the first wave arrived, the boat had reached a position about 1,300 feet northwest of the cabin, in the water at least 70 feet deep. No lowering or any other unusual dis-

[3] Perroud, P. H., 1957, The solitary wave reflection along a straight vertical wall at oblique incidence: Calif. Univ., (Berkeley), Ph.D. thesis. 93 p.

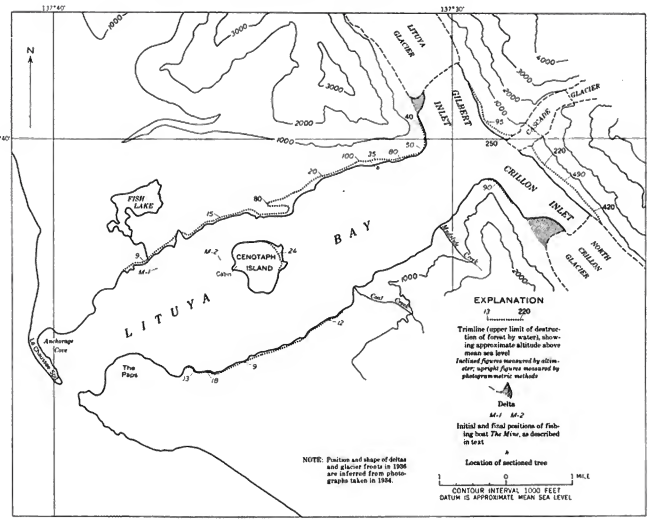

Figure 17. Map of Lituya Bay showing setting and effects of 1936 giant waves.

turbance of the water surface was noticed up to this time.

The first wave raised *The Mine* about 50 feet above normal water level; out of the lee of the island, to the north and south, the wave was possibly 50 feet higher. Immediately after the passing of the first wave the water surface fell below normal level. Huscroft's seining boat, anchored nearby in 48 feet of water, touched bottom. The first wave was followed at estimated 2-minute intervals by the second and third waves, each larger than the preceding one. The water surface receded below normal level after each of these waves also. Smaller waves continued for about half an hour after the third large wave passed. The direction of wave movement was always toward the mouth of the bay; there was no sloshing of the water back and forth in the bay. Floating logs and ice appeared around the boat about half an hour after the third large wave passed.

ACCOUNTS OF BERNARD V. ALLEN AND JAMES HUSCROFT

The more complete of two newspaper articles based on the account of Allen (Alaska Daily Press, 1936) states that he and Huscroft were awakened at 7:00 a.m. on October 27, 1936, by a roar like "the drone of 100 airplanes at low altitude," to find the water already up to their cabin on Cenotaph Island. As seen from a higher, safer point on the island, the water is described by Allen as sweeping over the shore in 3 waves of increasing altitude, at an estimated velocity of about 20 knots (23 miles per hour). In the published account the maximum height of the waves is given at 250 feet, but in a shorter account recorded in the log book of Osa Nolde (Caroline Jensen, written communication, Dec. 23, 1958) Allen stated that the waves reached a height of from 150 to 200 feet. These accounts agree in most respects with the recollections of Fredrickson; in the log book, however, Allen described the weather in

Lituya Bay on October 27, 1936, as cool, with rain, hail, thunder, and lightning.

The observations attributed to Huscroft by Williams (1938) differ from the other accounts in the following respects: Huscroft was preparing breakfast in his cabin at the time the roar was first heard; the water rushed toward the entrance in a single "mountainous tidal wave" followed by an immense "back wave," and then by waves that surged and resurged over the length of the bay a number of times. This was on a morning in the fall of 1936, during a period of unusually heavy rainfall.

EFFECTS OF THE WAVES

The observations attributed to Huscroft by Williams of Lituya Bay by the 1936 waves, as shown on figure 17, was mapped from field observations made by members of U.S. Geological Survey field parties in 1952–53, from single-lens vertical photographs at a scale of about 1:40,000, taken in 1948 by the U.S. Navy, and from an oblique aerial photograph taken in 1937 by Bradford Washburn. The upper limit of wave destruction around much of the inner part of the bay is readily seen on the 1948 vertical aerial photographs due to the difference in tone, texture, and average height of the vegetation growing above and below the trimline. Around the outer part of the bay and on some steep slopes near the head of the bay, however, field examination was required to determine the effects of the 1936 wave. At several places on steep slopes in the upper part of the bay the upper limit of wave destruction was no longer recognizable even in the field, due to the scarcity of large trees. The altitude of the trimline was measured at 14 points by means of a hand-carried altimeter, and at other points using the Kelsh plotter.

The identity of the trimline with the known 1936 wave was confirmed by tree ring counts in two ways: (a) sections cut in 1953 from the largest trees among the three principal types growing below the trimline on the northwest shore near point *h* (fig. 17), showed the following ages: cottonwood, 17 years; alder, 15 years; spruce, 14 years; (b) a section cut from a tree just above the trimline at point *h* (fig. 17, pl. 8*A*), showed, on the side toward the bay, an injury believed to have been caused by debris carried by the waves (pl. 8*B*). The section showed 17 annual growth rings outside the injury. The tree-ring counts were made by R. M. Godman of the Alaska Forest Research Center R. F. Taylor, written communications, Oct. 26 and Nov. 20, 1953). The second method (see page 77), was used to date the oldest known trimline in Lituya Bay. The assumption that the injuries were caused by the waves was convincingly confirmed by the many similarly damaged trees found along the trimline of the 1958 wave (pl. 6*A*).

The trimline of the 1936 waves has a maximum height of 490 feet or more above sea level on the northeast wall of Crillon Inlet (pl. 9*A*). The exact upper limit of wave destruction could not be determined by field examination in this area in 1953, due to the scanty growth of trees on the steep slope and to the possibility that the alinement of trees at the position tentatively mapped as the trimline was accidental. The position mapped in the field was later confirmed by an aerial photograph taken in 1937 by Bradford Washburn, on which the slope below the trimline is virtually bare of vegetation. Destruction of the forest extended to a maximum distance of 2,000 feet from the shoreline in the reentrant northeast of Cenotaph Island. Along a 1-mile segment midway along the bay—the same reference interval cited for the 1958 wave on page 60—the band of destruction on the north and south shores averages 50 feet in width and extends to an average altitude of 10 feet. The total area between the trimlines of the 1936 waves and the high tide shoreline is about 0.8 square mile.

Much of the evidence of destruction by the 1936 waves was obliterated by the wave in 1958. Short segments of the 1936 trimline still remained above the 1958 trimline from Cascade Glacier northwest about 1,500 feet and about 3,000 feet along the northeast wall of Crillon Inlet.

The total destruction of the forest up to a sharp trimline by the 1936 waves is mentioned in all of the available eyewitness accounts and is recorded in photographs taken during the latter part of 1936 by Tom Smith. One of these photographs is reproduced as plate 9*B*. Allen (Alaska Daily Press, 1936) reported that trees and shrubs were cleared away to a maximum altitude of 400 feet. The same article reported that within a few days uprooted trees had drifted along the beach as much as 50 miles south of Lituya Bay. Fredrickson (written communication, Sept. 1958) said that although not many trees were felled in the outer part of the bay, the water flowed for some distance out through the forest. Crabs and clams were found as much as half a mile back from the beach north of the mouth of the bay. According to Fredrickson most of the trees felled by the waves were washed out by the roots but still had roots, limbs and bark attached after the waves had passed. This difference in the damage caused by the 1936 waves, as compared to that caused by the 1958 wave is confirmed also by other eyewitness accounts and by the photographs taken by Smith.

One of the accounts attributed to Allen (Alaska Daily Press, 1936) describes the 1936 "flood" as "cutting a new bank from the soil and stone, and hurling rocks and trees." Williams (1938, p. 18), either from information furnished by Huscroft or from his own observations in 1937, states that "corrasion was complete down to bedrock, including all forest growth and even boulders 10 feet or more in diameter." This was not true in all areas below the trimline, for the photographs taken by Smith show stretches northwest of Cascade Glacier and along the north shore of the bay where many trees were left lying at or near their original positions. Even after the 1958 wave the bedrock was not exposed at many places touched by the 1936 waves. In 1952–53 scarps as much as 4 feet high were seen at a few places along the 1936 trimline; at most places, however, evidence indicated removal of not more than a thin soil layer containing the root systems of the trees. The erosive power of the 1936 waves, even at the head of the bay, was much less than that of the 1958 wave.

The 1936 waves (only the third wave according to Fredrickson and to one account by Allen) washed into Huscroft's cabin on the west shore of Cenotaph Island without causing much damage, but destroyed at least two small frame buildings nearby. Two triangulation stations established by the U.S. Coast and Geodetic Survey in 1926 could not be found in 1940 (U.S. Coast and Geodetic Survey "Lithographic List of Descriptions of Triangulation Stations, Alaska No. 57," not dated). One was on the north shore near Cenotaph Island marked by bronze disks set in boulders and one was on the south shore at Coal Creek marked by concrete blocks. Don Tocher (oral communication, Sept. 2, 1958) suggested that these markers may have been carried away or moved by the 1936 waves.

NATURE AND CAUSE OF THE WAVES

All eyewitness accounts agree that the 1936 waves were preceded by or accompanied by a loud noise, and the two most detailed accounts agree that there were three waves of increasing size in the vicinity of Cenotaph Island, with estimates of maximum height ranging from 100 to 250 feet. The account of one of the men on the boat, in a better position for observation than the men on the island, indicates that the roaring noise from the head of the bay was heard as much as half an hour before the first wave was sighted. This account also indicates that the waves were spaced about 2 minutes apart, and were followed by recession of the water below normal level. One observer on the island estimated the rate of water movement (not necessarily the speed of the waves) at about 23 miles per hour. The time required for the first wave to travel from near the head of the bay to the west side of Cenotaph Island, as estimated by one observer on the boat, gives a speed of about 22 miles per hour. Evidence preserved in the trimlines indicates that the waves were generated at or near the head of Crillon Inlet, where at least one of them dashed up on the valley wall to a height of 490 feet or more. The maximum height of the trimlines near Cenotaph Island is 24 feet, suggesting that the observers' estimates of the height of the waves at this position in the bay is too large.

Possibly significant in the consideration of the origin of the 1936 waves is the fact that they occurred "during a period of unusually heavy rainfall" (Williams, 1938, p. 18). Although two eyewitness accounts differ as to the weather on the day of the waves, the weather records at other places in southeastern Alaska do indicate that the occurrence of these waves was preceded by heavy rainfall (U.S. Weather Bureau, 1938). At the two coastal stations nearest Lituya Bay—Sitka (fig. 14), and Cape St. Elias, about 260 miles northwest of Lituya Bay—precipitation averaged 45 percent above normal for the entire month of October 1936, and 150 percent above normal for the 6-day period preceding October 27. At the three nearest inland stations—Juneau, Haines, and Skagway (fig. 14)—precipitation averaged 42 percent above normal for the month of October, and 111 percent above normal for the 6-day period preceding October 27. These departures are based on weather records through 1957 (U.S. Weather Bureau, 1958).

Allen, in both the published account (Alaska Daily Press, 1936) and in the account related to Nolde (Jensen, Caroline, written communication, Dec. 23, 1958), attributed the 1936 destructive "flood" and waves in Lituya Bay to the sudden draining of an ice-dammed lake in the basin of North Crillon Glacier. Williams (1938, p. 18) presented this hypothesis in detail, showing in a diagram the supposed course followed by the wall of water as it rushed down the surface of the glacier and into the head of Crillon Inlet. Williams (written communication, Mar. 3, 1954) stated that when he visited Lituya Bay after the "flood" (in 1937) he climbed along the sides of the Crillon Glacier and noticed the highwater marks there.

Floods due to the sudden draining of ice-dammed lakes are a frequent and well-known phenomenon in southern Alaska, and it is understandable that this hypothesis was proposed and generally accepted as the cause of the destruction in Lituya Bay in 1936. In papers given orally in 1954 the writer presented evidence opposing the ice-dammed lake hypothesis as follows: North Crillon Glacier is an actively moving,

much crevassed stream of ice that has an average gradient of about 500 feet per mile; its drainage basin, now mapped from vertical aerial photographs and well known from aerial and ground observations (D. L. Rossman, written communication, 1957), lacks any topographic configuration in which a large body of water could be ponded, unless it is a chamber concealed beneath the glacier. An aerial photograph taken by Bradford Washburn in June 1937, less than a year after the supposed "flood," shows no derangement of the surficial moraine patterns on the surface of the lower part of North Crillon Glacier, such as certainly should have occurred if water had flowed down over the surface of the ice as inferred by Williams. The high-water marks mentioned by Williams may have been the scars of fresh rockslides.

Crillon Lake, into which the South Crillon Glacier discharges (pl. 2), has been mentioned also as the lake that drained at the time of the 1936 waves. Seismic investigation by Goldthwait (1936, p. 508), indicates, however, that the bedrock sill on the divide beneath the drainage of North Crillon Glacier into Lituya Bay and South Crillon Glacier into Crillon Lake is about at the same level as the surface of the lake.

The writer, after reviewing the evidence available in 1954, concluded that serious objections could be raised against many of the possible causes of the 1936 waves that had been suggested until then, and that conclusive support could not be marshaled for any of them. Despite the additional evidence obtained since then about the 1936 waves and despite the wealth of information gained from the 1958 wave, this opinion is still held as this report is written. It is necessary therefore, as in 1954, to present several possible causes, some more convincing than others, but none definitely proven.

SUDDEN DRAINING OF AN ICE-DAMMED BODY OF WATER

The writer has already given convincing arguments opposing the hypothesis of surface drainage from an ice-dammed lake in the North Crillon Glacier basin, although this hypothesis perhaps best explains the roaring sound heard before the waves were seen.

Two other variations of this hypothesis warrant consideration: (a) The water could have been ponded in a chamber within or beneath the North Crillon Glacier, or on the divide separating the drainage of the North and South Crillon Glaciers, then suddenly released beneath the glacier or through an ice tunnel below sea level in the tidal front of North Crillon Glacier. This might account for the sudden upwelling immediately in front of the glacier. However it seems unlikely that a chamber of sufficient size could form in a glacier as active as North Crillon. Also, if the chamber were very high in the glacier, as would be required to obtain a substantial hydraulic head, it seems unlikely that the water could have jetted out rapidly enough to generate giant waves. (b) A partly subglacial lake is present now, and existed in 1936 in the trench tributary to Gilbert Inlet, just northwest of the sharp bend in the Lituya Glacier (pl. 2). Aside from the probability of relatively slow drainage from this lake, it is also unlikely that drainage from beneath the Lituya Glacier would set up waves that rose highest at the opposite end of the trough forming the head of Lituya Bay.

FAULT DISPLACEMENT

In 1954, displacement along the Fairweather fault was suggested as a possible cause of the 1936 "flood wave," although evidence of an earthquake was lacking (Miller, 1954). Through the eyewitness accounts that were obtained since then, the date and approximate hour of occurrence of the 1936 waves are now known and it is possible to state definitely that no earthquake was felt in Lituya Bay and that no earthquake with an epicenter near Lituya Bay was recorded at that time on seismographs at Sitka, Alaska, or more distant stations (Tocher, Don, written communication, Aug. 1, 1958). Perry Byerly (oral communication, Jan. 22, 1954) believes that fault displacement sufficiently large to cause the waves could not fail to have caused an earthquake that would have been felt in the bay and recorded at seismographic stations more distant than Sitka. Therefore, it seems that fault displacement can be ruled out as a cause for the 1936 waves.

ROCKSLIDE, AVALANCHE, OR LANDSLIDE

The roaring sound reported by three eyewitnesses to the 1936 waves and said by one of the observers to have come from the head of the bay and to have preceded the waves, suggests a rockslide or avalanche. Some of the observed differences between the 1936 and 1958 waves, particularly the occurrence of three waves of increasing size in 1936, and the much higher velocity of the 1958 wave, might be advanced as an argument against a common origin. On the other hand, these differences in the wave patterns might be due to differences in the location of the sliding or falling rock mass and the manner in which it entered the water. This was demonstrated in 1934 in Tafjord, Norway, where a rockfall generated waves of about the same height and velocity as the 1936 waves in Lituya Bay, and where three waves of increasing height were observed (Kaldhol and Kolderup, 1937; table 1, this report). Three waves reportedly were generated also by two other landslides into Norwegian fiords, Lang-

fjord in 1746 and Norddalsfjord in 1938 (Jørstad, 1956, p. 326, 330–331).

By analogy with the 1958 wave, a falling mass that caused the 1936 waves in Lituya Bay should have come from the southwest wall of Crillon Inlet, opposite the high point on the trimline. None of the previously published eyewitness accounts mention any evidence that a large mass of rock or ice had fallen into Lituya Bay at the time of the 1936 waves, and Fredrickson (written communication, Sept. 1958) states that he did not notice any such evidence when he went to the head of the bay a short time after the waves had occurred. Comparison of the trilens photographs of Lituya Bay taken in 1929 by the U.S. Navy with the 1948 vertical photographs indicate that sliding had occurred on the valley wall above and just south of the front of North Crillon Glacier at some time between 1929 and 1948. This slide scar, however, is directly above the delta that formed in front of North Crillon Glacier before 1929, and some evidence of a large slide in 1936 should have been preserved on the delta and should be visible in the 1948 photographs. The 1929 and 1948 photographs show scattered large blocks of rock on the delta surface, also small talus cones along the base of the cliff, suggesting that sliding in this area has taken place frequently but in small increments.

Elsewhere on both walls of Crillon Inlet the correspondence between the 1929 and 1948 photographs is so close, even as to individual trees, gulleys, and other distinctive patterns, as to definitely eliminate the possibility that a large slide occurred during this interval. Small fields of permanent snow and ice are on the northeast wall of Crillon Inlet above 3,400 feet altitude, but these too show close correspondence in shape and size on photographs taken by Bradford Washburn in 1934 and 1937, eliminating the possibility of a large avalanche. There is a possibility that a rockslide or avalanche of ice fell on the North Crillon Glacier causing movement that was transmitted through the glacier to the tidal front. This possibility may be eliminated at least for the lower 2 miles of the glacier by inspection of the 1937 photographs; it seems unlikely that any movement higher on the glacier would be transmitted to the front.

The photographs indicate the occurrence of small rockslides into Gilbert Inlet from both the southwest and northeast sides, and into Lituya Bay between Mudslide Creek and Crillon Inlet, at some time between 1929 and 1948, but these locations are all incompatible with the trimline pattern of the 1936 waves. If the writer's interpretations of the photographs are correct, and falling or sliding of a mass of a size greater than a few thousand cubic yards into Crillon Inlet is required to generate the 1936 waves, then landsliding or avalanching may virtually be eliminated as a possible cause.

SUBMARINE SLIDING

Submarine slides (submarine "landslides") have long been included among two or more hypothetical causes of tsunamis in the oceans. For example, Gutenberg (1939), and Shepard, Macdonald and Cox (1950, p. 394–395), offer opposing viewpoints. The tsunami associated with the 1908 earthquake in the Straits of Messina has been attributed to a turbidity current originating in a submarine slump (Heezen, 1957). Recent laboratory experimental work indicates that submarine slides are capable of generating tsunamis (Wiegel, 1955).

Soundings in Crillon and Gilbert Inlets indicate slopes of as much as 28°, through vertical distances of nearly 500 feet. Unconsolidated material was available in 1936 in the deltas built out from the fronts of both North Crillon and Lituya Glaciers, and may have been present in substantial thickness at other places around the head of the bay. Submarine slides could also have occurred in bedrock. Perhaps one of the most attractive aspects of submarine sliding as a possible cause of the 1936 waves is that it cannot be definitely disproved because the evidence, if any, is hidden beneath the bay. Considering the magnitude of the slopes available and the probability that a large submarine slide would involve material at least partly above water, submarine sliding seems unlikely as the cause of the 1936 waves, however. Unless two or more slides occurred in close succession, or the waves were reflected at the head of the bay, it is difficult to account for the observed fact that the third wave, rather than the first, was the largest.

MOVEMENT OF A TIDAL GLACIER FRONT

The trimlines at the head of Lituya Bay show clearly that at least the largest of the 1936 waves was generated at or near the tidal front of North Crillon Glacier, and attained maximum height on the northeast wall of Crillon Inlet within 3,500 feet of the glacier front. This evidence, reinforced by the known generation of waves at the fronts of other glaciers that discharge into water, lends strong support to some kind of movement of the Crillon Glacier front as the cause of the 1936 waves. Three types of movement must be considered: (a) calving of ice from the subaerial part of a glacier front into the water; (b) calving and sudden surfacing of ice from a submarine projection of a glacier front; and (c) almost instantaneous forward movement of a glacier front. One aspect of the 1936 wave pattern, the occurrence of three waves of increasing

A. Trees washed out and turned upslope by water at altitude of 1,720 feet. Small slides occurred on steep slope at right during the 1958 earthquake, but destruction of forest in middle and lower left part of view is due mainly to water

B. West side of spur; note washed appearance of bedrock at lower right, in contrast to slide area just below trimline at *t*. Height of view, from bay at lower left to upper right corner, is about 1,200 feet

SPUR SOUTHWEST OF GILBERT INLET, AUGUST 1958

A North shore of Lituya Bay between Cenotaph Island and Gilbert Inlet, showing forests of different ages in zone denuded by 1936 giant waves (shore to *h*), in upper part of zone denuded by giant wave about 1874 (*h* to *j*), in upper part of zone denuded by giant wave in 1853 or 1854 (*j* to *k*), in upper part of recently glaciated zone (*k* to *m*), and above lateral moraine at *m*. Photograph taken in 1953

B. Section cut in 1953 from spruce tree growing just above trimline of 1936 giant waves (loc. *h*, in *A* and in fig. 17). There are 17 growth rings outside injury on right

A. Crillon Inlet and head of Lituya Bay in 1952; Trimline begins above tidal front of North Crillon Glacier; altitude 490 feet at *i*. Front of Cascade Glacier at left margin

B. Destruction to an altitude of about 90 feet at head of Lituya Bay, half a mile northwest of Cascade Glacier. Photograph by Tom Smith in 1936

DESTRUCTION OF FOREST BY 1936 GIANT WAVES

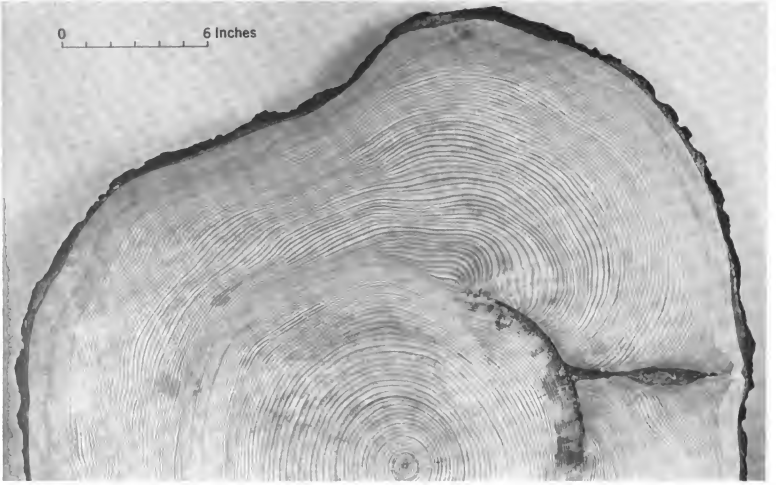

SECTION CUT IN 1953 FROM SPRUCE TREE GROWING JUST ABOVE TRIMLINE OF 1853-54 GIANT WAVE

There are 100 growth rings outside injury on right. Locality (L), on figure 19

height in the vicinity of Cenotaph Island, could be explained either by repeated movements of any of these three types, or by interference, refraction or reflection of waves near the point of generation at the head of the bay. Calving from an ice front could have caused the roaring sound reported by eyewitnesses, although it seems unlikely that calving could have occurred continuously for as much as half an hour before the first wave was sighted.

No photographs showing the North Crillon Glacier front shortly before or shortly after the occurrence of the 1936 waves are available, but oblique aerial photographs taken by Bradford Washburn in the summer of 1934 and in June 1937 show little change in the position and configuration of the northeast half of the front. The delta and southwest half of the front on Crillon Inlet are not shown on the 1937 photographs. Based on the photographs taken in 1934, and assuming little change in the following 2 years, the tidal front of North Crillon Glacier at a time just preceding the occurrence of the 1936 waves was a nearly vertical wall of ice about 2,700 feet long and 200 to 300 feet above water level, extending across about half of the total width of Crillon Inlet (fig. 17). If the ice front extended to the bottom of the inlet, as seems likely, its maximum height below water level was about 290 feet.

Calving of subaerial ice into water has been observed at the fronts of many glaciers discharging into lakes, rivers, bays, and even into the open ocean in Alaska, as well as in many other parts of the world. From observation or indirect evidence such calving has formed waves capable of eroding as much as 5 feet above high tide a mile or more from the ice front (Tarr, 1909, p. 33–34), but according to available data no waves even approaching the magnitude of the 1936 waves in Lituya Bay have resulted from glacier calving in Alaska. If calving were the cause of the giant waves in 1936, such waves should occur with greater frequency, not only in Lituya Bay but also at the fronts of many other tidal glaciers in Alaska. This would be true unless, as suggested by C. C. Bates (written communication, Apr. 7, 1955), simultaneous calving from two or more glacier fronts is a further requirement.

In the course of the model study of Lituya Bay, R. L. Wiegel and Don Tocher found that rotational fall of a partly submerged weight with a flat face, simulating the Crillon Glacier tidal front, formed wave traces that compare closely in configuration to the trimlines on the walls of Crillon Inlet. The maximum height reached by the wave in the model, however, was about equal to the height of the face of the weight above water level. This gives some basis for doubting that ice falling from the Crillon Glacier front could have raised a wave to a height much greater than the height of the front. C. C. Bates (written communication, Apr. 7, 1955) suggested that although ice falling from the front of North Crillon Glacier might provide only about 10 percent of the necessary volume increment, the remainder of the rise indicated by the trimline on the northeast shore of Crillon Inlet might come from uprush or local refraction effects.

Submarine calving from the glacier front was suggested as a possible cause of the 1936 waves by W. O. Field, Jr. (written communication, Dec. 5, 1952). Evidence of ice projecting below water level as much as 1,000 feet beyond the subaerial part of glacier fronts has been reported for glaciers in the Yakutat Bay area (Russell, 1891, p. 101–102; Tarr, 1909, p. 31–32). Field states that waves 25 feet or more in height are formed by calving of projecting submarine ice masses at the front of Muir Glacier in Glacier Bay. The configuration of the submarine parts of the tidal ice fronts in Lituya Bay is not known. The possibility that the deltas in front of the Lituya Glacier may have been underlain by ice was mentioned on page 60. In the few hours that either or both the North Crillon and Lituya Glacier fronts were in sight during the 1952, 1953, and 1958 field investigations, the writer did not see any calving of submarine ice. The appearance of the delta in front of North Crillon Glacier in the 1948 vertical photographs does not give evidence of disturbance by the sudden rise of an ice mass beneath it, and the remaining tidal part of the glacial front seems to be too small to provide a mass of sufficient size to generate the 1936 waves.

Slippage of an ice mass over its floor is generally accepted by glaciologists as a major mechanism of movement for glaciers on slopes (Sharp, 1954, p. 826). However, an instantaneous advance of a glacier front of more than a few inches has not been proven. Prospectors in Disenchantment Bay reported that during the largest of the Yakutat Bay earthquake shocks, on September 10, 1899, the tidal front of the Hubbard Glacier advanced or was thrust forward from one-half to three-quarters of a mile, but Tarr and Martin (1912, p. 16) believed this to be an erroneous interpretation of the enormous calving of ice from the glacier front. It seems likely that forward movement of the Crillon Glacier front of a few feet or even a few tens of feet would be required to raise a wave to the height indicated by the 1936 trimline in Crillon Inlet. Such movement of the glacier front should have disrupted the surface of the glacier for some distance above the front to such an extent that the changes should be evident on photographs taken in 1937 and later. An oblique aerial photograph taken by Bradford Wash-

burn in June 1937 shows no unusual crevassing or disruption of the surficial moraine patterns on North Crillon Glacier.

TSUNAMI IN THE OCEAN

Perry Byerly and J. P. Eaton (oral communication, Jan. 22, 1954) offered the suggestion that wave motion from a tsunami generated at sea might be transmitted either through the narrow entrance or through the spit at the mouth of Lituya Bay, causing a seiche wave or some other type to form inside the bay. In further support of this suggestion Byerly (written communication, Feb. 1, 1954) called attention to the following statement by McNown (1952, p. 163): "It has been amply proved that the motion produced in a port can have an amplitude not only equal to but even a number of times greater than the amplitude of the wave that produces it. Furthermore, from theoretical considerations, this amplitude can occur equally well with an entrance width that is extremely small."

According to tide-gage records (Neuman, 1938, p. 26) no tsunami occurred in the northeastern Pacific Ocean in October 1936. It is difficult, also, to understand how wave motion introduced at the mouth of Lituya Bay could have been transmitted without any obvious surface effects to the head of the bay, there to be amplified into three giant waves that traveled out the bay at high velocity.

OTHER POSSIBLE CAUSES

For the sake of completeness several other agents capable of generating waves are mentioned, although there is little or no evidence to recommend them as possible causes of the 1936 waves in Lituya Bay. Submarine volcanic activity is known to have given rise to large tsunamis in the sea, as, for example, the destruction of Krakatoa in 1883 (Williams, 1941, p. 255–256, 261). Waves caused by tidal action and by wind are well known. As examples of water waves set in motion by air waves, Press (1956) cited a sea wave with a 2-foot amplitude that followed the Krakatoa explosion, and a 10-foot wave at Chicago in 1954. Finally, Olaf Holtedahl (oral communication, 1957) suggested that a falling meteorite be added to the list of possible causes.

WAVES BETWEEN 1854 AND 1916

EYEWITNESS ACCOUNTS

When the writer first visited Lituya Bay in 1952 stories of "floods" were heard from several fishermen who anchored their boats in the bay. One described catastrophic floods caused by breaking of a glacial lake near the head of the bay in 1890 and again in 1928. Another mentioned a flood about 1899 that destroyed a native village and a fish saltery near the mouth of the bay, and a second flood about 1928, when Huscroft was living on Cenotaph Island. Others reported that both floods occurred after sharp earthquakes. It is clear now that these accounts referred at least in part to the 1936 and 1853–54 waves, but the mention of dates 1890–99, of earthquakes, and of a saltery near the mouth of the bay suggest the occurrence of another wave of intermediate age. In 1958 James Betts of Angoon, Alaska reported that his grandfather had experienced a flood or wave in Lituya Bay in 1899 (Tom Smith, oral communication, Aug. 1958). The writer has been unable to obtain further information on this report.

OTHER EVIDENCE

Possible evidence for the occurrence of at least one giant wave in Lituya Bay between the 1853–54 wave and the 1936 waves was first noticed during the 1953 field investigation, on the north shore near the mouth of the creek draining from Fish Lake. At this locality, in a narrow belt midway between the 1936 and 1853–54 trimlines, the spruce and hemlock trees appeared to be a little smaller in average size than in the forest adjoining and just below the 1853–54 trimline. This impression was not tested at the time by sectioning the trees. In the course of later study of ground photographs taken in 1917, photographs of the north shore of the bay between Cenotaph Island and Gilbert Inlet (J. B. Mertie, nos. 604, 605, 619, and 620, U.S. Geological Survey Photolibrary, Denver) showed not only the 1853–54 trimline but also, in the interval about 0.8 to 1.8 miles west of Gilbert Inlet, a probable lower trimline that had about the same height and configuration as the 1936 trimline in the same area. This segment can be identified with certainty as a trimline on a photograph taken in 1894 by a Canadian Boundary Survey party (McArthur no. 128; print loaned by W. O. Field, Jr., Mar. 3, 1959). The lower trimline in this area shows faintly on the 1929 trilens photographs and on these can be traced westward along the north shore, with decreasing certainty, to the locality of the field observation near Fish Lake. The eastward extent of this trimline near Gilbert Inlet is also uncertain. It probably falls to or near the shoreline, as shown on figure 18, but the photograph taken in 1894 suggests that it may rise eastward to or nearly to the 1853–54 trimline in this area.

Possible trimlines that may be at least in part younger than the definitely identified trimline on the north shore are shown in ground photographs taken in 1916 by Trevor Davis (oral communication, July 1958) near Cascade Glacier and on the spurs southwest of Gilbert and Crillon Inlets, and in photographs of the north shore of Anchorage Cove taken in 1917 (Mertie nos. 98, 99). The supposed trimline at Cas-

cade Glacier is recognizable on the 1929 trilens photographs and can be projected about a mile to the southeast as an irregular lower limit of scattered clumps and groves of spruce trees. A few scattered spruce trees of about the same size are standing below this line, however. None of these supposed trimlines shown on 1916 and later photographs can be recognized on the few copies of 1894 photographs that are available, but because of incomplete coverage and the poor quality of some of the prints, their existence at that time cannot be disproved.

DATES

The lower trimline definitely identified in a photograph of the north shore of Lituya Bay taken in 1894 indicates that at least one giant wave occurred before this date but later than the 1853–54 wave. The stage of vegetation growth below the lower trimline, as shown on the photograph, suggests that the trimline was formed about midway in the interval 1854 to 1894. Hence the "evidence of flooding and washing" noted in 1874 by Dall (1883, p. 203) may have resulted from this wave.

The other possible trimlines shown on 1916–17 photographs, on the basis of the previously mentioned unsubstantiated eyewitness account and on the basis of the stage of vegetation growth, are attributed tentatively to a wave occurring in 1899. The occurrence during that year of the great Yakutat Bay earthquakes and the report of a great amount of drift timber and muddy water in the ocean between Cape Fairweather and Yakutat 2 days after the largest of the earthquake shocks (Tarr and Martin, 1912, p. 79) are further evidence for this date. The absence of any reference to Lituya Bay among the many reports of those who experienced the Yakutat Bay earthquakes probably means either that no report was received by Tarr and Martin (1912, p. 65–68) or that no one was in Lituya Bay at that time, because the shocks were felt throughout a large area in southern Alaska and adjacent Canada.

EFFECTS OF THE WAVES

The trimlines plotted on figure 18 were reconstructed mainly from the 1916 photographs by Davis and the 1929 trilens photographs. Altitudes on the trimlines were obtained by transferring points by inspection to the 1948 vertical photographs, from which the approximate height above water level was then estimated or measured photogrammetrically. Trimlines formed by two different waves were tentatively identified. The older wave apparently destroyed all or nearly all vegetation up to a sharp trimline for a distance of 4 miles or more along the north shore. A maximum altitude of 80 feet and a maximum width of 2,100 feet back from the high-tide line were measured for this trimline. The younger wave destroyed vegetation to a maximum altitude of about 200 feet on the northeast shore of Crillon Inlet and to lesser heights on the spurs southwest of Gilbert and Crillon Inlets, and possibly to a height of a few feet on the north shore of Anchorage Cove. On the south shore of Lituya Bay, west of Mudslide Creek, destruction of vegetation by either wave, if any, must have been limited to a narrow zone bordering the beach. The total area of substantial destruction of vegetation below all of the tentatively identified trimlines in less than 0.4 square mile. Most of the evidence of destruction by the waves between 1854 and 1916 was removed by the 1936 wave and any remaining evidence was wiped out by the 1958 wave.

NATURE AND CAUSE OF THE WAVES

Photographs taken in 1894 by McArthur (nos. 105A, 128) show fresh, bare surfaces on the upper slopes of the northeast wall of Gilbert Inlet and the valley of Mudslide Creek, suggesting that slides had occurred in these areas not long before. It is doubtful that the older wave was generated by a slide from the northeast wall of Gilbert Inlet, because McArthur's photographs do not show a trimline on the opposite shore of Gilbert Inlet. By analogy with the 1958 wave, destruction of vegetation should have been greatest there. A slide in the valley of Mudslide Creek could account for the maximum known destruction obliquely opposite on the north shore of the bay, and also for the absence of a conspicuous trimline in the inlets at the head of the bay.

The trimline of the wave inferred to have occurred about 1899, as reconstructed from photographs, compares most closely in magnitude and configuration with the trimline of the 1936 waves. It seems likely, therefore, that the 1899 (?) wave was generated in Crillon Inlet, possibly by the same unknown mechanism that caused the 1936 waves. However, if a wave did occur at the time of one of the great earthquake shocks in 1899, displacement along the Fairweather fault warrants consideration as a possible cause. By analogy with the 1958 wave, a rockslide into Crillon Inlet must also be considered. St. Amand (1957, p. 1357–59) suggested that at least one of the earthquakes in 1899 resulted from movement on the Fairweather fault. Evidence in support of this suggestion was found by Tocher and Miller (1959) after the 1958 earthquake. New surface breaks were seen from the air near the scarps on Nunatak Fiord described by Tarr and Martin (1912, p. 37-40); along the Fairweather fault southeast of Lituya Bay

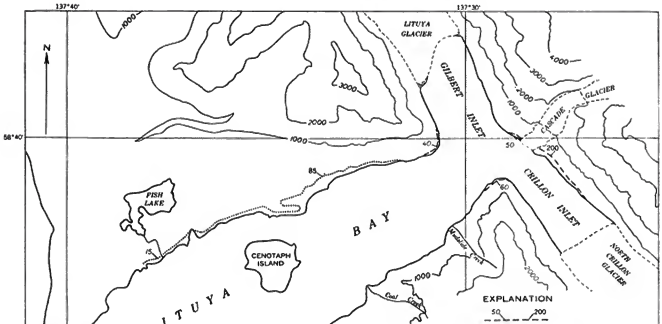

FIGURE 18.—Map of Lituya Bay, showing trimlines of one or more giant waves that occurred between 1854 and 1916.

much of the new breakage had taken place along old scarps. The few oblique photographs taken at the head of Lituya Bay at the turn of the century are not adequate to either prove or disprove the occurrence of a rockslide in Crillon Inlet.

WAVE IN 1853 OR 1854

EYEWITNESS ACCOUNTS

Williams (1938, p. 19) related the formation of the oldest trimline in Lituya Bay to an old Indian story about the catastrophic destruction of a village near the entrance. The source of this legend was not cited. Emmons (1911, p. 294–298) and de Laguna (1953, p. 55) were told the story of the meeting between La Perouse and the Tlingit in Lituya Bay in 1786 by natives living at Yakutat, near Juneau, and at Angoon. Emmons (1911, p. 295) also recorded the Tlingit legend about a monster who dwelt in Lituya Bay near the entrance and who, with his assistant, caused tidal waves by grasping the surface of the water and shaking it as if it were a sheet. De Laguna (written communication, Nov. 19, 1957) was told a story about a flood in Dry Bay that killed a great many people, possibly between 1850 and 1860, and also the story of a village near Dry Bay that was abandoned about 1850 because eight canoe loads of men from the village were lost in Lituya Bay when their canoes tipped over. W. A. Soboleff (oral communication, June 7, 1958) was unable to find any specific information about Lituya Bay among the people of Tlingit origin in the Juneau area, other than that the Indians had left the bay for an unknown reason and at an unknown date. These stories may indeed refer to the giant wave that formed a trimline in Lituya Bay in 1853 or 1854, but some of the stories might also refer to incidents related to the treacherous tidal current in the entrance or to an earlier or later wave.

None of these stories are of any value for determining the nature and cause of the 1853–54 wave or for dating the wave more accurately.

OTHER EVIDENCE

The only positive evidence now known for the occurrence of a giant wave in Lituya Bay in 1853–54—the destruction of vegetation along the shores—is clearly recorded on many photographs taken between 1894 and 1954. The evidence was also studied in the field in 1952–53. Only two segments of the 1853–54 trimline, totaling about a mile in length, remain on the north shore of the bay since the 1958 wave.

DATE

An approximate date of late 1853 or early 1854 for the occurrence of the oldest known giant wave in Lituya Bay was obtained from a tree ring count using the second method described on page 69. A section cut by Rossman and Plafker from a large spruce tree growing just above the oldest trimline at point *L* on figure 19 showed an injury on the side toward the bay (pl. 10). According to R. L. Godman of the Alaska Forest Research Center (R. F. Taylor, written communication, Oct. 26, 1953) the injury occurred after the end of the 1853 growing season and before the beginning of the 1854 growing season, or between mid-August and the early part of May. Rossman and Plafker estimated the age of the largest spruce tree seen in the forest below the trimline at this site in 1953 to be about 92 years.

EFFECTS OF THE WAVE

The trimline formed by the 1853-54 wave, as shown on figure 19, was mapped from field observations in 1952 and 1953, and from the single-lens verticle photographs taken in 1948. The altitude of the trimline was measured on the ground at 12 points with an altimeter, and at other points with a Kelsh plotter. Destruction of the forest by the 1853-54 wave seems to have been complete up to a sharp trimline that is easily seen on the 1948 vertical photographs and on oblique photographs (pl. 8*A*) of the north shore west of Gilbert Inlet, around Cenotaph Island, and from Coal Creek west on the south shore. These trimlines seem to intersect the beach about 1½ miles inside the entrance, on the north shore, and about 2 miles inside the entrance on the south shore. A trimline to a maximum height of 18 feet was identified by field examination in 1953 for a short distance along the steep slope north of The Paps. In 1953, along both shores in the outer part of the bay, and on La Chaussee Spit, spruce trees older than 100 years were found growing to the edge of the forest above the beach.

Field examination in 1953 indicated that on the spur southwest of Gilbert Inlet the trimline sloped down, and also became gradually less well defined toward the east. This is confirmed by McArthur's photograph (no. 128), taken in 1894. No evidence of the trimline was found, either in the field or on the photographs, along the walls of Gilbert and Crillon Inlets or on the south shore between Crillon Inlet and Mudslide Creek. This could be due to the scarcity of large trees on these steep slopes, but probably the wave had little effect at the head of the bay or along the south shore at Mudslide Creek.

Destruction of the forest on the shores of Lituya Bay by the giant wave in 1853 or 1854 extended to a maximum height of 395 feet above mean sea level and to a maximum horizontal distance of 2,500 feet inland from the high-tide shoreline, a total area of at least 1 square mile. In the 1-mile long segment used as a reference for comparison with the other waves (p. 60, 69) the band of destruction on the north and south shores averages about 620 feet in width and about 80 feet in altitude. Scarps as much as 25 feet high were seen at a few places along the trimline of the 1853–54 wave. These scarps, plus the evidence of the effects on the forest, indicate that the erosive power of the giant wave in 1853 or 1854 was comparable to that of the 1958 wave, although it did not affect as large an area. Part of the trees remained standing at the sites of the native dwellings shown at the shore near the entrance of the bay on the map of La Perouse (1798, opposite p. 146). However, the water almost certainly inundated these sites and may have destroyed the village, as indicated by native legend and by the observations in 1874 by Dall (1883, p. 203).

NATURE AND CAUSE OF THE WAVE

At the present time (1959) the only basis for speculation on the nature and cause of the 1853–54 wave is a comparison of its effects on the vegetation with the effects of the two most recent giant waves in Lituya Bay. In extent and thoroughness of its destruction, the 1853–54 wave compares most closely with the 1958 wave. From the configuration of its trimline the 1853–54 wave probably was generated at or near the head of the bay, but either at a different point or by a different cause than the 1958 wave.

A rockslide from the steep wall on the south side of Lituya Bay at the present position of or just east of Mudslide Creek (fig. 19) seemingly would best account for the maximum known height of destruction almost directly opposite on the north shore of the bay. It would also account for the minimum destruction or total lack of destruction of vegetation on the south

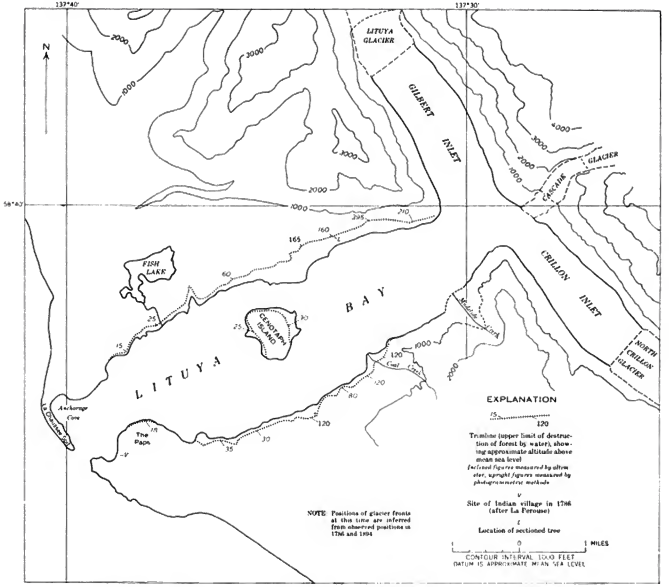

FIGURE 19.—Map of Lituya Bay showing setting and effects of giant wave that occurred in 1853 or 1854.

shore in the vicinity of Mudslide Creek, in Gilbert Inlet and in Crillon Inlet. The valley of Mudslide Creek, and particularly the east wall of the valley, is an area of active sliding at the present time, and sliding in the past probably played an important part in the formation of the valley. Photographs taken in 1894 by McArthur (nos. 105A and 128) show that the shape of the Mudslide Creek valley was similar to that shown on the 1948 vertical photographs, so any major sliding must have occurred before 1894. The sketch map of Lituya Bay made in 1874 and issued in 1875 as U.S. Coast Survey Chart 742 is almost identical to the La Perouse map in the part of the bay east of Cenotaph Island, indicating that little or no resurveying was done in the upper part of the bay. Hence a comparison of these maps gives no information on the possible occurrence of a large slide at Mudslide Creek between 1786 and 1874. The modern U.S. Coast and Geodetic Survey chart of Lituya Bay (no. 8505) shows a more pronounced bulge in the shoreline at Mudslide Creek than does the La Perouse map. The difference is slight and, in view of the small scale and questionable accuracy of the La Perouse map, only suggests but does not prove that a large slide occurred there sometime after 1786.

No major earthquakes in the region adjoining Lituya Bay are known to have been reported between 1847 (Dall, 1870, p. 342) and 1862 or 1863 (Musketov and

Orlov, 1893, p. 349, 386). The paucity of records for this period in Alaska, however, cannot be taken as proof that no earthquake occurred in conjunction with the 1853–54 wave in Lituya Bay.

POSSIBILITY OF FUTURE WAVES

Giant waves have occurred in Lituya Bay at least four times, and possibly five times within 105 years, or on the average, once every 21 to 26 years. Hence, based on the historical record only, the odds against one of these waves occurring on any single day spent in the bay are comfortably large (about 9,000 to 1). The writer believes that the odds may be much less than this at the present time because of a larger than average potential for slides resulting from (a) shaking and ground breakage associated with the 1958 earthquake; (b) removal of vegetation and unconsolidated deposits by the 1958 wave. Areas especially susceptible to sliding are outlined in figure 20. The rockslide on the northeast wall of Gilbert Inlet in 1958 created new unstable slopes at the head of the slide scar and along its southeast margin. Planes of weakness parallel to bedding or schistosity in the upper part of the 1958 rockslide area continue southeastward toward Cascade Glacier; Tocher, in August 1958 (oral communication) from the air noticed open fractures along some of these planes just southeast of the slide scar. In the field during the same month the writer found many open fractures above and generally parallel to steep slopes at altitudes ranging from 1,700 to 2,500 feet along the crests of the spurs southwest of Gilbert and Crillon Inlets. Destruction of vegetation by the 1958 wave will result in accelerated erosion of unconsolidated deposits by running water for some time to come, and therefore in further undermining of steep and unstable slopes.

Further movement along the Fairweather fault, particularly of the magnitude of the 1958 movement, could cause new slides from steep slopes around the head of Lituya Bay. Slides could also be started by freezing and thawing of water in the open fractures during the spring or fall, by unusually heavy rainfall, or merely by rock or soil failure without any triggering mechanism. In addition to the subaerial slides there may be at least one other mechanism, not yet identified, that has generated one or more giant waves in Lituya Bay in the past and might do so again in the future.

Whatever the odds against their occurring during any given short period of time, the giant waves probably will occur in Lituya Bay in the future; this potential danger should be known to those who enter the bay. Steady increase in the permanent and transient population of Alaska, as well as the development of the Glacier Bay National Monument, under normal circumstances, would result in steadily increasing use of Lituya Bay as a harbor for small boats and landing place for amphibious aircraft and, eventually, in permanent settlement. Before the 1958 wave the U.S. National Park Service was considering Lituya Bay as a site for a ranger station, for, despite the then known hazard of the entrance and the somewhat vague history of earlier waves, the bay is advantageously located on the coastline of the Glacier Bay National Monument and affords the only protected anchorage for many miles in either direction along the coast (Mitchell, L. J., written communication, Mar. 13, 1959). The giant waves thus have increased the difficulty of providing safe access to this part of the National Monument, but at the same time they have greatly enhanced the interest in the bay and its value for recreational and scientific purposes.

SUMMARY AND CONCLUSIONS

A rockslide triggered either by movement on the Fairweather fault or the accompanying shaking, on July 9, 1958 plunged into Gilbert Inlet, causing water to surge over the opposite wall of the inlet to an altitude of about 1,740 feet and generating a gravity wave that moved out from the head of Lituya Bay at a speed of about 100 miles per hour. Field investigation indicates that this surge and the giant water wave were primarily responsible for the nearly total destruction of the forest up to a sharp trimline that has a maximum altitude of about 1,720 feet opposite the rockslide and extends along the shores of the bay to the mouth. This conclusion is supported by R. L. Wiegel's study of a model of Lituya Bay and his calculations from existing theory and data on wave hydraulics.

The giant waves that rose to a maximum height of 490 feet in Lituya Bay on October 27, 1936 were generated in Crillon Inlet by some disturbance other than the previously reported flood of water from an ice-dammed lake in the basin of North Crillon Glacier. The waves of 1936 were not associated with an earthquake, and evidence is lacking that a large subaerial slide into Crillon Inlet caused them. Among other possible causes, movement of a tidal glacier front or submarine sliding seem the most plausible, but none are conclusively supported by the information at hand. Further study of a hydraulic model of Lituya Bay will probably be the most fruitful method of solving the problem of the origin of the 1936 waves. However, the necessary clue or clues may be found in contemporary photographs or observations not available in the present investigation, or in the literature on similar waves elsewhere.

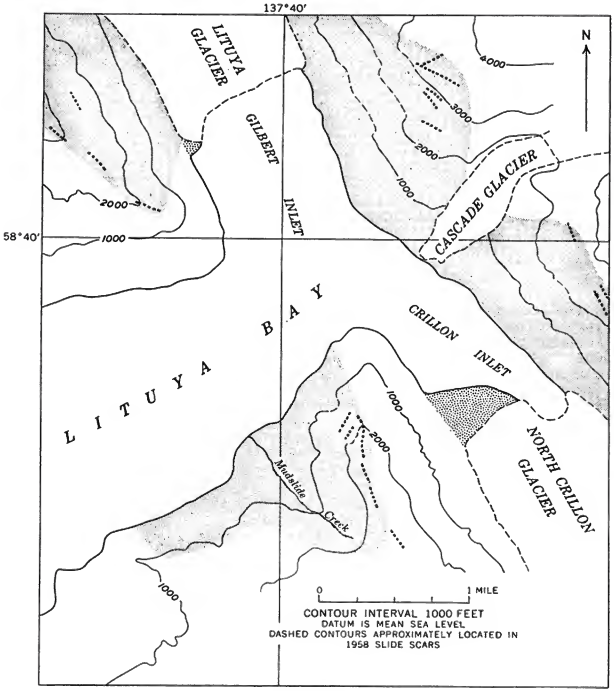

EXPLANATION

Open fractures seen or photographed in August 1958

Areas belived to be especially susceptible to sliding

Delta

FIGURE 20.—Map of head of Lituya Bay, showing open fractures and areas believed to be especially susceptible to sliding.

Unsubstantiated oral accounts, and a possible trimline shown on photographs taken in 1916 and later, suggest that a wave 200 feet high may have been generated by a disturbance in Crillon Inlet at the time of one of the great earthquakes in 1899.

A trimline having a maximum altitude of about 80 feet on the north shore of Lituya Bay, shown clearly in photographs taken in 1894, records a giant wave that occurred after 1854 and is tentatively dated about 1874. The configuration of the trimline, as partly reconstructed from photographs, suggests sliding in the vicinity of Mudslide Creek as the cause of this wave.

A trimline having a maximum height of 395 feet on the north shore records the earliest known giant wave in Lituya Bay. Based on a tree-ring count, this wave occurred in late 1853 or early 1854. Configuration of the trimline suggests sliding in the vicinity of Mudslide Creek as the cause. No major earthquakes are known to have occurred in southern Alaska during 1853 or 1854.

The fact that giant waves have occurred more frequently in Lituya Bay than in other seemingly similar bays may be due to the following factors in combination: (a) Presence of an active fault under water at the head of the bay; (b) presence of recently glaciated, steep slopes on highly fractured and sheared rocks along the fault zone; (c) presence of deep water immediately below the steep slopes in and near the fault zone; (d) heavy rainfall and frequent freezing and thawing. The glaciers discharging into the head of the bay along the fault zone may also contribute to generation of the waves, but little direct evidence is available now to support this.

The potential for generation of localized but enormously destructive waves by the falling or sliding of solid masses into water deserves wider recognition by geologists, by engineers concerned with the planning of dams and reservoirs, and by anyone concerned with the safety or permanency of structures or equipment near the water level in lakes or bays that adjoin steep slopes. Many of the fiordlike inland waterways of southeastern Alaska, for example, have the necessary topographic and hydrographic requirements and seemingly are susceptible to the occurrence of localized waves comparable in magnitude to those in Lituya Bay, although much less frequently than in Lituya Bay.

The 1958 giant wave in Lituya Bay affords geologists and biologists an example of catastrophic destruction of plant and animal life, and also an opportunity to study the rate and nature of reestablishment of marine life in the intertidal and nearshore zones, and of plant life in the recently denuded zone above the shoreline.

REFERENCES CITED

Alaska Daily Press, 1936, 250-foot wave sweeps shore of Lituya Bay; 4 men endangered: Alaska Daily Press, Juneau, v. 39, no. 2437 (Nov. 5), p. 5.

Alaska Sportsman, 1958, Where hell breaks loose: Alaska Sportsman, Juneau, v. 24, no. 10 (October), p. 6–10.

Alaska Weekly, 1936, Wall of water sweeps Lituya; bay region hit by wave 250 feet high; much damage reported: Alaska Weekly, Seattle, Wash.; v. 39, no. 35 (Nov. 27), p. 3.

Bancroft, H. H., 1886, History of Alaska: San Francisco, Calif., 775 p.

Boursin, Henry, 1893, Mining and other industries of Alaska, *in* Report on population and resources of Alaska at the eleventh census, 1890: Washington, U.S. Government Printing Office, p. 229–241.

Brazee, R. J., and Jordan, J. N., 1958, Preliminary notes on southeastern Alaska earthquake: Earthquake Notes, v. 29, no. 3, p. 36–40.

Brigham, A. P., 1906, A Norwegian landslip: Geog. Soc. Bull. Philadelphia, v. 4, p. 292–296.

Buddington, A. F., and Chapin, Theodore, 1929, Geology and mineral deposits of southeastern Alaska: U.S. Geol. Survey Bull. 800, 398 p.

Bugge, Arne, 1937, Fjellskred fra topografisk og geologisk synspunkt: Norsk geog. tidsskr., Oslo, v. 6, no. 6, p. 342–360, 14 figs.

Carpe, Allen, 1931, The conquest of Mount Fairweather: London, Alpine Jour., v. 43, p. 221–231.

Daily Alaska Empire, 1958a, Earthquake kills three; Idaho Inlet couple missing; comparable to 'Frisco quake (by Assoc. Press): Daily Alaska Empire, Juneau, v. 92, no. 14,008 (July 10), p. 1.

——— 1958b, Lituya Bay shoreline stripped clean by huge tidal wave, ice slides: Daily Alaska Empire, Juneau, v. 92, no. 14,009 (July 11), p. 1.

——— 1959, Survey teams to study Lituya Bay earthquake area: Daily Alaska Empire, Juneau, v. 93, no. 14,227 (Mar. 31), p. 1.

Dall, W. H., 1870, Alaska and its resources: Boston, Mass., Lee and Shepard, 627 p.

——— 1878, Report on Mount St. Elias, Mount Fairweather, and some of the adjacent mountains (Alaska), *in* U.S. Coast Survey Rept. 1875: U.S. 44th Cong., 1st Sess., H. Ex. Doc. 81, p. 157–188.

——— 1883, *in* U.S. Coast and Geodetic Survey Pacific Coast Pilot, Alaska, pt. 1, p. 202–204.

de Laguna, Frederica, 1953, Some problems in the relationship between Tlingit archaeology and ethnology: Soc. Am. Archaeology, Mem. 9 (supp. to Am. Antiquity), v. 18, no. 3, pt. 2, p. 53–57.

Eckel, E. B., ed., 1958, Landslides and engineering practice: Highway Research Board Spec. Rept. no. 29 (NAS-NCR Pub. 544), 232 p.

Emmons, G. T., 1911, Native account of the meeting between La Perouse and the Tlingit: Am. Anthropologist, n. ser., v. 13, p. 294–298.

Fons, W. L., and Pong, W. Y., 1957, Tree breakage characteristics under static loading; ponderosa pine: U. S. Dept. Agriculture, Div. Fire Research, Forest Service, Interim Tech. Rept. AFSWP-867, 51 p.

Goldthwait, R. P., 1936, Seismic soundings on South Crillon and Klooch Glaciers: London, Geog. Jour., v. 87, p. 496–517.

Grye, George, Miller, D. J., and Payne, T. G., 1951, Possible future petroleum provinces of North America; chapter on Alaska: Am. Assoc. Petroleum Geologists Bull., v. 35, p. 151–168.

Gutenberg, Beno, 1939, Tsunamis and earthquakes: Seismol. Soc. America Bull., v. 29, p. 517–526.

Heezen, B. D., 1957, 1908 Messina earthquake, tsunami, and turbidity current [abs.]: Geol. Soc. America Bull., v. 68, p. 1743.

Henrickson, E. L., 1959, Alaskan adventure: Voice [Carleton Alumni], v. 24, no. 4 (Jan.), p. 14–19.

Holmsen, Gunnar, 1936, De siste bergskred i Tafjord og Loen, Norge: Svensk geog. årsbok, årg 12, p. 171–190, 5 figs., 1 pl., Lund.

Holtedahl, Olaf, 1953, Norges Geologi: Norges Geologiske Undersökelse, no. 164, v. 2, p. 1044–1048, figs. 461–462.

International Boundary Commission, 1952, Joint report upon the survey and demarcation of the boundary between Canada and the United States from Tongass Passage to Mount St. Elias: U.S. Dept. State, Washington, 365 p.

Ippen, A. T., and Mitchell, M. M., 1957, The damping of the solitary wave from boundary shear measurements: Mass. Inst. Tech. Hydrog. Lab. Tech. Rept. no. 23, 50 p.

Jørstad, F. A., 1956, Fjellskredet ved Tjelle; et 200-års minne: Naturen årg 80, no. 6, p. 323–333.

Kaldhol, H. and Kolderup, N. H., 1937, Skredet i Tafjord 7. april 1934: Bergens Museums Årbok 1936, nat. rekke, v. 2, no. 11, 15 p., 4 figs., map.

Kennedy, G. C., and Walton, M. S., 1946, Geology and associated mineral deposits of some nitrabasic rock bodies in southeastern Alaska: U.S. Geol. Survey Bull. 947–D, p. 65–84.

Klotz, O. J., 1899, Notes on glaciers of southeastern Alaska and adjoining territory: Geog. Jour., v. 14, p. 523–534.

La Perouse, J. F. de G., 1798, The voyage of La Perouse round the world in the years 1785, 1786, 1787, and 1788, arranged by M. L. A. Milet-Mureau: London, printed for John Stockdale, v. 1, A1–A—4, p. 1–290. (English translation of the 1st ed. in French, Paris, Imprimerie de la République, 1797. The section on Alaska is reproduced also in Le voyage de LaPérouse sur les côtes de l'Alaska et de la Californie (1786), avec une introduction et des notes par Gilbert Chinard: Baltimore, Md., Johns Hopkins Press, p. 1–144, 1937).

Leet, L. D., 1948, Causes of catastrophe: New York, McGraw-Hill, 232 p.

McNown, J. S., 1952, Waves and seiche in idealized ports, *in* Gravity Waves, a symposium: Natl. Bur. Standards Circ. 521, p. 153–164.

Mertie, J. B., Jr., 1931, Notes on the geography and geology of Lituya Bay, Alaska: U.S. Geol. Survey Bull. 836–B, p. 117–135.

Miller, D. J., 1953, Preliminary geologic map of Tertiary rocks in the southeastern part of the Lituya district, Alaska: U.S. Geol. Survey open-file report.

——— 1954, Cataclysmic flood waves in Lituya Bay, Alaska (abs.): Geol. Soc. America Bull., v. 65, p. 1346; 5th Alaskan Sci. Conf., Anchorage, Sept. 7–10, 1954; Proc., 1957, p. 56–57.

Muskatov, I., and Orlov, A., 1893, Catalog of earthquakes of the Russian Empire: Contr. Russian Geog. Soc., in general geography, v. 26, 582 p.

Neuman, Frank, 1938, United States earthquakes, 1936: U.S. Coast and Geod. Survey Pub. no. 610, 45 p.

Ogawa, Takuji, 1924, Notes on the volcanic and seismic phenomena in the volcanic district of Shimabara, with a report on the earthquake of December 8th, 1922: Kyoto Imp. Univ., Mem. Coll. Sci., ser. B., v. 1, p. 201–254.

Omori, F., 1907, Note on the eruptions of the Unsen-daké in the 4th year of Kansei (1792): Imp. Earthquake Inv. Committee Bull., Tokyo, v. 1, p. 142–144.

Petroff, Ivan, 1884, Report on the population, industries, and resources of Alaska: Tenth Census of the United States, v. 8, 189 p.

Press, Frank, 1956, Volcanoes, ice, and destructive waves: Engineering and Science, v. 20, no. 2 (Nov.), p. 26–28, 30.

Prins, J. E., 1958a, Characteristics of waves generated by a local disturbance: Am. Geophys. Union Trans., v. 39, p. 865–874.

——— 1958b, Water waves due to a local disturbance: Proc. 6th Conf., Coastal Engineering, Council Wave Research, Eng. Found., Berkeley, Calif., p. 147–162.

Reid, H. F., 1908, The variations in glaciers, XII: Jour. Geology, v. 16, p. 46–55.

Russell, I. C., 1891, An expedition to Mount St. Elias: Natl. Geog. Mag., v. 3, p. 53–204.

Seismological Society of America Bulletin, 1958, Seismological notes: Seismol. Soc. America Bull., v. 48, p. 403–407.

Sharp, R. P., 1954, Glacier flow: a review: Geol. Soc. America Bull., v. 65, p. 821–838.

Sharpe, C. F. S., 1938, Landslides and related phenomena: New York, Columbia Univ. Press, 137 p.

Shelikof, G. I. [Shelekhof], 1812, Voyages: St. Petersburg; [English translation by Ivan Petroff], Bancroft Library, Calif. Univ.

Shepard, F. P., Macdonald, G. A., and Cox, D. D., 1950, The tsunami of April 1, 1946: Scripps Inst. Oceanography Bull., v. 5, no. 6, p. 391–528.

St. Amand, Pierre, 1957, Geological and geophysical synthesis of the tectonics of portions of British Columbia, the Yukon Territory, and Alaska: Geol. Soc. America Bull., v. 68, p. 1343–1370.

Tarr, R. S., 1909, The Yakutat Bay region, Alaska: Physiography and glacial geology: U.S. Geol. Survey Prof. Paper 64, pt. 1, p. 1–144.

Tarr, R. S., and Martin, Lawrence, 1912, Earthquakes at Yakutat Bay, Alaska, in September, 1899, with a preface by G. K. Gilbert: U.S. Geol. Survey Prof. Paper 69, 135 p.

Tocher, Don, and Miller, D. J., 1959, Field observations on effects of Alaska earthquake of 10 July, 1958: Science, v. 129, no. 3346, p. 394–395.

Ulrich, Howard, [as told to Haynes, V.], 1958, Night of terror: Alaska Sportsman, v. 24, no. 10 (October), p. 11, 42–44.

U.S. Coast and Geodetic Survey, 1935, Tide tables, Pacific Coast and Indian Ocean for the year 1936: ser. no. 576, p. 65.

——— 1942, Chart 8505, Lituya Bay.

——— 1952, Coast Pilot, Southeast Alaska, p. 474.

——— 1957, Tide tables, West coast of North and South America, 1958, p. 120, 182.

U.S. Congress, 1904, Proceedings of the Alaskan Boundary Tribunal: U.S. 58th Cong., 2d Sess., Doc. No. 162, atlas, pt. 3, sheet no. 16.

U.S. Weather Bureau, 1938, Climatological data, Alaska, summary for 1936: v. 22, no. 13, p. 69–79.

——— 1958, Climatological data, Alaska, summary for 1957: v. 43, no. 13, p. 204–215.

Washburn, Bradford [H. B., Jr.], 1935, The conquest of Mount Crillon: Natl. Geog. Mag., v. 67 p. 361–400.

——— 1936, The Harvard-Dartmouth Alaskan expeditions: London, Geog. Jour., v. 87, p. 481–495.

Wiegel, R. L., 1955, Laboratory studies of gravity waves generated by movement of a submerged body: Am. Geophys. Union Trans., v. 36, p. 759–774.

Wiegel, R. L., and Beebe, K. E., 1956, The design wave in shallow water: Jour. Waterways Div., Am. Soc. Civil Engineers, v. 82, no. WW1, paper 910, 21 p.

Wiegel, R. L., Beebe, K. E., and Moon, James, 1957, Ocean wave forces on circular cylindrical piles: Jour. Hydrol. Div., Am. Soc. Civil Engineers, v. 83, no. HY2, paper 1190, 36 p.

Wiegel, R. L., and Skjei, R. E., 1958, Breaking wave force prediction: Jour. Waterways Div., Am. Soc. Civil Engineers, v. 84, no. WW2, paper 1573, 14 p.

Williams, Howel, 1941, Calderas and their origin: Calif. Univ. Pub., Bull. Dept. Geol. Sci., v. 25, p. 239–346.

Williams, Jay [J. P.], 1938, Lituya the bewitcher: Alaska Sportsman, v. 2, no. 2 (February), p. 6, 18–19, *incorporated with little change in Williams, J. P.*, 1952, Alaskan Adventure: Harrisburg, Pa., Stackpole Co., p. 133–138.

Wood, H. O., 1914, On the earthquake of 1868 in Hawaii: Seismol. Soc. America Bull., v. 4, p. 169–203.

INDEX

Page

Acknowledgments ... 53
Aerial observations ... 53, 59, 64, 65, 69, 75, 79
equipment for ... 53
Aerial photographs, evidence for giant waves ... 53, 57, 59, 60, 64, 69, 71, 77, 79, 81
Age determinations, radiocarbon ... 55
Alaska Forest Research Center ... 53, 69, 77
Allen, B. V., account by ... 67, 68
Anchorage Cove ... 58, 59, 74, 75
Angoon, Alaska ... 74, 76

Boats in area of giant waves, *Badger* ... 57, 58, 59
Eerie ... 57
L'Astrolabe ... 56
La Boussole ... 56
Steven R. Capps ... 53
Sunmore ... 57, 58
Bonider till ... 55

Calving of ice ... 72, 73
Cape Fairweather ... 75
Cape Spencer ... 54, 59
Cape St. Elias ... 70
Cascade Glacier ... 54, 60, 61, 69, 70, 74, 79
Cenotaph Island ... 54, 55, 56, 57, 58, 59, 62, 68, 67, 68, 70, 74, 77, 78
Coal Creek ... 55, 62, 63, 70, 77
Crillon Glacier ... 70, 72, 73
Crillon Inlet ... 54, 55, 59, 60, 61, 62, 63, 64, 65, 69, 70, 72, 73, 74, 75, 77, 78, 79, 81
Crillon Lake ... 55, 71

Destruction by waves, marine invertebrates ... 62, 69
vegetation ... 57, 60, 62, 69, 75, 77, 79; pl. 54
works of man ... 62, 63, 70, 74, 76, 77
Disenchantment Bay ... 67, 73
Dixon Harbor ... 53, 59
Dry Bay ... 76

Earthquake, epicenter ... 55
on July 9, 1958 ... 53, 55, 57, 58, 59, 64, 79
origin ... 55, 57
Earthquakes, between 1847 and 1862 or 1863 ... 78, 81
in Japan ... 67
in Norway ... 67
in Washington ... 67
Yakutat Bay, 1899 ... 55, 75
Erosion, unconsolidated deposits ... 57, 69, 79
wave of 1936 ... 70
Exploration of area, American ... 56
French ... 55, 56
Russian ... 56
Eyewitness accounts ... 56, 57, 58, 59, 67, 68, 76

Fairweather fault, displacement ... 55, 63, 65, 71, 75, 79
relative movement ... 53, 55
Fairweather Range ... 53, 54, 55
Field observations ... 55, 56, 64, 69, 77, 79
Fish Lake ... 54, 60, 62, 67, 74
Forest, age ... 54, 55, 57, 77
Fredrickson, F. H., eyewitness account ... 67, 68
Future waves, susceptible areas ... 79, 80

Geography of area ... 53, 54
Geologic setting ... 55
Giant waves, interpretation ... 53, 63, 64, 65, 67
Gilbert Inlet ... 55, 59, 60, 61, 62, 63, 64, 65, 71, 74, 75, 77, 78, 79; pl. 4*B*
Glacial drift ... 55
Glaciation, post-Wisconsin ... 55
Glacier Bay ... 53, 59, 73
Glacier Bay National Monument ... 53, 57, 79
Gulf of Alaska ... 51, 56, 57

Haines, Alaska ... 70
Harbor Point ... 62, 63
History of area ... 51, 53, 55, 56
Hubbard Glacier, tidal front ... 73
Huscroft, James, account by ... 67, 68

Ice blocks, floating, dimensions ... 59
Ice-dammed lakes ... 70, 71, 79

Juneau, Alaska ... 53, 70, 76

Ketchikan newspaper ... 67
Krusof Island ... 59

La Chaussee Spit ... 54, 57, 59, 63, 77
La Perouse expedition ... 51, 55, 56
map and chart ... 56, 77, 78
Lituya Bay, geography ... 53, 61
laboratory model ... 73, 79
location ... 53
Lituya Glacier, dimensions ... 54, 59
location ... 55, 61, 71
movement ... 58, 59, 60, 72, 73
origin ... 54

Metamorphic rocks, diorite ... 55
schist ... 55, 65
slate ... 55
Moraines ... 54, 55, 71, 74
Mudslide Creek ... 58, 61, 63, 64, 72, 75, 77, 78, 81
Muir Glacier ... 73

North Crillon Glacier ... 54, 55, 56, 60, 61, 70, 71, 72, 73, 74, 79
Number of waves, evidence ... 57
Nunatak Fiord ... 55, 75

Palma Bay ... 55
Petroleum investigations ... 51
Photogrammetric methods ... 60, 65, 75, 77
Placer gold ... 56
Precipitation ... 54, 69, 70, 81

Reforestation, sequence ... 54, 55, 69, 75
Rockslides, cause ... 67, 75, 78, 79
Crillon Inlet ... 72, 76
Gilbert Inlet ... 60, 61, 63, 64, 65, 72, 75, 76, 79
Mudslide Creek ... 75, 77, 81
volume ... 65, 72

Salisbury Sound ... 59
Sedimentary rocks, age ... 51, 55
graywacke ... 55
Seiche, wave motion ... 63, 74
Sitka, Alaska ... 58, 59, 70, 71
Sitka National Monument ... 53
Sitka Sound ... 59
Skagway, Alaska ... 70
Solomon Railroad ... 54
South Crillon Glacier ... 71
St. Elias Mountains ... 53, 55
Submarine contours ... 54
Submarine sliding ... 72
Swanson, W. A., account by ... 58, 59

Temperature ... 54
Tertiary rocks ... 51, 55

Page
The Paps ..... 54, 77; pl. 2
Tidal current, velocity 52, 54, 57, 76
Tidal glacier front, movement 72, 79, 81
Tlingit tribe, language 54
legend 76, 77
population 56
Trees, generic and specific names 54
Alnus, sp. 54
Chamaecyparis nootkatensis 54
Picea sitchensis 54
Populus trichocarpa 54
Salix, sp. 54
Tsuga heterophylla 54
mertensiana 54
Trimlines, age 51, 52, 55, 57, 69, 74, 75
altitude 51, 53, 54, 60, 61, 63, 64, 69, 75, 77, 79, 81
as evidence of waves 57
cause 52
definition 60
Tsunamis 59, 64, 67, 72, 74
Turbidity currents 72

Ulrich, H. G., account by 57, 58

Page
U.S. Coast and Geodetic Survey, aerial observations 53
soundings by 54

Wave on July 9, 1958, cause 53, 59, 63, 79
effect on tide gage 57, 59
erosive effect 62
height 57, 58, 59, 64, 79
progress 57
sources of information 57
velocity 57, 59, 63, 79
Wave on October 27, 1936, causes 71, 72, 73, 74, 79
erosive effect 70
height 68, 69, 70, 71, 73, 79
velocity 68, 70, 71
Wave in 1853 or 1854, age 77
cause 77
Waves in other parts of the world 66, 67
Wiegel, R. L., quoted 63, 64, 65

Yakutat, Alaska 53, 54, 59, 75
Yakutat Bay 55, 67, 73, 75

Zones of denudation ..... 54, 60, 62, 64, 65; pl. 8

○

Early Cretaceous (Albian) Ammonites From the Chitina Valley and Talkeetna Mountains, Alaska

By RALPH W. IMLAY

SHORTER CONTRIBUTIONS TO GENERAL GEOLOGY

GEOLOGICAL SURVEY PROFESSIONAL PAPER 354-D

The Early Cretaceous (Albian) ammonites in southern Alaska have strong affinities with those in California and Oregon but are in part of Boreal and Eurasian origin

UNITED STATES GOVERNMENT PRINTING OFFICE, WASHINGTON : 1960

UNITED STATES DEPARTMENT OF THE INTERIOR

FRED A. SEATON, *Secretary*

GEOLOGICAL SURVEY

Thomas B. Nolan, *Director*

For sale by the Superintendent of Documents, U.S. Government Printing Office
Washington 25, D.C. - Price 50 cents (paper cover)

CONTENTS

	Page
Abstract	87
Introduction	87
Biologic analysis	87
Stratigraphic summary	88
Talkeetna Mountains	88
Chitina Valley	88
Ammonite faunules and correlations	89
Leconteites modestus and *Puzosigella* faunule	89
Moffitites robustus and *Leconteites deansi* faunule	91
Ammonite faunules and correlations—Continued	Page
Brewericeras breweri and *B.* cf. *B. hulenense* faunule	91
Freboldiceras singulare faunule	92
Other Albian faunules	93
Comparisons with other faunas	93
Geographic distribution	93
Summary of results	93
Systematic descriptions	97
References	111
Index	113

ILLUSTRATIONS

[Plates follow index]

PLATE 11. *Phyllopachyceras, Calliphylloceras, Anagaudryceras, Valdedorsella?, and Hypophylloceras.*
12. *Callizoniceras, Kossmatella, Ptychoceras,* and *Tetragonites.*
13. *Moffitites.*
14. *Beudanticeras, Moffitites,* and *Freboldiceras.*
15. *Kennicottia.*
16. *Puzosia* and *Beudanticeras.*
17. *Desmoceras?* and *Brewericeras.*
18. *Parasilesites, Hulenites, Arethoplites?,* and *Lemuraceras.*
19. *Leconteites, Aucellina, Puzosigella,* and *Cleoniceras.*

	Page
FIGURE 21. Correlation of the Albian faunas of the Chitina Valley and Talkeetna Mountains	90
22. Index map of the principal areas	94
23. Index map showing Albian localities in the Chitina Valley	95
24. Index map showing Albian localities in the Talkeetna Mountains	97

TABLES

	Page
TABLE 1. Ammonite genera in the Albian beds of the Chitina Valley, Talkeetna Mountains, Alaska, showing biological relationships and relative numbers available for study	88
2. Localities at which ammonites were collected from the Albian strata of the Chitina Valley and Talkeetna Mountains	96
3. Geographic distribution of early and middle Albian ammonites from the Chitina Valley and Talkeetna Mountains, Alaska	98

SHORTER CONTRIBUTIONS TO GENERAL GEOLOGY

EARLY CRETACEOUS (ALBIAN) AMMONITES FROM THE CHITINA VALLEY AND TALKEETNA MOUNTAINS, ALASKA

By Ralph W. Imlay

ABSTRACT

The Early Cretaceous (Albian) ammonites of the Chitina Valley and Talkeetna Mountains, Alaska, belong to four faunules ranging in age from early to early middle Albian.

The lowest faunule in the Chitina Valley is characterized by *Leconteites modestus* (Anderson) and by species of *Puzosigella* that permit a close correlation with the *Leconteites leconteí* zone of California and Oregon and hence with the early Albian of Eurasia. *Mofflites crassus* Imlay, n. sp., also may be characteristic of this faunule.

The next higher faunule in the Chitina Valley is characterized by *Mofflites robustus* Imlay and *Leconteites deussi* (Whiteaves). It is probably only slightly younger than the *Leconteites leconteí* zone of California and Oregon. The next higher Albian faunule in the Chitina Valley is characterized by a coarsely ribbed variant of *Brewericeras breweri* (Gabb) that suggests approximate correlation with the *Brewericeras hulencase* zone in California. An early Albian age for this faunule is indicated by the ammonites *Valdedorsella*, *Parasilesites*, and subgenus *Subarethoplites*.

In the Talkeetna Mountains the only Albian representative is the *Freboldiceras singulare* faunule, which is characterized by excellently preserved specimens of *Beudanticeras glabrum* (Whiteaves), *Freboldiceras singulare* Imlay, and *Lemuroceras talkeetnanum* Imlay, n. sp. These are either identical with or closely related to ammonites in the western interior of Canada beneath beds that contain *Gastroplites*. The faunule is probably younger than the *Lemuroceras belli* zone of Canada and the *Brewericeras breweri* faunule of the Chitina Valley, but the evidence is not conclusive. If it is younger, its age is probably early middle Albian.

The Albian ammonite faunules of the Chitina Valley have a provincial aspect owing to the presence of genera not yet found outside the Pacific coast of North America. These include *Mofflites*, *Kossmatella*, *Brewericeras*, *Leconteites*, *Puzosigella*, *Hulenites*, and *Parasilesites*. A marine connection with the boreal province through Canada or Alaska is indicated, however, by the presence of such ammonites as *Lemuroceras (Subarethoplites)* and *Callizonoceras*. In addition the faunules include many genera that are distributed nearly worldwide, or that do not characterize any particular province. The Albian ammonites of the Talkeetna Mountains likewise exhibit a provincial aspect, but in contrast to those from the Chitina Valley, the relationships are strong with the western interior of Canada and with northern Alaska.

These faunal relationships imply that the Albian sea that covered southern Alaska had broad connections with seas in the western interior of the continent, in California and Oregon, and in Asia.

INTRODUCTION

This study of the Early Cretaceous (Albian) ammonites of the Chitina Valley and Talkeetna Mountains in the southeastern part of the main body of Alaska is based on collections made by members of the Geological Survey since 1899. Thanks are due to Leo G. Hertlein and Dallas G. Hanna, of the California Academy of Sciences in San Francisco, for the privilege of examining the type specimens of certain Albian ammonites. Correlations with Albian beds in California were influenced by discussions with Michael Murphy of the University of California at Riverside. Some notes on the Cretaceous of the Chitina Valley prepared by Don J. Miller, of the U.S. Geological Survey, were very useful in determining the stratigraphic distribution of the Albian faunules.

The Albian ammonites of the Chitina Valley and Talkeetna Mountains are of exceptional interest because they are highly varied, and well preserved and represent an association of ammonites that occur elsewhere in distinct faunal provinces and are associated with plants that paleobotanists maintain are of Jurassic age. Description of the ammonites is justified, therefore, as documentation of their Albian age and that of the associated plants, as an aid in geologic mapping, and as a means of interpreting local geologic history in terms of events elsewhere. The fact that the ammonite faunules are derived from various provinces should prove useful in making interregional and intercontinental correlations.

BIOLOGIC ANALYSIS

The Albian ammonites from the Chitina Valley and Talkeetna Mountains include 379 specimens, of which 308 are specifically identified and 61 are compared to

described species. Among these the Phylloceratidae are represented by 28, the Tetragonitidae by 40, the Ptychoceratidae by 2, the Desmoceratidae by 205, the Silesitidae by 5, the Kossmaticeratidae by 4, and the Hoplitidae by 95. The distribution of these specimens by genera, subfamilies, and families is shown in table 1.

The table shows that the Desmoceratidae is the dominant family as regards individuals, species, and genera. It is characterized by the presence of such genera as *Moffitites*, *Freboldiceras*, *Kennicottia*, and *Brewericeras*, which have not been recorded outside the Pacific coast of North America. It includes, however, such Old World genera as *Valdedorsella*, *Callizoniceras*, *Puzosia*, and *Desmoceras*. The species of *Beudanticeras* present have certain peculiarities that distinguish them from European species, but are judged not to be of sufficient importance to warrant generic differentiation.

TABLE 1.—*Ammonite genera in the Albian beds of the Chitina Valley and Talkeetna Mountains, Alaska, showing biological relationships and relative numbers available for study*

Family	Subfamily	Genus	Specimens
Phylloceratidae	Phylloceratinae	*Phyllopachyceras*	4
		Hypophylloceras	1
	Callophylloceratinae	*Callophylloceras*	23
Tetragonitidae	Gaudryceratinae	*Anagaudryceras*	32
	Kossmatellinae	*Kossmatella*	3
	Tetragonitinae	*Gabbioceras*	1
		Tetragonites	4
Ptychoceratidae		*Ptychoceras*	2
Desmoceratidae	Puzosiinae	*Valdedorsella*	2
		Callizoniceras	11
		Moffitites	38
		Freboldiceras	4
		Kennicottia	16
		Puzosia	92
	Beudanticeratinae	*Beudanticeras*	9
		Beudanticeras (*Grantziceras*)	5
		Brewericeras	27
	Desmoceratinae	*Desmoceras*	1
Silesitidae		*Parasilesites*	5
Kossmaticeratidae		*Hulenites*	4
Hoplitidae	Cleoniceratinae	*Cleoniceras*	1
		Puzosigella	16
		Leconteites	73
	Gastroplitinae	*Lemuroceras*	1
		Lemuroceras (*Subarethoplites*)	2
		Arethoplites?	2

Next in importance is the family Hoplitidae in which the genera *Puzosigella* and *Leconteites* dominate in individuals and in species. These genera have not yet been reported elsewhere than the Pacific coast of North America. Of particular importance is the presence of typical representatives of the genera *Cleoniceras* and *Lemuroceras*. There are also, two specimens belonging to *Subarethoplites* Casey (1954, p. 111) which is herein considered to be a subgenus of *Lemuroceras*.

The families Phylloceratidae and Tetragonitidae are of comparatively minor importance, and the other families in table 1 are represented only by single species and a few specimens. It is interesting, however, that *Parasilesites* and *Hulenites* have not been recorded outside the Pacific coast of North America.

The absence of *Pseudoleymeriella* Casey (1957, p. 35; Whiteaves, 1893b, p. 444, pl. 7, figs. 2, 2a, b), which occurs in early Albian beds in the Queen Charlotte Islands, as well as the absence of *Douvilleiceras*, which is common in California, possibly reflects insufficient collecting.

STRATIGRAPHIC SUMMARY

TALKEETNA MOUNTAINS

Albian ammonites have been found in the Talkeetna Mountains at only two places, one near the head of Billy Creek and the other near the head of Flume Creek. They occur in concretions in the basal 125 feet of a shale and siltstone unit above 150 feet of sandstone that contains coaly beds of unknown age. This sandstone overlies 550 feet of sandstone of Valanginian age that overlies the Nelchina limestone of Valanginian age. From the siltstone 250 feet above the concretions, specimens of *Inoceramus* of Late Cretaceous age have been obtained. There is a possibility that the concretions have been reworked from older beds (Arthur Grantz, written communication, Dec. 29, 1958). Nevertheless, the presence of Albian ammonites, even locally, in the Talkeetna Mountains suggests that Albian beds once existed nearby and may now exist in the subsurface of the Copper River basin east of the mountains.

CHITINA VALLEY

Albian beds in the Chitina Valley have been identified only in the upper (eastern) 50 to 60 miles of the valley east of the Kuskulana River. The main areas of outcrop, from west to east, occur near Kuskulana Pass, along Fohlin and Bear Creeks west of Kennicott Glacier, near the head of McCarthy Creek, and near the foot of Nizina Glacier. Several other areas of outcrop occur from 25 to 35 miles south of the Nizina Glacier near the headwaters of Young Creek and near the mouth of Canyon Creek. The extent of outcrop in most of these areas is not known. However, the numerous collections obtained near Kuskulana Pass and the creeks immediately to the west are all of Albian age except for some fossils obtained 5,800 feet S. 39° E. of the mouth of Slatka Creek (Mes. loc. 8939) that are probably of Late Cretaceous age. In the area along Fohlin and Bear Creeks, all the Albian fossils were obtained near or north of Bear Creek and its east-northeast projection.

The total thickness of the Albian beds in the Chitina Valley is not known, but it is probably only a few hundred feet. In the section measured by Moffit (1938,

Digitized by Google

p. 71) on Fourth of July Creek west of Kennicott Glacier, only the lower 150 to 250 feet of massive brown sandstone and crumbly gray shale have furnished Albian fossils. The thickness of Albian beds at the head of McCarthy Creek must be slight also because that area has furnished many collections of Late Jurassic (Oxfordian to Kimmeridgian) age (USGS Mes. locs. 11373, 11374, 11376, 11378, 11380, 14032, 14034, 14035, 14495–14497) and Early Cretaceous (Valanginian) age (USGS Mes. locs. 2172, 2209, 11375, 11377, 14031, 14500–14502), but only one collection (USGS Mes. loc. 6313) of Albian age. That collection was from a sandstone, but the preservation of the fossils indicates that they were obtained from a concretion in the sandstone. A collection at the bend of Young Creek (Mes. loc. 9492), obtained from concretions in brown sandstone, is younger than any of those obtained on Fohlin Creek, Bear Creek, or near Kuskulana Pass, but the thickness of the stratigraphic unit involved is not known.

The 352 feet of sandstone and shale exposed at the base of the Cretaceous near the mouth of Canyon Creek (Moffit, 1938, p. 73) (Mes. locs. 9481, 9485–9487) contains fossils of late Albian to Cenomanian ages, according to Tatsuro Matsumoto (1959, p. 85, 86), and are therefore appreciably younger than the early Albian beds exposed in a similar appearing sequence at the base of the Cretaceous on Fourth of July Creek. Interestingly, Mesozoic locality 9489, about 3 miles west of the mouth of Canyon Creek, contains early Albian fossils identical with those near the base of the Cretaceous on Fourth of July, Bear, and Fohlin Creeks. Judging from published illustrations (Moffit, 1938, pl. 2; Moffit and Overbeck, 1918, fig. 2, on p. 27, and pl. 3), Mesozoic locality 9489 should be somewhat lower stratigraphically than locality 9487 at the mouth of Canyon Creek along the same belt of outcrops, but the stratigraphic interval between these localities cannot be measured from the map. These occurrences suggest, however, that the basal beds of the Cretaceous sequence in the Chitina Valley are of different ages from place to place and that the Albian part of the sequence is not very thick.

AMMONITE FAUNULES AND CORRELATIONS

LECONTEITES MODESTUS AND PUZOSIGELLA FAUNULE

This faunule (fig. 21) is represented in the Chitina Valley near Bear, Fohlin, and Fourth of July Creeks at USGS Mesozoic localities 8877, 9971, 11389, and 14468 by the ammonites *Leconteites modestus* (Anderson), *Puzosigella* cf. *P. rogersi* (Hall and Ambrose), *P.* cf. *P. perrinsmithi* (Anderson), *P.* cf. *P. taffi* (Anderson), and *Anagaudryceras aurarium* (Anderson). The faunule may be represented, also, by *Moffitites crassus* Imlay, n. sp., obtained 1 mile north of Bear Creek at USGS Mesozoic locality 14487 and 3½ miles southeast of Kuskulana Pass at USGS Mesozoic locality 14477.

These ammonites are usually associated with many specimens of the pelecypod *Aucellina* (Moffit, 1938, pl. 10, figs. 4, 5), which genus in reports dealing with the Chitina Valley has generally been compared with "*Aucella*" *pallasi* (Keyserling), or "*Aucella*" *crassicollis* (Keyserling) (Martin, 1926, p. 336, 347, 348; Moffit, 1938, table facing p. 80). It includes all specimens previously assigned to "*Aucella*" except those from the Late Jurassic and Early Cretaceous (Valanginian) localities listed herein under the heading "Stratigraphic summary."

The localities listed under the *Leconteites modestus* faunule are all near the contact of Cretaceous with Triassic rocks and, judging from Moffit's map (1938, pl. 2), are distinctly lower stratigraphically than most of those of the succeeding faunule typified by *Moffitites robustus* Imlay. At a few places, however, the fossils of one faunule were found near those of the other, as at USGS Mesozoic localities 8877 and 8878. This is not surprising considering that the total thickness of beds involved in both faunules is not more than 300 feet in most places (Moffit, 1938, p. 71, 78).

The beds containing *Leconteites modestus* (Anderson) and *Puzosigella* spp. may be correlated with the *Leconteites lecontei* zone (Murphy, 1956, p. 2118, fig. 6) in California and Oregon because of the presence of the genera *Leconteites* and *Puzosigella* and of the species *Leconteites modestus* (Anderson). Also, the presence of *Anagaudryceras aurarium* (Anderson) is normal in that zone, although it ranges higher in California into the zone of *Brewericeras hulenense*.

The age of the *Leconteites lecontei* zone is either early or early middle Albian as shown by the presence of the ammonite *Douvilleiceras*, which in Europe ranges from the upper part of the *Leymeriella tardefurcata* zone into the middle of the *Hoplites dentatus* zone (Spath, 1930, p. 60–65; Collignon, 1949, p. 110–114; Breistroffer, 1947, p. 27, 28). An early Albian age for the *Leconteites lecontei* zone is favored, however, by the presence of *Silesites*, which normally occurs in beds older than Albian, and by the presence of *Douvilleiceras* in the next two overlying zones, which may be correlated with the upper part of the range of the genus in Europe. The presence of *Anagaudryceras* and *Tetragonites* indicates an age not older than Albian.

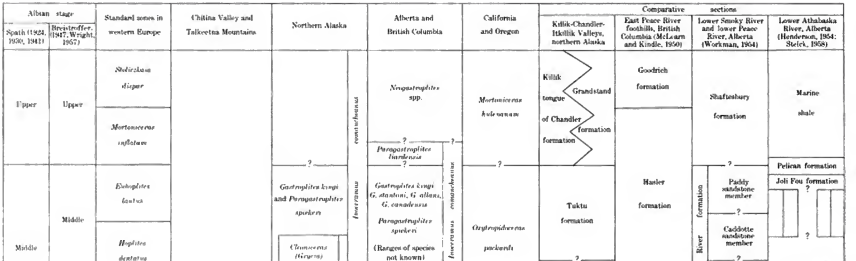

FIGURE 21.—Correlation of the Albian faunas of the Chitina Valley and Talkeetna Mountains.

MOFFITITES ROBUSTUS AND LECONTEITES DEANSI FAUNULE

This faunule (fig. 21) is represented in the Chitina Valley at many localities along Bear and Fohlin Creeks (USGS Mes. loc. 2147, 2191, 2201, 8872, 8873, 8875, 8876, 8878, 8880, 9966, 9967, 9967a, 9972, 9973, 9976, 9978, 14471, 14484, 14485), and at single localities along Fourth of July Creek (USGS Mes. loc. 14467), Trail Creek (USGS Mes. loc. 9950), and 3 miles west of the mouth of Canyon Creek (USGS Mes. loc. 9489). The most common ammonites are *Moffitites robustus* Imlay, *Kennicottia bifurcata* Imlay, *Leconteites deansi* (Whiteaves), *L. crassicostatus* Imlay, n. sp., and *Anagaudrycceras aurarium* (Anderson). Somewhat less common are *Phyllopachyceras* cf. *P. shastalense* (Anderson), *Calliphylloceras* cf. *C. aldersoni* (Anderson), *Ptychoceras* cf. *P. laeve* (Gabb), *Callizoniceras (Wollemanniceras) alaskanum* Imlay, n. sp., *C. (W.) fohlinense* Imlay, n. sp., *Kennicottia rugosa* Imlay, n. sp., *Puzosia* sp., and *Leconteites* aff. *L. deansi* (Whiteaves). These ammonites are associated with the pelecypod *Aucellina* (pl. 19, figs. 28–32) which locally occurs in great numbers and has been obtained at many more localities than the ammonites.

The *Moffitites robustus* faunule is of early Albian age—only a little younger than the underlying faunule containing *Leconteites modestus* (Anderson) and *Puzosigella*. This is indicated by the close stratigraphic association of the faunules and by the presence in both of the genus *Leconteites*, which in California has been found only in the *Leconteites lecontei* zone of early Albian age. Similarly, the presence of *Callizoniceras (Wollemanniceras)* is excellent evidence that the *Moffitites robustus* faunule is not younger than early Albian (Wright, 1957, p. L363).

The *Moffitites robustus* faunule is not correlated with either the *Leconteites lecontei* zone or the overlying *Brewericeras hulenense* zone in California (Murphy, 1956, p. 2118) because the only species in common with those zones is *Anagaudrycceras aurarium* (Anderson) and because those zones may be correlated respectively with the *Leconteites modestus* faunule and the *Brewericeras breweri* faunule of the Chitina Valley. Both stratigraphically and faunally, therefore, the *Moffitites robustus* faunule appears to occupy a position intermediate between the California zones in question. Such a position is not in conflict with recent studies in California. Inspection of the zonal map prepared by Murphy (1956, fig. 5 on p. 2109) for the Cottonwood area near Ono, Calif., shows that there is ample space stratigraphically for another faunule zone between the *Leconteites lecontei* and *Brewericeras hulenense* zones.

BREWERICERAS BREWERI AND B. CF. B. HULENENSE FAUNULE

This faunule is represented in the upper part of the Chitina Valley at USGS Mesozoic localities 9480 and 9492 near the head of Young Creek, at USGS Mesozoic locality 14514 near the foot of Nizina Glacier, and probably at USGS Mesozoic locality 6313 near the head of McCarthy Creek. The fossils at localities 9492 and 6313 were obtained from concretions in sandstone, but the characteristics of the beds at the other localities is not known. As all these localities are many miles from the localities that furnished *Leconteites* and *Moffitites*, the thickness of the stratigraphic unit involved is not known.

The fossils in the faunule characterized by *Brewericeras breweri* (Gabb) are listed by localities as follows:

Phyllopachyceras chitinanum Imlay, n. sp.	9492
Hypophylloceras cf. *H. californicum* (Anderson)	9492
Calliphylloceras nizinanum Imlay, n. sp.	9492
Anagaudrycceras sp. Indet.	6313
Kossmatella rappei Imlay, n. sp.	9492, 14514
Tetragonites aff. *T. timothranus* (Pictet)	9492
Valdedorsella? schitwarsi Imlay, n. sp.	9492
Puzosia alaskana Imlay, n. sp.	9492
Brewericeras breweri (Gabb)	9492
cf. *B. hulenense* (Anderson)	6313, 9492, 14514
Desmoceras sp. juv.	9492
Parasilesites bullatus Imlay, n. sp.	9492
irregularis Imlay, n. sp.	9492
Hulenites cf. *H. residei* (Anderson)	9480, 9492
Cleoniceras orerbecki Imlay, n. sp.	9492
Lemuroceras (Subarcthoplites) aff. *L. belli* McLearn	9492
Arcthoplites? sp.	9492

The only abundant ammonites among those listed are *Puzosia alaskana* Imlay, n. sp., *Calliphylloceras nizinanum* Imlay, n. sp., *Brewericeras breweri* (Gabb), and *B.* cf. *B. hulenense* (Anderson). All other species are represented by five specimens or less. Associated with these ammonites are many other mollusks (Moffit, 1918, p. 40), of which the most significant stratigraphically are small specimens of *Inoceramus* that resemble immature specimens of *I. comancheanus* Cragin (equals *I. anglicus* Woods). Also, of stratigraphic significance is the absence of the pelecypod *Aucellina*, which is abundant in the older beds containing *Leconteites* and *Moffitites*.

The beds in the Chitina Valley that contain *Brewericeras breweri* (Gabb) and *B.* cf. *B. hulenense* (Anderson) are considered to be approximately equivalent to the zone of *B. hulenense* in northern California (Murphy, 1956, p. 2118, fig. 6) because they both contain the same coarsely ribbed variant of *B. breweri* (Gabb) that was illustrated by Whiteaves (1876, p. 21, pl. 1, figs. 2, 2a, 3, 3a) from the Queen Charlotte Islands. Also, the specimens herein compared to *B. hulenense* (Anderson) are probably immature examples of that

species rather than of *B. haydeni* (Gabb). Otherwise the Alaskan *Brewericeras breweri* faunule differs from the ammonites in the *B. hulenense* zone in California by the absence of the genus *Douvilleiceras* and the presence of the genera *Valdedorsella*, *Parasilesites*, *Hulenites*, *Cleoniceras*, and *Lemuroceras (Subarethoplites)*.

The *Brewericeras hulenense* zone in California may be correlated with the *Douvilleiceras mammillatum* zone in Europe on the basis of containing an abundance of *Douvilleiceras* and of being in the middle of the local range of *Douvilleiceras*. Similarly the underlying *Leconteites leconteí* zone may be correlated with the lowest occurrence of *Douvilleiceras* in Europe in the upper part of the *Leymeriella tardefurcata* zone. If these correlations are correct, the age of the *B. hulenense* zone should be late early Albian, according to the classification used by Wright (1957, p. L128) and Breistroffer (1947, p. 51, 53), or early middle Albian, according to the classification used by Spath (1941, p. 668).

Concerning the age of the beds in Alaska that contain *Brewericeras breweri* (Gabb), an early rather than middle Albian age is indicated by the presence of such genera as *Valdedorsella* and *Lemuroceras (Subarethoplites)*. Of these, *Valdedorsella* has not been found above the lower Albian in Europe; *Parasilesites* belongs in a family that is not known above the lower Albian; and the subgenus *Subarethoplites* occurs in northern Alaska about 600 feet below the lowest known occurrence of *Cleoniceras*, which ranges through more than 2,500 feet of strata (Imlay, 1960).

FREBOLDICERAS SINGULARE FAUNULE

This faunule is represented in the Talkeetna Mountains by the ammonites *Tetragonites* sp., *Freboldiceras singulare* Imlay, *Beudanticeras glabrum* (Whiteaves), *B. (Grantziceras) multiconstrictum* Imlay; and *Lemuroceras talkeetnanum* Imlay, n. sp. The faunule is of unusual interest because of the excellent preservation of the specimens, because its component species show close affinities with Albian species in the western interior of Canada and in India, and because its genera and species have no known affinities with the Albian ammonites of California or Oregon, although they occur in the same marine basin as the Albian ammonites of the Chitina Valley that are closely related to ammonites in California and Oregon.

The age of the ammonite faunule in question from the Talkeetna Mountains is either early Albian or early middle Albian on the basis of comparisons with similar ammonites in the western interior of Canada. The presence of *Beudanticeras glabrum* (Whiteaves) indicates a correlation with Albian beds in Canada below the lowest occurrence of the ammonite *Gastroplites* in the Harmon shale member of the Peace River formation (Henderson, 1954, p. 2285, 2286; Stelck and others, 1956, p. 10, 12). The resemblance of *Freboldiceras singulare* Imlay to "*Lemuroceras*" *irenense* McLearn (1945, pl. 5, fig. 5; 1948, p. 2) from the upper part of the Moosebar formation of British Columbia (Stelck and others, 1956, p. 10) suggests an age slightly younger than that of *Lemuroceras (Subarethoplites) belli* McLearn (1945, pl. 3, figs. 17, 18; 1948, p. 2) from the Clearwater formation and the upper part of the Loon River formation (McLearn and Kindle, 1950, p. 86, 93). However, the resemblance of *Lemuroceras talkeetnanum* Imlay, n. sp., to *Lemuroceras* cf. *L. indicum* Spath (McLearn, 1945, pl. 5, fig. 4) from the lower part of the Loon River formation (Stelck and others, 1956, p. 6, 11, 14) suggests an age slightly older than that of *Lemuroceras belli* McLearn.

The fact that *Lemuroceras talkeetnanum* Imlay, n. sp., is remarkably similar to *L. indicum* (Spath) (1933, p. 801, pl. 129, fig. 5) from India and Madagascar (Collignon, 1949, p. 68, 69, pl. 12, figs. 2, 2a, b, pl. 14, fig. 2) suggests that it is of nearly the same age as that species and that the *Freboldiceras singulare* faunule may be correlated with the Old World *Douvilleiceras mammillatum* zone. As just discussed, however, correlation with that zone seems reasonable, also, for the *Brewericeras hulenense* zone in California and for the *B. breweri* faunule in the Chitina Valley which have an entirely different ammonite assemblage than the faunule in the Talkeetna Mountains. This difference is especially significant for correlation purposes considering that the Albian beds of the Talkeetna Mountains and of the Chitina Valley were deposited in the same basin and, therefore, that the ammonites in those beds should not differ greatly provided they are of the same age.

Therefore, the Albian fossils from the Talkeetna Mountains are either slightly younger or slightly older than the *Brewericeras breweri* faunule in the Chitina Valley. The matter cannot be settled definitely on the basis of available evidence, but a younger age is suggested by the fact that in northern Alaska the beds containing *Lemuroceras belli* McLearn are underlain by beds containing Albian ammonites that are considerably different than those in the Talkeetna Mountains. Accordingly the *Freboldiceras singulare* faunule is probably younger than the *Lemuroceras belli* zone of Canada and northern Alaska and should be sought in the upper part of the Moosebar formation and in the Gates formation of British Columbia and in the Notikewin member of the Peace River formation of Alberta. Such a correlation would agree with the general

resemblance of *Freboldiceras singulare* Imlay to "*Lemuroceras*" *irenense* McLearn.

OTHER ALBIAN FAUNULES

Some fossil collections of late Albian to Cenomanian ages have been obtained from the valley of the Nizina Glacier (USGS Mes. locs. 14038, 14040, 14511, 14515) and about 30 miles south-southeast of that glacier in an area northwest of Gibraltar Hill (USGS Mes. locs. 9481, 9485–9487). Most of the fossils were considered to be of Albian age by Imlay and Reeside (1954, p. 230), but recent studies by Matsumoto (1959, p. 85, 86) show that USGS Mesozoic locality 9481 contains fossils of probable Cenomanian age and that the other localities contain long-ranging species that could be of late Albian or of Cenomanian age. A definite age determination must await additional collecting. Considering these age limitations, it is interesting that plant fossils obtained from USGS Mesozoic localities 9481 and 9486 and from many localities of early to middle Albian age in the Chitina Valley have been identified by F. H. Knowlton as definitely Late Jurassic (Moffit and Overbeck, 1918, p. 42, 44; Martin, 1926, p. 336–346; Moffit, 1938, p. 88).

COMPARISONS WITH OTHER FAUNAS

The Albian ammonites from the Chitina Valley belong in the same faunal province as the Albian ammonites of California and Oregon as shown by the presence of the genera *Brewericeras*, *Hulenites*, *Puzosigella*, and *Leconteites*. However, some kind of faunal connection with the western interior of Canada and with northern Alaska is shown by the presence of *Lemuroceras* (*Subarethoplites*) in association with *Brewericeras*. Also the presence of *Callizoniceras*, known elsewhere only from Greenland and northwest Europe, suggests some kind of connection through Canada or northern Alaska with the boreal province. The genera *Moffitites* and *Kennicottia* have not yet been reported from California or Oregon but are present in U.S. Geological Survey collections from the Queen Charlotte Islands and may be expected farther south. Most of the other genera are widely distributed in many parts of the world.

The few Albian ammonites from the Talkeetna Mountains in contrast with those from the Chitina Valley belong in the same faunal province as the Albian ammonites of the western interior of Canada and of northern Alaska and have not yet been found in California and Oregon. This is shown by the presence of *Beudanticeras glabrum* (Whiteaves), which is common in the western interior of Canada, and of species of *Beudanticeras*, *Freboldiceras*, and *Lemuroceras* that are closely similar to Canadian species. Such a relationship is surprising because any Albian beds in or near the Talkeetna Mountains must have been deposited in the same marine sedimentary basin as the Albian beds of the Chitina Valley. These facts mean either that there was some mixing of the Albian faunas of the interior region, which are of boreal origin, with those of the Pacific coast during Albian time or that the faunas were actually not distinct. In this connection the presence of a species of *Lemuroceras* in the Talkeetna Mountains similar to *L. indicum* (Spath) from India and Madagascar (Spath, 1933, pl. 128, figs. 4a, b, 5a, b; Collignon, 1949, pl. 12, figs. 2, 2a, b, pl. 14, figs. 2) and to a species from the western interior of Canada (McLearn, 1945, pl. 5, fig. 4) suggests that the Albian ammonite faunules of the western interior of Canada and of northern Alaska may have had a much wider distribution than now realized.

In summation, the Albian ammonite assemblage in southern Alaska is predominantly related to the Albian ammonite assemblage in California and Oregon, but includes some genera and species that are boreal in origin, and others that occur in Albian beds in many parts of the world.

GEOGRAPHIC DISTRIBUTION

The occurrence by area and locality of the 45 species described in this report is indicated in table 3. The position of the two known areas of lower to middle Albian rocks in the southeastern part of the main body of Alaska is shown in figure 22, and the general position of each locality is shown in figures 23 and 24. The positions of such localities as 2147, 2173, 2191, 2201, and 6313 may be in error by a mile or more because of inadequate field descriptions. Descriptions of the individual localities are given in table 2. This list does not include any localities mentioned in the text under such ages as Late Jurrassic, Early Cretaceous (Valanginian), or late Albian to Cenomanian. The description of such localities may be found in U.S. Geological Survey Bulletin 894 on pages 83–88.

SUMMARY OF RESULTS

The Early Cretaceous (Albian) ammonites from the Talkeetna Mountains and the upper part of the Chitina Valley discussed herein are well preserved and highly varied. They include 24 genera and 45 species. Of these species 18 are described as new. Of the 24 genera, 4 were described as new in a preliminary paper (Imlay, 1959) published during the course of this study.

Among the Albian ammonites the family Desmoceratidae is dominant in numbers, genera, and species. It is characterized by the genera *Moffitites*, *Freboldiceras*,

FIGURE 22.—Index map of the main areas of Albian fossils in the southeastern part of the main body of Alaska.

Kennicottia, and *Brewericeras*, which have not been recorded outside of the Pacific coast of North America. It includes, also, the Old World genera *Callizoniceras*, *Puzosia*, *Beudanticeras*, and probably *Valdedorsella* and *Desmoceras*. Next in importance among the Albian ammonites is the family *Hoplitidae*. It is characterized by the genera *Leconteites* and *Puzosigella*, which have been found to date only on the Pacific coast of North America, but includes the widely distributed genera *Cleoniceras* and *Lemuroceras*. Of considerable lesser importance are the Phylloceratidae and Tetragonitidae. The Ptychoceratidae, Silesitidae, and Kossmaticeratidae are represented by only a few specimens.

The Albian beds include four ammonite faunules. In the Chitina Valley the faunules, from oldest to youngest, are characterized by 1, *Leconteites modestus* (Anderson) and *Puzosigella* spp.; 2, *Mofffitites robustus* Imlay and *Leconteites deansi* (Whiteaves); 3, *Brewericeras breweri* (Gabb) and *B.* cf. *B. hulenense* (Anderson). In the Talkeetna Mountains occurs a fourth faunule characterized by *Freboldiceras singulare* Imlay. This faunule is probably younger than the other faunules, but the evidence is not conclusive. The two lower faunules are associated with the pelecypod *Aucellina*.

The faunule characterized by *Leconteites modestus* and *Puzosigella* spp. is correlated with the *Leconteites leconteí* zone in California and Oregon and is of early Albian age.

The faunule characterized by *Mofffitites robustus* Imlay and *Leconteites deansi* (Whiteaves) is considered to be intermediate in age between the *Leconteites leconteí* zone and the *Brewericeras hulenense* zone in California. An age not younger than earlier Albian is indicated by the presence of the genus *Callizoniceras*.

The faunule characterized by *Brewericeras breweri* (Gabb) and *B.* cf. *B. hulenense* (Anderson) is approximately equivalent to the *Brewericeras hulenense* zone in California because it contains the coarsely ribbed variant of *Brewericeras breweri* (Gabb) identical with that in the *B. hulenense* zone. The faunule in the Chitina Valley differs in other respects, however, and may not be an exact equivalent. Its age, judging by the presence of the ammonites *Valdedorsella?*, *Parasilesites*, and *Lemuroceras (Subarcthoplites)* is not younger than early Albian.

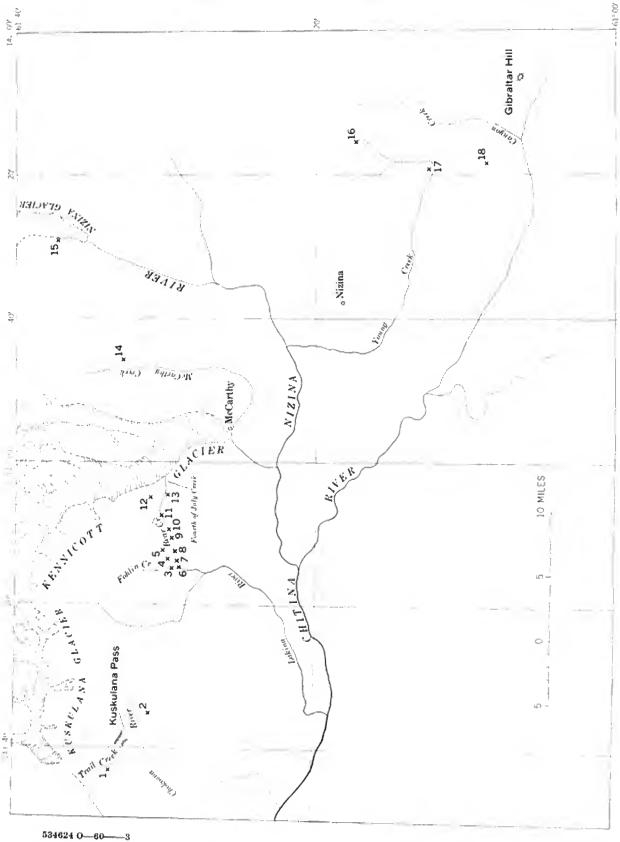

FIGURE 23.—Index map showing Albian localities in the Chitina Valley.

TABLE 2.—*Localities at which ammonites were collected from the Albian strata of the Chitina Valley and the Talkeetna Mountains*

Locality on figs. 2 and 3	Geological Survey Mesozoic localities	Collectors' field Nos.	Collector, year of collections, description of locality, and lithologic features
1	9950	32	Moffit, F. H., 1916. On west side of Trail Creek at altitude of 3,500 ft, Chitina Valley.
2	14477	AM–F14	Moffit, F. H., 1928. Near head of Chokosna River, 1 mile up southern tributary that joins river at the Kuskulana Trail, Chitina Valley.
3	8873	57	Martin, G. C., and Overbeck, R. M., 1914. East bank of Fohlin Creek, 4,900 ft north of mouth of Bear Creek, Chitina Valley.
3	8875	60	Martin, G. C., and Overbeck, R. M., 1914. East bank of Fohlin Creek about 6,800 ft north of Bear Creek, Chitina Valley.
3	8876	61	Martin, G. C., and Overbeck, R. M., 1914. East bank of Fohlin Creek 5,500 ft north of Bear Creek, Chitina Valley.
3	14484	28AM–F21	Moffit, F. H., 1928. Fohlin Creek 1 mile north of Bear Creek. Near Mes. loc. 8873, Chitina Valley.
3	14485	28AM–F22	Moffit, F. H., 1928. Fohlin Creek 100 yds north of Mes. loc. 14484, Chitina Valley.
4	9971	54	Moffit, F. H., 1916. At falls on first northern tributary of Bear Creek at altitude of 3,200 ft and a little more than 1 mile from Bear Creek, Chitina Valley.
4	14487	28AM–F24	Moffit, F. H., 1928. First northern tributary of Bear Creek, 1 mile above its mouth, Chitina Valley.
5	14471	AM–F8	Moffit, F. H., 1928. About 1½ miles north of Bear Creek and the same distance east of Fohlin Creek, Chitina Valley.
6	9976	59	Moffit, F. H., 1916. On Fohlin Creek 125 ft above mouth of Bear Creek, Chitina Valley.
6	9978	61	Moffit, F. H., 1916. On Fohlin Creek, 1,300 ft upstream from Mes. loc. 9976, Chitina Valley.
7	2147	3	Rohn, Oscar, 1899. Creek between Lakina River and Fohlin Creek between camps 11 and 12, Chitina Valley.
7	2191	1048	Schrader, F. C., and Spencer, A. C., 1900. Creek tributary to the Lakina River half a mile above crossing of old trail between Lakina and Kennicott Rivers, Chitina Valley.
7	2201	5	Schrader, F. C., and Spencer, A. C., 1900. Old trail between Lakina and Kennicott Rivers, Chitina Valley.
7	9966	----------	Moffit, F. H., 1916. Half a mile above mouth of Bear Creek on first tributary from north, Chitina Valley.
7	9967	50	Moffit, F. H., 1916. A little upstream from Mes. loc. 9966, Chitina Valley.
7	9967a	50	Moffit, F. H., 1916. Float from Mes. loc. 9967, Chitina Valley.
8	2173	6	Rohn, Oscar, 1899. Small canyon between camp 13 and the Kennicott Glacier, Chitina Valley.
8	9972	55	Moffit, F. H., 1916. On Bear Creek at altitude of 2,850 ft about half way from Fohlin Creek to Fourth of July Pass. Soft, gray sandstone containing nodular masses, Chitina Valley.
8	9973	55	Moffit, F. H., 1916. On Bear Creek near Mes. loc. 9972, Chitina Valley.
9	8872	55	Martin, G. C., and Overbeck, R. M., 1914. Float in Bear Creek about 2½ miles above its mouth, Chitina Valley.
10	8877	62	Martin, G. C., and Overbeck, R. M., 1914. Bear Creek about 3 miles above mouth, Chitina Valley.
10	8878	63	Martin, G. C., and Overbeck, R. M., 1914. 100 yds above Mes. loc. 8877 on Bear Creek, Chitina Valley.
11	8880	65	Martin, G. C., and Overbeck, R. M., 1914. Bear Creek about 400 ft below summit of Fourth of July Pass, Chitina Valley.
12	14466	28AM–F4	Moffit, F. H., 1928. Northern tributary of Fourth of July Creek 1½ miles from its mouth, Chitina Valley.
12	14467	28AM–F4a	Moffit, F. H., 1928. Same as Mes. loc. 14466.
12	14468	28AM–F5	Moffit, F. H., 1928. Near Mes. loc. 14466, Chitina Valley.
13	11389	10	Moffit, F. H., 1922. On Fourth of July Creek 2 miles from Kennicott Glacier, Chitina Valley.
14	6313	9	Moffit, F. H., 1909. McCarthy Creek. Base of Kennicott formation.
15	14514	28AM–F51	Moffit, F. H., 1928. West side of Nizina Glacier 1 mile from its lower end. Chitina Valley.
16	9480	14	Moffit, F. H., and Overbeck, R. M., 1915. Float from upper part of east branch of Young Creek, Chitina Valley.
17	9492	34	Moffit, F. H., and Overbeck, R. M., 1915. From concretions in sandstone in bluffs on north side of Young Creek west of big bend at altitude of 3,450 ft and half a mile above foot of trail to the Chitina River, Chitina Valley.
18	9489	31	Moffit, F. H., and Overbeck, R. M., 1915. From nodules in sandstone near south end of trail from Chitina Valley to Young Creek at altitude of 1,900 ft, Chitina Valley.
19	24877	53AGz137	Grantz, A. and Fay, L. F., 1953. Concretions in basal siltstone of the Matanuska formation overlying the Nelchina limestone near head of Billy Creek, Talkeetna Mts. (A–2) quad., lat 62°01′40½″ N., long 147°39′18″ W., Talkeetna Mts.
21	25320	54AGz53	Grantz, A., 1954. Concretions in basal siltstone of the Matanuska formation overlying the Nelchina limestone near the head of Flume Creek. Talkeetna Mts. (A–2) quad. lat 62°00′41″ N., long 147°34′46″ W., Talkeetna Mts.
20	25329	54AGz56L	Grantz, A., 1954. Concretions in basal siltstone of the Matanuska formation overlying the Nelchina limestone near the head of Flume Creek. Talkeetna Mts. (A–2) quad., lat 62°00′41″ N., to lat 62°00′43″ N., long 147°34′46″ W., to long 147°34′54″ W., Talkeetna Mts.

Digitized by Google

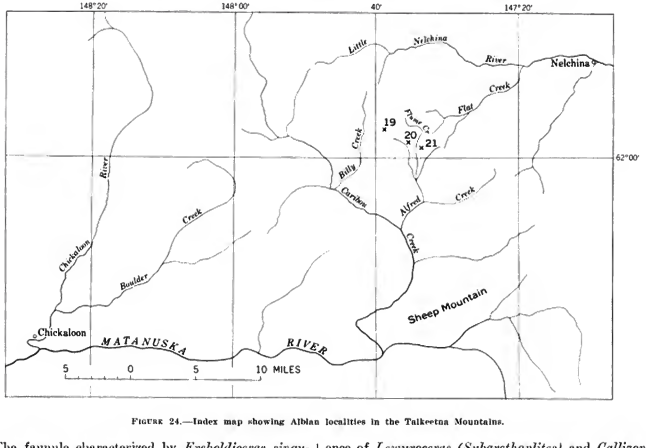

FIGURE 24.—Index map showing Albian localities in the Talkeetna Mountains.

The faunule characterized by *Freboldiceras singulare* Imlay contains Albian ammonites that are unlike those in the Chitina Valley or in California, but are identical with or closely similar to species in the western interior of Canada. The faunule is correlated with beds in Canada that overlie the zone of *Lemuroceras belli* and underlie the zone of *Gastroplites kingi*, but the evidence is not conclusive. If this correlation is correct, it is probably younger than the *Brewericeras breweri* faunule in the Chitina Valley on the basis that that faunule contains a species of *Lemuroceras* that occurs in the zone of *Lemuroceras belli* in northern Alaska.

Other ammonite faunules of late Albian age are possibly represented in the Chitina Valley at certain localities near the base of Nizina Glacier and near the mouth of Canyon Creek. The collections on hand, however, contain only long-ranging species that could be of Cenomanian age.

The Albian ammonites from the Chitina Valley belong to the same faunal province as the Albian ammonites of California and Oregon as shown by the presence of the genera *Brewericeras*, *Hulenites*, *Puzosigella*, and *Leconteites*. A possible connection with the boreal province is indicated, however, by the presence of *Lemuroceras (Subarcthoplites)* and *Callizoniceras*. In contrast the Albian ammonites from the Talkeetna Mountains belong to the same faunal province as those in the western interior of Canada and in northern Alaska. It appears, therefore, that the Albian sea that covered the areas now occupied by the Chitina Valley and Talkeetna Mountains had broad connections with the seas in the western interior of the continent and in California. Careful stratigraphic collecting from the Albian beds in the Chitina Valley would probably furnish the evidence for precise interregional correlations.

SYSTEMATIC DESCRIPTIONS

Class CEPHALOPODA
Genus PHYLLOPACHYCERAS Spath, 1925

Phyllopachyceras chitinanum Imlay, n. sp.

Plate 11, figures 1–5

This species is represented only by the holotype. Whorls ovate in section, a little higher than wide, widest near middle of flanks, becoming stouter during growth. Flanks gently convex, rounding evenly into umbilical wall and into arched venter. Umbilicus extremely narrow. Body chamber occupies three-fifths of a whorl and appears to be nearly complete.

TABLE 3.—*Geographic distribution of early Albian ammonites from the Chitina Valley and Talkeetna Mountains, Alaska*

[Numbers 1-21 refer to numbers on figs. 23 and 21. Higher numbers are Geological Survey Mesozoic locality numbers]

	Chitina Valley																																	Talkeetna Mountains		
	Kennicott formation																												Undivided Lower Cretaceous					Matanuska formation		
	1	2	3					4		5	6		7						8			9	10		11	12			13	14	15	16	17	18	19	20	21
	9950	14477	8873	8875	8876	14484	14485	9971	14487	14471	9976	9978	2147	2191	2201	9966	9967	9967a	2173	9972	9973	8672	8877	8878	8880	14466	14467	14465	11589	6313	14514	9480	9492	9489	24877	25320	25329
Phyllopachyceras chitinanum Imlay, n. sp.																																	X				
cf. *P. shastalense* (Anderson)			X				X													X																	
Hypophylloceras cf. *H. californicum* (Anderson)																																	X				
Calliphylloceras nizinanum Imlay, n. sp.																																	X				
cf. *C. aldersoni* (Anderson)																				X																	
Anagaudryceras aurarium (Anderson)			X			X	X	X							X																						
cf. *A. aurarium* (Anderson)	X															X									X									X			
sp. indet.																										X				X							
Kossmatella cappsi Imlay, n. sp.																															X		X				
Gabbioceras sp.											X																										
Tetragonites aff. *T. timotheanus* (Pictet)																																	X				
sp. indet.																																			X	X	
Ptychoceras cf. *P. laeve* (Gabb)																				X		X															
Valdedorsella? *whiteavesi* Imlay, n. sp.																																	X				
Callizoniceras (*Wollemanniceras*) *alaskanum* Imlay, n. sp.			X								X																										
(*W.*) *fohlinense* Imlay, n. sp.							X																														
Moffitites robustus Imlay			X	X	X	X	X			X		X	X	X				X						X										X			
cf. *M. robustus* Imlay, n. sp.																			X	X							X										
crassus Imlay, n. sp.		X							X															X													
Freboldiceras singulare Imlay																																			X		
Kennicottia bifurcata Imlay			X			X				X										X																	
rugosa Imlay, n. sp.							X																											X			
Puzosia alaskana Imlay, n. sp.																																	X				
Puzosia sp. indet.			X																	X																	
Beudanticeras glabrum (Whiteaves)																																			X		
(*Grantziceras*) *multiconstrictum* Imlay																																			X	X	X
Brewericeras breweri (Gabb)																																	X				
cf. *B. hulenense* (Anderson)																														X	X		X				
Desmoceras sp. juv.																																	X				
Parasilesites bullatus Imlay																																	X				
irregularis Imlay, n. sp.																																	X				
Hulenites cf. *H. reesidei* (Anderson)																										X						X	X				
Cleoniceras overbecki Imlay, n. sp.																																	X				
Puzosigella cf. *P. rogersi* (Hall and Ambrose)																							X														
cf. *P. perrinsmithi* (Anderson)																													X								
cf. *P. taffi* (Anderson)																												X	X								
Leconteites modestus (Anderson)								X																					X								
deansi (Whiteaves)															X			X		X		X															
sp.						X											X				X				X												
cf. *L. deansi* (Whiteaves)			X			X									X					X		X		X													
Lemuroceras talkeetnanum Imlay, n. sp.																																			X		
sp. juv. cf. *L. dubium* Collignon						X																															
(*Subarcthoplites*) aff. *L. belli* McLearn																																	X				
Arcthoplites? sp.																																	X				

The ornamentation on the adapical part of the body whorl consists of nearly microscopic raised lines. These are replaced adorally at a diameter of about 31 mm by low rounded ribs on the venter. Toward the aperture the ribs become stronger and originate at various heights on the middle and upper parts of the flanks. All ribs are of equal strength on the venter which they cross nearly transversely. The suture line has the tetraphyllic first and second lateral saddles that are typical in the genus.

The holotype has a maximum diameter of 38 mm. At a diameter of 35 mm, it has a whorl height of 22 mm and a whorl thickness of 21 mm. At the adapical end of the body chamber, the whorl height is 13 mm, and the whorl thickness is 10.5 mm.

This species compared with *Phyllopachyceras theresae* (Anderson) (1938, p. 141, pl. 12, figs. 4, 5) from California has a stouter whorl section, a smaller umbilicus, and finer, denser ribbing. It is particularly characterized by its stout whorl section.

Type: Holotype USNM 130142.
Locality: USGS Mes. loc. 9492.

Genus HYPOPHYLLOCERAS Salfeld, 1924

Hypophylloceras cf. H. californicum (Anderson)

Plate 11, figure 29

One laterally crushed septate specimen bears ribbing similar to that on *H. californicum* (Anderson) (1938, p. 143, pl. 12, fig. 7), but the characteristics of that species are not known sufficiently to permit identification. *H. onoense* (Stanton) (1896, p. 76; Anderson, 1928, p. 142, pl. 11, figs. 1, 2) has much finer ribbing.

Figured specimen: USNM 130132.
Locality: USGS Mes. loc. 9492.

Genus CALLIPHYLLOCERAS Spath, 1927

Calliphylloceras nizinanum Imlay, n. sp.

Plate 11, figures 6–12

This species is represented by 20 specimens, of which most are small and septate. Whorls ovate in section, higher than wide, highly involute. Flanks gently convex, converging above to a rather narrowly rounded venter. Umbilicus extremely narrow; wall steep. Body chamber represented by three-fourths of a whorl.

Surface of shell covered with very fine striae that incline forward on the flanks in a gently flexous manner and arch forward on the venter. Surface of mold marked by sigmoidal constrictions that are barely evident at a diameter of 25 mm, but become fairly strong adorally, and arch forward on the venter. Six constrictions are present on the body chamber. Fine lirae are visible only on the venter. The suture line is typical of the genus.

The small paratype shown on plate 11, figures 10 and 11, at a diameter of 33 mm, has a whorl height of 19 mm, a whorl thickness of 15 mm, and an umbilical width of 3 mm. On the holotype at a diameter of 46 mm, the corresponding dimensions are 30, 21, and 4 mm.

This species is distinguished from *C. aldersoni* (Anderson) (1938, p. 143, pl. 11, figs. 3–6) by its constrictions and growth striae arching forward more strongly on the venter, by lacking flexuous raised lines on the flanks, and by having a higher whorl section.

Types: Holotype USNM 130138. Paratype USNM 130139.
Locality: USGS Mes. loc. 9492.

Calliphylloceras cf. C. aldersoni (Anderson)

Plate 11, figs. 13–17

Three specimens very closely resemble *C. aldersoni* (Anderson) (1938, p. 143, pl. 11, figs. 3–6) from California as far as their preservation and small size permit comparison. Their flanks converge rapidly toward a narrowly rounded venter and are covered with fine flexuous raised lines that arch forward gently on the venter, and the internal molds bear five flexuous constrictions.

Figured specimen: USNM 130161.
Locality: USGS Mes. loc. 9672.

Genus ANAGAUDRYCERAS Shimizu, 1934

Anagaudryceras aurarium (Anderson)

Plate 11, figures 18, 19, 24

Lytoceras (Kossmatella?) aurarium Anderson, 1938, Geol. Soc. America Spec. Paper 16, p. 151, pl. 20, figs. 1, 2.

This species is represented in the Chitina Valley by 28 specimens that agree very well with the original description and illustrations by Anderson except for the presence of very fine, forwardly inclined regularly spaced lirae. These are visible only on a few specimens in places where some of the shell is preserved.

Type: Plesiotype USNM 130154.
Localities: USGS Mes. locs. 2201, 8873, 9971, 14484, 14485. Fragments possibly belonging to this species occur at Mes. locs. 8880, 9489, 9950, 9966.

Genus KOSSMATELLA Jacob, 1907

Kossmatella cappri Imlay, n. sp.

Plate 12, figures 17–22

Three specimens of this species are on hand. Whorls in young stages depressed ovate and much wider than high, in adult specimens becoming subquadrate and higher than wide, embracing preceding whorls about two-fifths. Flanks on inner whorls strongly convex, rounding evenly into nearly vertical umbilical wall and into broadly rounded venter. Flanks on adult body chamber somewhat flattened, rounding fairly rapidly into steep umbilical wall and into moderately arched venter. Umbilicus moderate in width, wall steeply inclined to nearly vertical. Body chamber incomplete, represented by slightly more than half a whorl.

The entire surface of the shell is covered with fine forwardly inclined lines. In addition both shell and mold are marked by regular forwardly inclined constrictions that are most pronounced on the inner whorls and near the aperture of the adult body chamber. The constrictions on the inner whorls demarcate prominent lateral bulges that become much less prominent adorally on the penultimate whorl. The adult body whorl has 15 constrictions.

The suture line has fairly symmetrical bifid saddles and a bifid first lateral lobe.

At a diameter of 63 mm, the largest specimen from Alaska has a whorl height of 29 mm, a whorl thickness of 25 mm, and an umbilical width of 20 mm. At a diameter of 58 mm the same measurements are 25, 22, and 17 mm respectively.

The Alaskan specimens in general appearance are similar to *Kossmatella agassizianum* (Pictet) as figured by Jacob (1908, pl. 2, figs. 8–10) and differ mainly by having much weaker bulges and by their constrictions inclining adapically near the umbilicus. They show even greater resemblance to *Kossmatella gainesi* (Anderson) (1938, p. 153, pl. 20, figs. 3–5) from California, from which they differ by the presence of lateral bulges on their inner whorls and by fewer constrictions.

The species is named in honor of S. R. Capps in recognition of many years of study of Alaskan geology.

Types: Holotype USNM 130160. Paratypes USNM 130140.
Localities: USGS Mes. locs. 9492, 14514.

Genus TETRAGONITES Kossmat, 1895

Tetragonites aff. T. timothesanus (Pictet)

Plate 12, figures 24–28

Some Alaskan specimens of this genus differ from *T. timotheanus* (Pictet) (in Pictet and Roux, 1847, p. 39, pl. 2, figs. 6a–b, pl. 3, figs. 1a–c) by having parallel, instead of convergent flanks. They have been described in detail by Matsumoto (1959, p. 77–79, pl. 22, figs. 1a–c, 2a–c) in a paper dealing mainly with Cenomanian ammonites from the upper part of the Chitina Valley. In that paper most of the occurrences listed are from localities of late Albian to Cenomanian age, but Mesozoic locality 9492, which is either of early Albian or early middle Albian age, is also included. The specimens figured herein are all from Mesozoic locality 9492.

Figured specimen: USNM 130131.

Genus PTYCHOCERAS d'Orbigny, 1842

Ptychoceras cf. P. laeve (Gabb)

Plate 12, figure 23

Two small internal molds show parts of two closely appressed limbs that belong mostly to the body chamber. The smaller limb is much depressed. The larger limb is nearly circular in section. The surface is nearly smooth, being marked only by faint growth lines and by several constrictions. The constrictions near the adoral end of the larger limb are bordered by a rounded rib that is most prominent on the venter.

These specimens differ from *P. laeve* (Gabb) (1869, p. 144, pl. 25, figs. 21, 21a, b) in being much smaller, but possibly belong to that species.

Figured specimen: USNM 130163.
Localities: USGS Mes. locs. 8872, 9972.

Genus VALDEDORSELLA Breistroffer, 1947

Valdedorsella? whiteavesi Imlay, n. sp.

Plate 11, figures 20–23, 25–28

?*Ammonites* (sp. undet.). Whiteaves, 1876, Geol. Survey Canada Mesozoic Fossils, v. 1, p. 47, pl. 3, figs. 4, 4a.

Two small ammonites from the Chitina Valley greatly resemble a small ammonite from the Queen Charlotte Islands described by Whiteaves (1876, p. 47, pl. 3, figs. 4, 4a) and are possibly identical. They have in common a broadly rounded, depressed whorl section, a small deep umbilicus, a rounded umbilical margin, and 6 or 7 sigmoidal constrictions that arch forward on the venter. On the specimens from the Chitina Valley, each constriction is posteriorly bordered by a low rounded rib that is slightly swollen at the umbilical margin. Also, a few weaker riblets occur on the venter between the constrictions.

The suture line is rather simple. Its saddles are slender and bifid; its first lateral lobe is trifid and slightly shorter than the ventral lobe; and its auxiliaries descend regularly to the umbilicus.

The holotype at a maximum diameter of 11.5 mm has a whorl height of 6.5 mm, a whorl thickness of 8.5 mm, and an umbilical width of 2 mm.

Except for a broader whorl section *V.? whiteavesi* Imlay, n. sp. greatly resembles *V. getulina* (Coquand) as illustrated by Pervinquiere (1907, p. 154, pl. 6, figs. 16a–c) from beds near the Aptian-Albian boundary in Tunisia. *V. houreqi* (Collignon) (1937, p. 18, pl. 2, figs. 6, 6a, b, 7, 7a, b) from Madagascar is less depressed and has stronger ribbing and wider saddles, and its constrictions cross the venter nearly transversely instead of arching forward. *V. akuschaensis* (Anthula) (1899, p. 104, pl. 8, figs. 3a–c) from the Caucasus is more compressed and has wider saddles, but is difficult to compare because of its larger size.

The specimens from the Chitina Valley show some resemblances also to the upper Albian *Puzosia chirichensis* Pervinquiere (1907, p. 152, pl. 6, figs. 17–20), which species Breistroffer (1947, p. 60) assigns to *Lunatodorsella*, a subgenus of *Desmoceras*. That subgenus is distinguished, however, by a craterlike umbilicus, a rather sharp umbilical edge, and straighter constrictions.

The range of *Valdedorsella*, according to Wright (1956, L363), is Hauterivian to Aptian. Collignon (1937, p. 19) notes that *V. getulina* (Coquand) exists in both the Barremian and the Aptian of the Mediterranean region, but predominates in the Aptian. He notes that *V. akuschaensis* (Anthula) occurs in Aptian beds in the Caucasus and above the Aptian in the Clansayes beds in the province of Drôme in southern France.

This occurrence in the Clansayes beds is interesting because it indicates that the genus *Valdedorsella* ranges at least as high as the Aptian-Albian boundary. Whether the Clansayes beds are placed at the top of the Aptian (Breistroffer, 1947, p. 11–20) or at the base of the Albian (Spath, 1941, p. 668; Collignon, 1949, p. 109), they are not much older than the beds in the Chitina Valley, Alaska, that contain the lower Albian ammonites herein described.

Types: Holotype USNM 130145. Paratype USNM 130146.
Locality: USGS Mes. loc. 9492.

Genus CALLIZONICERAS Spath, 1923
Subgenus WOLLEMANNICERAS Breistroffer, 1947

Callizoniceras (Wollemanniceras) alaskanum Imlay, n. sp.

Plate 12, figures 11–16

The species is represented by six specimens. The holotype has been laterally crushed at the adapical end of the body whorl and slightly depressed at the adoral end. Shell small, moderately compressed. Whorls ovate depressed, becoming less depressed adorally, embracing about one-half of preceding whorls. Flanks convex, rounding evenly into broadly arched venter and into umbilical wall. Umbilicus moderate in width; wall steeply inclined at base. Body chamber on holotype is represented by three-fifths of a whorl and appears to be nearly complete.

The ornamentation consists partly of gently flexous, rounded ribs of moderate strength that tend to fade on the venter. It includes some rather strongly flexuous, pronounced constrictions that arch forward on the venter and are bordered by flared ribs that are particularly prominent on the venter. The primary ribs begin low on the umbilical wall and incline forward to near the middle of the flanks where about half of them bifurcate. A few primary ribs bifurcate considerably below the middle of the flanks. All ribs, forked and single, curve forward strongly on the upper parts of the flanks, arch forward on the venter, and weaken ventrally. On the paratypes the ribs do not quite fade out on the venter. On the holotype the venter of the body chamber is nearly smooth except near the aperture where the ribbing becomes a little stronger. Tubercles are not present. Seven to eight constrictions occur on each whorl. The suture line is too poorly preserved to be traced.

The paratype (pl. 12, figs. 13, 14) at a diameter of 23 mm has a whorl height of 9 mm, a whorl thickness of 11 mm, and an umbilical width of 6.5 mm. The holotype has a more compressed whorl section but has been somewhat deformed.

This species has the general appearance of *Callizoniceras (Wollemanniceras) keilhacki* Wollemann (1907, p. 36, pl. 5, figs. 4, 4a, 5, 5a; Casey, 1957, pl. 7, figs. 4, 4a, 5). It differs by having a more depressed whorl section, less flexuous constrictions and ribs, a greater number of forked ribs, and perhaps denser ribbing.

Types: Holotype USNM 130165. Paratypes USNM 130166a, b.
Localities: USGS Mes. locs. 8873, 9976.

Callizoniceras (Wollemanniceras) fohlinense Imlay, n. sp.

Plate 12, figures 1–10

The species is represented by five specimens. Shell small, compressed. Whorls subquadrate, a little higher than wide, embracing about one-half. Flanks gently convex on inner whorls, becoming flattened during growth. Venter highly arched. Umbilicus moderate in width, shallow; wall low, steeply inclined on inner whorls, becoming vertical on outer whorls; umbilical edge evenly rounded on inner whorls, abruptly rounded on outer whorl. Body chamber unknown.

The ornamentation consists of thick, gently flexuous ribs and constrictions that incline forward on the flanks, arch forward strongly on the venter, and become progressively stronger and more flexuous during growth. On the smaller whorls (pl. 12, fig. 6) the ornamentation consists of variably spaced unbranched ribs that begin low on the umbilical wall, are strong on the flanks, and nearly disappear on the venter. At a diameter of about 13 mm some short ribs are intercalated high on the flanks. At greater diameters many ribs branch near the middle of the flanks, others are indistinctly connected with secondary ribs, and a few remain unbranched. The ribs and constrictions on the venter are much weaker than on the flanks at all stages of growth, but become a little stronger during growth. Generally the ribs bordering the constrictions on the venter are a little stronger than the other ribs.

The suture line is simple. The auxiliaries do not descend toward the umbilicus as in *Callizoniceras (Wollemanniceras) keilhacki* Wollemann (1907, pl. 5, fig. 5a), but rather trend radially as in *C. hoyeri* (Von Koenen) (1902, pl. 38, fig. 6c).

The holotype at a diameter of 27 mm has a whorl height of 10.7 mm, a whorl thickness of 9.5 mm, and an umbilical width of 8 mm.

This species compared with *C. alaskanum* Imlay, n. sp., has a subquadrate rather than a depressed ovate whorl section and has stronger more flexuous ribs. It bears much greater resemblance to the paratype of *C. keilhacki* (Wollemann) (1907, pl. 5, figs. 4a, 4b), but appears to have more forked ribs and a less rounded whorl section.

Types: Holotype USNM 130155. Paratypes USNM 130156.
Locality: USGS Mes. loc. 14484.

Genus MOFFITITES Imlay, 1959

The original description of this genus is as follows:

> This genus is characterized by an inflated shell, moderate involution, a whorl section that changes from ovate to coronate during growth, by flexuous ribs and constrictions that arch forward strongly on the venter, by frequent bifurcation of the primary ribs into somewhat weaker secondary ribs near the middle of the flanks, by a tendency of the secondary ribs to weaken and become striate as they near the middle of the venter, by the occurrence of flared ribs adjacent to the constrictions, and by having a desmoceratid suture line whose auxiliaries descend gradually toward the umbilical seam.

It differs from the new genus *Kemicottia* with which it is associated by being much more inflated, by having much stronger primary ribs, and by a tendency of its secondary ribs to become striate on the venter. Its ornamentation bears some resemblance to that of *Pseudohaploceras* Hyatt (1900, p. 500), but it is easily distinguished by having regularly furcating ribs and a coronate whorl section. It resembles *Valdedorsella* Breistroffer (1947, p. 60) in shape and involution, but the differentiation of its ribs into primaries and secondaries and the considerable strength of its primary ribs permit easy separation of the genera. The same features distinguish it readily from genera within the Holcodiscidae such as *Astieridiceras* Kilian (1910, p. 265).

The type species of *Moffitites* is *Moffitites robustus* Imlay, n. sp.

This genus is named for Fred H. Moffit in recognition of his many important contributions to Alaskan geology as a member of the U.S. Geological Survey.

Moffitites robustus Imlay

Plate 13, figures 1–13

Moffitites robustus Imlay, 1959, Jour. Paleontology, v. 33, no. 1, p. 181–182, pl. 29, figs. 9–14.

The original description follows:

The species is represented by 30 specimens. Shell stout, moderate in size. Whorls ovate depressed, becoming stouter during growth, embracing about three-fifths. Flanks gently convex on immature specimens, becoming highly convex on adults. Venter highly arched in immature specimens, becoming broadly rounded on adults. Umbilicus moderate in width; wall inclined steeply, fairly high, rounding evenly into flanks. Body chamber incomplete, but represented by at least half a whorl.

The ribbing is gently flexuous on the flanks, is arched forward on the venter, and is variable in density. The primary ribs are moderate in strength, are triangular in section, become stronger ventrally, and are generally narrower than the interspaces. They begin low on the umbilical wall, incline forward slightly on the wall and on the lower third of the flanks, and then recurve gently near the middle of the flanks where they pass into, or are replaced by much weaker secondary ribs.

On immature specimens some of the primary ribs bifurcate near the middle of the flanks. Others remain single on the flanks, but may be separated from each other, or from forked ribs by 1 or 2 secondary ribs that arise freely on the upper parts of the flanks. On the penultimate and body whorls most of the primary ribs bifurcate near the middle of the flanks and many of the pairs of secondary ribs are separated on the venter by 1 or 2 intercalated ribs. In many specimens the secondary ribs tend to weaken and become striate along the midventral area, but this tendency varies considerably from one specimen to another and from whorl to whorl. Tubercles are not present at any growth stage.

All whorls are marked by 6 to 8 constrictions that are flexuous on the flanks and arch forward on the venters. The constrictions are inconspicuous on the immature whorls, but become more pronounced adorally. On the outer whorls the constrictions are generally bounded by 1 or 2 swollen primary ribs on the flanks and by a forwardly projected swelling on the venter.

The suture line is desmoceratid in plan. Its auxiliaries descend gradually toward the umbilical seam as in *Desmoceras*, *Pseudohaploceras* or *Valdedorsella*.

The holotype at a diameter of 97 mm has a whorl height of 43 mm, a whorl thickness of 52 mm, and an umbilical width of 31 mm. At a diameter of 66 mm the other dimensions are 30, 40, and 20 mm respectively. On paratype USNM 129875b at a diameter of 56 mm the other dimensions are 24, 37, and 18 mm respectively.

Types: Holotype USNM 129874. Paratypes USNM 129875a, b, 129876a, b.

Occurrence: USGS Mes. locs. 2147, 2191, 8873, 8875, 8876, 8878, 9489, 9976a, 9978, 14471, 14484, 14485. Fragments that possibly belong to this species occur at Mes. loc. 2173, 9971, and 14467.

Moffitites crassus Imlay, n. sp.

Plate 14, figures 3–7

This species is represented by three specimens. It differs from *Moffitites robustus* Imlay, n. sp., by having a somewhat less depressed whorl section, much sparser, coarser ribbing, and fewer intercalated ribs on the upper part of the flanks, and the secondary ribs do not become striate on the venter. The holotype has 26 primary ribs and only 2 secondary ribs for each primary. Specimens of *M. robustus* Imlay at a comparable size have from 33 to 35 primary ribs and a little more than 2 secondary ribs for each primary.

The holotype at a diameter of 35.5 mm has a whorl height of 16.5 mm, a whorl thickness of 16.5 mm, and an umbilical width of 8.5 mm. The suture line is not preserved.

Types: Holotype USNM 130175. Paratype USNM 130176.
Localities: USGS Mes. locs. 8878, 14477, 14487.

Genus FREBOLDICERAS Imlay, 1959

The original description is as follows:

This genus resembles *Callizoniceras* Spath (1923, p. 35) from the upper Barremian to lower Albian of Europe (Von Koenen, 1902, p. 58, pl. 9, figs. 5a–c, p. 60, pl. 28, figs. 5a, b, 6a–c, 7; Wollemann, 1907, p. 36, pl. 5, figs. 4, 4a, 5, 5a; Brinkmann, 1937, p. 8–10, figs. 4, 5). It differs by being more involute; by its whorl section being higher and more narrowly rounded; by its primary ribs being more regularly-spaced, more swollen, and confined generally to the lower part of the flanks; by its constrictions being less regularly-spaced; and by having fewer secondary ribs. Its smooth body chamber and large size may be other distinctions. Its suture is very simple and closely resembles that of *Callizoniceras*. The type species of *Freboldiceras* is *Freboldiceras singulare* Imlay, n. sp.

Freboldiceras singulare Imlay

Plate 14, figures 8–17

Freboldiceras singulare Imlay, 1959, Jour. Paleontology, v. 33, no. 1, p. 182, 183, pl. 30, figs. 1–7.

The original description is as follows:

Four specimens of this species have been found in the Talkeetna Mountains at one locality. Shell compressed, discoidal,

Whorls subovate in section, considerably higher than wide, thickest near umbilicus, embracing about two-thirds. Flanks gently convex in their lower parts, but tapering above to a narrowly rounded venter. Umbilicus fairly narrow, wall steeply inclined, rounding evenly into flanks. Body chamber represented by at least three-fifths of a whorl.

The ornamentation of the septate parts of the shell consist mostly of prominent, flexuous, regularly-spaced primary ribs, of deep, irregularly-spaced constrictions, and of flexuous striae. The primary ribs begin high on the umbilical wall, incline forward and become swollen near the umbilical edge, and then curve forward near the middle of the flanks where most of them pass into bundles of striae that arch forward gently on the flanks and venter. The primary ribs that adjoin constrictions continue across the flanks and venter, but are more prominent on the internal mold than on the shell. Some specimens at a few places have single, short secondary ribs that are intercalated between the primary ribs and continue across the venter. Where shelly material is preserved its surface is covered with fine, flexuous striae that is coarser on the primary ribs than on the interspaces. The periphery of the internal mold is strongly undulating. Wherever the shell is preserved the periphery is nearly smooth.

The adult body chamber is nearly smooth. Faint flexuous striae are present in a few places where shell layers are present. On the penultimate whorl the primary ribs become much weaker adorally and are barely visible near the last-formed septa.

The suture-line is very simple. It greatly resembles that of the genus *Callizoniceras* (Wollemann, 1907, pl. 5, fig. 5a; Y. Koenen, 1902, pl. 9, fig. 5c, pl. 38, figs. 6, 7; Chapuit, 1920, pl. 1, figs. 4a, b) in its broad first lateral saddle, in its first lateral lobe being slightly deeper than the ventral lobe, and in its auxiliary saddles not being retracted adapically near the umbilicus. In fact the auxiliaries ascend slightly as they approach the umbilical seam.

The holotype at a diameter of 55 mm, has a whorl height of 24 mm, a whorl thickness of 19 mm and an umbilical width of 14 mm.

This species resembles *Lemuroceras irenense* McLearn (1945, pl. 5, fig. 5, 1948, p. 2) from the Moosebar formation of British Columbia, and probably belongs in the same genus. The preservation of the holotype of *L. irenense* is not sufficient, however, to prove whether the resemblances are accidental or reflect generic relationships.

Types: Holotype USN 129868. USNM 129869a-e.
Occurrence: USGS Mes. loc. 21877.

Genus KENNICOTTIA Imlay, 1959

The original description is as follows:

This genus is characterized by being fairly involute, by the presence of persistent primary ribs that bifurcate fairly regularly near the middle of the flanks, by having flexuous ribs and constrictions that arch forward strongly on the venter, by the presence of some flared ribs adjoining the constrictions, by reduction of the secondary ribs along the midline of the venter, and by its suture line having regularly descending auxiliary lobes. It shows resemblance to *Pseudohaploceras* Hyatt (1900, p. 570) in amount of involution, whorl shape, suture-line, presence of flexuous constrictions and ribs, and presence of bifurcating ribs. It differs, however, by having a more subquadrate whorl section, a vertical umbilical wall, flatter flanks, weaker constrictions and flared ribs, and stronger, more regularly bifurcating primary ribs. It differs from *Valdedorsella* (Briestroffer, 1947, p. 60) in its whorl section being subquadrate instead of round and by the presence of bifurcating ribs. It differs from *Puzosia* by being considerably more involute, by the presence of bifurcating primary ribs, and by the auxiliary lobes of its suture line descending regularly instead of abruptly. The type species of *Kennicottia* is *Kennicottia bifurcata* Imlay, n. sp.

Kennicottia bifurcata Imlay

Plate 15, figures 1–6

Kennicottia bifurcata Imlay, 1959, Jour. Paleontology, v. 33, n. 1, p. 183, 184, pl. 30, figs. 8–13.

The original description is as follows:

This species is represented by 13 specimens. Whorls subovate in immature specimens, becoming subquadrate in adult, embracing about three-fifths. Flanks gently convex, becoming less so during growth, rounding into highly arched venter. Umbilicus fairly narrow; wall low, vertical at base, rounding evenly into flanks. Body chamber unknown.

The ribbing is gently flexuous on the flanks and arched forward strongly on the venter. The primary ribs are somewhat stronger than the secondary ribs. They begin low on the umbilical wall, are highest on the edge of the wall and become rather broad ventrally. Most primary ribs bifurcate near the middle of the flanks, but some remain single, and some are indistinctly connected with secondary ribs. The secondary ribs are reduced in strength along the midline of the venter.

From 6 to 7 weak flexuous constrictions occur per whorl. They become more conspicuous adorally and are most conspicuous on the venter. On the adoral part of the holotype, they are bounded by swollen ribs.

The suture line is desmoceratid in type. Its regularly descending auxiliary lobes contrast with the retracted auxiliaries in *Puzosia*, but are comparable with those in *Pseudohaploceras*.

The holotype at a diameter of 63 mm has a whorl height of 29 mm, a whorl thickness of 25 mm, and an umbilical width of 15 mm.

This species has a general resemblance to *Puzosia subquadrata* Anderson (1938, p. 186, pl. 45, figs. 3–5) from California, but differs by having much stronger primary ribs that bifurcate fairly regularly, by its ribbing being less flexuous, by its umbilical wall rounding more evenly into the flanks, and by its auxiliary lobes descending much more gradually toward the umbilical seam (compare Anderson, 1938, p. 183, text, fig. 3, no. 6).

Types: Holotype USNM 129870. Paratype USNM 129871.
Occurrence: USGS Mes. locs. 8873, 9972, 14471, 14484.

Kennicottia rugosa Imlay, n. sp.

Plate 15, figures 7–13

The species is represented by three specimens. Shell fairly large for genus, moderately compressed. Whorls subquadrate in section, becoming stouter during growth, embracing about three-fifths of preceding whorls. Flanks gently convex, becoming less so during growth, rounding evenly into broadly arched venter. Umbilicus fairly narrow; wall moderate in height, vertical at base, inclined above, and rounding

rather abruptly into flanks. Body chamber incomplete, but represented by at least half a whorl.

The ribbing is flexuous on the flanks, arched forward on the venter, and somewhat reduced in strength along the midventral lines. The primary ribs begin at the umbilical seam, and incline forward gently on the lower part of the flanks, and generally divide near the middle of the flanks into pairs of weaker secondary ribs that arch forward considerably. Some secondary ribs are indistinctly connected with the primary ribs, and some arise freely above the middle of the flanks.

About 8 to 9 flexuous constrictions occur on each whorl. These constrictions are inconspicuous on the smaller whorls, but become more prominent during growth. Some constrictions on the penultimate and body whorls are bounded by swollen ribs that on the venter may become flared.

The suture line is poorly preserved and cannot be traced.

The holotype at its adoral end has a whorl height of 58 mm and a whorl thickness of 51 mm. The paratype shown on plate 15, figures 7, 8, 11, at a diameter of 42 mm, has a whorl height of 20.5 mm, a whorl thickness of 18 mm, and an umbilical width of 10 mm.

This species is distinguished from any species of *Puzosia* by being more involute and by having persistent primary ribs of which most divide near the middle of the flanks. It differs from *K. bifurcata* Imlay, n. sp., by having a stouter whorl section, coarser, sparser ribbing, and a more abruptly rounded umbilical edge.

Types: Holotype USNM 130152. Paratypes USNM 130153a, b.
Localities: USGS Mes. locs. 9489, 14485.

Genus PUZOSIA Bayle, 1878

Puzosia alaskana Imlay, n. sp.

Plate 16, figures 1–13

The species is represented by about 90 specimens. Whorls elliptical in section, higher than wide, widest near the umbilicus, embracing about one-half of preceding whorls. Flanks flattened, converging slightly toward the highly arched venter. Umbilicus moderate in width; wall steeply inclined in early growth stages, becoming vertical in adult, rounding evenly into flanks in early stages, but abruptly in adult. Body chamber represented by three-fifths of a whorl.

The ornamentation on immature specimens consists of strongly flexuous striae, riblets, and constrictions that arch forward considerably on the venter. They curve forward on the umbilical wall and base of the flanks, curve backward slightly below the middle of the flanks, and then curve forward strongly on the upper part of the flanks. The riblets are most pronounced on the venter and upper parts of the flanks, but many of the constrictions are bounded on one, or on both, sides by riblets that begin at the umbilical margin. The constrictions number from 6 to 7 per whorl and are much more conspicuous on the internal molds than on the shell.

During growth the constrictions become more deeply impressed and more strongly arched on the venter. The ribbing weakens on the lower part of the flanks, but becomes stronger on the venter and on the upper part of the flanks. On the adult body chamber there are from 18 to 12 ribs between successive constrictions. Generally the ribs bordering the constrictions on the venter are somewhat swollen.

The suture line descends fairly rapidly toward the umbilicus. It is characterized by the second lateral saddle being a little higher than the first lateral saddle. This feature occurs in the genus *Melchiorites* as figured by Fallot (1920, p. 255–257) as well as in *Puzosia* (see Spath, 1923, pl. 2, fig. 3e).

The holotype at a diameter of 41 mm has a whorl height of 17 mm, a whorl thickness of 13 mm, and an umbilical width of 13.5 mm. The same dimensions of the small paratype shown on plate 16, figure 11, are 29, 12, 10, and 8.5 mm, respectively.

This species shows resemblances with the genera *Melchiorites*, *Puzosia*, and *Hulenites*. In lateral view it resembles *Puzosia quenstedti* Parona and Bonarelli (1897, p. 81, pl. 11, figs. 3a, b) from the Albian of Europe, but its ribs and constrictions arch forward much more on the venter, and it develops an abrupt instead of an evenly rounded umbilical edge. The pattern of its ornamentation and the shape of its umbilical edge is so similar to that of *Hulenites reesidei* (Anderson, 1938, p. 187, pl. 38, figs. 2, 3) from the late Aptian to early Albian of California as to suggest that the two species are closely related. It may be distinguished from *H. reesidei*, however, by being more compressed, by having more projected ornamentation on the venter, by its ribs showing no tendency to fade on the venter, and by the ribs on the immature whorls being much finer and more flexuous. It also shows considerable resemblance to ribbed species of *Melchiorites*—such as *M. indigenes* Anderson (1938, p. 184, pl. 67, fig. 3, pl. 68, fig. 2) from the Aptian of California, but it is distinguished by developing an abrupt umbilical edge and finer, denser, more sigmoidal ribbing.

Types: Holotype USNM 130143. Paratypes USNM 130144.
Locality: USGS Mes. loc. 9492.

Genus BEUDANTICERAS Hitzel, 1905

Beudanticeras glabrum (Whiteaves)

Plate 16, figures 14–21

Placenticeras glabrum Whiteaves, 1889, Contr. to Canadian Paleontology, v. 1, pt. 2, p. 172, pl. 24, figs. 1, 1a, b.

Desmoceras affine var. *glabrum* Whiteaves, 1893, Royal Soc. Canada, 1st ser., v. 10, p. 115, pl. 9.

Beudanticeras glabrum (Whiteaves). McLearn, 1931, Royal Soc. Canada, Trans., ser. 3, v. 25, sec. 4, p. 3.

?*Beudanticeras* cf. *B. glabrum* Whiteaves. McLearn, 1945, Geol. Survey Canada Paper 44–17 (2d ed.), pl. 4, figs. 2, 3.

Beudanticeras glabrum (Whiteaves). Warren, 1947, Jour. Paleontology, v. 21, p. 121, pl. 30, figs. 1–4.

Nine specimens of *Beudanticeras*, obtained in the Talkeetna Mountains, very closely resemble the original type specimen described by Whiteaves in their narrowly rounded whorl section, very narrow umbilicus, broad asymmetrical first lateral lobe, low, broad saddles, and numerous auxiliary lobes. Furthermore, five of the specimens are nearly as smooth as the type, being marked only by fine flexuous striae that are barely visible under oblique lighting. The other four differ from the type, however, by having riblets and weak bulges on the flanks. In addition several of the specimens bear one or more weak constrictions per whorl.

The presence of striae and riblets on some of the specimens from the Talkeetna Mountains agrees with the observations of Warren (1947, p. 121) based on specimens of *Beudanticeras glabrum* (Whiteaves) from the Lower Mackenzie River valley in Canada. In his specimens, however, the ornamentation is most conspicuous near the umbilical border and constrictions are absent.

These differences are probably not of specific value considering that the number and strength of constrictions is a variable characteristic in many species of *Beudanticeras*, that the determination of the presence of weak constrictions may be difficult on poorly, preserved specimens, and that the distribution of riblets on the flanks may reflect individual variations. The fact that most of the specimens from the Talkeetna Mountains agree very well in their characteristics with the holotype of *B. glabrum* (Whiteaves) is herein given more weight than the minor differences in ornamentation mentioned above.

This species is characterized by its umbilicus being narrower and its saddles broader and lower than in most species that have been assigned to the genus *Beudanticeras*. The narrowness of the umbilicus is comparable, however, with that of *B. sutherlandi* (Etheridge) (Whitehouse, 1928, p. 202, pl. 25, fig. 4) from Australia, which species differs from *B. glabrum* by its stouter whorls. Furthermore the sutural pattern is similar to that in *B. laevigatum* (J. de C. Sowerby) (Spath, 1923, p. 56) from England; this species differs by its wider umbilicus and stouter whorls. Because of these similarities *B. glabrum* is herein considered as belonging within the range of variation of *Beudanticeras*, although possessing peculiar characteristics somewhat different from typical species of *Beudanticeras* in Europe. The differences are no greater than among certain Jurassic ammonites from western North America that Arkell (in Arkell and Playford, 1954, p. 596–597) assigns to genera based on European species even though they possess certain features that are not characteristic of the types.

Type: Plesiotypes USNM 130149.
Locality: USGS Mes. loc. 24877.

Subgenus GRANTZICERAS Imlay, 1960

Beudanticeras (Grantziceras) multiconstrictum Imlay

Plate 14, figures 1, 2

Beudanticeras (*Grantziceras*) *multiconstrictum* Imlay, 1960, U.S. Geol. Survey Prof. Paper 335 (*in press*).

This species is characterized by many regularly spaced falciform constrictions, by broadly bundled striae on its flanks, and by a scaphitoid body chamber. Its largest specimens are considerably larger than any described European species of *Beudanticeras*, but are only about half as large as *B. affine* (Whiteaves) from Canada and northern Alaska. It resembles *B. affine* more closely than any other described species of *Beudanticeras*, but differs by having nearly twice as many constrictions per whorl, a somewhat wider umbilicus, a shorter second lateral lobe, and a more compressed whorl section.

Types: Holotype USNM 128721. Paratypes USNM 128722, 128723.
Localities: USGS Mes. locs. 24877, 25320, 25329.

Genus BREWERICERAS Casey, 1954

Brewericeras breweri (Gabb)

Plate 17, figures 5–10, 12, 13

Ammonites breweri Gabb, 1864, Paleontology Calif. v. 1, p. 62, pl. 10, fig. 7.

Gabb, 1869, Gabb, Paleontology Calif., v. 2, p. 130, pl. 19, fig. 5b, pl. 20, fig. 5.

Gabb, Whiteaves, 1876, Geol. Survey Canada Mesozoic Fossils, v. 1, p. 21, pl. 1, figs. 2, 2a, 3, 3a.

Beudanticeras breweri (Gabb). Anderson, 1938, Geol. Soc. America Spec. Paper 16, p. 189, pl. 43, fig. 3, pl. 44, figs. 1, 2.

Brewericeras breweri (Gabb). Casey, 1954, Washington Acad. Sci. Jour., v. 44, no. 4, p. 112.

The 13 Alaskan specimens of this species on hand are all compressed, have flattened flanks, a highly arched venter, a vertical or nearly vertical umbilical

wall, and a fairly sharp umbilical rim. They all develop sigmoidal ribs that bear extremely weak, forwardly inclined swellings at the umbilical edge, that are prominent and sparse on the upper part of the flanks, and are reduced in strength on the venter and on the lower parts of the flanks. They show considerable variation, however, in strength of ribbing and in the stage of growth at which ribs first appear. In some specimens sigmoidal ribs appear at a diameter as small as 20 mm. In other specimens ribs first appear at a diameter of 50 mm. The costate parts of internal molds bear constrictions that are conspicuous only on the venter. The suture line is similar to that of the genus *Beudanticeras*.

Type: Pleslotype USNM 130133.
Locality: USGS Mes. loc. 9492.

Brewericeras cf. B. hulenense (Anderson)

Plate 17, figures 11, 14–16

Beudanticeras hulenense Anderson, 1938, Geol. Soc. America Spec. Paper 16, p. 190, pl. 44, figs. 3, 4.
Brewericeras hulenense (Anderson). Casey, 1954, Washington Acad. Sci. Jour., v. 44, no. 4, p. 112.

Associated with *B. breweri* (Gabb) at Mesozoic locality 9492 are some ammonites that are possibly only a smooth variant of that species. They differ, however, by having a smaller umbilicus, slightly flatter flanks, and much weaker, finer ribbing that develops at a later growth stage. In addition the larger specimens have a slightly raised umbilical rim. These specimens have hitherto been assigned to "*Ammonites*" *haydeni* Gabb (Martin, 1926, p. 346; Moffit 1938, table opposite p. 80; Imlay and Reeside, 1954, p. 229), but their whorl sections compare in stoutness with those of *B. hulenense* (Anderson) (1938, pl. 44, fig. 4) rather than with those of *B. haydeni* (Gabb) (1864, p. 62, pl. 10, fig. 8a), which has similar weak ornamentation.

Figured specimens: USNM 130130, 130159.
Localities: USGS Mes. loc. 9492, 14514.

Genus DESMOCERAS Zittel, 1884

Desmoceras? sp. juv.

Plate 17, figures 1–4

The species is represented by one internal mold. The specimen is small and has a subquadrate whorl section. At a diameter of 26 mm, its whorl height is 13 mm, its whorl thickness is 14 mm and its umbilical width is 4 mm. The adoral part of the internal mold is marked by two conspicuous gently flexuous constrictions that arch forward slightly on the venter. Between the constrictions on the venter are faint riblets. The suture line is typical of *Desmoceras*.

This species differs from *D. voyi* Anderson (1938, p. 180, pl. 40, figs. 4–8) by having a subquadrate instead of an ovate whorl section. It is so much smaller than the figured specimens of *D. merriami* (Anderson) (1902, p. 103, pl. 6, figs. 135–138; 1938, p. 181, pl. 43, figs. 1, 2) that comparisons with that species would be meaningless.

Figured specimen: USNM 130135.
Locality: USGS Mes. loc. 9492.

Genus PARASILESITES Imlay, 1959

The original description (Imlay, 1959, p. 184) is as follows:

This genus is characterized by its fairly evolute shell, wide, shallow umbilicus, strongly flexuous ribs and constrictions, presence of umbilical bullae, occasional rib furcation on the flanks, and by the auxiliaries of its suture line descending only slightly. It differs from the Barremian genus *Silesites* by the presence of umbilical bullae, by the furcation of some ribs low on the flanks, by the ribs being inclined forward strongly at the edge of the umbilicus, and perhaps by its auxiliaries not curving adorally. It differs from the upper Aptian-lower Albian genus *Neosilesites* by the presence of umbilical bullae, by its ornamentation being much more sigmoidal, by its ribs branching much lower on the flanks, and by its primary ribs not splitting into many fine secondary ribs on the upper parts of the flanks. The suture line of *Parasilesites* is similar to that on small specimens of *Silesites* and *Neosilesites* (Fallot 1920a, p. 54, 55; 1920b, p. 209–213). The tendency in the Silesitidae (Wright, 1957, p. L372) for the auxiliaries to curve forward in advance of the first saddle, as illustrated by Uhlig (1883, pl. 18, figs. 11–14), does not bar *Parasilesites* from that family considering that the tendency, as discussed by Fallot (1920b, p. 209) is general only among adults. The type species of *Parasilesites* is *Parasilesites bullatus* Imlay, n. sp.

Parasilesites bullatus Imlay

Plate 18, figure 1–8

Parasilesites bullatus Imlay, 1959, Jour. Paleontology, v. 33, no. 1, p. 184, pl. 29, figs. 1–8.

Only two specimens of this species are known. Whorls ovate in section, a little higher than wide, embracing about two-fifths. Flanks gently convex, rounding evenly into highly arched venter. Umbilicus fairly wide, shallow; umbilical wall low, steeply inclined, rounding evenly into flanks. Body chamber incomplete, represented by at least half a whorl.

The innermost whorls, exposed in the umbilicus of the type specimens, are marked by 7 or 8 deep, forwardly inclined constrictions and by faint forwardly inclined riblets. On the penultimate whorl the riblets are a little stronger and more flexuous, and number from 5 to 7 between successive constrictions. Those riblets adjoining constrictions are a little larger than the others and some of them bear weak bullae near the umbilical margin. On the body whorl both constrictions and ribs become stronger, many ribs are bullate, and some rib branching occurs at the bullae. On both the penultimate and body whorls the ribs and constrictions arch forward on the venter and most of the ribs are somewhat weakened on the venter. The venter of the internal mold at the beginning of the

body chamber bears a distinct groove that has a length of only 8 mm. The ribs end abruptly at this groove and some terminate in swellings. The groove may represent a deformity and probably is not of specific importance.

The suture line is very simple. Its auxiliaries descend only slightly toward the umbilical seam. The ventral lobe is nearly as long as the first lateral lobe.

The holotype at a diameter of 27 mm has a whorl height of 9 mm, a whorl thickness of 8 mm, and an umbilical width of 11.5 mm.

The species is characterized by developing distinct umbilical bullae, by having fairly regularly-spaced constrictions and ribs, and by some of the ribs bifurcating from the bullae. The small paratype resembles *Silesites puzosiaformis* Anderson (1938, p. 191, pl. 20, figs. 9, 10) from the early Albian of California, but is stouter, has coarser ribbing, more and deeper constrictions, and bears weak umbilical bullae.

Types: Holotype USNM 129872. Paratype USNM 129873.
Occurrence: USGS Mes. loc. 9492.

Parasilesites irregularis Imlay, n. sp.

Plate 18, figures 9–17

This species is represented by three specimens. Shell compressed, discoidal. Whorls subquadrate in section, higher than wide, embracing about one-third. Flanks flattened, rounding evenly into moderately arched venter. Umbilicus fairly wide, shallow; wall low, steeply inclined, rounding evenly into flanks. Body chamber represented by at least half a whorl. Aperture sinuous and has a pronounced ventral projection.

The ornamentation of the septate whorls, exposed in the umbilicus of the holotype, consists of 9 deep, flexuous constrictions between which lie from 2 to 5 prominent, irregularly spaced, single flexuous ribs. The ribs adjoining the constrictions are somewhat stronger than the other ribs and many of them are swollen on the umbilical edge. Both constrictions and ribs weaken considerably on the venter and arch forward gently on the venter.

On the flanks of the body chamber the constrictions and ribs become more flexuous, stronger, and more irregularly spaced. Many of the ribs are distinctly bullate at the umbilical edge. On the venter both constrictions and ribs arch forward strongly, the constrictions are narrow and deep, and the ribs are highly variable in strength. Most of the ribs bordering the constrictions on the venter are swollen. Between these ribs are bundles of riblets or striae that arise from the flank ribs on the margin of the venter and tend to fade out on the venter or to pass into swollen ribs.

The suture line is very simple, and its auxiliaries descend only slightly toward the umbilicus.

The holotype at an estimated diameter of 24 mm has a whorl height of 8 mm, a whorl thickness of 7 mm, and an umbilical width of 10 mm.

The presence of umbilical bullae readily distinguish this species from all species of *Silesites*, but its irregular ribbing bears some resemblance to that of *S. vulpes* (Coquand) as figured by Uhlig (1883, p. 111, pl. 18, figs. 8, 9) from the Barremian of the Carpathian Mountains.

Types: Holotype USNM 130147. Paratypes USNM 130148.
Locality: USGS Mes. loc. 9492.

Genus HULENITES Matsumoto, 1955

Hulenites cf. H. reesidei (Anderson)

Plate 18, figures 18–21

The genus *Hulenites* (Matsumoto, 1955, p. 122) is represented in the Chitina Valley by 4 specimens, of which 1 is much smaller than the other 3. Shell compressed, discoidal. Whorls ovate in section, higher than wide, becoming higher during growth, embracing about one-half preceding whorls. Flanks gently convex, becoming flatter during growth, rounding evenly into highly arched venter. Umbilicus moderately wide, shallow; umbilical wall low, vertical at base, rounding rather abruptly into flanks. Body chamber incomplete, represented by at least half a whorl.

The inner whorls, exposed in the umbilicus, bear many deep, forwardly inclined constrictions, but otherwise are smooth. The outer whorl of the smaller figured specimen has nine flexuous constrictions that arch forward strongly on the venter and become more deeply impressed during growth. Weak, forwardly inclined riblets are barely visible on the upper part of the flanks and on the venter. The outer whorl of the larger specimens bears constrictions that are deep near the umbilicus and shallow on the venter. Between successive constrictions are from 7 to 12 fine, forwardly inclined ribs that begin below the middle of the flanks, arch forward on the venter, and weaken along the midventral line. Some of the ribs bordering the constrictions are swollen.

The suture line cannot be traced accurately.

The larger specimen illustrated at a diameter of 33 mm has a whorl height of 13.5 mm, a whorl thickness of 11 mm, and an umbilical width of 12 mm.

The largest specimens from the Chitina Valley are comparable in size with the small paratype of *Hulenites reesidei* (Anderson) (1938, p. 187, pl. 38, fig. 3) from California. They appear to have finer ribbing, a stouter whorl section, and a wider umbilicus. As these differences are all minor and as the range of variation in *H. reesidei* (Anderson) is unknown, the establishment of the Alaskan specimens of *Hulenites* as a distinct species does not seem justified at present.

Figured specimen: USNM 130134.
Localities: USGS Mes. loc. 9480, 9492, 14466.

Genus CLEONICERAS Parona and Bonarelli, 1896

Cleoniceras overbecki Imlay, n. sp.

Plate 19, figures 36–39

One small specimen of *Cleoniceras* has been found in the Chitina Valley. Whorl compressed, much higher than wide, widest at umbilical edge, embracing about three-fourths of preceding whorls. Flanks flat, converging from umbilical edge to narrowly rounded venter. Umbilicus narrow; wall low, vertical at base, steeply inclined above, rounding abruptly into flanks. Body chamber unknown.

The umbilical edge bears 15 weak bullae that become weaker adorally. From these bullae pass weak, slightly flexuous ribs that incline forward on the flanks and arch forward on the venter. Some ribs remain single, but many bifurcate on the lower third of the flanks. Other ribs arise freely between the lower third and the middle of the flanks. All ribs become stronger ventrally, but are reduced somewhat in strength along the midventral line. There are 42 ribs on the upper part of the flanks, or nearly 3 secondary ribs for each primary.

The suture line cannot be traced. The figured specimen at a diameter of 38 mm has a whorl height of 18 mm, a whorl thickness of 10 mm, and an umbilical width of 7.5 mm.

The Alaskan species somewhat resembles the small specimen of *Cleoniceras cleon* (d'Orbigny) (1841, pl. 84, fig. 3) from France. That species, however, judging from a plaster replica of a typical specimen furnished by Raymond Casey of the British Geological Survey, has more prominent bullae and much stronger, more flexuous ribs. *C. bicurvatoides* (Sinzow) (1909, p. 29, pl. 2, figs. 7–18) from southern Russia has much more flexuous ribs and less prominent umbilical bullae. *C. baylei* (Jacob) at a comparable size, as figured by Spath (1925, p. 93; 1923, pl. 4, figs. 6a, b), has a much stouter whorl section. *C. leightonense* Spath (1942, p. 701, 702, text fig. 247) is similar in shape and ornamentation, but is not strictly comparable because of the much greater size of the type. The adoral weakening of the ribs and bullae on the Alaskan species indicates that it loses its ornamentation at a much smaller size than does *C. leightonense* Spath.

The Alaskan specimen is the only one yet described from the Pacific coast of North America that fits the definition of *Cleoniceras* in all particulars. As its characteristics do not match those of the described species of *Cleoniceras* from Eurasia, it is deemed worthy of specific rank even though its adult characteristics are unknown.

This species is named in honor of R. M. Overbeck, who collected many of the ammonites from the Chitina Valley described herein.

Type: Holotype USNM 130141.
Locality: USGS Mes. loc. 9492.

Genus PUZOSIGELLA Casey, 1954

Puzosigella cf. P. rogersi (Hall and Ambrose)

Plate 19, figures 33–35

Three specimens from the Chitina Valley probably belong to "*Sonnratia*" *rogersi* Hall and Ambrose (1916, p. 69) as interpreted by Anderson (1938, p. 197, pl. 20, figs. 6, 7). They are closely similar to the small plesiotype figured by Anderson on his plate 20, figure 6, but differ from the larger specimen figured by Anderson by losing their umbilical bullae at an earlier growth stage and by having finer, more closely spaced secondary ribs. Such differences appear to be normal for the species judging from the specimens in the Geological Survey collections from Oregon and California. As these collections show that the genus *Puzosigella* is characterized by considerable variability, the validity of the species discussed by Anderson should be established thoroughly before additional species are described. The Alaskan specimens may represent a distinct species from any described, but such cannot be proved now. The presence of the genus *Puzosigella* in Alaska is itself of stratigraphic importance as *Puzosigella* in California and Oregon is restricted to beds of early Albian age.

Figured specimen: USNM 130168.
Locality: USGS Mes. loc. 8877.

Genus LECONTEITES Casey, 1954

This genus includes shells that are compressed and moderately involute and that develop a vertical umbilical wall. The shell is marked by flexuous ribs that are arched forward considerably on the venter and are reduced in strength along the midventral line. Bifurcation near the middle of the flanks is common. Weak flexuous constrictions that may be bordered by flared ribs on the venter are more evident on the internal mold than on the shell. The most finely ribbed species develop a sharp umbilical rim and weak umbilical bullae. The more coarsely ribbed species develop an abruptly rounded umbilical rim and more or less swollen primary ribs. The genus *Puzosigella* Casey (1954, p. 110) differs from *Leconteites* mainly by having more prominent umbilical bullae, by the flanks ribs originating in bundles at these bullae, and by possessing many, rather conspicuous, narrow constrictions on immature specimens.

Leconteites modestus (Anderson)

Plate 19, figures 4–6

Cleoniceras modestum Anderson, 1938, Geol. Soc. America Spec. Paper 16, p. 193, pl. 50, figs. 2–4.

This species is represented in the Chitina Valley by three specimens that compare closely in shape and ribbing with the paratypes from California figured by Anderson on his plate 50, figures 3 and 4. They all differ from the type specimens of *L. lecontei* (Anderson) (1938, p. 192, pl. 38, fig. 4, pl. 47, figs. 3–5) by having weaker less flexuous ribs and less conspicuous umbilical tubercles. However, collections on hand from California and Oregon suggest that *L. modestus* is merely a smooth variant of *L. lecontei*. This matter cannot be settled until larger collections are available. Illustrations of *L. lecontei* (Anderson) are shown on plate 19, figures 1–3, for comparison with the Alaskan specimens of *L. modestus* (Anderson) and *L. deansi* (Whiteaves) described herein.

Type: Pleslotypes USNM 130172, 130173.
Localities: USGS Mes. loc. 9971, 11389.

Leconteites deansi (Whiteaves)

Plate 19, figures 7–14

Olcostephanus (*Astieria*) *deansi* Whiteaves, 1893, Canadian Record Science p. 442–444, pl. 7, figs. 1, 1a.

The species is represented by 35 specimens. Shell small, discoidal, compressed. Whorls subovate, higher than wide, embracing about three-fifths. Flanks flattened below, converging slightly above to narrowly round venter. Umbilicus fairly narrow; wall low, vertical, rounding rather abruptly into flanks on inner whorls, but developing a rim on adult body chamber. The body chamber represents about three-fifths of a whorl.

The ribbing is fine and strongly flexuous. The primary ribs incline forward on the umbilical wall and on the lower third of the flanks where they recurve and then pass into pairs of slightly weaker secondary ribs that incline forward strongly on the venter. Bifurcation on the inner whorls occurs on the lower third of the flanks, but during growth the points of furcation rise to the middle of the flanks. In a few places furcation occurs at or near the umbilical edge. Many pairs of secondary ribs are separated by single ribs that arise above the middle of the flanks. All ribbing is much reduced in strength on the venter, even where shelly material is preserved. Tubercles are not present, although some of the primary ribs on the body whorl are faintly swollen at the umbilical edge. Each whorl is marked by five or six weak constrictions that are most evident on the venter.

The suture line is imperfectly preserved. It is characterized by the first lateral lobe being much longer than the ventral lobe. Its general plan is similar to that of *L. lecontei* (Anderson) (1938, p. 183, text fig. 3, no. 5, pl. 47, fig. 3), but its major lobes and saddles are more slender and less frilled, and its auxiliary lobes are much smaller.

The specimen shown on plate 19, figures 9–11, has been only slightly compressed. At a diameter of 40 mm, its whorl height is 18.5 mm, its whorl thickness is 13.5 mm, and its umbilical width is 10 mm. These dimensions are similar to those of the holotype.

L. deansi (Whiteaves) in general appearance is similar to *Leconteites lecontei* (Anderson) (see pl. 19, figs. 1–3) from the early Albian of California and Oregon, but may be distinguished by having stronger primary ribs, by lacking tubercles, and by developing a sharp umbilical rim at a much later growth stage.

Type: Pleslotypes USNM 130164, 130170.
Localities: USGS Mes. locs. 2201, 8872, 9967a, 9972. Fragmentary specimens possibly belonging to *L. deansi* (Whiteaves) were found at Mes. locs. 8873, 8880, 9967, 9973, 14484.

Leconteites cf. L. deansi (Whiteaves)

Plate 19, figures 15–27

From the same beds as specimens assigned to *L. deansi* (Whiteaves) and in part from the same localities (Mes. loc. 8872, 9972) have been obtained 25 specimens of *Leconteites* that differ from *L. deansi* by having much stronger primary ribs, a slightly wider umbilicus, a stouter whorl section, and rounder flanks (pl. 19, figs. 19–27). These features would ordinarily be sufficient to justify assigning them to a distinct species. However, the presence at other localities (Mes. locs. 2201, 14484) of 4 specimens (pl. 19, figs. 16–18) that are intermediate in appearance suggest that the 25 stout, coarsely ribbed specimens are merely an extreme variana of *L. deansi* (Whiteaves). Their status cannot be settled definitely by the specimens on hand.

Figured specimens: USNM 130158, 130162, 130169, 130174.
Localities: USGS Mes. loc. 2201, 8872, 8873, 8878, 9972, 14484.

Genus LEMUROCERAS Spath, 1942

Lemuroceras talkeetnanum Imlay, n. sp.

Plate 18, figures 34–41

?*Lemuroceras* cf. *L. indicum* Spath. McLearn, 1945, Geol. Survey Canada Paper 44–17 (2d ed.), pl. 5, fig. 4.

This species is represented by two specimens that retain some of the inner shelly layer. On this layer feather structures is well shown at one place (Arkell, in Arkell, Kummel and Wright, 1957, p. L92). The whorls are subquadrate in section and higher than wide

and embrace about three-fifths of preceding whorl. The flanks are flattened, but become gently convex on the body chamber. The venter is nearly flat on the sutured part of the shell and gently rounded on the body chamber. The umbilicus is moderately narrow; the umbilical wall is low and steeply inclined and rounds evenly into the venter. The body chamber is represented by half a whorl and appears to be complete.

The ribbing on the septate part of the body whorl is prominent, widely spaced, and strongly flexuous. About half of the ribs arise on the umbilical wall, are most prominent at the umbilical edge, incline forward strongly low on the flanks, recurve near the middle of the flanks, and arch forward strongly on the upper part of the flanks and on the venter. The remaining ribs either arise freely near, or below, the middle of the flanks, or are indistinctly connected with the longer ribs at about the top of the lower third of the flanks. All ribs are equally strong on the venter, and all are slightly reduced in strength along the midventral line.

The ribbing on the body chamber fades out rapidly toward the aperture and becomes less strongly arched on the venter. Near the aperture only weak lines of growth are visible where the shell is preserved and the internal mold is quite smooth.

The body chamber has been crushed laterally and cannot be measured. At the beginning of the body chamber, the whorl height is 17 mm, and the whorl thickness is 13 mm.

The suture line is quite similar to that of *L. aburense* (Spath) (1933, p. 801, pl. 129, fig. 5) from India. The first lateral lobe is a little longer than the ventral lobe. The first lateral saddle is very wide. The other lobes and saddles are relatively much smaller. The auxiliaries descend slightly toward the umbilicus.

This species is remarkably similar to *L. indicum* (Spath) (1933, p. 801, pl. 128, figs. 4a, b, 5a, b) from India and Madagascar (Collignon, 1949, p. 68, 69, pl. 12, figs. 2, 2a, b, pl. 14, fig. 2). It is distinguished from that species mainly by being more involute and by its ribs arching forward more strongly on the venter. It appears, also, to have flatter flanks, but that may be a result of compression. The primary ribs are not nearly so prominent at the umbilical edge as in the holotype of *L. indicum* (Spath), or in the ammonite fragment figured by McLearn (1945, pl. 5, fig. 4), from the western interior of Canada, but the ribs are of nearly the same strength as on the paratype of *L. indicum* (Spath) (1933, pl. 128, fig. 5a).

Types: Holotype USNM 13015. Paratype USNM 130150.
Locality: USGS Mes. loc. 24877.

Lemuroceras? sp. juv. cf. L. dubium Collignon

Plate 18, figs. 26–29

One small specimen has a subquadrate whorl section, flattened flanks and venter, a moderately wide umbilicus, and a low vertical umbilical wall that rounds evenly into the flanks.

The ribs are strongly flexuous on the flanks and arch forward moderately on the venter. Most ribs begin on the umbilical wall and remain single on the flanks. About one-third of the ribs bifurcate at, or below, the middle of the flanks, or are indistinctly connected with secondary ribs. A few secondary ribs arise freely on the flanks. The secondary ribs are as strong, or nearly as strong, as the primary ribs. All ribs are slightly reduced in strength along the midventral line. Six weak constrictions are present, but are conspicuous only on the venter.

At a diameter of 25 mm, the whorl height is 10 mm, the whorl thickness is 8 mm, and the umbilical width is 7.5 mm.

The suture line is not preserved.

This specimen is assigned to *Lemuroceras* rather than to *Leconteites* because of the characteristics of its ribbing, but it does have a vertical wall, a feature which is characteristic of *Leconteites*. Its appearance in lateral view is similar to that of *L. dubium* Collignon from Madagascar (1949, p. 74, pl. 15, figs. 2, 2a, b), but it has fewer secondary ribs and more primary ribs per whorl, is more compressed, and has a vertical umbilical wall.

Figured specimen: USNM 130157.
Locality: USGS Mes. loc. 14484.

Subgenus SUBARCTHOPLITES Casey, 1954, revised Imlay

Subarcthoplites Casey (1954, p. 111) based on *Lemuroceras belli* McLearn (1945, pl. 3, figs. 17, 18) from the western interior of Canada was considered by its author to be more similar to the boreal genus *Arcthoplites* than to *Lemuroceras* from India and Madagascar. The discovery of adult specimens of *Lemuroceras belli* McLearn in northern Alaska shows, however, that it differs from *Arcthoplites* by lower points of rib branching, by the presence of constrictions, and by its ribs fading on the body chamber instead of becoming coarser. In these respects it is identical with typical species of *Lemuroceras* from India and Madagascar. *Lemuroceras belli* McLearn differs from the typical species only by having rounder flanks, less flexuous ribbing, and a less abrupt change in the direction of ribbing on the lower part of the flanks. These differences are slight and are not considered worthy of more than subgeneric rank.

Lemuroceras (Subarcthoplites) aff. L. belli McLearn

Plate 18, figures 23, 30–33

Two immature specimens of *Lemuroceras* from the Chitina Valley differ from *L. belli* McLearn (1945, pl. 3, figs. 17, 18; 1948) by being more compressed and by having weaker ribs that bifurcate less commonly and are more widely spaced on the venter.

The small specimens from the Chitina Valley each have about one-third of a whorl of body chamber. On the septate part of the shell the primary ribs incline forward strongly on the umbilical wall and on the lower third of the flank where most of them either bifurcate or are indistinctly connected with a secondary rib. All ribs curve backward near the middle of the flanks and then arch forward gently on the venter. On the body chamber, furcation becomes less common and secondary ribs become fewer. All ribs continue across the venter with only slight reduction in strength as compared with the ribs on the flanks.

The suture line has a very wide first lateral saddle and a wide trifid first lateral lobe that is only slightly longer than the ventral lobe. The auxiliaries are curved slightly adorally. The pattern of the suture is similar to that of *L. aburense* (Spath) (1933, pl. 129, fig. 5) from India.

Figured specimen: USNM 130136.
Locality: USGS Mes. loc. 9492.

Arcthoplites? sp.

Plate 18, figures 22, 24, 25

Two fragments bear high, thin, widely spaced ribs similar to those on the outer whorl of *Arcthoplites jachromensis* (Nikitin) (1888, p. 57, pl. 4, fig. 1) from the lower or middle Albian of Russia. On the venter of the internal mold the ribs arch forward and become a little broader and lower. In places where the shell is preserved the ribs are much thicker than on the internal mold. As the lower parts of the flanks are not preserved, the fragments could be assigned as readily to *Tetrahoplites* or *Pseudosonneratia* as to *Arcthoplites*.

Figured specimen: USNM 130137.
Locality: USGS Mes. loc. 9492.

REFERENCES

Anderson, F. M., 1938, Lower Cretaceous deposits in California and Oregon: Geol. Soc. America Spec. Paper 16, 339 p., 85 pls., 6 figs.

——— 1902, Cretaceous deposits of the Pacific Coast: California Acad. Sci. Proc., 3d ser., v. 2, 126 p., illus.

Anthula, D. J., 1899, Über die Kreidefossilien des Kaukasus: Beitr. Paläontologie Oesterr.-Ungarns u. des Orients, v. 12, p. 55–102, pls. 2–7.

Arkell, W. J. and Playford, P. E., 1954, The Bajocian ammonites of western Australia: Royal Soc. London Philos. Trans., ser. B, Biological Sciences, no. 651, v. 237, p. 547–605, pls. 27–40.

——— *in* Arkell, W. J., Kummel, Bernhard, and Wright, C. W., 1957, Mesozoic Ammonoidea: Treatise on Invertebrate Paleontology, part L, Mollusca 4, 490 p., illus.

Breistroffer, Maurice, 1947, Zur las zones d'Ammonites dans l'Albian de France et d'Angleterre: Grenoble Univ., Lab. geologie, Travaux, v. 26, p. 1–88.

Brinkmann, Roland, 1937, Biostratigraphie des Leymericlienstammes nebst Bemerkungen zür Paläogeographie des Nordwestdeutschen Alb: Hamburg Min. geol. Staatsinst. Mitt., no. 16, p. 1–18, figs. 1–12.

Casey, Raymond, 1954, New Genera and subgenera of Lower Cretaceous ammonites: Washington Acad. Sci. Jour., v. 44, no. 4, p. 106–115, 1 pl.

——— 1957, The Cretaceous ammonite genus *Leymericlia*, with a systematic account of its British occurrences: Palaeontology, v. 1, pt. 1, p. 29–59, pls. 7–10, 6 text figs.

Chaput, M. E., 1920, Les Desmoceratides du Paleocretace. Revision du genre Desmoceras *in* Kilian, Wilfred, and others, Contributions a l'etude des céphalopodes paléocrétacés du Sud-Est de la France: Mém. Carte géol. det. France, p. 167–180, 1 pl.

Collignon, Maurice, 1937, Les ammonites pyriteuses de l'Aptien D'Antanatana-mirafy: Paléont. de Madagascar, 22, Annales de paléontologie, p. 107–132, pls. 1–3.

——— 1949, Recherches sur les faunes Albiennes de Madagascar I-L'Albien d'ambarimaninga (Madagascar); Annales geol. Serv. des Mines de Madagascar, part 16, 128 p., 22 pls., 29 text figs.

Fallot, Paul, 1920a, La faune des marnes aptiennes et albiennes de la region d'Andraitx, Majorque: Trab. Mus. Nac. de ciene. Nat. ser. geol., no. 26 (Madrid), p. 1–68, pls. 1–3.

——— 1920b, Remarques sur le genre Sibesites *in* Kilian, Wilfred, and others, Contributions a l'etude des céphalopodes paléocrétacés du Sud-Est de la France: Mém. Carte geol. det. France, p. 207–226, 7 text figs.

Gabb, W. M., 1864, Description of the Cretaceous fossils: California Geol. Survey, Paleontology, v. 1, p. 56–236, pls. 1–32.

——— 1869, Cretaceous and Tertiary fossils: California Geol. Survey, Paleontology, v. 2, 299 p., pls. 1–36.

Hall, E. B., and Ambrose, A. W., 1916, Description of new species from the Cretaceous and Tertiary of the Telsa, Pleasanton, San Jose and Mount Hamilton quadrangles, California: Nautilus, v. 30, p. 68–71.

Henderson, W. R. S., 1954, Cretaceous and some Triassic beds of northeastern British Columbia, Canada: Am. Assoc. Petroleum Geologists Bull., v. 38, no. 11, p. 2269–2289, 6 figs.

Hyatt, Alpheus, 1900, Cephalopoda *in* Zittel, K. A., Textbook of Palaeontology: 1st English ed. transl. Eastman, C. R., p. 502–592, figs. 1049–1235.

Imlay, R. W., 1959, New genera of Early Cretaceous (Albian) ammonites from Alaska: Jour. Paleontology, v. 33, no. 1, p. 179–185, pls. 29, 30, 2 tables.

——— 1960, Characteristic Early Cretaceous megafossils from northern Alaska: U.S. Geol. Survey Prof. Paper 335 (in press).

Imlay, R. W., and Reeside, J. B., Jr., 1954, Correlation of the Cretaceous formations of Greenland and Alaska: Geol. Soc. America Bull., v. 65, p. 223–246, 1 correlation table.

Jacob, Charles, 1908, Étude sur quelques ammonites du Crétacé Moyen: Soc. geol. France, Paleont. Mém. no. 38, for 1907, 63 p., 9 pls.

Koenen, A. von, 1902, Die Ammoniten des Norddeutschen Neocom (Valanginien; Hauterivien, Barremien und Aptien); Preuss. geol. Landesanstalt Abh., N. F., no. 34, 451 p., 55 pls.

Killian, Wilfred, 1907–1913, Unterkreide (Palaeocretacicum) *in* Frech, F., Lethaea Geognostica, II, Mesozoicum, v. 3 (Kreide), 398 p., pls. 1–14.

Martin, G. C., 1926, The Mesozoic Stratigraphy of Alaska, U.S. Geol. Survey Bull. 776, 493 p., 13 figs.

Matsumoto, Tatsuro, 1955, Family Kossmaticeratidae from Hokkaido and Saghalien: Japanese Jour. Geology and Geography, v. 26, nos. 1, 2, p. 115–164, pls. 8–10.

——— 1959, Cretaceous ammonites from the upper Chitina Valley, Alaska. Mem. Fac. Sci. Kyushu Univ., ser. D, and Geology, v. 8, no. 3, p. 49–90, pls. 12–29, 16 text figs.

McLearn, F. H., 1931, The Gastroplites and other Lower Cretaceous faunas of the northern Great Plains: Royal Soc. Canada Proc. and Trans. 3d ser., v. 25, sec. 4, p. 1–8, pls. 1, 2, 1 text fig.

——— 1945, Revision of the Lower Cretaceous of the western interior of Canada: Canada Geol. Survey Paper 44–17 (2d ed.), 14 p., 2 tables, 12 pls.

——— 1948, New Lower Cretaceous species from Alberta and northeastern British Columbia: Appendix to Canada Geol. Survey Paper 44–17, 2 p.

McLearn, F. H., and Kindle, E. D., 1950, Geology of northeastern British Columbia: Canada Geol. Survey Mem. 259, 236 p., 8 pls., 16 text figs., 1 map, 6 tables.

Moffit, F. H., 1938, Geology of the Chitina Valley and adjacent area Alaska: U.S. Geol. Survey Bull. 894, 137 p., 16 pls., 1 map.

Moffit, F. H., and Overbeck, R. M., 1918, The Upper Chitina Valley, Alaska, *with* A description of the igneous rocks: U.S. Geol. Survey Bull. 675, 82 p., 13 pls., 2 figs.

Murphy, M. A., 1956, Lower Cretaceous stratigraphic units of northern California: Am. Assoc. Petroleum Geologists Bull., v. 40, p. 2098–2119, 6 figs.

Nikitin, S. N., 1888, Les vestiges de la période crétacée dans la Russie centrale: Com. Geol. St. Petersbourg. Mem., v. 5, no. 2, p. 166–205, pls. 1–5, map.

Orbigny, Alcide d', 1840–1842, Paléontologie de Française: Terrains Crétacés, v. 1, 662 p., 148 pls.

Parona, C. F., and Bonarelli, Guido, 1897, Fossili Albiani d'Escragnolles del Nizzardo e della Liguria occidentale: Palaeontogr. Italica, v. 2, p. 53–112, pls. 10–14.

Pervinquière, L., 1907, Études de paléontologie tunisienne, 1 Céphalopodes des terrains secondaires. (Carte geol. Tunisie), Système Crétacique, p. 43–428, pls. 1–27.

Pictet, F. J., and Roux, W., 1847–53, Description des mollusques fossiles qui se trouvent dans les grès verts des environs de Genève; Soc. phys. et hist. nat. Genève, v. 1, pt. 4, 286 p., pls. 26–43.

Sinzow, I. T., 1909, Beiträge zur Kenntniss des südrussischen Aptien und Albien: Verh. russ. k. Min. Gesell. St. Petersburg, ser. 2, v. 47, p. 1–48, pls. 1–4.

Spath, L. F., 1923–1943, A monograph of the Ammonoidea of the Gault: Palaeontogr. Soc., 2 v., 787 p., 72 pls., 248 text figs., 4 tables.

——— 1927–33, Revision of the Jurassic cephalopoda fauna of Kachh (Cutch): Palaeontologia Indica new ser. v. 9, 6 pts., 945 p., 130 pls.

——— 1930, The fossil fauna of the Semana Range and some neighboring areas: part V. The Lower Cretaceous ammonoidea; with notes on Albian cephalopoda from Hazara: Palaeontologia Indica, new ser., v. 15, p. 51–66, pls. 8, 9.

Stanton, T. W., 1895, Contributions to the Cretaceous Paleontology of the Pacific Coast, The fauna of the Knoxville beds: U.S. Geol. Survey Bull. 133, 132 p., 20 pls. [1896].

Stelck, C. R., Wall, J. H., Bahan, W. G., and Martin, L. J., 1956, Middle Albian foraminifera from Athabasca and Peace River Drainage areas of western Canada: Research Council of Alberta Rept. 75, 60 p., 5 pls., 2 figs.

Uhlig, Victor, 1883, Die Cephalopodenfauna der Wernsdorfer Schichten: K. Akad. Wiss., Math.-natnrh. Kl., Denks. v. 46, p. 1–166 (128–290), 32 pls.

Warren, P. S., 1947, Cretaceous fossil horizons in the Mackenzie River valley: Jour. Paleontology, v. 21, no. 2, p. 118–123, pls. 29, 30.

Whiteaves, J. F., 1876, On some invertebrates from the coal-bearing rocks of the Queen Charlotte Islands: Canada Geol. Survey, Mesozoic Fossils, v. 1, p. 1–92, pls. 1–10.

——— 1889, On some Cretaceous fossils from British Columbia, the northwest territory and Manitoba: Canada Geol. Survey, Contr. to Canadian Paleontology, v. 1, p. 151–196, pls. 20–24.

——— 1893a, Notes on the ammonites of the Cretaceous rocks of the district of Athabasca, with descriptions of four new species: Royal Soc. Canada Proc. and Trans., 1 ser., v. 10, sec. 4, p. 111–121, pls. 8–10.

——— 1893b, Descriptions of two new species of ammonites from the Cretaceous rocks of the Queen Charlotte Islands: Canadian Record Science, v. 5, p. 441–446, pl. 7.

Whitehouse, F. W., 1928, Additions to the Cretaceous ammonite fauna of eastern Australia, part 2 (Desmoceratidae): Mem. Queensland Museum, v. 9, pt. 2, p. 200–206, pls. 25, 26.

Wollemann, A., 1907, Die Fauna des mitteren Gaults von Algermissen: Jahrb. Preuss. Geol. Landesanstalt u. Bergakademie für 1903, v. 24, p. 22–42, pls. 4, 5.

Wright, C. W., *in* Arkell, W. J., Kummel, Bernhard, and Wright, C. W., 1957, Mesozoic Ammonoidea: Treatise on Invertebrate Paleontology, part L, Mollusca 4, 490, p., illus.

INDEX

[Italic numbers indicate descriptions]

A — Page

abyssus, *Lemuroceras* ... 110, 111
affine, *Beudanticeras* ... 105
glabrum, *Desmoceras* ... 105
aguanizianum, *Kossmatella* ... 99
akuchaensis, *Valdedorsella* ... 100
alaskana, *Puzosia* ... 91, 98, *104*, pl. 16
alaskanum, *Callizoniceras* ... 101
Callizoniceras (*Wollemanniceras*) ... 91, 98, *101*, pl. 12
Albian ammonites, geographic distribution ... 98
Albian faunules ... 93
alderoni, *Calliphylloceras* ... 91, 98, *89*, pl. 11
Ammonite faunules and correlations ... 89–93
Ammonites ... 100
breweri ... 105
haydeni ... 105
Anagaudryceras ... 88, 89, 99
aurarium ... 89, 91, 98, *89*, pl. 11
sp. indet. ... 91, 98
anglicus, *Inoceramus* ... 91
Arethophites ... 88, 110, 111
jachromensis ... 111
sp. ... 91, 98, *111*, pl. 18
(*Antiera*) *denusi*, *Oleostephanus* ... 109
Asteridiscus ... 102
Aucella ... 89
crassicollis ... 89
pallasi ... 89
Aucellina ... 89, 91, 94
Aucellina sp. ... pl. 19
aurarium, *Anagaudryceras* ... 89, 91, 98, *89*, pl. 11
Lytoceras (*Kossmatella*) ... 99

B

baylei, *Cleoniceras* ... 108
Bear Creek ... 88, 89, 91, 96
belli, *Lemuroceras* ... 92, 97, 110, *111*, pl. 18
Lemuroceras (*Subarethophites*) ... 91, 92, 98, 111, pl. 18
Beudanticeras ... 88, 93, 94, 105, 106
affine ... 105
breweri ... 105
glabrum ... 92, 93, 98, *105*, pl. 16
hulenense ... 106
lacrisanum ... 105
sutherlandi ... 105
(*Granziceras*) ... 88
multiconstrictum ... 92, 98, *105*, pl. 14
Beudanticeratinae ... 88
bicurvatoides, *Cleoniceras* ... 108
bifurcata, *Kennicottia* ... 91
Billy Creek ... 88, 96
Biologic analysis ... 87–88
breweri, *Ammonites* ... 105
Beudanticeras ... 105
Brewericeras ... 91, 92, 94, 98, *103*, pl. 17
Brewericeras ... 88, 93, 94, 97, 105
breweri ... 91, 92, 94, 98, *105*, pl. 17
faunule ... 91, 92, 97
haydeni ... 91, 105
hulenense ... 89, 91, 94, 98, *106*, pl. 17
zone ... 91, 92, 94, 98
bullaiva, *Parasiteites* ... 91, 98, *106*, pl. 18

C — Page

californicum, *Hypophylloceras* ... 91, *88*, pl. 11
Calliphylloceras ... 88, 99
alderoni ... 91, 98, *89*, pl. 11
nizinsanum ... 91, 98, *88*, pl. 11
Calliphylloceratinae ... 88
Callizoniceras ... 88, 93, 91, 97, 101, 102, 103
alaskanum ... 101
hogeri ... 101
(*Wollemanniceras*) ... 91
alaskanum ... 91, 98, *101*, pl. 12
fokiinense ... 91, 98, *101*, pl. 12
keilhecki ... 101
Canyon Creek ... 88, 89, 91, 97
cappei, *Kossmatella* ... 91, 98, *99*, pl. 12
Cephalopoda ... 97
chirichensis, *Puzosia* ... 100
Chitina River ... 96
Chitina Valley ... 88–89
chilinanum, *Phyllopachyceras* ... 91, 97, 98, pl. 11
Chokosna River ... 96
Clamsnyes beds ... 100
Clearwater formation ... 92
clean, *Cleoniceras* ... 108
Cleoniceras ... 88, 92, 94, 108
baylei ... 108
bicurvatoides ... 108
clean ... 108
leightonense ... 108
modestum ... 109
overbeki ... 91, 98, *108*, pl. 19
Cleoniceratinae ... 88
comanchensis, *Inoceramus* ... 91
Copper River basin ... 88
Correlations and ammonite faunules ... 89–93
crassiodiscus, *Aucella* ... 89
crassicostatus, *Leconieites* ... 91
crassus, *Mallotites* ... 89, 98, *102*, pl. 14

D

deanni, *Leconieites* ... 91, 94, 98, *109*, pl. 19
Oleostephanus (*Antiera*) ... 109
Desmoceras ... 88, 91, 100, 102, 106
affine glabrum ... 105
merriami ... 106
rogi ... 106
sp. juv. ... 91, 98, *106*, pl. 17
Desmoceratidae ... 88, 93
Desmoceratinae ... 88
Douvilleiceras ... 88, 89, 92
mammillatum zone ... 92
dubium, *Lemuroceras* ... 98, *110*, pl. 18

F

Flume Creek ... 88, 96
Fohlin Creek ... 88, 89, 91, 96
fokiinense, *Callizoniceras* (*Wollemanniceras*) ... 91, 98, *101*, pl. 12
Fourth of July Creek ... 89, 91, 96
Fredholmiceras ... 88, 93, *102*
simulare ... 92, 93, 94, 97, 98, *102*, pl. 14
faunule ... 92–93

G — Page

Gaudryceras ... 88
sp. ... 98
gaunesi, *Kossmatella* ... 99
Gastroplites ... 92
kingi ... 97
Gastroplitinae ... 88
Gates formation ... 92
Geographic distribution, Albian ammonites ... 98
giesiana, *Valdedorsella* ... 100
Gibraltar Hill ... 93
glabrum, *Beudanticeras* ... 92, 93, 98, *105*, pl. 16
Desmoceras affine ... 105
Placenticeras ... 105
Granziceras ... 105
(*Granziceras*), *Beudanticeras* ... 88
multiconstrictum, *Beudanticeras* ... 92, 98, *105*, pl. 14
Guadryceratinae ... 88

H

Harmon shale member, Peace River formation ... 92
haydeni, *Ammonites* ... 106
Brewericeras ... 91, 106
Hoplites deniatus zone ... 89
Hoplitidae ... 88, 94
howeoji, *Valdedorsella* ... 100
hogeri, *Callizoniceras* ... 101
hulenense, *Beudanticeras* ... 106
Brewericeras ... 89, 91, 94, 98, *106*, pl. 17
Hulenites ... 88, 92, 93, 97, 104, 107
occidei ... 91, 98, 104, *107*, pl. 18
Hypophylloceras ... 88, 98
californicum ... 91, 98, pl. 11
onoense ... 98

I

indicum, *Lemuroceras* ... 92, 93, 109
indigenus, *Melchiorites* ... 104
Inoceramus ... 88, 91
anglicus ... 91
comanchensis ... 91
irenense, *Lemuroceras* ... 92, 93, 103
irregularis, *Puzositeites* ... 91, 98, *102*, pl. 18

J

jachromensis, *Arethophites* ... 111

K

keilhecki, *Callizoniceras* (*Wollemanniceras*) ... 101
Kennicott formation ... 98
Kennicott Glacier ... 88, 89, 96
Kennicott River ... 96
Kennicottia ... 88, 93, 94, 102, 103
bifurcata ... 91, 98, *103*, 104, pl. 15
rugosa ... 91, 98, *104*, pl. 15
kingi, *Gastroplites* ... 97
Kossmatella ... 88, 99
aguanizianum ... 99
cappei ... 91, 98, 89, pl. 12
gaunesi ... 99
(*Kossmatella*) *aurarium*, *Lytoceras* ... 99
Kossmatellinae ... 88
Kossmaticeratidae ... 88, 94

Page

Kuskulana Pass 88, 89
Kuskulana River 88

L

laevi, *Psychoceras* ..... 91, 98, *100*, pl. 12
laevilyrum, *Neudanticeras* 105
Lakina River 96
leconteii, *Leconteites* 109
Leconteites 88, 89, 91, 93, 94, 97, *108*, 110
crassicostatus 91
deani ..... 91, 94, 98, *109*, pl. 19
faunule 91–92
leconteii 109
zone 89, 91, 92, 94
modestus ..... 89, 91, 94, 98, *109*, pl. 19
faunule 89, 91
sp. 98
leightonense, *Cleoniceras* 108
Lemuroceras 88, 93, 94, 97, 109, 110
abiesense 110, 111
belli ..... 92, 97, 110, *111*, pl. 18
zone 92
dubium ..... 98, *110*, pl. 18
indicum 92, 93, 109
irenense 92, 93, 103
taltecnanum ..... 92, 98, *109*, pl. 18
(*Subarethoplites*) *belli* 88, 92, 93, 94, 97
belli ..... 91, 92, 98, *111*, pl. 18
Leymeriella tardefurcata zone 89, 92
Loon River formation 92
Lunatodorsella 100
Lytoceras (*Kossmatella*) *aurarium* 99

M

McCarthy Creek 88, 89, 91, 96
Mulanuska formation 95, 98
Melchiorites 104
indipensis 104
meririami, *Desmoceras* 106
modestum, *Cleoniceras* 109
modestus, *Leconteites* ..... 89, 91, 94, 98, *109*, pl. 19
Moffitites 88, 91, 93, *101*
crassus ..... 88, 98, *102*, pl. 14
robustus ..... 91, 94, 98, *102*, pl. 13
faunule 91–92
Moosebar formation 92
multiconstrictum, *Neudanticeras* (*Granticeras*) ..... 92, 98, *105*, pl. 14

N

Nelchina limestone 88, 96
Neoilestes 106
Nizina Glacier 88, 91, 93, 95, 97
nitinanum, *Calliphylloceras* ..... 91, 98, *99*, pl. 11
Notikewin member, Peace River formation 92

O

Oleostephanus (*Astieria*) *deanni* 109
onoense, *Hypophylloceras* 98
orethecki, *Cleoniceras* ..... 91, 98, *108*, pl. 19

P

pallavi, *Aucella* 89
Parasilerites 88, 92, 94, *106*
bullatus ..... 91, 98, *106*, pl. 18
irregularis ..... 91, 98, *107*, pl. 18
Peace River formation, Harmon shale member 92
Notikewin member 92
perrinsmithi, *Puzosiella* 89, 98
Phylloceratidae 88, 94
Phylloceratinae 88
Phyllopachyceras 88, 97
chitinanum ..... 91, 97, 98, pl. 11
shastalense 91, 98
thereae 98
Placenticeras glabrum 105
Pseudohaploceras 102, 103
Pseudolegmeriella 88
Pseudosonneratia 111
Psychoceras 88, 100
laevi ..... 91, 98, *100*, pl. 12
Ptychoceratidae 88, 94
Puzosia 88, 94, 103, 104
alaskana ..... 91, 98, *104*, pl. 16
chirichenkii 100
quenstedti 104
subquadrata 103
sp. 91
sp. indet. 98
puzosiaformis, *Silesites* 107
Puzosiella 88, 89, 91, 93, 94, 97, 108
faunule 89, 91
perrinsmithi 89, 98
rogersi ..... 89, 98, *108*, pl. 19
taffi 89, 98
spp. 89, 94
Puzosiinae 88

Q

Queen Charlotte Islands 88, 91, 93, 100
quenstedti, *Puzosia* 104
raridki, *Holcoites* ..... 91, 98, 104, *107*, pl. 18
robustus, *Moffitites* ..... 91, 94, 98, *102*, pl. 13
rogersi, *Puzosiella* ..... 89, 98, *108*, pl. 19
Sonnratia 108
rugosa, *Kossmatella* ..... 91, 98, *103*, pl. 15

S

shastalense, *Phyllopachyceras* 91, 98
Silesites 89, 106, 107
puzosiaformis 107
vulpes 107
Silesitidae 88, 94
singulare, *Freboldiceras* ..... 92, 93, 94, 97, 98, *102*, pl. 14
Slatka Creek 88
Sonnratia rogersi 108
Stratigraphic summary 88–89
Subarethoplites 92, *110*
(*Subarethoplites*) *belli*, *Lemuroceras* 91, 92, 98
Lemuroceras 88, 92, 93, 94, 97
subquadrata, *Puzosia* 103
Summary of results 93–97
sutherlandi, *Neudanticeras* 105
Systematic descriptions 97–111

T

taffi, *Puzosiella* 89, 98
Talkeetna Mountains 88
taltecnanum, *Lemuroceras* ..... 92, 98, *109*, pl. 18
Tetragonites 88, 89, 100
timotheanus ..... 91, 98, *100*, pl. 12
sp. 92
sp. indet. 98
Tetragonitidae 88, 94
Tetragonitinae 88
Tetrahoplites 111
thereae, *Phyllopachyceras* 98
timotheanus, *Tetragonites* ..... 91, 98, *100*, pl. 12
Trail Creek 91, 96

V

Valdedorsella 88, 92, 94, 100, 102, 103
alaskaensis 100
getulina 100
hourcqi 100
whiteavesi ..... 91, 98, *100*, pl. 11
vogi, *Desmoceras* 106
vulpes, *Silesites* 107

W

whiteavesi, *Valdedorsella* ..... 91, 98, *100*, pl. 11
Wollemanniceras 101
(*Wollemanniceras*) *alaskanum*, *Callizoniceras* ..... 91, 98, *101*, pl. 12
Callizoniceras 91
fohlinense, *Callizoniceras* ..... 91, 98, *101*, pl. 12
keilhacki, *Callizoniceras* 101

Y

Young Creek 88, 89, 91, 96

PLATES 11–19

Digitized by Google

PLATE 11

[Figures natural size unless otherwise indicated]

FIGURES 1–5. *Phyllopachyceras chitinanum* Imlay, n. sp. (p. 97).
Holotype USNM 130142, from USGS Mes. loc. 9492. Suture line drawn from adapical end of body chamber.

6–12. *Calliphylloceras nizinanum* Imlay, n. sp. (p. 99).
All specimens from USGS Mes. loc. 9492.
6, 10, 11. Paratype USNM 130139a.
7, 8. Holotype USNM 130138.
9. Paratype USNM 130139b.
12. Paratype USNM 130139c.

13–17. *Calliphylloceras* cf. *C. aldersoni* (Anderson) (p. 99).
All specimens from USGS Mes. loc. 9972.
13. Specimen USNM 130161a showing traces of finely ribbed shell.
14. Specimen USNM 130161b.
15–17. Ventral, cross section, and lateral views of specimen USNM 130161c.

18, 19, 24. *Anagaudryceras aurarium* (Anderson) (p. 99).
Both specimens from USGS Mes. loc. 14485.
18, 19. Immature septate specimen, USNM 130154a.
24. Adult specimen USNM 130154b showing fine striations on the shell and deep constrictions on the mold. Body chamber represented by three-fifths of a whorl.

20–23, 25–28. *Valdedorsella? whiteavesi* Imlay, n. sp. (p. 100).
Both specimens from USGS Mes. loc. 9492.
20–23, 25. Holotype, USNM 130145. Suture line drawn at diameter of 11.5 mm. Note figures 21 and 22 are identical views at different magnifications.
26–28. Paratype USNM 130146.

29. *Hypophylloceras* cf. *H. californicum* (Anderson) (p. 98)
Specimen USNM 130132, from USGS Mes. loc. 9492.

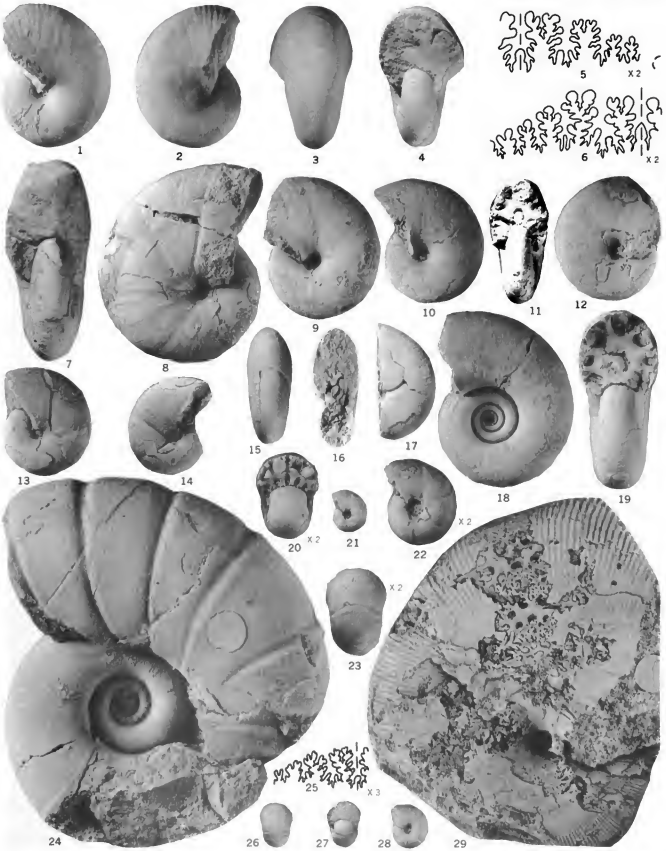

PHYLLOPACHYCERAS, CALLIPHYLLOCERAS, ANAGAUDRYCERAS, VALDEDORSELLA?, AND HYPOPHYLLOCERAS

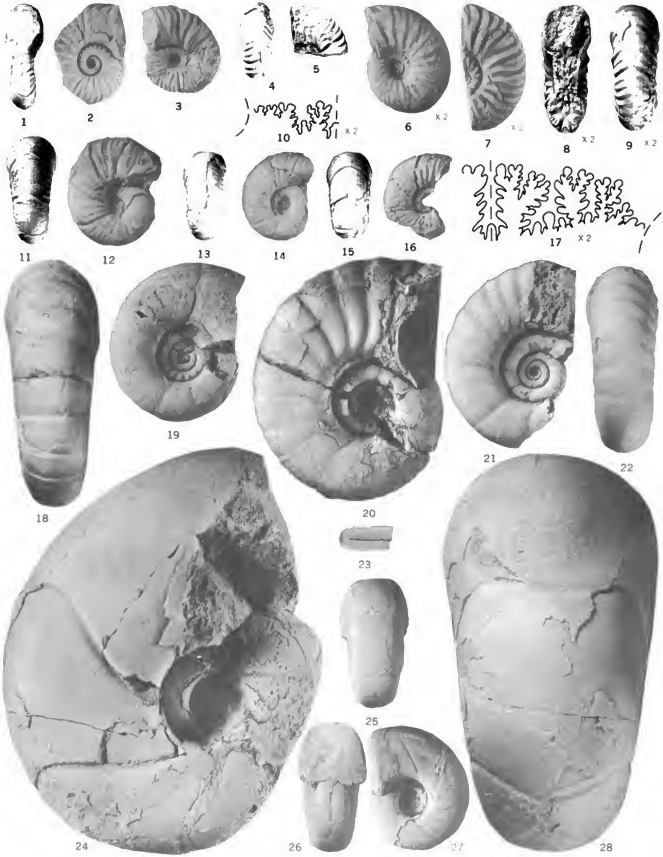

CALLIZONICERAS, KOSSMATELLA, PTYCHOCERAS, AND *TETRAGONITES*

PLATE 12

[Figures natural size unless otherwise indicated]

FIGURES 1–10. *Callizoniceras* (*Wollemanniceras*) *fohlinense* Imlay, n. sp. (p. 101).
All specimens from USGS Mes. loc. 14484.
1, 2, 10. Holotype USNM 130155.
3. Paratype USNM 130156a.
4, 5. Paratype USNM 130156b.
6. Paratype USNM 130156c. Weaker ribbed than the holotype.
7–9. Paratype USNM 130156d. Stronger ribbed than the holotype.

11–16. *Callizoniceras* (*Wollemanniceras*) *alaskanum* Imlay, n. sp. (p. 101).
Both paratypes from USGS Mes. loc. 8873.
11, 12. Holotype USNM 130165, from USGS Mes. loc. 9976.
13, 14. Paratype USNM 130166a.
15, 16. Paratype USNM 130166b.

17–22. *Kossmatella cappsi* Imlay, n. sp. (p. 99).
Both paratypes from USGS Mes. loc. 9492.
17, 19. Paratype USNM 130140a.
21, 22. Paratype USNM 130140b.
18, 20. Holotype USNM 130160, from USGS Mes. loc. 14514.

23. *Ptychoceras* cf. *P. laeve* (Gabb) (p. 100).
Specimen USNM 130163, from USGS Mes. loc. 9972.

24–28. *Tetragonites* aff. *T. timotheanus* (Pictet) (p. 100).
Both specimens from USGS Mes. loc. 9492.
24, 28. Adult showing three-fifths of a whorl of body chamber, USNM 130131a.
25–27. Immature specimen USNM 130131b.

PLATE 13

[Figures natural size unless otherwise indicated]

FIGURES 1–13. *Moffitites robustus* Imlay. (p. 102).

1–3, 5. Septate paratype USNM 129875a, from USGS Mes. loc. 9972, is slenderer than most specimens of the species.

4, 9. Small septate paratype USNM 129876a, from USGS Mes. loc. 14485.

6–8. Normally stout septate paratype USNM 129875b, from USGS Mes. loc. 9972. Note tendency of ribs to become threadlike on the venter.

10, 13. Holotype USNM 129874, from USGS Mes. loc. 2191. About three-fifths of a whorl belongs to the body chamber.

11, 12. Lateral views of paratype USNM 129876b, from USGS Mes. loc. 14485. Shows characteristic ribbing on inner whorls.

1

2

3

4

5

6

7

8

9

10

11

12

13

MOFFITITES ROBUSTUS

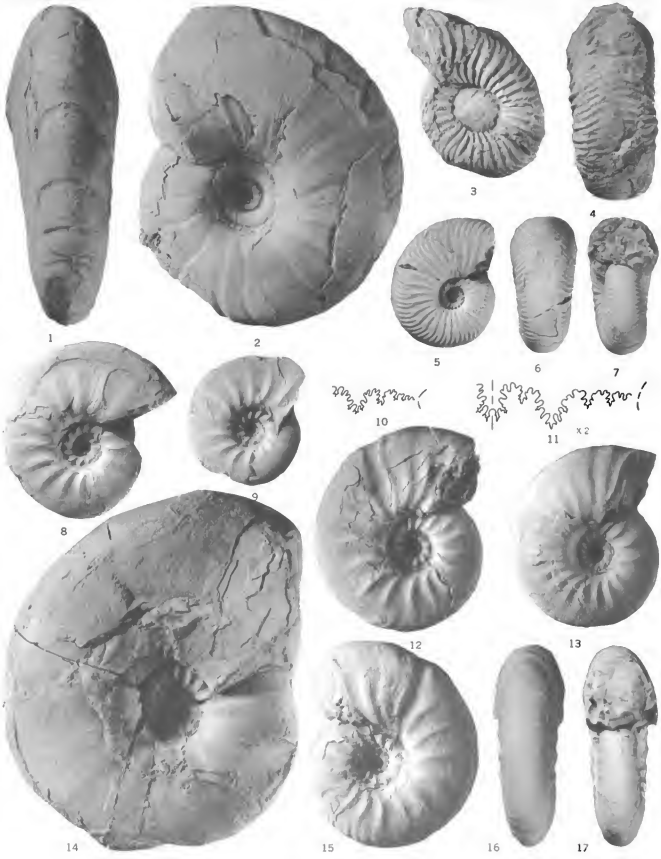

BEUDANTICERAS, MOFFITITES, AND FREBOLDICERAS

PLATE 14

[Figures natural size unless otherwise indicated]

FIGURES 1, 2. *Beudanticeras* (*Grantziceras*) *multiconstrictum* Imlay (p. 105).
Holotype USNM 128721, from USGS Mes. loc. 24877.

3–7. *Moffitiles, crassus* Imlay, n. sp. (p. 102).
3, 4. Paratype USNM 130176, from USGS Mes. loc. 14487.
5–7. Holotype USNM 130175, from USGS Mes. loc. 8878.

8–17. *Freboldiceras singulare* Imlay (p. 102).
All specimens from USGS Mes. loc., 24877.
8–10. Lateral views and suture line of paratype USNM 129869a.
11, 12, 15–17. Holotype USNM 129868. Note fine striations on shell. Suture line drawn at whorl height of 15 mm.
13. Paratype USNM 129869b.
14. Paratype USNM 129869c. The smooth body chamber occupies about three-fifths of a whorl.

PLATE 15

[Figures natural size unless otherwise indicated]

FIGURES 1–6. *Kennicottia bifurcata* Imlay (p. 103).

1–5. Holotype USNM 129870, from USGS Mes. loc. 9972. Suture line drawn at diameter of 63 mm.

6. Paratype USNM 129871, from USGS Mes. loc. 8873. Shows furcation of ribs on inner whorls.

7–13. *Kennicottia rugosa* Imlay, n. sp. (p. 103).

7, 8, 11. Paratype USNM 130153a, from USGS Mes. loc. 14485.

9, 10. Paratype USNM 130153b, from USGS Mes. loc. 14485.

12, 13. Holotype USNM 130152, from USGS Mes. loc. 9489.

KENNICOTTIA BIFURCATA AND *K. RUGOSA*

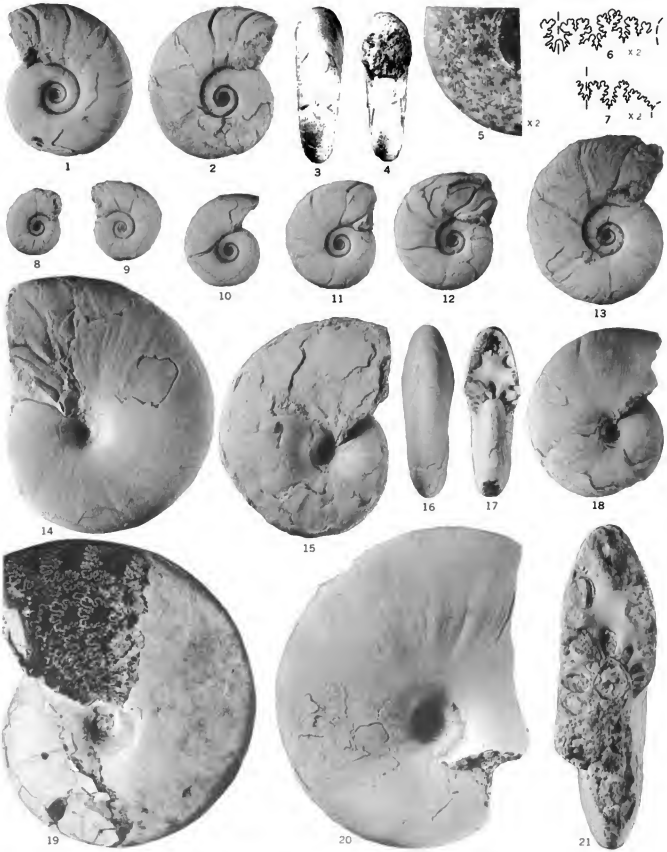

PUZOSIA ALASKANA AND *BEUDANTICERAS GLABRUM*

PLATE 16

[Figures natural size unless otherwise indicated]

FIGURES 1–13. *Puzosia alaskana* Imlay, n. sp. (p. 104).

1–4. Holotype USNM 130143, from USGS Mes. loc. 9492.

5–13. Paratypes USNM 130144, from USGS Mes. loc. 9492. Lateral views 8 to 13 shows differences in strength of ribbing and in constrictions. The suture lines were drawn from the specimen shown in figure 5.

14–21. *Beudanticeras glabrum* (Whiteaves) (p. 105).

Plesiotypes USNM 130149, from USGS Mes, loc. 24877. Figures 14 and 19 represent fairly smooth specimens. Figure 15 represents a specimen with large bulges or ribs. Figures 16 to 18 show prominent constrictions. Figures 20 and 21 represent a specimen that develops weak lateral bulges. All these specimens are septate.

PLATE 17

[Figures natural size unless otherwise indicated]

FIGURES 1–4. *Desmoceras*? sp. juv. (p. 106).

Specimen USNM 130135, from USGS Mes. loc. 9492. Suture drawn at whorl height of 10 mm.

5–10, 12, 13. *Brewericeras breweri* (Gabb) (p. 105).

Plesiotypes USNM 130133, from USGS Mes. loc. 9492. Figures 5–7 represent a typical specimen. Figure 8 illustrates feather structure on the septate part of the shell and likewise bears ribbing typical of the species. Figures 9 and 10 and figure 13 represent two specimens in which coarse ribbing appears at an earlier growth stage than is typical in the species. The suture line was drawn at the adapical end of the body chamber from the specimen shown on figures 5–7.

11, 14–16. *Brewericeras* cf. *B. hulenense* (Anderson) (p. 106).

11. Specimen USNM 130139, from USGS Mes. loc. 14514.

14–16. Specimens USNM 130130, from USGS Mes. loc. 9492.

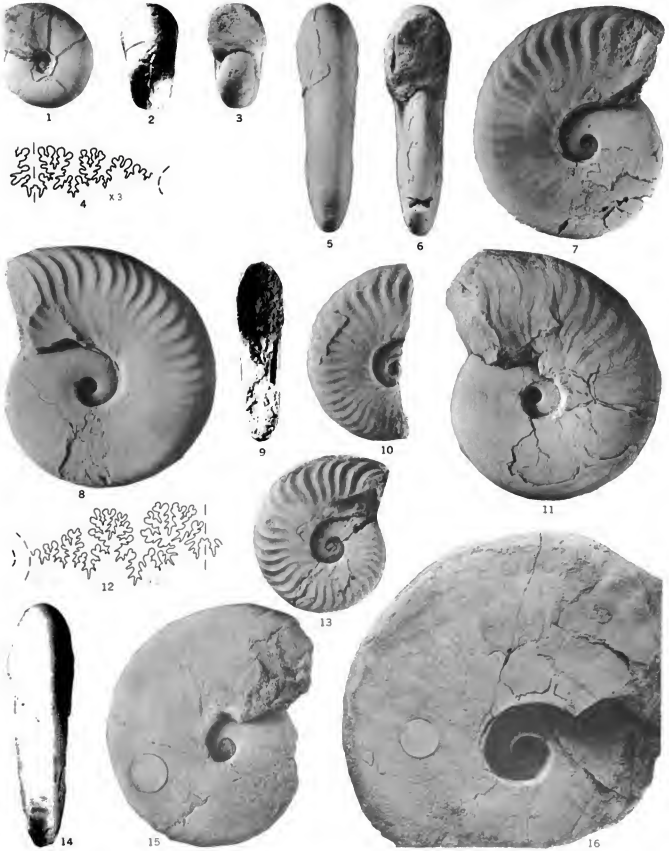

DESMOCERAS? SP., *BREWERICERAS BREWERI*, AND *B. HULENSE*

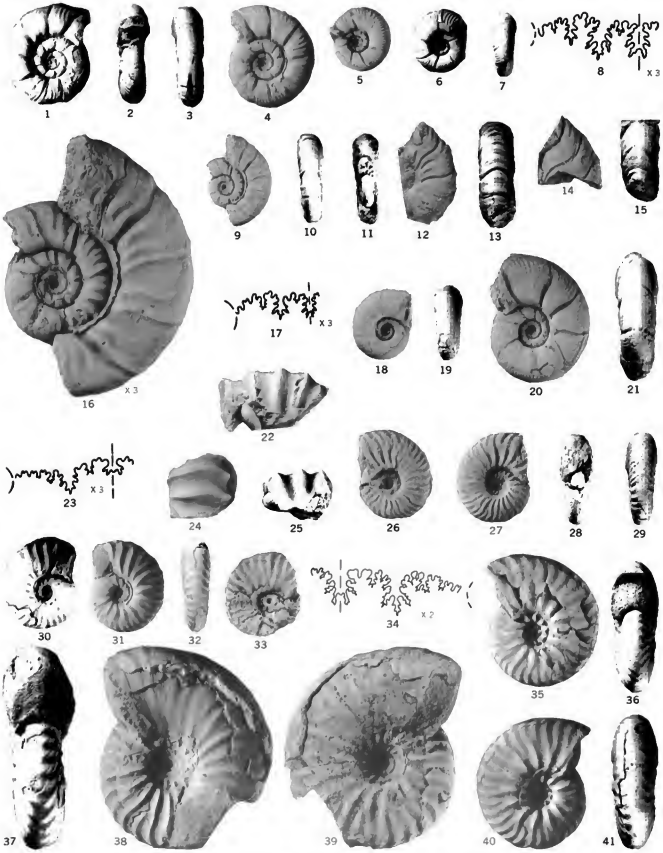

PARASILESITES, HULENITES, ARCTHOPLITES, AND LEMUROCERAS

PLATE 18

[Figures natural size unless otherwise indicated]

FIGURES 1–8. *Parasilesites bullatus* Imlay (p. 106).
1–4, 8. Holotype USNM 129872, from USGS Mes. loc. 9492.
5–7. Paratype USNM 129873, from USGS Mes. loc. 9492.

9–17. *Parasilesites irregularis* Imlay, n. sp. (p. 107).
All types are from USGS Mes. loc. 9492.
9–11, 16, 17. Lateral, ventral, and apertural views and suture line of holotype USNM 130147. Suture line drawn at diameter of 13 mm. Note that figure 16 is an enlargement of figure 9.
12, 13. Paratype USNM 130148a.
14, 15. Paratype USNM 130148b.

18–21. *Hulenites* cf. *H. reesidei* (Anderson) (p. 107).
Specimens USNM 130134, from USGS Mes. loc. 9492.

22, 24, 25. *Arethoplites*? sp. (p. 111).
Specimen USNM 130137, from USGS Mes. loc. 9492. Figures 24 and 25 represent ventral and lateral views of one specimen.

23, 30–33. *Lemuroceras (Subarethoplites)* aff. *L. belli* McLearn (p. 111).
Both specimens from USGS Mes. loc. 14484.
23, 30–32. Specimen USNM 130136a. Suture line drawn at diameter of 19 mm.
33. Specimen USNM 130136b.

26–29. *Lemuroceras*? sp. juv. cf. *L. dubium* Collignon (p. 110). Specimen USNM 130157, from USGS Mes. loc. 14484.

34–41. *Lemuroceras talkeetnanum* Imlay, n. sp. (p. 109).
34, 37–39. Holotype USNM 130151, from USGS Mes. loc. 24877. Suture line drawn at whorl height of 14 mm.
35, 36, 40, 41. Paratype USNM 130150, from USGS Mes. loc. 24877.

PLATE 19

[Figures natural size unless otherwise indicated]

FIGURES 1–3. *Leconteites leconteí* (Anderson) (p. 109).
Plesiotype USNM 130171, from gulch emptying into Hulen Creek a little east of Ono, Calif. Inserted for comparison with species of *Leconteites* from Alaska. Note tubercles at umbical edge.

4–6. *Leconteites modestus* (Anderson) (p. 109).
4, 5. Plesiotypes USNM 130172, from USGS Mes. loc. 9971.
6. Plesiotype USNM 130173, from USGS Mes. loc. 11389.

7–14. *Leconteites deansi* (Whiteaves) (p. 109).
7, 8. Plesiotype USNM 130164a, from USGS Mes. loc. 9972.
12–14. Plesiotype USNM 130164b, from USGS Mes. loc. 9972. Suture line drawn at whorl height of 10.5 mm.
9–11. Plesiotype USNM 130170, from USGS Mes. loc. 2201.

15–27. *Leconteites* cf. *L. deansi* (Whiteaves) (p. 109).
15, 20, 21. Specimen USNM 130162a, from USGS Mes. loc. 9972.
16, 17. Specimen USNM 130158, from USGS Mes. loc. 14484.
18. Specimen USNM 130169, from USGS Mes. loc. 2201.
19, 23, 24, 27. Four specimens USNM 130174, from USGS Mes. loc. 8872. These show changes in ribbing during growth.
22. Specimen USNM 130162b, from USGS Mes. loc. 9972.
25, 26. Specimen USNM 130162c, from USGS Mes. loc. 9972.

28–32. *Aucellina* sp. (p. 91).
Both specimens from USGS Mes. loc. 8873.
28–30 Left and right valves and anterior view of both valves of an average-sized specimen, USNM 130167a.
31, 32 Left and right valves of a large specimen, USNM 130167b.

33–35 *Puzosigella* cf. *P. rogersi* (Hall and Ambrose) (p. 108).
Three specimens USNM 130168, from USGS Mes. loc. 8877, show changes in ribbing during growth.

36–39 *Cleoniceras overbecki* Imlay, n. sp. (p. 108).
Holotype USNM 130141, from USGS Mes. loc. 9492. Note elongate tubercles at umbilical edge.

LECONTEITES, AUCELLINA, PUZOSIGELLA, AND *CLEONICERAS*

Interpretation of the Composition of Lithium Micas

By MARGARET D. FOSTER

SHORTER CONTRIBUTIONS TO GENERAL GEOLOGY

GEOLOGICAL SURVEY PROFESSIONAL PAPER 354-E

Relations of lithian muscovites ana lepidolites, and of siderophyllites, protolithionites, zinnwaldites, and lepidolites, based on published analyses

UNITED STATES GOVERNMENT PRINTING OFFICE, WASHINGTON : 1960

UNITED STATES DEPARTMENT OF THE INTERIOR

FRED A. SEATON, *Secretary*

GEOLOGICAL SURVEY

Thomas B. Nolan, *Director*

For sale by the Superintendent of Documents, U.S. Government Printing Office
Washington 25, D.C.

CONTENTS

	Page
Abstract	115
Introduction	115
Calculation of formulas	115
Aluminum lithium micas	116
Interpretation of composition of lepidolites based on end members	116
Compositional changes shown by the analyses	117
Hypothetical Li-(octahedral Al) replacement ratios	117
Relation of Li to other constituents in calculated formulas	119
Relation between Li and octahedral Al	119
Relation between $(Li-R^{+2})$ and Si	121
Relation between Li and total Al	121
Relation between Li and occupied octahedral sites in excess of 2.00	122
Relation between Li_2O and F	122
Relation between Li_2O content, octahedral occupancy, and structure	122
Discussion	126
Ferrous lithium micas	127
Previous interpretations of composition	127
Compositional changes shown by analyses	129
Ferrous lithium micas—Continued	
Relation between ferrous lithium micas, siderophyllites, and aluminian lepidomelanes	129
Compositional relations in siderophyllites and ferrous lithium micas	130
Relation between Li and trivalent octahedral cations	130
Relation between Li and Fe^{+3}	130
Relation between Li and Si	131
Hypothetical Fe^{+2}-Li replacement ratios	131
Siderophyllite-lepidolite isomorphous series	132
Siderophyllites and lepidomelanes	134
Protolithionites	135
Zinnwaldites	136
Ferroan lepidolite (cryophyllite)	136
Relation between aluminum lithium micas and ferrous lithium micas	137
Unusual lithium micas	139
Summary	140
References cited	141
Index	147

ILLUSTRATIONS

	Page
FIGURE 25. Relation between octahedral sites occupied by Li and vacated by Al in aluminum lithium micas	120
26. Relation between $(Li-R^{+2})$ and Si in aluminum lithium micas	121
27. Relation between the number of formula sites occupied by Li and R^{+2} in aluminum lithium micas	122
28. Relation between Li and octahedral occupancy in excess of 2.00 in aluminum lithium micas	123
29. Relation between Li_2O and F in aluminum lithium micas	123
30. Relation between F and H_2O+ in aluminum lithium micas	123
31. Relation between Li occupancy, octahedral occupancy, and structural type in Stevens' and Berggren's samples	125
32. Histograms of selected formulas showing the relation of lithian muscovites and lepidolites	127
33. Relation between Li, $R^{+2}(Fe^{+2}, Mn^{+2}, Mg)$, and octahedral R^{+3} (Al, Fe^{+3}) + Ti^{+4} in aluminum lithium micas	128
34. Relation between Li and octahedral R^{+3} cations in siderophyllites and ferrous lithium micas	130
35. Relation between Li and Fe^{+3} in siderophyllites and ferrous lithium micas	130
36. Relation between Li and Si in siderophyllites and ferrous lithium micas	131
37. Relation between Li, $R^{+2}(Fe^{+2}, Mn^{+2}, Mg)$, and octahedral R^{+3}(Al, Fe^{+3}) + Ti^{+4} in siderophyllites and ferrous lithium micas	131
38. Histograms of selected formulas representing steps in the siderophyllite-lepidolite series	134
39. Relation between Li, $R^{+2}(Fe^{+2}, Mn^{+2}, Mg)$, and octahedral R^{+3}(Al, Fe^{+3}) + Ti^{+4} in lithium micas	138

TABLES

Page

TABLE 1. Relation between Li_2O content, octahedral occupancy, and structure of lithium micas analyzed by Stevens ---- 124
2. Comparison of Li occupancy, Li-(octahedral Al) replacement ratio, and structure ---- 126
3. Selected formulas illustrating relation between lithian muscovites and lepidolites ---- 126
4. Selected formulas representing steps in the siderophyllite-lepidolite series ---- 133
5. Analyses of lithian micas that do not fit in the aluminum lithium or ferrous lithium series ---- 139
6. Analyses, with data for writing formulas, of aluminum lithium micas used in interpretation of composition (in order of increasing Li_2O content) ---- 142
7. Analyses, with data for writing formulas, of siderophyllites and ferrous lithium micas used in interpretation of composition (in order of increasing Li_2O content) ---- 144
8. Analyses, with data for writing formulas, of siderophyllites and ferrous lithium micas not used in interpretation of composition (in order of increasing Li_2O content) ---- 146

SHORTER CONTRIBUTIONS TO GENERAL GEOLOGY

INTERPRETATION OF THE COMPOSITION OF LITHIUM MICAS

By Margaret D. Foster

ABSTRACT

A study of more than 100 analyses of lithium micas reported in the literature indicates that, compositionally, most of the lithium micas may be interpreted as if derived by isomorphous replacement from muscovite or siderophyllite.

Starting with muscovite, analyses and formulas of aluminum lithium micas, arranged in order of increasing Li content, are characterized by decrease in octahedral Al and in tetrahedral Al and by increase in Si and in octahedral occupancy. These changes can be interpreted as the result of progressive replacement of octahedral Al by Li, in ratios varying between 2 and 3 Li for 1 octahedral Al. The aluminum lithium micas are not, however, members of a continuous isomorphous series. The series is interrupted about halfway between an octahedral occupancy of 2.00 and 3.00 by a change in structure from muscovite to lepidolite. The term "lithian" muscovite is given to aluminum lithium micas having a muscovite structure.

Starting with siderophyllite, or other trioctahedral micas having high Fe^{+2} and very low Mg content, analyses and formulas of ferrous lithium micas, arranged in order of increasing Li content, are characterized by decrease in Fe^{+2}, decrease in tetrahedral Al, increase in Si, and increase in octahedral occupancy. These changes can be interpreted as the result of progressive replacement by Li^{+1} of Fe^{+2}, at an average replacement ratio of 2.0 Li^{+1} for 1.5 Fe^{+2}. As there is less difference between the number of positive charges carried by the replacing cations and the replaced cations than in the aluminum lithium micas, the change in composition and the increase in octahedral occupancy is less in the ferrous lithium micas. The prototype, siderophyllite, is structurally trioctahedral, and, as replacement tends to increase octahedral occupancy, the ferrous lithium micas are also trioctahedral and no structural adjustments are necessary. The ferrous lithium mica series is, therefore, not broken as is the aluminum lithium mica series. Varietal definitions based on octahedral sites occupied by Li^{+1} in the half-cell formula are: lithian siderophylite, having fewer than 0.25 sites occupied by Li^{+1}, protolithionite, having between 0.25 and 0.75 sites occupied by Li^{+1}, zinnwaldite, having between 0.75 and 1.25 sites occupied by Li^{+1}, and lepidolite, having more than 1.25 sites occupied by Li^{+1}.

The high-Li members of both series are lepidolites. Thus lepidolites may be interpreted as if derived from muscovite or from siderophyllite.

INTRODUCTION

This study of the compositional and layer-charge relations of lithium-bearing micas is an extension of similar studies by the writer of the compositional and layer-charge relations of the dioctahedral potassium micas (Foster, 1956) and of the trioctahedral micas (Foster, 1960). In the study of the dioctahedral potassium micas, the effect of octahedral replacement of trivalent by bivalent cations on the charge relation and composition of the constituent layers was studied in detail, and it was shown that these micas can be classified and correlated on the basis of the relation between the charges on their tetrahedral and octahedral layers, and that these micas are members of, and form, a trisilicictetrasilicic series. In the study of the trioctahedral micas, the effect of octahedral replacement of bivalent by trivalent cations on the charge relations and composition of the constituent layers was studied in detail and it was shown that the trioctahedral micas accommodate the additional number of positive charges carried by trivalent cations, compared with bivalent cations, in two quite different ways, and that the phlogopites, biotites, siderophyllites, and lepidomelanes form a complete magnesium-replacement system, in which Mg^{+2} is gradually and completely replaced by bivalent and trivalent cations.

It is the purpose of the present paper to present a similar study of the composition and layer-charge relations of the lithium micas.

CALCULATION OF FORMULAS

For the present study about 80 analyses of aluminum lithium micas and about 45 analyses of ferrous lithium micas were collected from the literature, and formulas were calculated from these analyses by the method devised by Marshall (1949, p. 58) and modified by the author. This method is described in detail in a previous paper of this series (Foster, 1960). Most of the discussion of the compositional characteristics of these analyses in the present paper is based on the calculated half-cell formulas.

Attention is directed to the order in which the groups and the cations within the group are written. First the octahedral group, enclosed in parentheses, is written,

with the cations in that group noted in order of decreasing valence (except Ti, which is written after Al). Then the tetrahedral group, also enclosed in parentheses, is written, again with the cations noted in order of decreasing valence. Above each group the charge is written. After these two groups, which indicate the cationic composition of the layers, the anionic composition, $O_{10}(OH,F)_2$, is written and the whole is bracketed, thus indicating the composition of the composite layer. After the upper part of the closing bracket, the total negative charge on the composite layer is noted. This is followed by a notation in parentheses of the interlayer cation content, with the positive charge carried by these cations written at the top of the closing parenthesis, and the total number of positions occupied by these cations written at the bottom. The interlayer cations are written last, rather than first, which is the more conventional position, because the amount and charge of the interlayer cations are dependent on and must neutralize the charge on the composite layer.

The negative charge on the composite layer and the positive charge on the interlayer cations should be close to 1.00 in the half-cell formula. In evaluating the dependability of the formulas used in this study a variation of plus or minus 0.10 was permitted in these values. Formulas in which the negative charge on the composite layer and the interlayer cationic charge were greater or less than 1.00 by more than 0.10 were not used in the study unless the number of sites occupied by the interlayer cations was less than 1.10. For example, in a few formulas the negative composite-layer charge and the interlayer cationic charge were greater than 1.10, but because of the presence of bivalent interlayer cations (Ca), the number of interlayer sites occupied was less than 1.10. Such formulas were included in the study. The analyses of aluminum lithium micas that were used in the study and data from which their calculated formulas can be written are given in table 6, in order of increasing lithium content, and analyses of the ferrous lithium micas used in the study, with data for writing their calculated formulas, are given in table 7.

Some analyses of ferrous lithium micas were not used in the study. In most of these analyses, which are given in table 8, the alkali content is high compared with the octahedral and tetrahedral cations; in the rest it is low. These discrepancies may be due to faulty analysis, particularly failure to determine lithium properly, or to nonhomogeneous or contaminated samples.

Any error in the Li determination has a double effect, as Li is an octahedral cation and the other alkalies are interlayer cations. If the Li is not completely separated, the part not separated is reported as Na; thus the Na reported is too high, the alkalies calculated as interlayer cations are also too high, and the octahedral cations are too low. If the determination of Li errs on the high side, the other alkalies reported are too low, and the octahedral cations are too high. If the sample is not homogeneous, it is possible that the part taken for determination of the alkalies might be higher or lower in alkalies than the part taken for determining the other constituents, SiO_2, Al_2O_3, Fe_2O_3, and MgO.

ALUMINUM LITHIUM MICAS

INTERPRETATION OF COMPOSITION OF LEPIDOLITES BASED ON END MEMBERS

In recent years, following Stevens (1938) and Winchell (1942), there has been a strong tendency to interpret lepidolites as isomorphous mixtures of various end members. Stevens found that the composition of the 17 samples upon which he based his study closely approximates that of isomorphous mixtures of polylithionite,

$$(Al_{1.00}Li_{2.00})Si_4O_{10}(OH)_2K_{1.00},$$

with biotite,

$$F^{2+}_{2.00}(Si_{2.00}Al_{1.00})O_{10}(OH)_2K_{1.00},$$

lithium muscovite,

$$(Al_{1.50}Li_{1.50})(Si_{3.00}Al_{1.00})O_{10}(OH)_2F_{1.00},$$

and muscovite,

$$Al_{2.00}(Si_{3.00}Al_{1.00})O_{10}(OH)_2K_{1.00},$$

Stevens considered that in such solid solutions the end members would not be present as individual end-member unit cells, but that the ions of which the end members are composed would be distributed uniformly throughout the structure. The selection of end members to interpret the composition of lepidolites is an arbitrary one. As Stevens (1938, p. 623) remarks:

> Other combinations of four end members which express the compositions equally well are: polylithionite, zinnwaldite (assuming its formula to be $K\text{-}LiR''Al\text{-}AlSi_3O_{10}F_2$), lithium muscovite, and muscovite; polylithionite, taeniolite ($K\text{-}LiR_3''\text{-}Si_4O_{10}F_2$), lithium muscovite, and muscovite. In addition, 5 or 6 of the above end members may be taken, depending on what end members are used to express the bivalent ion content.

Winchell (1942) interpreted lepidolites as isomorphous mixtures of polylithionite, paucilithionite (identical with Stevens' lithium muscovite), and protolithionite ($K_2LiFe_4Al_2Si_4O_{20}F_4$). He calculated 28 lithium micas to these end members and found that Li_2O was deficient in all but 1 and that the average deficiency in Li_2O was almost 1 percent by weight (0.91). However, if some muscovite was assumed to be present also, the deficiency in Li_2O could be eliminated and the

composition satisfactorily explained. Winchell considered muscovite to be present, not in solid solution but as a discrete mineral which might be so intimately intergrown or intermixed as to be difficult to detect optically.

Lepidolite and muscovite are, indeed, often intimately associated. In Stevens' study of lepidolites, five samples are discarded because small flakes of lepidolite in them were found to contain minute inclusions of muscovite. Winchell believed that muscovite may coexist with lepidolite in units too small to be detected optically. Ginzburg and Berkhin (1953) believe that considerable lepidolite in pegmatitic rocks has been derived from metasomatic replacement of muscovite and biotite. By incomplete replacement reactions, heterogeneous mixtures of the primary mica with lepidolite have been, they believe, analyzed as one mica type. Pale-violet lepidolites from muscovite in pegmatites from the Kalbinsk Chains, or from Turkestan, often contain relict inclusions of muscovite and intimate graphic intergrowths with this primary muscovite. However, the amount of muscovite that Winchell had to assume to be present to account for the deficiency in lithium content—more than 10 percent in 20 out of 28 samples—is such that its presence could easily be detected by X-rays. For example, Stevens' sample 8 (36, table 6), with an Li_2O content of 5.11 percent, was estimated by Winchell to contain 29.9 percent muscovite. X-ray study by Hendricks and Jefferson (1939) of this sample showed it to have a one-layer lepidolite structure. They did not report the presence of any muscovite in this sample nor in any other of Stevens' samples that had more than 5 percent of Li_2O. They found, however, that Stevens' sample 1 (21, table 6), with a Li_2O content of 2.70, was structurally a muscovite. They found samples 2–5 (22, 23, 24, and 29, table 6), too fine grained for study. Later study of X-ray and Weissenberg photographs by Levinson (1953) confirmed Hendricks and Jefferson's findings with respect to Stevens' samples. In addition Levinson showed that Stevens' samples 2–5 were mixtures of 2-layer muscovite and 6-layer lepidolite. These studies of the crystal structure of lepidolites show that deficiency of Li in them, as compared with end members, cannot always be explained by assumption of admixture with muscovite. It is probable that some materials that have been analyzed as "lepidolites" have contained some occluded or interlayered muscovite, but the work of Hendricks and Jefferson and Levinson demonstrates that lepidolites have characteristic optical properties and structures, and that they are not mixtures of end members as interpreted by Winchell and Stevens.

COMPOSITIONAL CHANGES SHOWN BY THE ANALYSES

The analyses given in table 6 indicate a general increase in SiO_2 content, decrease in Al_2O_3 content, decrease in H_2O+ content, and increase in F content with increase in Li_2O content. Some of the analyses in which Li_2O is very low have only 45 percent or even less of SiO_2, as compared with SiO_2 contents of more than 55 percent in those in which Li_2O is high. On the other hand, analyses which are very low in Li_2O content have the highest amounts of Al, more than 35 percent, whereas those highest in Li_2O content are lowest in Al_2O_3 content, some having only 15 percent or even less. Similarly, analyses very low in Li_2O content have a H_2O+ content of 4 percent or more but a low content of F, less than 0.5 percent, and analyses that contain high amounts of Li_2O are very low in H_2O+, 0.5 percent or less, but have high contents of F, 8 percent or more. These relations are reflected in the data for the calculated formulas which are included in the table. These formulas indicate also that octahedral occupancy increases from about 2 sites in aluminum lithium micas very low in Li_2O to about 3 sites in those containing the highest amounts of Li_2O. These, in general, orderly compositional variations accompanying increase in Li_2O content suggest the sort of isomorphous substitution that characterizes other members of the mica group, such as the substitution of bivalent and other trivalent ions for aluminum in the muscovites (Foster, 1956) and the substitution of trivalent and other bivalent cations for magnesium in the phlogopites and biotites (Foster, 1960, p. 16–32). A similar replacement system among the aluminum lithium micas was suggested by Levinson (1953, p. 88) on the basis of his work on the structure of the micas.

HYPOTHETICAL LI-(OCTAHEDRAL AL) REPLACEMENT RATIOS

Theoretically, Li can be accommodated in muscovite micas in 4 different ways: occupancy of vacant octahedral sites, replacement of 1 ion of Al by 1 ion of Li, replacement of 1 ion of Al by 2 ions of Li, and replacement of 1 ion of Al by 3 ions of Li. The first 3 methods of accommodation necessitate layer-charge readjustments, Li being univalent and Al trivalent; the fourth method does not, as the 3 positive charges carried by 3 Li ions exactly balance the 3 positive charges of the replaced Al ion. However, it does necessitate increase in octahedral occupany, as do also the first and third methods.

In attempting to explain a form of muscovite having as much as 3.3 percent of Li_2O, Levinson (1953, p. 93) speculated as to whether it is possible for such a large amount of Li to replace Al isomorphously in the

muscovite structure. He concluded that because of similarity in atomic radii, Al=1.43 A (angstrom units), Li=1.51 A, the substitution is possible but not necessary as Li could occupy vacant octahedral positions. The effect of this sort of accommodation of Li can be illustrated by Stevens' (1938, p. 615) sample 1 (21, table 6), which Levinson found to have a normal muscovite structure and which contains 2.70 percent of Li_2O. This amount of Li_2O is equivalent to 0.73 octahedral positions in the calculated formula. If this number of vacant octahedral positions in the primary muscovite formula

$$[(\underbrace{Al_{1.84}Fe^{+3}_{0.01}Fe^{+2}_{0.02}Mg_{0.01}Mn^{+2}_{0.12}}_{2.00})^{-0.15}(Si_{3.16}Al_{0.84})^{-0.85}O_{10}(OH,F)_2]^{-1.00}K^{+1.00}_{1.00},$$

which has the same bivalent-ion content as Stevens' sample, were to be occupied by Li, with no replacement of Al,

$$[(\underbrace{Al_{1.84}Fe^{+3}_{0.01}Fe^{+2}_{0.02}Mg_{0.01}Mn^{+2}_{0.12}Li_{0.73}}_{2.73})^{+0.85}(Si_{3.42}Al_{1.58})^{-1.58}O_{10}(OH,F)_2]^{-1.00}K^{+1.00}_{1.00},$$

certain other changes in layer-charge relations and in the composition of the tetrahedral layer necessarily follow. The addition of 0.73 positive charges to the octahedral layer changes the negative charge of 0.15 previously on that layer to a positive charge of 0.58. This positive charge on the octahedral layer requires an increase in the negative tetrahedral charge to 1.58, by increase in Al content and decrease in Si content, in order to preserve the total composite-layer charge at −1.00. Thus a lithium-containing muscovite in which Li merely occupies vacant octahedral positions would, in general, be characterized by a positive octahedral charge and a negative tetrahedral charge in excess of 1.00 by an amount equivalent to the positive octahedral charge, by a decrease in Si equivalent to the increase in negative tetrahedral charge, and by a 1:1 relation between the number of positions occupied by Li and the increase (above 2.00) in occupied octahedral positions. These characteristics are quite different from those shown by the calculated formulas. As illustrated in figures 26 and 28, particularly, the formulas exhibit an increase, not decrease, in Si content with increase in Li content, and an approximate 2:1 ratio between the number of positions occupied by Li and the increase (above 2.00) in the number of octahedral sites occupied. The compositional and charge relations shown in these figures, therefore, indicate that Li is not accommodated in the structure by simple occupancy of vacant octahedral sites by Li. In the actual formula for Stevens' sample 1 (21, table 6)

$$[(\underbrace{Al_{1.58}Fe^{+3}_{0.01}Fe^{+2}_{0.02}Mg_{0.01}Mn^{+2}_{0.12}Li_{0.73}}_{2.47})^{-0.20}(Si_{3.16}Li_{0.84})^{-0.84}O_{10}(OH,F)_2]^{-1.04}K(Na,Rb,Cs)^{+1.01}_{1.01},$$

the octahedral charge is negative, not positive, Si is greater than 3.00, not less, and the ratio of positions occupied by Li to the increase (above 2.00) in the number of octahedral sites occupied is about 5:3, not 1:1. Furthermore, simple occupancy of vacant octahedral sites by Li, with no replacement of Al, cannot explain the amounts of Li found in many aluminum lithium micas. The limit of octahedral occupancy possible, 1.00 octahedral position, is equivalent to only about 3.75 percent of Li_2O, whereas many aluminum lithium micas contain more than 5 percent of Li_2O.

If the Li content of Steven's sample 1 is added to the primary mica above, in the replacement ratio of 1 Li for 1 octahedral Al, the following irrational formula results:

$$[(\underbrace{Al_{1.11}Fe^{+3}_{0.01}Fe^{+2}_{0.02}Mg_{0.01}Mn^{+2}_{0.12}Li_{0.73}}_{2.00})^{-1.61}Si_4O_{10}(OH,F)_2]^{-1.61}K^{+1.61}_{1.61}.$$

The deficiency in positive charges in the octahedral layer is so great that the negative charge on the layer is 1.61, and, even with complete filling of the tetrahedral layer with Si, the charge on the composite layer is also −1.61, instead of −1.00. The greatest amount of Li that can substitute for octahedral Al, ion for ion, in an ideal muscovite, and produce a rational formula, is 0.50:

$$[(\underbrace{Al_{1.50}Li_{0.50}}_{2.00})^{-1.00}Si_4O_{10}(OH,F)_2]^{-1.00}K^{+1.00}_{1.00}$$

Any greater degree of substitution at this ratio results

in too great a negative octahedral charge and composite-layer charge. This Li limit is too low to account for the composition of many aluminum lithium micas.

A 2:1 Li-(octahedral Al) replacement ratio for the amount of Li present in Stevens' sample 1 in the primary muscovite above results in a formula,

$$[\underbrace{(\overset{-0.50}{Al_{1.43}Fe^{+3}_{0.01}Fe^{+2}_{0.02}Mg_{0.01}Mn^{+2}_{0.12}Li_{0.73}})}_{2.37}(\overset{-0.50}{Si_{3.50}Al_{0.50}})O_{10}(OH,F)_2]^{-1.00}\,K^{+1.00}_{1.00},$$

which resembles more closely the characteristics of the calculated formulas as illustrated in figures 25, 26, and 28; namely, a decrease in Al (IV) content, increase in Si content, and an increase in total octahedral positions occupied which is about one-half the number of lithium positions occupied. The end member for this ratio of replacement would have the formula,

$$[\underbrace{(\overset{-1.00}{Al_{1.00}Li_{2.00}})}_{3.00}\overset{0.00}{Si_4}O_{10}(OH,F)_2]^{-1.00}\,K^{+1.00}_{1.00}.$$

In this formula the ratio of positions occupied by Li to the increase in octahedral positions occupied is 2:1, the increase in Si is also equivalent to half the increase in Li, and the decrease in total Al is equivalent to the increase in Li. These changes can be expressed in the equation

$$n\mathrm{Li}+n\ 0.5\ \mathrm{Si}+0.5\ n\mathrm{Oct.Site}=n\mathrm{Al}. \qquad \text{(A)}$$

This ratio of replacement permits the admission of enough Li into the structure to account for the composition of the highest amounts of Li that have been reported in lepidolites. This formula represents the composition of polylithionite, one of the Li end members used by both Stevens and Winchell in their interpretation of the composition of lepidolites.

Substitution of 3 Li cations for 1 octahedral Al in the primary muscovite for Stevens' sample 1 produces a formula,

$$[\underbrace{(\overset{-0.14}{Al_{1.60}Fe^{+3}_{0.01}Fe^{+2}_{0.02}Mg_{0.01}Mn^{+2}_{0.12}Li_{0.73}})}_{2.49}(\overset{-0.86}{Si_{3.14}Al_{0.86}})O_{10}(OH,F)_2]^{-1.00}\,K^{+1.00}_{1.00},$$

which is very close to that calculated from the analysis of this sample, suggesting that the Li-(octahedral Al) replacement ratio for this sample is very close to 3:1. The end-member formula for this ratio of replacement,

$$[\underbrace{(\overset{0.00}{Al_{1.50}Li_{1.50}})}_{3.00}(\overset{-1.00}{Si_{3.00}Al_{1.00}})O_{10}(OH,F)_2]^{-1.00}\,K^{+1.00}_{1.00},$$

has the same tetrahedral group as muscovite. As 1.5 cations carrying 1.5 positive charges replace 0.5 cation of Al, which also carries 1.5 positive charges, there is no change in layer-charge relations. The compositional changes involved in this ratio of replacement of Li for octahedral Al may be expressed as

$$1.5n\mathrm{Li}+n\mathrm{Oct.Site}=0.5n\mathrm{Al} \qquad \text{(B)}$$

Stevens called this hypothetical end member lithium muscovite and Winchell called it paucilithionite. Neither name is satisfactory. Muscovite is a heptaphyllic or dioctahedral mica, whereas the above formula is that of an octaphyllic or trioctahedral mica. Winchell used the prefix pauci because the formula represents the minimum tenor of Li in a lepidolite end member. However, the use of this prefix, which means small or little, for an end member containing more than 5 percent of Li_2O, and in which one-half of the available octahedral sites are occupied by Li, too much minimizes its lithian character. The prefix also exaggerates the difference between this hypothetical end member and polylithionite, which contains about 7.5 percent Li and in which two-thirds of the octahedral sites are occupied by Li. The three Li ions occupying octahedral sites in the unit-cell formula,

$$[\underbrace{(\overset{0.00}{Al_{3.00}Li_{3.00}})}_{6.00}(\overset{-2.00}{Si_{6.00}Al_{2.00}})O_{20}(OH,F)_4]^{-2.00}\,K^{+2.00}_{2.00},$$

suggests the name "trilithionite" as more appropriate for this hypothetical end member. This name also suggests the 3:1 Li-(octahedral Al) replacement ratio of this end member.

This discussion of the possible methods of accommodating Li in the muscovite structure shows that simple occupancy of vacant octahedral sites in muscovite by Li or replacement of 1 octahedral Al by 1 Li either produce irrational formulas for end members or produce end-member formulas whose Li content is too low to be applicable to the interpretation of the composition of some lepidolites. Replacement of octahedral Al by Li in the ratio of 2 or 3 for 1 produces rational end-member formulas capable of interpreting the composition of these micas.

RELATION OF LI TO OTHER CONSTITUENTS IN CALCULATED FORMULAS

RELATION BETWEEN LI AND OCTAHEDRAL AL

The relation between the number of octahedral positions occupied by Li and the number of octahedral

positions assumed to have been vacated by Al in formulas of analyzed aluminum lithium micas is shown in figure 25. In a study of the dioctahedral micas (Foster, 1956) it was found that octahedral occupancy in these micas is always close to 2.00 and that replacement of Al by other trivalent and by bivalent cations is ion for ion. Consequently, in calculating the number of octahedral-Al positions replaced by Li it was assumed that 2.00 octahedral sites were occupied in the primary muscovite, and that replacement of octahedral Al by Fe^{+3}, Fe^{+2}, Mg, and Mn was ion for ion—such as 1 ion of Fe^{+3} for 1 of Al, 1 of Fe^{+2} for 1 of Al. The difference, then, between 2.00 and the number of octahedral sites occupied by Al and these other octahedral cations is assumed to represent the number of octahedral-Al cations replaced by the Li present. All but a few of the points fall between line B, which represents the 2:1 Li-(octahedral Al) replacement ratio and leads to the end member polylithionite, and line C, which represents the 3:1 Li-(octahedral Al) replacement ratio and leads to the end member trilithionite.

In the formulas represented by points lying between these 2 lines, therefore, the Li-(octahedral Al) replacement ratio is between 2 and 3. The location of the points indicates that in most of the formulas the ratio is between 2.3 and 2.8. Only 1 of the formulas represented by points that fall outside the area embraced between lines B and C contains more than 2.0 percent Li_2O. This formula, in which the Li-(octahedral Al) replacement ratio is 1.9, is closest in composition to the end member, polylithionite. The other points that fall outside the area between lines B and C fall below line C, indicating that in the formulas that they represent, the Li-(octahedral Al) replacement ratio is greater than 3. In most of these formulas, however, the ratio is quite close to 3, and the discrepancy may be due to slight analytical error, particularly in the determination of Li_2O, to lack of homogeneity in the sample, or to error in assuming that the octahedral occupancy in the primary muscovite was exactly 2.00 in calculating the number of Al sites replaced. The amount of replaced Al in these formulas is so small that an error in octahedral occupancy in the primary muscovite of as little as 0.03 less than 2.00 could account for the high Li-(octahedral Al) ratio in them.

It has been shown that accommodation of Li by replacement of octahedral Al in the ratio of 2 for 1 involves compositional changes in accordance with equation A, $n\text{Li}+0.5n\text{Si}+0.5n\text{Oct.Site}=n\text{Al}$. In other words, for each ion of Li or fraction thereof added, half as many Si ions are added and half as many additional octahedral sites are occupied, but the loss in total Al ions (octahedral and tetrahedral) is the same as the gain in Li ions. It was also shown that in accommodation of Li by replacement of octahedral Al in the ratio of 3.0 for 1.0 involves compositional changes in accordance with equation B, $1.5n\text{Li}+n\text{Oct.Site}=0.5n\text{Al}$. Thus for each 1.5 ion of Li or fraction thereof

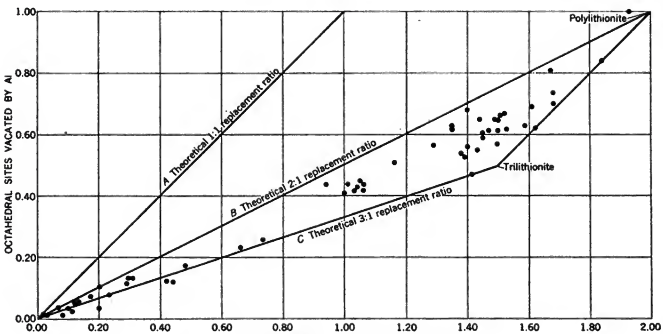

FIGURE 25.—Relation between octahedral sites occupied by Li and vacated by Al in aluminum lithium micas.

added, two-thirds as many octahedral sites are occupied and there is a loss in octahedral Al ions equivalent to one-third the gain in Li ions. This manner of adjustment involves no change in Si content. As the Li-(octahedral Al) replacement ratios in the analyses studied are, for the most part, between 2 and 3, it would be expected that they would show compositional changes between those specified by equations A and B, and that the closer the replacement ratio in any particular formula is to 2 or 3, the closer the compositional changes indicated by that formula will be to equation A or B, respectively.

RELATION BETWEEN (LI–R^{+2}) AND SI

The relation between (Li—R^{+2}) and Si in the aluminum lithium micas studied is shown in figure 26. If, except for Li, the octahedral layer were entirely occupied by trivalent ions, Li in the formulas would have been plotted directly against the increase (above 3.0) in Si. However, the octahedral groups in the formulas are not made up entirely of trivalent ions plus Li, but also contain varying amounts of bivalent ions, and some of the positive charges carried by Li compensate for the deficiency in charge, compared with Al, of these ions. For example, in the formula for analysis 34, table 6,

$$[(\underbrace{Al_{1.29}Fe_{0.01}^{+3}Mn_{0.16}^{+2}Li_{1.38}}_{2.84})(Si_{3.38}Al_{0.62})O_{10}(OH,F)_2]^{-1.62}K(Na,Rb,Cs)_{1.03}^{+1.03}.$$

0.17 of the positive charges carried by Li compensate for the deficiency of the number of positive charges present in the octahedral layer compared with the number carried by the same number of trivalent ions. The effect on the Si content is as though 1.21 and not 1.38 ions of Li were present. In order to eliminate the effect of the variable amounts of R^{+2} ions present in the formulas, Si is plotted against (Li—R^{+2}) in figure 26, not against Li alone. In some of the formulas in which Li is very low, the positive charges added by Li do not entirely compensate for the deficiency in octahedral charge due to the bivalent ions present.

In figure 26 all but a few of the points representing the (Li—R^{+2}):Si relation in the formulas fall between line A, which represents the 2:1—Li:Si relation found in formulas in which the Li-(octahedral Al) replacement ratio is 2, and line B, the baseline, which represents the 1.5:0—Li:Si relation found in formulas in which the Li-(octahedral Al) replacement ratio is 3. Thus the (Li—R^{+2}):Si relation in most of the formulas is consistent with that to be expected in formulas for aluminum lithium micas in which the Li-(octahedral Al) replacement ratio is between 2 and 3.

RELATION BETWEEN LI AND TOTAL AL

The relation between the number of octahedral sites occupied by Li and the total number of formula sites occupied by Al is shown in figure 27. Except for some

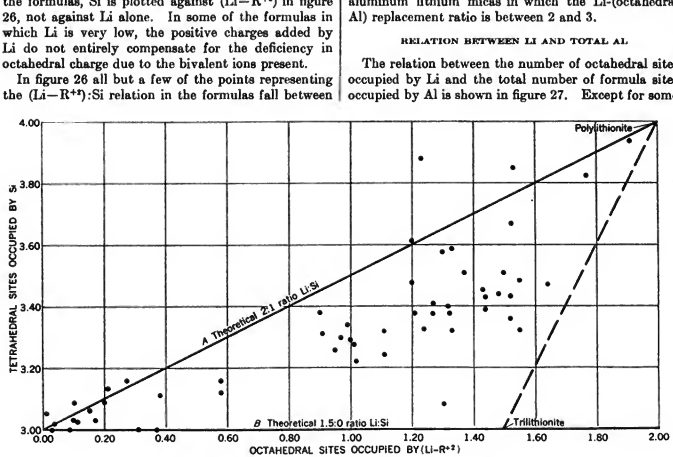

FIGURE 26.—Relation between (Li—R^{+2}) and Si in aluminum lithium micas.

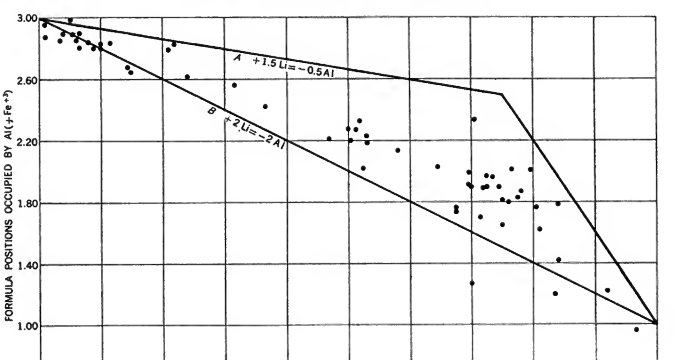

FIGURE 27.—Relation between the number of formula sites occupied by Li and R^{+3} in aluminum lithium micas.

points representing formulas with a low content of Li, almost all the points representing the Li:Al relation in the calculated formulas of the analyses studied fall between lines A and B. Line A represents the Li:Al relation, as compared with muscovite, in formulas in which the Li-Al replacement ratio is 3.0; line B represents the Li:Al relation when the Li-Al replacement ratio is 1.0. The location of most of the points, therefore, indicates a decrease in Al with increase in Li that is in accordance with the Li:Al relation to be expected in formulas in which the Li-Al replacement ratio is between 2 and 3.

RELATION BETWEEN LI AND OCCUPIED OCTAHEDRAL SITES IN EXCESS OF 2.00

The relation between Li and the number of octahedral sites occupied in excess of 2.00 is shown in figure 28. In aluminum lithium micas in which the Li-(octahedral Al) replacement ratio is 2, the number of octahedral positions occupied in excess of 2.00 is theoretically one-half the number of octahedral positions occupied, as represented by line B (fig. 28); in aluminum lithium micas in which the Li-(octahedral Al) replacement ratio is 3, the number of octahedral positions occupied in excess of 2.00 is theoretically in the ratio of 1.5 Li to 1.0 octahedral position, as represented by line A (fig. 28). In accordance with the Li-(octahedral Al) replacement ratios found in the calculated formulas, most of the points representing the relation between the number of octahedral sites occupied by Li and the total number of octahedral sites occupied in excess of 2.00 fall between the two lines.

RELATION BETWEEN Li_2O AND F

A casual inspection of the Li_2O and F values in the analyses in table 6 shows a general increase in F content with increase in Li_2O content. The grouping of the points in figure 29 along the line representing a 1:1 ratio between Li_2O and F indicates a tendency toward a 1:1 relation in these constituents in aluminum lithium micas. Considering the difficulties inherent in the determination of both Li_2O and F, some of the discrepancies shown in figure 29 are probably more to be attributed to error in determination than to other than a 1:1 relation between Li_2O and F. Increase in F content is accompanied by decrease in H_2O+ content (fig. 30).

RELATION BETWEEN Li_2O CONTENT, OCTAHEDRAL OCCUPANCY, AND STRUCTURE

The variations in composition accompanying increase in Li content shown in figures 25, 26, 27, and 28 are those to be expected if Li were substituted for octahedral

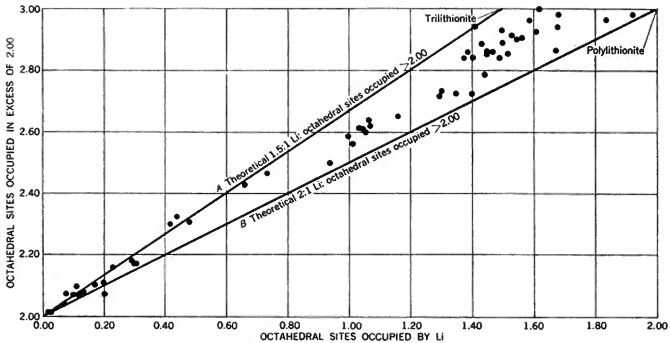

FIGURE 28.—Relation between Li and octahedral occupancy in excess of 2.00 in aluminum lithium micas.

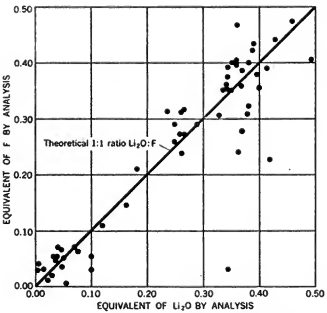

FIGURE 29.—Relation between Li_2O and F in aluminum lithium micas.

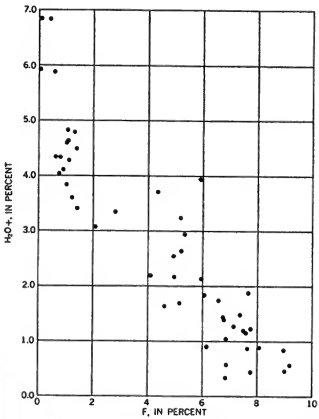

FIGURE 30.—Relation between F and H_2O+ in aluminum lithium micas.

Al in muscovite in ratios varying between 2 and 3 Li for 1 octahedral Al. Compositionally, therefore, these micas resemble members of an isomorphous series that starts with muscovite. However, the increase in octahedral occupancy from 2.00 in muscovite to 3.00 in some lepidolites and in the theoretical end members, poly-

lithionite and trilithionite, raises the problem of structural continuity.

Information as to the structure of aluminum lithium micas is furnished by Hendricks and Jefferson's study of Stevens' lepidolite samples (1939, p. 761), and by Levinson's study of aluminum lithium micas (1953) that varied in Li_2O content from a few tenths of a percent to more than 7 percent. Included among the micas studied by Levinson were most of Stevens' samples. Except for a few samples in a restricted range of Li_2O content, both investigators found that the mica samples studied were not mixtures, as postulated by Stevens (1938) and Winchell (1942), but that each consisted of one structural form. Hendricks and Jefferson found that Stevens' sample 1 (21, table 6), which has an Li_2O content of 2.70 percent, has a muscovite structure, but that his samples 6–10 and 12–17, which contain between 5.04 and 7.26 percent Li_2O, all have lepidolite structures. Also, samples 2–5 of Stevens' suite, which contain between 3.51 and 3.96 percent Li_2O and fall, in Li_2O content, between sample 1, with a muscovite structure, and 6, with a lepidolite structure, were too fine grained for the type of study made by them. Levinson (1953, p. 99) speculated that it seemed likely that "* * * these fine-grained micas owe their macrostructural defects to small-scale variations in their crystal structure which itself probably is assignable to their chemically transitional position in the muscovite-lepidolite series." In order to test this hypothesis, he made detailed powder X-ray studies of these fine-grained micas and found that they all are combinations of 2-layer muscovite and 6-layer lepidolite forms, with the 6-layer[1] lepidolite form predominating over the 2-layer muscovite form in all the samples. As a result of his study of the aluminum lithium micas, Levinson concluded that micas with less than 3.3 percent Li_2O have muscovite structure; those with 3.4 to 4.0 percent Li_2O have mixed structures, and that those with more than 4.0 percent Li_2O have lepidolite structure.

Data for correlation of structure with the number of sites occupied by Li and octahedral cations in Stevens' samples are given in table 1. These data show that in the half-cell formula for Stevens' sample 1, which has a muscovite structure, octahedral occupancy is 2.47; in Stevens' 2, 3, 4, and 5, which are combinations of muscovite and lepidolite forms, octahedral occupancy is 2.50 to 2.62 sites; and in Stevens' other samples, all of which have lepidolite structures, octahedral occupancy is greater than 2.70. Thus the samples that are combinations of forms, giving evidence of transition in structural type, have octahedral occupancies about halfway between 2.00 and 3.00. In these samples, Li occupancy is close to one octahedral site. These relations between Li occupancy, octahedral occupancy, and structural type in Stevens' and Berggren's samples, which were also included in Levinson's study, are shown graphically in figure 31.

[1] Smith and Yoder (1956, p. 215) renamed this $2M_1$.

TABLE 1.—*Relation between Li_2O content, octahedral occupancy, and structure of lithium micas analyzed by Stevens*

Stevens (1938)		Li sites	Octahedral occupancy	Structure	
Specimen	Li_2O (percent)			Hendricks and Jefferson (1939)	Levinson (1953)
1	2.70	0.73	2.47	Muscovite	Normal muscovite.
2	3.51	.94	2.50	Too fine grained for study.	6-layer lepidolite and 2-layer muscovite.
3	3.70	1.00	2.59	do	Do.
4	3.81	1.03	2.57	do	Do.
5	3.96	1.06	2.62	do	Do.
6	5.04	1.35	2.72	6-layer monoclinic	6-layer monoclinic (and lithian muscovite).
7	5.05	1.38	2.84	do	Not available.
8	5.11	1.35	2.73	1-layer	1-layer.
9	5.32	1.44	2.79	do	Not available.
10	5.39	1.50	2.93	do	Do.
11	5.51	1.49	2.84	Not available	Do.
12	5.64	1.52	2.85	6-layer monoclinic	Do.
13	5.76	1.56	2.90	1-layer	1-layer.
14	5.89	1.61	2.92	3-layer hexagonal	3-layer hexagonal.
15	6.18	1.68	2.94	1-layer	1-layer.
16	6.84	1.84	2.96	do	Do.
17	7.26	1.93	2.93	do	Do.

Just as the transitional samples consist of a combination of forms, the values reported for various constituents on analysis are composite values made up of the amounts of these constituents contributed by muscovite and lepidolite forms present. For example, the value for Li_2O found on analysis in these samples is a composite value made up of Li_2O contributed by the muscovite present, in which the Li_2O content may be less than 3.0 percent, and of Li_2O contributed by the lepidolite present, in which the Li_2O content may be more than 4.0 percent. Thus the Li_2O values in the area of mixed forms which suggest a continuity in Li content in figure 31, for example, between aluminian lithium micas of muscovite structure and those of lepidolite structure are deceptive, and there is actually a gap in Li content between these two types of aluminum lithium micas. Similarly, all the other analytical values reported for these mixed-form samples are composite values. Therefore, both the compositional and structural continuity of the aluminum lithium series is broken at the point at which change in structure takes place, and the isomorphous series that starts with muscovite extends only to an octahedral occupancy of about 2.45 sites and an Li occupancy just short of 1.00 octahedral site.

Following Schaller (1930), these aluminum lithium micas having muscovite structures are termed "lithian" muscovites. Levinson applied this term to a new variation of the muscovite polymorph which he observed in muscovite containing at least 3.3 percent

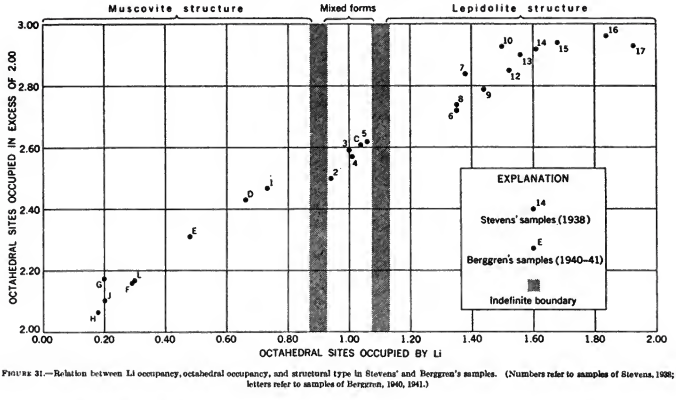

FIGURE 31.—Relation between Li occupancy, octahedral occupancy, and structural type in Stevens' and Berggren's samples. (Numbers refer to samples of Stevens, 1938; letters refer to samples of Berggren, 1940, 1941.)

Li_2O and possibly as much as 4.3 percent Li_2O. In so doing he applied a chemical term to a structural variation, whereas Schaller had proposed the use of the adjectival ending "ian" to names of chemical elements to describe a variety in which there was minor and variable replacement of an essential element by an analogous element, as chromian muscovite, or vanadian muscovite. According to this usage a lithian muscovite is a muscovite containing some Li in place of Al, not a muscovite having a slight structural variation over a limited range of Li_2O content, as used by Levinson.

Because of their different structure, and the break in compositional continuity in the transition area, the lepidolites do not belong to the aluminum lithium isomorphous series that starts with muscovite. However, in composition they can be interpreted as if they were a continuation of this series, that is, on the basis of Li replacement of octahedral Al in muscovite in ratios varying between 2 and 3 Li for 1 octahedral Al. This continuation in type and order of replacement beyond the structural transition zone is illustrated in figures 25 through 31.

Available information on Li content and octahedral occupancy, Li-(octahedral Al) replacement ratios, and structure in Stevens' samples and in Berggren's samples that were studied by Levinson, listed in table 2, shows no consistent correlation between replacement ratio and structure in lithian muscovites and lepidolites. Lithian muscovites have Li-(octahedral Al) replacement ratios ranging from 1.5 to 2.9; lepidolites with 6-layer structures have Li-(octahedral Al) replacement ratios ranging from 2.1 to 2.8, and those with 1-layer structures have Li-(octahedral Al) replacement ratios ranging from 1.9 to 2.6. Apparently, therefore, micas in which the Li-(octahedral Al) replacement ratio is 2 are not distinct structurally from micas in which this replacement ratio is 3.

Three polymorphic variations were found among the lepidolites: the 6-layer monoclinic, the 1-layer, and the 3-layer hexagonal. Levinson correlated the 6-layer monoclinic polymorph with lepidolites containing 4.0 to 5.1 percent Li_2O (equivalent to about 1.05 to 1.40 octahedral sites in half-cell formulas), and the 1-layer polymorph with those having more than 5.1 percent Li_2O. However, Hendricks and Jefferson (1939) concluded that there is no apparent correlation between the different lepidolite polymorphs and composition. Thus Stevens' sample 12 (47, table 6), with 5.64 percent Li_2O, has a 6-layer monoclinic structure whereas others with lower Li_2O content (table 1) have 1-layer lepidolite structures. Nor is there, apparently, any relation among lepidolites, between octahedral occupancy and the different lepidolite polymorphs. As shown in table 2, octahedral occupancy in the 6-layer lepidolites studied ranges between 2.72 and 2.96; that

in the 1-layer lepidolites ranges between 2.73 and 2.96. Hendricks and Jefferson also found that the 6-layer and 1-layer polymorphs cannot be distinguished optically.

TABLE 2.—*Comparison of Li occupancy, Li-(octahedral Al) replacement ratio, and structure*

Sample			Li_2O (percent)	Li sites	Octahedral occupancy	Replacement ratio	Structure
Table 6	Other reports: Identification	Other reports: Author					
11	H	Berggren, 1940	0.69	0.15	2.05	1.5	Muscovite.
13	J	Berggren, 1941	.76	.20	2.10	2.0	Do.
15	F	Berggren, 1940	1.10	.29	2.16	2.3	Do.
16	L	Berggren, 1941	1.1	.30	2.17	2.3	Do.
19	E	Berggren, 1940	1.8	.48	2.31	2.8	Do.
20	D	do	2.45	.66	2.43	2.9	Do.
21	1	Stevens, 1938	2.70	.73	2.47	2.8	Do.
33	6	do	5.04	1.35	2.72	2.1	6-layer and muscovite.
34	7	do	5.05	1.38	2.84	2.6	6-layer.
47	12	do	5.64	1.52	2.85	2.3	Do.
53	A	Berggren, 1940	5.95	1.59	2.96	2.5	Do.
36	8	Stevens, 1938	5.11	1.35	2.73	2.2	1-layer.
39	9	do	5.33	1.44	2.79	2.3	Do.
42	10	do	5.39	1.51	2.93	2.6	Do.
50	13	do	5.78	1.56	2.90	2.4	Do.
54	15	do	6.18	1.66	2.94	2.3	Do.
57	16	do	6.84	1.84	2.96	2.1	Do.
58	17	do	7.26	1.93	2.93	1.9	Do.

DISCUSSION

On the basis of chemical evidence alone, the aluminum lithium micas can be considered as if they were members of an isomorphous series, starting with muscovite, in which Li replaces octahedral Al in the ratio of from 2 to 3 Li for 1 octahedral Al. However, structural evidence indicates that the series is not continuous, either structurally or compositionally, but is broken about halfway between muscovite and polylithionite in a zone in which octahedral occupancy is about 2.50 to 2.60 sites and Li occupancy is about 0.95 to 1.05 sites. In this zone the samples are mixed structural forms, muscovite and lepidolite, whereas samples with octahedral occupancy less than 2.50 sites or greater than 2.60 sites are 1 structural form only. As the samples in this zone are mixtures of forms, the analytical values which suggest continuity in composition are composite values and do not actually represent the composition of single-form aluminum lithium micas having an octahedral occupancy of between 2.50 and 2.60 sites. Consequently, the compositional continuity is broken. The aluminum lithium micas, therefore, are members of 2 related series: the lithian muscovite series, which starts with muscovite and extends to micas having an Li occupancy of about 0.85 octahedral sites and an octahedral occupancy of about 2.50 sites, and the lepidolite series, which starts with a lepidolite having an Li occupancy of about 1.10 octahedral sites and an octahedral occupancy of about 2.65 sites and extends to a lepidolite having an Li occupancy of from 1.80 or more octahedral sites and an octahedral occupancy of about 3.00 sites. Selected formulas are given in table 3 that show the relation of lithian muscovites and lepidolites. This relation is shown graphically by histograms in figure 32.

The chemical composition of both the lithian muscovites and lepidolites can be interpreted in the same way; that is, as if they were derived from muscovite by the replacement of octahedral aluminum by lithium in a ratio varying between 2 and 3 Li for 1 octahedral. The other compositional changes that characterize

TABLE 3.—*Selected formulas illustrating relation between lithian muscovites and lepidolites*

	Number in table 6	Formula	Li-(octahedral Al) replacement ratio
Lithian muscovites	2	$[\underbrace{(Al_{1.94}Fe^{+3}_{0.02}Fe^{+2}_{0.04})}_{2.01}(Si_{3.00}Al_{1.00})O_{10}(OH)_2]^{-1.04}(K,Na,Ca/2)^{+1.08}_{1.03}$	2.0
	16	$[\underbrace{(Al_{1.71}Fe^{+3}_{0.07}Fe^{+3}_{0.04}Mg_{0.02}Mn^{+2}_{0.01}Li_{0.32})}_{2.17}(Si_{3.13}Al_{0.87})O_{10}(OH)_2]^{-1.03}(K,Na,Rb,Cs,Ca/2)^{+1.08}_{1.05}$	2.3
	21	$[\underbrace{(Al_{1.88}Fe^{+3}_{0.01}Fe^{+2}_{0.02}Mg_{0.01}Mn^{+2}_{0.12}Li_{0.73})}_{2.47}(Si_{3.16}Al_{0.84})O_{10}(OH)_2]^{-1.04}(K,Na,Rb,Cs)^{+1.01}_{1.01}$	2.8
Mixed structural forms			
Lepidolites	34	$[\underbrace{(Al_{1.24}Fe^{+3}_{0.01}Mn^{+2}_{0.16}Li_{1.38})}_{2.84}(Si_{3.38}Al_{0.62})O_{10}(OH)_2]^{-1.03}(K,Na,Rb,Cs)^{+1.03}_{1.03}$	2.6
	52	$[\underbrace{(Al_{1.32}Fe^{+3}_{0.07}Mg_{0.01}Mn^{+2}_{0.04}Li_{1.61})}_{2.92}(Si_{3.48}Al_{0.52})O_{10}(OH)_2]^{-1.04}(K,Na,Rb,Cs)^{+1.02}_{1.02}$	2.3
	57	$[\underbrace{(Al_{1.08}Fe^{+3}_{0.01}Mg_{0.02}Mn^{+2}_{0.04}Li_{1.84})}_{2.96}(Si_{3.83}Al_{0.17})O_{10}(OH)_2]^{-1.04}(K,Na,Rb,Cs)^{+1.04}_{1.06}$	2.1

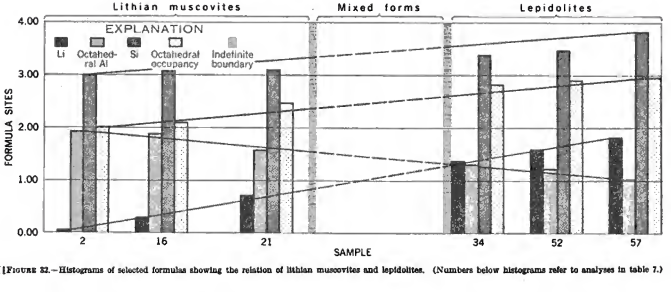

FIGURE 32.—Histograms of selected formulas showing the relation of lithian muscovites and lepidolites. (Numbers below histograms refer to analyses in table 7.)

these micas—increase in silica and decrease in the tetrahedral Al with increase in Li content—are necessitated by the disparity in positive charges carried by the replacing Li and replaced octahedral Al.

The interpretation of the composition of these micas postulated by Stevens (1938) and Winchell (1942), as mixtures of end members, is not borne out by the structural work of Hendricks and Jefferson (1939) and Levinson (1953).

The relation between Li, $R^{+2}(Fe^{+2},Mn^{+2},Mg)$, and octahedral $R^{+3}(Al,Fe^{+3})+Ti^{+4}$ is shown in figure 33, in which the percentages of occupied octahedral sites occupied by Li, $R^{+2}(Fe^{+2},Mn^{+2},Mg)$, and octahedral $R^{+3}(Al,Fe^{+3})+Ti^{+4}$ in each formula are plotted on a triangular diagram. In this diagram ideal muscovite falls at the lower left corner, which represents 100-percent occupancy of the octahedral layer by $Al(+Fe^{+3})$, trilithionite is represented by a point midway along the left side of the triangle, and polylithionite is represented by a point two-thirds of the way up the left side of the triangle. The points representing octahedral occupancy of the calculated formulas of lithian muscovites and lepidolites are distributed along the left side of the triangle from the lower left corner, which represents muscovite, to the point representing polylithionite. Because of the small amounts of FeO, MnO, and (or) MgO found in most lepidolites, few of these points fall on the outside boundary, as do trilithionite and polylithionite. However, all fall between the outside boundary and the line representing 10 percent of bivalent octahedral cations, Fe^{+2}, Mn^{+2}, and Mg.

FERROUS LITHIUM MICAS

PREVIOUS INTERPRETATIONS OF COMPOSITION

Both Kunitz (1924, p. 409) and Winchell (1927, p. 274) regarded lepidolite and protolithionite as end members of a series characterized by decrease in Li content and increase in Fe^{+2}, with protolithionite representing the Fe^{+2}-high, Li-free end of the series. Intermediate members were known as zinnwaldites. Kunitz believed that lepidolite, $KH_2Al_2Le(SiO_4)_3$, contained a special group (2Li,Si), denoted as Le, that was completely replaceable by $3Fe^{+2}$ to form protolithionite. Winchell considered that lepidolite was miscible in all proportions with protolithionite in the crystal state, and that the natural lepidolites, zinnwaldites, and protolithionites were made up of various proportions of the end members. He regarded cryophyllite, a lithium mica described by Cooke (1867) from Cape Ann, Mass., as doubtful. At that time Winchell considered these minerals heptaphyllites, but later (1942, p. 117) he recognized them as octaphyllites and, furthermore, included some lithium in his formula for protolithionite.

Hallimond (1925, p. 311) also believed that lepidolite, zinnwaldite, and protolithionite form a series. However, as indicated by his formulas, $R_2O{\cdot}Li_2O{\cdot}2Al_2O_3{\cdot}6SiO_2{\cdot}2H_2O$, for lepidolite, and $K_2O{\cdot}Li_2O{\cdot}3RO{\cdot}2Al_2O_3{\cdot}6SiO_2{\cdot}2H_2O$, for protolithionite, this series is characterized merely by addition of RO, the Li_2O content remaining constant. Thus Hallimond's series was not a replacement series. The two zinnwaldites reported by Dana, he states, might be regarded as

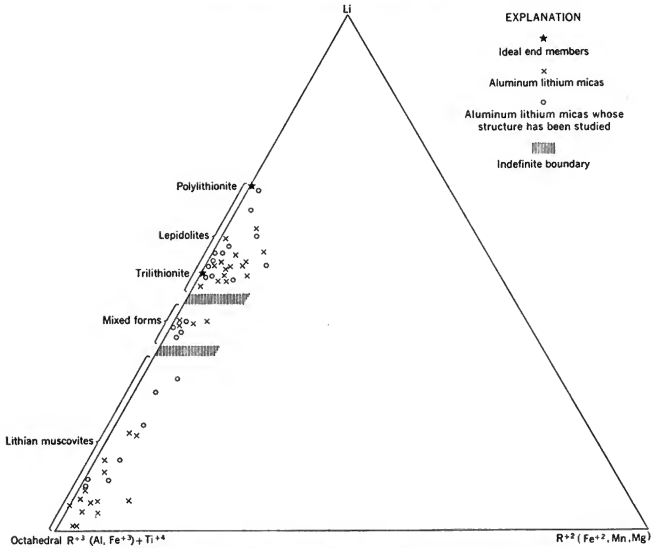

FIGURE 33.—Relation between Li, $R^{+3}(Fe^{+3},Mn^{+3},Mg)$, and octahedral $R^{+3}(Al,Fe^{+3})+Ti^{+4}$ in aluminum lithium micas.

consisting chiefly of the compound $K_2O{\cdot}Li_2O{\cdot}RO{\cdot}2Al_2O_3{\cdot}6SiO_2{\cdot}2H_2O$ or, alternately, as mixtures of lepidolite and protolithionite. He believed that cryophyllite bears the same relation to lepidolite that phengite bears to muscovite.

A classification by Ginzburg and Berkhin (1953) includes the ferrous lithium micas as part of a series of which lepidolite is the high-Li end member and biotite is the Li-free end member. In this series the transition from biotite to lepidolite is supposed to be marked by the replacement of $2Mg^{+2}$ by Li and Al^{+3}.

Thus four kinds of series have been proposed to interpret the composition and relation of the ferrous lithium micas: the lepidolite-protolithionite series of Kunitz (1924, p. 409), in which the Le group (2Li,Si) is completely replaced by $3Fe^{+2}$; the lepidolite-protolithionite series of Winchell, in which the end members are miscible in all proportions and form intermediate members; the lepidolite-protolithionite series of Hallimond, in which Fe^{+2} is additive but Li remains constant; and the biotite-lepidolite series of Ginzburg and Berkhin, in which 2Mg is replaced by (Li+Al). In none of these series are the limits in composition between lepidolite, cryophyllite, zinnwaldite, and protolithionite defined.

The clearest definition of the limits of composition between protolithionite, zinnwaldite, and cryophyllite is that stated in Hey (1955, p. 208). Hey gives the same formula $2[K_2(Li,Fe^{+2},Al)_6(Si,Al)_8O_{20}(F,OH)_4]$ for all three, excepting only that Fe^{+3} is included in the (Li,Fe^{+2},Al) group in his formulas for protolithionite and cryophyllite, but he qualifies the formulas by observations on the amounts of Li, Fe^{+3}, and Si typically present. Thus in protolithionite, zinnwaldite, and cryophyllite, Li occupies 1–2, ≈2, and ≈2½ formula

positions, respectively; Fe occupies ≈1½, ≈1½, and ≈1 (including Fe^{+3}) formula positions, respectively; and Si 5½–6, ≈6½, and ≈7 formula positions, respectively. Following Dana (1892, p. 626), Hey gives zinnwaldite species status, with protolithionite and cryophyllite being considered varieties of zinnwaldite.

COMPOSITIONAL CHANGES SHOWN BY ANALYSES

The analyses of ferrous lithium micas vary considerably in SiO_2 and Al_2O_3 content, although there is a general increase in SiO_2 content and decrease in Al_2O_3 content with increase in Li_2O content. However, these relations are not as consistent as in the aluminum lithium micas. The Fe_2O_3 content is quite variable in ferrous lithium micas having less than 3.5 percent of Li_2O; in ferrous lithium micas having more than 3.5 percent of Li_2O, Fe_2O_3 is generally low or absent. FeO is also quite variable, but, in general, decreases with increase in Li_2O content. All but 1 of the ferrous lithium micas included in the study that contained less than 2 percent of Li_2O have more than 15 percent of FeO, those with between 2.0 and 3.0 percent of Li_2O have between 9.0 and 14.0 percent of FeO, and those with more than 3 percent of Li_2O have between 6.0 and 12.6 percent of FeO. MgO is generally low. Many of the analyses contain less than 0.5 percent, and few contain more than 1.0 percent. Only 1 analysis has a significant amount, 5.23 percent.

In most of the formulas calculated from the analyses the number of octahedral sites occupied is greater than 2.60. These micas are, therefore, trioctahedral or octaphyllic micas, not heptaphyllic micas as was formerly assumed by Winchell (1927, p. 274).

RELATION BETWEEN FERROUS LITHIUM MICAS, SIDEROPHYLLITES, AND ALUMINIAN LEPIDOMELANES

In their principal compositional characteristics, their low MgO content with high FeO content, their octahedral occupancy, and their octahedral-tetrahedral charge relations, the ferrous lithium micas with low Li_2O content resemble siderophyllites and lepidomelanes, which are the low-Mg members of the phlogopite-biotite-siderophyllite (or lepidomelane) Mg replacement system (Foster, 1960, p. 30). The similarity in composition is illustrated by the following formulas:

A. Siderophyllites and aluminian lepidomelanes

Number in table 7

1 ---------- $\underbrace{[(Al_{0.99}Ti_{0.01}Fe^{+3}_{0.05}Fe^{+2}_{1.32}Mg_{0.05}Mn^{+2}_{0.02})}_{2.44}(Si_{2.97}Al_{1.03})O_{10}(OH,F)_2]^{-1.09}K(Ca/2)^{+1.10}_{0.98}$ (−0.06; −1.03)

2 ---------- $\underbrace{[(Al_{0.73}Fe^{+3}_{0.08}Fe^{+2}_{1.88}Mg_{0.01}Mn^{+2}_{0.02}Li_{0.10})}_{2.82}(Si_{2.65}Al_{1.35})O_{10}(OH,F)_2]^{-1.00}K(Na,Ca/2)^{+0.99}_{0.98}$ (+0.35; −1.35)

4 ---------- $\underbrace{[(Al_{0.44}Ti_{0.09}Fe^{+3}_{0.49}Fe^{+2}_{1.38}Mg_{0.03}Mn^{+2}_{0.06}Li_{0.15})}_{2.64}(Si_{2.81}Al_{1.19})O_{10}(OH,F)_2]^{-0.95}K(Na,Ca/2)^{+0.96}_{0.87}$ (+0.24; −1.19)

B. Ferrous lithium micas (Li_2O < *1.5 percent*)

9 ---------- $\underbrace{[(_{1.06}Ti_{0.03}Fe^{+2}_{1.12}Mg_{0.01}Mn^{+2}_{0.04}Li_{0.42})}_{2.68}(Si_{2.76}Al_{1.24})O_{10}(OH,F)_2]^{-1.18}K(Na,Ca/2)^{+1.15}_{1.04}$ (+0.06; −1.24)

10 ---------- $\underbrace{[(Al_{0.71}Fe^{+2}_{0.23}Fe^{+2}_{1.24}Mg_{0.03}Mn^{+2}_{0.10}Li_{0.45})}_{2.76}(Si_{2.93}Al_{1.07})O_{10}(OH,F)_2]^{-1.06}K(Na,Ca/2)^{+1.08}_{1.06}$ (+0.01; −1.07)

11 ---------- $\underbrace{[(Al_{0.37}Ti_{0.03}Fe^{+3}_{0.31}Fe^{+2}_{1.44}Mg_{0.02}Mn^{+2}_{0.02}Li_{0.47})}_{2.86}(Si_{2.89}Al_{1.11})O_{10}(OH,F)_2]^{-0.92}K(Na,Ca/2)^{+0.90}_{0.88}$ (+0.19; −1.11)

In both these groups Mg is insignificant and Fe^{+2} is the dominant octahedral cation, but the amount of Fe^{+2} present varies greatly. In some siderophyllites and in some of the ferrous lithium micas, Al is the principal trivalent octahedral cation, in others in both groups there are significant amounts of trivalent iron. Indeed some low-Mg, high-Fe^{+2} trioctahedral micas, lepidomelanes, contain trivalent iron as the greatly dominant octahedral cation. In formulas calculated from analyses of ferrous lithium micas, the dominant trivalent octahedral cation is usually Al, some contain considerable Fe^{+3}, but Fe^{+3} is not greatly dominant in any of the calculated formulas studied. In the study of the phlogopite-biotite-siderophyllite (or lepidomelane) system (Foster, 1960), it was found that replacements of Mg by bivalent iron (Fe^{+2}), and by the trivalent ions, Al and Fe^{+3}, proceed quite independently; a given degree of replacement by Fe^{+2} has no relation to the

degree of replacement by Al or Fe^{+3}, nor has the degree of replacement by Al any relation to the degree of replacement by Fe^{+3}.

The octahedral charge in the siderophyllites and the ferrous lithium micas is usually positive, but it may be about neutral or even slightly negative, depending on how the additional positive charges carried by trivalent octahedral cations (as compared with the number of charges carried by bivalent cations) have been accommodated in the structure (Foster, 1960, p. 16), and the negative tetrahedral charge may be considerably greater than 1.00, close to 1.00, or less than 1.00, depending on the octahedral charge. Octahedral occupancy also varies considerably, depending also on how the additional positive charges of trivalent octahedral cations have been accommodated.

The similarity in characteristics of siderophyllites and ferrous lithium micas suggests that the siderophyllites are the prototypes from which the ferrous lithium micas are derived. It should be noted here that most analyses of siderophyllites and lepidomelanes include small amounts of Li_2O. Some materials that have been called siderophyllite contain as much as 1 percent of Li_2O.

COMPOSITIONAL RELATIONS IN SIDEROPHYLLITES AND FERROUS LITHIUM MICAS

RELATION BETWEEN LI AND TRIVALENT OCTAHEDRAL CATIONS

The relation between the number of formula sites occupied by Li and by trivalent octahedral cations (Al and Fe^{+3}) in siderophyllites and ferrous lithium micas is shown in figure 34. The number of octahedral sites occupied by trivalent cations is more variable, and in general lower, in the siderophyllites and aluminian lepidomelanes and in the ferrous lithium micas having less than 1.5 percent of Li_2O (about 0.5 octahedral sites), than in ferrous lithium micas containing more than 1.5 percent Li_2O. In the latter the octahedral trivalent cationic content is remarkably constant over

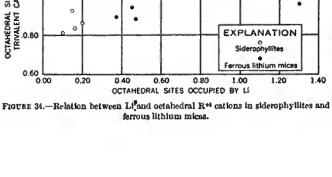

FIGURE 34.—Relation between Li and octahedral R^{+3} cations in siderophyllites and ferrous lithium micas.

a range in Li_2O content of from 1.5 to 4.8 percent. This relative constancy in octahedral trivalent cationic content suggests that these cations are not involved in the addition of Li to the structure.

RELATION BETWEEN LI AND FE^{+2}

The relation between Li and Fe^{+2} in siderophyllites and ferrous lithium micas is shown in figure 35, in

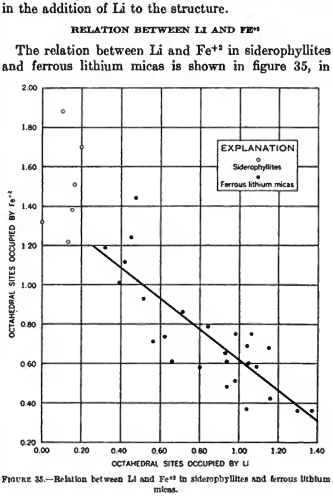

FIGURE 35.—Relation between Li and Fe^{+2} in siderophyllites and ferrous lithium micas.

which the number of octahedral sites occupied by Fe^{+2} is plotted against the number of sites occupied by Li. The Fe^{+2} content of siderophyllites (including ferrian siderophyllites and aluminian lepidomelanes) varies greatly, as does also that of the ferrous lithium micas. Even those containing about the same amount of Li vary greatly in Fe^{+2} content. In general, however, there is a sharp downward trend of the points with increase in Li content, which is suggestive of replacement. The ratio of replacement is, however, difficult to determine because of the great variation in Fe^{+2} content in ferrous lithium micas having low Li content, as well as in the siderophyllites from which they are hypothetically assumed to have been derived, as indicated by the great variation in Fe^{+2} content in the siderophyllites at hand. Thus there is no definite point of departure with respect to Fe^{+2} content from which to calculate Fe^{+2} replacement as there was with respect to Al content and Al replacement in the lepidolites.

RELATION BETWEEN LI AND SI

The relation between Li and Si in siderophyllites (including aluminian lepidomelanes) and ferrous lithium micas is shown in figure 36, in which the number of formula sites occupied by Si is plotted against the number of formula sites occupied by Li. As in Fe^{+2} content, the Si content varies greatly, even in micas having about the same Li content. This difference in Si content in samples having about the same Li content is due to the manner in which the additional charges carried by trivalent octahedral cations are accommodated in the structure (Foster, 1960, p. 16). If the additional positive charges are accommodated predominantly as a positive charge on the octahedral layer and neutralized by a negative tetrahedral charge which is greater than 1.00 by an amount about equivalent to the positive octahedral charge, the Si is considerably lower than if the additional positive charges are predominantly neutralized by anions associated with unoccupied octahedral sites. This variation in Si content, owing to differences in the way in which the additional positive charges were accommodated, in ferrous lithium micas with about the same Li content is illustrated in the formulas for analyses 22 and 23, table 7, that follow:

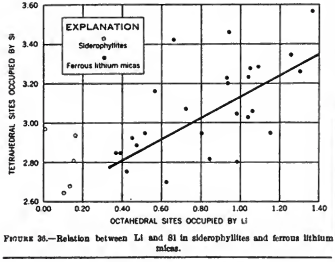

FIGURE 36.—Relation between Li and Si in siderophyllites and ferrous lithium micas.

$$[\underbrace{(Al_{0.80}Ti_{0.02}Fe^{+3}_{0.52}Fe^{+2}_{0.75}Mg_{0.10}Li_{0.96})}_{2.99}]^{+0.19}(Si_{2.80}Al_{1.20})O_{10}(OH,F)_2]^{-1.20}K(Na,Ca/2)^{+1.03}_{0.97}$$

$$[\underbrace{(Al_{1.16}Ti_{0.07}Fe^{+3}_{0.61}Mg_{0.02}Mn^{+2}_{0.02}Li_{0.94})}_{2.76}]^{-0.18}(Si_{2.20}Al_{0.80})O_{10}(OH,F)_2]^{-0.80}K(Na,Ca/2)^{+1.09}_{0.96}$$

The Li_2O content in the micas represented by these formulas is almost the same, 3.39 and 3.40, respectively. But the SiO^2 content of analysis 22 is only 39.04 percent, as compared with 46.37 percent in 23. In 22, octahedral occupancy is complete. Univalent Li compensates for 0.98 of the additional 1.19 positive charges carried by Al, Fe^{+3}, and Ti^{+4}; the remainder form a positive charge (+0.19) on the octahedral layer that is neutralized by an equivalent increase, above 1.00, in the negative tetrahedral charge. In 23, only 2.76 octahedral sites are occupied. Univalent Li compensates for 0.94 of the 1.24 additional positive charges carried by Al and Ti; the rest are neutralized by negative charges associated with unoccupied octahedral sites. However, the 0.24 unoccupied sites make 0.48 such negative charges available, and as only 0.30 are need to neutralize the uncompensated additional positive charges, the octahedral layer is left with a negative charge of −0.18. In order that the unit layer charge be close to −1.00, the negative tetrahedral charge must be less than 1.00 by the same amount. Because, therefore, of the different ways in which the additional positive charges carried by trivalent cations are accommodated in the structure in such trioctahedral micas as the ferrous lithium micas, there is considerable variation in Si content, even in those in which the Li_2O content is the same. However, despite such differences in SiO_2 content, the upward trend of the points in figure 36 suggests that increase in Li content is accompanied by increase in Si content, although the angle of trend of increase is less than the angle of trend of decrease in Fe^{+3} content.

HYPOTHETICAL FE+2-LI REPLACEMENT RATIOS

If Li replaces Fe^{+2} in the ratio of 2:1, the number of positive charges carried by octahedral cations is not changed, and, consequently, the octahedral and tetrahedral charges and Si are unchanged, but the octahedral occupancy is increased by one-half the number of Li cations added. This is illustrated in the following formulas, in which 1.00 Li is substituted for 0.50 Fe^{+2} in the formula for analysis 4, table 7.

$$[\underbrace{(Al_{0.44}Ti_{0.09}Fe^{+3}_{0.49}Fe^{+2}_{1.38}Mg_{0.03}Mn^{+2}_{0.06}Li_{0.18})}_{2.64}]^{+0.24}(Si_{2.81}Al_{1.19})O_{10}(OH,F)_2]^{-1.19}K(Na,Ca/2)^{+0.95}_{0.57},$$

$$[\underbrace{(Al_{0.44}Ti_{0.09}Fe^{+3}_{0.49}Fe^{+2}_{0.88}Mg_{0.03}Mn^{+2}_{0.06}Li_{1.18})}_{3.14}]^{+0.24}(Si_{2.81}Al_{1.19})O_{10}(OH,F)_2]^{-1.19}K(Na,Ca/2)^{+0.96}_{0.57}.$$

The octahedral-tetrahedral charge relation and the Si are the same in the second formula as in the first, but octahedral occupancy is increased by 0.5 and is greater than 3.00.

If, on the other hand, Li replaces Fe^{+2} ion for ion in the formula for 4, above,

$$\frac{[(Al_{0.44}Ti_{0.09}Fe^{+3}_{0.49}Fe^{+2}_{0.33}Mg_{0.03}Mn^{+2}_{0.06}Li_{1.18})^{-0.76}}{2.64}(Si_{3.81}Al_{0.19})^{-0.19}O_{10}(OH,F)_2]^{-0.95}K(Na,Ca/2)^{+0.96}_{0.87},$$

the octahedral occupancy remains the same, but the layer-charge relation is greatly altered, and there is an increase in Si equivalent to the increase in Li and the decrease in Fe^{+2}. The increase in Si, equivalent to the increase in Li and to the decrease in Fe^{+2}, is greater than indicated by the comparative angles of trend of the points in figures 35 and 36, which indicate that the general increase in Si is generally less than the decrease in Fe^{+2}. The negative octahedral charge is considerably greater, and the negative tetrahedral charge is considerably less, than in any of the calculated formulas of ferrous lithium micas.

Neither of these types of replacement of Fe^{+2} by Li, therefore, correlates well with the characteristics of the ferrous lithium formulas nor with the degree of Si-increase, Fe^{+2}-decrease relation suggested in figures 35 and 36. Substitution of Li for Fe^{+2} in the 2:1 ratio results in no change in Si content; substitution of Li for Fe^{+2} in the 1:1 ratio results in a greater increase in Si than indicated by figure 36. This suggests that the replacement ratio lies between 2:1 and 1:1. In the formula below, a replacement ratio of 2:1.5 (1 Li for 0.75 Fe^{+2}) in the formula for analysis 4, table 7, is assumed.

$$\frac{[(Al_{0.44}Ti_{0.09}Fe^{+3}_{0.49}Fe^{+2}_{0.18}Mg_{0.03}Mn^{+2}_{0.06}Li_{1.18})^{-0.26}}{2.99}(Si_{3.81}Al_{0.19})^{-0.69}O_{10}(OH,F)_2]^{-0.95}K(Na,Ca/2)^{+0.96}_{0.87}.$$

In this formula, the increase in Si (+0.5) is equivalent to one-half the increase in Li content (+1.0) and to two-thirds the decrease in Fe^{+2} content (0.75). This relation between Li and Si is about that suggested by the trend of the points in figure 36, and the relation between Si increase and Fe^{+3} decrease is comparable to the relative trend of points in figures 35 and 36. The octahedral-tetrahedral charge relation in this formula and the octahedral occupancy are also comparable with those found in the calculated formula for ferrous lithium micas (the data for writing these calculated formulas are included in table 7). The replacement ratio probably varies considerably, possibly as much as from 2:1 to 1:1 Li for Fe^{+2} in certain specimens of ferrous lithium micas, but a replacement ratio of about 2:1.5 Li for Fe^{+2} best explains in general the amount of decrease in Fe^{+2}, the amount of increase in Si, the octahedral occupancy, and the octahedral-tetrahedral charge relations found in calculated formulas of ferrous lithium micas.

The changes in composition that take place in replacement of Fe^{+2} by Li in this ratio can be expressed briefly as $4nLi+2nSi=3nFe^{+2}+2n$ tetrahedral Al. Octahedral trivalent cations, Al and Fe^{+3}, are not involved in the replacement, as is indicated in figure 34.

SIDEROPHYLLITE-LEPIDOLITE ISOMORPHOUS SERIES

The relation between Li, $R^{+2}(Fe^{+2},Mn^{+2},Mg)$, and octahedral $R^{+3}(Al,Fe^{+3})+Ti^{+4}$ in siderophyllites and aluminian lepidomelanes and ferrous lithium micas is shown in figure 37, in which the percentages of occupied octahedral sites occupied by Li, $R^{+2}(Fe^{+2},Mn^{+2},Mg)$, and octahedral $R^{+3}(Al,Fe^{+3})+Ti^{+4}$ in each of the calculated formulas used in this study are plotted on a triangular diagram. The points representing siderophyllites and aluminian lepidomelanes occupy an area at the base of the triangle just to the right of the center. Only one point, representing a siderophyllite in which no Li_2O was reported, falls on the baseline. The other five points, which represent siderophyllites and lepidomelanes which contain small amounts of Li_2O, fall a little above the baseline. The points representing the the ferrous lithium micas fall in a band trending diagonally upward from the area occupied by siderophyllites and aluminian lepidomelanes toward the point representing polylithionite. Calculated formulas representing progressive stages of replacement of ferrous iron by Al in the siderophyllite-lepidolite isomorphous series are given in table 4 and are represented graphically in histograms in figure 38. Both the formulas and histograms illustrate the progressive changes in composition that take place with increase in Li content, particularly decrease in Fe^{+2} content and increase in Si content.

The slight hiatus between points (fig. 37)representing siderophyllites and aluminian lepidomelanes and those representing ferrous lithium micas serves to differentiate the former and protolithionite, but differentiation between protolithionites and zinnwaldites must be on an arbitrary basis, as there is no hiatus between points representing these varietics.

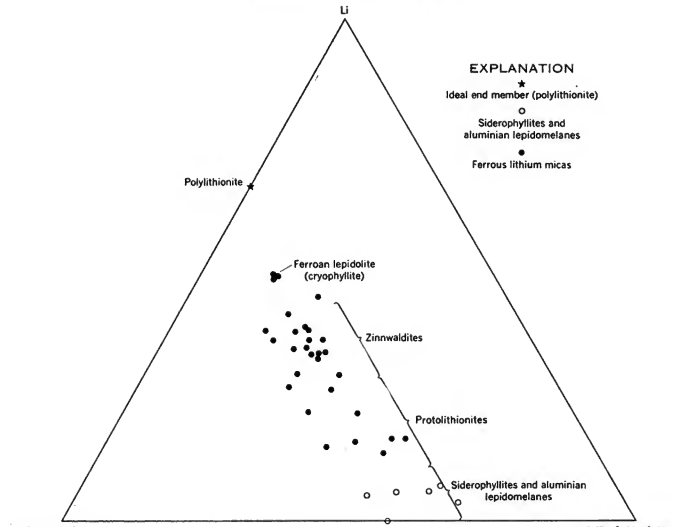

FIGURE 37.—Relation between Li, $R^{+3}(Fe^{+3},Mn^{+3},Mg)$, and octahedral $R^{+3}(Al,Fe^{+3})+Ti^{+4}$ in siderophyllites and ferrous lithium micas.

TABLE 4.—*Selected formulas representing steps in the siderophyllite-lepidolite series*

Number in table 7	*Formula*	*Li_2O (percent)*
3	$[(\underbrace{Al_{0.52}Ti_{0.01}Fe^{+3}_{0.62}Fe^{+2}_{1.22}Mg_{0.09}Mn^{+2}_{0.02}Li_{0.13}}_{2.61})(Si_{2.68}Al_{1.32})_{O_{10}(OH,F)_2}]^{-1.07}\ K(Na,Ca/2)^{+1.06}_{0.99}$ (+0.25, −1.32)	0.39
9	$[(\underbrace{Al_{1.06}Ti_{0.03}Fe^{+3}_{1.12}Mg_{0.01}Mn^{+2}_{0.04}Li_{0.42}}_{2.68})(Si_{2.76}Al_{1.24})_{O_{10}(OH,F)_2}]^{-1.13}\ K(Na,Ca/2)^{+1.15}_{1.04}$ (+0.06, −1.24)	1.44
15	$[(\underbrace{Al_{1.04}Fe^{+3}_{0.05}Fe^{+2}_{0.87}Mg_{0.06}Li_{0.71}}_{2.73})(Si_{3.07}Al_{0.93})_{O_{10}(OH,F)_2}]^{-1.09}\ K(Na)^{+1.08}_{1.08}$ (−0.16, −0.93)	2.42
18	$[(\underbrace{Al_{1.08}Fe^{+3}_{0.04}Fe^{+2}_{0.68}Mn^{+2}_{0.10}Li_{0.92}}_{2.82})(Si_{3.21}Al_{0.79})_{O_{10}(OH,F)_2}]^{-0.95}\ K(Na)^{+0.94}_{0.94}$ (−0.16, −0.79)	3.28
31	$[(\underbrace{Al_{1.11}Fe^{+3}_{0.01}Fe^{+2}_{0.42}Mn^{+2}_{0.12}Li_{1.16}}_{2.82})(Si_{3.35}Al_{0.65})_{O_{10}(OH,F)_2}]^{-1.05}\ K(Na)^{+1.07}_{1.07}$ (−0.40, −0.65)	4.18
35	$[(\underbrace{Al_{0.90}Fe^{+3}_{0.31}Fe^{+2}_{0.34}Mn_{0.02}Li_{1.28}}_{2.85})(Si_{3.56}Al_{0.43})_{O_{10}(OH,F)_2}]^{-0.99}\ K(Na)^{+1.00}_{1.00}$ (−0.57, −0.42)	4.99

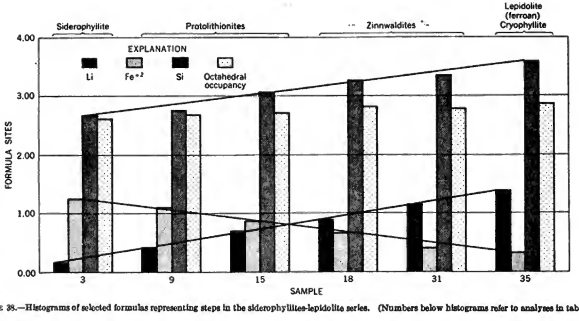

FIGURE 38.—Histograms of selected formulas representing steps in the siderophyllites-lepidolite series. (Numbers below histograms refer to analyses in table 7.)

SIDEROPHYLLITES AND LEPIDOMELANES

Siderophyllites and lepidomelanes are the high-Fe^{+2}, low-Mg members of the trioctahedral Mg replacement system of which phlogopite, $Mg_{3.0}(Si_{3.0}Al_{1.0})O_{10}(OH,F)_2K_{1.0}$, is the high-Mg, low-$Fe^{+2}$ member (Foster, 1960, p. 24). Heretofore it has been assumed that the high-Fe^{+2} end member of a Mg-Fe^{+2} replacement series is annite, $Fe^{+2}_{3.0}(Si_{3.0}Al_{1.0})O_{10}(OH,F)_2K_{1.0}$, the Fe^{+2} analog of phlogopite, but a study of analyses of natural trioctahedral micas showed that no natural representative of such a mica has been recorded in the literature, that replacement of Mg by Fe^{+2} is also always accompanied by more or less replacement by Al and Fe^{+3}, and, consequently, that the low-Mg, high-Fe^{+2} end of the system is represented not by annite but by siderophyllite, in which the principal octahedral trivalent cation is dominantly Al, and lepidomelane, in which it is Fe^{+3}. High-Fe^{+2}, low-Mg trioctahedral micas that contain both octahedral Al and Fe^{+3} are termed ferrian siderophyllites, or aluminian lepidomelanes, depending on whether octahedral Al or Fe^{+3} is dominant. In some formulas the amounts of octahedral Al and of Fe^{+3} present are about equal.

In most of the formulas calculated from analyses of ferrous lithium micas, Al is the predominent trivalent octahedral cation, although in a few formulas Fe^{+3} is equal to, or slightly greater than, the octahedral Al. However, in none is Fe^{3} greatly dominant over tri-octahedral Al. This suggests that the siderophyllites, ferrian siderophyllites, and aluminian lepidomelanes are prototypes of these minerals, but not lepidomelanes, in which Fe^{+3} is greatly predominant.

The available calculated formulas of these prototypes vary considerably in content of Fe^{+2}, Fe^{+3}, and octahedral Al. In the analyses at hand, Fe^{+2} ranges from 1.22 to 1.88 occupied sites and averages 1.50, Fe^{+3} ranges from 0.05 to 0.62 and averages 0.36, and octahedral Al ranges from 0.44 to 0.99 and averages 0.57. Total trivalent octahedral cations (R^{+3}) range from 0.81 to 1.14 occupied octahedral sites and average 0.93. The reciprocal extremes in R^{+3} and Fe^{+2} content are illustrated in the following formulas for analyses 2 and 3, table 7,

$$[(\underbrace{Al_{0.72}Fe^{+3}_{0.08}Fe^{+2}_{1.58}Mg_{0.01}Mn^{+2}_{0.02}Li_{0.10}}_{2.82})(Si_{2.62}Al_{1.38})O_{10}(OH,F)_2]^{-1.00}K(Na,Ca/2)^{+0.99}_{0.98},$$

$$[(\underbrace{Al_{0.52}Ti_{0.01}Fe^{+3}_{0.62}Fe^{+2}_{1.22}Mg_{0.09}Mn^{+2}_{0.02}Li_{0.13}}_{2.81})(Si_{2.68}Al_{1.32})O_{10}(OH,F)_2]^{-1.07}K(Na,Ca/2)^{+1.08}_{0.99}.$$

The first formula, calculated from analysis 2, table 7, has the highest Fe^{+2} content and the lowest octahedral-R^{+3} content of the available analysis of siderophyllites and aluminian lepidomelanes; the second formula, calculated from analysis 3, table 7, has the lowest Fe^{+2} and the highest octahedral R^{+3}. Thus siderophyllite, the prototype of the ferrous lithium micas, varies greatly in Fe^{+2}, Fe^{+3}, and Al content, just as ferrous lithium micas that contain about equal amounts of Li may vary widely in these constituents.

In all but one of the analyses of siderophyllite the presence of a small amount of Li is reported.

PROTOLITHIONITES

Kunitz (1924, p. 409) considered protolithionite the lithium-free member of a ferrous lithium mica series of which lepidolite was the high-Li end member, with a formula, $KH_2AlFe_3^{+2}Si_3O_{12}$, that is identical with Winchell's formula for annite. At this time Winchell (1927, p. 274) also considered protolithionite Li free, but heptaphyllic (or dioctahedral), with the formula $H_4K_2Fe_3^{+2}Al_4Si_5O_{22}$. Later Winchell (1942, p. 117) recognized it as octaphyllic (or trioctahedral) and used is as an end member, representing the maximum tenor of bivalent cations together with a minimum tenor of Li, in interpreting the composition of lepidolites. In the formula which he then assigned to protolithionite, $K_2LiFe_4^{+2}Al_3Si_6O_{20}F_4$, Li occupies 1 unit-cell formula site. Hey (1955, p. 208) observes that Li occupies between 1 and 2 sites in the unit-cell formula.

Perhaps because of these considerable differences in the Li content in published formulas for protolithionite, published analyses for materials called protolithionite also vary considerably in Li content. No analyses purported to be those of protolithionite were discovered in which no Li_2O was reported, but one published as that of a protolithionite contained only 0.32 percent of Li_2O ($\lessgtr$0.10 octahedral site in the half-cell formula), and another contained only 0.39 percent of Li_2O. On the other hand, another analysis reporting 4.57 percent of Li_2O ($\lessgtr$1.30 octahedral sites in the half-cell formula) was also called that of a protolithionite. The literature indicates, therefore, a state of considerable confusion as to the Li_2O content of protolithionite.

In the present study the Li content of protolithionite is defined as 0.5 ± 0.25 octahedral sites in the half-cell formula, or 1.00 ± 0.50 sites in the unit-cell formula. This Li content is based on the Li content in the formula used by Winchell in 1942 and on Hey's statement as to the Li content of protolithionite. A range is given for Li because these micas are interpreted as belonging to an isomorphous series, the members of which contain varying amounts of Li. This is the range bracketed opposite protolithionite in figure 37. The permissible site occupancy given is equivalent to a range of from about 0.75 to about 2.50 percent in Li_2O content. Ferrous lithium micas containing a little Li_2O but less than 0.75 percent, like those represented by points near the baseline in figure 37, are considered lithian siderophyllites, or lepidomelanes, depending on the Al and Fe^{+3} content. Those containing more than 2.50 percent of Li_2O are considered zinnwaldites or ferroan lepidolites.

In the protolithionite analyses 7–15, table 7, Li varies from 1.19 to 2.42 percent Li_2O, equivalent to a variation in octahedral sites of from 0.37 to 0.71 in the half-cell formula. FeO, as in the siderophyllites, is quite variable, ranging from 10.20 to 21.97 percent (0.61 to 1.44 octahedral sites in the half-cell formula). The octahedral content of trivalent cations, Al and Fe^{+3}, with Al usually dominant, is considerably more constant, varying only between 0.91 and 1.21 octahedral sites. These ranges in content of the principal octahedral cations can be expressed as follows:

$$(R^{+3}_{1.10\pm0.20}, Fe^{+2}_{1.00\pm0.40}, Li_{0.50\pm0.25}).$$

Winchell assumes full octahedral occupancy in the formula for protolithionite that he used in 1942 in his interpretation of the composition of lepidolites. In this formula, recast in the half-cell notation used herein,

$$[\underbrace{(\overset{0.00}{Al_{0.5}Fe^{+2}_{2.0}Li_{0.5}})}_{3.00}(\overset{-1.00}{Si_{3.0}Al_{1.0}})O_{10}(OH)_2]^{-1.00}\,K^{+1.00}_{1.00},$$

the excess in positive charges carried by Al (as compared with the number of positive charges carried by bivalent cations) is exactly compensated by the deficiency in positive charges carried by Li, and the octahedral layer is neutral. All the charge on the unit composite layer is on the tetrahedral layers owing to the substitution of Al for one Si cation. However, in all the formulas calculated from analyses of natural protolithionites, the octahedral trivalent cations, Al and Fe^{+3}, with usually a little Ti, are considerably in excess of Li, so that there are extra positive octahedral charges to be accommodated in the structure. In most of the calculated formulas the greater part of the additional positive charges are neutralized by negative charges associated with unoccupied octahedral sites, and there is only a slight positive charge on the octahedral layer to be neutralized by an equivalent negative charge in excess of 1.00 on the tetrahedral layers. In these formulas, octahedral occupancy ranges between 2.63 and 2.88, and Si is less than 3.00, and ranges between 2.72 and 2.95. However, in three of the calculated formulas for protolithionites the octahedral layer has a negative charge, and Si is greater than 3.00. Exclusive of one formula in which Si is exceptionally high (3.43 tetrahedral sites), the range in the number of tetrahedral sites occupied by Si in the calculated formulas for protolithionite is from 2.72 to 3.17, approximately 2.95 ± 0.25.

The number of octahedral sites occupied by Fe^{+2} in the formulas calculated from analyses of protolithionite, as here defined, is generally higher than that specified by Hey (1955, p. 208). Hey's value for Fe^{+2}, 0.75 sites in terms of the half-cell formula, corresponds with

only the lower part of the range for Fe^{+2} found in the calculated formulas, 0.60 to 1.40. On the other hand, Hey's value for Si, 2.75 to 3.00 in terms of a half-cell formula, agrees fairly well with the Si content of the calculated formulas, 2.70 to 3.20. Hey indicates that protolithionites contain little Fe^{+2}, but more than half of the analyses had more than 2.5 percent of Fe_2O_3 and one had as much as 7.81 percent of Fe_2O_3.

ZINNWALDITES

Zinnwaldite was considered an intermediate member of the lepidolite-protolithionite system by Kunitz (1924, p. 409), Winchell (1927, p. 274), and Hallimond (1925, p. 311), and was not assigned a definite formula. Hey (1955, p. 208) gives the formula 2 $[K_2(Li,Fe,^{+2}Al)_5(Si,Al)_8O_{20}(F,OH)_4]$ for zinnwaldite, with the observation that there is often considerable deficiency in the (Li,Fe^{+2},Al) group, and that typically $Li \approx 2$, $Fe^{+2} \approx 1\frac{1}{2}$, and $Si \approx 6\frac{1}{2}$. On the basis of the Li content in this formula, the Li content of zinnwaldite is herein defined as 1.0 ± 0.25 octahedral sites in the half-cell formula, or 2.00 ± 0.50 octahedral sites in the unit-cell formula. Again a range is given because these micas, as members of an isomorphous series, contain varying amounts of Li, as well as of the other constituents. This is the range bracketed opposite zinnwaldite in figure 37. The defined range in octahedral-site occupancy is equivalent to a Li_2O content of from about 2.50 to about 4.50 percent.

In the zinnwaldite analyses 16–31, table 7, Li_2O varies from 2.62 to 4.18 percent, equivalent to octahedral-site occupancies of 0.80 to 1.16 in the half-cell formulas. FeO is generally lower than in the protolithionites and not quite so variable, ranging from 6.35 to 12.22 percent (0.37 to 0.79 octahedral sites in the half-cell formulas). In general, the contents of Li_2O and FeO in these analyses bear a reciprocal relation to each other: the lower contents of Li_2O are associated with the higher contents of FeO, and vice versa. The octahedral content of the trivalent cations Al and Fe^{+3} in the half-cell formulas for zinnwaldites is quite constant, varying only between an occupancy of 1.07 and 1.26 sites, with no apparent relation between octahedral R^{+3} and Li content. In most of the analyses of zinnwaldite the amount of Fe_2O_3 present is very small, and octahedral Al is the greatly dominant R^{+3} cation in the formulas calculated from these analyses, but several analyses contain significant amounts of Fe_2O_3, and in the formulas calculated from these analyses Fe^{+3} may occupy about as many or even more octahedral sites than Al. The ranges in octahedral content of the principal cations in half-cell formulas for zinnwaldites are summarized in the following expression:

$$(R^{+3}_{1.15\pm0.10}, Fe^{+2}_{0.55\pm0.20}, Li_{1.00\pm.25}).$$

Octahedral occupancy in the zinnwaldites is generally between 2.75 and 3.00. Only 1 calculated formula for a zinnwaldite (21, table 7) had an octahedral occupancy significantly lower than 2.75. This formula has an octahedral occupancy of only 2.62. In most of the calculated formulas the octahedral charge is negative. Consequently, Si in these formulas is generally in excess of 3.00 and ranges from 3.03 to 3.46. However, in 3 calculated formulas (17, 22, and 25, table 7) the octahedral group had a positive charge, and Si was less than 3.00—2.82, 2.80, and 2.95. Thus the range in the number of tetrahedral sites occupied by Si in the calculated formulas for zinnwaldites is quite wide, 2.80–3.46, or 3.15 ± 0.35.

The amounts of Fe^{+2} and Si in the calculated formulas herein defined as those of zinnwaldite differ somewhat from the amounts indicated by Hey (1955, p. 208) as present in zinnwaldite. Hey's value for Fe^{+2}, about $1\frac{1}{2}$ sites in the unit-cell formula, represents the high end of the range of Fe^{+2} present in the calculated formulas. The median value for Fe^{+2} present, in terms of the unit-cell formula, is much closer to 1.00 (1.10) than to 1.5 octahedral sites. Hey's value for Si, about $6\frac{1}{2}$ sites in the unit-cell formula, is somewhat higher than the median and average value for Si found in the calculated formulas, which is 6.3. Hey's formula for zinnwaldite includes no Fe^{+3}, although his formulas for protolithionite and cryophyllite both include Fe^{+3}. As pointed out above, some of the calculated formulas containing the amounts of Li to be found in zinnwaldite, as defined by Hey, contain appreciable amounts of Fe^{+3}.

FERROAN LEPIDOLITE (CRYOPHYLLITE)

The name cryophyllite was given by Cooke (1867, p. 217) to a micaceous mineral found in the granite ledges that form the extremity of Cape Ann, Mass. Cooke's analyses of two types of this material showed them to have virtually the same chemical composition. Later, in 1886, three different types of cryophyllite from Cape Ann were analyzed by R. B. Riggs (Clarke, 1886, p. 358). These three types were also virtually identical in chemical composition and were similar to those analyzed by Cooke, except that Riggs obtained somewhat higher values for Li_2O—4.81, 4.87, and 4.99 percent, compared with Cooke's 4.05 and 4.06 percent. No other occurrence of a ferrous lithium mica having a comparable Li_2O content has been reported in the literature. On the basis of these analyses, particularly those of Riggs, cryophyllite has been considered a variety of zinnwaldite (Dana, 1892, p. 626, and Hey, 1955, p. 208) with a somewhat higher Li and lower Fe^{+}_{2} content. The relation between cryophyllite and zinnwaldites is shown in figure 37.

The formula calculated from the average of Riggs' 3 analyses (33, 34, and 35, table 7),

$$[(\underbrace{Al_{0.92}Fe^{+3}_{0.16}Fe^{+2}_{0.38}Mg_{0.02}Li_{1.36}}_{2.84})^{-0.60}(Si_{3.58}Al_{0.42})^{-0.42}O_{10}(F,OH)_2]^{-1.02}K(Na)^{+1.05}_{1.05},$$

has a Li content similar to that of Stevens' sample 7 (34, table 6), a 6-layer lepidolite,

$$[(\underbrace{Al_{1.29}Fe^{+2}_{0.01}Mn^{+2}_{0.16}Li_{1.38}}_{2.84})^{-0.41}(Si_{3.38}Al_{0.62})^{-0.62}O_{10}(F,OH)_2]^{-1.03}K(Na,Rb,Cs)^{+1.03}_{1.03},$$

and does not greatly exceed Stevens' sample 10 (42, table 6), a 1-layer lepidolite,

$$[(\underbrace{Al_{1.10}Ti_{0.01}Fe^{+3}_{0.02}Fe^{+2}_{0.15}Mn^{+2}_{0.15}Li_{1.50}}_{2.93})^{-0.50}(Si_{3.48}Al_{0.52})^{-0.52}O_{10}(F,OH)_2]^{-1.02}K(Na,Rb,Cs)^{+0.99}_{0.99},$$

in content of R^{+2} cations. In the formula for cryophyllite, R^{+2} is made up almost entirely of Fe^{+2}; in the formula for Stevens' sample 10, R^{+2} is made up equally of Fe^{+2} and Mn^{+2}. These two formulas also have about the same ocatahedral-R^{+3} content, although in the cryophyllite formula Fe^{+3} occupies 0.16 octahedral sites and in Stevens' sample 10 only 0.03 octahedral sites. Thus Li_2O content and the relation between Li, Fe^{+2}(Mg, Mn^{+2}), and R^{+3}(Al, Fe^{+3}) in the material called cryophyllite are comparable with that in some lepidolites. It is, therefore, recommended that the material known as cryophyllite be considered a ferroan variety of lepidolite, and that the name cryophyllite be discarded.

RELATION BETWEEN ALUMINUM LITHIUM MICAS AND FERROUS LITHIUM MICAS

The relation between the aluminum lithium micas and the ferrous lithium micas is illustrated in figure 39 (which combines fig. 33), which shows the Li, R^{+2}(Fe^{+2}, Mn^{+2}, Mg), and octahedral R^{+3}(Al, Fe^{+3})+Ti^{+4} relation in aluminum lithium micas, and figure 37, which shows the same relation in ferrous lithium micas. Lepidolites are aluminum lithium micas and, as such, were discussed with other aluminum lithium micas, and their composition was interpreted as if derived from muscovite by replacement of octahedral Al by Li. However, figure 39 shows that complete, or almost complete, replacement of Fe^{+2} in siderophyllite also produces lepidolites. Thus the lepidolite composition can be interpreted as the result of two different series of replacements.

The following equations show the general course of evolution of lepidolite from muscovite and from siderophyllite, using the average Li-(octahedral Al) and Li-Fe^{+2} replacement ratios found in the natural micas:

Muscovite to lepidolite

Muscovite $[Al^{0.00}_{2.00}(Si_{3.00}Al^{-1.00}_{1.00})O_{10}(OH)_2]^{-1.00}\ K^{+1.00}_{1.00}$

Lithian muscovite $[(\underbrace{Al_{1.80}Li_{0.50}}_{2.30})^{-0.10}(Si_{3.10}Al^{-0.90}_{0.90})O_{10}(OH,F)_2]^{-1.00}\ K^{+1.00}_{1.00}$

Mixed structures

Lepidolite $[(\underbrace{Al_{1.40}Li_{1.50}}_{2.90})^{-0.30}(Si_{3.30}Al^{-0.70}_{0.70})O_{10}(F,OH)_2]^{-1.00}K^{+1.00}_{1.00}$

Siderophyllite to lepidolite

Siderophyllite $[(\underbrace{R^{+3}_{1.05}Fe^{+2}_{1.50}}_{2.55})^{+0.15}(Si_{2.85}Al^{-1.15}_{1.15})O_{10}(OH)_2]^{-1.00}\ K^{+1.00}_{1.00}$

Protolithionite $[(\underbrace{R^{+3}_{1.05}Fe^{+2}_{1.12}Li_{0.50}}_{2.67})^{-0.19}(Si_{3.19}Al^{-0.81}_{0.81})O_{10}(OH,F)_2]^{-1.00}\ K^{+1.00}_{1.00}$

Zinnwaldite $[(\underbrace{R^{+3}_{1.05}Fe^{+2}_{0.75}Li_{1.00}}_{2.80})^{-0.35}(Si_{3.35}Al^{-0.65}_{0.65})O_{10}(OH,F)_2]^{-1.00}\ K^{+1.00}_{1.00}$

Lepidolite (ferroan) $[(\underbrace{R^{+3}_{1.05}Fe^{+2}_{0.37}Li_{1.50}}_{2.92})^{-0.61}(Si_{3.61}Al^{-0.39}_{0.39})O_{10}(F,OH)_2]^{-1.00}\ K^{+1.00}_{1.00}$

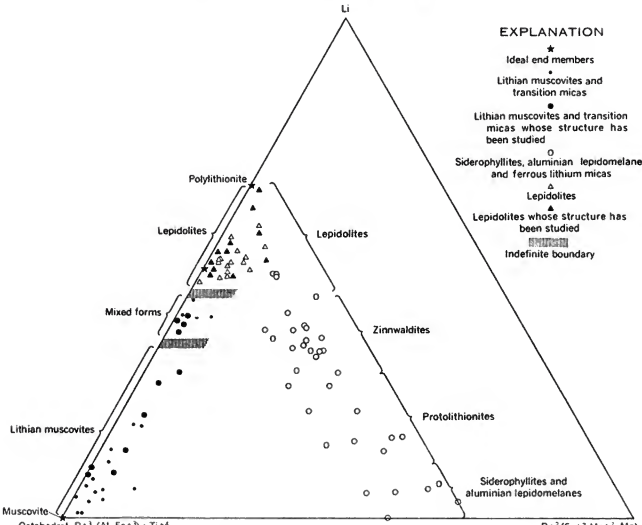

FIGURE 39.—Relation between Li, R^{+2} (Fe^{+2}, Mn^{+2}, Mg), and octahedral R^{+3}(Al, Fe^{+3})+Ti^{+4}, in lithium micas.

Replacement of octahedral Al in muscovite by Li in the ratio of 2 Li for 1 octahedral Al leads to polylithionite,

$$[\underbrace{(\overset{-1.00}{Al_{1.00}}\overset{0.00}{Li_{2.00}})}_{3.00}Si_{4.00}O_{10}F_2]^{-1.00}\ K^{+1.00}_{1.00},$$

as the high-Li end of the series, but in the natural aluminum lithium micas studied the replacement ratio varied between 2 and 3 Li for 1 octahedral Al. In the series above, therefore, the replacement ratio used is 2.5 Li for 1.0 octahedral Al. At this replacement ratio the greatest number of octahedral sites that Li can occupy is 1.68, with Al occupying 1.33 sites. Among the formulas for lepidolite, only 2 (57 and 58, table 6) had a higher Li occupancy, 1.84 and 1.93 sites, respectively. In these 2 formulas the Li-(octahedral Al) replacement ratio is 2.0, and they are close to polylithionite. Aside from these 2 formulas, the lepidolite formula having the highest Li occupancy is 56, table 6, in which Li occupies 1.68 sites and Al(+Mn^{+2}) occupies 1.30 sites, and the Li-(octahedral Al) replacement ratio is 2.4. This formula, therefore, is almost identical with that of the high-Li end of the series shown above, in which the Li-(octahedral Al) replacement ratio is 2.5.

The series of formulas shown for the evolution of lepidolite from siderophyllite is based on the averages of the formulas at hand for siderophyllite, protolithionite, and zinnwaldite. The generalized formulas for these averages show an average replacement ratio of 2.0 Li for 1.5 Fe^{+2}. Extension of this series of formulas at the same replacement ratio to the highest Li occupancy produces a formula,

$$[\underbrace{(\overset{+3}{R}_{1.68}\overset{+2}{Fe}_{0.11}\overset{-0.78}{Li_{1.185}})}_{3.01}\overset{-0.22}{(Si_{3.78}Al_{0.22})}O_{10}(F,OH)_2]^{-1.00}\ K^{+1.00}_{1.00},$$

which is cloee to polylithionite and very like the formula for 57, table 6,

$$\underset{2.96}{[(Al_{1.08}\overset{-0.57}{R^{+3}_{0.07}}Li_{1.84})}(Si_{3.83}\overset{-0.17}{Al_{0.17}})O_{10}(F,OH)_2]^{-1.00}K(Na,Rb,Cs)^{+1.00}_{1.00}$$

These two series of formulas, one starting with muscovite, the other with siderophyllite, produce formulas for lepidolite that have the same Li occupancy but which differ considerably in octahedral-R^{+3} occupancy. They also differ in Fe^{+2} content, but this is not so significant as the difference in octahedral-R^{+3} content, because the ferrous lithium micas themselves differ considerably in Fe^{+2} content and could produce a lepidolite containing little or no Fe^{+2}. On the other hand, the octahedral-R^{+3} content in the lepidolite formulae and the range of octahedral-R^{+3} occupancy found in ferrous lithium micas may serve to suggest the source of certain lepidolites.

In some of the calculated formulas of lepidolites in which Li occupies fewer than 1.60 sites, octahedral Al is higher than that found in any of the calculated formulas for siderophyllite, protolithionite, or zinnwaldite. Such lepidolites may be interpreted as derivations of muscovite. In other lepidolite formulas having fewer than 1.60 sites occupied by Li, octahedral Al occupancy ie comparable with that in calculated formulas for siderophyllites and ferrous lithium micas in which octahedral R^{+3} is made up almost entirely of Al. Such lepidolites can be interpreted as possibly derived from siderophyllite. The very low Fe^{+3} content of these lepidolites indicates, however, a highly aluminian siderophyllite as the possible source. None could have been derived from eiderophyllite containing significant amounts of Fe^{+3}, or from aluminian lepidomelane, as can some of the protolithionites and zinnwaldites.

In the two lepidolite formulas in which Li occupancy ie greater than 1.70 sites (57 and 58, table 6), the lepidolites they represent can be interpreted as having been derived either from muscovite, at a Li-(octahedral Al) replacement ratio of 2:1, or from eiderophyllite.

UNUSUAL LITHIUM MICAS

Four analysee of lithium micas can not be interpreted as if derived by replacement from either muscovite or siderophyllite. One of these ie the analysis of the rare mica, taeniolite, made by Stevens (Miser and Stevene, 1938, p. 106) from Magnet Cove, Ark. (1, table 5). The formula calculated from this analysis,

$$\underset{2.89}{[(Al_{0.08}Ti_{0.01}\overset{-0.96}{Fe^{+3}_{0.02}}\overset{+2}{Fe^{+2}_{0.01}}Mg_{1.92}Li_{0.81})}(Si_{3.97}\overset{-0.03}{Al_{0.03}})O_{10}(F,OH)_2]^{-1.01}(K_{0.90},Na_{0.08})^{+0.99}_{0.99},$$

resembles that of a phlogopite in which about 0.84 Mg had been replaced by 0.84 Li,

$$\underset{2.89}{[(Al_{0.08}Ti_{0.01}\overset{-0.10}{Fe^{+3}_{0.02}}\overset{+2}{Fe^{+2}_{0.01}}Mg_{2.77})}(Si_{3.13}\overset{-0.87}{Al_{0.87}})O_{10}(OH)_2]^{-0.97}(K_{0.90},Na_{0.08})^{+0.98}_{0.98}.$$

The deficiency in the amount of positive charge carried by the Li cations results in a negative charge on the octahedral layer, which necessitates an equivalent decrease in the negative charge on the tetrahedral layers. The eample ie very low in both octahedral and tetrahedral Al, and Si, which occupies almost all the tetrahedral sites, ie quite high. This specimen is very close to the ideal high-Li end member of a hypothetical phlogopite-taeniolite ceries,

$$[M_{3.00}(\overset{0.00}{Si_{3.00}}\overset{-1.00}{Al_{1.00}})O_{10}(OH)_2]^{-1.00}K^{+1.00}_{1.00}$$

$$\downarrow$$

$$\underset{3.00}{[(Mg_{2.50}\overset{-0.50}{Li_{0.50}})}(Si_{3.50}\overset{-0.50}{Al_{0.50}})O_{10}(OH)_2]^{-1.00}K^{+1.00}_{1.00}$$

$$\downarrow$$

$$\underset{3.00}{[(Mg_{2.00}\overset{-1.00}{Li_{1.00}})}Si_4O_{10}(OH)_2]^{-1.00}K^{+1.00}_{1.00}$$

This specimen has a 1-layer etructure (monoclinic hemihedral), as determined by Hendricks and Jefferson (1939, p. 758).

TABLE 5.—*Analyses of lithian micas that do not fit in the aluminum lithium or ferrous lithium series*

	1	2	3	4
SiO_2	58.82	42.02	35.81	36.97
TiO_2	.11	1.35	1.46	2.64
Al_2O_3	1.29	18.75	20.03	17.51
Fe_2O_3	.40	.66	.13	2.26
FeO	.24	8.29	21.83	14.81
MnO	----------	.27	1.19	.22
MgO	18.18	9.35	5.23	5.45
CaO	----------	.93	----------	None
Li_2O	3.10	1.20	.93	.65
NaO	.64	.73	.22	.46
K_2O	10.44	8.54	9.09	8.48
Rb_2O	----------	1.80	----------	1.46
Cs_2O	----------	.47	----------	1.12
H_2O-	.09	.15	1.87	.32
H_2O+	.59	2.44		2.48
F	8.56	4.34	.76	3.17
Total	102.46	101.85	99.27	101.01
(O = F)	-3.60	-1.83	-.32	-1.33
Total	99.86	99.72	98.95	99.68

1. Magnet Cove, Ark. (Miser and Stevens, 1938, p. 106). Associated with clay and novaculite.
2. Kings Mountain, N.C. (Hess and Stevens, 1937, p. 1044, analysis 1). From mica schist at contact with spodumene pegmatite.
3. Middletown, Conn. (Dana, 1892, p. 520, analysis 29).
4. Tin Mountain, S. Dak. (Hess and Stevens, 1937, p. 1044, analysis 2).

The formulas calculated from analyses 2, 3, and 4, table 5,

$$[(\underbrace{Al_{0.65}Ti_{0.07}Fe^{+3}_{0.04}Fe^{+2}_{0.50}}_{2.66}Mg_{1.03}Mn^{+2}_{0.02}Li_{0.35})(Si_{3.05}Al_{0.95})O_{10}(OH,F)_2]^{-1.15}K(Na,Rb,Cs,Ca/2)^{+1.14}_{1.06},$$

$$[(\underbrace{Al_{0.51}Ti_{0.08}Fe^{+3}_{0.01}Fe^{+2}_{1.39}}_{2.94}Mg_{0.59}Mn^{+2}_{0.08}Li_{0.28})(Si_{2.71}Al_{1.29})O_{10}(OH,F)_2]^{-1.01}K(Na)^{+1.02}_{1.02}, \text{ and}$$

$$[(\underbrace{Al_{0.39}Ti_{0.15}Fe^{+3}_{0.13}Fe^{+2}_{0.94}}_{2.78}Mg_{0.96}Mn^{+2}_{0.01}Li_{0.20})(Si_{2.82}Al_{1.18})O_{10}(OH,F)_2]^{-1.00}K(Na,Rb,Cs)^{+1.00}_{1.00},$$

respectively, resemble biotites in which some Fe^{+2}, or Mg, has been replaced by Li.

SUMMARY

The composition of most lithium micas can be interpreted as if derived from muscovite, by the replacement of octahedral Al by Li, or from siderophyllite, by the replacement of Fe^{+2} by Li. In the aluminum lithium micas Li replaces octahedral Al in ratios varying between 2 and 3 Li for 1 octahedral Al, with an average replacement ratio of about 2.5. Increasing Li content is, therefore, accompanied by increasing octahedral occupancy, from 2.00 in muscovite to about 3.00 in some lepidolites. Correlation of calculated formulas with the structural work of Hendricks and Jefferson and of Levinson indicates that a change in structure to the lepidolite structure takes place when the octahedral occupancy is about half way between 2.00 and 3.00 and Li occupancy is about 1.00 (equivalent to about 3.75 percent Li_2O). Because of the disparity between the amount of positive charge carried by the replacing Li cations and the replaced Al cations, increase in Li content is also accompanied by increase in the amount of negative charge on the octahedral layer and by decrease in tetrahedral Al and increase in Si, with consequent decrease in the negative charge on the tetrahedral layers. Thus the chemical characteristics of the aluminum lithium micas with increase in Li are: decrease in both octahedral Al and tetrahedral Al, increase in Si, and increase in octahedral occupancy. However, the aluminum lithium micas are not members of a continuous series; the series is broken at about the halfway point by the structural change necessitated by increase in octahedral occupancy.

Starting with siderophyllite (ferrian siderophyllite, or aluminian lepidomelane), the ferrous lithium micas form a series in which Li progressively replaces Fe^{+2} in an approximate ratio of 2.0 Li for 1.5 Fe^{+2}. Ferrous lithium micas in which Li occupies fewer than 0.25 octahedral sites are termed lithian siderophyllites, lithian ferrian siderophyllites, or lithian aluminian lepidomelanes, depending on the Fe^{+3} content; those in which Li occupies between 0.25 and 0.75 sites are defined as protolithionites; those in which Li occupies between 0.75 and 1.25 sites are defined as zinnwaldites; and those in which Li occupies more than 1.25 sites are considered lepidolites. Thus the high-lithium mica described by Cooke, and named cryophyllite, is considered a ferroan lepidolite. The greatest number of octahedral sites that can be occupied by Li, at the approximate Li-Fe^{+2} replacement ratio and at the average octahedral R^{+3} content found in these micas, is 1.85,

$$[(\underbrace{R^{+3}_{1.65}Fe^{+2}_{0.11}}_{3.01}Li_{1.85})(Si_{3.78}Al_{0.22})O_{10}(F,OH)_2]^{-1.00}K^{+1.00}_{1.00}.$$

In siderophyllites and protolithionites, R^{+3} may consist entirely of Al or may contain significant amounts of Fe^{+3}, but in most zinnwaldites R^{+3} is made up predominantly of Al. Fe^{+3} is low in all the lepidolites. In this series, as in the aluminum lithium mica series, increasing Li content is accompanied by increasing octahedral occupancy, but the increase is not as great, and the ferrous lithium micas are trioctahedral throughout, except perhaps for some siderophyllites and protolithionites in which octahedral occupancy is less than 2.50. Increase in octahedral negative charge and decrease in tetrahedral negative charge also accompany increase in Li content. Thus the compositional characteristics of the series are increase in Li content, decrease in Fe^{+2} content, decrease in octahedral Al content, and increase in Si content.

The two series join in lepidolite. Lepidolites derived from siderophyllite would be expected to be lower in octahedral and tetrahedral Al, for the same Li content, than lepidolites derived from muscovite; they would also be higher in Fe^{+2}, although not necessarily, as the ferrous lithium micas vary considerably in Fe^{+2} content. The ideal end member of both series is polylithionite,

$$[(\underbrace{Al_{1.00}Li_{2.00}}_{3.00})Si_{4.00}O_{10}F_2]^{-1.00}K^{+1.00}_{1.00}.$$

REFERENCES CITED

Berggren, Thelma, 1940, Minerals of the Varuträsk pegmatite, pt. 15—Analyses of mica minerals and their interpretation: Geol. Fören Stockholm Förh., v. 62, p. 182–193.

——— 1941, Minerals of the Varuträsk pegmatite, pt. 25—Some new analyses of lithium-bearing mica minerals: Geol. Fören. Stockholm Förh., v. 63, p. 262–278.

Buryanova, E. S., 1940, An account of the mineralogy of granite pegmatites from the Korosten plutone massif in Volhynia and of a study of their iron biotites: Mineralog. obshch., Leningrad, Zapiski, ser. 2, v. 69, p. 519–540.

Clarke, F. W., 1886, Researches on lithia micas, pt. 2—The iron-lithia micas of Cape Ann: Am. Jour. Sci., 3d ser., v. 32, p. 358–361.

——— 1910, Analyses of rocks and minerals from the laboratory of the U.S. Geological Survey, 1880–1908: U.S. Geol. Survey Bull. 419, 323 p.

Cooke, J. P., Jr., 1867, On cryophyllite, a new mineral species of the mica family, with some associated minerals in the granite of Rockport, Massachusetts: Am. Jour. Sci., 2d ser., v. 43, p. 217–230.

Dana, E. S., 1892, The system of mineralogy, 6th ed.: New York, John Wiley and Sons, 1104 p.

Duparc, Louis, Wunder, M., and Sabot, R., 1910, Les minéraux des pegmatites des environs d'Antsirabé a Madagascar: Mem. Soc. phys. et histoire nat. Genéve, v. 36, p. 363–410.

Foster, M. D., 1956, Correlation of dioctahedral potassium micas on the basis of their charge relations: U.S. Geol. Survey Bull. 1036–D, p. 57–67.

——— 1960, Interpretation of the composition of trioctahedral micas: U.S. Geol. Survey Prof. Paper 354–B.

Ginzburg, A. I., and Berkhin, S. I., 1953, On the composition and chemical constitution of the lithium micas: Mineralog. Muzeya. Akad. Nauk U.S.S.R. Trudy, v. 5, p. 90–131.

Hallimond, A. F., 1925, On the chemical classification of the mica group, 1. The acid micas: Mineralog. Mag., v. 20, p. 305–318.

Heinrich, E. W., and Levinson, A. A., 1953, Studies in the mica group; Mineralogy of the rose muscovites: Am. Mineralogist v. 38, p. 25–49.

Hendricks, S. B., and Jefferson, M. E., 1939, Polymorphism of the micas: Am. Mineralogist, v. 24, p. 729–771.

Hess, F. L., and Stevens, R. E., 1937, A rare-alkali biotite from Kings Mountain, North Carolina: Am. Mineralogist, v. 22, p. 1040–1044.

Hey, M. H., 1955, An index of mineral species and varieties, 2d rev. ed.: London, British Museum (Nat. History), 728 p.

Kunitz, Wilhelm, 1924, Die Beziehungen zwischen der chemischen Zusammensetzung und der physikalisch-optischen Eigenschaften innerhalb der Glimmergruppe: Neues Jahrb. Mineralogie, Geologie, u. Paläontologie, Beilage-Band 50, p. 365–413.

Levinson, A. A., 1953, Studies in the mica group; relationship between polymorphism and composition in the muscovite-lepidolite series: Am. Mineralogist, v. 38, p. 88–107.

Litvin, O. I., 1956, The lithium-ferrous micas from pegmatites of Volhynia: Kiev Derzhav. Univ. Nauk. Zapiski, v. 15, no. 2, Zbirnik Geol. no. 6, p. 119–128.

Marshall, C. E., 1949, The colloid chemistry of the silicate minerals: New York, Academic Press, 195 p.

Meng, H. M., and Chang, K., 1935, Geology of the Hsianghualing tin deposits, Lingwu, Hunan: Nat. Research Inst. Geology (Acad. Sinica), Mem., no. 15, p. 15–72.

Miser, H. D., and Stevens, R. E., 1938, Taeniolite from Magnet Cove, Arkansas: Am. Mineralogist, v. 23, p. 104–110.

Nockolds, S. R., and Richey, J. E., 1939, Replacement veins in the Mourne Mountains granites, N. Ireland: Am. Jour. Sci., v. 237, p. 27–47.

Pehrman, Gunnar, 1945, Die Granitpegmatite von Kimito (S.W.-Finnland) und ihre Minerale: Acad. Aboensis math. et phys. Acta 15, no. 2, 84 p.

Saldanha, Reynaldo, 1946, O estudo da jazida de wolframita de Inhandjara: São Paulo Univ., Fac. Filosofia Bol. 60 (Mineralogica, no. 8), p. 1–95.

Schaller, W. T., 1930, Adjectival ending of chemical elements used as modifiers to mineral names: Am. Mineralogist, v. 15, p. 566–574.

Shibata, H., 1952a, Spodumene and ambligonite from the Bunsen Mine and other localities in Korea: Tokyo Bunrika Daigaku, Sci. Repts., sec. C., v. 2, no. 11, p. 145–154.

——— 1952b, Mineralizations in granite-pegmatites in Japan and Korea: Tokyo Bunrika Daigaku, Sci. Repts., sec. C., v. 2, no. 12, p. 155–206.

Shilin, L. L., 1953, On lithium micas from pegmatites of alkaline magmas: Mineralog. Muzeya. Akad. Nauk U.S.S.R. Trudy, v. 5, p. 153–163.

Simpson, E. S., 1927, Contributions to the mineralogy of Western Australia: Royal Soc. Western Australia Jour., v. 13, p. 37–48.

Smith, J. V., and Yoder, H. S., Jr., 1956, Experimental and theoretical studies of the mica polymorphs: Mineralog. Mag., v. 31, p. 209–235.

Stelzner, A. W., 1896, Contribution on the lead ore of Freiberg and the tin ore of the Erzgebirge: Zeitschr. prakt. Geologie. v. 4, p. 377–412.

Stevens, R. E., 1938, New analyses of lepidolites and their interpretation: Am. Mineralogist, v. 23, p. 607–628.

Stevens, R. E., and Schaller, W. T., 1942, The rare alkalies in micas: Am. Mineralogist, v. 27, p. 525–537.

Tsyganov, E. M., 1954, The lithium micas of Volhynia: Mineralog. Obshch., Leningrad, Zapiski, ser. 2, v. 83, no. 4, p. 383–397.

Ukai, Yasuo, Nishimura, Shinichi, and Hashimoto, Yoshikazu, 1956, Chemical studies of the lithium micas from the pegmatite of Minagi, Okayama Prefecture: Mineralog. Jour. Japan, v. 2, no. 1, p. 27–38.

Walker, T. L., and Parsons, A. L., 1924, Pegmatite minerals from New Ross, Nova Scotia: Toronto, Univ., Studies, Geol. ser., no. 17, p. 46–50.

Wells, R. C., 1937, Analyses of rocks and minerals from the laboratory of the United States Geological Survey, 1914–1936: U.S. Geol. Survey Bull. 878, 134 p.

Winchell, A. N., 1927, Further studies in the mica group: Am. Mineralogist, v. 12, p. 267–279.

——— 1942, Further studies of the lepidolite system: Am. Mineralogist, v. 27, p. 114–130

TABLE 6.—*Analyses, with data for writing formulas, of aluminum lithium micas used in interpretation of composition*

[In order of increasing Li_2O content]

Analysis [1]	Percent																
	SiO_2	Al_2O_3	TiO_2	Fe_2O_3	FeO	MgO	MnO	Li_2O	CaO	Na_2O	K_2O	Rb_2O	Cs_2O	H_2O+	H_2O-	F
1	45.54	36.36	0.07	0.25	0.02	0.07	0.80	0.06	0.09	0.37	10.76	.....	.....	4.35	0.55	0.62
2	44.85	37.30	.04	.40	.45	Tr.	.02	.07	.22	1.10	10.20	.....	.....	4.36	.00	.79
3	44.10	33.04	.14	2.95	.50	.33	.03	.24	.36	.75	9.73	.....	.....	5.90	1.64	.56
4	45.22	37.46	.....	Tr.	.56	.38	.71	.32	.10	1.19	10.71	.....	.....	3.63		.73
5	44.80	37.72	.....	.67	.....	.....	.....	.38	.....	.91	10.07	0.82	0.09	4.32		.20
6	42.30	35.56	.05	.97	1.30	.18	.01	.40	.04	.96	9.31	.....	.....	6.85	4.09	.37
7	45.03	36.33	.02	.14	.02	.05	.41	.41	.09	.69	10.50	.79	.06	4.56	.79	1.01
8	43.63	32.54	.14	2.62	1.63	1.06	.....	.46	.....	1.05	8.92	.53	<.20	3.85	2.43	1.00
9	45.24	36.85	.01	.09	.02	.08	.12	.49	.00	.64	10.08	.86	.20	4.12	.46	.91
10	45.60	35.96	.03	.10	.02	.05	.37	.63	.08	.59	10.52	.....	.....	4.81	.44	1.31
11	46.01	35.64	.00	.13	.00	.04	.09	.69	1.12	1.88	8.19	1.20	.20	4.05	.05	.94
12	45.18	35.76	.15	.00	1.52	.07	.11	.73	.00	.88	9.95	.57	Tr.	4.48	.38	.88
13	46.17	35.57	.00	.15	.08	.00	.04	.76	.00	.56	10.37	1.1	.3	4.06	.12	.76
14	42.90	31.00	.46	4.79	.70	.22	.00	.80	.60	.51	8.90	.....	.....	6.84	3.06	.07
15	47.64	34.22	.00	.10	.....	.28	.05	1.10	.00	.47	10.40	.55	.78	3.21	.10	1.21
16	46.24	32.37	.10	1.34	1.14	.19	.09	1.1	.10	.79	10.16	1.3	.2	3.41	.69	1.41
17	41.82	32.58	.25	.88	.94	.10	.00	1.51	.68	.30	9.50	.....	.....	6.50	4.38	1.02
18	43.24	33.90	.24	.56	1.35	.26	.01	1.53	.90	.12	10.21	.....	.....	5.90	2.36	.08
19	46.20	33.08	.00	.00	1.20	.14	.28	1.80	.00	.63	10.09	1.37	.41	3.06	.34	2.06
20	46.34	32.47	.06	.00	1.05	.00	.35	2.45	.36	.5	9.46	1.5	.2	3.32	.42	2.82
21	47.00	30.60	Tr.	.26	.41	.13	2.04	2.70	Tr.	.77	9.52	1.93	.18	2.18	.26	4.09
22	49.50	28.06	Tr.	.....	1.11	.00	.54	3.51	.00	1.27	10.32	1.11	.13	2.15	.27	6.98
23	48.58	28.93	Tr.	.....	1.04	.00	.92	3.70	Tr.	.87	10.02	.91	.16	2.56	.54	4.93
24	50.20	28.18	Tr.	.....	1.04	.00	.28	3.81	Tr.	.64	9.91	1.55	.11	2.18	.18	4.97
25	46.52	28.80	.....	.40	.24	.02	.07	3.87	.13	.13	8.02	3.73	.08	1.72		5.18
26	48.68	29.62	.00	.10	.00	.00	.28	3.9	.00	1.3	10.05	1.5	.2	1.64	.14	4.60
27	50.30	25.49	Tr.	.05	1.30	.38	.53	3.90	.24	.95	10.13	1.39	.17	1.84	.08	6.03
28	49.14	27.66	.00	.....	3.43	.03	1.22	3.95	Tr.	.40	10.13	1.17	.62	2.54		5.21
29	49.20	28.40	Tr.	.....	1.05	.12	.65	3.96	Tr.	.77	9.93	1.56	.12	1.76	.14	6.32
30	49.62	27.30	.....	.31	.07	.....	.55	4.34	.....	2.17	8.03	2.44	.72	1.52		5.45
31	51.52	25.96	.....	.31	.....	.02	.20	4.90	.16	1.06	11.01	.....	.....	1.35		5.80
32	48.94	22.21	.00	1.55	1.32	.03	.75	4.99	.10	.53	8.62	3.8	1.08	1.46	0.88	6.09
33	53.45	22.15	Tr.	.....	1.16	.14	.32	5.04	.00	.74	9.58	1.56	.48	1.29	.41	7.22
34	49.58	23.87	.06	.....	1.21	.00	2.78	5.05	.00	.87	10.14	1.62	.09	1.22	.51	7.49
35	49.19	24.81	.08	.....	3.24	.05	2.51	5.10	Tr.	.52	10.25	1.78	.19	1.21		6.89
36	54.69	22.83	Tr.	.....	1.11	.00	.14	5.11	.00	.57	9.53	1.64	.17	1.02	.31	6.86
37	57.44	15.50	.....	.50	.....	1.70	Tr.	5.16	.64	.64	8.69	.....	.....	4.28	3.68	1.04
38	51.88	20.65	.21	.79	1.99	.00	2.01	5.26	.00	.51	10.55	.....	.....	1.80		7.63
39	51.70	23.97	Tr.	.....	1.04	.00	.17	5.33	Tr.	.89	10.79	.42	.41	1.21	.26	7.76
40	53.16	23.54	.00	.46	1.27	.06	.79	5.34	.04	1.10	10.97	.....	.....	1.39	.79	6.75
41	49.28	21.36	.63	.....	.....	.73	.87	5.36	.26	.66	11.24	.32	.....	.87		8.92
42	50.31	19.95	.22	.49	2.55	.02	2.63	5.39	Tr.	.59	10.14	.97	.06	.86	.66	7.65
43	49.14	21.99	.08	.44	.24	.58	1.41	5.41	.06	.52	9.82	.....	.....	3.25	3.51	4.81
44	50.92	23.12	.00	.06	.00	.06	.52	5.5	.00	.55	9.75	2.0	.66	.57	.05	6.86
45	51.10	23.98	Tr.	.04	.02	.00	.13	5.51	Tr.	.63	10.25	1.35	.48	1.50	.64	7.36
46	48.95	20.12	.13	.40	.18	.32	1.32	5.57	.07	.72	10.18	.....	.05	2.96	3.68	6.28
47	52.58	22.32	.....	.01	.00	.28	.57	5.64	Tr.	.59	10.11	1.04	.67	1.35	.30	7.56
48	49.18	18.85	.12	.42	.16	1.24	1.77	5.67	.26	.06	10.37	.....	.....	3.94	3.86	5.93
49	50.60	23.42	.00	.28	.02	.00	.15	5.7	.00	.35	9.08	3.2	.93	.79	.09	6.15
50	51.25	22.71	.01	.....	3.07	.08	.61	5.78	Tr.	.65	9.90	2.00	.08	.90	.34	8.08
51	51.67	22.05	.06	.....	1.04	.30	1.47	5.83	.00	1.03	11.18	.....	.....	.44		8.22
52	51.07	22.05	.06	.....	1.23	.09	.76	5.89	Tr.	.82	9.70	1.38	.09	.96		7.13
53	49.80	25.56	.00	.08	.00	.22	.38	5.95	.00	.4	9.67	1.97	1.2	.38	.50	6.85
54	51.40	17.95	.02	.....	8.21	.30	2.06	6.18	Tr.	.72	10.28	1.22	.24	.58	.81	9.19
55	58.56	14.97	.36	.43	.....	1.30	.14	6.31	.22	.84	10.03	.....	.....	2.72	.88	4.34
56	52.37	23.01	.04	.08	.....	.....	.68	6.37	.....	.90	11.19	.....	.....	.....	.59	8.26
57	57.03	15.55	.03	.....	3.12	.22	.72	6.84	Tr.	.44	10.65	1.35	.40	.49	.74	9.90
58	59.56	12.04	.48	.13	.42	.34	.03	7.26	Tr.	.53	11.04	1.14	None	.47	.73	7.73

Note and footnotes at end of table.

TABLE 6.—*Analyses, with data for writing formulas, of aluminum lithium micas used in interpretation of composition*—Continued

[In order of increasing Li_2O content]

Analysis [1]	Percent			Octahedral positions occupied by—								Octahedral charge	Tetrahedral charge	Composite layer charge	Interlayer cations	
	Total	O=F_2	Adjusted total	Al	Ti	Fe^{+3}	Fe^{+2}	Mg	Mn^{+2}	Li	Total				Charge	Positions
1	100.11	−0.26	99.85	1.92	0.00	0.01	0.00	0.01	0.06	0.02	2.01	−0.07	−0.95	−1.02	+1.00	1.00
2	100.30	−.33	99.97	1.94	.00	.02	.03	.00	.00	.02	2.01	−.04	−1.00	−1.04	+1.05	1.03
3	100.30	−.33	100.00	1.75	.01	.15	.03	.00	.04	.07	2.04	−.07	−.95	−1.02	+1.02	.99
4	101.06	−.31	100.75	1.85	.....	.00	.03	.04	.....	.08	2.07	−.06	−1.03	−1.09	+1.06	1.06
5	[2] 100.39	−.05	100.31	1.93	.....	.03	.....	.....	.....	.10	[2] 2.07	+.01	−1.02	−1.01	+1.00	1.00
6	101.11	−.15	100.96	1.81	.00	.06	.07	.02	.....	.12	2.07	−.12	−1.00	−1.12	+1.12	1.03
7	100.90	−.42	100.48	1.90	.00	.01	.00	.05	.02	.11	2.09	−.02	−.98	−1.00	+1.00	.99
8	100.13	−.42	99.71	1.68	.01	.14	.09	.11	.....	.13	2.15	+.03	−.98	−.96	+.95	.85
9	100.24	−.38	99.86	1.93	.00	.00	.00	.01	.01	.13	2.08	−.04	−.97	−1.01	+.99	.99
10	100.41	−.55	99.86	1.90	.00	.01	.00	.00	.03	.17	2.10	−.06	−.94	−1.00	+.99	.98
11	100.46	−.23	100.23	1.86	.00	.01	.00	.00	.01	.18	2.06	−.19	−.94	−1.13	+1.15	1.07
12	100.66	−.32	100.29	1.85	.01	.00	.05	.00	.01	.20	2.17	+.03	−.97	−.94	+.90	.89
13	100.04	−.22	99.72	1.89	.00	.01	.00	.00	.00	.20	2.10	−.10	−.91	−1.01	+1.01	1.01
14	100.55	−.03	100.52	1.60	.02	.25	.04	.02	.00	.22	2.15	−.02	−.97	−.99	+.96	.91
15	100.39	−.41	99.75	1.84	.00	.00	.....	.03	.00	.29	2.16	−.13	−.84	−.97	+.98	.98
16	100.63	−.59	100.04	1.71	.00	.07	.06	.02	.01	.30	2.17	−.18	−.87	−1.05	+1.06	1.04
17	100.77	−.43	100.34	1.74	.02	.05	.06	.01	.00	.44	2.32	+.03	−1.02	−.99	+1.03	.98
18	100.71	−.02	100.69	1.73	.01	.03	.05	.03	.00	.42	2.30	−.04	−1.02	−1.06	+1.05	.98
19	100.76	−.57	99.89	1.73	.00	.00	.07	.01	.02	.46	2.31	−.13	−.89	−1.02	+1.02	1.02
20	101.21	−1.19	100.03	1.89	.00	.00	.06	.00	.02	.56	2.43	−.11	.86	−.99	+1.03	1.01
21	102.06	−1.72	100.34	1.55	.00	.01	.03	.01	.12	.73	2.47	−.20	−.84	−1.04	+1.01	1.01
22	102.96	−2.52	100.44	1.54	.....	.01	.00	.03	.08	.94	2.50	−.42	−.89	−1.31	+1.10	1.10
23	102.15	−2.06	100.08	1.54	.00	.....	.00	.00	.05	1.00	2.59	−.25	−.74	−1.02	+1.01	1.01
24	102.05	−2.09	99.96	1.54	.00	.....	.00	.00	.02	1.01	2.57	−.33	−.66	−.99	+.99	.99
25	102.71	−2.18	100.53	1.56	.....	.02	.01	.00	.00	1.03	2.61	−.20	−.71	−.91	+.94	.93
26	102.08	−1.94	100.14	1.44	.00	.01	.00	.00	.02	1.04	2.51	−.27	−.78	−1.05	+1.06	1.05
27	102.78	−2.54	100.24	1.40	.00	.00	.08	.04	.03	1.05	2.60	−.45	−.62	−1.07	+1.09	1.05
28	102.63	−2.19	100.43	1.49	.00	.....	.02	.00	.07	1.06	2.64	−.29	−.70	−.99	+.98	.96
29	103.27	−2.75	100.52	1.51	.00	.....	.00	.01	.04	1.06	2.62	−.31	−.72	−1.03	+1.02	1.03
30	102.83	−2.29	100.23	1.44	.....	.02	.00	.....	.03	1.15	2.65	−.40	−.68	−1.08	+1.09	1.09
31	101.89	−2.44	99.45	1.39	.....	.02	.....	.00	.02	1.29	2.72	−.44	−.62	−1.06	+1.08	1.07
32	103.15	−2.82	100.33	1.21	.00	.08	.09	.00	.04	1.39	2.81	−.48	−.60	−1.08	+1.08	1.05
33	102.78	−3.04	99.74	1.32	.00	.....	.01	.01	.03	1.35	2.72	−.50	−.42	−.91	+.99	.99
34	103.19	−3.15	100.04	1.29	.00	.....	.01	.00	.16	1.38	2.84	−.41	−.62	−1.03	+1.03	1.03
35	102.82	−2.90	99.92	1.32	.00	.....	.01	.00	.14	1.39	2.86	−.35	−.67	−1.02	+1.03	1.03
36	102.98	−2.99	100.00	1.36	.00	.....	.01	.00	.01	1.35	2.73	−.53	−.41	−.94	+.94	.94
37	[4] 99.70	−.43	99.27	1.12	.....	.03	.....	.....	.17	.00	1.40	2.72	−.81	−.12	−.93	+.93	.88
38	103.39	−3.22	100.17	1.16	.01	.04	.11	.00	.12	1.43	2.87	−.47	−.49	−.96	+.98	.98
39	102.98	−3.27	99.71	1.34	.00	.....	.00	.00	.01	1.44	2.79	−.52	−.55	−1.07	+1.06	1.06
40	102.71	−3.22	99.49	1.25	.00	.02	.07	.01	.04	1.45	2.85	−.47	−.62	−1.09	+1.12	1.09
41	103.80	−3.76	99.74	1.26	.....	.03	.....	.07	.05	1.45	2.86	−.44	−.68	−1.12	+1.10	1.08
42	102.55	−3.22	99.33	1.10	.01	.02	.15	.00	.16	1.50	2.93	−.50	−.52	−1.02	+.99	.99
43	102.17	−2.15	100.01	1.19	.00	.03	.01	.09	.08	1.50	2.89	−.51	−.60	−1.11	+1.08	1.01
44	102.64	−2.80	99.75	1.26	.00	.00	.00	.00	.03	1.47	2.86	−.39	−.51	−1.00	+1.00	1.00
45	102.88	−3.10	99.78	1.34	.00	.....	.00	.00	.01	1.49	2.84	−.47	−.56	−1.03	+1.03	1.03
46	100.54	−2.22	98.32	1.40	.01	.03	.01	.00	.07	1.41	2.96	−.07	−.92	−.99	+1.00	.95
47	101.83	−2.52	99.31	1.31	.00	.....	.00	.....	.02	1.52	2.85	−.51	−.49	−1.00	+1.00	1.00
48	101.83	−2.50	99.33	1.10	.01	.02	.01	.13	.11	1.62	3.00	−.48	−.49	−.97	+.99	.97
49	102.76	−2.59	100.17	1.36	.00	.01	.00	.01	.03	1.53	2.91	−.34	−.64	−.98	+.98	.98
50	103.46	−3.40	100.06	1.20	.00	.....	.00	.01	.03	1.56	2.90	−.46	−.57	−1.03	+1.02	1.02
51	103.26	−3.19	99.90	1.24	.00	.....	.00	.03	.06	1.55	2.90	−.51	−.57	−1.08	+1.08	1.08
52	100.23	−3.00	97.23	1.25	.00	.....	.01	.00	.04	1.51	2.92	−.52	−.52	−1.04	+1.02	1.02
53	102.95	−3.49	99.47	1.33	.00	.....	.00	.01	.02	1.59	2.95	−.34	−.68	−1.02	+.99	.99
54	104.16	−3.87	100.29	1.10	.00	.....	.01	.03	.12	1.68	2.94	−.70	−.33	−1.03	+1.04	1.04
55	[5] 103.10	−1.83	101.27	1.01	.07	.03	.....	.13	.27	1.68	3.16	−.86	−.88	−1.03	+1.03	1.02
56	103.35	−3.45	100.00	1.26	.00	.01	.....	.....	.04	1.68	2.98	−.46	−.53	−.99	+1.05	1.05
57	[6] 103.72	−3.79	99.93	1.05	.00	.....	.01	.02	.04	1.84	2.96	−.87	−.17	−1.04	+1.04	1.04
58	103.43	−3.26	100.17	.88	.02	.01	.02	.03	.00	1.93	[2] 2.93	−1.03	−.06	−1.09	+1.08	1.06

The numbers in the footnotes below are in percent.
[1] See descriptions on pages 144 for origin of samples and source of analyses.
[2] Includes 0.21 MnO_2, <0.01 octahedral position.
[3] Total Fe reported as FeO.
[4] Includes 0.09 F_2O_3 and 0.34 SO_3.
[5] Includes 0.05 Cl.
[6] May be present as Fe_2O_3.
[7] Includes 0.04 P_2O_5, 0.34 SO_3, and 0.02 Cl.
[8] Includes 0.14 Nb_2O_5, <0.00 octahedral position.
[9] Includes 1.62 Nb_2O_5, <0.04 octahedral position.

(Notes to table 6 are on page 144)

NOTES TO TABLE 5

1. Apache, Petaca, N. Mex. (Heinrich and Levinson, 1953, p. 43, no. 4).
2. Russia, locality not given (Ginzburg and Berkhin, 1953, p. 85).
3. Yamanoo, Tsukuba, Japan (Shibata, 1952b, p. 153, no. 12).
4. Londonderry, Western Australia (Simpson, 1927, p. 46).
5. Harding mine, 9½ miles east of Embudo, N. Mex. (Wells, 1937), p. 108, B. Corrections of percentages of alkalies by Stevens and Schaller, 1942, p. 527.
6. Yamanoo, Tsukuba, Japan (Shibata, 1952b, p. 153, no. 11).
7. White Spar mine No. 1, Gunnison County, Colo. (Heinrich and Levinson, 1953, p. 43, no. 2).
8. Kimito, southwest Finland (Fehrman, 1945, p. 36).
9. Pitillo, Rociada, N. Mex. (Heinrich and Levinson, 1953, p. 43, no. 5).
10. Brown Derby No. 1 mine, Gunnison County, Colo. (Heinrich and Levinson, 1953, p. 43, no. 3).
11. Varutträsk, Sweden (Berggren, 1940, p. 183, H.). Normal muscovite structure.
12. Varutträsk, Sweden (Berggren, 1940, p. 183, G). Normal muscovite structure.
13. Varutträsk, Sweden (Berggren, 1941, p. 264, J). Normal muscovite structure.
14. Naratare, Fukuoka Pref., Japan (Shibata, 1952b, p. 154, no. 19).
15. Varutträsk, Sweden (Berggren, 1940, p. 185, F).
16. Varutträsk, Sweden (Berggren, 1941, p. 264, L). Normal muscovite structure.
17. Bunsen mine, South Kankyō-nando, Korea (Shibata, 1952b, p. 154, no. 21).
18. Bunsen mine, South Kankyō-nando, Korea (Shibata, 1952b, p. 154, no. 22).
19. Varutträsk, Sweden (Berggren, 1940, p. 185, E). Normal muscovite structure.
20. Varutträsk, Sweden (Berggren, 1940, p. 185, D). Normal muscovite structure.
21. Manitoba, Canada (Stevens, 1938, p. 615, no. 1, U.S. Natl. Mus. No. 97535). Normal muscovite structure.
22. Katerina mine, Pala, San Diego County, Calif. (Stevens, 1938, p. 615, no. 2). Transitional structure (combination of forms).
23. Stewart mine, "40 acres," Pala, San Diego County, Calif. (Stevens, 1938, p. 615, no. 3). Transitional structure (combination of forms).
24. Panama-Pacific-Exposition mine, Chihuahua Valley, east of Oak Grove, San Diego County, Calif. (Stevens, 1938, p. 615, no. 4). Transitional structure (combination of forms).
25. Norway, Maine (Clarke, 1910, p. 287, F).
26. Varutträsk, Sweden (Berggren, 1940, p. 183, C). Normal muscovite structure.
27. Rema, Moravia, Czechoslovakia (K. E. Stevens written communication, 1938, U.S. Geol. Survey Lab. Record No. D-789).
28. Mt. Apatite, Auburn, Maine (Winchell, 1942, p. 115, no. 17, U.S. Natl. Mus. No. 80230).
29. Stewart mine, San Diego County, Calif. (Stevens, 1938, p. 615, no. 5). Transitional structure (combination of forms).
30. Auburn, Maine (Clarke, 1910, p. 287, D).
31. Black Mountain, Rumford, Maine (Clarke, 1910, p. 287, A).
32. Kimito, southwest Finland (Fehrman, 1945, p. 36).
33. Stewart mine, Pala, San Diego County, Calif. (Stevens, 1938, p. 615, no. 6). Structure, 6-layer lepidolite.
34. Ohio City, Colo. (Stevens, 1938, p. 615, no. 7, U.S. Natl. Mus. No. 97893). Structure, 6-layer lepidolite.
35. Ohio City, Colo. (Winchell, 1942, p. 115, no. 10).
36. Himalaya mine, Mesa Grande, San Diego County, Calif. (Stevens, 1938, p. 615, no. 8). Structure, 1-layer lepidolite.
37. Locality not given (Shilin, 1953, p. 155).
38. Wakefield, Quebec, Canada (Winchell, 1942, p. 115, no. 26).
39. San Diego mine, Mesa Grande, San Diego County, Calif. (Stevens, 1938, p. 615, no. 9). Structure, 1-layer lepidolite.
40. Aiabashta, Urals (Winchell, 1942, p. 115, no. 18).
41. New Rosa, Nova Scotia (Walker and Parsons, 1924, p. 49).
42. Wakefield, Quebec, Canada (Stevens, 1938, p. 615, no. 10). Structure, 1-layer lepidolite.
43. Urushiko, Kōgen-dō, Korea (Shibata, 1952b, p. 155, no. 23).
44. Rozena, Moravia (Berggren, 1941, p. 271, F).
45. Stewart mine, Pala, San Diego County, Calif. (Stevens, 1938, p. 615, no. 11). Structure not determined.
46. Yagatani, Fukuoka Pref., Japan (Shibata, 1952b, p. 154, no. 20).
47. Stewart mine, Pala, San Diego County, Calif. (Stevens, 1938, p. 615, no. 12). Structure, 6-layer lepidolite.
48. Bunsen mine, South Kankyō-nando, Korea (Shibata, 1952a, p. 150).
49. Utö, Sweden (Berggren, 1941, p. 265).
50. Himalaya mine, Mesa Grande, San Diego County, Calif. (Stevens, 1938, p. 615, no. 13). Structure, 1-layer lepidolite.
51. Longsdiernsuk, Julianehaab district, Greenland (Stevens, 1938, p. 615, no. 17, U.S. Natl. Mus. No. 94314). Structure, 1-layer lepidolite.

TABLE 7.—*Analyses, with data for writing formulas, of sideraphyllites and ferrous lithium micas used in interpretation of composition*

[In order of increasing H_2O content]

Analysis [1]	Percent															
	SiO_2	Al_2O_3	TiO_2	Fe_2O_3	FeO	MgO	MnO	Li_2O	CaO	Na_2O	K_2O	H_2O+	H_2O-	F	Total
1	39.60	22.80	0.21	0.79	20.98	0.46	0.29	.....	1.52	Tr.	8.95	2.63	0.24	2.03	100.59
2	33.50	22.30	.06	1.44	28.54	.10	.33	0.32	.14	0.46	8.90	1.66	.08	.89	[2] 98.91
3	32.52	19.07	.31	10.08	17.54	.70	.21	.99	.72	.31	8.53	3.17	3.21	2.36	99.22
4	35.25	17.24	1.51	8.15	30.61	.28	.69	.48	1.10	.27	7.21	2.99	2.74	1.67	100.43
5	36.52	18.44	4.99	.78	7.73	22.81	.62	.74	.80	.35	.44	7.68	3.03	2.30	1.97	101.53
6	31.96	17.06	.68	7.44	24.12	.29	.71	.59	.48	.51	7.41	5.95	2.94	1.59	100.84
7	37.39	20.96	1.62	2.37	18.10	1.19	.....	1.19	.48	1.01	8.04	3.24	.....	.....	[3] 98.17
8	36.00	23.63	.....	4.84	16.17	.21	1.29	.....	.43	1.68	9.40	.98	.54	3.80	[4] 100.72
9	35.60	27.60	.64	.....	18.50	.12	.66	1.44	1.50	1.37	8.15	3.06	.04	1.68	101.86
10	35.54	19.81	.....	3.98	19.53	.27	1.59	1.47	.25	.88	9.64	1.59	.....	5.75	100.28
11	36.91	18.20	.55	5.18	21.97	.20	.29	1.48	.29	.28	8.29	4.51	.....	3.15	101.17
12	43.70	22.96	.23	.89	11.67	.....	1.96	1.92	.....	.74	9.64	1.55	.08	5.62	[4] 101.53
13	37.12	22.37	Tr.	7.81	12.03	2.20	3.21	2.10	1.05	.81	8.60	2.13	.....	.21	99.84
14	38.26	23.73	.....	.21	10.30	.....	2.21	2.44	.....	.16	10.47	.60	.40	2.46	[4] 101.04
15	41.73	22.76	.....	.98	14.34	.55	.....	2.42	.....	.67	10.51	1.44	.....	6.46	101.80
16	38.83	22.27	.13	4.49	9.07	.58	1.66	2.62	1.18	.48	9.53	H_2O-+	H_2O+	3.92	100.99
17	36.41	19.37	.14	10.06	12.23	.63	3.97	2.69	.99	.15	8.99	2.93	3.74	4.79	101.22
18	45.87	22.50	.....	.60	11.66	.....	1.75	3.28	.....	.42	10.46	0.94	.....	7.94	[5] 105.53
19	45.23	21.78	.....	.47	11.25	.23	1.73	3.23	.....	.78	9.46	.97	.....	7.86	102.63
20	45.44	21.84	.....	1.41	10.06	.....	1.80	3.36	.....	.54	10.58	.....	.....	7.62	103.74
21	45.53	20.02	.16	.32	7.10	.....	.37	3.27	.97	2.45	8.35	2.27	.54	6.12	99.34
22	39.04	23.56	.57	4.10	12.42	.67	.....	3.39	.78	.71	8.51	3.25	.....	.....	99.30
23	46.37	23.43	1.30	.....	10.05	.21	.35	3.40	.50	1.22	8.57	3.60	.27	2.25	102.44
24	42.62	23.61	Tr.	1.66	8.58	.99	4.02	3.41	.82	.52	9.41	1.96	.26	2.78	100.33
25	43.59	25.60	1.35	.....	11.80	.14	.73	3.70	.42	1.30	7.73	4.05	.55	1.24	101.43
26	45.26	25.34	1.52	.....	12.40	.20	.73	3.70	.45	1.28	7.66	4.60	1.20	1.28	101.76
27	46.80	24.00	.....	.50	6.85	.....	1.38	3.73	.24	1.72	9.30	.88	.....	8.63	103.94
28	46.74	21.78	.....	1.10	10.22	.65	.37	3.72	.50	.54	10.37	.86	.....	7.42	103.35
29	45.88	20.80	.....	.97	9.65	.13	1.74	3.78	.....	.96	9.11	1.43	.....	5.12	99.56
30	41.60	25.70	.76	.....	11.25	.12	.22	3.43	.50	2.33	8.03	4.40	.86	1.58	102.25
31	43.40	21.02	.....	.24	7.19	.....	1.57	4.19	.08	1.12	10.45	.64	.24	2.24	[6] 100.83
32	45.98	18.04	.22	3.56	6.00	1.59	2.49	4.57	1.83	.25	9.85	.86	1.14	5.66	101.95
33	51.46	16.22	.....	2.21	7.63	.17	.06	4.81	Tr.	.89	10.62	1.12	.....	7.44	102.66
34	51.92	16.89	.....	2.63	6.59	.24	.48	4.87	.12	.87	10.70	1.81	.....	6.78	103.72
35	52.17	16.39	.....	4.11	5.99	Tr.	.32	4.99	Tr.	.63	10.48	1.46	.....	7.69	102.66

Note and footnotes at end of table.

TABLE 7.—*Analysis, with data for writing formulas, of siderophyllites and ferrous lithium micas used in interpretation of composition*—Continued

[In order of increasing Li_2O content]

Analysis [1]	Percent		Octahedral positions occupied by—								Octahedral charge	Tetrahedral charge	Composite-layer charge	Interlayer cations	
	O=F_2	Adjusted total	Al	Ti	Fe[+3]	Fe[+2]	Mg	Mn[+2]	Li	Total				Charge	Positions
1	−0.85	99.95	0.99	0.01	0.05	1.32	0.05	0.02	.....	2.44	−0.06	−1.03	−1.09	+1.10	0.98
2	−.37	98.54	.73	.00	.08	1.88	.01	.02	0.10	2.83	+.35	−1.35	−1.00	+.99	.98
3	−.99	98.23	.52	.01	.62	1.22	.09	.02	.13	2.61	+.25	−1.32	−1.07	+1.06	.99
4	−.70	99.73	.44	.09	.69	1.38	.03	.06	.15	2.64	+.24	−1.19	−.95	+.96	.87
5	−.54	99.69	.36	.05	.47	1.51	.06	.05	.18	2.68	+.13	−1.06	−.93	+.92	.89
6	−.67	100.17	.39	.00	.47	1.70	.04	.05	.20	2.85	+.36	−1.21	−.85	+.96	.92
7	.....	.....	.72	.09	.16	1.19	.14	.....	.37	[2] 2.68	+.05	−1.16	−1.11	+1.07	1.03
8	−1.60	99.12	.94	.....	.27	1.01	.....	.02	.39	2.63	+.08	−1.16	−1.07	+1.06	1.06
9	−.70	101.10	1.06	.03	.....	1.12	.01	.04	.42	2.68	+.05	−1.24	−1.18	+1.15	1.04
10	−2.42	100.96	.71	.....	.23	1.24	.03	.10	.45	2.76	+.01	−1.06	−1.08	+1.08	1.06
11	−1.33	99.94	.57	.03	.31	1.41	.02	.07	.47	2.86	+.19	−1.11	−.92	+.90	.89
12	−2.33	99.21	1.32	.02	.03	.71	.....	.12	.56	2.57	−.22	−.83	−1.05	+1.04	1.04
13	−.09	99.55	.05	.00	.43	.74	.24	.20	.62	2.88	+.22	−1.26	−1.06	+1.08	1.00
14	−2.27	99.77	1.16	.....	.01	.61	.....	.04	.65	2.48	−.53	−.87	−1.10	+1.07	1.07
15	−2.72	99.08	1.04	.....	.05	.87	.05	.....	.71	2.73	−.16	−.93	−1.09	+1.08	1.08
16	−1.61	99.38	.95	.01	.25	.58	.04	.11	.80	2.74	+.10	−1.05	−1.15	+1.10	1.08
17	−2.02	102.20	.60	.01	.58	.79	.07	.13	.84	2.92	+.10	−1.18	−1.08	+1.08	1.00
18	−3.34	102.19	1.05	.....	.04	.68	.....	.10	.92	2.82	−.16	−.79	−.95	+.94	.94
19	−3.36	100.27	1.05	.....	.02	.68	.02	.10	.92	2.79	−.27	−.75	−1.05	+1.01	1.01
20	−3.21	100.53	1.05	.....	.07	.59	.....	.11	.95	2.77	−.29	−.75	−1.04	+1.02	1.02
21	−2.85	96.66	1.15	.01	.02	.48	.....	.02	.94	2.62	−.51	−.54	−1.05	+1.07	.99
22	.....	.....	.80	.03	.33	.75	.10	.....	.98	2.99	+.19	−1.20	−1.01	+1.03	.97
23	−1.07	101.37	1.19	.07	.....	.61	.02	.02	.94	2.76	−.18	−.80	−.98	+1.00	.98
24	−1.17	99.16	1.04	.00	.06	.51	.10	.24	.98	2.93	−.02	−.95	−.97	+1.02	.99
25	−.54	100.91	1.08	.07	.....	.69	.01	.04	1.04	2.93	+.04	−.97	−.93	+.91	.88
26	−.54	101.22	1.01	.07	.....	.75	.02	.04	1.06	2.95	−.01	−.94	−.95	+.95	.91
27	−3.63	100.31	1.23	.....	.03	.37	.....	.08	1.04	2.75	−.28	−.77	−1.05	+1.08	1.08
28	−3.17	100.19	1.08	.....	.06	.60	.....	.02	1.05	2.81	−.29	−.72	−1.01	+1.00	1.00
29	−2.16	97.40	1.04	.....	.06	.58	.01	.10	1.09	2.87	−.26	−.72	−.98	+.96	.96
30	−.67	100.58	1.09	.04	.....	.68	.01	.01	1.15	2.98	−.02	−1.05	−1.07	+1.07	1.08
31	−1.04	99.79	1.11	.....	.01	.42	.....	.12	1.16	2.82	−.40	−.65	−1.05	+1.07	1.07
32	−2.38	99.57	.77	.01	.19	.36	.16	.14	1.20	2.93	−.46	−.74	−1.20	+1.20	1.07
33	−2.13	99.53	.91	.....	.12	.44	.02	.00	1.35	2.84	−.64	−.42	−1.06	+1.07	1.07
34	−2.83	99.87	.94	.....	.14	.38	.00	.01	1.36	2.81	−.66	−.42	−1.08	+1.07	1.08
35	−2.96	100.60	.90	.....	.21	.34	.00	.02	1.38	2.85	−.57	−.42	−.99	+1.00	1.00

The numbers in the footnotes below are in percent.

[1] See descriptions below for origin of samples and source of analyses.

[2] Contains 0.03 P_2O_5.

[3] Contains 0.32 SiO_2 (<0.01 octahedral position), and 0.60 undissolved residue.

[4] Contains 0.75 B_2O_3.

[5] Contains 1.04 RbO and 0.10 Cs_2O.

[6] Contains 0.08 P_2O_5.

[7] Contains 0.08 P_2O_5.

[8] Contains 2.48 B_2O_3.

NOTES TO TABLE 7

1. New Castle, Ireland (Nockolds and Richey, 1939, p. 39). In greisen veins cutting aplite veins in granite.
2. Yagenyama, Japan (Shibata, 1952b, p. 162, no. 7). In topaz vein in granite pegmatite.
3. Eidsu mine, Nuegi District, Japan (Shibata, 1952b, p. 162, no. 6). In greisen.
4. Hachiman, Nuegi District, Japan (Shibata, 1952b, p. 161, no. 1). In granite pegmatite.
5. Hachiman, Nuegi District, Japan (Shibata, 1952b, p. 161, no. 2). In pegmatite.
6. Hachiman, Nuegi District, Japan (Shibata, 1952b, p. 161, no. 3). In pegmatite.
7. Wilaschbusa, Germany (Steiner, 1896, p. 241). From granite.
8. Lingwu, Hunan, China (Meng and Chang, 1935, p. 57). In pneumatolytic-metamorphosed rocks (greisen).
9. Volhynia, Russia (Tsyganov, 1954, p. 398, no. 9). From topaz pegmatite.
10. Zinnwald, Erzegebirge, Bohemia (Kunitz, 1924, p. 413).
11. Volhynia, Russia (Buryanova, 1940, p. 532–533). From granite pegmatite.
12. Morefield mine, Amelia, Va. (Watts, 1937, p. 113).
13. Near Jundai, northwest of São Paulo, Brazil (Baldanha, 1946, p. 49). In quartz veins in gneiss, microgranitic quartz-porphyry, and greisen.
14. Lingwu, Hunan, China (Meng and Chang, 1935, p. 57). In pneumatolytic-metamorphosed rock (greisen).
15. Altenburg, Saxony, Germany (Kunitz, 1924, p. 413, no. 7).
16. Yamanota, Nuegi District, Japan (Shibata, 1952b, p. 162, no. 5). In pegmatite.
17. Hachiman, Nuegi District, Japan (Shibata, 1952b, p. 161, no. 4). In pegmatite.
18. Zinnwald, Erzegebirge, Bohemia (Dana, 1892, p. 620, no. 1).
19. Zinnwald, Erzegebirge, Bohemia (Kunitz, 1924, p. 413).
20. Zinnwald, Erzegebirge, Bohemia (Dana, 1892, p. 620, no. 2).
21. Volhynia, Russia (Litvin, 1956, p. 120, no. 15). From pegmatite.
22. Elbeinsdorf, Erzegebirge, Bohemia (Scheiner, 1896, p. 391).
23. Volhynia, Russia (Tsyganov, 1954, p. 398, no. 1). From pegmatite.
24. Locality not given (Ginsburg and Berkhin, 1953, p. 105).
25. Volhynia, Russia (Litvin, 1956, p. 120, no. 10). From pegmatite.
26. Volhynia, Russia (Litvin, 1956, p. 120, no. 9). From pegmatite.
27. Cassiterite Creek, Cape York, Alaska (Clarke, 1910, p. 287, no. M). W. T. Schaller, analyst.
28. Zinnwald, Erzegebirge, Bohemia (Winchell, 1942, p. 115, no. 24).
29. Ambatofotsi, Madagascar (Duparc, Wunder, and Sabot, 1910, p. 369). From pegmatite.
30. Volhynia, Russia (Tsyganov, 1954, p. 398, no. 2). From pegmatite.
31. Lingwu, Hunan, China (Meng and Chang, 1935, p. 56). In pneumatolytic-metamorphosed rock (greisen).
32. Sakihama, Okinai, Iwate Pref., Japan (Shibata, 1952b, p. 162, no. 17).
33. Cape Ann, Rockport, Mass. (Clarke, 1886, p. 358, no. B). R. B. Riggs, analyst.
34. Cape Ann, Rockport, Mass. (Clarke, 1886, p. 358, no. A). R. B. Riggs, analyst.
35. Cape Ann, Rockport, Mass. (Clarke, 1886, p. 358, no. C). R. B. Riggs, analyst.

TABLE 8.—*Analyses, with data for writing formulas, of ferrous lithium micas not used in interpretation of composition*

[In order of increasing Li_2O content]

Analysis [1]	Percent														
	SiO_2	Al_2O_3	TiO_2	Fe_2O_3	FeO	MgO	MnO	Li_2O	CaO	Na_2O	K_2O	H_2O+	H_2O-	F	Total
1	32.53	17.90	0.88	4.45	30.93	0.13	0.49	0.77	0.20	0.10	7.19	3.57	.....	1.21	100.35
2	37.65	16.80	1.10	.32	22.26	2.91	.39	1.21	1.36	3.57	5.54	2.17	0.26	4.28	100.84
3	37.53	24.35	.30	7.29	11.78	.44	.27	1.73	.30	2.24	10.03	1.23	.....	4.26	102.27
4	47.00	28.75	1.40	.....	11.50	.21	.64	1.85	.24	1.77	5.35	4.20	.41	3.09	103.41
5	36.30	20.30	1.60	.....	26.50	.16	.53	2.01	.17	2.80	8.70	2.80	.28	1.68	102.21
6	35.80	19.80	1.64	.....	27.80	.20	.....	2.02	1.75	2.28	5.85	3.00	.30	1.68	102.20
7	47.10	24.80	.80	.....	12.30	.15	.....	2.30	.22	1.60	8.28	4.47	.22	3.33	103.56
8	41.78	21.46	.57	.28	13.36	.47	.38	2.45	2.71	2.64	6.12	1.91	.24	5.95	102.30
9	48.80	21.21	Tr.	2.78	6.16	.57	4.80	2.89	.72	1.29	8.99	.44	.38	5.78	[3] 103.47
10	41.10	25.22	.80	.....	14.10	.03	.72	2.74	.20	1.95	9.80	4.05	.09	2.95	103.71
11	43.00	24.65	.71	.....	11.60	.05	.....	2.86	1.18	2.28	9.01	3.90	.15	2.38	101.97
12	45.34	18.40	.19	1.06	9.95	.28	.63	3.51	1.25	2.78	7.63	2.09	.36	6.32	99.69
13	46.58	24.10	.....	.69	4.28	.49	1.34	3.56	.66	.84	10.51	1.89	.....	7.90	102.77
14	43.50	28.00	1.35	.....	11.80	.14	.73	3.70	.42	1.20	7.73	4.05	.55	1.28	101.45

Analysis [1]	Percent		Octahedral positions occupied by—								Octahedral charge	Tetrahedral charge	Composite layer charge	Interlayer cations	
	O+F	Adjusted total	Al	Ti	Fe^{+3}	Fe^{+2}	Mg	Mn^{+2}	Li	Total				Charge	Positions
1	−0.51	99.84	0.49	0.06	0.03	2.16	0.01	0.03	0.26	2.04	+0.46	−1.28	−0.82	+0.82	0.80
2	−1.80	99.04	.46	.06	.02	1.44	.34	.02	.38	2.72	−.34	−1.08	−1.42	+1.41	1.80
3	−1.90	100.47	.86	.02	.42	.72	.03	.02	.51	2.60	+.01	−1.24	−1.23	+1.26	1.26
4	−1.30	102.11	1.28	.07	.....	.66	.02	.04	.51	2.58	+.07	−.79	−.72	+.74	.72
5	−.70	101.51	.53	.09	.....	1.70	.02	.03	.62	2.99	+.07	−1.30	−1.23	+1.22	1.19
6	−.70	101.50	.50	.09	.....	1.77	.03	.....	.62	3.01	+.08	−1.28	−1.20	+1.19	1.04
7	−1.40	102.16	1.24	.04	.....	.71	.01	.....	.84	2.64	−.04	−.76	−.80	+.80	.78
8	−2.50	99.80	.90	.03	.01	.94	.02	.05	.72	2.67	−.41	−.95	−1.36	+1.27	1.16
9	−2.43	101.04	1.00	.00	.15	.36	.06	.29	.73	2.59	−.40	−.77	−1.17	+1.18	1.12
10	−1.24	102.47	1.06	.04	.....	.84	.00	.04	.78	2.77	−.12	−1.07	−1.19	+1.18	1.15
11	−1.09	100.88	1.11	.04	.....	.69	.00	.....	.81	2.65	−.32	−.95	−1.27	+1.31	1.22
12	−2.66	97.03	.92	.01	.06	.61	.03	.04	1.04	2.71	−.62	−.66	−1.30	+1.31	1.21
13	−3.33	99.44	1.24	.....	.04	.23	.05	.08	1.00	2.66	−.40	−.75	−1.15	+1.17	1.12
14	−.54	100.91	1.08	.07	.....	.69	.01	.04	1.04	2.93	+.04	−.97	−.93	+.91	.88

[1] See descriptions below for origin of samples and source of analyses.
[2] Contains 2.04 percent (Rb,Cs)$_2O$.

NOTES TO TABLE 8

1. Volhynia, Russia (Buryanovs, 1940, p. 222–223).
2. Volhynia, Russia (Litvin, 1956, p. 120, no. 6). From pegmatite.
3. Geyer, Saxony, Germany (Dana, 1892, p. 527, no. 2).
4. Volhynia, Russia (Tsyganov, 1954, p. 386, no. 3). From pegmatite.
5. Volhynia, Russia (Tsyganov, 1954, p. 386, no. 10). From pegmatite.
6. Volhynia, Russia (Tsyganov, 1954, p. 386, no. 11). From pegmatite.
7. Volhynia, Russia (Tsyganov, 1954, p. 386, no. 6). From pegmatite.
8. Volhynia, Russia (Litvin, 1956, p. 120, no. 7). From pegmatite.
9. Minagi, Okayama Pref., Japan (Ukai, Nishimura, and Hashimoto, 1956, p. 32 no. 2).
10. Volhynia, Russia (Tsyganov, 1954, p. 386, no. 8). From pegmatite.
11. Volhynia, Russia (Tsyganov, 1954, p. 386, no. 4). From pegmatite.
12. Volhynia, Russia (Litvin, 1956, p. 120, no. 14). From pegmatite.
13. New Ross, Nova Scotia (Walker and Parsons, 1924, p. 49). From pegmatite.
14. Volhynia, Russia (Tsyganov, 1954, p. 386, no. 5). From pegmatite.

INDEX

Page

Aluminian lepidomelanes 130, 131, 132, 134, 138
lithium micas 124, 129
Aluminum lithium micas 115, 116, 117, 120, 121, 122, 124, 126, 138, 140
and ferrous lithium micas, relation 137
Anionic composition of micas 116
Annite 134

Berggren, Thelma 125
Berkhin, S. I. *See* Ginzburg, A. I. and Berkhin, S. I.
Biotite 115, 116, 128, 140
Biotite-lepidolite series 127, 128

Clarke, F. W 136
Compositional changes shown by the analyses 117, 129
relations in siderophyllites and ferrous lithium micas 130
Compositions, previous interpretations 127
Cooke, J. P. Jr 127, 136, 140
Cryophyllite 127, 128, 129, 135, 137, 140
Cryophyllite-zinnwaldite relation 137

Dana, E. S 127, 129, 136
Dioctahedral mica 119
potassium micas 115, 120

Fe^{+3}-Li replacement ratios 131
Ferrian siderophyllites 130, 134
Ferrous lepidolites 135, 136, 140
Ferrous lithium micas 116, 116, 127, 128, 129, 130, 131, 132, 135
siderophyllites, and aluminian lepidomelanes, relation 129, 140
Formulas, calculation of 115
Foster, M. D 115, 117, 129, 130, 131

Ginzburg, A. I. and Berkhin, S. I. 117, 128

Hallimond, A. F 127, 136, 139
Hendricks, S. B. and Jefferson, M. E 117, 124, 125, 127, 129, 140
Heptaphyllitic micas 119, 127, 129, 135
Hey, M. H 128, 129, 135, 136

Interlayer cations 116

Jefferson, M.E. *See* Hendricks, S. B., and Jefferson, M. E.

Kunitz, Wilhelm 127, 135, 136

Le (2 Li, Si) 127, 128
Lepidolite series 126
structure 117, 124
Lepidolites, interpretation of composition 115, 126, 136
Lepidolite-muscovite association 117
Lepidolite-protolithionite series 127, 128
Lepidomelanes 115, 135
Levinson, A.A 117, 124, 125, 127, 140
Lithian muscovites 115, 124, 125, 126
interpretation of composition 125, 126
Lithian siderophyllites 135, 140

Page

Lithium and occupied octahedral sites relation 122
and octahedral Al, relation between 119, 138
Li and Si relation 121
Li and total Al relation 121
Lithium and trivalent octahedral cations, relation 130
Li, effect on formula calculation 116
Lithium micas 115
Lithium micas, unusual 139
Lithium muscovite 118, 119
Li-(octahedral Al) replacement ratio 117, 120, 121, 122, 125, 137, 138, 140
Lithium, relation to other constituents in calculated formulas 119
Li and Fe^{+3} relation 130
Li – R^{+3} and Si relation 121
Liδ and F relation 122
Liδ content, octahedral occupancy, and structure 122

Magnesium-replacement system 115, 129
Marshall, C. E 115
Miser, H. D 139
Mixed structure 124, 126
Muscovite 116, 117, 119, 123, 124, 125, 126, 127, 128, 139, 140
Muscovite structure 118, 124

Octahedral group 115
Octahedral replacement of bivalent by trivalent cations 115
Octahedral replacement of trivalent by bivalent cations 115
Octaphyllite micas 119, 127, 129, 135

Pancilithionite 116, 119
Phengite 128
Phlogopite 115, 139
Phlogopite-taeniolite series 139
Polylithionite 116, 119, 120, 126, 127, 132, 138, 139, 140
Protolithionite 116, 127, 129, 132, 135, 138, 139, 140

Riggs, R.B 136

Schaller, W. T 124
Siderophyllite 126, 130, 131, 132, 133, 134, 137, 138, 139, 140
Siderophyllite-lepidolite isomorphous series 132
Siderophyllites and lepidomelanes 115, 134
Stevens, R. E 116, 117, 118, 124, 127, 139
Structure of aluminum lithium micas 124
polymorphic variations in 125
transition in 124

Taeniolite 116, 139
Tetrahedral group 116
Transitional samples 124
Trilithionite 119, 120, 124, 127
Trioctahedral micas 115, 119
Trisilicic-tetrasilicic series 115
Trivalent octahedral cations 130, 131, 132

Winchell, A. N 116, 117, 124, 127, 129, 135, 136

Zinnwaldite 127, 129, 132, 135, 136, 139, 140

Zones and Zonal Variations in Welded Ash Flows

By ROBERT L. SMITH

SHORTER CONTRIBUTIONS TO GENERAL GEOLOGY

GEOLOGICAL SURVEY PROFESSIONAL PAPER 354-F

A concept of zonation in ash flows based on degree of welding and type of crystallization

UNITED STATES GOVERNMENT PRINTING OFFICE, WASHINGTON : 1960

UNITED STATES DEPARTMENT OF THE INTERIOR

FRED A. SEATON, *Secretary*

GEOLOGICAL SURVEY

Thomas B. Nolan, *Director*

For sale by the Superintendent of Documents, U.S. Government Printing Office
Washington 25, D.C.

CONTENTS

	Page
Abstract	149
Introduction	149
Acknowledgments	150
Eruption and emplacement	150
Welding	151
Crystallization	151
The zones	153
Zone of no welding	154
The zones—Continued	Page
Zone of partial welding	154
Zone of dense welding	154
Zones of crystallization	155
Cooling unit	157
Composite sheet	158
Influence of buried topography	158
References cited	158

ILLUSTRATIONS

PLATE 20. Diagrams showing zones of some ash-flow cooling units ..... In pocket

21. Zones of no welding, partial welding, and dense welding, and their approximate crystalline equivalents .. Facing page 152

SHORTER CONTRIBUTIONS TO GENERAL GEOLOGY

ZONES AND ZONAL VARIATIONS IN WELDED ASH FLOWS

By Robert L. Smith

ABSTRACT

Welded tuffs are recognized as special parts of ash flows, other pyroclastic flows, or, more rarely, air-fall deposits. Ash flows may be emplaced at any temperature below a maximum eruption temperature. Those emplaced above a minimum welding temperature may show any and all degrees of welding and crystallization.

Three basic zones are recognized, the *zones of no welding, partial welding*, and *dense welding*. In sheets where the zone of dense welding occurs, the zones of no welding and partial welding will have upper and lower counterparts.

Cooling of welded ash flows may result in sheets that range from completely glassy (except for phenocrysts and inclusions) to mostly crystalline.

Crystallization superimposed on the zonal patterns produced by welding results in another set of zones that is controlled in part by degree of welding.

Three principal types of crystallization that take place during the cooling history are recognized. These in order of frequency of occurrence, are devitrification, vapor-phase crystallization, and granophyric crystallization. The *zone of devitrification* is common to most crystallized welded tuffs and frequently occupies most of the zones of dense welding and partial welding. The *zone of vapor-phase crystallization*, where present, occupies the porous parts of the welded tuff sheets and reaches its maximum development in the upper zone of partial welding where it overlaps the zone of devitrification. The *zone of granophyric crystallization* is probably confined to cooling units several hundreds of feet thick where it will divide the devitrified zone into upper and lower parts. Fumarolic alteration may be found in the upper zone of no welding.

Single ash flows may cool with the formation of a basic pattern of zones. This pattern is illustrated and described both for those sheets which remain glassy and for those in which crystallization has occurred. These flows are called *simple cooling units*.

Successive ash flows, emplaced quickly enough to bridge the cooling gap between flows, will form a stack of flows that may also cool to form the zonal pattern of a simple cooling unit. The gaps or hiatuses, here called partings, may contain or consist of lump pumice layers, flow surfaces reworked by wind or water, airfall pyroclastic material, other deposits, or minor erosional unconformities.

Compound cooling units consist of multiple flow units with or without visible partings and which show zonal patterns that depart from the patterns of the simple cooling units. Horizontal separation of compound cooling units into separate cooling units suggests the existence of a hypothetical unit, the *composite sheet*, which could have time-stratigraphic significance.

Buried topography can have a profound influence on the zonation of certain ash-flow cooling units. Very hot ones, because of their high compactability potential, will show less zonal change than colder ones, although they will show greater surface expression of the buried topography. Abrupt changes in relief, especially if the buried topographic high rises to the top of the zone of dense welding, can cause horizontal changes, in a short distance, that may be difficult to interpret.

INTRODUCTION

In this report, welded tuffs are considered to be special parts of ash flows, other pyroclastic flows, or more rarely, air-fall deposits (not to be confused with fused tuffs, p. 155). Most students of welded tuffs have recognized vertical variations of texture, specific gravity, color, mineralogy, and other properties within the deposits. Horizontal variations are rarely emphasized because complete ash-flow sheets have not been mapped, particularly in detail. Mapping of complete sheets has not been done because of the generally large areal extent of the sheets, they may be of only casual interest to the mapping problem, or because erosion, and cover by younger rocks, limits their area of exposure.

The uniform and unsorted character of ash-flow deposits has been cited as a criterion for their recognition. Although this is generally true, the complex emplacement and cooling history of many such deposits may produce various textural and mineralogical facies that bear little or no resemblance to the original materials of the ash flows. These variations are zonal and normally show a consistent pattern of transitions both vertically and horizontally in uniform ash flows which have had an unimpeded cooling history. Once this zonal pattern is clearly understood for simple cooling units, progress can be made in interpreting aberrant patterns in more complex deposits.

549220—60

The purpose of this report is to describe the zones and the simple zonal patterns by means of 4 simplified diagrams (pl. 20 *A–D*) and a brief text. The diagrams are not intended to represent specific welded ash flows but are simply hypothetical models. They were constructed to illustrate, in part, the writer's concept of simple ash-flow cooling units. The scales used give an order-of-magnitude relation among the different zones that is probably realistic for some natural sheets. The most difficult characteristics to generalize are the horizontal changes, because a cooling unit may range from less than a mile to many tens of miles in length, or from less than a square mile to hundreds and perhaps thousands of square miles in area. The true nature of the distal ends is generally problematical. They are rarely preserved or recognized in prehistoric sheets and there appears to be a wide variation in historic "nuée ardente" deposits, from "snub noses" to thin tapered ends often measurable in inches.

The diagrams were constructed based on the assumption that some cooling took place in the direction of thinning. Although this is probably a common condition it is by no means necessarily true for all flows. Some widespread ash-flow cooling units show only slight effect of cooling or thinning over tens of miles whereas others show marked effects in only a few miles. The direction of thinning may be related to the surface underlying the flow or it may reflect a change away from the source area. These facts, among others, indicate the need for a critical examination of accepted concepts on the mechanics of eruption and emplacement of ash flows.

The use of welded tuffs for correlation purposes presents many pitfalls to the geologist, but with careful work a high degree of success should be achieved. The potential importance of these rocks as stratigraphic marker beds cannot be overemphasized, considering their possible long-distance continuity in terrane where lensing and facies changes, in sedimentary and other volcanic deposits, are common.

The presentation of hypothetical diagrams without documentation leaves much to be desired. Also much of this report may seem academic concerning very young and undeformed welded ash flows. However, this study should have practical merit where applied to mapping and interpreting problems in highly deformed areas. It should also be useful in regions where ash-flow sheets from different sources overlap, and in the vicinity of some ore deposits where the geologist must locate relative spatial position within a rock body. In the vicinity of most ore deposits, alteration of different types will further complicate matters, but this difficulty may be overcome if the geologist has a clear understanding of the normal characteristics of the unaltered rocks. The zonal patterns will be extremely important for detailed geochemical studies.

ACKNOWLEDGMENTS

The writer is indebted to Clarence S. Ross with whom he has studied welded tuffs for many years and with whom he has written a more comprehensive report (Ross and Smith, 1960). Much of the material in the present report is an outgrowth of this earlier study, although the writer is solely responsible for the organization of the data and theory as presented here. The writer is especially indebted to Roy A. Bailey, also a close working companion of many years, who has been a most helpful critic. Of the many other Geological Survey colleagues who have aided the writer's studies special thanks are due C. A. Anderson and Harry W. Smedes for their constructive criticisms.

ERUPTION AND EMPLACEMENT

Much could be written about the eruption of pyroclastic materials that are emplaced as hot sheetlike bodies and whose slow cooling may result in deposits that show striking physical and chemical differences from the initially erupted material. However, the main purpose of this report is to discuss the more obvious characteristics of the deposits after they have cooled. It is well recognized that these deposits were, for the most part, emplaced as hot avalanchelike masses or particulate flows, many if not all of which contained hot gas and many of which were autoexplosive. The evidence for flowage as the principal mechanism for emplacement of these deposits has been cited by many authors; the most fundamental papers are those by Fenner (1923), Marshall (1935), and Gilbert (1938). In the present report, the basic unit of most of these deposits is referred to as an ash flow.

Ash flows can probably be emplaced at any temperature below a maximum eruption temperature. However, there will be a temperature of emplacement below which no visible physical or chemical changes will take place during cooling. This temperature may be referred to as the minimum welding temperature and will vary from place to place with changes in the variables that control the lower limit of the softening range of the glass.

Nonwelded ash flows are important, but those emplaced at temperatures above their minimum welding temperatures are of greater interest.

A single ash flow may be the only unit of cooling, or two or more ash flows, with or without intercalated air-fall beds or other partings, may combine to form

the cooling unit. A deposit that can be shown to be a *cooling unit* in one place, may by division horizontally, become two or more cooling units, separated by chill zones, air-fall pyroclastic rocks, sedimentary deposits, erosional unconformities, or lava flows. The writer will refer to this complex rock body as the *composite sheet*. The complexities inherent in such a scheme are infinite and the geologic implications will be obvious.

WELDING

The welding process must begin immediately after emplacement if the ash flow or any part of it, comes to rest above its minimum welding temperature. Welding continues until it is complete or until the process is stopped by cooling or crystallization of the glass.

In the present report welding is briefly defined as that process which promotes the union or cohesion of glassy fragments. The degree of welding may range from incipient stages marked by the sticking together or cohesion of glassy fragments at their points of contact and within the softening range of the glass to complete welding marked by the cohesion of the surfaces of glassy fragments accompanied by their deformation and the elimination of pore space, and perhaps ultimate homogenization of the glass.

Incipient welding may be recognized in some very young and fresh glassy tuffs by brittle rather than crumbly fracture, although the rock is very porous. However, this criterion is not entirely dependable because other types of induration may cause the rock to break in a similar manner.

Where the distinction between nonwelded and incipiently welded tuff is necessary, the boundary should be placed at, or close to, that point where deformation of glassy fragments becomes visible. Deformation of pumiceous fragments and shards is the only positive criterion of welding in the tuffs which have crystallized, particularly in older rocks.

Incipient welding presumably takes place in most welded tuffs before the deformation of glass fragments becomes visible, because the deformation accompanying welding is related primarily to lithostatic load pressure, especially at the lower temperatures. In practice the transition between visible deformation and obviously nonwelded tuff can be located in most tuffs within a few feet or at most a few tens of feet.

Even the sillars (Fenner, 1948, p. 883), those columnar-jointed, largely crystalline, but very porous tuffs, which are believed to be indurated by crystallization rather than by welding (Fenner, 1948, p. 883; Jenks and Goldich, 1956, p. 157), were probably incipiently welded before they crystallized. Specimens of salmon and white sillars kindly given to C. S. Ross and the writer by Fenner, are interpreted by the writer to be incipiently welded. Some of the specimens of salmon sillar show practically no crystallization but are firmly coherent. They show slight deformation of shards in thin sections and incipient compaction foliation in hand specimens. The white sillar, on the other hand, is completely crystalline and could represent salmon sillar that has crystallized in the vapor-phase zone of a cooling unit.

The sillar-type tuffs were probably emplaced at temperatures as high as that of many densely welded tuffs but the load pressure within the deposits was insufficient to cause obvious visible deformation of the glass before crystallization (white sillar) or cooling below the minimum welding temperature (salmon sillar) began. If these tuffs could be traced horizontally into thicker cooling units, the degree of welding would increase greatly.

The transition from incipient to complete welding is one of progressive loss of pore space accompanied by an increase in deformation of the shards and pumiceous fragments (pl. 21*A–F*). The progressive flattening of shards and pumice produces the streaky foliate structure long known as eutaxitic structure, which can be seen in outcrop, hand specimen, and under the microscope.

In most welded tuffs complete welding is probably achieved by simple load deformation, without stretching of particles, other than that necessary for local accommodation to available space. Crinkling or crenulation around crystal or rock fragments is common, and in many pumice-rich or inclusion-rich tuffs wavy eutaxitic foliation is normal.

Flattened pumiceous fragments, depending on their primary shape, are normally disclike in the plane of flattening. However, in some tuffs, usually in the lower part of the cooling unit, the fragments are elongate rather than disclike and show a preferred orientation. In most such examples probably some mass flowage has taken place in the sheet during welding. In welded tuffs of this kind observed by the writer, the stretching could have been accomplished by mass movement of from less than a few inches to a maximum of a few feet. Such mass flowage might be related to buried topography, earth movements during welding, or other factors, and more rarely, might be of greater magnitude.

CRYSTALLIZATION

Crystallization of the glass takes place in many ash flows subsequent to, or perhaps in part synchronous

with, the welding process. Physically and (or) chemically different environments within the cooling unit may give rise to different types of crystallization. These may, depending on the degree of their development, be recognized as distinct, although overlapping, entities, and together with the degree of welding, can be potential guides to relative position within a deposit.

Three principal categories of crystallization which may take place during cooling are recognized by the writer. In order of frequency of occurrence, these are devitrification, vapor-phase crystallization, and granophyric crystallization. Throughout the report the term "cooling-history crystallization" refers to these three types, and to fumarolic alteration unless otherwise specified. The principal categories of cooling-history crystallization may be defined as follows:

Devitrification.—Crystallization of glass to form spherulitic and axiolitic intergrowths and aggregates, chiefly of cristobalite and feldspar. This crystallization is confined within glass fragments or massive glass. It is common to all crystallized silicic welded tuffs.

Vapor-phase crystallization.—The growth of crystals, from a vapor phase, in pore spaces. Vapor-phase crystallization is, in general, a coarser grained crystallization than devitrification, and is commonly manifest in the porous upper parts of welded ash flows where it is contemporary with, or follows, devitrification. In rhyolitic ash flows the predominant vapor-phase minerals are alkalic feldspar, tridymite, and cristobalite.

Granophyric crystallization.—In silicic welded tuffs granophyric crystallization is characterized by groundmass quartz intergrown with, or as blebs associated with, alkalic feldspar and minor accessory minerals. The aggregate shows granophyric or micrographic textures similar to those shown by many slowly cooled rhyolitic flows, domes, and shallow intrusive rocks.

Granophyric crystallization (quartz) has never been seen by the writer in fresh unaltered welded tuffs that were less than about 600 feet thick. However, many older deposits and ultimately all deposits will probably contain quartz as the groundmass silica mineral, through conversion of critobalite and tridymite.

A fourth category of cooling-history crystallization or, probably more precisely, alteration, should be rec-

---

EXPLANATION OF PLATE 21

ZONES OF NO WELDING, PARTIAL WELDING, AND DENSE WELDING, AND THEIR APPROXIMATE CRYSTALLINE EQUIVALENTS

Specimens *A–F* show transition from zone of no welding to zone of dense welding. Specimens *G–L* show approximate crystalline equivalents in zones of partial welding and dense welding. *A–E*, from Battleship Rock, Jemez Springs quadrangle; *G–I*, from the Bandelier rhyolite tuff (Smith, 1938), Jemez Mountains, N. Mex.

A. Zone of no welding. Pumice blocks and lapilli in an unconsolidated ashy matrix. Some accidental rock fragments.

B. Zone of partial welding (upper part of upper zone). Shows incipient compaction foliation. Fracture takes place through, rather than around pumice fragments. Matrix ash more gray than in *A*.

C. Zone of partial welding (upper zone). Compaction foliation well developed, pumice fragments darker with less pore space and more vitreous luster than in *B*. By contrast, the ashy matrix still has a dull luster and hackly fracture.

D. Zone of partial welding (lower part of upper zone). Collapsed pumice lenticles and matrix ash have vitreous luster and conchoidal fracture although pore space is still about 20 percent.

E. Zone of partial welding (near transition to zone of dense welding). Collapsed pumice lenticles obsidianlike without pores although traces of former vesicles can still be seen in thin section.

F. Zone of dense welding. Dense black obsidianlike glass of virtually zero porosity. Collapsed pumice fragments only faintly visible in hand specimen. Their boundaries are visible in thin section but former vesicular structures have been partly to completely homogenized by welding. From km 153, Taxco Highway, Central Mexico. Collected by Carl Fries, Jr.

G. Vapor-phase zone (upper part of upper zone of partial welding). Slight compaction foliation; completely devitrified. Pumice fragments crystallized into drusy growths of tridymite and alkalic feldspar and some cristobalite. The pumice-tube structure is well preserved. Approximate crystalline equivalent to *B*. Very similar, except for fragment size, to white ash described by Fenner.

H. Vapor-phase zone (upper zone of partial welding). Compaction foliation well developed. Pumice-tube structure not as well preserved in this plane, but very obvious in the plane of flattening. Approximate crystalline equivalent to *C*.

I. Devitrified zone (zone of dense welding). Some collapsed pumice fragments visible. In thin section this specimen shows coarse axiolitic devitrification.

J. Devitrified zone near base (zone of dense welding). Fine-grained devitrification of a dense black glass. Only faint traces of original pyroclastic character preserved in hand specimen. Perfect preservation of shards and flattened pumice fragments in thin section. Crystalline equivalent to *F*. Matahina ash flow, Rangitaiki Gorge, North Island, New Zealand. Collected by R. A. Bailey.

K. Specimen showing the effect of gas trapped during welding. The rock belongs in the zone of dense welding but the collapsed pumice fragments are miarolitic and coarsely crystalline. From the lower part of Enlows' (1955) member 6, Rhyolite Canyon formation, Bonita Canyon, Chiricahua National Monument, Ariz.

L. Lithophysal cavities in the devitrified zone of dense welding. This rock is composed of fine-grained pyroclastic materials which probably caused lithophysae to form instead of miarolitic cavities in pumice fragments. From the Ammon quadrangle, Idaho.

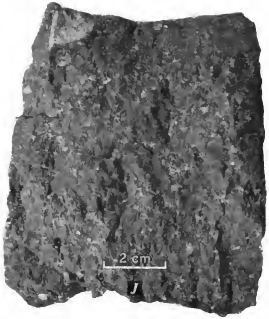
2 cm
J

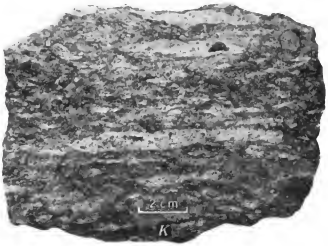
2 cm
K

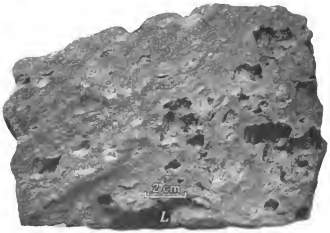
2 cm
L

Digitized by Google

ognizable in many deposits. This little-studied and generally unrecognized (in older deposits) process is fumarolic alteration. Some geologists may argue that this process is not basically different from vapor-phase crystallization, but the products are notably different and, generally belong to lower temperature and pressure environments.

Devitrification of the glass after initial cooling, and other forms of low-grade alteration need much discussion, but these should be considered in well-documented papers. Correct interpretation of cooling-history processes is obstructed by post-cooling-history, hydration, devitrification or other alteration of glass, oxidation of iron, and conversion of tridymite and cristobalite to opal, chalcedony, or quartz, and related processes. Some of these processes take place during as well as after cooling, and the knowledge necessary to always distinguish between the two has not yet been acquired. In Pleistocene and Recent rocks the problems are minor or nonexistent, but in some Pliocene and in most Miocene and older formations many physical and chemical properties of the rocks seem to have been affected by processes that occurred after cooling. Depth of burial and ground-water conditions are extremely important factors. Many geologists consider these altered rocks to be fresh and unaltered.

These alteration effects are often of regional extent and can best be interpreted as low-grade metamorphic reactions.

THE ZONES

All ash flows in which welding or crystallization have taken place show zonal variations in texture, color, or other features. These variations are dependent upon such factors as temperature, thickness of the deposit, composition of the ash, amount and composition of volatile constituents, and the ratio of pumice fragments to shards.

Any system that includes several variables where one variable can change the entire appearance of a rock body, or any part of it, is a very flexible system, and must be treated as such. The chance that two or more welded ash flows will show no differences as a whole is extremely slight. On the other hand, the close similarities that commonly exist between some welded ash flows may be confusing and it may be impossible to distinguish between their equivalent zonal facies. Differentiation may then be dependent upon detailed petrographic studies of phenocrystic minerals coupled with careful field study.

The zones shown in plate 20 are those which can be easily recognized or inferred in the field. Recognition of minor zones depends on the microscopic study; they are briefly mentioned in the following discussions of the individual major zones. All zone boundaries are transitional, some more abruptly than others. In general the boundaries of the basal zones are more sharply defined than those of the upper zones.

The ordered sequence of overlapping zones is best visualized by examining first the zones formed during the welding process without crystallization upon cooling. If welding proceeds to completion in any part of an ash flow, three distinct zones will be formed. These are the *zone of no welding*, the *zone of partial welding*, and the *zone of dense welding* (pl. 20 *A*,*B*). The *upper* zones of no welding and partial welding will be separated from the *lower* zones of no welding and partial welding by the zone of dense welding. Where sufficient lateral thinning of the ash flow occurs, such as the normal distal ends and margins, points will be reached where the upper and lower zones of partial welding will merge and grade into the nonwelded mantle of the deposit.

This simple pattern of zones is illustrated in plate 20*A* and *B*. Plate 20*B* shows the zonal relations in an extremely hot and moderately thin ash flow whereas plate 20*A* shows the zonal relations in a thicker ash flow emplaced at much lower temperature. Plate 20*B* also shows an additional zone which represents an early stage of crystallization. This additional zone in no way affects the comparison of the other zones illustrated in plate 20*A* and *B*. An ash flow emplaced at a temperature too low for welding is not shown, but is represented by the nonwelded mantle (pl. 20*A*). All transitions between this low-temperature extreme and the hot, densely welded type shown in plate 20*B* can occur. However, as temperature and thickness are increased together, a point will be reached where crystallization begins; thus the type of tuff illustrated in plate 20*B* can never reach great thickness and remain glassy throughout during cooling.

The glass of densely welded tuff that is of the order of thickness shown in plate 20*A* and *B* will probably be charged with spherulites or lithophysae or both, although these may vary in number and character with the initial gas content.

Crystallization usually follows, but may in part, accompany the welding process. This crystallization may occur in a narrow zone confined to the deep interior of the cooling unit or as a broad zone which may overlap, horizontally at least, all other zones formed during welding. All transitions between the two extremes may occur.

The character of crystallization is strongly influenced by the degree of welding of that part of the tuff upon which it is superimposed, the rate of cooling of the ash flow, and the amount and composition of vola-

tile materials that it contains. Differences in character of crystallization, then, add another set of zones controlled in part by the zones already formed during welding, and in part by other factors.

ZONE OF NO WELDING

The *zone of no welding* is that part of an ash flow in which no welding has taken place (pl. 21*A*). This zone may comprise the entire ash flow or only a small part. Most single ash-flow cooling units have a nonwelded top and bottom (pl. 20*A*), although in some of the very hot flows the nonwelded bottom may not be present under the entire sheet (pl. 20*B* and *C*). In these very hot ash flows densely or partly welded tuff may extend to the base of the unit, especially near the source area.

The nonwelded zone will probably contain some incipiently welded tuff, especially in the crystalline units, because as mentioned on page 151, the only practical way to locate the zone boundary is by megascopic detection of deformation or compaction foliation. Incipient welding occurs at some point before this.

The nonwelded zone is commonly the least spectacular part of a welded ash flow, but is probably the most important zone because it is the only one that shows the original character of the erupted materials. Its preservation is necessary to such measurements as initial density and porosity, size analyses, and to the nature of the primary glass. For the most accurate characterization of the magma, chemical analyses should be made of pumice from this zone (pl. 21*A*), providing that the rocks are fresh and the pumice is not foreign material. Most middle to early Tertiary and apparently all known pre-Cretaceous ash-flow tuffs show some alteration in this zone beyond simple hydration of the glass and are not too helpful in understanding the chemistry of the primary magma.

ZONE OF PARTIAL WELDING

The *zone of partial welding* includes all material ranging from that which shows incipient welding to that which has lost virtually all its pore space (pl. 21*B–E*). This zone shows a greater diversity of textures than any of the other zones because of the wide range in porosity and degree of deformation of its glassy parts. The boundary between the zones of partial and dense welding is discussed below.

Further subdivision of the zone might have practical application in some welded ash flows. For example, a measure of the degree of collapse of pumice fragments can be an important factor in determining the relative vertical position of material in the sheet.

In some cooling units the upper zone of partial welding may extend horizontally for many miles without much apparent change in thickness as long as it is underlain by a zone of dense welding.

The zone of partial welding is best developed in colder ash flows (pl. 20*A*) and is poorly developed in very hot ash flows (pl. 20*B*). The thickness of this zone is therefore, in a general way, an index of the emplacement temperature of the ash flows.

ZONE OF DENSE WELDING

Ideally the *zone of dense welding* should be defined as that zone in which complete coalescence of the glassy fragments has resulted in the elimination of all pore space. A dense black glass or vitrophyre is the normal product of this process (pl. 21*F*). Actually it will be a rare welded tuff that is completely pore free, exclusive of the *vitrophyre zone* in some sheets, because of processes other than welding that help determine the final character of the rock. Entrapped or exsolved gas, for example, causing the formation of lithophysal (pl. 21*L*) or other types of cavities, may inhibit complete loss of pore space in this zone during welding. However, in the groundmass surrounding these porous areas, complete welding of the shards will show that the rock is in the zone of dense welding. The boundary between the zone of dense welding and the upper zone of partial welding marks a plane below which the rock is pore free, or potentially pore free were it not for entrapped gas, and above which the rock would be porous, with or without gas entrapment. Crystallization of a pore-free glass may result in a slightly porous rock. All these factors must be considered in distinguishing the zone of dense welding from the zone of partial welding.

If the welded tuff remains glassy upon cooling, all the zones and zonal transitions are generally well defined and simple, although in the simple cooling units the transitions above the zone of dense welding are less sharply defined than those below. However, when crystallization takes place, the upper transitions may become obscure, and the exact location of the zone boundaries in some sheets will be largely subjective, particularly in crystal-rich quartz latites and rhyodacites.

The transition from partial to dense welding in glassy welded tuffs is best shown by changes in the pumice fragments present in most ash flows. In fresh rocks and those that have had a simple cooling history, the pumiceous fragments and blocks change by decreasing porosity and a general darkening of color until they become black and obsidianlike (pl. 21*A–F*).

The darkening of the pumiceous fragments precedes the darkening of the shardy matrix. For field purposes the end stage of the welding process is a dense black glass in which the pumiceous fragments and the matrix are megascopically indistinguishable.

Complete welding is not achieved until the pumiceous fragments, shards, and glass dust are homogenized; all grain boundaries disappear and, exclusive of crystals and inclusions, a completely homogenous glass is formed. This *zone of homogenization* can only be proven by microscopic study in conjunction with field study, and will be found only rarely, probably for the following reasons: (a) In ash flows initially thin enough or cold enough to remain uncrystallized after cooling, temperatures and pressures high enough to cause homogenization of the glass particles are rare; (b) in thick cooling units where a zone of complete homogenization might occur, this zone will likely crystallize on cooling and may be indistinguishable from nonhomogenized welded tuff whose vitroclastic structure has been obliterated by crystallization. Partial homogenization of tube structures in pumice fragments is common in some glassy welded tuffs but complete homogenization is rare. Tube structures refer to tubular vesicles which are more common than spherical vesicles in pumice from tuffs of silicic composition. These tubes are sometimes so fine that they present a fibrous appearance and cause the pumice to have a silky luster. The writer has never seen complete obliteration of shard boundaries in glassy rocks but it will no doubt be found, and it is for this reason that the point of homogenization is emphasized.

The vitrophyre zone generally shows a transition downward through a partly welded zone to a nonwelded base which may range from almost zero to many feet in thickness. However, some flows were emplaced at such high temperature that the vitrophyre zone extends to the base of the cooling unit and, in some vertical sections, may extend below the base of the unit as a fused zone in underlying glassy pyroclastic deposits (pl. 20*D*). This fused selvage will probably never be more than a few feet thick. If the underlying material is bedded ash, the bedding may still be preserved in the vitrophyre. An excellent example of this basal fusion has been described by Boyd.[1]

The vitrophyre zone (pl. 20*C* and *D*) is often the most useful part of a cooling unit for mapping purposes, especially in complexly faulted rocks, as it provides a useful marker unit.

[1] Boyd, F. R., 1957, Geology of the Yellowstone rhyolite plateau: Ph. D. thesis, Harvard Univ., 134 p.

ZONES OF CRYSTALLIZATION

A large proportion of welded ash flows have crystallized to some degree upon cooling. Crystallization may be incipient or intensely pervasive. Incipient crystallization may be marked by growths of minute spherulites in the zone of dense welding, or by the presence of vapor-phase or fumarolic minerals in scattered fine-grained growths in the upper porous zones. Crystallization may also be so extensive throughout the cooling unit that only a very thin chilled base, top, and distal end of the unit will remain glassy after cooling. Crystallization in most welded ash flows will fall somewhere between the two extremes (pl. 20*C*).

Devitrification is the most common crystallization process and in most cooling units the products of devitrification will be present throughout the entire crystalline zone. However, in some porous rocks these products will be subordinate to those of vapor-phase crystallization because of intense vapor-phase activity.

In rhyolitic tuffs, devitrification consists of the simultaneous crystallization of cristobalite and alkalic feldspar to form submicroscopic spherulitic and axiolitic intergrowths of these minerals plus minor accessory minerals. This devitrification process is confined within shards or glass masses, whereas crystallization by growth of crystals into pore spaces is a different process related to the movement of vapors and transfer of material. Without pore space, vapor-phase crystallization cannot take place. Thus in densely welded tuff that has not entrapped large quantities of gas, devitrification is the dominant and commonly the only process of crystallization. For this reason the writer refers to the crystallized part of the zone of dense welding as the *devitrified zone* (pl. 21*I* and *J*). The crystalline porous zone is referred to as the *vapor-phase zone* (pl. 21*G* and *H*), if it contains crystal growths in the pore spaces, or if it is probable that it had crystal growths in the pore spaces.

The ideal boundary between that part of the zone of devitrification that contains the vapor-phase zone, and that part in which the vapor phase does not occur is the boundary between the zone of dense welding and the upper zone of partial welding (pl. 20*C*). The abrupt appearance of the lower boundary of the vapor-phase zone will depend on the sharpness of transition between the glassy zones before crystallization. In some tuffs this transition may take place within a few feet, whereas in others it may be so broad that it may be difficult to detect at all.

Some of the features that may mark this transition are: (a) The upward appearance of vapor-phase minerals; (b) a visible upward increase in porosity; (c)

a downward change in color or shading of color from light to dark; (d) a downward change from coarse to fine joint spacing; and (e) the zone of dense welding is usually a better cliff former in crystalline tuffs.

Curves derived from density or porosity measurements of vertical sections of simple cooling units may sometimes show that a porosity gradient exists in the zone of dense welding. Ideally the porosity of a vertical section of a cooling unit should show no change in the zone of dense welding. However, the ideal is not usually achieved except in the vitrophyre zone or in the basal part of some devitrified zones. Thus in some cooling units, there is a slight, perhaps irregular, but steady increase in porosity upward from a point near the base of the devitrified zone to the top of the zone of dense welding. Above this point the porosity increases more rapidly and the transition is marked on porosity curves by a change in slope of the curve. The writer suggests that where this porosity gradient does exist in the zone of dense welding, it reflects a lithostatic pressure gradient, but exists owing to the direct or indirect effects of entrapped gas that acted as a deterrent to uniform completion of the welding process.

Thick hot gas-rich ash flows may weld so fast that gas is entrapped throughout all but a relatively thin basal zone. Pumice fragments commonly serve as loci for the entrapped gas, and crystallization of these gives rise to streaky eutaxitic folia, some of which are cavernous and more coarsely crystalline than the densely welded groundmass shards surrounding them (pl. 21*K*). Unless these tuffs are very young and fresh, it may be difficult or impossible to differentiate between the vapor-phase crystallization around the entrapped-gas cavities and the true continuous vapor-phase zone above the zone of dense welding. Thus in some ash-flow cooling units recognition of the vapor-phase zone may be of questionable importance. However, in others differentiation of the vapor-phaze zone, from vapor-phase crystallization in lenticular or lithophysal cavities in the zone of dense welding, may be highly important for the following reasons: (a) Stratigraphic significance; (b) petrologic and mineralogic interest; (c) because this zone is one of active rising vapors and it is here that changes may take place in chemical composition due to vapor-phase transfer of materials. Preliminary investigations indicate that appreciable chemical differences (in both major and minor elements) may be found between this and other zones.

Mafic phenocrysts, especially biotite, hornblende, and orthopyroxene, are commonly in part or wholly destroyed by the crystallization processes. Their former presence may be confirmed by the distribution of opaque oxides, relicts, and their existence in the vitric zones. In extreme examples a new generation of mafic minerals may be formed (biotite, amphibole, fayalite, and others).

In fresh rhyolitic rocks the appearance of tridymite with drusy feldspar usually indicates the presence of a vapor-phase zone (pl. 21*G* and *H*). Commonly these crystal druses are localized in pumice fragments and show varying degrees of lenticularity depending on the amount of flattening of the pumice fragment during welding. The former pumice-tube structures are often preserved in these crystal aggregates and can be seen in the field by the unaided eye. In older or less fresh rocks (middle Tertiary and older) these vapor-phase crystals have commonly been replaced by opal, chalcedony, quartz or other minerals and their original structure may no longer be recognizable.

The writer believes that most of the groundmass quartz that is seen in some welded tuffs is probably secondary, having formed through the conversion of cristobalite or tridymite by diagenetic or low-grade metamorphic processes. However, sometimes quartz is seen deep in the interior of the devitrified zone of very thick ash-flow cooling units, where it is probably primary in the sense that it formed during the cooling history of the cooling unit. The textures formed are similar to those seen in granophyric rocks. Conditions might exist within very hot thick ash flows where quartz would form in preference to cristobalite as the groundmass silica mineral, or early formed cristobalite might be converted to quartz during later stages of cooling. This would give rise to a *zone of granophyric crystallization* separating the devitrified zone into upper and lower parts.

Poor preservation or complete obliteration of vitroclastic textures might be expected in very thick cooling units. Several variables are involved hence the minimum thickness of tuff necessary for the formation of this zone is problematical. The writer has never seen what he would interpret to be primary groundmass quartz in any welded tuff unit less than about 600 feet thick.

Speculation on the probable nature of a very hot gas-rich cooling unit that is 2,000 feet or more thick seems warranted. No doubt thicknesses of this magnitude will be found. Welding would be almost instantaneous throughout most of the sheet and much gas would be entrapped. Slow cooling could be expected and a long stage of deuteric activity would produce a granophyric groundmass in which former pyroclastic textures could be completely destroyed.

Without excellent exposures to reveal the contact relations, such a rock body could easily be interpreted

as an intrusive mass. Even the contacts might be expected to show injection phenomena. Some ash flows are hot enough to cause fusion of underlying glassy ash or to weld almost completely against low porosity rocks that are relatively fast heat conductors. Such welded material under high load could inject cracks and crevices. Crystallization might also extend to the base of such a rock body. The zone of granophyric crystallization might then occupy a large proportion of the cooling unit.

Any ash flow that contains hot gas or is emplaced at a temperature high enough to crystallize on cooling should give off gas at its surface. The amount, composition, and temperature of this gas, along with other factors, will determine the degree of alteration of the surface and upper parts of the deposit including joint cracks. By this reasoning, and by analogy with historic ash-flow deposits such as the Valley of Ten Thousand Smokes (Zies, 1929, p. 1–79) and the Komagatake deposits (Kozu, 1934, p. 164–174), many ash flows should show a *zone of fumarolic alteration* transitional with the vapor-phase zone and with, perhaps, more intense alteration localized by deep joints. Surface sublimates and some near-surface alteration products are probably rapidly reworked by water entering the deposits. Some are no doubt removed entirely, but others are probably lodged in the soft tops of the cooling units.

Where these ash-flow tops are preserved in rocks of silicic composition, pale but decidedly variegated color patterns may indicate the presence of former fumarolic activity. These color patterns are in contrast to the uniform chalky white, gray, pink, lavendar, red, brown, or purplish groundmass colors of the vapor-phase zone. Mild fumarolic alteration has been recognized in prehistoric deposits by Gilbert (1938, p. 1851–1854), Williams (1942, p. 86–87), and Mackin (1952, p. 1337–1338).

COOLING UNIT

Unimpeded cooling of ash flows emplaced above the minimum welding temperature results in a deposit that shows a pattern of zones resembling closely (a) plate 20*A*, *B*, or *C*; (b) some intermediate stage between the diagrams; or (c) a vertical segment of these diagrams or intermediate stages. Such deposits may be called *simple cooling units*. Multiple flow units may also form a simple cooling unit provided they are emplaced in such rapid succession that there is no hiatus in cooling which cannot be bridged by successive flows (pl. 20*D*).

In a given vertical section of a simple cooling unit it may be impossible to distinguish between flow units, and the recognition of partings between them may only be possible because of horizontal changes in the sheet. Partings that exist in the nonwelded and partly welded zones will probably be easily seen. However, those occurring in the densely welded zone, especially after crystallization, may be invisible for many miles, depending on the characteristics of the partings.

Partings between successive ash flows within a single cooling unit may be marked by the following: (a) Concentrations of lump pumice; (b) fine- to coarse-bedded air-fall ash, lapilli, or blocks; (c) bedded ash from a reworking of the surface of the ash flow by wind or water; and (d) minor erosional unconformities. In the absence of these criteria, the ash flows may in places be distinguished on the basis of abrupt changes in their physical or chemical makeup. Such properties as grain size, phenocryst ratios, chemical or mineralogical composition, color and inclusions should be considered. In some densely welded tuffs where partings between ash flows are obscure, preferential weathering or slight irregularities in density or porosity may suggest their presence. Any, all, or none of these highly variable factors may be significant in a simple cooling unit.

Pronounced deviations in the pattern of zones as outlined for simple cooling units seem to indicate breaks in the cooling history of given cooling units and suggest compound cooling. These *compound cooling units* can show infinite variation between simple cooling units and separate cooling units. In other words, a simple cooling unit may, by horizontal gradation, become a compound cooling unit which, in turn, may grade into two or more simple or compound cooling units.

A few of the more obvious features that suggest compound cooling are: (a) Reversal of relative thickness of upper and lower zone of partial welding; (b) extensive development of vapor-phase zone below a devitrified zone of dense welding with a transitional contact between the two zones; (c) basal nonwelded zone which is many times thicker than overlying zones; (d) visible reversals in density or porosity within the zones of welding exclusive of those related to differing mineral facies; (e) extensive development of columnar joints below a zone of dense welding.

Some of the factors contributing to compound cooling are: (a) Unequal areal distribution of individual ash flows; (b) degree of development of some of the phenomena which cause the partings listed above; (c) successive emplacement of ash flows of radically different temperatures; and (d) periodicity of eruptions.

The cooling unit, either simple or compound, is probably the logical map unit in most unmetamorphosed

rocks. It is a closely limited time unit as well as a genetic rock unit. Distinguishing between individual flow units is generally not practical and is impossible in many situations. In many areas, mapping of at least the more spectacular zones of the cooling unit is practical, and in detailed studies, recognition and mapping of the zones as integral parts of a unit may help solve many problems of structure and stratigraphy.

COMPOSITE SHEET

A hypothetical unit, the *composite sheet*, is discussed because its existence seems inevitable now that many of the diverse characteristics of the cooling units are known. The writer has examined ash-flow deposits which can be explained only on the assumption that they are part of a unit of higher rank than the cooling units. The evidence consists of observed horizontal change of compound cooling units into separate cooling units. That is, the composite sheet is composed of cooling units that may range horizontally through any or every stage from a single- or multiple-flow simple cooling unit, multiple-flow compound cooling unit, to cooling units that are separated by erosional unconformities, other volcanic or sedimentary deposits, or local hiatuses in time sufficient to allow cooling of one unit before another is emplaced on top of it. Detailed mapping for documentation of this concept is necessary.

At any given time during its emplacement cycle the composite sheet is visualized as undergoing continuous cooling throughout some of its few tens to few thousands of square miles of area. The merging or overlap of composite sheets or cooling units from different source areas would give rise to many complexities. The time-stratigraphic importance of such a relation might be very great, especially if air-fall deposits can be related to the ash-flow sheets.

INFLUENCE OF BURIED TOPOGRAPHY

The zonal variations expected to occur where a simple cooling unit is superimposed on a high or low feature in the underlying topography are shown in plate 20*D*. The effects are the same as would be expected from normal horizontal thinning or thickening, but the changes are more abrupt.

The changes due to buried topography may be striking in regions of high relief, but in regions of low relief they are more subtle. For example, the distribution of outcrops of a persistent dense glass zone may suddenly become erratic. One explanation might be that the cooling unit was emplaced on an irregular surface such that the tops of the buried topographic high areas were roughly coincident with the level in the cooling unit that marks the transition from the zone of dense welding to the upper zone of partial welding. A dense black glass could not form over any topographic high that reached this transition level. In sheets of this type, buried topography will also be reflected by gentle irregularities in the surface of the cooling unit.

Other variables being equal, the thickness of the cooling unit (producing load pressure) at any point controls the amount and degree of welding at that point. Thus the percent of total compaction will be greater in the thicker parts of the unit, and it is this differential compaction that results in surface expression of buried topography. If two cooling units of equal emplacement thickness are of different compactability, the one with the higher compactability will show the more irregular surface over equivalent buried topography.

By careful consideration of plate 20*D*, the effect of buried topography can be predicted for other zones and different topographic environments. The extreme abruptness of changes in the cooling-unit surface and the zones as shown in plate 20*D* is due to the vertical exaggeration of the projection.

Some cooling units (map units) can change abruptly over a buried escarpment, resulting in thick welded tuff on one side and a thinner nonwelded or only partly welded tuff on the other. As shown in plate 20*D*, the thick side of the buried escarpment contains a vitrophyre zone and a devitrified zone of dense welding, whereas the other side is predominantly a "sillar" type of tuff (p. 151). If such a situation as this were to be found in deformed and eroded terrane, with poor exposures, the chances of correct interpretation would probably be small even for experienced geologists. It would present difficulties even under ideal field conditions. Infinite variation is possible, especially if compound cooling or composite sheet effects are involved.

REFERENCES CITED

Enlows, H. E., 1955, Welded tuffs of Chiricahua National Monument, Arizona: Geol. Soc. America Bull., v. 66, no. 10, p. 1215–1246.

Fenner, C. N., 1923, The origin and mode of emplacement of the great tuff deposit in the Valley of Ten Thousand Smokes: Natl. Geog. Soc., Contr. Tech. Papers, Katmai ser., v. 1, no. 1, 74 p.

——— 1948, Incandescent tuff flows in southern Peru: Geol. Soc. America Bull., v. 59, no. 9, p. 879–893.

Gilbert, C. M., 1938, Welded tuff in eastern California: Geol. Soc. America Bull., v. 49, no. 12, p. 1829–1862.

Jenks, W. F., and Goldich, S. S., 1956, Rhyolitic tuff flows in southern Peru: Jour. Geology, v. 64, p. 156–172.

Kozu, Shukusuke, 1934, The great activity of Komagatake in 1929: Tschermaks mineralog. petrog. Mitt., v. 45, p. 133–174.

Mackin, J. H., 1952, Hematite veinlets in an ignimbrite in the Iron Springs district, southwestern Utah [abs.]: Geol. Soc. America Bull., v. 63, no. 12, pt. 2, p. 1337–1338.

Marshall, Patrick, 1935, Acid rocks of Taupo-Rotorua volcanic district: Royal Soc. New Zealand trans., v. 64, p. 323–375.

Ross, C. S., and Smith, R. L., 1960, Ash-flow tuffs: their origin, geologic relations, and identification: U.S. Geol. Survey Prof. Paper 366, in press.

Smith, H. T. U., 1938, Tertiary geology of the Abiquiu quadrangle, New Mexico: Jour. Geology, v. 46, p. 933–965.

Williams, Howel, 1942, The geology of Crater Lake National Park, Oregon, with a reconnaissance of the Cascade Range southward to Mount Shasta: Carnegie Inst. Washington Pub. 540, 162 p.

Zies, E. G., 1929, The Valley of Ten Thousand Smokes; 1, The fumarolic incrustations and their bearing on ore deposition; 2, The acid gases contributed to the sea during volcanic activity: Natl. Geog. Soc., Contr. Tech. Papers, Katmai ser., v. 1, no. 4, 79 p.

○

Deposition of Uranium in Salt-Pan Basins

By KENNETH G. BELL

SHORTER CONTRIBUTIONS TO GENERAL GEOLOGY

GEOLOGICAL SURVEY PROFESSIONAL PAPER 354-G

Prepared on behalf of the United States Atomic Energy Commission and published with permission of the Commission

UNITED STATES GOVERNMENT PRINTING OFFICE, WASHINGTON : 1960

UNITED STATES DEPARTMENT OF THE INTERIOR

FRED A. SEATON, *Secretary*

GEOLOGICAL SURVEY

Thomas B. Nolan, *Director*

For sale by the Superintendent of Documents, U.S. Government Printing Office
Washington 25, D.C. - Price 20 cents (paper cover)

CONTENTS

	Page
Abstract	161
Introduction	161
Uranium in evaporite minerals and deposits	162
Summary	169
Literature cited	169

TABLES

	Page
TABLE 1. Uranium content of typical deposits of anhydrite and gypsum	164
2. Chemical and mineralogic determinations on samples from a drill core of an evaporite deposit	166
3. Uranium contents of euxenic dark shales and enclosing dolomites and anhydrite for the Paradox basin	168

DEPOSITION OF URANIUM IN SALT-PAN BASINS

By Kenneth G. Bell

ABSTRACT

Drainage waters carry minute quantities of uranium into oceans, inland seas, and lakes, and when bodies of water evaporate completely in desiccating salt-pan basins, the uranium must be deposited together with all other dissolved materials. The ratio of uranium to total evaporite sediments is approximately $1:2 \times 10^7$. The distribution of uranium in salt-pan basin sediments is not completely known. Some organic-rich muds, and phosphatic sediments deposited in desiccating basins may contain uranium in amounts as large as 0.0X percent. Uranium may be adsorbed on clays that are deposited with some evaporite sediments. These muds, phosphatic sediments, and clays may remove nearly all of the dissolved uranium from the water of some basins. Anhydrite, gypsum, halite, and potassium-bearing evaporite minerals probably are the least uraniferous of all rocks in the earth's crust; their uranium contents generally are less than 0.00001 percent. Within salt-pan basins where oxidizing conditions tend to prevail, and no significant amounts of organic-rich muds, clays, and phosphatic sediments are deposited, highly soluble uranium salts remain in solution and are deposited only as the basin finally is completely desiccated. These final highly soluble evaporite sediments are not likely to be preserved because they are subject to removal by wind erosion and leaching.

INTRODUCTION

Waters draining lands commonly carry minute amounts of dissolved uranium. Unless drainage waters have traversed highly uraniferous terranes, their contents of uranium generally are fractions of a part per billion (Fix, 1956; Judson and Osmond, 1955; Adams, 1954; Rona and Urry, 1952). This uranium is carried into lakes, inland seas, and the oceans.

Ocean water contains traces of uranium; the amounts vary slightly, depending upon total salinity, depth, and position with respect to shore line. Uranium contents ranging from 0.36 to 3.5 parts per billion (ppb), oil 0.36 to 3.5×10^{-9}, for ocean water from different localities have been reported by various authors (Hernegger and Karlik, 1935; Föyn and others, 1939; Koczy, 1950; Nakanishi, 1952; Rona and Urry, 1952; Stewart and Bentley, 1954; Rona and others, 1956). There are few published data on the uranium contents of waters from saline lakes and inland seas. Stewart and Bentley (1954) have reported uranium contents of 4.7 to 5.3 micrograms per liter (4.7 to 5.3 ppb) in water samples from Great Salt Lake, Utah. Some samples from the Salton Sea, Calif., that were analyzed in the U.S. Geological Survey laboratories contained about 10 ppb of uranium (Butler, A. P., Jr., written communication, 1947). Tourtelot (1955) has stated that highly alkaline water from lakes in western Nebraska contains 12 to 100 ppb of uranium. The concentration of uranium in ocean water is about a 10-fold increase over that in drainage waters, and the concentration in some saline lake waters is greater.

The amount of uranium that can be deposited within a salt-pan basin normally is very small. If the figure of 0.1 ppb, indicated by Fix (1956) to be approximately the average uranium content for water of major streams in the United States, is considered to represent drainage waters in general, then 10 billion tons, or 7.4 million acre-feet, of water must evaporate for each ton of uranium deposited during complete desiccation. An approximate comparison between the amount of uranium and the total amount of evaporite sediments that can be deposited from a given volume of water can be obtained by considering the composition of the ocean. If the quantity of 35 grams per kilogram (35,000,000 ppb) for the total salinity of ocean water (Sverdrup and others, 1942, p. 176–177 and 219) and a uranium content of 1.5 ppb are used, and desiccation is assumed to be complete, a simple calculation shows that for every ton of uranium deposited about 23 million tons of evaporite sediments are deposited. If the uranium is assumed to be uniformly distributed in the evaporite sediments the content would be less than 0.00001 percent.

If an undrained basin that initially held a lake, an inland sea, or a detached body of ocean water becomes completely desiccated, all the dissolved material is deposited, mostly in the form of saline or evaporite sediments; a minute portion of the dissolved matter may be adsorbed on clastic and organic sediments. Uni-

form, uninterrupted desiccation would cause progressive deposition of the most abundant minerals in the general sequence: calcium carbonate (as calcite or limestone) and calcium phosphate (as forms of apatite or dispersed in other minerals), calcium sulfate (as gypsum and anhydrite), sodium chloride (as halite), potassium chloride (as sylvite), and magnesium chlorides and sulfates; other less abundant minerals may be deposited. This idealized sequence rarely is obtained because desiccation generally is neither uniform nor uninterrupted; cyclic repetition of parts of the sequence may occur many times, mainly because of influxes of water into the basin. An important result of influxes of water is the increasingly high concentration of very soluble salts in the residual liquid as desiccation reduces the volume and causes precipitation of slightly and moderately soluble salts (evaporite minerals); the influxes also may bring substantial amounts of detrital and organic sediments into the basin. Complete desiccation can be expected to result in deposition of a final, uppermost thin layer containing the most soluble evaporite minerals.

Some minerals and compounds in an evaporite sequence may be intermixed to a considerable degree. Calcium phosphate is likely to be dispersed in calcite (or limestone). Calcite and gypsum or anhydrite may be intimately mixed or occur in alternating, thin, relatively pure layers. Sylvite commonly is mixed with halite. After desiccation has ceased, redistribution of material may result in the formation of secondary minerals that may be intermixed with the primary minerals; polyhalite, carnallite, and other minerals that are double salts may be formed in this manner. Redistribution of material may tend to concentrate some elements in thin zones. The physical chemistry of the formation of evaporite minerals, both during and after desiccation, is not fully known.

There is no analytical evidence that conclusively indicates that uranium minerals are deposited from saline water simultaneously with anhydrite, gypsum, halite, sylvite, and other minerals of similar solubility. As desiccation proceeds and minerals of increasing solubility are deposited, the concentration of uranium in the water should increase, and uranium minerals should be deposited with the final, most soluble evaporite minerals. Clays, shales, and organic sediments that are interbedded with some evaporite sediments commonly contain slightly greater amounts of uranium, probably held by adsorption or chemically combined with organic matter, than the evaporite minerals themselves. Any calcium phosphate minerals that are deposited can be expected to contain small amounts of uranium held in isomorphous substitution for calcium.

Most of the uranium that enters lakes, inland seas, and oceans with drainage waters probably is carried as highly soluble uranyl ions or in complex ions containing a uranyl radical. Inasmuch as uranium salts that might be present in lake or ocean waters are highly soluble, a tremendous concentration of such ions must occur before any evaporite uranium minerals are deposited. The hydrous forms of uranyl chloride ($UO_2Cl_2 \cdot 3H_2O$) and uranyl sulfate ($2UO_2SO_4 \cdot 7H_2O$) are soluble to the extent of several parts of the salt to one part of water; sodium and potassium chlorides are soluble to the extent of about 0.35 parts of the salt to one part of water at 20° C (Chemical Rubber Publishing Co., 1956, p. 622–623, 596–597, 570–571). The deposition of halite, sylvite, and other saline minerals of similar solubility begins long before saturation points of hydrous uranyl salts are reached.

A desiccating body of water, particularly if it is shallow, generally is well aerated and therefore maintains an oxidizing environment. This condition is indicated by the common presence of ferric oxides as impurities in evaporite sediments. The oxidizing environment maintains the dissolved uranium in the highly soluble uranyl form. A reducing environment, caused by stagnation of part of the body of water or by an influx of putrefying organic matter, is either a local or a temporary condition. Where a reducing environment exists some uranium may be reduced to the tetravalent state and be deposited with organic-rich muds, or some uranium in the uranyl state may be sorbed by organic matter and subsequently become reduced to the tetravalent state. Many evaporite deposits include no sediments that could have been deposited only under reducing conditions. Reduction or sorption of uranyl uranium and its incorporation in nonsaline reduzates is strictly the result of a local condition that exists temporarily during desiccation of some salt-pan basins. It is probable that in most basins only a small part of the uranium in the water is removed by this mechanism.

Shortly after the desiccation of a salt-pan basin begins, the water becomes permanently saturated with the carbonate ion in equilibrium with calcium except for short intervals occurring immediately after large influxes of water. The carbonate ion is an effective agent for holding the uranyl ion in solution. Whether or not it plays a significant role in maintaining the solubility of uranium in desiccating basins is a moot question. It is probable that the concentration of

carbonate ion considerably exceeds that of the uranyl ion until possibly such time as desiccation is almost complete. The excess of carbonate ion enhances the solubility of the uranyl ion, but in an oxidizing environment the uranyl ion is so soluble that the presence of carbonate may not be significant. Also, little seems to be known concerning the effect of the carbonate ion on the adsorption of uranium by clays and other substances.

URANIUM IN EVAPORITE MINERALS AND DEPOSITS

Thin beds of limestone or marlstone may be deposited during the initial stage of desiccation in a salt-pan basin. The uranium content of such limestone and marlstone generally is in the order of 0.0001 percent, or less, except where the rock is appreciably phosphatic.

Ocean water contains phosphorus in amounts ranging from 0.001 to 0.1 mg per kg, or 1 to 100 ppb (Sverdrup and others, 1942, p. 176). Complete precipitation of this phosphorus in the form of marine apatite produces about 0.005 to 0.5 milligrams of the phosphate mineral. The waters of some lakes and inland seas contain more phosphorus than the ocean waters. It has been established that marine phosphatic sediments generally contain small and variable amounts of uranium, and some phosphatic sediments deposited from saline lake waters are also uraniferous. Investigations by Altschuler and others (1958) have shown that sedimentary marine apatite typically contains between 0.005 and 0.02 percent uranium that is considered to be in the apatite structure in isomorphous substitution for calcium. Deposition of phosphatic sediments from saline waters therefore provides a mechanism for removal of uranium.

Pure phosphate minerals are not characteristic constitutents of evaporite deposits because the small quantities of phosphates present generally are dispersed in other evaporite minerals, but all the dissolved phosphate must be deposited in any basin that becomes completely desiccated. The relatively low solubility of the phosphate minerals causes them to be deposited simultaneously with the carbonate minerals, and consequently in an evaporite sequence a large portion of the phosphatic constituents are deposited early and are found in thin beds of slightly phosphatic marlstone or limestone. By use of the values given by Sverdrup and others (1942, p. 176) for the phosphorus content of ocean water and the data of Altschuler and others (1958) for the uranium content of marine phosphatic sediments it can be seen that the phosphatic constituent removes a variable portion of the available uranium (0.005 to 0.5 milligrams of phosphate mineral containing between 0.0000003 and 0.0001 milligrams of uranium, whereas the available uranium averages approximately 0.002 milligrams per kilogram of ocean water). Phosphatic sediment that rests upon the bottom for a long period of time continues to take up uranium, and reworked marine apatite may contain as much as 0.1 percent of this element (Altschuler and others, 1958). Under some conditions the phosphatic sediments may remove essentially all of the uranium from the saline water; under other conditions only a small fraction of the available uranium may be removed. Evaporite minerals that are deposited after the bulk of the carbonate minerals generally contain mere traces of phosphates; such minute quantities of uranium as are in gypsum, anhydrite, halite, and sylvite could be associated with phosphatic impurities.

Large amounts of calcium sulfate minerals are deposited during the early stages of desiccation of salt-pan basins that initially are filled with ocean water. Gypsum is deposited during desiccation of lakes and inland seas that are characterized by sulfate-rich waters. Many thick deposits of anhydrite and gypsum occur in nearly pure form, that is, they contain less than 20 percent of other materials. If organic matter and clays are not the major impurities, these deposits are essentially devoid of uranium. As indicated below, the sulfate minerals hold only minute traces of uranium, and the uranium content of impure anhydrite and gypsum rocks is contained in the clay, organic matter, and other substances, and not in the sulfate minerals.

Many deposits of anhydrite become partly or wholly converted to gypsum by the hydrating action of ground and surface waters, therefore, a question arises concerning the possibility that uranium might be leached during the hydration. This action undoubtedly can occur, but it is probable that the anhydrite held no significant amount of uranium. Gamma-ray logs of test wells drilled through evaporite sequences indicate that anhydrite and halite strata show, in general, the lowest levels of radioactivity of all sedimentary rocks. Examples of this low radioactivity are found in gamma-ray logs of many wells drilled through evaporite-mineral deposits in the Paradox basin of southwestern Colorado and southeastern Utah and in the Delaware basin of southeastern New Mexico.

On the west slope of the Humboldt Range, Pershing County, Nev., there are large outcrops of gypsum, one of which has an area of about a square mile. The principal impurities in this gypsum are carbonate minerals. The outcrops are covered by a layer of weath-

ered gypsum a few inches thick mixed with a small amount of wind-deposited sediment derived mostly from dust and salt flats of the adjacent Humboldt Sink. Radioactivity measurements made on the outcrops with a scintillation counter gave readings of approximately 0.003 milliroentgens per hour when the instrument was held about 2 feet above the weathered gypsum surface. The readings were almost nil where taken inside some prospect tunnels. The small amount of energy measured on the outcrop probably was predominately cosmic radiation. A similar condition exists in White Sands National Monument, N. Mex., where dunes of gypsum sand cover large areas. A scintillation counter gave no measurable reading during a traverse of some of these dunes (A. P. Pierce and J. W. Mytton, U.S. Geological Survey, oral communication, 1957).

Secondary uranium minerals have been found in a few bedded gypsum deposits, for example in the Paradox member of the Hermosa formation in Gypsum Valley, San Miguel County, Colo., and in the Brule formation, Dawes County, Nebr. These uranium minerals are epigenetic and have been introduced by ground and surface waters. The Brule formation is nonmarine, and its gypsiferous member was deposited from a lake of sulfate-rich water in which the salinity apparently did not reach the point where minerals more soluble than gypsum were deposited. A field examination in sec. 3, T. 34 N., R. 47 W. showed that anomalous radioactivity, and uranium minerals, occur at scattered points along the gypsum outcrop where there are intermittent ground-water seeps. The flow of water is insufficient to make surface streams, except during unusually wet periods, but does cause small landslides and collapse of steep slopes. The uranium minerals are carnotite, autunite, and sabugalite $[Hal(UO_2)_4(PO_4)_4 \cdot 16\ H_2O]$ (Dunham, 1955). They are concentrated on the surfaces of the outcrops and in the thin soil mantle where the ground water evaporates. Where there is no evidence of ground-water seepage, neither anomalous radioactivity nor uranium minerals can be found.

Two samples of the bedded gypsum from the Brule formation contained 0.0008 and 0.0001 percent of uranium (Nos. 260461 and 260462, table 1). Sample no. 260461 was light brown, had a strong fetid odor, and contained a small amount of organic matter that probably had sorbed the apparently anomalous amount of uranium; sample 260462 was white and odorless. The samples contained about 5 percent of acid-insoluble matter. The waters that formed the Brule lake drained a terrane characterized by sedimentary deposits containing an abundance of volcanic ash and therefore probably contained greater-than-average quantities of uranium. This condition is reflected in the abnormally high uranium content of the gypsum. It is unlikely that the minute, although anomalous, amount of uranium in this gypsum accounts for the secondary uranium minerals on the surfaces of the outcrops and in the topsoil. It is more likely that the uranium in the secondary minerals is leached from tuffaceous clays in the vicinity and is deposited on the outcrops and in the topsoil where the water evaporates.

Anhydrite is anomalously radioactive within or in the vicinity of some petroleum and natural gas fields, for example, in the Permian formations of the Panhandle field of Texas. Investigations have shown that the radioactivity originates in uraniferous organic substances that have been epigenetically emplaced in secondary anhydrite; the primary anhydrite, which was deposited as an evaporite sediment, is no more uraniferous than primary anhydrite found elsewhere (A. P. Pierce, U.S. Geological Survey, oral communication, 1957).

The uranium contents of some typical deposits of anhydrite and gypsum are presented in table 1. Three samples (Nos. 252251, 252252, and 260461) contained small amounts of organic matter. These three samples contained anomalous quantities of uranium, which possibly were sorbed by the organic matter.

Saline minerals, such as halite, sylvite, carnallite, and others of similar solubility contain so little uranium that the amount cannot be determined with pre-

TABLE 1.—*Uranium content of typical deposits of anhydrite and gypsum*

[Analysts: D. L. Ferguson, H. H. Lipp, W. J. Mountjoy, C. G. Angelo, J. P. Schuch, and E. J. Fenelly.]

Sample No.	Material	Acid-insoluble matter percent	SO_4 percent	Uranium percent
252250	Anhydrite	.....	.....	0.0001
252251	do	.....	.....	.0004
252254	do	.....	.....	.0002
260459	Gypsum	10.2	35.5	.0001
260460	Anhydrite	.5	36.9	.0001
260461	Gypsum	5.0	40.1	.0008
260462	do	5.9	41.6	.0001

NOTE.—Sources of samples:

252250. Sample of core chips, Shell Oil Co.'s Desert Creek No. 1 well, SW¼SE¼NW¼ sec. 2, T. 42 S., R. 23 E., San Juan County, Utah, depth 5,123½ ft.

252251. Same as source of sample 252250; depth 5,124½ ft.

252254. Sample of core chips, Reynolds Metal Co.'s Hatch No. 1, sec. 4, T. 39 S., R. 24 E., San Juan County, Utah, depth 5,797–5,799 ft.

260459. Sample from prospect tunnel, W½ sec. 27, T. 26 N., R. 32 E., Pershing County, Nev.

260460. Sample from abandoned Regan mine, approximately 12 miles south of Yerington, Nev.

260461. Sample from outcrop of gypsiferous member of Brule formation, W½ sec. 3, T. 34 N., R. 47 W., Dawes County, Nebr.

260462. Sample from same locality as sample 260461.

cision by standard methods of chemical analysis. There are but few published data on this subject. Kemény (1941) has reported that the uranium contents of rock salt, sylvite, and carnallite from Germany and Austria, determined by radiometric methods, average 0.0006 percent (6×10^{-10} g/g). Gentner and others (1954) have reported a uranium content of 0.00001 percent (1×10^{-10} g/g) for sylvite from Buggingen, Germany; the determination was made by a method of counting alpha tracks on an emulsified plate. A few samples of potash ores, consisting mainly of halite, sylvite, and polyhalite, from the Carlsbad district, New Mexico, have been tested for uranium in the Geological Survey laboratories. The uranium contents of the samples were less than 0.0001 percent, so no attempt was made to determine them precisely. All uranium determinations by the Geological Survey laboratories were made by fluorometric methods.

These meager data do not indicate enrichment of uranium in evaporite sediments. They do not warrant any conclusions regarding the proportionate rate at which uranium is deposited during stages of desiccation represented by halite and sylvite.

The clays and the iron and aluminum oxides that are deposited with saline minerals probably as a rule are considerably more uraniferous than the saline minerals themselves. Some information about the distribution of uranium between water-soluble evaporite minerals and water-insoluble matter was obtained by analyzing several samples taken from a drill core recovered from potassium-bearing beds in the Salado formation of Permian age, Delaware basin, N. Mex. The samples were cut from a 19-foot length of core from a stratigraphic section that includes two thin zones having large contents of clays. The clays evidently were deposited when large influxes of sediment-bearing water entered the basin. The analytical data are presented in table 2.

The sections of core were split lengthwise, and one part was crushed and mixed to provide material for analysis. Uranium in the total sample was determined by a fluorometric method. The samples were then separated into water-soluble saline minerals, water-insoluble but acid-soluble saline minerals, and water- and acid-insoluble matter by the following procedure: The samples were leached by weighing 1 gram of the substance into a tared sintered glass crucible of medium porosity, 10 ml of water were added, the slurry was stirred briefly, and the resulting solution was drawn by vacuum into a volumetric flask; this procedure was repeated ten times for a total of 100 ml of water; the water-soluble evaporite minerals, such as halite and sylvite, and a small portion of the slightly water-soluble minerals, such as polyhalite and anhydrite, were dissolved in the water leachate; the crucible and contents were then dried under a vacuum of less than 1 cm of mercury in a desiccator containing anhydrous calcium sulfate, were weighed, and the leaching procedure repeated with 1:1 hydrochloric acid; the acid leachate contained most of the polyhalite and the calcium sulfate minerals, as well as phosphate and carbonate minerals; the water- and acid-insoluble matter remaining in the crucible consisted of clay minerals and other clastic sediments, which were then dried and weighed.

An attempt was made to determine the uranium contents of the water-soluble leachates by the fluorometric method, but the quantities of uranium present were below the threshold of the procedure used, or less than 0.00002 percent. Uranium in the acid leachates was determined, but there is no assurance that the values obtained are indicative of the uranium contents of the water-insoluble but acid-soluble minerals; some of this uranium may have been adsorbed on clays and was removed by the acid. Uranium in the water- and acid-insoluble matter was obtained by difference, and again there is no assurance that the values indicate the true quantities of uranium because some uranium may have been removed by the acid.

The data presented in table 2 indicate that most of the uranium is concentrated in the water-insoluble but acid-soluble matter and the water- and acid-insoluble matter. The water-soluble matter contains extremely small amounts of uranium, the amount being less than 0.00002 percent of the total sample for all samples analyzed. The uranium contents of the water-insoluble but acid-soluble matter are very small and show a positive correlation with the total uranium contents of the samples; the latter feature may be an indication of extraction of uranium from the water- and acid-insoluble matter by the acid.

One sample (No. 254465, table 2) is of especial interest because it represents a clay-rich zone about 6 inches thick. Unfortunately about three-quarters of the material from this zone was lost during drilling; that which was recovered was completely consumed in the various chemical analyses. The megascopically visible constituents of the sample were coarse crystalline halite, sylvite, and polyhalite, and galls and stringers of greenish-gray clay consisting of montmorillonite, illite, and kaolinite and (or) chlorite. The analytical data (table 2) indicate the presence of a surprisingly large amount of uranium; two splits of the core contained 0.0078 and 0.038 percent uranium,

TABLE 2.—*Chemical and mineralogic determinations on samples from a drill core of an evaporite deposit Potash Company of America drill-hole-151, Sec. 12, T. 20 S., R 33 E., Lea County, N. Mex.*

[Analysts: W. T. Mountjoy, H. H. Lipp, and C. G. Angelo, U.S. Geological Survey. Clay minerals indentified by A. J. Gude, U.S. Geological Survey.]

Sample No.	Sample interval (depth)	Principal minerals	Water-soluble saline minerals	Water- and acid-insoluble matter	Acid-soluble but water-insoluble saline minerals (by difference) [1]	Uranium (as percent of total sample)				Chemical composition (as percent of total sample)													
											Water leachate						Acid leachate of water-insoluble matter [1]						Approximate summation
						Total	In water leachate	In acid leachate	In insoluble matter (minimum by difference)	$CO_3^=$	Ca^{++}	Mg^{++}	Na^{++}	K^+	$SO_4^=$	Cl^-	Ca^{++}	Na^+	K^+	$SO_4^=$	$PO_4^{\equiv}$	
254463	2,258 ft 0 in to 2,262 ft 4 in.	Halite	99.85	0.10	0.05	0.00008	<0.00002	<0.00001	0.00005	.....	0.56	0.29	35.75	3.98	2.85	52.28	0.06	<0.02	0.02	<0.02	<0.0005		101.8
254464	2,262 ft 4 in. to 2,263 ft 8 in.	Polyhalite	67.2	.05	32.15	.00012	<.00002	.00002	.00008	.....	9.18	2.80	1.12	10.00	43.50	1.78	3.78	.02	2.78	17.50	.007		91.3
[1] 254465	2,263 ft 8 in to 2,264 ft 2 in.	Halite, sylvite, montmorillonite, Illite, kaolinite and (or) chlorite, carbonate minerals.	71.6	19.4	9.00	.038	.....	.....	.....	2.61	1.60	3.06	9.14	9.17	7.60	27.85	1.70	<.02	.07	1.06	.....		53.2
						<.0078	<.00002	.....	.....	.....	.....	.....	.....	.....	.....	.....	.....	.....	.....	.....	.041		
						.....	.....	5.04	.....	.....	.....	.....	.....	.....	.....	.....	.....	.....	.....	.....	.....		
254466	2,264 ft 2 in to 2,264 ft 10 in.	Halite	99.49	.47	.04	.00006	<.00002	<.00001	.00003	.....	.47	.29	35.75	4.90	2.05	56.45	.04	<.02	<.02	.05	<.0005		100.5
254467	2,264 ft 10 in to 2,268 ft.	Halite, sylvite	99.05	.88	.07	.00004	<.00002	<.00001	.00001	.....	.12	.62	22.25	22.60	2.12	52.10	.04	<.02	<.02	.02	.001		101.0
254468	2,268 ft to 2,273 ft 6 in.	Halite, sylvite, clay minerals.	94.3	3.9	1.80	.00065	<.00002	.00007	.00056	.....	.24	.47	26.25	14.00	1.38	52.00	.78	.15	.02	.75	.009		99.9
254469	2,273 ft 6 in to 2,274 ft 6 in.	Halite, sylvite, montmorillonite, Illite, kaolinite and (or) chlorite.	61.9	32.7	5.40	.00011	<.00002	<.00001	.00008	.....	.56	2.07	13.40	4.42	3.30	28.90	.24	<.02	.08	.29	.004		90.2
254470	2,274 ft 6 in to 2,277 ft.	Halite	98.3	.89	.81	.00004	<.00002	<.00001	.00001	.....	.71	.34	36.75	1.62	3.30	55.95	.17	.02	.02	.38	<.0005		100.2

[1] Acid-soluble but water-insoluble saline minerals include carbonate and phosphate minerals, and part of any polyhalite, gypsum, and anhydrite in the sample.

[2] Mg^{++} and Cl^-, were present, are in amounts of less than 0.01 percent in all samples.

[3] Partial analyses were made of three portions of the sample.

or 78 and 380 (ppm); the acid-soluble matter of a third split, obtained after removing water-soluble matter, contained an amount of uranium corresponding to 0.040 percent (400 ppm) of the sample. The range of values is attributed to the coarse heterogeneous character of the material and the improbability of making three identical splits of the core. This sample contained about 19 percent water- and acid-insoluble matter, about 2.6 percent carbonate as $CO_3^{=}$, and about 0.041 percent phosphate as $PO_4^{\equiv}$.

Above average quantities of uranium and phosphate were found in the second thin clay-rich zone represented by samples 254468 and 254469 (table 2). The amount of uranium in sample 254468 was 0.00065 percent (6.5 ppm) and of phosphate as $PO_4^{\equiv}$ was 0.009 percent (90 ppm).

These clay-rich samples contained no visible uranium minerals and no fluorescent substance. Some uranium undoubtedly was combined with the phosphate constituent, but the amounts of uranium found seem to be considerably in excess of what reasonably could be accounted for by this combination. Some of the uranium could have been adsorbed on clays, and a finely dispersed uranium mineral could have been present.

The clay-rich zones undoubtedly represent interruptions in the desiccation of the basin caused by large influxes of water carrying dissolved matter and much fine-grained sediment. Such influxes could have resulted from occasional floods that washed the adjacent terrain. When the floods subsided, desiccation immediately was resumed; fine-grained suspended clastic sediments settled to the bottom and became mixed with the initial evaporite layer which contained some phosphatic and carbonate constituents. This action provided at least two mechanisms for removal of uranium from the basin water, adsorption on clays, and combination with phosphatic constituents. It seems probable that most of the uranium thus removed was already in the basin prior to the influx that brought in the clays.

Stagnant, anaerobic conditions may exist temporarily within the water of parts of some desiccating salt-pan basins. If there is an influx of fine-grained clastic sediments and organic matter during such periods, organic-rich dark muds or limy muds may be deposited and ultimately become shales. Some of such shales that are slightly phosphatic may be anomalously radioactive and contain uranium in the range of 0.00X to 0.0X percent. On the other hand, organic-rich muds can be deposited in oxidizing environments, and subsequently a zone in which reducing conditions exist may form in them although the uppermost layer of mud and the water above it remain in an oxidizing condition; under these circumstances the reducing zone is insulated from the main body of water, and the only uranium that can be sorbed is that in the connate water, consequently the muds do not become significantly enriched in uranium. Uranium-rich muds generally are deposited in reducing environments, and if the bottom surface remains in a reducing condition, sorption of uranium in a particular layer may continue for as long as water can move freely past or through it.

In the Paradox basin of southwestern Colorado and southeastern Utah some thin beds of euxenic dark-gray and black shale are interspersed among the carbonate and saline deposits of the Paradox member of the Hermosa formation. They are good marker beds for stratigraphic correlation because they show anomalously high radioactivity on gamma-ray logs. The characteristics and possible origin of these dark-shale beds have been discussed by Wengerd and Strickland (1954). The uranium contents of a few samples of some of these dark-shale beds and of the dolomites and anhydrite that enclose them have been determined. These data are presented in table 3. The samples were chipped from drill cores and represent the only material that was available at the time of this investigation. The most uraniferous sample, No. 252252, contained 0.0057 percent uranium. In general, the uranium contents of these shale beds are about an order of magnitude higher than those of the enclosing dolomites and anhydrite. Probably some uranium is sorbed by organic matter and phosphatic sediments and thereby is removed from the saline during the deposition of sediments such as those that formed the shales in the Paradox member. This mechanism operates only temporarily in a few basins and probably removes only a small part of the dissolved uranium from the water.

TABLE 3.—*Uranium contents of euxenic dark shales and enclosing dolomites and anhydrite from the Paradox basin.*

[Analysts: G. G. Angelo, J. P. Schnob, and E. J. Fennelly]

Sample No.	Depth (feet)	Description	Uranium percent
Shell Oil Co.'s North Boundary Butte No. 1 Well, C SW¼ NE¼ sec. 33, T. 42 S., R. 22 E., San Juan County, Utah			
252220	4,212	Limy gray shale	0.0009
252221	4,615	do	.0007
252222	4,617	do	.0009
252223	4,618½	do	.0013
252224	4,620½	Shale and dolomite, anhydrite	.0005
252225	4,621½	Dolomite	.0004
252226	4,622	do	.0011
252227	4,623	do	.0003
252228	4,628	Dolomite, anhydrite	.0003
252229	4,626	Limy gray shale	.0006

TABLE 3.—*Uranium contents of euxenic dark shales and enclosing dolomites and anhydrite from the Paradox basin*—Continued

Sample No.	Depth (feet)	Description	Uranium percent
Superior Oil Co.'s No. 1-28 Navajo Well, C NW¼ NW¼ sec. 28, T. 41 S., R. 26 E., San Juan County, Utah			
252230	6,048–6,049	Shaly dolomite	0.0008
252231	6,053–6,054	.....do	.0006
252232	6,055–6,056	Gray shale	.0007
252233	6,056–6,057	.....do	.0007
252234	6,057–6,058	.....do	.0008
252235	6,058–6,059	.....do	.0006
252236	6,059–6,060	Black shale	.0008
252237	6,061–6,062	.....do	.0010
252238	6,062–6,063	.....do	.0010
252239	6,063–6,064	.....do	.0010
252240	6,064–6,065	.....do	.0012
252241	6,065–6,066	.....do	.0007
252242	6,067–6,068	.....do	.0006
252243	6,068–6,069	.....do	.0007
252244	6,069–6,070	.....do	.0011
252245	6,070–6,071	.....do	.0032
252246	6,071–6,072	.....do	.0013
252247	6,072–6,073	Shaly dolomite	.0007
252248	6,073–6,074	Dolomite	.0002
Shell Oil Co.'s Desert Creek No. 1 Well, SW¼ SE¼ NW¼ sec. 2, T. 42 S., R. 22 E, San Juan County, Utah			
252249	5,122½	Anhydrite	0.0001
252250	5,124½	.....do	.0001
252251	5,126	Gray shale	.0004
252252	5,127	Black shale	.0057
252253	5,128½	Dolomite	.0001
Reynolds Metal Co.'s Hatch No. 1 Well, sec. 4, T. 39 S., R. 24 E., San Juan County, Utah			
252254	5,797–5,799	Anhydrite	0.0002
252255	5,799–5,799¼	Black shale	.0017
252256	5,799¼–5,800	Shaly dolomite	.0003

The data presented above indicate that the distribution of uranium in sediments deposited in desiccating salt-pan basins is not uniform and is not completely known. In attempting to determine the distribution, a major difficulty arises from the fact that the amounts of uranium and its compounds involved are very small in comparison to the total bulk of sediments. It is known that in some salt-pan-basin deposits uranium is not uniformly distributed among the various sedimentary materials but is relatively enriched in clays, in phosphatic sediments, and in some beds of organic-rich, dark shale that were deposited in reducing environments. It is possible that in some basins essentially all of the dissolved uranium can be removed from solution by inclusion in clays and phosphatic and organic sediments. Within basins where such sediments are not deposited, or are deposited in very small amounts, it seems most likely that a substantial part of the uranium must remain in solution until the bittern finally evaporates.

The probability that the concentration of uranium increases continuously in the water of some salt-pan basins even though substantial amounts of clays, phosphatic sediments, and carbonate and evaporite minerals are deposited is indicated by the comparatively high concentrations of uranium in the waters of the Salton Sea, Calif., and Great Salt Lake, Utah. Much of the water entering Great Salt Lake drains terranes to the east and northeast that are composed in part of highly phosphatic formations (Phosphoria and Park City formations). Rather extensive deposits of calcareous oolites that contain small amounts of phosphatic material are found along parts of the shore, and the oolites still are being formed; black, organic-rich clays are being deposited along other parts of the shore (Eardley, 1938). The uranium contents of the oolites and black clays are unknown. Even though these sediments are types that commonly are enriched in uranium from solution, the lake water has about twice the concentration of uranium as does ocean water. The concentration of uranium in the Salton Sea (10 ppb) is about four times that of ocean water.

It already has been pointed out that within desiccating salt-pan basins oxidizing conditions tend to prevail and reducing conditions tend to be localized and often are of brief duration. As a consequence, most of the dissolved uranium is maintained in the highly soluble uranyl state. The uranyl salts are so highly soluble that it is reasonable to assume that the water in a basin must evaporate completely to cause deposition of uranium that is not sorbed by clays, organic matter, and phosphatic sediments. If the water never evaporates completely it is unlikely that any uranium salts will be deposited. If a basin becomes completely desiccated, a small but appreciable amount of uranium minerals should be deposited in a final layer of highly soluble evaporite minerals. Such uraniferous deposits apparently are unknown; the reason is that they are readily susceptible to removal.

The surface of a dried-up basin, or even a partly dried-up basin, is subject to wind erosion that can remove considerable amounts of sediment. Anyone who has been in the vicinity of the Bonneville salt flats of Utah, or the smaller salt flats in the Carson and Humboldt Sinks of Nevada, in the Mohave and Death Valley areas of California, or the bolsons of west Texas on windy days can attest to the fact that wind moves large amounts of evaporite minerals. An indication of the amount of evaporite material that can be so moved is given by Eardley and others (1957, p. 1151) in discussing wind erosion in the Bonneville basin of Utah. They stated: "The writers postulate that the wind removes about 3,000,000 tons of salt annually from the Great Salt Lake desert. This is carried by the wind out of the drainage basin." It is reasonable to assume that an exposed layer of uraniferous evaporite minerals could be removed by wind within a very short period.

Uraniferous evaporite minerals would have to be covered by some other kind of sediment immediately after they were deposited in order to be preserved from wind erosion. Even then, these very soluble minerals would be leached by the first passage of water through the sediments. This water would remove the highly soluble salts, including uranium salts, from the places of initial deposition and transport them laterally or downward, thereby dispersing them through much larger volumes of rock and sediment, or it would bring them to the surface to form deposits of efflorescent minerals that subsequently would become dispersed.

There is little possibility that a final deposit of uranium-rich evaporite sediments can be preserved in a salt-pan basin.

SUMMARY

In summary, it can be stated that evaporite sediments deposited in salt-pan basins are probably the least uraniferous of all rocks. Their uranium contents average less than 0.00001 percent. This condition results from (1) the paucity of uranium in ocean and surface waters, (2) the oxidizing environments that generally exist within the evaporating bodies of water, (3) the great solubility of uranyl chlorides and sulfates and uranyl carbonate complexes, and (4) the likelihood that any uraniferous evaporite sediments that might be deposited are removed by wind erosion or by leaching. Analytical work that would indicate whether uranium is deposited at a fairly uniform rate throughout the desiccation of a salt-pan basin or tends to remain in solution until the basin finally dries out has not been done. Theoretical considerations indicate that in some basins most of the uranium can be removed from solution through sorption by clays, phosphatic sediments and organic-rich muds; in other basins the bulk of the uranium should remain in solution until such time as desiccation is almost complete.

LITERATURE CITED

Adams, J. A. S., 1954, Uranium contents of Wisconsin rivers and their use in geochemical prospecting [abs.]: Geol. Soc. America Bull., v. 65, p. 1225.

Altschuler, Z. S., Clarke, R. S., Jr., and Young, E. S., 1958, Geochemistry of uranium in apatite and phosphorite: U.S. Geol. Survey Prof. Paper 314-D, 50 p.

Chemical Rubber Pub. Co., 1956, Handbook of chemistry and physics: 38th ed. Cleveland. 3206 p.

Dunham, R. J., 1955, Uranium minerals in Oligocene gypsum near Chadron, Dawes County, Nebr.: U.S. Geol. Survey TEI-625, 31 p., issued by U.S. Atomic Energy Comm. Tech. Inf. Service Ext., Oak Ridge, Tenn.

Eardley, A. J., 1938, Sediments of Great Salt Lake, Utah: Am. Assoc. Petroleum Geologists Bull., v. 22, p. 1305–1411.

Eardley, A. J., Gvosdetsky, Vasyl, and Marsell, R. E., 1957, Hydrology of Lake Bonneville and sediments and soils of its basin: Geol. Soc. America Bull., v. 68, p. 1141–1201.

Fix, P. F., 1956, Hydrogeochemical exploration for uranium, *in* Contributions to the geology of uranium and thorium by the United States Geological Survey and Atomic Energy Commission for the United Nations International Conference on peaceful uses of atomic energy, Geneva, Switzerland 1955: U.S. Geol. Survey Prof. Paper 300, p. 667–671.

Föyn, E., Karlik, B., Petterson, H., and Rona, E., 1939, Radioactivity of sea water: Nature, v. 143, p. 275–276.

Gentner, W., Goebel, K., and Prig, R., 1954, Argonbestimmungen an Kalium-Mineralien. III. Vergleichende Messungen nach der Kalium-Argon- und Uran-Helium Methode: Geochim. et Cosmochim. Acta, v. 5, p. 124–133.

Hernegger, Friedrich, and Karlik, Berta, 1935, Die quantitative Bestimmung sehr kleiner Uranmengen un der Urangehalt des Meerwassers: Sitzungsberichte Academie der Wissenschafter in Wien, Math.-naturw. Kl. Abt. IIa, v. 144, p. 217–225.

Judson, Sheldon, and Osmond, J. K., 1955, Radioactivity in ground and surface water: Am. Jour. Sci., v. 253, p. 104–116.

Kemény, Etel, 1941, Uran- und Radiumgehalt von Steinsalz und Sylvin: Sitzungsberichte Akademie der Wissenschafter in Wien, Math.-naturw. Kl., Abt. IIa, v. 150, p. 193–207.

Koczy, Gerta, 1950, Weitere Uranbestimmungen an Meerwasserproben: Sitzungsberichte Akademie der Wissenschafter in Wien, Math.-naturw. Kl., Abt. IIa, v. 158, p. 113–121.

Nakanishi, Masaki, 1952, Fluorometric microdetermination of uranium. V. The uranium content of sea water: Chem. Soc. Japan, Bull., v. 24, p. 36–38.

Rona, Elizabeth, Gilpatrick, L. O., and Jeffrey, L. M., 1956, Uranium determination in sea water: Am. Geophysical Union, Trans., v. 37, p. 697–701.

Rona, Elizabeth, and Urry, W. D., 1952, Radioactivity of ocean sediments. VIII. Radium and uranium content of ocean and river waters: Am. Jour. Sci., v. 250, p. 241–262.

Stewart, D. C., and Bentley, W. C., 1954, Analysis of uranium in sea water: Science, v. 120, p. 50–51.

Sverdrup, H. V., Johnson, M. W., and Fleming, R. H., 1942, The oceans. Their physics, chemistry and general biology: New York, Prentice-Hall, Inc., 1087 p.

Tourtelot, H. A., 1955, Uranium content of water in the Great Plains region of Nebraska and in adjacent states [abs.]: Geol. Soc. America Bull., v. 66, p. 1627–1628.

Wengerd, S. A., and Strickland, J. W., 1954, Pennsylvania stratigraphy of Paradox salt basin, Four Corners region, Colorado and Utah: Am. Assoc. Petroleum Geologists Bull., v. 38, p. 2157–2199.

O

Foraminifera From Onotoa Atoll Gilbert Islands

By RUTH TODD

SHORTER CONTRIBUTIONS TO GENERAL GEOLOGY

GEOLOGICAL SURVEY PROFESSIONAL PAPER 354-H

Ecologic study of Recent assemblages from beaches, reefs, and shallow lagoon floor

UNITED STATES GOVERNMENT PRINTING OFFICE, WASHINGTON : 1961

UNITED STATES DEPARTMENT OF THE INTERIOR

STEWART L. UDALL, *Secretary*

GEOLOGICAL SURVEY

Thomas B. Nolan, *Director*

For sale by the Superintendent of Documents, U.S. Government Printing Office
Washington 25, D.C.

CONTENTS

	Page		Page
Abstract	171	Examination of fish contents	182
Introduction	171	Foraminifera from pits	184
Material studied	171	Local distribution of *Calcarina* and *Baculogypsina*	186
Locality data	173	Notes on selected species	186
Fauna	176	References cited	188
Wet samples	181	Index	189

ILLUSTRATIONS

[Plates 22–25 follow index]

PLATE 22. Recent benthonic Foraminifera from Onotoa Atoll.
23. Recent benthonic Foraminifera from Onotoa Atoll.
24. Recent planktonic Foraminifera from Onotoa Atoll.
25. Foraminifera sands from Onotoa Atoll.

FIGURE 40. Map of Onotoa showing locations of samples studied and major occurrences and relative abundance of *Calcarina* and *Baculogypsina* 172
41. Diagrammatic sections of 7 dug pits on the northern main island of Onotoa Atoll 185

TABLES

TABLE 1. Distribution of Recent Foraminifera of Onotoa Atoll 177
2. Occurrence of Foraminifera in stomach and gut contents of fish from the lagoon at Onotoa Atoll 183

SHORTER CONTRIBUTIONS TO GENERAL GEOLOGY

FORAMINIFERA FROM ONOTOA ATOLL, GILBERT ISLANDS

By Ruth Todd

ABSTRACT

The distribution of 168 species and varieties of smaller Foraminifera is recorded within the lagoon and on the reefs and beaches of Onotoa Atoll as represented by 33 surface samples and 23 pit samples. Nearly all the species are well known in shallow-water sediments of the tropical Pacific; 7 are indeterminate; none are described as new. The lagoon collecting localities were all but one from depths no greater than 20 feet, and mostly from areas protected from the open ocean. Preservation in alcohol of 24 samples permitted a staining process to be used and an estimate to be made of the very small live-dead ratio, and determination of the living places of certain of the species.

Recognition of two major distinctive habitats—(a) reef surfaces and their adjacent slopes and (b) limesand bottom of the lagoon—is based in part on the relative abundance of species and in part on the presence of live (stained) specimens.

Four species—*Calcarina spengleri*, *Baculogypsina sphaerulata*, *Amphistegina madagascariensis*, and *Marginopora vertebralis*—make up quantitatively most of the foraminiferal material in the reef sediments. Major foraminiferal constituents of the lagoon sediments are, in quantitative order: *Amphistegina madagascariensis*, *Heterostegina suborbicularis*, *Marginopora vertebralis*, and *Elphidium striato-punctatum*. Quantitatively insignificant because of their smaller size, but common or abundant in most samples, are many species of miliolids and several species in each of the following families: Textulariidae, Peneroplidae, Buliminidae, Discorbidae, Cymbaloporidae, Anomalinidae, and Planorbulinidae. Globigerinids are present, but only rarely, and appear to have come in from the open ocean through breaks in the reef. Seventeen other families are represented mostly by rare or scattered occurrences.

Stomach and gut contents of 22 fish were found to contain Foraminifera tests nearly as varied as the naturally occurring fauna. The fact that most of the individual fish did not contain as great a variety as the composite of all the fish suggests a rather localized feeding area for each fish.

Seven pits provide short sections—a maximum of 10 feet—into the sediments that make up the northern main island. These sediments are interpreted as beach sands overlying and transitional to reef flat deposits.

INTRODUCTION

Onotoa Atoll is a "dry" atoll (referring to its rainfall [Cloud, 1952, p. 10–15]) in the southern part of the Gilbert Islands. It is elongate northwest-southeast and bordered nearly continuously on the northeast (windward) and south sides by narrow islands but either open to the ocean or protected by discontinuous living coral reefs on the southwest side (fig. 40). Its dimensions are roughly 12 miles long and 4 to 5 miles wide. Latitude and longitude at its northwestern end are 1°46′ S. and 175°30′ E. Its physical description may be found in a preliminary report by Preston E. Cloud, Jr. (1952), who in 1951 made the collections upon which this study is based.

Acknowledgments.—I am indebted to Preston E. Cloud, Jr., for making available the well-documented material and to John E. Randall for the identifications of the fishes studied. For helpful suggestions and discussions I am grateful to Preston E. Cloud, Jr., and to Richard Cifelli. Invaluable help in preparation of material and tabulation of results was received from Doris Low. The illustrations of the individual specimens of Foraminifera were made by Elinor Stromberg.

MATERIAL STUDIED

Samples were studied from the following areas of Onotoa Atoll:

(1) Area open to ocean on west (leeward) side of atoll (7 samples from depths between 3 and 18 feet);
(2) Lagoon:
  (a) Southern part (8 samples from depths between 6 and 17 feet, with 1 exception, f11683 [GOC–55] collected from 48 feet)
  (b) Central and northern part (7 samples from depths down to 20 feet);
(3) Reef areas (3 samples from leeward side of atoll and 2 from windward);
(4) Southern part of atoll (4 samples of fine sediment and incipient beachrock);
(5) Islands along the east (windward) side of atoll
  (a) Beach sands (4 samples)
  (b) Material from pits having depths from 20 inches to 11½ feet. The pits start in beach sands, in which many of the specimens are severely corroded (13 samples), and penetrate through progressively richer transitional sediments (7 samples) into sediments of a reef-flat horizon (3 samples).

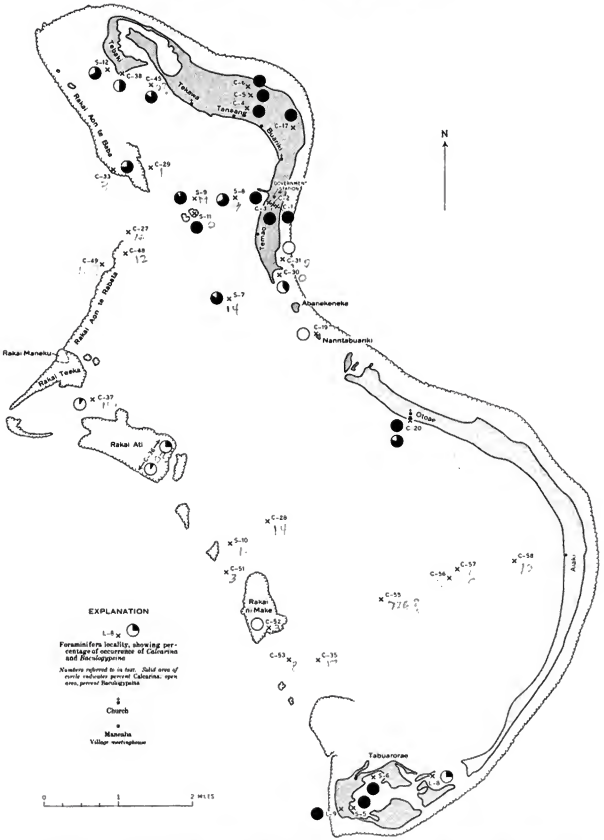

FIGURE 40.—Map of Onotoa showing locations of samples studied and major occurrences and relative abundance of *Calcarina* and *Baculogypsina*.

LOCALITY DATA

The following locality and sample descriptions, taken from P. E. Cloud's field notes, are arranged in order of their U.S. Geological Survey Foraminifera locality numbers. They include pertinent details of the various environments from which the Foraminifera from Onotoa Atoll, Gilbert Islands, were derived.

U.S.G.S. loc. No. — *Field localities and descriptions*

f11639–f11643. GOC–1. Southern part of northern main island, about 1,100 ft S. 41° E. from east (inshore) end of lagoon-side jetty at Government Station and 325 ft inshore from sea beach along line bearing S. 87° W. at Pacific Science Board campsite. Pit in which water level fluctuated with tide. Pit section in descending order, with unit thicknesses, is:

f11639. GOC–1A. 99+ percent medium-grained *Calcarina* sand, dark brownish gray from organic matter. Roots very abundant, up to seven-eighths of an inch in diameter. Foraminifera worn or eroded by organic acids. Subaerial accumulation?. Top 9–10 in.

f11640. GOC–1B. 99+ percent medium-grained dark-tan *Calcarina* sand, abruptly gradational to f11639 (GOC–1A). Sample f11640 differs only in organic content, abundance of roots, and good preservation of *Calcarina*, suggesting only slight transportation. Roots moderately abundant, as much as one-half of an inch in diameter, cutting off abruptly at base. Subaerial accumulation?. Thickness, 16–17 in.

f11641. GOC–1C. Similar to f11642 (GOC–1D), which follows, but has alternating layers of semi-indurated to indurated material. Basal 1–4 in. indurated. Roots rarely extend into unit C. Probably deposited along beach near reef flat. Thickness, 7–10 in.

f11642. GOC–1D. Weakly indurated to nonindurated medium-grained limesand, 80± percent well-preserved *Calcarina* and 20± percent other Foraminifera and detrital $CaCO_3$, much of it quite fine grained. Other Foraminifera include *Marginopora*. Color is light tan to flesh. Thickens where f11641 (GOC–1C) thins and unit C apparently represents incipient beachrock at top of unit D. No roots. Probably deposited along beach near reef flat. Thickness, 14–17 in.

f11643. GOC–1E. Zone of *Heliopora*. About 70 percent blue coral of which much may be but none is certainly in position of growth; 30± percent interstitial limesands are coarse to fine grained, light tan to flesh, of detrital $CaCO_3$ and Foraminifera. *Marginopora* abundant; *Calcarina* common; echinoid spines occasional. Interpreted as reef-flat horizon, built up to about low tide level and then overrun by beach of f11642 (GOC–1D). No roots. 16 in. above watermark. Thickness, 25 in.

f11644–f11649. GOC–2. Southern part of northern main island, about 940 ft S. 25° E. from east (inshore) end of lagoon-side jetty at Government Station and 660 ft inshore from sea beach along line bearing S. 87° W. at Pacific Science Board campsite. Pit similar to GOC–1. Pit section in descending order, with unit thicknesses, is:

f11644. GOC–2A. Medium- to fine-grained limesand, dark brownish gray from organic matter. Worn *Calcarina* about 60 percent; remainder of detrital fines. Roots uncommon. Some stones as much as three-fourths of an inch in diameter. Top 5 in.

f11645. GOC–2B. Medium-grained limesand. Worn *Calcarina* about 70 percent with occasional pebbles as much as three-eighths of an inch in upper 7 in. Up to 95+ percent worn *Calcarina* below. Remainder is detrital $CaCO_3$. Tan to flesh colored; darker above than below. Roots abundant, as much as three-eighths of an inch in diameter. Thickness, 19 in.

f11646. GOC–2C. Loose $CaCO_3$ gravel composed of 50 percent $CaCO_3$ pebbles as much as 2½ in. long and 50 percent worn *Calcarina* and detrital $CaCO_3$. Roots abundant, as much as one-fourth of an inch in diameter. Thickness, 11 in.

f11647. GOC–2D. Strongly indurated flesh-colored granule sandstone, of varied detrital $CaCO_3$. One loose sand layer 2–4 in. from base. Roots very rare. Thickness, 15 in.

f11648. GOC–2E. Very fine grained flesh-colored detrital limesand. No roots. Thickness, 6 in.

f11649. GOC–2F. Zone of *Heliopora*. Essentially same as f11643 (GOC–1E). No roots. Reef flat horizon? Thickness, 51 in.

f11650–f11653. GOC–3. Southern part of northern main island, about 870 ft S. 3° E. (true) from east (inshore) end of lagoon-side jetty at Government Station and 340 ft inshore from lagoon beach along line bearing N. 87° E. through Pacific Science Board campsite strip. Pit similar to GOC–1 and GOC–2. Pit section in descending order, with unit thicknesses, is:

f11650. GOC–3A. Dark-brownish-gray organically enriched limesand similar to f11644 (GOC–2A). Roots common. Top 8 in.

f11651. GOC–3B. Similar to f11650 (GOC–3A) but with less organic matter and only dark-tan to light-brown color. Roots abundant as much as one-half of an inch in diameter. Subsoil. Thickness, 6 in.

None. GOC–3C. Medium-grained flesh-colored (pinkish-tan) limesand with occasional granules and small pebbles (to one-half of an inch in diameter). Mostly 90 percent worn and smooth *Calcarina* but with occasional Foraminifera of other sorts, echinoid spines, algal fragments, small mollusks, and detrital $CaCO_3$. Many roots, upper part. Thickness, 38 in.

U.S.G.S. loc. No.	Field localities and descriptions
f11652.	GOC-3D. Similar to GOC-3C but has fairly numerous pebbles (one-half of an inch maximum diameter) and granules; small gastropods relatively common, and *Marginopora* common. Thickness, 20 in.
None.	GOC-3E. Pinkish-gray granule gravel of fragmentary ramose calcareous algae with interstitial *Calcarina* sand (worn smooth). Thickness, 10 in.
f11653.	GOC-3F. Similar to f11652 (GOC-3D). Thickness, 40 in.
None.	GOC-3G. Zone of large head-forming crustose corallines and occasional astraeiform corals and interstitial sand like f11652 (GOC-3D) and f11653 (GOC-3F). Only algae and corals sampled. Thickness, 8 in.
None.	GOC-3H. Similar to f11652 (GOC-3D) and f11653 (GOC-3F). (Field observation, no sample taken.) Thickness, 8 in.
f11654–f11655.	GOC-4. North-central part of northern main island, about 1,000 ft east-northeast from Taneang-Tekawa Maneaba. Section in area of fine clastic limesand that makes fine-grained loamy soil—at this place dry. Pit section in descending order, with unit thicknesses, is:
f11654.	GOC-4A. Very fine grained brownish-gray (from organic matter) limesand; grades down to f11655 (GOC-4B). Roots common, as much as five-eighths of an inch in diameter. Top 10 in.
f11655.	GOC-4B. Pinkish-yellow clastic limesand—mostly fine grained, with <10 percent *Calcarina* but local patches contain abundant *Calcarina*. Only occasional roots in upper part. Thickness, 26 in.
f11656.	GOC-5. North-central part of northern main island, about 1,700 ft northeast from Taneang-Tekawa Maneaba. Area of pebble coral gravel with interstitial limesands. Stony and hard to dig. Dug down only 20 in., of which top 10 in. is organic-rich, brownish-gray soil with plentiful roots. Lower 10 in. pinkish yellow.
f11657–f11659.	GOC-6. North-central part of northern main island, about 2,400 ft north-northeast from Taneang-Tekawa Maneaba. Section in area of fine clastic limesands locally with thin gravel veneer at surface and locally of old dune sand material near shore. Pit section in descending order, with unit thicknesses, is:
f11657.	GOC-6A. Organic-rich, dark-gray-brown limesand, 20± percent worn *Calcarina*, few small pebbles (as much as one-half of an inch in diameter), many small roots. Top 6 in.
f11658.	GOC-6B. Dark-tan limesand, 30–40 percent worn *Calcarina*, many roots as much as one-half of an inch in diameter; no pebbles. Thickness, 10 in.
f11659.	GOC-6C. Flesh-colored medium-grained limesand, 10–25 percent badly worn *Calcarina*. Thickness, 14 in.

U.S.G.S. loc. No.	Field localities and descriptions
f11660–f11661.	GOC-17. Central part of northern main island, about 2,100–2,200 ft due east from Buariki Maneaba. Area of fine clastic limesilt on which water lies close to surface, hardpan tends to form, ground water is brackish, and soil is generally poor. Pit section in descending order, with unit thick-nesses, is:
f11660.	GOC-17A. Fine medium-grayish-tan limesand and limesilt. Many roots as much as three-eighths of an inch in diameter. Few *Calcarina*. Top 9 in.
f11661.	GOC-17B. Light-tan medium-grained limesand, 10–15 percent *Calcarina*. Roots mainly in top inch or two but some to bottom. Thickness, 15 in.
f11662.	GOC-19. Beach sand on the northwest shore of islet of Nanntabuariki. Excellently preserved *Baculogypsina* and *Marginopora* washed in from adjacent reef flats to north and east.
f11663–f11664.	GOC-20. Southern main island, section above beach just south of Otose village Maneaba, lagoon shore. Section in descending order, with unit thicknesses, is:
f11663.	GOC-20A. Limesand, 20± percent *Calcarina*, scattered pebbles as much as 2 in long. Top 24 in.
f11664.	GOC-20B. Shell bed, limesand (50 percent *Calcarina*) matrix—small *Cardium* most abundant. Goes laterally to a pebble gravel. Thickness, 6 in.
None.	GOC-20C. Limesand, 40–50 percent *Calcarina*, occasional pebbles as much as 2 in long. Thickness, 15 in.
f11665.	GOC-27. About 9,200 ft S. 72° W. from offshore end of Government Station jetty (on southern part of northern main island) just south of main passage out of lagoon (Rawa ni Karoro) where coral shoals known as Aon te Rabata begin to deepen. Collection from area where reef knolls and patches rise above the limesand bottom at 16 ft depth. Most specimens from a low coral patch about 14 ft below the surface.
f11666.	GOC-28. Slightly less than 4 miles N. 85° W. from Aiaki Maneaba in outer lagoon. Reef patches and knolls rising above limesand bottom (at 14 ft) to within 6 ft of water surface. Fish taken from on and near reef knolls and sediment taken from bottom.
f11667.	GOC-29. About 1 mile S. 32° W. from Tekawa church at lagoon margin of south end of reef stretch known as Aon te Baba. Collection from reef patches rising above limesand bottom (at a depth of 9 ft reduced to mean low tide) to within 1 ft of surface. Much *Halimeda*, many sheetlike crustose corallines red on under sides. Limesand very fine to limesilt at centers of open areas.
f11668.	GOC-30. *Heliopora* flat at south end of the northern main island. At +1 ft low tide, tops of living *Heliopora* and few *Porites lobata* seen were just flush with water surface.

U.S.G.S. loc. No.	Field localities and descriptions
f11669.	GOC-31. Southeast end of northern main island. Scrapings from green algal crust on inner flat of windward reef about midway out (east) on reef flat from center of cove at southeast end of island. Sediment-binding green algae are matted with *Baculogypsina*, *Marginopora*, and other Foraminifera.
f11670.	GOC-33. About 7,100 ft S. 50° W. from Tekawa church at seaward edge of Aon te Baba reef north of main boat passage. Reef area is broad and irregular, fronted seaward by area of limesand 18 ft deep at midtide or about 15 ft reduced to mean low tide. (At collecting locality reef itself at general depth of 3 ft at mean low tide, with holes to depth of 8 ft at mean low tide.) Medium-grained limesand with ripple marks parallel to reef front. Slopes gradually seaward with off-lying reef patches.
f11671–f11672.	GOC-35. About 8,600 ft N. 18° W. from Tabuarorae Maneaba in 17 ft of water at mean low tide.
f11671.	GOC-35a. South bottom sample.
f11672.	GOC-35b. North bottom sample. Area of many coral patches on limesand-gravel bottom. Anchored for first sample (f11671 GOC-35a) of limesand-gravel over an area richly floored with red bushy crustose coralines, but dragged anchor and drifted northwest about 100 yd where collected second bottom sample (f11672, GOC-35b) of relatively pure limesand.
f11673–f11674.	GOC-36. Southeast end of reef area known as Rakai Ati (south side of big westward point of reef near center of atoll). A flourishing reef; collection from reef flat northeastward in shoal waters, from strip about one-half of a mile long running clear across the reef.
f11673.	GOC-36a. Seaward or southwestward ±500 ft is area of much coral in small and large patches with interspersed coarse limesand having a considerable gravel fraction of granule and pebble size.
f11674.	GOC-36b. Lagoonward or northeastward ±500 ft is mostly sand with scattered coral patches.
f11675.	GOC-37. About one-third of the distance between the north point of the reef area known as Rakai Ati and the east end of Rakai Maneku, at inner part of point of reef that projects westward from near the center of Onotoa Atoll. Sediment sample taken from hole about 10–12 ft deep.
f11676.	GOC-38. Lower beach at southwest corner of Tebaki, north end of northern main island. Sandy lagoon beach.
f11677.	GOC-45. Area of *Thalassia* patches on coarse limesand bottom off northwest end of outer rib of elevated beachrock at north Tekawa, northwest Onotoa Atoll.
f11678.	GOC-48. About 10,000 ft S. 62° W. from lagoon end of Government Station jetty at north end of reefy shoal area known as Aon te Rabata. Coral patches rising to within 5 ft of surface from lesser (30–50 percent of area) intervening areas of limesand bottom, 12 ft.
f11679.	GOC-49. About 12,000 ft S. 63° W. from lagoon end of Government Station jetty, on the seaward side of the north end of a reefy shoal area known as Aon te Rabata, in patch reefs rising to within 6 ft of surface Limesand bottom at 18 ft deep.
f11680.	GOC-51. About 3¼ miles N. 31° W. from Tabuarorae Maneaba near center of Te Rawa ni Bao, a pass in south part of leeward reef. Collected from thickly set coral masses rising from 15 ft (sounded at low tide) of water to within about 8–10 ft of surface locally. Bottom of coral-algal rock and living corals and algae with minor pockets of very coarse limesand and calcareous gravel. Sediment sample taken in shoal area lagoonward in about 3 ft of water from hole containing coarse limesand and gravel.
f11681.	GOC-52. About 12,000 ft N. 30° W. from Tabuarorae Maneaba at south end of Rakai ni Make, a reef area in southern part of leeward reef. Collected corals, algae, mollusks, and sample of coarse limesand and gravel, the latter from a hole in about 3 ft of water.
f11682.	GOC-53. About 9,300 ft N. 30° W. from Tabuarorae Maneaba in southern part of Te Rawa Tekatobibi, a pass through south end of leeward reef. Collected from coral patches and knolls rising to occasional maximum of within 4 ft of surface from a bottom sounded at 18 ft.
f11683	GOC-55. About 13,400 ft S. 75° W. from Aiaki Maneaba in deep central part of the lagoon. Impalpably fine limemud from bottom of low scattered dead and living coral patches on intervening limemud and limesand about 30–40 percent sediments and 60–70 percent coral.
f11684.	GOC-56. About 8,300 ft S. 76° W. from Aiaki Maneaba on reef patch in the central lagoon. Complex mass of living coral with patches of limesand and fine gravel on surface, perhaps 150–200 yd in diameter, rising from surrounding bottom of ±18 ft. Depths on knoll 4–10 ft at mean low tide, with coral heads rising to within 1 ft of surface. Sediment sample from mean low tide depth of ±6 ft.
f11685.	GOC-57. About 7,500 ft S. 80° W. from Aiaki Maneaba on reef patch in central lagoon. Habitat, bottom types, and depth range similar to f11684 (GOC-56), but much more limesand and less coral. Depth of sediment sample at ±6 ft at mean low tide datum.

U.S.G.S. loc. No.	Field locations and descriptions
f11686.	GOC–58. About 3,600 ft S. 80° W. from Aiaki Maneaba on reef patch in central lagoon. Generally similar to f11684 (GOC–56) and f11685 (GOC–57) but smaller and deeper and contains even less coral than f11685 (GOC–57). Bottom at ±10 ft at mean low tide datum, with patchy coral. Collected bottom sample at 15 ft mean low tide datum from limesand slope leading off to slightly deeper water.
f11687.	51–L–8. Southeast end of Tabuarorae islet corresponding to Aontebeke land area. Weakly bonded limesand along beach.
f11688.	51–L–9. Southwest end of Mangaia land area, Tabuaurorae islet. Low, narrow north-trending ridge in area of lush vegetation, apparently most easterly of a set of older dunesand ridges—±500 ft long, about 60 ft across from intertrough to intertrough. Only one of set that seems phosphatic.
f11689.	51–S–5. Central Tabuarorae islet. West end of tidal flats encircled by islet.
f11690.	51–S–6. Tabuarorae islet. Near center of north arm of tidal flats encircled by islet.
f11691.	51–S–7. About 4,400 ft N. 86° W. from northwest corner of Abanekeneke, sediment taken in about 14 ft of water at mean low tide datum.
f11692.	51–S–8. About 1,400 ft S. 60° W. from lagoon end of Government Station jetty. Drag sample of limesand bottom between sparse dead and living coral, taken in about 9 ft of water at mean low tide datum.
f11693.	51–S–9. About 4,200 ft S. 79° W. from lagoon end of Government Station jetty. Fine limesand bottom at 20 ft depth at mean low tide datum. Patches of growing coral mostly to about 10–15 ft in diameter and only 1–2 ft above bottom.
f11694.	51–S–10. About 3½ miles N. 30° W. from Tabuarorae Maneaba. From coarse- to medium-grained limesand bottom about 10 ft deep with coral pinnacles rising to within 6 ft of surface.
f11695.	51–S–11. About 4,600 ft S. 65° W. from lagoon end of Government Station jetty. Limesand bottom of reentrant or depression in large lagoon reef patch.
f11696.	51–S–12. West side of Tebaki, northwest Onotos Atoll. Center of clean limesand area between southwestward extending limesand spits.

FAUNA

A total of 168 species and varieties have been found in the Onotoa samples. In table 1 the samples are grouped, according to similarity of environment, in the following categories:

1. Area open to ocean on west (leeward side)
2. Lagoon
3. Reef areas
4. Islands along east side of atoll.

In the last category are included both modern beach sands and material from a series of dug pits inshore from the sea beach. Samples from the pits are grouped according to similarity of composition and in order of increasing variety of species. With this arrangement, the samples fall into three subdivisions: those interpreted as beach sands, those interpreted as reef flat sediments, and those transitional between these two types of deposits.

As the Onotoa species are nearly all well known and well illustrated (Cushman, Todd, and Post, 1954; Todd, 1957; Todd and Low, 1960), complete formal descriptions are not included in this report and only a selected few are illustrated. In a later section, certain species that are not found in these three Professional Papers are discussed and selected references included for them.

Major constituents of the Onotoa fauna are:

Amphistegina madagascariensis d'Orbigny
Baculogypsina sphaerulata (Parker and Jones)
Calcarina spengleri (Gmelin)
Elphidium striato-punctatum (Fichtel and Moll)
Homotrema rubrum (Lamarck)
Heterostegina suborbicularis d'Orbigny
Marginopora vertebralis Blainville

Besides these, the following species, although they make up negligible amounts of the population, are found in most of the samples except the beach sand:

Acervulina inhaerens Schultze
Cibicidella variabilis (d'Orbigny)
Cornuspira planorbis Schultze
Cymbaloporetta bradyi (Cushman)
C. squammosa (d'Orbigny)
Elphidium advenum var. *dispar* Cushman
E. crispum (Linné)
Gaudryina (*Siphogaudryina*) *rugulosa* Cushman
Haddonia torrestensis Chapman
Neoconorbina patelliformis (Brady)
Planorbulina acervalis Brady
Pyropilus rotundatus Cushman
Quinqueloculina polygona d'Orbigny
Reussella simplex (Cushman)
Rosalina candeiana d'Orbigny
Schlumbergerina alveoliniformis (Brady)
Siphogenerina raphana (Parker and Jones)
Spirolina arietina (Batsch)
Spiroloculina angulata Cushman
Tretomphalus concinnus (Brady)
T. planus Cushman
Triloculina irregularis (d'Orbigny)
T. oblonga (Montagu)

The remaining 138 species and varieties are rare for the most part, and their occurrences are scattered or single occurrences. Among them, however, are a few species whose distribution shows a restricted, and possibly significant pattern.

TABLE 1.—*Distribution of Recent Foraminifera of Onotoa Atoll*

[A indicates abundant; C, common; R, rare. Symbol printed in boldface indicates presence of live specimens]

	Area open to ocean on west (leeward side)							Lagoon															Reef areas					Southern part of atoll			
								Southern							Central and northern								Leeward			Windward					
	GOC-33	GOC-27	GOC-48	GOC-49	GOC-37	GOC-51	GOC-53	GOC-35a	GOC-35b	GOC-55	GOC-56	GOC-57	GOC-58	GOC-28	51-S-10	51-S-7	51-S-8	51-S-9	51-S-11	GOC-29	GOC-45	51-S-12	GOC-52	GOC-30a	GOC-30b	GOC-30	GOC-31	51-L-8	51-L-9	51-S-5	51-S-6
Hyperamminidae:																																
Sagenina frondescens (Brady)		R																							R								
Lituolidae:																																
Ammobaculites sp. (pl. 22, fig. 1)																				R											
Textulariidae:																																
Textularia agglutinans d'Orbigny	R	R		R			R			R	R	R			R			R		R			R				R				
alveata Todd				R				R	R		R	R				?													
candeiana d'Orbigny		R					R																									
dupla Todd	R	?					C		R											R												
foliacea Heron-Allen and Earland											R																				
foliacea var. *oceanica* Cushman									C		R	R																			
Verneuilinidae:																																
Gaudryina cf. *G. pauperata* Earland																							R								
(*Siphogaudryina*) *rugulosa* Cushman (pl. 25, fig. 5b)	R	C	C	R	C	C	A			R	R	C	R	R	C				R				C			R					
(*Siphogaudryina*) *siphonifera* (Brady)																									R							
Valvulinidae:																																
Valvulina davidiana Chapman	R	R	R	R						R	R	R		R						R		R									
Clavulina angularis d'Orbigny	R	R	R	C	R					R		R						R	R	C						R					
Miliolidae:																																
Quinqueloculina agglutinans d'Orbigny			R								R		R				R		R			?		R						
anguina Terquem var. *arenata* Said			R	R	R					R		R		R		R	R	C	R	C												
bertheloliana d'Orbigny							R								R																	
bidentata d'Orbigny (pl. 22, fig. 2)	R	R	R	R						R	R	R	R	R	R	R	R	R		R	R				?						
disterquesta Cushman	R				R										R				R	R							R				
cf. *Q. ferussaci* d'Orbigny				R					R		R			R						R		R									
neostriatula Thalmann	R	R									R	R	R				R	R	R		R	R	R	R		R	R					
polygona d'Orbigny (pl. 22, fig. 5)			R	R							R		R	C		R	R		R		R		R									
sulcata d'Orbigny	R		R	R	R		R			R		R	R			R		R		C		R									
lobus Todd	R	R	R		R							R	C	R	R		R		R		R			R		R	R					
Triloculina bicarinata d'Orbigny	R			R		R	R		R													R									
cuneata Karrer	R	C									R							R		R	R	C									
cariandi Cushman			R	R							R					R	R		R		R											
incisura Todd					R		R					R	R		R	R				R		R	R		R	C	R			R	R
irregularis (d'Orbigny)	C	R	R	C	R	R	R	R		R	R	R	R	R	R		R	R		R	R	C	R		R	R					
kerimbatica (Heron-Allen and Earland)	R	R	R										R	R			R				R		R	C		R	R					
marshallana Todd		R					R		R															C		R							
oblonga (Montagu)			R	R	R		R			R	R	R	R					R	R	R	A	R	R	R		R	R				R	R
spinata Cushman																				R					?							
subplanciana Cushman	R				R						R		?										R								
transversestriata (Brady)																				R											
tricarinata d'Orbigny																		R							R							
trigonula (Lamarck)	R			R																				R							
Spiroloculina angulata Cushman	R	R	R	R	R	R		R		R		R			R	R	R		C	R		C		R	?		R			
clara Cushman	R			R										R	R		C	R		R		C	R		R							
clara var. *lirata* Cushman																R														
communis Cushman and Todd	?					R														R			R								
corrugata Cushman and Todd																																
eximia Cushman			R		R										R														
rugosa Cushman and Todd																				R											
sensata Cushman and Todd			R																	R		R								
Massilina planata Cushman		R			R					R				R					R	R											

	From islands along east side of atoll																										
	Beach sands				Pits inshore from sea beach (see text fig. 1)																						
					Interpreted as beach sands													Transitional sediments							Interpreted as reef flats		
	GOC-38	GOC-19	GOC-20A	GOC-20B	GOC-1A	GOC-2A	GOC-3A	GOC-3B	GOC-3D	GOC-3F	GOC-4A	GOC-5	GOC-6A	GOC-6B	GOC-6C	GOC-1B	GOC-2B	GOC-4B	GOC-17A	GOC-17B	GOC-1C	GOC-2C	GOC-1D	GOC-2D	GOC-1E	GOC-2E	GOC-2F
Hyperamminidae:																										
Sagenina frondescens (Brady)																										
Lituolidae:																										
Ammobaculites sp. (pl. 22, fig. 1)																										
Textulariidae:																										
Textularia agglutinans d'Orbigny		R		R					R						R	R	R				R		R		R	R	R
alveata Todd																										
candeiana d'Orbigny																	?						R		R	R	R
dupla Todd																										R		R
foliacea Heron-Allen and Earland																										
foliacea var. *oceanica* Cushman																										
Verneuilinidae:																										
Gaudryina cf. *G. pauperata* Earland																										
(*Siphogaudryina*) *rugulosa* Cushman (pl. 25, fig. 5b)	R									C	R						R				R			R			R	R
(*Siphogaudryina*) *siphonifera* (Brady)																										
Valvulinidae:																										
Valvulina davidiana Chapman	R			R																						
Clavulina angularis d'Orbigny																									R	R	R
Miliolidae:																										
Quinqueloculina agglutinans d'Orbigny																										
anguina Terquem var. *arenata* Said																										
bertheloliana d'Orbigny																										
bidentata d'Orbigny (pl. 22, fig. 2)	?																					R	R	C	R	R
disterquesta Cushman																										
cf. *Q. ferussaci* d'Orbigny																	?			C					R		
neostriatula Thalmann																		R								
polygona d'Orbigny (pl. 22, fig. 5)																	R				C	R	R	R	A	A	C
sulcata d'Orbigny																											R
lobus Todd	R																R	R	R	R	R	R	R	R	R	R	R
Triloculina bicarinata d'Orbigny																				?							
cuneata Karrer																C				R	A		A		R	A	R
cariandi Cushman																				R							
incisura Todd	R	R														C	C	R	R	C	C	A	C	C	A	C	C
irregularis (d'Orbigny)											R						R	R	R	R	R	R	R	R		R	R
kerimbatica (Heron-Allen and Earland)			R														C		R		R	R	C	R	A	C	C
marshallana Todd																	?			R				R	R		
oblonga (Montagu)	R			R	R				R	R						C	R			R	C	A	A	C	C	C	C
spinata Cushman																										
subplanciana Cushman																				R							R
transversestriata (Brady)																									R		R
tricarinata d'Orbigny																										
trigonula (Lamarck)																									R		
Spiroloculina angulata Cushman																R	R	R		R	R	R	R	C	C	R	C
clara Cushman	R																									
clara var. *lirata* Cushman																										
communis Cushman and Todd																										
corrugata Cushman and Todd																					R	R	R		R	R	R
eximia Cushman																										
rugosa Cushman and Todd																										
sensata Cushman and Todd																											R
Massilina planata Cushman																										

TABLE 1.—*Distribution of Recent Foraminifera of Onotoa Atoll*—Continued

[A indicates abundant; C, common; R, rare. Symbol printed in boldface indicates presence of live specimens]

	Area open to ocean on west (leeward side)						Lagoon														Reef areas				Southern part of atoll			From islands along east side of atoll																									
									Southern							Central and northern								Leeward			Windward						Beach sands				Pits inshore from sea beach (see text fig. 1)																					
																																					Interpreted as beach sands													Transitional sediments							Interpreted as reef flats		
	GOC-33	GOC-27	GOC-48	GOC-49	GOC-37	GOC-51	GOC-53	GOC-35a	GOC-35b	GOC-55	GOC-56	GOC-57	GOC-58	GOC-28	51-S-10	51-S-7	51-S-8	51-S-9	51-S-11	GOC-29	GOC-45	51-S-12	GOC-32	GOC-36a	GOC-36b	GOC-30	GOC-31	51-L-8	51-L-9	51-S-5	51-S-6	GOC-38	GOC-19	GOC-20A	GOC-20B	GOC-1A	GOC-2A	GOC-3A	GOC-3B	GOC-3D	GOC-3F	GOC-4A	GOC-5	GOC-6A	GOC-6B	GOC-6C	GOC-1B	GOC-2B	GOC-4B	GOC-17A	GOC-17B	GOC-1C	GOC-2C	GOC-1D	GOC-2D	GOC-1E	GOC-2E	GOC-2F
Miliolidae—Continued																																																										
Hauerina diversa Cushman				R							**R**	R						R		R			R																													R							
involuta Cushman	R	R	R	R	R								R				R	R		R					R																																		
milletti Cushman				R			?				**R**	R	R			R		**R**		R			**R**																																				
pacifica Cushman	**R**	R		R			R												R	R			?	**R**																									R											
serrata Cushman	R								R	?									R																																					
speciosa (Karrer)					R										R				R																																					
Schlumbergerina alveoliniformis (Brady)	R	C	R	C	R		R		R	R	**R**	C	**R**	R	**R**	R	C	C	R	C	C	R	**R**		**R**						R																		R	R						R	R
Ammomassilina alveoliniformis (Millett)		R																R																																						
Articulina elongata Cushman																					R																																					
pacifica Cushman			R					R		R				R						R																																					
Nubeculina divaricata (Brady)		?	C	R	R									R	R				R	R			R																																		
Miliolinella australis (Parr)	R					**R**													R		R		R	R																																		
labiosa (d'Orbigny)	R	R	R	R			R				**R**	**R**			R					C		R	R		**R**	R						R										R							R	R	R		R	R	R	R	C	R
oceanica (Cushman)	R																**R**		C			R		R	R	R						R																R				R	R		R			R
Pyrgo denticulata (Brady)									R																																															R	R
Ophthalmidiidae:																																																										
Cornuspira planorbis Schultze			R	R	R				R	R	**R**	**R**	R	R		**R**		**R**		**R**	R	R	C		**R**	R	R			R											R					R	R		R		R	R	C	C	R	R	R
Planispirinella exigua (Brady)												R				R		R		R												R																									
Wiesnerella auriculata (Egger)																					R																																					
Parrina bradyi (Millett)	R				R										**R**		**R**		R			**R**		**R**	R																								R	R	R					R	R	R
Fischerinidae:																																																										
Fischerina pellucida Millett (pl. 22, fig. 6)													**R**								R																																					
Placopsilinidae:																																																										
Placopsilina bradyi Cushman and McCulloch																								R																																		
? sp. (pl. 22, figs. 3, 4; pl. 25, fig. 5d)			R		R				R				R				**R**	R																																						
Haddonia torresiensis Chapman		C		R	R	**R**		R			R	**R**	R	R	R		R		R				**R**			C					R	C		R	R	R			R							C			R	R	R		A	R	R	A	R
Idelloidina aggregata Carter																																																											R
Polymorphinidae:																																																										
Sigmomorphina terquemiana (Fornasini)																								R																																		
Camerinidae:																																																										
Heterostegina suborbicularis d'Orbigny (pl. 25, fig. 5a)	A	A	C	C	A	A	A	A	A	A	A	A	C	A	A	C	C	A	A	A	C	C	A	C	C	R		R	C	C	R	C	R	R	C	R		R	C	A	C	C	C	R	C	C		R	R	C	C	R	C	C	R		R	C
Peneroplidae:																																																										
Peneroplis ellipticus d'Orbigny		R		R					R	R	**R**	**R**		R	**R**	R	R	**R**		R	R	R			**R**			R																														
proteus d'Orbigny (pl. 22, fig. 7)			R													R	R			R																															R						
Spirolina acicularis (Batsch)																	R		R		R																																							R
arietina (Batsch)	R	C	R	**R**	**R**	**R**		R	R	R		R	R	R	R		R	**R**		R	C	C	**R**	**R**	R	R	**R**			R		R			R						R				R		R	R	**R**	**R**	R			R			R
Monalysidium politum Chapman			R												?		R			R	R	R																																				
Sorites marginalis (Lamarck)		C	R	R								R	R	R		C	R			R		R								R																					R		R	R			R		R
Marginopora vertebralis Blainville	C	C	C	A	A	**R**	R	C	C	C	A	A	A	C	C	C	A	A	R	C	C	A	C	**R**	A	A	A	A		R	R	A	A	C	C	C	C		R	A	R	C	R				C	C	C	C	C	C	R	A	C	A	A	A
Alveolinellidae:																																																										
Borelis pulchrus (d'Orbigny)		**R**		R		R	R							R	R		R	R													R																										
Heterohelicidae:																																																										
Bolivinella folium (Parker and Jones)													R		R		R		R		R																																					
Buliminidae:																																																										
Buliminella milletti Cushman								R					R				R									R																												R	R	R	R	R
Buliminoides williamsonianus (Brady)				R			C									R				R																																					
Fissurina lacunata (Burrows and Holland)																					R																																					
lagenoides (Williamson)			R																																																						
milletti Todd								R																																														?				

Bolivina compacta Sidebottom			R														R			R			R			R					R										R											R	R		R	C	R	C
rhomboidalis (Millett)			R	R								R				R		R		R			R		R	R																						R				R	R	R	C	R	R	R
striatula Cushman																						R																														R		R	R	C	C	C
subexcavata Cushman and Wickenden					R		R	R			R	R				R		R		R	R	R	R			R																										R		R	R			
tortuosa Brady	R				R		R					R				R		R		R		R	R	R	R	R	R														R							R	R	R			R	R	R	R	R	R
(*Loxostomum*) *limbata* Brady	R				R				?	R	R					R			R	R						R																						R		R				R	R			R
(*Loxostomum*) *mayori* Cushman																		R		R						R																						R								R		
Reussella simplex (Cushman)	R	C	C	R	R	R	R		R	R	R	R	R	R		R	R	R	R	C			R																			R						R			R			R		R		R
Chrysalidinella dimorpha (Brady) (pl. 22, fig. 10)																															R																											
Uvigerina porrecta Brady																				R																																						
Siphogenerina raphana (Parker and Jones)	R	R	R	R	R		R		R	R		R					R			R		R	R								R					R						R						R	R		R	R	R	R	R	R	R	R
Rectobolivina? sp. (pl. 22, fig. 8)									R																																							R				R		R	R		R	R
Spirillinidae:																																																										
Spirillina decorata Brady				R														R							R							R																										
denticulo-granulata Chapman (pl. 23, fig. 5)				R		R														R																																						
inaequalis Brady	R															R										R																																
tuberculato-limbata Chapman	R			R													R					R																														R						
vivipara Ehrenberg				R	R															R			R			R																										R		R	R	R	R	R
vivipara var. *revertens* Rhumbler							R													R			R	R																												R			R		R	R
Conicospirillina trochoidea Cushman																																																										R
sp. (pl. 23, figs. 3, 4)					R																						R																					R						R		R		
Patellina advena Cushman																																																										R
advena var. *altiformis* Cushman																										R																																
Discorbidae:																																																										
Rotalina candeiana d'Orbigny	R	R	R	R	R		R			R		R			R	R	R	R	R	R		R	R	R	R	R	R			R	C			R		R											R	R	R	R	R	C	R	C	R	R	R	R
concinna (Brady)	R	C		C	R						R	R	R	R		R				C			R		C	C	R																														R	R
orientalis (Cushman)																																																							R		R	
Neoconorbina frustata (Cushman)																																																						R		?		
patelliformis (Brady)	R	R	R	R	R	R	R	R		R		R		R	R	R	C	C		C	R	R	R	R	R	R	R																						R	R	R							R
terquemi (Rzehak)	R						C	R												C					R	R																									R				R	R		
tuberocapitata (Chapman)	R																R																																									
Strakina sp.		R				R					R									R			R																																			R
Rotaliidae:																																																										
Streblus beccarii (Linné)			R							R			R		R	R	R	R	R	R		R			R			R			R																		R	C	A							
beccarii tepida (Cushman)		R					R									R				R			R																																			
Poroeponides cribrorepandus Asano and Uchio	R	R	R	C		R	R		R	R			R		R			R		R																										R												R
Epistomaroides polystomelloides (Parker and Jones)				R	R					R				R						R					R		?																							R	R					R		?
Siphonia tubulosa Cushman			R		R											R		R								R																																
Siphoninoides echinatus (Brady)		R			R														R																																							
Elphidiidae:																																																										
Elphidium advenum (Cushman)										R				R		R	R	R		R	R	R						R						R																				R	R			
advenum var. *dispar* Cushman	R	R	R	R	R		R		R	R		R		R		R		R		C		R	R		R																															R	R	R
crispum (Linné)	R	C	R	C	R	R	R	R	R	R	R	R		R	R	R	R	R	R	R		C	C	R	R					R	R		R	R	R													R	R		C				R	R	R	C
milletti (Heron-Allen and Earland)																																																								R		R
cf. *E. poeyanum* (d'Orbigny) (pl. 23, fig. 1)			R							R			R		R	R				R			?								R																											
simplex Cushman																R		R																													R	C		R	R	R	R	C	C	R	R	C
striato-punctatum (Fichtel and Moll)	R	A	C	C	C	R		R	R	A	C	C	C	A	C	A	A	A	A	A	C	C			C						R	C		R	C																							
Nonionidae:																																																										
Nonion pacificum (Cushman)	R	R	R		R		R													R			R																	R																		
Nonionella sp. Todd, 1957																				R																																						
Pegidiidae:																																																										
Pegidia dubia (d'Orbigny)																																																									R	
Sphaeroidia papillata Heron-Allen and Earland		R																																																								
Amphisteginidae:																																																										
Amphistegina madagascariensis d'Orbigny (pl. 25, figs. 4, 6)	A	A	C	A	A	A	A	A	A	A	A	A	A	A	A	A	A	A	A	A	A	A	A	A	A	A	C	C	A	A	C	A	A	C	C	C	C	C	C	A	A	C	C	C	C	C	R	A	C	A	C	C	C	C	C	R	A	C
Calcarinidae:																																																										
Calcarina spengleri (Gmelin) (pl. 25, figs. 7-9)	A	R	R	R	R		R	R	R			R	R	R		A	A	C	C	R	A	A		R	C	C		C	A	A	A	A		A	A	A	A	C	C	A	A	A	A	A	A	A	A	A	A	A	A	A	A	A	A	A	A	A
Baculogypsina sphaerulata (Parker and Jones) (pl. 25, figs. 1, 2)	C	R	R	R	C	R						R			R	R	R	R			R	R	C	A	A	A	A	A				A	C		R																							
Cymbaloporidae:																																																										
Cymbaloporetta bradyi (Cushman)	A	C	R	C	R		C	R	R	R	R	R	R	R	R	R	R	R	R	A	R	R	C	R	C	C	C			R						R			R	C	C							R	R		R	R	R	R	R		C	R
squammosa (d'Orbigny)			R			R	R	R				R			R		R					R	R		R		R	R			R	R	R						R		R						R	C				C		C	R	C	C	C
Pyropilus rotundatus Cushman (pl. 22, fig. 9)	R		R	R							R	R		R		R	R			R			R																									R				R				R	R	R
Tretomphalus concinnus (Brady) (pl. 24, fig. 4)		R	R	R			R	R		R			R	R	R			R		C			R		C															R												R		R	R		R	R
planus Cushman (pl. 24, fig. 6)	R	R	R	C	R			R		R						R		R		R			R		R	R																										C				C	C	C
Cassidulinidae:																																																										
Cassidulina minuta Cushman	R						R																R	R																																		
Epistominella tubulifera (Heron-Allen and Earland)	R	R		R		R	R													R			R		R	R																														R		
Robertinidae:																																																										
Allialina translucens (Cushman) (pl. 23, fig. 2)				R			R																		R																																	

TABLE 1.—*Distribution of Recent Foraminifera of Onotoa Atoll*—Continued

[A indicates abundant; C, common; R, rare. Symbol printed in boldface indicates presence of live specimens]

| | Area open to ocean on west (leeward side) | | | | | | Lagoon | | | | | | | | | | | | Reef areas | | | | Southern part of atoll | | | From islands along east side of atoll | | | | | | | | | | | |

The species *Textularia foliacea* Heron-Allen and Earland, with its variety *oceanica*, appears to be restricted to the central deeper part of the lagoon where the bottom is covered by fine to coarse limesand between patches of coral. *Streblus beccarii* (Linné) is a large robust form unknown in typical form in the Marshall Islands but is found fairly commonly around Saipan Island. At Onotoa Atoll it is present in some of the lagoonal sediments. It probably is not a reef dweller. The rare occurrences of *Bolivinella folium* (Parker and Jones) are all from limesand bottom in the central part of the lagoon.

Examples of the Foraminifera typical of the limesand bottom of the lagoon are illustrated on plate 25, figures 4–6.

In general, the Onotoa fauna shows rather close correspondence in species composition to the faunas of other areas of the central Pacific. Comparisons with shallow-water faunas around Saipan, Mariana Islands, (Todd, 1957), and inside the lagoons of four atolls (Bikini, Eniwetok, Rongelap, and Rongerik) in the northern Marshall Islands (Cushman, Todd, and Post, 1954) are of interest. At Saipan the material was collected from depths mostly not greater than 38 feet—depths comparable to those at Onotoa which were mostly shallower than 20 feet. In the Marshall Islands most of the samples came from depths greater than 60 feet. No striking differences in fauna were observed between Saipan and Onotoa when the rarer occurrences from each area are left out of consideration. In the Marshall Islands, on the other hand, where the material came from significantly greater depths than did the Onotoa material, three species that are unknown at Onotoa are present with more than scattered occurrences. Their absence at Onotoa may signify an upper depth limitation for them, somewhere between 20 and 60 feet. The species are *Operculina ammonoides* (Gronovius), *Calcarina hispida* Brady, and *Anomalinella rostrata* (Brady).

WET SAMPLES

Twenty-four of the Onotoa samples were treated with alcohol when collected in 1951 and preserved wet in order that distinction between living specimens and empty tests would be possible. By this means an estimate of which species actually lived in various locations and which species may have been deposited there as empty tests could be made.

In the spring of 1957, after approximately 6 years, the samples were processed by staining in rose bengal solution as described by Walton (1952, p. 58). Relatively few specimens (such as of the order of 1 percent) gave a positive reaction to the stain. It is unknown whether or not a 6-year interval between collection and processing may affect the apparent live-dead ratio. To me it seems doubtful that it had an appreciable effect on the Onotoa samples, as the stained specimens observed were mostly very clearly and unmistakable stained.

On table 1, the record of live specimens is indicated by the abundance symbol being printed in bold face. An A or C printed in bold face does not of course mean that the live specimens were abundant or common, but merely that among the abundant or common specimens were some live (stained) ones.

With the stained individuals forming so small a percentage of the total specimens present, it is not unreasonable to assume that evidence for these live specimens would be frequently missed. This assumption may be the explanation for the "lack" of stained specimens of a particular species in certain samples where unstained specimens of that species are common to abundant. The following common to abundant species are those of which living specimens probably occurred but were missed in the samples studied.

Amphistegina madagascariensis d'Orbigny
Baculogypsina sphaerulata (Parker and Jones)
Calcarina spengleri (Gmelin)
Cymbaloporetta bradyi (Cushman)
C. squammosa (d'Orbigny)
Elphidium striato-punctatum (Fichtel and Moll)
Heterostegina suborbicularis d'Orbigny
Marginopora vertebralis Blainville
Schlumbergerina alveoliniformis (Brady)
Spirolina arietina (Batsch)

The assumption that specimens of the foregoing species lived where they occur commonly to abundantly seems, therefore, a safe one.

The two major distinctive habitats that are recognizable at Onotoa on the basis of the relative abundance of species in the sediments are the surfaces and slopes of reefs and the limesand bottom of the lagoon. Presence and absence of stained specimens (that is, collected as living individuals) of certain species in samples from these two areas confirms the distinction between these two habitats. The major inhabitants of reef surfaces and the slopes adjacent to reefs seem to be (in order of abundance):

Calcarina spengleri (Gmelin)
Baculogypsina sphaerulata (Parker and Jones)
Amphistegina madagascariensis d'Orbigny
Marginopora vertebralis Blainville
Cymbaloporetta bradyi (Cushman)
C. squammosa (d'Orbigny)

The major inhabitants of the limesand bottom of the lagoon seem to be (in order of abundance):

Amphistegina madagascariensis d'Orbigny
Heterostegina suborbicularis d'Orbigny
Marginopora vertebralis Blainville
Spirolina arietina (Batsch)

Cymbaloporetta bradyi (Cushman)
C. squamosa (d'Orbigny)
Elphidium striato-punctatum (Fichtel and Moll)
Schlumbergerina alveoliniformis (Brady)

Minor inhabitants of the limesand floor include four large arenaceous species, *Valvulina davidiana* Chapman, *Haddonia torresiensis* Chapman, and the two large species of *Gaudryina* (*Siphogaudryina*); a variety of miliolids; the peneroplids *Peneroplis ellipticus* d'Orbigny and *Sorites marginalis* (Lamarck); several buliminids including *Reussella simplex* (Cushman) and a few species of *Bolivina;* a few discorbids including several species of *Rosalina* and *Neoconorbina;* several species of *Elphidium;* a few forms belonging in the Cymbaloporidae (*Pyropilus rotundatus* Cushman and two species of *Tretomphalus*); and several species of the families Anomalinidae and Planorbulinidae that are usually attached forms.

In addition, the following species are present as live specimens in the lagoon but seem to be locally restricted, their local restriction being obvious from the limited distribution of their empty tests as well as of stained specimens:

Buliminoides williamsonianus (Brady)
Cassidulina minuta Cushman
Epistomaroides polystomelloides (Parker and Jones)
Epistominella tubulifera (Heron-Allen and Earland)
Placopsilina? sp.
Poroeponides cribrorepandus Asano and Uchio
Siphoninoides echinatus (Brady)
Spirillina (several species)
Streblus beccarii (Linné)
Textularia dupla Todd
T. foliacea Heron-Allen and Earland
T. foliacea var. *oceanica* Cushman

As for the remaining 76 species present in the 24 wet samples, for which no evidence of living specimens was found, with but two exceptions the species are rare with scattered occurrences. One interpretation of these 76 may be that the specimens did not live precisely where found and the empty tests were deposited there after having been washed in from another, probably nearby, location. However, the possibility of missing stained specimens, in assemblages where the species in question occurs rarely, is very great. Thus a second interpretation is that evidence of live specimens was missed in many of these rare occurrences.

The two exceptions where species were not rare are *Spiroloculina clara* Cushman and *Homotrema rubrum* (Lamarck). Specimens of *Spiroloculina clara* were probably washed into their collecting localities as empty tests. In *Homotrema rubrum* the red original color of the test would preclude recognition of any red stain if present. Furthermore, it is unlikely that broken-off fragments of such permanently attached forms as *Homotrema* would retain their protoplasm for long. However, in other less firmly or less permanently attached forms, such as *Planorbulina* and *Acervulina*, staining proved that at least some of the detached specimens were still alive when collected.

EXAMINATION OF FISH CONTENTS

Stomach and gut contents of 22 fishes were examined for their Foraminifera, and many species were found in several of them (table 2). The fishes fall into five groups as follows:

Trigger fishes:
- Nos. 2–4. *Rhinecanthus aculeatus* (Linnaeus)
- 8. *R. rectangulus* (Bloch and Schneider)
- 5–7. *Balistapus undulatus* (Park)
- 20. *Melichthys buwia* (Günther)

Surgeon fishes:
- Nos. 16. *Acanthurus gahhm* (Forskål)
- 17. *Ctenochaetus striatus* (Quoy and Gaimard)
- 18. *C. cyanoguttatus* Randall

Parrot fishes:
- Nos. 9–15. *Scarus* sp.

File fish:
- No. 21. *Cantherines sandwichensis* (Quoy and Gaimard)

Puffers:
- Nos. 22, 24. *Arothron nigropunctatus* (Bloch)

From Cloud's observations in the field (written communication July 24, 1959), the feeding habits of these groups of fish are as follows: Trigger fishes and surgeon fishes browse mostly on algae and coral, but they also eat small echinoids and take in considerable amounts of the bottom sediment. The parrot fishes browse on algae, coral, and coral-algal rock, occasionally breaking off large chunks. The file fishes and puffers seem to eat mainly coral.

It can be seen from the occurrence table that a greater variety of Foraminifera species is found in the trigger and surgeon fishes (in which the habit of taking in bottom sediment is present) than in those fishes that ordinarily browse only on the various plants and animals that grow up from the lagoon floor.

In general, a larger proportion of attached forms are found in the stomach and gut contents than are found in the bottom sediments. In only one sample, however, was any foraminiferal material obviously bitten off by a fish: a large fragment of *Planorbulinoides retinaculatus* (Parker and Jones) found in one of the trigger fishes. Probably most of the specimens were taken in as a part of the bottom sediment incidental to the obtaining of other food. In some samples a large proportion of the specimens of *Amphistegina* still retain their light-green color and fresh appearance, suggesting they were living when taken in by the fish.

The composite fauna from the several fish examined is one characteristic of shallow conditions. The most abundant species is *Amphistegina madagascariensis* d'Orbigny, which is the dominant species in most

TABLE 2.—*Occurrence of Foraminifera in stomach and gut contents of fish from the lagoon at Onotoa Atoll*

	Trigger fishes									Surgeon fishes		Parrot fishes								File fish	Puffers	
	Rhiperoanthus sandwichensis (Lidstone)	*Balistapus undulatus* (Park)	*Melichthys niger* (Bloch)	*Acanthurus xanthopterus* (Cuvier)	*Ctenochaetus striatus* (Quoy and Gaimard)	*C. spongiolaris* Randall	*Sparus* sp.													*Cantherines sandwichensis* (Streets) (Lidstone)	*Arothron nigropunctatus* (Bloch)	
	2	3	4	8	5	5a	6	7	20	16	17	18	9	10	11	12	13	14	15	21	22	24
Textulariidae:																						
Textularia candeiana d'Orbigny										X												
Verneuilinidae:																						
Gaudryina cf. *G. pauperata* Earland	X				X																	
Valvulinidae:																						
Clavulina angularis d'Orbigny					X		X															
multicamerata Chapman	X																					
Miliolidae:																						
Quinqueloculina bidentata d'Orbigny										X												
neostriata Thalmann	X											X										
sulcata d'Orbigny	X							X														
Triloculina cuneata Karrer	X				X																	
incisura Todd																					X	
irregularis (d'Orbigny)	X		X	X	X	X		X		X												
karinabella (Heron-Allen and Earland)			X																			
oblonga (Montagu)	X				X		X	X		X		X										
subpoeyanana Cushman			X									X										
terquemiana (Brady)		X																				
trigonula (Lamarck)										X												
Spiroloculina angulata Cushman	X				X							X										
elora Cushman	X																					
Hauerina involuta Cushman												X										
milletti Cushman	X																					
pacifica Cushman												X									X	
Schlumberperina alveoliniformis (Brady)			X																			
Miliolinella australis (Parr)										X												X
labiosa (d'Orbigny)																					X	
Ophthalmidiidae:																						
Cornuspira planorbis Schultze	X																					
Parrina bradyi (Millett)	X																				X	
Camerinidae:																						
Heterostegina suborbicularis d'Orbigny	X	X	X		X		X	X		X	X	X				X		X				X
Peneroplidae:																						
Peneroplis dilipticus d'Orbigny			X																			
proteus d'Orbigny	X											X										
Sporolina orientina (Batsch)	X	X										X										
Marginopora vertebralis Blainville	X	X	X	X	X	X	X	X		X	X	X										
Buliminidae:																						
Stainera striatula Cushman	X																					
Bimonella simplex (Cushman)					X					X		X										
Siphogenerina raphana (Parker and Jones)					X																	
Entomobrinna? sp.										X												
Spirillinidae:																						
Spirillina vivipara Ehrenberg								X														
Coniospirillina sp.							X															
Discorbidae:																						
Rotalina caudeiana d'Orbigny					X			X		X	X	X									X	
concinna (Brady)	X						X															
rugosa d'Orbigny	X																					
Neoconchina patelliformis (Brady)								X		X		X										
Strabilina sp.							X	X														
Rotaliidae:																						
Nonion becarii (Linné)			X																			
Poroeponides cribronepunctus Asano and Uchio								X		X												
Elphidiidae:																						
Elphidium adversum (Cushman) var. *dispar* Cushman	X																					
crispum (Linné)					X	X				X	X	X										
simplex Cushman	X							X														
striato-punctatum (Fichtel and Moll)	X																					
Amphistegintidae:																						
Amphistegina madagascariensis d'Orbigny	X	X	X	X	X	X	X	X	X	X	X	X			X	X	X	X	X		X	X
Calcarinidae:																						
Cubicarina spengleri (Gmelin)	X	X	X	X				X		X	X								X			
Baculogypsina sphaerulata (Parker and Jones)		X			X	X		X		X	X					X						
Cymbaloporetidae:																						
Cymbaloporetta bradyi (Cushman)	X		X		X		X	X	X			X	X								X	
symmetrica (d'Orbigny)	X	X			X	X	X	X	X	X	X		X								X	
Tretomphalus concinnus (Brady)					X		X	X	X		X									X	X	
planus Cushman	X			X				X														
Globigerinidae:																						
Globigerinoides ruber (d'Orbigny)								X														
secaldiri (Brady)							X															
Anomalinidae:																						
Cibicides lobatulus (Walker and Jacob)					X															X		
Cibicidella variabilis (d'Orbigny)							X	X	X	X											X	X
Planorbulinidae:																						
Planorbulina acervalis Brady					X			X														
Planorbulinella retinaculata (Parker and Jones)		X		X	X																X	
Acervulina inhaerens Schultze	X				X			X	X													
Homotremidae:																						
Homotrema rubrum (Lamarck)		X		X		X	X	X	X	X		X	X	X					X		X	X

shallow waters of the tropical Pacific. The next most abundant species is *Heterostegina suborbicularis* d'Orbigny. Abundance of these two forms is known to vary greatly from place to place, possibly for reasons related to gregarious habit of Foraminifera. Likewise, their abundance varies greatly in the stomach and gut contents. Fish No. 15, for example, contained more specimens of *Heterostegina* than of any other genus of Foraminifera.

Miliolids are much more abundant than buliminids in the samples under discussion. Peneroplids (except for *Marginopora vertebralis* Blainville, a species that appears to live more abundantly on the reef flats than on the bottom of the lagoon) are rare, and arenaceous forms are almost completely missing. Globigerinids are also very rare in the stomach and gut contents. Quite a large proportion of the specimens found in the stomach and gut contents are attached forms, such as *Neoconorbina, Rosalina, Cymbaloporetta, Cibicides, Cibicidella, Acervulina, Planorbulina, Planorbulinoides*, and *Homotrema*.

In the bottom sediments, specimens of *Tretomphalus* are found in fair abundance; those with float chambers accompanied by rather large numbers of the *Rosalina*-stages without float chambers. The morphogenetic relationship between these two forms was demonstrated and clearly illustrated by Myers (1943, pl. 3), who also presented other observations regarding the biology and ecology of the genus *Tretomphalus*. Myers concluded (1943, p. 21) that the planktonic stage of *Tretomphalus* was very brief and lasted usually no more than 18 hours unless the specimen became encrusted with minute algae or other organisms, in which case it would remain afloat indefinitely. If not thus supported, a planktonic specimen would promptly sink to the bottom after the escape of the gametes through the large pores in the spherical float chamber. Thus in a tropical environment where there is no marked seasonal temperature fluctuation and where the water temperature of about 29° C is well above the 18° C observed to be the minimum temperature for development of the floating stages of *Tretomphalus* (Myers, 1943, p. 22), a steady supply of the fragile specimens with float chambers might be expected to be constantly added to the bottom sediments.

The *Rosalina* stages of *Tretomphalus*, however, presumably did not live in the bottom sands or muds but attached to algae or any sort of stemmed structure and thus could have been obtained by the fish as it browsed. Nevertheless, most of both forms of this genus were probably taken in as a part of the bottom sediment rather than in the process of browsing on algae or coral (Cloud, 1952, p. 26; 1959, p. 398–399, pls. 130, 131).

The trigger and surgeon fishes, most of which contain a large proportion of reef-dwelling Foraminifera, such as *Baculogypsina, Calcarina*, and *Marginopora*, may be interpreted as being frequenters of reef flats and reef fronts. Other fishes, whose stomachs are free or nearly free of those large genera, probably fed mostly in patch reefs and sandy areas. The observation that certain fish had consumed large proportions of one or the other, but usually not both, of the two major genera (*Calcarina* and *Baculogypsina*) that inhabit the reef flats suggests that individual fish may be quite restricted in their food-gathering travels.

Study of stomach and gut contents of sedentary animals might throw additional light on the probable dwelling places of various species of Foraminifera, whether on algae of various kinds, or on coral, or in the sands or muds of the lagoon bottom.

Table 2 gives the species of Foraminifera found in the 22 samples of fish stomach and gut contents. In only three samples were species found in the fish that were not also found in the bottom sediments:

1. *Clavulina multicamerata* Chapman in fish No. 2. It differs from *C. angularis* d'Orbigny in a rounded cross section toward the apertural end instead of a triangular section throughout.
2. *Triloculina terquemiana* (Brady) in fish No. 3.
3. *Rosalina rugosa* d'Orbigny in fish No. 2. It differs from *R. candeiana* d'Orbigny in having very coarse perforations, which may prove to be not a specific distinction.

FORAMINIFERA FROM PITS

Samples were examined from seven pit sections well away from the beach. All the pits were shallow, three in the southern part and four in the central part of the northern main island. (See USGS locs. f11639–f11661.) None of the four pits (GOC–4, GOC–5, GOC–6, and GOC–17) in the central part of the island exceeded 3 feet in depth. The other three pits (GOC–1, GOC–2, and GOC–3) were deeper: about 6 feet, 9 feet, and 11 feet, the deepest sample studied from the last hole, however, being at 10 feet.

Omitting the pit at GOC–17, all the excavations started in soil composed of nearly pure *Calcarina* sand, much darkened by organic matter, and in which roots were common. Some, but not all, of the specimens of *Calcarina* were much worn, presumably by abrasion before final deposition. The specimens also show the effects of corrosion by organic acids in the soil, in that many of the shells are porous with openings into the chamber cavities (pl. 25, fig. 7). The dark stain and porosity of the shells was not observed in material obtained from below a depth of about 1 foot.

The uppermost sections of the pits at GOC–1, GOC–2, and GOC–4 and the entire section of the pits

at GOC-3, GOC-5, and GOC-6 are interpreted as beach sands. (See fig. 41.) These sands are composed of *Calcarina* with lesser amounts of *Amphistegina*, *Marginopora*, and *Heterostegina*. Minor elements, such as miliolids and species of *Bolivina* and *Cymbaloporetta*, increase with depth in pits GOC-3 and GOC-6. In the lower sections of these pits the orange color of the sand and good preservation of specimens is similar to that of modern beach sands, and there is only slight evidence of abrasion. Presumably the species in these pits lived not far from where they were deposited.

In pits GOC-1, GOC-2, and GOC-4 the beach sands are gradually transitional into sediments with a much smaller proportion of *Calcarina* and a greater variety of other Foraminifera. Nevertheless, even with the change, *Calcarina* remains the predominant element to the bottom of all the pits. (See pl. 25, figs. 8, 9.) These richer and more varied sediments are interpreted as a reef-flat horizon which was built up to become progressively shallower and finally to be overrun by the sediments of an adjacent beach—sediments that now overlie it in the pits. The transition between beach sands and reef-flat sediment, however, occurs at different depths in the various pits. For example, the pit at GOC-3, although sampled to a greater depth than any other pit, did not—even at a depth of 10 feet—reach the rich fauna of the reef flat horizon (fig. 41).

The pit at GOC-17 was dug through limesand and limesilt throughout, and the entire 2-foot section is in sediments transitional between those of a reef-flat horizon and beach sands. No beach sands overlie the surface at GOC-17.

In addition to the pits on the northern main island, a small section is exposed above the beach on the lagoon side of the southern main island at GOC-20. Material in the 3¾-foot section is beach sand (pl. 25, fig. 3), slightly richer and less well worn than that occurring in the area of the pits on the northern main island.

A few of the species found in the pits were not found in the lagoon sediments. None of them occur more than very rarely and all are known as Recent species:

Adelloidina aggregata Carter
Conicospirillina trochoidea Cushman
Elphidium milletti (Heron-Allen and Earland)
Neoconorbina frustata (Cushman)
Patellina advena Cushman
Pegidia dubia (d'Orbigny)
Rosalina orientalis (Cushman)
Spiroloculina corrugata Cushman and Todd

Among the species found rather consistently in the lagoon and reef sediments, the following are conspicuous by their absence from the pits:

Baculogypsina sphaerulata (Parker and Jones)
Elphidium striato-punctatum (Fichtel and Moll)
Hauerina involuta Cushman
Spiroloculina clara Cushman
Valvulina davidiana Chapman

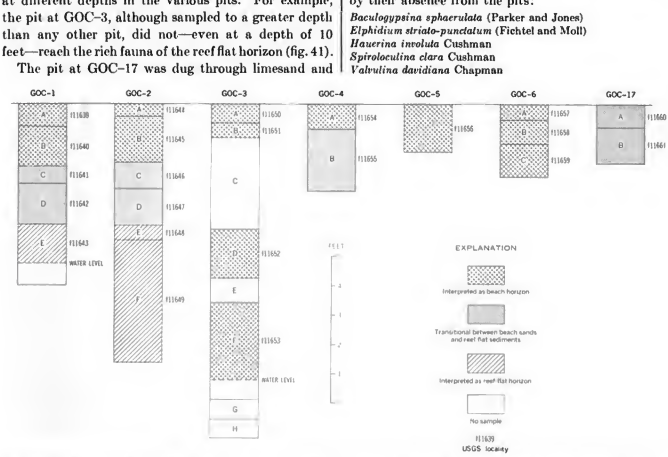

FIGURE 41.—Diagrammatic sections of seven dug pits on the northern main island of Onotoa Atoll. For detailed illustrations of Foraminifera sands of GOC-1D see pl. 25, fig. 9; of GOC-2F, pl. 25, fig. 8; GOC-6A, pl. 25, fig. 7.

For the last four species listed it is probable that a shallow reef-flat horizon is not the preferred habitat (see occurrence of these species in table 1), and hence their absence is not unexpected. For *Baculogypsina sphaerulata*, on the other hand, its absence in an environment known to be its preferred habitat is surprising and suggests the existence of some prohibitive factor, as discussed in the following section.

LOCAL DISTRIBUTION OF *CALCARINA* AND *BACULOGYPSINA*

With but two exceptions, the more abundant species at Onotoa seem to be distributed more or less uniformly, though in varying proportions depending upon the facies. The two exceptions are *Calcarina spengleri* (Gmelin) and *Baculogypsina sphaerulata* (Parker and Jones). Both of these two species are believed to be mainly reef dwellers although some live specimens were also found in the bottom sediments adjacent to reefs and in some beach sands (f11676, GOC–38) and coarse shallow sediments (f11677, GOC–45) of the lagoon.

Figure 40 shows the 27 localities where either one or both of these species was found to constitute a significant part of the Foraminifera population. Symbols indicate the approximate relative abundance of these species to each other (not to the total fauna). In table 1 it will be observed that either or both are present in many other samples, but less abundantly.

It may be seen that in the overall picture *Calcarina* dominates. It is present to the exclusion of *Baculogypsina* in 11 of the localities. In only 3 localities is *Baculogypsina* present alone, while in the remaining 13 localities the 2 genera are found together, though possibly not living together. Even though live specimens were found in the same sample, easy transport over short distances by means of surf or currents leaves the possibility open that the two genera do not occupy precisely the same ecological niche. In general the samples where *Baculogypsina* is predominant are from localities in or near breaks in the reef and away from land areas (pl. 25, figs. 1, 2).

I have no theories as to the reason for the separate geographic occurrence, here and elsewhere, of these two genera. I believe it is more than a chance distribution, and more than a result of incomplete collection of or examination of samples. In each of the seven pits (f11639–f11661, GOC–1 to GOC–17) only *Calcarina* was found. As two of these pits (GOC–2 and GOC–3) afford sections of about 9 and 10 feet, respectively, the sediments penetrated probably represent deposition over a considerable period of time. The fact that only *Calcarina* was found in all the pit samples suggests that *Baculogypsina* may have been a comparatively late comer to this atoll. However *Baculogypsina* is not a late comer in the general area of the western Pacific as is evidenced by the fact that at Bikini and Eniwetok atolls it is found in the shallow drillings but is not present in the Recent fauna.

NOTES ON SELECTED SPECIES

Chrysalidinella dimorpha (Brady)

Plate 22, figure 10

Chrysalidinella dimorpha (Brady). Cushman, 1945, Cushman Lab. Foram. Research Contr., v. 21, p. 52, pl. 8, figs. 21, 22.

This species is characterized by its elongate and straight-sided form. Only a single specimen was found.

Elphidium cf. E. poeyanum (d'Orbigny)

Plate 23, figure 1

Rare specimens found in several of the lagoon samples are distinctive in having a nearly transparent wall, uninflated test, and very short retral processes. In these characteristics they are similar to *Elphidium poeyanum* (d'Orbigny) (Cushman, 1939, p. 54, pl. 14, figs. 25, 26), a common species of the West Indian region. They are easily distinguishable from *E. simplex* Cushman, which has an umbilical plug, a milky wall, and a tendency toward inflation of the later chambers. I have not observed this very transparent species elsewhere in the western Pacific.

Globigerina cf. G. inflata d'Orbigny

Plate 24, figure 1

Rare specimens in the lagoon samples, mostly in those samples from areas open to the ocean on the southwest, seem related to *Globigerina inflata* d'Orbigny (Cushman, 1946, p. 16, pl. 3, fig. 3; pl. 4, figs. 1–4). They are close coiled with four chambers making up the final whorl and have a large, arched and rimmed aperture that opens into the umbilicus.

Globigerina inflata was not found in the *Globigerina* oozes around the Marshall Islands, nor was it observed among the rare globigerinids found in the shallow sediments around Saipan. Its nearest reported occurrence seems to be the Mid-Pacific seamounts (Hamilton, 1953, p. 222).

Globigerinita glutinata (Egger)

Plate 24, figure 3

Globigerinita glutinata (Egger). Phleger, Parker, and Peirson, 1953, Swedish Deep-Sea Exped. Repts., v. 7, Sediment cores from the North Atlantic Ocean, no. 1, p. 16, pl. 2, figs. 12–15.

Rare specimens of this small globigerinid occur in the lagoon and in the area open to the ocean. One

occurrence was from sediments interpreted as a reef-flat horizon from the bottom of one of the pits.

Neoconorbina terquemi (Rzehak)

Rosalina orbicularis Terquem, 1876, Essai Classement Animaux Plage Environs Dunkerque, Paris, fasc. 2, p. 75, pl. 9, fig. 4.
Rosalina terquemi Rzehak, 1888, Austria Geol. Reichsanst., Verh., p. 228.
Conorbina orbicularis (Terquem). Parker, 1954, Harvard Coll. Mus. Comp. Zoology Bull., v. 111, no. 10, p. 522, pl. 8, figs. 13, 14.

This species is type of the genus *Neoconorbina;* the name *terquemi* was proposed to differentiate Terquem's species from one described earlier under the name by d'Orbigny.

The species occurs in a few of the lagoon and reef-flat samples, in some samples fairly commonly. Their low, flat, scalelike shape suggests they were attached in life.

Nubeculina divaricata (Brady)

Nubeculina divaricata (Brady). Cushman, 1932, U.S. Natl. Mus. Bull. 161, pt. 1, p. 48, pl. 11, figs. 5, 6.

This miliolid with arenaceous coating is generally recognizable only when its uncoated tubular neck is preserved. It was found in a few of the lagoon and reef samples.

Placopsilina bradyi Cushman and McCulloch

Placopsilina bradyi Cushman and McCulloch, 1939, Allan Hancock Pacific Exped., v. 6, no. 1, p. 112, pl. 12, figs. 14, 15.
Placopsilina cenomana Brady [not d'Orbigny] 1884 [part], *Challenger* Rept., Zoology, v. 9, p. 315, pl. 36, fig. 1 [not figs. 2?, 3].

Several specimens of this permanently attached form were found on the surfaces of shells and algae from the reef edge (f11681, GOC–52). They consist of a series of coarsely agglutinated chambers, initially coiled, then in a uniserial arrangement and an irregularly winding course.

The first mention of this species (see second reference in synonymy) included two and possibly three types of forms under the name *Placopsilina cenomana:* figure 1, coarsely arenaceous, white, and with transverse measurements of 0.30–0.45 mm; figure 3, arenaceous, orange, and with transverse measurements of 0.04–0.08 mm; and figure 2 possibly differing in being either finely arenaceous or not agglutinated. The distinction between the very small orange one and the larger white one was recognized by the erection in 1920 of *P. confusa* Cushman (1920, p. 71, pl. 14, fig. 6) for the former, leaving the latter in *P. cenomana* d'Orbigny. The original description of *P. bradyi*, however, included all three of Brady's figures in synonymy, probably by oversight, as no mention of *P. confusa* is made, and the description, figures, and a paratype in the U.S. National Museum collection (USNM 35815) all indicate that a form equivalent to Brady's figure 1 (not fig. 3) is meant to carry the name of *P. bradyi*.

As comparison of type material of the two species, *P. confusa* and *P. bradyi*, indicates possible if not probable specific differences between the two, the name *P. bradyi* is retained for the Onotoa specimens.

Placopsilina? sp.

Plate 22, figures 3, 4; plate 25, figure 5d

Rare fragments of irregularly curving cylindrical agglutinated tubes, consisting of uniserial chambers varying in height but usually quite low and uneven in shape, were found in three lagoon samples. One unbroken end shows a smooth, round, and unrimmed apertural opening in the depressed center of the final chamber. These fragments may be the upward-growing parts of attached specimens of *Placopsilina*.

Quinqueloculina polygona d'Orbigny

Plate 22, figure 5

Quinqueloculina polygona d'Orbigny, 1839, *in* De la Sagra, Histoire physique, politique et naturelle de l'Île de Cuba, Foraminifères, p. 198, pl. 12, figs. 21–23.
Cushman, 1932 [part], U.S. Natl. Mus. Bull. 161, pt. 1, p. 25, pl. 6, fig. 6 [not fig. 5].

Typical specimens of this angular miliolid that was described from shore sands of Cuba are present, sometimes abundantly, in the Onotoa samples.

Rectobolivina? sp.

Plate 22, figure 8

Rectobolivina sp. Todd, 1957, U.S. Geol. Survey Prof. Paper 280–H, p. 290–291 (table)

In the Onotoa material, particularly that from the reef-flat horizons in pits GOC–1 and GOC–2, are rare specimens that are questionably referred to this genus. They are identical with some from Tanapag lagoon, Saipan. They are always in association with *Siphogenerina raphana* (Parker and Jones) from which they are distinguishable by their much smaller size (0.35–0.55 mm long), slenderer form (0.10–0.20 mm wide), more translucent wall, proportionally longer multiserial stage (becoming biserial but twisted in the present material), and the slightly indented sutures and hence slightly lobulated outline. They may prove to be related to *Siphogenerina raphana*, possibly being included in the same species.

Rosalina candeiana d'Orbigny

Rosalina candeiana d'Orbigny, 1839, *in* De la Sagra, Histoire physique, politique et naturelle de l'Île de Cuba, Foraminifères, p. 97, pl. 4, figs. 2–4.
Discorbis opima Cushman, 1933, Cushman Lab. Foram. Research Contr., v. 9, p. 88, pl. 9, fig. 3.

This is the commonest of the discorbids found at Onotoa, occurring in nearly all the lagoon samples and on the reef flats. It is too fragile to persist in the beach sands. As is typical of the family Discorbidae, specimens were probably loosely attached by their ventral surfaces during life, but not cemented, so that as empty tests they were easily washed down into the bottom sediments.

Rosalina concinna (Brady)

Discorbina concinna Brady, 1884, *Challenger* Rept., Zoology, v 9, p. 646, pl. 90, figs. 7, 8.
Discorbis micena Cushman, 1933, Cushman Lab. Foram. Research Contr., v. 9, p. 89, pl. 9, fig. 5.

This small circular scalelike species was also attached during life. It is almost surely the early stage of the species of *Tretomphalus* that is called *T. concinnus* (Brady), referring to the same Brady reference as above. Thus the separation of these two forms is wholly artificial and a matter of convenience. In most samples where either is common, the two forms occur together.

Rosalina orientalis (Cushman)

Discorbis orientalis Cushman, 1926, B. P. Bishop Mus. Bull. 27, p. 130 [imprint date 1925].
Todd, 1957, U.S. Geol. Survey Prof. Paper 280–H, p. 290–291 (table), pl. 90, fig. 13.

Comparison with the types indicates that this species is merely a high-spired form of *Rosalina candeiana*.

Spiroloculina rugosa Cushman and Todd

Spiroloculina rugosa Cushman and Todd, 1944, Cushman Lab. Foram. Research Spec. Pub. 11, p. 66, pl. 9, figs. 9–13.

A single specimen of this species with its distinctively rugose wall was observed in f11667, GOC–29.

Spiroloculina venusta Cushman and Todd

Spiroloculina venusta Cushman and Todd, 1944, Cushman Lab. Foram. Research Spec. Pub. 11, p. 60, pl. 8, figs. 16, 17.

This species was found rarely in the lagoon samples.

Svratkina sp.

Epistominella sp. D, Todd, 1957, U.S. Geol. Survey Prof. Paper 280–H, p. 292–293 (table), pl. 92, fig. 2.
Svratkina sp. A, Todd and Low, 1960, U.S. Geol. Survey Prof. Paper 260–X, p. 840.

The genus *Svratkina* was erected (Pokorný, 1956, p. 257) for specimens that had been previously reported under various other names from Australia, Europe, and America and from the Eocene (if not older) to the Recent. This compact and close-coiled genus is distinguished by large pores, particularly on the dorsal side, the pores sometimes surrounded by tubular necks, and by the aperture being a long, narrow opening extending from the umbilicus along the base of the apertural face to a depression beneath the periphery where it widens and extends upward into the apertural face.

The first reference cited above is to specimens of this genus from Recent lagoon sediments of Saipan; the second to specimens from the upper part of the Eniwetok drill holes in the Marshall Islands. Identical specimens are found rarely at Onotoa. They seem very close to the type of the genus, *Discorbis tuberculata* (Balkwill and Wright) var. *australiensis* Chapman, Parr, and Collins, but may prove to be distinct when sufficient material becomes available.

REFERENCES CITED

Cloud, P. E., Jr., 1952, Preliminary report on geology and marine environments of Onotoa Atoll, Gilbert Islands: Natl. Acad. Sci., Natl. Research Council, Pacific Sci. Board, Atoll Research Bull. 12, p. 1–73, figs. 1–8.
——— 1959, Geology of Saipan, Mariana Islands. Part 4, Submarine topography and shoal-water ecology: U.S. Geol. Survey Prof. Paper 280–K, p. 361–445, pls. 2, 120–139, figs. 36–43.
Cushman, J. A., 1920, The Foraminifera of the Atlantic Ocean. Part 2, Lituolidae: U.S. Natl. Mus. Bull. 104, pt. 2, p. 1–111, pls. 1–18.
——— 1939, A monograph of the foraminiferal family Nonionidae: U.S. Geol. Survey Prof. Paper 191, p. 1–100, pls. 1–20.
——— 1946, The species of *Globigerina* described between 1839 and 1850: Cushman Lab. Foram. Research Contr., v. 22, p. 15–21, pls. 3, 4.
Cushman, J. A., Todd, Ruth, and Post, R. J., 1954, Recent Foraminifera of the Marshall Islands: U.S. Geol. Survey Prof. Paper 260–H, p. 319–384, pls. 82–93, figs 116–118.
Hamilton, E. L., 1953, Upper Cretaceous, Tertiary, and Recent planktonic Foraminifera from Mid-Pacific flat-topped seamounts: Jour. Paleontology, v. 27, p. 204–237, pls. 29–32, figs. 1–5.
Myers, E. H., 1943, Biology, ecology, and morphogenesis of a pelagic foraminifer: Stanford Univ. Pubs., Biol. Sci., v. 9, no. 1, p. 1–30, pls. 1–4.
Pokorný, Vladimir, 1956, New Discorbidae (Foraminifera) from the upper Eocene brown Pouzdřany marl, Czechoslovakia: Prague, Univ. Carolina, Geologica, v. 2, no. 3, p. 257–278, figs. 1–15.
Todd, Ruth, 1957, Smaller Foraminifera, *in* Geology of Saipan, Mariana Islands. Part 3, Paleontology: U.S. Geol. Survey Prof. Paper 280–H, p. 265–320, pls. 2, 4, 64–93, tables 1–4.
Todd, Ruth, and Low, Doris, 1960, Smaller Foraminifera from Eniwetok drill holes: U.S. Geol. Survey Prof. Paper 260–X, p. 799–861, pls. 255–264, text figs. 256–259, tables 1–7.
Walton, W. R., 1952, Techniques for recognition of living Foraminifera: Cushman Found. Foram. Research Contr., v. 3, pt. 2, p. 56–60.

INDEX

[Italic numbers indicate descriptions]

Page

A

Abanekeneke ... 176
Acanthurus gahm ... 182, 183
acervalis, Planorbulina ... 176, 180, 183
Acervulina ... 182, 184
inhaerens ... 176, 180, 183
sp. ... 180
acicularis, Spirolina ... 178
Acknowledgments ... 171
aculeatus, Rhinecanthus ... 182, 183
adnexa aliformis, Patellina ... 179
Patellina ... 179, 183
adnexum dispar, Elphidium ... 176, 179, 183
Elphidium ... 179
aequisiderella, Globigerinella ... 180
aequitinans, Quinqueloculina ... 177
Textularia ... 177
aggregata, Rotaloidina ... 178, 183
Aiaki Maneaba ... 174, 175, 176; pl. 25
Allaitina transiuens ... 179; pl. 23
aliformis, Patellina adnexa ... 179
alveata, Textularia ... 177
Alveolinellidae ... 178
alveolinformis, Ammomassilina ... 178
Schlumbergerina ... 176, 178, 181, 182, 183
Ammobaculites sp. ... 177; pl. 22
Ammomassilina alveolinformis ... 178
ammonoides, Operculina ... 181
Amphistegina ... 182, 185; pl. 25
madagascariensis ... 176, 179, 181, 182, 183; pl. 25
Amphistiginidae ... 179, 183
anguina arenata, Quinqueloculina ... 177
angularis, Clavulina ... 177, 183, 184
angulata, Spiroloculina ... 176, 177, 183
Anomalina abbreviata ... 180
Anomalinella rostrata ... 181
Anomalinidae ... 180, 182, 183
Aon te Baba ... 174, 175; pl. 25
Aontebeke land area ... 176
Aon te Rabata shoals ... 174, 175
arenata, Quinqueloculina anguina ... 177
arietina, Spirolina ... 176, 178, 181, 183
arthrron nigropunctatum ... 182, 183
Articulina elongata ... 178
pacifica ... 178
auriculata, Wiesnerella ... 178
australiensis, Discorbis tuberculata ... 188
australis, Miliolinella ... 178, 183

B

Baculogypsina ... 172, 174, 175, 184, 186; pl. 25
sphaerulata ... 176, 179, 181, 183, 185, 186; pl. 25
Balistapus undulatus ... 182, 183
Baliolodina aggregata ... 178, 183
Beach sands ... 171, 176, 183, 186; pl. 25
beccarii, Strebina ... 179, 181, 182, 183
tepida, Strebina ... 179
bertheliana, Quinqueloculina ... 177
biarinata, Triloculina ... 177
bidentata, Quinqueloculina ... 177, 183; pl. 22
Bikini atoll, Marshall Islands ... 181, 186
Biloculina ... 182, 183
compacta ... 179
(*Lacrostomum*) *limbata* ... 179
major ... 179
rhombeidalis ... 179
striatula ... 179, 183
subscoaula ... 179
tortuosa ... 179
Biloculinella falcum ... 178, 181
Borelis pulchrus ... 178

C

Calcarina ... 172, 173, 174, 184, 185, 186; pl. 25
hispida ... 181
spengleri ... 176, 179, 181, 183, 185; pl. 25
Calcarinidae ... 179, 183
Camerinidae ... 178, 183
candeiana, Rosalina ... 176, 179, 183, 181, *188*
Textularia ... 177, 183
Cauthernes sandwichensis ... 182, 183
Cauthum ... 174
Cassidulina minuta ... 179, 182
Cassidulinidae ... 179
ceanomas, Placopsilina ... 187
Chrysolidinella dimorpha ... 179, *186*; pl. 22
Cibicidella ... 184
variabilis ... 176, 180, 183
Cibicides ... 184
cicatricosa ... 180
lobatulus ... 180, 183
mayori ... 180
pseudoungerianus ... 180
cicatricosa, Cibicides ... 180
clara lirata, Spiroloculina ... 177
Spiroloculina ... 177, 182, 183, 185
Clavulina angularis ... 177, 183, 184
multicamerata ... 183, 184
communis, Spiroloculina ... 177
compacta, Biloculina ... 179
concinna, Discorbina ... 188
Rosalina ... 179, 183, *188*
concinnus, Tretomphalus ... 176, 179, 183, 188; pl. 24
confusa, Placopsilina ... 187
conglobatus, Globigerinoides ... 180
Conicospirillina trochoides ... 179, 183
sp. ... 179, 183; pl. 23
Conorbina orbicularis ... 187
Cornuspira planorbis ... 176, 178, 183
corrugata, Spiroloculina ... 177, 183
cribroepondes, Poroponides ... 179, 182, 183
crispum, Elphidium ... 176, 179, 183
Ctenochaetus cyanoguttatus ... 182, 183
striatus ... 182, 183
cuneata, Triloculina ... 177, 183
cyanoguttatus, Ctenochaetus ... 182, 183
Cymbaloporetta ... 184, 185
bradyi ... 176, 179, 181, 182, 183
spinosa ... 176, 179, 181, 182, 183
Cymbaloporidae ... 179, 182, 183

D

davidiana, Valvulina ... 177, 182, 185
decorata, Spirillina ... 179
denticulata, Pyrgo ... 178
denticulo-granulata, Spirillina ... 179; pl. 23
dimorpha, Chrysolidinella ... 179, *186*; pl. 22
Discorbinae ... 179, 183, 188
Discorbina concinna ... 188
Discorbis micros ... 188
spinea ... 188
orientalis ... 188
tuberculata australiensis ... 188
bradyi, Cymbaloporetta ... 176, 179, 181, 182, 183
Perrina ... 178, 183
Placopsilina ... 178, *187*
Buariki Maneaba ... 174
Buliminella millettii ... 178
Buliminidae ... 178, 183
Buliminoides williamsonianus ... 178, 182
bulloides, Globigerina ... 180
bunion, Melichkys ... 182, 183

C

Calcarina ... 172, 173, 174, 184, 185, 186; pl. 25
hispida ... 181
spengleri ... 176, 179, 181, 183, 185; pl. 25
Calcarinidae ... 179, 183
Camerinidae ... 178, 183
candeiana, Rosalina ... 176, 179, 183, 181, *188*
Textularia ... 177, 183
Cauthernes sandwichensis ... 182, 183
Cauthum ... 174
Cassidulina minuta ... 179, 182
Cassidulinidae ... 179
ceanomas, Placopsilina ... 187
Chrysolidinella dimorpha ... 179, *186*; pl. 22
Cibicidella ... 184
variabilis ... 176, 180, 183
Cibicides ... 184
cicatricosa ... 180
lobatulus ... 180, 183
mayori ... 180
pseudoungerianus ... 180
cicatricosa, Cibicides ... 180
clara lirata, Spiroloculina ... 177
Spiroloculina ... 177, 182, 183, 185
Clavulina angularis ... 177, 183, 184
multicamerata ... 183, 184
communis, Spiroloculina ... 177
compacta, Biloculina ... 179
concinna, Discorbina ... 188
Rosalina ... 179, 183, *188*
concinnus, Tretomphalus ... 176, 179, 183, 188; pl. 24
confusa, Placopsilina ... 187
conglobatus, Globigerinoides ... 180
Conicospirillina trochoides ... 179, 183
sp. ... 179, 183; pl. 23
Conorbina orbicularis ... 187
Cornuspira planorbis ... 176, 178, 183
corrugata, Spiroloculina ... 177, 183
cribroepondes, Poroponides ... 179, 182, 183
crispum, Elphidium ... 176, 179, 183
Ctenochaetus cyanoguttatus ... 182, 183
striatus ... 182, 183
cuneata, Triloculina ... 177, 183
cyanoguttatus, Ctenochaetus ... 182, 183
Cymbaloporetta ... 184, 185
bradyi ... 176, 179, 181, 182, 183
spinosa ... 176, 179, 181, 182, 183
Cymbaloporidae ... 179, 182, 183

D

davidiana, Valvulina ... 177, 182, 185
decorata, Spirillina ... 179
denticulata, Pyrgo ... 178
denticulo-granulata, Spirillina ... 179; pl. 23
dimorpha, Chrysolidinella ... 179, *186*; pl. 22
Discorbinae ... 179, 183, 188
Discorbina concinna ... 188
Discorbis micros ... 188
spinea ... 188
orientalis ... 188
tuberculata australiensis ... 188
dispar, Elphidium adnexum ... 176, 179, 183
distorqueata, Quinqueloculina ... 177
Distribution of *Calcarina* and *Baculogypsina*, local ... 186
Distribution of Recent Foraminifera ... 177-180
divaricata, Nubecularia ... 178, *187*
diversa, Haurina ... 178
dubia, Pegida ... 179, 185
dupla, Textularia ... 177, 182

E

earlandi, Triloculina ... 177
echinatus, Siphoninoides ... 179, 182
eggeri, Globigerina ... 180; pl. 24
ellipsiana, Peneroplis ... 178, 182, 183
elongata, Articulina ... 178
Elphididae ... 179, 183
Elphidium ... 182
adnexum ... 179
dispar ... 176, 179, 183
crispum ... 176, 179, 183
millettii ... 179, 185
poeyanum ... 179, *186*; pl. 23
simplex ... 179, 183, 186
striato-punctatum ... 176, 179, 181, 182, 183, 185; pl. 25
Eniwetok atoll, Marshall Islands ... 181, 186, 188
Epistomaroides polystomelloides ... 179, 182
Epistominella tubulifera ... 179, 182
sp. ... 188
Examination of fish contents ... 182-184
eriqua, Planispirinella ... 178
eximia, Spiroloculina ... 177

F

Fauna ... 176-181
fernandei, Quinqueloculina ... 177
Fischerina pellucida ... 178; pl. 22
Fischerinidae ... 178
Flosculina lacunata ... 178
inornata ... 178
millettii ... 178
foliacea oceanica, Textularia ... 177, 181, 182
Textularia ... 177, 181, 182
folium, Biloculinella ... 178, 181
frondescens, Sagrina ... 177
frustata, Neoconorbina ... 179, 185

G

gahm, Acanthurus ... 182, 183
Gandryina pauperata ... 177, 183
(*Siphogandryina*) ... 182
rugulosa ... 176, 177; pl. 25
siphonifera ... 177
glabrata, Anomalina ... 180
Globigerina bulloides ... 180
eggeri ... 180; pl. 24
inflata ... 180, *186*; pl. 24
Globigerinella aequilateralis ... 180
Globigerinidae ... 180, 183
Globigerinoides glutinata ... 180, *186*; pl. 24
Globigerinoides conglobatus ... 180
ruber ... 180, 183
sacculifer ... 180, 183
globula, Gypsina ... 180
glutinata, Globigerinoides ... 180, *186*; pl. 24
Government Station ... 173, 174, 175, 176; pl. 25
Gypsina globula ... 180
plana ... 180
vesicularis ... 180

H — Page

Haddonia torresiensis 176, 178, 182
Halimeda 174
Haueriina diversa 178
involuta 178, 183, 185
miliolii 178, 183
pacifica 178, 182, 184
serrata 178
speciosa 178
Haliopora 173, 174
Heterohelicidae 178
Heterostegina ..... 184, 185; pl. 25
suborbicularis ..... 176, 178, 181, 183, 184; pl. 25
hispida, Calcarina 181
Hamotrema 182, 184
rubrum 176, 180, 182, 183
Hemotremidae 180, 183
Hyperamminidae 177

I

inaequalis, Spirillina 179
inciura, Triloculina 177, 183
infinita, Globigerina ..... 180, *186*; pl. 24
inhaerens, Acervulina 176, 180, 183
Introduction 171
involuta, Haueriina 178, 183, 185
irregularis, Triloculina 176, 177, 183
Islands along east side 171, 176, 177–180

K

kerimbatica, Triloculina 177, 183

L

labiosa, Miliolinella 178, 183
lacunata, Fissurina 178
lagenoides, Fissurina 178
Lagoon 171, 176, 177–180, 181, 182, 184
Leeward side 171, 176, 177–180
limbata, Rotalina (Laxostomum) 179
linata, Spiroloculina clara 177
Lituolidae 177
lobata, Peritea 174
lobatulus, Cibicides 180, 183
Locality data 173–176
(Laxostomum) limbata, Rotalina 179
mayori, Rotalina 179

M

madagascariensis, Amphistegina ..... 176, 179, 181, 182, 183; pl. 25
Mangan land area 176
marginalis, Sorites 178, 182
Marginopora ..... 173, 174, 175, 184, 185; pl. 23
vertebralis 176, 178, 181, 183, 184
Marianna Islands 181
Marshall Islands 181, 186, 188
marshallana, Triloculina 177
Massilina planata 177
Material studied 171
mayori, Rotalina (Laxostomum) 179
Cibicides 180
Melichata tenuis 182, 183
micera, Discorbis 188
Mid-Pacific seamounts 186
Miliolidae 177, 178, 183
Miliolinella australis 178, 183
labiosa 178, 183
oceanica 178
milletti, Miliolinella 178
Elphidium 179, 183
Fissurina 178
Haueriina 178, 183
minuta, Cassidulina 179, 182
Monalysidium politum 178
multicamerata, Clavulina 183, 184

N

Nanntabuariki islet ..... 174; pl. 25
Neoconorbina 182, 184, 187
frustula 179, 185
patelliformis 176, 179, 183
terquemi 179, *187*
tuberculata 179
neostriatula, Quinqueloculina 177, 183
nigropunctatus, Arothron 182
Nonion pacificum 179
Nonionella sp. 179
Nonionidae 179
Notes on selected species 186–188
Nubeculina divaricata 178, *187*

O

obliquiloculata, Pullenialina ..... 180; pl. 24
oblonga, Triloculina 176, 177, 183
oceanica, Miliolinella 178
Textularia falcata 177, 181, 182
Operculina ammonoides 181
Ophthalmidiidae 178, 183
opima, Discorbis 188
orbicularis, Conorbina 187
Rosalina 187
Orbulina universa ..... 180; pl. 24
orientalis, Discorbis 188
Rosalina 179, 185, *188*
Otone village Maneaba ..... 174; pl. 25

P

Pacific Science Board campsite ..... 173; pl. 25
pacifica, Articulina 178
Haueriina 178, 183
pacificum, Nonion 179
papillata, Sphaeridia 179
Parrina bradyi 178, 183
patelliformis, Neoconorbina 176, 179, 183
Patellina advena 179, 185
advena california 179
pauperata, Gaudryina 177, 183
Pejidia dubia 179, 185
Peginidae 179
pellucida, Fischerina ..... 178, pl. 22
Peneroplidae 178, 183
Peneroplis elliptica 176, 182, 183
proteus ..... 178, 183; pl. 22
Pitts, Foraminifera from ..... 171, 176, 177–180, 184–186; pl. 25
Placopsilina 187
bradyi 178, *187*
cenomana 187
confusa 187
sp. ..... 178, 182, *187*, pls. 22, 25
Placopsilinidae 178
plana, Gypsina 180
planata, Massilina 177
Planispirinoides stigma 178
planorbis, Cornuspira 176, 178, 183
Planorbulina 182, 184
acervalis 176, 180, 183
rubra 180
Planorbulinidae 180, 182, 183
Planorbulinoides 184
retinaculatus 180, 182, 183
planus, Tretomphalus ..... 176, 179, 183; pl. 24
poeyanum, Elphidium ..... 179, *186*; pl. 23
politum, Monalysidium 178
polypona, Quinqueloculina ..... 176, 177, *187*; pl. 22
Polymorphinidae 179
polystomellidea, Epistomaroides 179, 182
Peritea lobata 174
Poroeponides cribrorepandus 179, 182, 183
porrecta, Uvigerina 179
proteus, Peneroplis ..... 178, 183; pl. 22
pseudoungerianus, Cibicides 180
pulchrus, Borelis 178
Pullenivirina obliquiloculata ..... 180; pl. 24
Pyrgo denticulata 178
Pyropilulu rotundatus ..... 176, 179, 182; pl. 22

Q

Quinqueloculina asplulinana 177
angulina arenata 177
bertheloiana 177
bidentata ..... 177, 183; pl. 22
Quinqueloculina—Continued — Page
distorquenta 177
farnsoeci 177
neostriatula 177, 183
polypona ..... 176, 177, *187*; pl. 22
sulcata 177, 183
tubus 177

R

Rakai Ati reef 175
Maneku 175
ni Make 175
raphana, Siphonoreria 176, 179, 183, 187
Rawa ni Karoro 174
rectangulus, Rhincanthus 182, 183
Rectobolivina sp. ..... 179, 183, *187*; pl. 22
Reef areas 171, 176, 177–180, 181, 184, 185
References cited 188
retinaculatus, Planorbulinoides 180, 182, 183
Reusella simplex 176, 179, 182, 183
reversens, Spirillina vivipara 179
Rhincanthus aculeatus 182, 183
rectangulus 182, 183
rhombeidalis, Bolivina 179
Raberiniidae 179
Rongelap atoll, Marshall Islands 181
Rongerik atoll, Marshall Islands 181
Rosalina 182, 184
candeana 176, 179, 183, 184, *188*
concinna 179, 183, *188*
orbicularis 187
orientalis 179, 185, *188*
rugosa 183, 184
terquemi 187
rostrata, Anomalinella 181
Rotalidae 179, 183
rotundatus, Pyropilus ..... 176, 179, 182; pl. 22
ruber, Globigerinoides 180, 183
rubra, Planorbulina 180
rubrum, Hamotrema 176, 180, 182, 183
rugosa, Rosalina 183, 184
Spiroloculina 177, *188*
rugulosa, Gaudryina (Siphogaudryina) ..... 176, 177; pl. 25

S

saccullifer, Globigerinoides 180, 183
Sagenina frondescens 177
Saipan Island 181, 186, 187, 188
sandwichensis, Cunherines 182, 183
Scarso sp. 182, 183
Schubertella sheeliniformis 176, 178, 181, 182, 183
serrata, Haueriina 178
Sigmamorphina terquemiana 179
simplex, Elphidium 179, 183, 186
Reusella 176, 179, 182, 183
(Siphogaudryina), Gaudryina 182
rugulosa, Gaudryina ..... 176, 177; pl. 25
siphonifera, Gaudryina 177
Siphonoreria raphana 176, 179, 183, 187
siphonifera, Gaudryina (Siphogaudryina) 177
Siphonina tubulosa 179, 182
Siphonoides echinatus 179, 182
Sorites marginalis 178, 182
Southern part of atoll 171, 177–180
speciosa, Haueriina 178
sphenjeri, Calcarina ..... 176, 179, 181, 183, 186; pl. 25
Sphaeridia papillata 179
sphaerulata, Varsiloppsina ..... 176, 179, 181, 183, 185, 186; pl. 25
spinata, Triloculina 177
Spirillina 182
decorata 179
denticulo-granulata ..... 179, pl. 22
inaequalis 179
tuberculato-limbata 179
vivipara 179, 183
reversens 179
Spirillinidae 179, 183
Spirolina acicularis 179, 183
arietina 176, 178, 181, 183

Page

Spiroloculina angulata 176, 177, 183
clara 177, 182, 183, 185
lirata 177
communis 177
corrugata 177, 185
eximia 177
rugosa 177, *188*
venusta 177, *188*
squammosa, Cymbaloporetta 176, 179, 181, 182, 183
Streblus beccarii 179, 181, 182, 183
beccarii tepida 179
striato-punctatum, Elphidium ..... 176, 179, 181, 182, 183, 185, pl. 25
striatula, Bolivina 179, 183
striatus, Ctenochaetus 182, 183
subexcavata, Bolivina 179
suborbicularis, Heterostegina ..... 176, 178, 181, 183, 184; pl. 25
subplanciana, Triloculina 177, 183
sulcata, Quinqueloculina 177, 183
Sarratkina sp. 179, 183, *188*

T

Tabuarorae islet ..... 176; pl. 25
Manraba 175, 176
Taneang-Tekawa Maneaba ..... 174, pl. 25
Tebaki 175, 176
Tekawa 175
church ..... 174, 175; pl. 25
tepida, Streblus beccarii 179
Te Rawa ni Bao 175
Te Rawa Tekatobibi 175

Page

terquemi, Neoconorbina 179, *187*
Rosalina 187
terquemiana, Sigmomorphina 178
Triloculina 183, 184
Textularia agglutinans 177
alveata 177
candeiana 177, 183
dupla 177, 182
foliacea 177, 181, 182
oceanica 177, 181, 182
Textulariidae 177, 183
Thalassia 175
terrestrensis, Haddonia 176, 178, 182
tortuosa, Bolivina 179
transluceus, Alliatina ..... 179; pl. 23
transversestriata, Triloculina 177
Tretomphalus 182, 184, 188
concinnus ..... 176, 179, 183, 188; pl. 24
planus ..... 176, 179, 183; pl. 24
tricarinata, Triloculina 177
trigonula, Triloculina 177, 183
Triloculina bicarinata 177
cuneata 177, 183
earlandi 177
incisura 177, 183
irregularis 176, 177, 183
kerimbatica 177, 183
marshallana 177
oblonga 176, 177, 183
spinata 177
subplanciana 177, 183

Triloculina—Continued Page

terquemiana 183, 184
transversestriata 177
tricarinata 177
trigonula 177, 183
trochidea, Conicospirillina 179, 185
tuberculata australiensis, Discorbis 188
tuberculato-limbata, Spirillina 179
tuberocapitata, Neoconorbina 179
tubulifera, Epistominella 179, 182
tubulosa, Siphonina 179
tubus, Quinqueloculina 177

U

undulatus, Halistapus 182, 183
universa, Orbulina ..... 180; pl. 24
Uvigerina porrecta 179

V

Valvulina davidiana 177, 182, 185
Valvulinidae 177, 183
variabilis, Cibicidella 176, 180, 183
venusta, Spiroloculina 177, *188*
Verneuilinidae 177, 183
vertebralis, Marginopora 176, 178, 181, 183, 184
vesicularis, Gypsina 180
vivipara reverens, Spirillina 179
Spirillina 179, 183

W

Wet samples 181–182
Wiesnerella auriculata 178
williamsonianus, Buliminoides 178, 182
Windward side 171

U. S. GOVERNMENT PRINTING OFFICE : 1961 O - 553580

PLATES 22–25

PLATE 22

FIGURE 1. *Ammobaculites* sp. (p. 177 tab.)
USNM 626873, × 56; USGS f11667, GOC–29.

2. *Quinqueloculina bidentata* d'Orbigny. (p. 177 tab.)
USNM 626883, × 44; USGS f11679, GOC–49; *a*, side view; *b*, apertural view.

3, 4. *Placopsilina*? sp. (p. 187)

3. USNM 626879, × 27; USGS f11678, GOC–48; *a*, *b*, opposite sides; *b*, attached surface; *c*, edge view showing terminal aperture.

4. USNM 626880, × 27; USGS f11678, GOC–48. Fragment of a terminal part that grew outward from initial attached portion.

5. *Quinqueloculina polygona* d'Orbigny. (p. 187)
USNM 626888, × 44; USGS f11683, GOC–55; *a*, side view; *b*, apertural view.

6. *Pischerina pellucida* Millett. (p. 178 tab.)
USNM 626874, × 40; USGS f11667, GOC–29.

7. *Peneroplis proteus* d'Orbigny. (p. 178 tab.)
USNM 626875, × 93; USGS f11667, GOC–29.

8. *Rectobolivina*? sp. (p. 187)
USNM 626872, × 140; USGS f11649, GOC–2F; *a*, side view; *b*, top view.

9. *Pyropilus rotundatus* Cushman. (p. 179 tab.)
USNM 626889, × 56; USGS f11684, GOC–56; *a*, dorsal view; *b*, ventral view; *c*, peripheral view.

10. *Chrysalidinella dimorpha* (Brady). (p. 186)
USNM 626890, × 88; USGS f11690, 51–S–6; *a*, side view; *b*, top view.

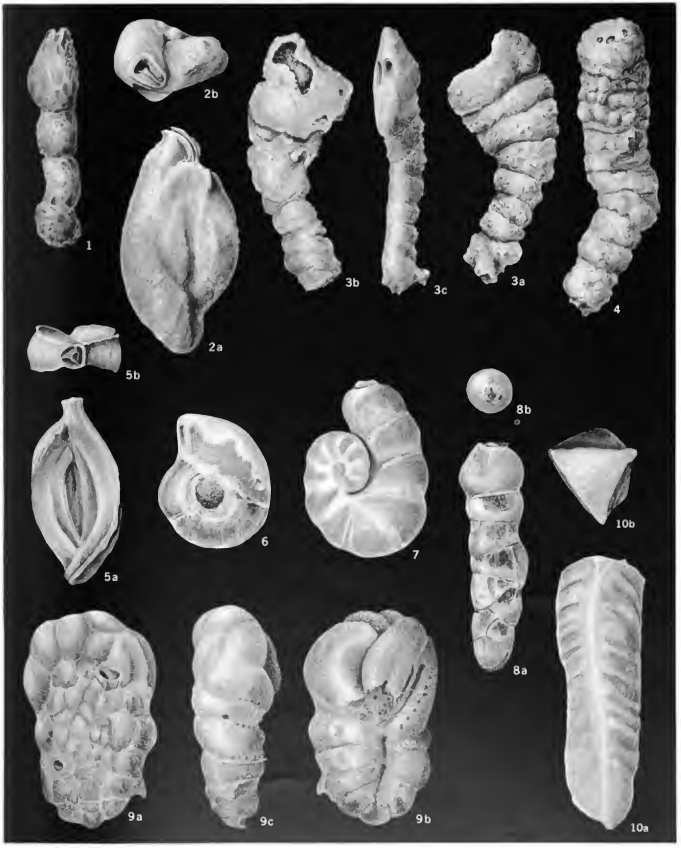

RECENT BENTHONIC FORAMINIFERA FROM ONOTOA ATOLL

PLATE 23

[*a*, Dorsal view; *b*, ventral view; *c*, peripheral view, except as indicated]

FIGURE 1. *Elphidium* cf. *E. poeyanum* (d'Orbigny). (p. 186)
USNM 626876, × 93; USGS f11667, GOC–29; *a*, side view; *b*, peripheral view.

2. *Alliatina translucens* (Cushman.) (p. 179 tab.)
USNM 626886, × 140; USGS f11679, GOC–49; *a*, side view; *b*, peripheral view.

3, 4. *Conicospirillina* sp. (p. 179 tab.)

3. USNM 626871, × 180; USGS f11667, GOC–29.

4. USNM 626870, × 220; USGS f11667, GOC–29.

5. *Spirillina denticulo-granulata* Chapman. (p. 179 tab.)
USNM 626881, × 93; USGS f11679, GOC–49.

RECENT BENTHONIC FORAMINIFERA FROM ONOTOA ATOLL

PLATE 24

[*a*, Dorsal view; *b*, ventral view; *c*, peripheral view]

FIGURE 1. *Globigerina* cf. *G. inflata* d'Orbigny. (p. 186)
USNM 626887, × 93; USGS f11679, GOC–49.

2. *Orbulina universa* d'Orbigny? (p. 180 tab.)
USNM 626891, × 112; USGS f11691, 51–S–7.

3. *Globigerinita glutinata* (Egger). (p. 186)
USNM 626877, × 194; USGS f11667, GOC–29.

4. *Tretomphalus concinnus* (Brady). (p. 179 tab.)
USNM 626885, × 93; USGS f11679, GOC–49. Side view.

5. *Globigerina eggeri* Rhumbler. (p. 180 tab.)
USNM 626878, × 112; USGS f11670, GOC–33.

6. *Tretomphalus planus* Cushman. (p. 179 tab.)
USNM 626884, × 70; USGS f11679, GOC–49. Side view.

7. *Pulleniatina obliquiloculata* (Parker and Jones). (p. 180 tab.)
USNM 626882, × 70; USGS f11679, GOC–49.

RECENT PLANKTONIC FORAMINIFERA FROM ONOTOA ATOLL

PLATE 25

[All figures × 16]

FIGURE 1. *Baculogypsina* sand from islet of Nanntabuariki on windward (northeast) side of Onotoa Atoll. USGS f11662, GOC–19. Fresh specimens washed onto beach from adjacent reef flat.

2. *Baculogypsina* sand from southeast end of Tabuarorae islet, south end of Onotoa Atoll. USGS f11687, 51–L–8. Well-worn specimens associated with *Amphistegina* and *Calcarina*.
3. *Calcarina*-bearing limesand from upper part of section above lagoon beach just south of Otoae village Maneaba, southern main island of Onotoa Atoll. USGS f11663, GOC–20A. Specimens mostly well preserved.
4. *Amphistegina*-bearing limesand from lagoon floor in northern part of lagoon, about 4,600 ft S. 65° W. from lagoon end of Government Station jetty, Onotoa Atoll. USGS f11695, 51–S–11. From bottom of reentrant or depression in large lagoon reef patch.
5. Miscellaneous Foraminifera from limesand bottom at 14 ft in outer part of lagoon of Onotoa Atoll, slightly less than 4 miles N. 85° W. from Aiaki Maneaba. USGS f11666, GOC–28. Among others, *Heterostegina suborbicularis* d'Orbigny (*a*), *Gaudryina* (*Siphogaudryina*) *rugulosa* Cushman (*b*), *Elphidium striato-punctatum* (Fichtel and Moll) (*c*), *Placopsilina*? sp. (*d*), and *Amphistegina madgascariensis* d'Orbigny (*e*) are recognizable.
6. *Amphistegina*-bearing limesand from seaward edge of Aon te Baba reef, west side of north end of Onotoa Atoll, about 7,100 ft S. 50° W. from Tekawa church. USGS f11670, GOC–33. Worn *Amphistegina* with associated *Heterostegina* and *Marginopora*.
7. Worn *Calcarina* beach sand, stained dark from organic matter and corroded by organic acids. From top 6 in. in pit GOC–6, north-central part of northern main island, about 2,400 ft north-northeast from Taneang-Tekawa Maneaba. USGS f11657, GOC–6A.
8. *Calcarina*-bearing sand interpreted as reef-flat horizon from bottom of 9-ft pit GOC–2, southern part of northern main island, about 940 ft S. 25° E. from east (inshore) end of lagoon-side jetty at Government Station and 660 ft inshore from sea beach along line bearing S. 87° W. at Pacific Science Board campsite. USGS f11649, GOC–2F.
9. *Calcarina* sand, interpreted as transitional between beach and reef flat, from near bottom of 6-ft pit GOC–1, southern part of northern main island, about 1,100 ft S. 41° E. from east (inshore) end of lagoon-side jetty at Government Station and 325 ft inshore from sea beach along line bearing S. 87° W. at Pacific Science Board campsite. USGS f11642, GOC–1D. Both fresh (with spines) and worn specimens.

1

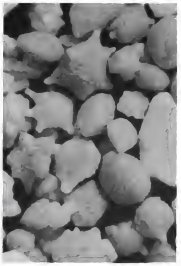
2

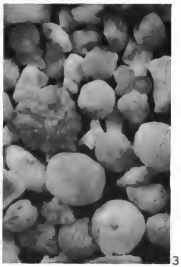
3

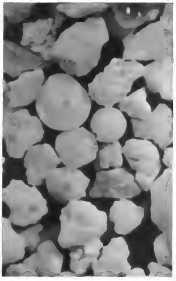
4

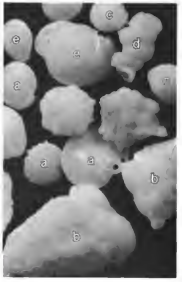

5

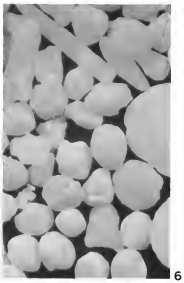
6

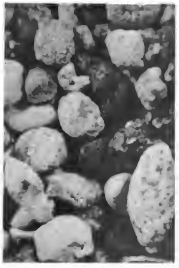
7

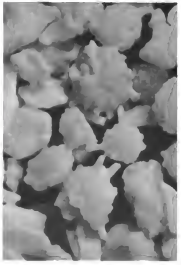
8

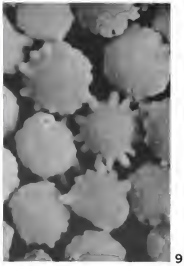
9

FORAMINIFERA SANDS FROM ONOTOA ATOLL

Occurrence and Significance of Marine Animal Remains in American Coal Balls

By SERGIUS H. MAMAY *and* ELLIS L. YOCHELSON

SHORTER CONTRIBUTIONS TO GENERAL GEOLOGY

GEOLOGICAL SURVEY PROFESSIONAL PAPER 354-I

A description of intermixtures of marine animals and land plants occurring in coal balls in Illinois, Iowa, Kansas, and Oklahoma

UNITED STATES GOVERNMENT PRINTING OFFICE, WASHINGTON : 1962

UNITED STATES DEPARTMENT OF THE INTERIOR

STEWART L. UDALL, *Secretary*

GEOLOGICAL SURVEY

Thomas B. Nolan, *Director*

For sale by the Superintendent of Documents, U.S. Government Printing Office
Washington 25, D.C. - Price 50 cents (paper cover)

CONTENTS

	Page
Abstract	193
Introduction	193
Previous work	194
Acknowledgements	194
Definition of coal balls	195
Occurrences of animal-containing coal balls	196
McAlester, Okla	196
Berryville, Ill	197
Southeastern Kansas	199
West Mineral	199
Stratigraphic relations of the coal balls	200
Franklin	201
Monmouth	201
Physical and biological features of coal balls	202
Normal coal balls	202
Homogeneous-mixed coal balls	203
Heterogeneous-mixed coal balls	204
Faunal coal balls	206
Chemical analyses	206
Laboratory methods	207
Preservation of the fossils	210
Interpretation of animal-containing-coal balls	211
Heterogeneous-mixed coal balls	211
Homogeneous-mixed and faunal coal balls	213
Alternative interpretations	215
Conclusions	216
References cited	216
Details of the samples and insoluble residues	217
Oskaloosa, Iowa	217
McAlester, Okla	218
Southeastern Kansas	218
West Mineral	218
Monmouth	219
Franklin	220
Berryville, Ill	220
Index	223

ILLUSTRATIONS

[Plates follow the index]

PLATE 26. Views at the Berryville, Ill., West Mineral, Kans., and Monmouth, Kans., coal ball localities.
27. Normal and mixed coal balls from Illinois and Kansas.
28. Faunal, mixed, and normal coal balls from West Mineral and Monmouth, Kans.
29. Homogeneous-mixed coal balls from West Mineral, Kans.
30. Heterogeneous-mixed coal balls from Berryville, Ill.
31. Mixed coal balls from Illinois and Iowa, and limestone from Illinois.
32. Faunal coal balls from Monmouth, Kans.
33. Representative spores and other plant remains recovered from insoluble residues.
34. Representative animal remains recovered from insoluble residues.

	Page
FIGURE 42. Geographic occurrence of mixed coal balls	197
43. Sketch of sawn surface of a normal coal ball	203
44. Sketch of sawn surface of a homogeneous-mixed coal ball	204
45. Sketch of sawn surface of a heterogeneous-mixed coal ball	205

TABLES

	Page
TABLE 1. Semiquantitative spectroscopic analyses of coal ball and limestone samples	206
2. Rapid rock analyses of coal ball and limestone samples	207
3. Distribution of animal groups and large spores in insoluble residues	208

SHORTER CONTRIBUTIONS TO GENERAL GEOLOGY

OCCURRENCE AND SIGNIFICANCE OF MARINE ANIMAL REMAINS IN AMERICAN COAL BALLS

By Sergius H. Mamay and Ellis L. Yochelson

ABSTRACT

Coal balls are mineralized nodular masses found within some coal seams. Although coal balls have been known for over 100 years, only botanical contents have been previously reported in detail. In this paper, occurrences of marine animal fossils associated with plant fossils in coal balls are described.

Three types of coal balls are here recognized: (a) normal coal balls, containing only plants; (b) mixed coal balls, containing both plants and marine animals; and (c) faunal coal balls, containing only animals. Mixed coal balls are homogeneous, if the plant and animal remains are mixed throughout the matrix, or heterogeneous, if the marine fraction is clearly segregated from the normal fraction.

Homogeneous-mixed coal balls were found near McAlester, Okla., near Oskaloosa, Iowa, and in parts of the southeastern Kansas coal fields. Heterogeneous-mixed coal balls were found near Berryville, Ill., and faunal coal balls were found at two localities in Kansas.

Coal balls are particularly common near West Mineral, Kans. They are abundant in the Fleming coal, of Des Moines age, and also occur in the underlying Mineral coal. Observations of mining waste suggest that mixed coal balls constitute 1 to 2 percent of the coal balls recovered, although none were found in place. There may be some positive correlation between abundance of coal balls and elevations or "highs" in the Fleming coal.

Semiquantitative spectroscopic analyses and rapid chemical analyses of selected coal balls are included in this report. These contain the most comprehensive data on the chemical composition of coal balls yet published.

Other samples were dissolved in formic acid; the residues are described. Uncompressed spores were recovered from many of the samples, along with diverse animal remains. Selected specimens of spores and animals are figured, and identifiable forms are tabulated.

The fossils are replaced by a variety of minerals, occasionally within the same coal ball. Spore fillings from a single coal ball may be pyritic or calcareous. Gastropods may be calcareous, pyritic, or baritic in the same sample. Pelecypods recovered are pyritic or baritic. Some echinoderm columnals, cephalopods, and brachiopods are pyritized, and others are calcareous.

The presence of marine animals within coal balls is evidence of transportation of material from a marine environment to a nonmarine environment. Though all coal balls have heretofore been considered concretionary in origin, mixed and faunal coal balls are, at least in part, of clastic origin. The swirled texture of some homogeneous-mixed coal balls is further evidence of transport.

It is suggested that heterogeneous-mixed coal balls were formed when mud rollers containing animal remains were brought into the coal swamp by temporary marine inundation and were secondarily surrounded by normal coal ball material. Some homogeneous-mixed coal balls may represent discrete lumps of transported fossiliferous mud. The animal content of still others may have been introduced into the coal swamp in a mud slurry. These temporary marine inundations may have provided a source of calcium carbonate for the formation of some normal coal balls.

INTRODUCTION

In a previous publication (Mamay and Yochelson, 1953) we briefly reported the occurrence of marine fossils associated with land plants in coal balls of Pennsylvanian age. Subsequent field observations and accummulation of additional material have made possible a more detailed report.

Although the occurrence of coal balls has been known for more than a century and although they have been noted in the coal fields of various European countries and of the United States and Great Britain, we are not aware of any authenticated reports, earlier than 1953, of faunal inclusions within coal balls.

Darrah (1939, p. 135) stated that "many of the Belgian and English coal balls contain fossil cephalopods," but he presented no further information. Coal ball deposits in England and Belgium are overlain by marine beds containing abundant fossiliferous nodules, in which goniatites are the predominating fossil; Stopes and Watson (1908) and Leclercq (1952) discussed in detail this relation of British and of Belgian coal ball deposits, respectively. Since extensive research has been done on both British and Belgian coal balls but no mention has been made of animals within the nodules, there is a possibility that Darrah

neglected to distinguish between roof-shale nodules and true coal balls.

Douville (1905), who discussed briefly the content of a few nodules from the coal fields of Yorkshire, England, recognized two types of coal balls, one containing only plant debris, the other containing sparse woody fragments among numerous marine shells. The second type were illustrated (Douville, 1905, pl. 6) as "Coal Balls du Yorkshire," but it is apparent that these specimens are actually roof nodules, distinct from the coal seam itself.

It may be that animal remains simply do not occur in coal balls of Europe or England. Alternative reasons may be the facts that the primary interests of most previous investigators were botanical and that most British studies were based on specimens obtained from professional collectors and were not seen in the field by the paleobotanists. The material on which the present report is based is unusual in that it contains not only the plant remains ordinarily associated with coal balls, but diverse assemblages of marine animal fossils as well. Because of its significance for the origin of coal balls, this material is described in detail.

PREVIOUS WORK

Although earlier workers, particularly W. C. Williamson, wrote many papers on the plant content of coal balls, it was not until 1908 that the geological aspects of coal balls were extensively discussed in the classical publication by Stopes and Watson (1908). Their paper reviewed all the pertinent information available at the time, and included several chemical analyses of coal balls. Stopes and Watson concluded that coal balls were formed in place, as a product of percolating marine waters.

Since the time of Stopes' and Watson's publication little has been written on the occurrence and formation of coal balls, However, many publications have dealt with the anatomy and morphology of plants preserved within coal balls, and a number of significant botanical facts have been reported. The years 1935–60 have seen a rapid expansion of this field of paleobotany in the United States, but a considerable waning of interest in England and Europe, where most of the early work was done.

Studies of coal balls in the United States were summarized in detail through 1950 by Andrews (1951). This summary includes a sketch of the history of coal ball research in Europe, as well as a brief discussion of the chemical composition and geological occurrences of coal balls.

The study reported here was started in 1952, when Mamay made a large collection of coal balls in southeastern Kansas and southern Illinois. Previously, Mamay's interests were centered on morphological aspects of the plant content of the coal balls, but his attention was drawn toward the geologic problems raised by the animal fossils found in a few of the coal balls. The presence of abundant gastropods among these faunas resulted in Yochelson's participation in the study, because of his interests in that group of animals. A preliminary account of this discovery was published (Mamay and Yochelson, 1953) because of the great rarity of known occurrences of marine animal remains within Paleozoic coal seams.

In May 1955, we studied field relations and collected more coal balls from previously known and from new localities. Interested paleobotanists contributed additional coal balls. Excellent examples of animal-containing coal balls were also found in previously unstudied coal balls collected near McAlester, Okla., by Charles B. Read. Laboratory studies were carried out during 1955 and 1956, and Mamay revisited some of the localities in 1957.

Two other short publications resulted from this study. Associated with the McAlester, Okla., coal balls were a number of calcareous fossiliferous nodules that presumably originated from the overburden of the Secor coal. The nodules contain a number of species of Foraminifera, some of which were epiphytic on a problematical alga, *Litostroma*. The Foraminifera were described and their depositional environment was discussed by Henbest (1958); Mamay (1959) described *Litostroma* in detail.

ACKNOWLEDGMENTS

Our colleagues Charles B. Read and James M. Schopf provided locality information and on several occasions helped us by their discussions of the coal balls. Emil Sandeen and Kenneth Moore of the Pittsburg and Midway Coal Co. and H. W. Compton of the Apex-Compton Coal Co. not only allowed access to their mining properties but provided valuable information regarding the occurrence of coal balls. Robert W. Baxter, University of Kansas, and Henry N. Andrews, Washington University, St. Louis, Mo., allowed us to examine their collections of coal balls and gave select specimens for study. Baxter also supplied geologic information and additional specimens from Monmouth, Kans., having visited that locality at our request in July 1957. We appreciate also the cooperation by other U.S. Geological Survey colleagues: Mona Frank and P. L. D. Elmore made the spectroscopic examinations and Paul W. Scott made the chemical analyses. Charles Milton identified several minerals, and S. O. Schlanger aided in interpretation of sedimentary

phenomena. Systematic identifications are to be credited as follows: Protozoa, Lloyd G. Henbest; Coelenterata and Bryozoa, Helen Duncan; Cephalopoda, Mackenzie Gordon, Jr.; Ostracoda, I. G. Sohn; Trilobita, A. R. Palmer; and conodonts, the late Wilbert H. Hass. David H. Dunkle of the U.S. National Museum examined the fish remains, and David Nicol, formerly of the U.S. National Museum, checked identification of the pelecypods. Robert M. Finks, Brooklyn College, identified sponge material, and R. M. Kosanke, Illinois State Geological Survey, checked spore identifications.

DEFINITION OF COAL BALLS

The results of this study show that coal balls are considerably more varied, texturally and biologically, than is ordinarily supposed. It is thus evident that some expansion of longstanding concepts is necessary, as well as some refinement and revision of definitions. Our emended definitions are presented here, before descriptions in detail of the various kinds of coal balls.

In classical usage (Stopes and Watson, 1908, p. 168) the term "coal balls" has been applied to nodular mineralized masses of petrified plant material that occur within coal seams. The balls are largely restricted to coals of Pennsylvanian or equivalent age,[1] and generally have been considered to be concretionary in origin. There are no known occurrences in anthracitic coals.

Coal balls are of various physical and chemical features. They may be calcareous, pyritic, dolomitic, sideritic, or even siliceous in composition. Within limits, coal balls with high proportions of calcium carbonate have the best preservation of cellular detail; as a general rule, high pyrite content results in poor preservation of the plant fossils. The balls may occur as small individuals no larger than a plum, or they may weigh as much as several hundred pounds and may form huge intergrown masses that displace the coal for areas of several square yards. The individual nodules may be spheroidal, approximately lenticular, or irregular in shape. At a few localities, particularly in England and Europe, spheroidal specimens are very abundant, but at others, flattened, roughly lenticular coal balls seem to predominate. Coal balls may occur anywhere between the upper and lower limits of a coal seam, but they are more common in the upper half. In many places they cause humps in the upper surface of the coal, where they are separated from the overlying rocks by only a thin veneer of coal. Their occurrence in a given coal seam may be either extremely sporadic or regular; many seams contain none at all.

Despite these varying factors, two primary features have been necessary for identification of a sedimentary rock as a coal ball, as heretofore understood: (a) that it contain histologically investigable fossil plant material, impregnated with and surrounded by a mineral matrix of nonvegetable origin, and (b) that it be indigenous to a coal seam.

Schopf (Whitehead and others, 1952, p. 290) reported an occurrence of coal ball limestone in a marine coquina above a coal seam. According to Schopf, this obviously formed within the precoal peat bed and was reworked into its present position; it thus is not in conflict with this definition.

This study shows that coal balls may vary as much in their enclosed organic remains as they do in any other measurable feature. Thus a realistic definition of coal balls should be expanded so that "inclusion of histologically investigable plant material" is replaced by "inclusion of fossil animal material, histologically investigable fossil plant material, or both, in varying proportions" as one of the two primary requisites for identification of a rock as a coal ball, its inclusion within the limits of a coal seam remaining the other. The definition is further emended to include in its scope objects of either clastic or concretionary origin, their inclusion within the coal seam rather than source of component fossils being the important factor.

Carrying this concept to an extreme, it might be argued that any fossiliferous lens in coal is a coal ball, but this is fallacious logic. Coal balls are relatively small, discrete masses of nodular aspect, usually but not always wholly concretionary. They generally show a vertical distribution throughout the coal, rather than a lateral continuity such as characterizes a split, parting, or lens within a coal. The essential feature of the primarily clastic coal balls is the exotic nature of some of their fossil content, which is foreign to the immediate environment of coal deposition. In no sense are the clastic coal balls a normal part of the sedimentary cyclothem characteristic of Pennsylvanian sedimentation. We believe that their presence within a coal seam along with the more usual, concretionary type of plant-containing coal balls is attributable to unusual, probably catastrophic and transitory means of landward redeposition, such as might be effected by violent storm wave or tidal wave action.

It is emphasized that this broadened definition of coal balls is made only on the basis of specimens that can be shown, by virtue of coal remnants on all or nearly all unfractured surfaces, to have originated within a coal seam. The various types of fossiliferous nodules that occur in the shaly or limy overburdens of

[1] Gothan (1911) reported masses of petrified plant material in German Tertiary brown coals, which he considered to be analogous to coal balls. The plants are preserved in siderite, however, and are not as well preserved as those in Carboniferous coal balls. Little more is known of this Tertiary occurrence

some coal seams are not regarded as coal balls because of their formation outside the coal seam. (See Stopes and Watson, 1908, p. 204–210, for discussion of goniatite-bearing nodules that occur in roof shales of some seams and occasionally contain well-preserved plant remains.)

The objects defined here as coal balls fall into three primary types, on the basis of biological content, and two subsidiary types, on the basis of textural features. The term "coal balls," unqualified, is used here for all these types. Although there is some intergradation in the relative proportions of plants to animals, for the sake of convenience coal balls may be classified as follows:

1. Normal coal balls: contain only plant fossils (pl. 27, fig. 1; pl. 28, fig. 2).
2. Mixed coal balls: contain both plant and animal fossils.
   (a) Homogeneous type: shows no distinguishable segregation of plant and animal fossils (pl. 27, figs. 2–4; pl. 28, fig. 3; pl. 29, figs. 1–3).
   (b) Heterogeneous type: shows distinct segregation of plant and animal fossils (pl. 30, figs. 1–3; pl. 31, fig. 1).
3. Faunal coal balls: contain exclusively zoological fossils (pl. 28, fig. 1; pl. 32, figs. 1–3).

Type 3 is very rare, and insofar as we know, has been found in significant quantities at only one locality. Type 2(a) (homogeneous-mixed) is by far the commonest type of animal-containing coal balls, while type 2(b) (heterogeneous-mixed) is, again, known to us from only one locality.

The following evidence supports this expanded concept of coal balls: In one coal ball (sample E–13, from Patik Mine, Iowa, pl. 31, fig. 4) animal remains are so rare as to be hardly noticeable on sawn surfaces, but acid solution produced a large number of small animal fossils, some of them unquestionably of marine origin. However, the plant debris is extremely well-preserved, and it is probable that casual inspection would lead to identification of the specimen as a normal coal ball.

It is possible to demonstrate a gradational series in which the proportion of animals to plants increases from the above-mentioned extreme in which animal remains are rare but present, to the point where plant remains are rare or even absent, as in some of the faunal coal balls. The faunal coal balls appear in the same seam with poorly preserved normal coal balls. There is no sharp line of demarcation between them and more intermediate specimens with higher proportions of plant fragments.

Comparison of normal coal balls from the Berryville, Ill., locality with the normal coal ball matrix surrounding the marine fraction of heterogeneous-mixed coal balls from the same locality indicates that the two are identical in physical composition, in texture, and in botanical content, as shown by study of peels and insoluble residues.

OCCURRENCES OF ANIMAL-CONTAINING COAL BALLS

Mixed coal balls were collected from localities in four States in the eastern interior and midcontinent coal basins: Illinois, Kansas, Oklahoma and Iowa. The Oklahoma deposit is no longer accessible. The Illinois specimens were found at a spot locality. The Kansas material, however, originates from an economically important mining area in the southeastern part of that State. This area has produced abundant coal balls from three different coal seams and has been the geographic source of much of the geologic information on the occurrence of mixed coal balls. The Iowa material consists of one coal ball from the Patik mine near Oskaloosa, presented to us by R. W. Baxter, University of Kansas.

Schopf (1941) published a chart showing important coal-ball stratigraphic levels in the United States and their correlation with European occurrences. Since this chart was prepared, only slight modifications in the correlations have been made (Moore and others, 1944; Wanless, 1956), so the chart is not repeated here. Geographic distribution of the mixed coal balls is shown in figure 42.

McALESTER, OKLA.

A small collection of coal balls from the Secor coal near McAlester, Okla., was made by C. B. Read in 1939. Only a few of the specimens were sectioned before 1953, and all those were of the normal type. Sectioning of the remainder showed that some were of the mixed type.

The collection was made at a small abandoned slope mine on the property of Mr. Joseph Lemont near the abandoned railroad station of Chambers, about 4 miles south-southeast of McAlester. The mine site is approximately at the common corners of secs. 26, 27, 34, and 35, T. 5 N., R. 14 E., Pittsburg County. This locality (USGS paleobotanical loc. 8764) was revisited by us in 1955, but only a few badly weathered loose coal balls were found. These all were of the normal type and no information was available regarding their original placement in the coal seam. The slag heap contained fragments of an impure bioclastic limestone. Similar limestone that was collected by Read corroborates a statement by Mr. Lemont that at the mining site the coal seam was overlain by a thin fossiliferous limestone.

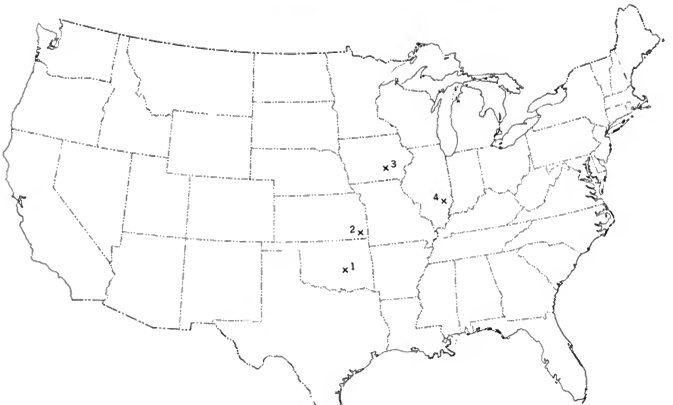

FIGURE 42. Geographic occurrences of mixed coal balls in the United States: 1. McAlester, Okla.; 2. southeastern Kansas; 3. Oskaloosa, Iowa; 4. Berryville, Ill.

Waste heaps of two other small abandoned mines in the nearby vicinity of the Lemont property (SW¼ SW¼SW¼ sec. 26 and NE¼NE¼NE¼ sec. 34) were also searched for coal balls but none were found; only a few large scaphopods and poorly preserved peleypods were found.

Along the highway between Hartshorn and McAlester, we examined several large abandoned strip pits in the McAlester coal in the McAlester shale, 1,200-2,500 feet below the base of the Boggy formation. A large abandoned strip pit where the Secor coal had been mined in the southern half of sec. 33, T. 5 N., R. 15 E., was also searched. None of these pits yielded coal balls.

The Secor coal is the oldest seam known by us to have produced mixed coal balls. According to Hendricks (1937), the Secor coal seam varies from 1 to 3 feet in thickness. It lies about 350 feet above the base of the Boggy formation in the Krebs group, of Des Moines age (Miser, 1954). Hendricks mentioned no fossiliferous limestone above the Secor coal; perhaps he did not observe it either because of its localized occurrence or because it is covered over large parts of the area.

BERRYVILLE, ILL.

The locality known in the literature as Berryville, Ill., was discovered by J. Marvin Weller in August 1936 (Schopf, 1956, written communication). It is on the farm of Ralph Brian, 6 miles south and 2 miles west of Sumner, Ill. (approximately SW¼NE¼NW¼ sec. 7, T. 2 N., R. 13 W., Lawrence County; USGS paleobotanical loc. 9190). Since its discovery, this deposit has become well known to students of coal ball floras of the United States and has provided them with an unusual quantity of excellently preserved plant fossils, many of which have been described. The deposit is of further interest as a source of heterogeneous-mixed coal balls.

The coal balls occur in a thin seam of coal, considered by Schopf (1941) and others to be the Calhoun coal, in the upper part of the McLeansboro group of Middle and Late Pennsylvanian age. The outcrop is limited, being exposed for a distance of less than 60 feet along the south bank and bed of a small intermittent stream. The streambank cuts into the side of a steep hill, and a thick alluvial overburden hampers efforts to excavate the coal balls. Intermittent flooding of the stream

erodes coal balls from the outcrop, so that collections may be made from float in the nearly dry streambed.

Several dozen fresh coal balls were collected at Berryville. Many of these were taken from the outcrop and broken in the field but none proved to be of the mixed type. A few heterogeneous-mixed specimens were found in float along the streambed, but these give no indication of their original position within the coal seam. The locality was revisited in 1957 by Mamay, who excavated heterogeneous-mixed coal balls in place and found that they extend throughout the thickness of the coal seam.

The outcrop area is shown on plate 26, figure 3. Because this exposure represents one of the few localities known to us where coal balls may be observed in place, the hillside adjacent to the outcrop was trenched and a section measured. The trench is seen along the right side of the photograph. The section consists of the following lithologic units:

Measured section at Berryville, Ill.

	Feet
Alluvium.	
Sandstone, light-gray, fine-grained; weathers dark gray; bedded in ½-in. laminae near base; becomes more massive upward	1.5
Shale, dark-brown, micaceous, with abundant fragmentary plant compressions; locally subfissile; poorly exposed	6.1
Limestone, dark-gray; highly crinoidal in a single massive bed; weathers very dark gray below and yellow iron stained above	1.0
Coal, moderately hard, banded, with blocky fracture; coal balls rare in lower 3 in., but become more numerous upward; some cause bulges in the upper surface of the seam. Average thickness of unit	2.0
Underclay, light-gray, slickensided with blocky structure; slightly arenaceous with scattered plant compressions; upper surface slightly irregular. Base not exposed, but thickness of unit at least	2.0
Total thickness measured	12.6

Examination of the coal seam face revealed the following distribution of the coal balls:

1. The relative abundance of the coal balls varies considerably within short horizontal distances; one spot may contain many, another a few feet away may have none.
2. Coal balls occur throughout the thickness of the seam.
3. Coal balls may occur at the base of the seam with only a thin film of coal below, and may even indent the subjacent underclay. Commonly, however, they seem to increase in abundance toward the top of the seam.
4. The coal balls that occur at the top of the seam may produce a bulge that protrudes into the overlying limestone. In all places observed, however, they were separated from the limestone by at least a thin film of coal.
5. The coal balls may be discrete lumps separated from each other by several inches or more of coal, or they may occur in large irregular intergrown masses that largely displace the coal seam for several square feet and contain only thin, irregularly oriented coal partings. One such mass is shown in plate 26, figure 2. This block of coal ball material, weighing perhaps a ton, stands isolated in the streambed. It consists of many closely associated, irregularly shaped but discrete masses of coal ball material separated from each other by thin streaks of coal. Although the overburden is completely eroded away, the intact condition of the underlying coal suggests that this mass is in its original position. It consists almost exclusively of the roots and other debris of the marattiaceous fern genus *Psaronius*, a dominant form in the Berryville flora.

Although nothing unusual was noted in the measured section, a somewhat involved sequence occurs a few yards downstream from the trench exposure (to the left of the trench in pl. 26, fig. 3). There the limestone overburden of the coal seam thickens abruptly to form a conspicuous mass approximately 5 feet thick. The coal beneath this limestone mass is reduced to approximately half its maximum thickness (see pl. 26, fig. 1), presumably by channeling, and the depression is filled with a mixture of detrital coal and limestone chunks, which grade into solid limestone above. A sample of the limestone blocks within the channel filling, when dissolved in acid, proved to contain almost the same type of plant and animal remains as the mixed coal balls. The coal immediately below the channel filling contains abundant limestone blocks; a representative sample included:

1. A typical, well-preserved normal coal ball containing a large undistorted fragment of the fructification of *Botryopteris*.
2. Several chunks, approximately 1 inch thick, composed of numerous particles of coal ball-like material in a coal groundmass and interbedded locally with stringers of coal. The brown coal ball particles are subangular to subrounded; they are closely packed and some are even molded into one another. The latter characteristic indicates that the particles were plastic when the rock was formed. The particles contain mostly well-preserved, uncompressed spores (see analysis of residue of sample E-15) and bits of cuticle, but no animal remains. They may represent an agglomeration of detrital coal ball material that was

finely divided at the time of channeling of the coal seam. Illustrations are given on plate 31.

3. Two pieces of gray crinoidal limestone, surrounded by coal and locally intermixed with or separated from the surrounding coal by brown petrified plant debris.

SOUTHEASTERN KANSAS

The southeastern Kansas coal field contains some of the richest known occurrences of coal balls in the United States (Andrews and Mamay, 1952), and consequently has been the geographic source of much of the information presented here. Several coal ball localities were visited by us in Cherokee and Crawford Counties; most of these were found by a systematic investigation of the strip-mining operations mapped by Abernathy (1946, pl. 1). A more up-to-date map of stripping operations in the area, published privately in 1952 by the Apex-Compton Coal Co., Inc., was also helpful in this search.

WEST MINERAL, KANS.

Investigations of this area were concentrated at the site of stripping operations of the Pittsburg and Midway Coal Co., at their Mine No. 19, in W½ sec. 5, T. 33 S., R. 22 E., Cherokee County. This site was selected because of the extensive scope of mining operations, the abundance of coal balls, and the relative freshness of the material.

In spite of the many coal balls found at the Pittsburgh and Midway mine, observations of their field relations were restricted by the sporadic occurrences of the coal balls and by the nature of the mining methods. Large-scale stripping operations are used because of the thickness of the overburden (as much as 50 feet); consequently, the relations of the coal to the overburden are usually concealed by slump from the steep walls of the pits.

The overburden is removed in long swaths of several thousands of square yards by either a dragline or an electric shovel. The upper surface of the coal is thoroughly cleaned. Once exposed, the coal is broken by a pinning machine, loaded, and taken to the tipple for washing and sizing.[2]

The mining procedure, while highly efficient, does not result in a clean working face, so that position of the coal balls within the coal is usually badly disturbed. The procedure also limits observations of the relation of the coal to the underlying sedimentary rocks, for little of the latter are removed. Furthermore, loading usually takes place shortly after breaking of the coal, so that one would have to be present at about the time the coal balls are uncovered to observe them in place.

In addition to the limitations imposed by the mining methods, three other factors restricted our observations. First, at the time of our visit, even though a large area of coal was exposed, few coal balls were being uncovered. Second, in 1955, mining was limited to a single pit, and it was not possible to make comparative observations at fresh exposures over a broader area. Third, as usual in large strip-mining operations, abandoned pits that might have contained good exposures of the coal and overlying strata in their walls were either refilled with overburden or flooded to levels above the coal.

Our observations, however, have been supplemented by those of the miners and pit operators. Particularly valuable information was derived from discussions with Emil Sandeen, mine superintendent of the Pittsburg and Midway Coal Co., and with Kenneth Moore, mining engineer, Mine No. 19, and from mining records of that company, to which we were given access.

The mining method necessarily results in contamination of the coal by coal ball material and minor amounts of underclay. Where the balls occur abundantly, they are a major nuisance since they are imbedded in the coal and must be loaded and transported to the washing plant for removal. The waste removed from the coal in the washing process varies from day to day, partly because of the sporadic occurrence of coal balls, and sometimes may constitute more than 30 percent of the gross tonnage mined. Coal balls form a large part of this impurity.

Despite the inconvenience of commercially worthless coal balls, their occurrence is not a total loss to the mine operators. The coal balls, being of much higher specific gravity than the coal, are easily removed in the washing plant. The coal balls are hauled from the tipple and piled in a nearby vacant area until they are needed for road construction. Their hardness and durability make them an excellent ballast for access mine roads, a fact that has been fully exploited at the Pittsburg and Midway mines, where this supply of ballast is seemingly endless! Part of one such pile, which was perhaps 6 feet high over an area of half an acre, is shown in plate 26, figure 4—a heap of possibly several thousand tons of almost pure, structurally preserved fossil material. Another indication of the abundance of coal balls at the Pittsburg and Midway mines was observed in a newly constructed roadbed, some 1,800 feet long, 50 feet wide, and 2 to 3 feet deep. It was estimated that between one-quarter and one-half of the volume consists of coal balls.

[2] Mine operations at the Pittsburg and Midway Mine are more completely described in Coal Age (1954).

STRATIGRAPHIC RELATIONS OF THE COAL BALLS

Two closely associated coal seams are mined by the Pittsburg and Midway Coal Co. These are the Fleming and the Mineral seams, both of which occur near the bottom of the upper one-third of the Cherokee shale of Des Moines age. The Fleming is the uppermost coal. It ranges from 12 to 18 inches in thickness and lies from 8 to 20 feet above the Mineral coal, the thickness of which ranges from 18 to 24 inches. Both seams locally contain coal balls, but the balls are far more abundant and widespread geographically in the Fleming coal.

The Mineral coal, although of more sporadic occurrence than the Fleming, apparently more consistently maintains a single stratigraphic level. It may be present directly beneath the Fleming coal, or present in an area where the Fleming coal is absent. On the other hand, the Mineral coal may be absent from an area that does contain the Fleming coal.

In contrast to the flat-lying Mineral coal, the Fleming coal undulates, varying in vertical distance from the underlying seam. It may be flat and almost parallel to the Mineral coal for a large area, but locally it rises to form structural "highs" that extend as much as 12 feet above its general level. The "highs" may form domes as much as 100 feet across or ridges extending along the seam for 500 to 1,500 feet (K. E. Moore, 1957, oral communication). They are usually accompanied by a thinning of the coal at their crests. In areas where the Mineral coal is generally absent, an isolated patch of it may be present directly below a "high" in the Fleming coal.

The overburden of the Mineral seam also differs from that of the Fleming seam. The Fleming coal is overlain by a dark-gray to black fine-grained marine shale, rich in productoid brachiopods (Williams, 1938, p. 105). According to Mr. Moore, a limestone is not known to overlie this seam at the Mine No. 19 area. On the other hand, over broad areas, the Mineral coal is overlain by a hard massive impure fossiliferous limestone as much as 20 inches thick, which may change laterally in a short distance to a black shale similar to that above the Fleming coal. At one exposure at Mine No. 19, we observed a limestone 20 inches thick directly above the Mineral coal; 50 feet away, the coal was overlain by the fossiliferous shale. No coal balls were observed in the coal beneath the limestone.

The coal balls show the following relations to the two coal seams:

1. Relative abundance of coal balls, in general, shows considerable local variation. At Mine No. 19, the dragline pit (sec. 6, T. 33 S., R. 22 E.) had produced few coal balls, while the shovel pit, less than two miles away (SW¼ sec. 32, T. 32 S., R. 22 E.), had produced many.
2. Of the two seams, the Fleming coal produces by far the most coal balls.
3. A previous statement by us (1953) that coal balls occur only beneath a marine limestone caprock is erroneous, as is strikingly illustrated by the abundance of coal balls in the Fleming coal, where a marine limestone cap is absent. Furthermore, there seems to be no correlation between limestone and coal balls in the Mineral coal, where both are known to occur. Thus it appears that the one condition found consistently in occurrences of coal balls is that the productive seam is directly overlain by a marine bed, regardless of its lithology. Feliciano (1924, p. 233) cast some doubt on this but did not present detailed evidence.
4. The coal balls are generally more abundant in the upper half of the seam, but are known to occur throughout the thickness of the coal. In some places they replace almost the entire coal seam over areas of many square yards.
5. In the Fleming coal the abundance of coal balls seems to be related to the elevation of the coal seam. It was brought to our attention by Messrs. Sandeen and Moore, as well as by several of the Pittsburg and Midway Coal Co.'s shovel operators, that coal balls in the Fleming seam are usually concentrated at the "highs." Mr. Moore stated that tipple waste from "high" areas of the Fleming coal usually is greater than that from "low" areas in the seam, and may reach as much as 37 percent of the total volume, a large part of this waste consisting of coal balls. Sporadic occurrence of coal balls within a given coal seam has been reported previously (Cady, 1936, p. 158; Andrews, 1951, p. 433) and probably is characteristic of all deposits containing coal balls. Whether these other sporadic occurrences are also associated with "highs" in the coal remains to be determined.

These facts may have some bearing on the overall problem of coal ball formation, but they shed no light on the outcrop relations of mixed coal balls to normal ones. However, it is known that the two types do occur very close to each other. Along one of the mine access roads at the West Mineral, Kans., locality, there had been dumped, intact, a nest of coal balls approximately 3 feet square and 1 foot thick. The lower surface of the nest bore a 2- to 3-inch layer of coal; its upper surface bore a thin film of coal, superposed by an inch or so of black fossiliferous shale whose surface undulations marked the positions of the individual coal balls. Several of these were broken from the upper

surface of the nest, and two proved to contain animal remains as well as moderately well preserved plant fragments; the rest of the collection consisted of normal coal balls with well-preserved plant structures. Thus it is at least known that mixed and normal coal balls may occur within 2 or 3 feet, horizontally, and a few inches, vertically, of each other.

Most of the mixed Kansas coal balls were collected from the roadbeds and ballast heaps of the Pittsburg and Midway Coal Co. Although it was not possible to observe the relation of mixed coal balls to normal coal balls or to arrive at any understanding of their real distribution, it was possible to gain some idea at least of their relative abundance. Mixed coal balls are no rarity at this particular locality, but, on the basis of examination of perhaps 4 or 5 miles of roadbed exposures and of the several large waste heaps in the area, we estimate that mixed coal balls constitute no more than 1 to 2 percent of all the coal balls spread about the Pittsburgh and Midway Coal Co.'s grounds.

The mixed coal balls show about the same range in size and shape as those of the normal specimens; several were more than 2 feet in greatest dimension and several hundred pounds in weight. Mixed coal balls were not concentrated at any one place, but were fairly evenly distributed among the normal coal balls and were found among the waste heaps and roadbeds of the abandoned Mine No. 15 as well as those of the then active Mine No. 19. This suggests an areal distribution approximating that of normal coal balls in the Fleming coal.

FRANKLIN, KANS.

Large heaps of coal balls were examined at the dumps of the Mackie-Clemens Mine No. 22 (SE¼ sec. 24, T. 28 S., R. 25 E., Crawford County) and Mine No. 23 (NW¼ sec. 21, T. 29 S., R. 25 E., Crawford County), east of Franklin, Kans. A few mixed specimens were found at the latter locality, an airline distance of nearly 30 miles from the Pittsburg and Midway Coal Co. pits.

Abernathy (1946) indicated the coal mined there to be the Mineral coal, but local inquiry indicated that the seam is considered by some miners to be the Fleming coal. On the basis of plant content and physical appearance, the coal balls examined there seem to be identical with those at West Mineral, where the Fleming coal yields most of the coal balls. Several other pits and dumps in this general area were examined without finding coal balls.

MONMOUTH, KANS.

The Bevier coal is exposed in an open-pit mine of the Apex-Compton Coal Co., in NW¼ sec. 12, T. 31 S., R. 22 E., Crawford County, near Monmouth, Kans. According to Abernathy (1946, p. 139) the Bevier coal lies above the Fleming and Mineral coals, about 100 feet below the top of the Cherokee shale. The roadbeds at the Monmouth pit, like those at the Pittsburg and Midway Coal Company, are composed largely of coal ball material, indicating regular and abundant occurrences of coal balls. But curiously enough, the coal balls themselves are predominately pyritized faunal coal balls or specimens containing negligible plant material. Only a few specimens of plant-bearing coal balls were found, and these are composed almost exclusively of fusinized wood fragments instead of the heterogeneous, calcified, and more or less well-preserved plant debris that occurs in normal coal balls. Thus it appears that the ratio of normal to animal-containing specimens at other deposits is almost reversed at the Apex-Compton mine, for the normal coal balls there constitute the smaller percentage, perhaps even a smaller percentage of the total than do the mixed coal balls at the Pittsburg and Midway pits.

The active pit was flooded at the time of our 1955 visit, and it was not possible to see the coal balls in place, but the following information regarding this curious occurrence was provided by H. W. Compton, owner of the mine:

1. A limestone has not been noted immediately above the coal in the Apex-Compton pits. The immediate overburden of the coal seam is a dark-gray slightly fissile shale containing productid brachipods, pectenoid pelecypods, and poorly preserved plant impressions near its contact with the coal. This shale ranges from 3 to 6 feet in thickness and is overlain by a 3- to 6-inch layer of medium dark-gray argilaceous unfossiliferous limestone; above the limestone is a light-gray nonfissile unfossiliferous shale. The overburden apparently lacks concretions and is generally very poor in fossils.
2. Coal balls are abundant and occur throughout the thickness of the seam. In some places they are so highly concentrated as to form sizable humps in the surface of the coal. As an exceptional example of the high proportion of the coal seam sometimes represented by coal ball material, Mr. Compton cited one particular pit, 80 feet wide and approximately one-half mile long, in which the coal was so heavily contaminated with coal balls that the pit was abandoned.
3. Although the surface of the coal seam shows some undulation, no correlation has been observed between the "highs" and coal ball occurrences, except where the elevations are actually caused by unusual concentrations of coal balls.

562661 O—62——3

In July 1957, Robert W. Baxter, University of Kansas, visited the Apex-Compton mine at our request, in order to study the field relation of the faunal coal balls under better conditions than those we found in 1955. Baxter's observations substantiate the above descriptions. He succeeded in observing, photographing, and collecting faunal coal balls in place at the working face of the coal seam, and forwarded us specimens and photographs for inclusion in this report. Part of the coal seam with two faunal coal balls in place is shown in plate 26, figure 5; sawn surfaces of these two specimens are shown in plate 32.

Baxter wrote us:

The seam exposed at the time of my visit averaged 16–18 inches thick. The swath of coal exposed while I was there was not over 60 yards long. In this area of mining, the Bevier seam is only 12–15 feet below the surface and the old pits are covered just about as fast as the coal is removed. Unfortunately, the area exposed was exceptionally clean of coal balls. The descriptions of Mr. Compton and three men who were working on the stripping shovel all tallied and agree that the coal balls tend to occur in pockets with a center of greatest density or abundance with gradually diminishing numbers towards the borders of the area. In the 16–18 inch seam they tend to occupy the entire seam from top to bottom in the pocket areas, the coal present being reduced to an embedding matrix. Just before we had arrived, the stripping shovel hit a small pocket occupying the entire thickness of the seam and had put the whole shovelful up on the far side of the pit. Samples of coal balls from this are being sent you. It was quite evident to me, from an examination of the almost intact shovelful, that the coal balls had filled the whole seam in that spot. There was a veneer of coal on all the coal ball material, but 90 percent of the shovelful was "rock."

Shortly after looking over the above, the stripping shovel exposed a large flat coal ball in place in the face of the seam with at least an inch of coal above it. A rounded, almost pure pyrite coal ball occurred slightly below it, deeper in the coal. Several pictures of the above exposure are enclosed and the two coal balls are being sent you.

Accordingly one can definitely say that these "coal balls" are abundant in the Bevier coal, usually in localized areas where they almost fill the seam, or in more isolated cases where they tend to occur in the upper part of the seam.

Regarding the underlying bed, Baxter wrote:

The coal seam lies on what I would consider a typical stigmarian underclay. Mr. Compton had the stripping shovel dig down into it for several feet. * * * Mr. Compton said the clay varied in thickness from up to 12 feet down to less than a foot thick, overlying a limestone layer. The depth of clay at the region of the picture was certainly over 3 feet.

Baxter observed that "none of the coal balls I saw, either in the pit or on the older dumps showed anything I could identify as plant material." He further stated:

While as indicated below, there is no doubt about the rather highly pyritized rock from this mine being coal ball material, in that it definitely occurs in the coal itself, it still seems quite different from most coal balls I am familiar with. For one thing, most of the rocks tend to occur as flat sheets, 2 to 3 inches thick. This makes it look suspiciously like similar fossiliferous rock from the overlying shale. However, there is no doubt that this occurs within the coal.[3] There is a smaller percentage of slightly rounded coal balls which almost always seem to be nearly pure pyrite.

In September 1957, Mamay revisited the Apex-Compton mine but made no significant additional observations, except that the overburden then exposed contained no fossiliferous rock with which the faunal coal balls could be compared.

Faunal coal balls were found at only one other locality, this being a small strip pit in the Bevier coal, owned by the Garrett Coal Co. and located in SE¼ sec. 34, T. 26 S., R. 25 E., Bourbon County, Kans. At this pit a few highly pyritized faunal coal balls were found in the uppermost 3 inches of the coal, which was about 18 inches thick. None were seen elsewhere in the seam, nor were any normal coal balls found.

PHYSICAL AND BIOLOGICAL FEATURES OF COAL BALLS

NORMAL COAL BALLS

The characteristics of normal coal balls were discussed thoroughly by Stopes and Watson (1908). A few comments are added here for the sake of completeness.

Normal coal balls show considerable range in the variety and preservation of their content, the quality of preservation being dependent on high percentages of calcium carbonate. Some contain little but roots or lycopodinean periderm, while others are rich in leaves and reproductive organs. A large number of samples from a given locality may give the investigator a reasonably sound basis for analysis of the local flora in terms of dominant and subdominant species.

Occasionally one finds a coal ball that consists of a single plant fragment. At the West Mineral locality, Mamay has found several well-preserved calcareous lycopod, medullosan, or psaronean stem fragments a foot or more long, surrounded by a film of coal and unaccompanied by other plant debris. The same locality yields large numbers of tiny "nucellar coal balls" (Roth, 1956), each of which consist of the internal parts of a single cordaitean seed.

Normal coal balls vary considerably in shape, some being nearly spherical. Specimens of this type seem to be most common in the English deposits but are rare in American deposits.

The contents of spheroidal coal balls usually show no layering or other textural peculiarities. Most com-

[3] Stopes and Watson reported apparently similarly shaped sheets of stone in the English coals; however, they considered the stone sheets, which they discussed only briefly and which contain only plant material, to be a "parallel formation to that of the normal coal balls" (Stopes and Watson, 1908, p. 176).

monly the plant fragments are uncompressed and otherwise undistorted.

Lenticular coal balls are common in American deposits. All degrees of lenticularity may be found, the most extreme having perhaps a ratio of less than one-quarter thickness to width. Some specimens are nearly circular in outline, relatively smooth-surfaced, and often slickensided. Coal balls of this type are common at the West Mineral, Kans., locality, some being nearly 2 feet in diameter. A West Mineral normal coal ball, irregular in shape but typical in composition, is shown diagrammatically in figure 43, and a lenticular specimen is illustrated on plate 28, figure 2.

Lenticularity is assumed to be the result of prelithification compaction, for lenticular specimens in place lie parallel to the bedding of the coal, with the laminae of the coal following the contours of the coal ball. This type of coal ball also presents the greatest consistency of relation of external shape to internal texture, for lenticular coal balls generally show distinct layering of the enclosed plant parts, the layering being almost parallel to the bedding of the coal. Stems with large or hollow pith cavities, such as the calamarians, are commonly flattened in lenticular coal balls. Furthermore, coal balls of this type commonly have a thin equatorial flange of well-preserved plant material that feathers out and disappears between laminae of the coal.

Aside from the spheroidal and the lenticular types of coal balls, there are no other regular or definable shapes that characterize these nodules. Coal balls have a variety of irregular shapes; angular external contours are, however, extremely rare. Specimens of irregular shape may show bedding or layering of their contents, but, on the other hand, commonly there is no definite arrangement of plant debris in the matrix.

Calcite-filled cracks, often penetrating nearly the entire width of a specimen, and concretionary mineralization patterns are common to all types of coal balls discussed thus far. Cracks may be abundant in a single specimen, and sometimes they fall into a roughly radial pattern that extends inward a variable distance from the periphery of the nodule. That such cracks often create a clean break in an otherwise undistorted and well-preserved plant axis suggests that they are probably compaction cracks, formed after initial mineralization had been completed.

HOMOGENEOUS-MIXED COAL BALLS

Homogeneous-mixed coal balls are mostly irregular in shape, although lenticular specimens have also been seen. Some homogeneous-mixed balls are slightly flattened, with layered alinement of the enclosed fossils, and in the lenticular specimens layering of fossils may be as clear as that often shown by plant debris in the lenticular normal coal balls. Calcite-filled cracks are common in homogeneous-mixed coal balls. A homogeneous-mixed coal ball is shown diagrammatically in figure 44 and others are illustrated on plates 27–29.

Animal and plant fossils may be randomly scattered through the entire coal ball, but in some the animals seem to be concentrated in poorly defined pockets. In samples of this sort the animal-containing pockets may be distinguished from the remainder of the coal ball by a slight difference in the color of the matrix, which

FIGURE 43.—Sketch of sawn surface of a normal coal ball from West Mineral, Kans., drawn from a peel preparation of specimen 9189–61E. Calcite-filled cracks are unstippled. Approximately $^{8}/_{10}$ natural size.

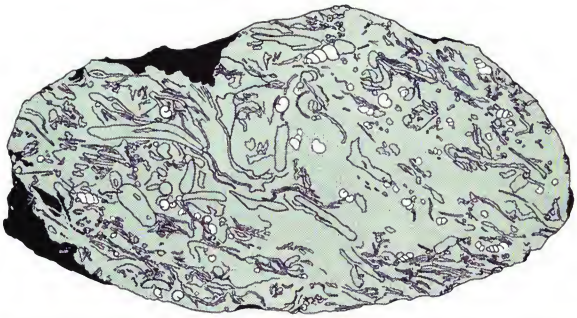

FIGURE 44.—Sketch of sawed surface of a homogeneous-mixed coal ball from West Mineral, Kans., drawn from a peel preparation of specimen 9189–120A. Unstippled areas represent animal remains. Natural size.

is not, however, sharply delineated from the surrounding matrix. Mixed coal balls with pockets of this type may also contain faunal and floral mixtures in other parts of the specimen.

Some homogeneous-mixed coal balls show a peculiar textural feature that is like the mixing together of two colors of cake batter and that we refer to as "swirled." This "swirling" consists of oriented lines of animal fossils. The lines nearly parallel each other, but are very irregular and bear no definite relation to the bedding plane of the coal where that feature can be inferred from the shape of the coal ball or adherent remnants of the surrounding coal. The swirl markings may also assume roughly concentric orientation, and may intergrade imperceptibly into coal ball matrix that shows no structure.

HETEROGENEOUS-MIXED COAL BALLS

Heterogeneous-mixed coal balls, which have been found only at Berryville, Ill., differ from all other types by showing a segregation of marine from nonmarine parts of the matrix; this segregation is illustrated in figure 45. Actually, this is not a simple segregation of plant from animals remains, for a certain amount of small resistant plant fragments (mostly well-preserved spores) is incorporated in the animal-containing matrix. However, this animal-containing matrix is surrounded by an area that contains only plant material and that in all aspects is typical of the matrix of a normal coal ball.

The marine masses, to which for want of a better term we refer as "cores," are of much interest, both structurally and biologically. They vary in form from elongate, more or less cylindrical rods that extend through the entire length of the coal ball, to irregularly shaped cores. The cylindroid type of marine core is illustrated in figure 45; others are shown on plates 30 and 31.

In the example shown in figure 45, as well as in several other examples, the coal ball is an elongate, slightly flattened specimen. The plant material shows perceptible flattening parallel to the long axis of the specimen. The marine core, which is slightly eccentric in position, extends through the whole length of the coal ball (approximately 16 inches) and is exposed at either end. It varies little in either its diameter (approximately 2½ inches) or its position relative to the center of the coal ball, and for the most part displays a sharp line of contact with the surrounding normal matrix. Here and there, however, a root or stem fragment or stringer of unrecognizable plant debris crosses the contact and extends a short distance into the core. In other specimens, though the contact between the core and the normal part of the coal ball is relatively clear, it is irregular and subangular in places.

The figured core is unusual in its deep embedment within the normal matrix and its nearly perfect cylindroid shape. Other cores are less regularly shaped and may constitute most of the coal ball. All cores, however, are surrounded by a layer of normal matrix with-

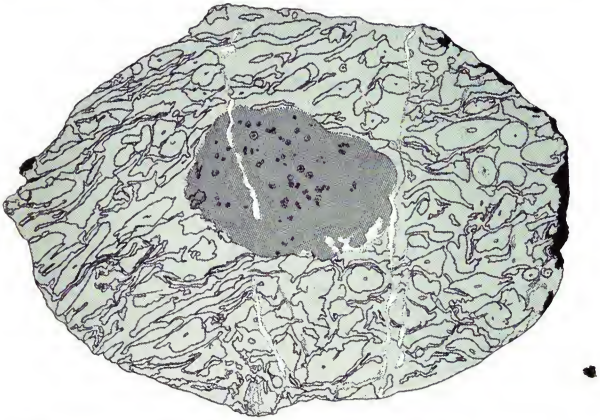

FIGURE 45.—Sketch of sawn surface of a heterogeneous-mixed coal ball, drawn from a peel preparation of specimen 9190–2 J. The marine core is indicated by dark stippling; calcite-filled cracks are unstippled. Natural size.

in a film of coal that indicates their original position below the upper limit of the coal seam.

Marine cores may extend nearly to the bottom of the seam. A large mass of coal balls, 2 feet long and 1 foot thick, was found in place by Mamay in 1957, and dug out of the coal. The bottom of this mass lay within an inch of the bottom of the coal seam, and it contains irregularly shaped but distinct cores through its whole thickness. One core reaches the lower surface of the thickest part of the coal ball mass, and thus was originally separated from the underclay by only an inch of coal.

Distinct bedding of the detrital fragments, both plant and animal, was observed within the marine core in several specimens. In one core (pl. 30, fig. 1) the fossil debris is arranged in easily discernible layers. The bedding may be flat and parallel to the less distinct bedding of the plant material in the surrounding normal matrix. However, for about 1 cm from the contact between the core and normal matrix, the bedding of the core is slightly warped. This warping suggests that the original lump of marine mud was still fairly plastic when deposited in the coal swamp. After deposition its inner bulk sagged slightly and produced the warped bedding planes.

Our interest in the specimen shown on plate 30 was increased by two facts: (a) The core itself is a roughly flattened body that stands "on edge" with its bedding planes extending across its smallest dimension. Thus the core presumably dropped into a deep but relatively narrow indentation in the surface of the peat, in such a way that its own bedding planes paralleled the surface of the bog. (b) The layer of coal surrounding this specimen also contains a second small normal coal ball with distinctly layered plant debris. This layering, however, is nearly perpendicular to that of the mixed specimen and indicates a precoalification disturbance of the peat, which distorted the bedding plane relations between these two adjacent coal balls.

The Berryville material is also distinctive because of its faunal content. As far as determinable, the faunas of the cores contain several elements identical with animals found in the limestone overlying the coal seam. The cores also contain many spores, cuticular fragments, and other plant remains. Although several samples of normal matrix surrounding the cores were carefully trimmed away from the latter and dissolved in acid, these samples produced no animal remains. It is therefore evident that the cores and surrounding nor-

mal matrices could not have been formed under identical depositional conditions. Further support for this line of reasoning may be seen in the results of chemical analyses of the two matrices (p. 207; table 2). These show that the Berryville core material contains Al_2O_3, which does not occur in the normal matrix or in any of the coal balls analyzed.

FAUNAL COAL BALLS

Specimens of faunal coal balls were noted in significant numbers only at the Monmouth, Kans., locality. They conform with the essential features of normal coal balls except that the contained fossils are of exclusively zoological origin. In shape they vary almost as much as normal coal balls, but have perhaps a higher proportion of lenticular or flattened specimens. Baxter (1957, written communication) noted that many of them are of sheetlike aspect. Their faunal contents may be roughly layered or scattered at random through the matrix, which may also contain stringers of coal. The animal remains are mostly small pyritized brachiopod fragments. As shown in tables 1 and 2, coal balls from this locality usually contain more pyrite than those from any other locality investigated.

CHEMICAL ANALYSES

In order to determine what chemical differences exist between normal and mixed coal balls, eight typical samples were selected for semiquantitative spectroscopic analysis and rapid rock analysis as described by Shapiro and Brannock (1956). The rock analyses were performed on samples as received, without preliminary drying. Samples of both normal and mixed coal balls were taken from West Mineral, Kans., McAlester, Okla., and Berryville, Ill.; a faunal coal ball from Monmouth, Kans., was analyzed. The Berryville material also included one sample from a heterogeneous-mixed coal ball and a piece of the limestone over the channel in the coal seam.

The rapid rock analyses (table 2) show some apparently consistent but small differences between normal and mixed coal balls in concentrations of SiO_2, FeS_2, K_2O, P_2O_5, Al_2O_3, $CaCO_3$ ($CaO+CO_2$) and MgO. These could reflect chemical makeup of animal fragments or other uncontrollable factors, and cannot safely be considered significant. The complete results are, however, presented as tables 1 and 2, for they represent the most detailed coal ball analyses known to us.

In reviewing the published record we found several chemical analyses of coal balls in papers treating primarily of the fossil floras. References to these are given to aid those who may wish to pursue the problem of the formation and chemical composition of coal balls. Analyses published prior to 1908 were summarized by Stopes and Watson (1908). An analysis of a single coal ball from Bohemia was presented by Kubart (1911, p. 1038). Leclercq (1925, p. 21) published one analysis of a coal ball from Belgium and subsequently analyses of three others (Leclercq 1952, p. 398). Zalessky and Tchirkova (1931, p. 590) published an analysis of a coal ball from the Kousnetzk basin of Russia. Teichmüller, Teichmüller, and Werner (1953, p. 145) published a summary of their work and that of others; they listed a dozen analyses for iron oxide, calcium carbonate, and magnesium carbonate in coal balls or "Torfdolomit" from the Ruhr area of Germany. So far as is known, Darrah (1939, p. 132) has presented the only published analysis of a coal ball from the United States.

TABLE 1.—*Semiquantitative spectroscopic analyses of coal ball and limestone samples*

[Analysts: Mona Frank and P. L. D. Elmore. Phosphorus may be present in these samples, but further work is necessary to assure positive identification. Sensitivity for phosphorus is 0.1]

Percentage	West Mineral, Kans., Fleming coal		Berryville, Ill., Calhoun coal			McAlester, Okla., Secor coal		Monmouth, Kans., Bevier coal
	Sample 145717, normal coal ball	Sample 145718, mixed coal ball	Sample 145719, normal coal ball	Sample 145720, marine-core from mixed coal ball	Sample 145721, marine-limestone above coal	Sample 145722, normal coal ball	Sample 145723, mixed coal ball	Sample 145724, faunal coal ball
>10	Ca	Ca	Ca	Ca	Ca	Ca	Ca	Fe
5-10								Ca
1-5	Fe, Mg	Fe			Mg	Fe, Mg	Fe	
.5-1		Mg	Fe, Mg	Fe, Mg	Al, Fe		Mg	
.1-.5	Si, Mn	Si	Si	Si, Al	Si, Mn	Si	Si, Al	Si, Mg
.05-.1	Al	Al, Mn	Mn	Sr, Na, Mn	Sr, Na		Mn	Al
.01-.05	V, Sr, Na, B, Ti	Sr, V, Na, Ti	Na, Sr, Al	Ba, Ti, V, B	Ba, Ti, V	Sr, Al, Mn, Na, V	Ba, Sr, Na, V	Mn, Na, Sr, Ba, Pb
.005-.01	Ni, Pb	B, Ni	Ti, B, Ni	Ni	B, Ni	B	B, Ti	Cu, Y, V
.001-.005	Ba, Mo	Pb, Cu, Ba	V, Ba	Pb, Cr, Cu, Mo	Cr	Ba, Ti		Mo, Sn, Ti, Zr
.0005-.001	Cr, Cu	Cr, Mo	Mo, Cr, Cu		Cu, Mo	Cr, Mo, Cu	Cr, Mo, Cu	Yb, Cr
.0001-.0005					Ag			

TABLE 2.—*Rapid rock analyses of coal ball and limestone samples*

[Analyst: Paul W. Scott]

Constituent	West Mineral, Kans., Fleming coal		Berryville, Ill., Calhoun coal			McAlester, Okla., Secor coal		Monmouth, Kans., Bevier coal
	Sample 145717, normal coal ball	Sample 145718, mixed coal ball	Sample 145719, normal coal ball	Sample 145720, marine core from mixed coal ball	Sample 145721, marine limestone above coal	Sample 145722, normal coal ball	Sample 145723, mixed coal ball	Sample 145724, faunal coal ball
SiO_2	0.21	0.80	0.35	1.8	2.9	0.31	1.3	1.1
Al_2O_3				.68	1.1		.46	
[1] FeO	1.3	.6	1.0	.9	2.7	.3	2.2	.0
MgO	2.8	1.0	1.8	1.4	2.8	3.4	2.3	.40
CaO	47.8	45.9	51.6	50.2	46.6	48.4	45.6	18.8
Na_2O	.09	.08	.08	.09	.14	.10	.08	.13
K_2O	.01	.03	.03	.09	.15	.02	.06	.05
TiO_2	.01	.02	.02	.03	.04	.02	.02	.01
P_2O_5	.10	.15	.08	.23	.17	.16	.19	.41
MnO	.34	.18	.27	.18	.47	.08	.18	.05
H_2O	.73	.50	.59	.36	.76	1.2	.52	.96
CO_2	40.5	37.1	42.4	40.4	40.2	40.8	39.7	14.8
Total S as FeS_2	4.5	11.2	.60	3.0	1.0	1.8	4.7	60.9
Total [2]	98	97	99	99	99	97	97	97

[1] Iron, exclusive of that required for calculation of FeS_2, calculated as FeO.
[2] Organic matter contained in all samples may account for differences between totals and 100 percent.

LABORATORY METHODS

Mixed coal balls from each of the various localities possess more or less distinctive physical and biological characteristics. To demonstrate these differences, a number of coal balls, as well as samples of associated rocks are described on pages 217–222. Faunal contents of the samples and spore identifications are summarized in table 3. Although small isospores or microspores were observed and are apparently abundant in some of the residues, these were not identified, because the larger spores were sufficient demonstration of the intermixture of land plants with marine animals.

Though animal remains in coal balls may easily be seen on cut or broken surfaces, such examination gives a generally incomplete picture of the biological composition of the assemblage. For this reason acid solution was used as the chief technique for releasing fossils from the coal-ball matrix.

When animal remains were first noted in the collection briefly described in 1953, commercial grade hydrochloric acid was used to isolate pyritized remains from the matrix. However, the diversity of animal groups represented in these residues suggested the presence of phosphatic fossils such as vertebrate bones, teeth and scales, and conodonts. Formic acid therefore was substituted for hydrochloric in our later studies, with the result that phosphatic fossils were recovered from many of the mixed coal balls.

Coal balls selected for acid solution were sawed into 1-inch thick slices; part of each coal ball was held in reserve for additional preparations if later desired. Because most of the fossils seen on the smoothed surfaces were relatively small, the slabs selected for acid solution were broken into small pieces to speed the reaction. Where it was evident that larger fossils were contained in the matrix, entire slabs were dissolved. Before the cores of marine sediment in the Berryville, Ill., coal balls were dissolved, surrounding normal parts were trimmed from the core so that the insoluble residue would not be contaminated with plant material from the normal coal ball matrix.

The samples were then weighed and placed in formic acid in covered containers. Strength of the acid was adjusted to prevent effervescence from damaging fragile specimens, and was maintained by daily recharging of the solution. Most samples required 7 to 10 days for complete solution of their soluble components. Samples high in calcium carbonate were generally reduced to fine- or medium-textured granular residues, but some with large amounts of pyrite were deeply corroded but not entirely disaggregated. The latter contributed little to faunal analyses because of generally poor preservation of the fossils.

The residues were washed in water, allowed to dry, and weighed to determine the proportions of soluble and insoluble components of the original sample. The residues were then sized through standard-size sieves down to 200-mesh size; this was done under water to keep breakage at a minimum. The graded residues were then dried and picked. In addition to the mixed coal balls, samples of limestone caprock, of normal coal balls, and of the normal matrix surrounding cores in the Berryville, Ill., specimens were also dissolved.

Samples from Berryville, Ill., were the most soluble: their residues ranged only from 0.2 to 5.4 percent of original sample weight. At the other extreme, residues of samples from Monmouth, Kans., ranged from 22.6 to 37.9 percent of sample weight. Because the solubility of the different samples showed meaningless variation, further details are omitted.

TABLE 3.—*Distribution of animal groups and large spores in insoluble residues*

Samples 9189–110 and 9190–1 were not etched in order to preserve calcareous coral specimens.
Locality of samples: E–1, 2, 17, Franklin, Kans.; 9189–110, E–9, 10, 12, 18, 23, 24, West Mineral, Kans.; E–7, 8, 20, 21, Monmouth, Kans.; E–11, 22, 30, 31, McAlester, Okla.; E–13, Oskaloosa, Iowa; E–3, 4, 19, 25–29, 9190–1, Berryville, Ill.; E–14, limestone overburden, West Mineral, Kans.; E–16, limestone overburden, McAlester, Okla.; E–5, limestone in channel, Berryville, Ill.; E–6, limestone overburden, Berryville, Ill.; E–15, limestone below channel, Berryville, Ill.

Fossil	Type of deposit and sample number																																			
	Homogeneous-mixed coal balls													Heterogeneous-mixed coal balls								Normal coal balls									Fusinal coal balls		Miscellaneous associated sedimentary deposits			
	E–1	E–2	9189–110	E–9	E–10	E–12	E–23	E–24	E–20	E–11	E–22	E–30	E–31	E–13	E–3	E–4	E–25	E–26	E–27	E–28	E–29	9190–1	E–17	E–18	E–21	E–19	E–30	E–7	E–8	E–14	E–16	E–5	E–6	E–15
Protozoa:																																				
Ammovertella? inclusa Cushman and Waters															×																					
Ammovertella cf. *A. labyrinthus* Ireland						×																														
Ammovertella? aff. *A. prodigalis* Ireland																																×				
Ammovertella sp.							×			×						×		×	×	×												×	×			
or *Serpulopsis* sp.							×	×		×						×																				
Ammovertella? sp.							×								×		×		×																	
or *Glomospira* sp.																																	×			
Genus aff. *Ammovertella*															×	×																	×			
Apertrinella sp.								×									×	×		×	×											×				
or *Calcitornella* sp.																			×																	
Apertrinella? sp.						×										×			×	×	×															
Cornuspira? sp.	×																											×								
or *Glomospira* sp.																												×								
Cornuspira? sp.									×																											
Endothyra or *Endotriyrenella?* sp.																												×								
Endothyrenella powersi? (Harlerton) sp.																	×																			
Globivalvulina sp.																														×	×					
Glomospira sp.									×										×																	
Serpulopsis aff. *S. insita* (White)																					×															
Serpulopsis? sp.																																				
Tetrataxis pauperata? (Worthin)	×																											×								
Thurammina aff. *T. rectangularis* Ireland																	×			×																
sp.																	×																			
Thurammina? sp.																														×	×		×			
Fusulinide indet.											×	×					×																×			
Porifera:																																				
Cf. *Pisetopoupia?* sp.							×																													
Hexactinellid spicule																×				×																
Coelenterata:																																				
Lophophyllid coral			×																			×														
Echinodermata:																																				
Crinoid stems	×	×					×									×		×	×	×	×							×			×		×			
Annelida:																																				
Arabellites sp.																																	×			
"*Spirorbis*" sp.						×				×	×	×				×				×																
Bryozoa:																																				
Rombiporella sp.																×			×																	
Trepostomatous bryozoans indet.										×						×			×													×				
Fenestella sp.																×		×	×	×																
Polypora sp. 1																×		×	×													×				
sp. 2																		×																		
sp. 3																		×																		
Penniretepora sp. 1															×	×		×	×	×	×											×				
sp. 2																		×			×											×				
Septopora sp.										×																										
Fhabdomeson sp.															×		×																			
Rhombocladia sp.															×		×	×	×	×	×											×				
Rhombopora sp.															×		×	×	×	×	×											×				
Brachiopoda:																																				
Lingulid indet.											×	×									×															
Orbiculoid indet.						×					×										×															
Rhipidomella? sp.																		×										×								
Derbyia sp.							×																													
Meekella sp.	×																											×								
Chonetid indet.		×				×													×																	
Marginifera sp.						×																														
Productid indet.					×	×	×								×		×	×	×	×	×									×		×				
Mollusca:																																				
Nuculana sp.																					×															
Nuculoid indet.																												×								
Pseudoleidon sp.							×	×	×	×	×	×				×	×				×															
Septimyalina sp.	×									×	×	×																								
Cf. *Leiopteria* sp.				×			×			×	×	×					×				×															
Schizodus sp.							×										×	×											×							
Aviculopecten sp.							×										×																			
Pectinoid indet.								×																												
Myalid indet.										×	×	×									×									×						
Permophorus sp.						×				×	×	×				×																				
Aviculella sp.						×									×			×		×																
Pelecypoda indet.						×		×												×										×						
Pelecypoda indet.					×	×	×	×		×	×	×	×		×	×																				
Knightites (*Retispira*) sp.					×			×																					×							
Bellerophontid indet.	×	×												×		×	×																			
Pleurotomaria sp.								×																												
Gastrioceras? sp.					×	×																						×	×							
Neilsonia? sp.								×																												
Shumardella sp.					×					×	×						×		×	×								×	×							
Steinkern cf. *Shumardella*						×	×					×						×										×	×							
Pleurotomarian indet.	×					×				×	×						×	×		×								×	×							
Cf. *Microdoma* sp.											×	×								×																
Euomphalus sp.						×	×																					×								

TABLE 3.—*Distribution of animal groups and large spores in insoluble residues*—Continued

Fossil	Type of deposit and sample number: Homogeneous-mixed coal balls													Heterogeneous-mixed coal balls							Normal coal balls						Faunal coal balls		Miscellaneous associated sedimentary deposits				
	E-1	E-2	9189-119	E-9	E-10	E-12	E-23	E-24	E-20	E-11	E-22	E-31	E-13	E-3	E-4	E-25	E-26	E-27	E-28	E-29	9190-1	E-17	E-18	E-21	E-19	E-30	E-7	E-8	E-14	E-16	E-5	E-6	E-15
Mollusca—Continued																																	
Naticopsis? sp.																											×						
Paleostylus (*Pseudozygopleura*) sp 1									×							×	×										×						
(*Pseudozygopleura*) sp 2																											×						
Cf. *Bulimorpha* sp.					×	×			×			×															×	×					
Meekospira sp.									×																		×	×					
Girtyspira sp.									×			×															×	×					
Subulitid indet.	×	×								×						×	×											×					
Donaldina sp.						×	×	×	×	×	×					×			×	×								×					
Steinkern cf. *Donaldina* sp.				×	×						×	×					×	×													×		
Low-spired gastropod indet.		×								×	×		×	×	×	×		×		×							×	×		×	×	×	
High-spired gastropods indet.											×	×				×			×														
Cf. *Endolobus* sp.							×																										
Mooreoceras sp.							×																										
Pseudorthoceras knoxense (McChesney)												×																					
Arthropoda:																																	
Ditomopyge sp.														×		×	×	×	×	×												×	
Cavellina sp.											×																						
Bairdia cf. *B. rhomboidalis* Hamilton																	×														×		
cf. *B. pompilioides* Harlton											×																						
cf. *B. garrisonensis* Upton of Kellett											×																						
sp.	×										×	×	×			×	×			×							×		×				
Bairdia? sp.										×																		×					
"*Bairdia*" cf. "*B.*" *oklahomensis* Harlton		×																															
aff. "*B.*" *texana* Harlton																	×		×										×				
sp.																															×		
Bairdiacypris? sp.																				×													
Fabalicypris sp.										×	×	×																					
Healdia sp.											×					×				×							×	×					
Paraparchites? sp.											×									×													
Sansabella sp.										×																							
Sansabella? sp.											×	×				×				×													
Monoceratina sp.													×																				
Kirkbya sp.													×				×			×													
Kirkbya? sp.																													×				
Knightina sp.											×					×																	
Amphissites centronotus (Ulrich and Bassler)													×	×		×			×										×		×		
sp.																				×													
Kegelites cf. *K. dattonensis* (Harlton)															×																		
Kellettina? sp.																			×														
Glyptopleura sp.	×	×																															
Hollinella sp.	×					×	×			×	×	×	×			×	×		×	×							×		×				
Genus indet A																													×				
Genus indet B																													×				
Genus indet.										×							×		×	×													
Chordata:																																	
Acanthodii											×																	×					
Cladodontii											×			×	×		×		×								×	×					
Selachii						×																											
Pleuracanthodii											×						×											×					
Bradyodonti											×																						
Actinopterygii	×	×							×	×	×																×	×		×			
Fish remains indet.							×					×	×							×												×	
Conodonts:																																	
Hindeodella sp.											×																						
Ozarkodina delicatula (Stauffer and Plummer)															×																		
Ozarkodina sp.																×																	
Neoprioniodus sp.																											×						
Roundya cf. *R. subacoda* (Gunnell)																											×						
Spathognathodus minutus? (Ellison)																×				×													
Gnathodus roundyi Gunnell																											×						
bassleri (Harris and Hollingsworth)													×																				
sp.		×																															
Cavusgnathus flexa Ellison											×					×																	
Idiognathodus magnificus Stauffer and Plummer											×																×	×					
cf. *I. magnificus* Stauffer and Plummer	×	×																															
Streptognathodus elegantulus Stauffer and Plummer														×	×	×															×		
Barlike conodont indet.	×			×							×						×			×													
Platelike conodont indet.									×		×																						
Bladelike conodont indet.																×																	
Large spores:																																	
Cystosporites varius (Wicher) Dijkstra												×								×													
sp.													×																				
Monoletes ovatus Schopf						×	×		×				×	×	×	×				×		×	×		×	×							
Parasporites cf. *P. maccabei* Schopf														×																			×
Spencerisporites sp.				×	×	×	×						×	×	×	×		×	×	×		×	×		×				×		×		×
Triletes auritus Zerndt						×			cf.	×																cf.[1]							
auritus var. *grandis* Zerndt												×	×	×	×	×	×	×	×	×											×		×
glabratus Zerndt														×	×	×	×	×	×	×											×		×
cf. *T. rugosus* (Loose) Schopf										×	×	×								×						×							
cf. *T. superbus* Bartlett				×	×	×	×	×					×																				
triangulatus Zerndt				×		×	×	×					×	×	×					×		×	×										
sp.																													×				
Large spore resembling *Lycospora*																															×		

[1] Specimens probably conspecific, but not complete enough for positive identification.

The technique described allows recovery of all but calcareous specimens. In order that important faunal elements should not be overlooked, nonpyritic specimens exposed on fractured surfaces were prepared for identification by mechanical methods. Most of the animal remains recovered by this method are pyritized; the calcareous ones constitute a minor element and consist largely of brachiopods and crinoid columnals.

It is probable that some specimens were destroyed or escaped observation during preparation. Nevertheless a sufficiently wide variety of animal groups are repeated in several coal balls from the same locality to favor the probability that most of the faunal elements are known.

PRESERVATION OF THE FOSSILS

Preservation of the plant fossils needs little discussion because, as is usual in coal ball petrification, there is little if any replacement of the original substance of cell walls. Woody tissues owe their excellent preservation to an impregnation and filling of the cell interiors, the dominant impregnating material usually being calcite. Waxy spore coats and cuticles, among the most resistant substances in the plant kingdom, are ordinarily preserved practically unchanged.

Most of the megaspores recovered from the acid residues are so little distorted by compression that their original shapes and external morphological features may be satisfactorily studied (pl. 33). Those from Berryville, Ill. (pl. 33, fig. 17), McAlester, Okla., and Oskaloosa, Iowa, are seen to be hollow when their coats are broken, a condition that we ascribe to dissolution of the original calcareous fillings of the spore cavities during treatment with acid. Megaspores from West Mineral, Kans., however, may be recovered in a hollow condition or their interiors may contain mineral fillings, usually calcitic, rarely pyritic (pl. 33, figs. 8, 9). The fact that some of the calcitic fillings remained intact after several days' treatment with acid can only be due to exclusion of the acid from contact with the surfaces of the filling, by the intact and impervious endosporal membrane or exospore, or by both. Specimens of *Triletes* cf. *T. superbus* recovered from the same coal ball were either hollow or were filled with pyrite or calcite.

Some of the megaspores are so well preserved that their endosporal membranes can be dissected out. Membranes removed from specimens of *Triletes* cf. *T. superbus* are thin and delicate, and almost invariably show a pattern of regularly distributed and shaped dark spots (pl. 33, fig. 10). The spots, which may represent vestiges of cellular organization, are always restricted to the proximal part of the membrane, and more concisely, to the circular area that is delimited by the arcuate ridges connecting termini of the triradiate sutures of the exospore. On the basis of their proximal positions these spots, despite their abundance in any one spore, were first interpreted as the remains of archegonia, but perhaps they are equivalent to the papillae in similar membranes of *Duosporites* described by Høeg, Bose, and Manum (1955).

Animal remains from most localities are generally replaced by pyrite, but preservation may also be calcareous, phosphatic, or baritic. Only in conodonts, scolecodonts, and fish is evidence of replacement lacking. Both conodonts and fish parts are phosphatic. The few scolecodonts found are black, highly lustrous, and resistant to all the common acids. They are apparently the original chitinlike substance.

Five other groups—the bryozoans, ostracodes, trilobites, worm tubes, and sponges—are consistently preserved in pyrite, almost invariably by replacement, but the few corals found remain calcareous. In the pyritic specimens, replacement ranges from fine to coarse grained.

Preservation of foraminifers is siliceous or pyritic. The thurammindis and tolypamminids had hard agglutinate shells, and in the acid residue the silica sand of many shells remains coherent because of silica cement which may be of secondary origin. The globivalulinids, originally calcareous, were not noted in other than pyritic preservation or chamber fillings. The fusulinid shells are mostly unaltered but their chamber fillings are pyritized or partly silicified.

Aside from the linguloids and orbiculoids, which are phosphatic and do not appear to be replaced, brachiopods from the West Mineral, Kans., samples are unaltered and require mechanical preparation; a few are, however, preserved in pyrite. All those from Monmouth, on the other hand, are pyritized.

Mollusks are present in all the faunas investigated. Pelecypods and gastropods are conspicuous faunal elements. The pelecypods, with two exceptions, are preserved only in pyrite. Cephalopods are calcareous except for the figured specimen (pl. 34, fig. 29). Mineralogic composition of this one was not determined because to do so would necessitate destroying part of the specimen. The specimen is insoluble in hydrochloric acid.

Preservation of the gastropods is perplexing. Although specific identifications are difficult because of the quality of the preservation, there is no apparent correlation between biological identity and mode of preservation of the gastropods. They may be preserved as actual shell replacements or as steinkerns; steinkern

preservation of some pelecypods and foraminifers has been seen but not of the other animals observed. Steinkerns may be phosphatic or pyritic and may fill calcareous shells, as shown by hollow casts surrounding the steinkerns on etched surfaces. Shell replacements are pyritic and filled with calcareous material, as shown by the hollow interiors of shell replacements recovered from the residues. Pyritic replacements are most common, but in one sample (Monmouth, Kans., E–20) replacements are composed of barite. A single coal ball may yield different individuals certainly of generic and probably of specific identity in all the types of preservation noted.

One further point with regard to the animal remains deserves mention here—the size of fragments or whole specimens, exclusive of those of ostracodes and conodonts. With the occasional exception of *Derbyia* and productoid brachiopod shells which may reach 3 cm or more in width, most of the animal material consists either of complete individuals or of fragments smaller than 1 cm in maximum measurement; more than half are 0.5 cm or less.

It is probable that mechanical sorting by wave or current action before original sedimentation and subsequent translocation to the swamp is the explanation for the consistently small size of animal fossils found in the coal balls and that the residues are not a representative sample of typical Pennsylvanian marine faunas.

Few of the specimens show evidence of abrasion or mechanical wear, and some of the more intricately ornamented ostracode shells are perfectly preserved. The one group in which worn specimens are common are the fish remains. The rounded corners and edges of many scales and dermal plates suggest considerable abrasion before final deposition.

Representative suites of plant and animal remains recovered from the acid residues are shown in plates 33 and 34, respectively. Plant material was photographed as recovered from the residues, without further chemical treatment.

INTERPRETATION OF ANIMAL-CONTAINING COAL BALLS

Because the marine animal remains contained in the mixed and faunal coal balls cannot be regarded as indigenous to the coal swamps, a fundamental conflict with commonly accepted theories of coal ball formation arises. Normal coal balls are considered by most authors to represent concretions formed in place, in accord with the conclusions of Stopes and Watson (1908). At variance with that hypothesis, however, Kindle (1934) preferred to compare coal balls with the so-called lake balls—mechanically accretionary, spheroidal masses of plant material whose formation has been observed in Recent aquatic environments. Kindle's analogy has not met with popular acceptance (Schopf, 1949, p. 81), but it is possible that his explanation may contain some acceptable points if applied to mixed coal balls. Obviously, any explanation of marine organisms in nonmarine strata must involve transportation of material. Rafting of coals has been suggested in explanation of the phenomena described here, but this explanation is highly improbable in view of the otherwise normal sedimentary relations of the coal seams that provided the mixed assemblages.

Some coal seams locally contain exotic materials such as igneous boulders and pebbles, and although these attract much interest, there seems to be no agreement regarding the mechanisms responsible for such inclusions; cataclysmic transportation, however, is a frequently suggested mechanism. The following discussion by Whitehead and others (1952, p. 290) demonstrates the necessity for resorting to unusual depositional circumstances by way of explanation.

W. L. Whitehead: A 15- or 20-foot tidal wave is not uncommon on some coasts during hurricanes or tsunamis. At these times submarine plants with hold-fasts can carry a 6-inch boulder 10 miles.

J. M. Schopf: Well, that certainly is a possibility. I should say that a number of these freakish and very difficult-to-explain occurrences must be explained by some cataclysmic method of the sort. I am not at all sure that the widespread partings aren't in that category too.

I. A. Breger: Shouldn't you get occasionally some marine evidence?

J. M. Schopf: You would think so—but let me tell you of an occurrence which puts the "shoe on the other foot." I have found coal-ball limestone, that is, the limestone characteristic of coal balls which must have originated no higher than within the upper portion of a coal-measures peat deposit—such coal-ball limestone has been found embedded in an unquestionable marine coquina overlying the coal. This is an example of the reverse direction in transportation. The coal-ball limestone must have originated within the precoal peat bed and then have been transported bodily into the marine bed above it. There are some strange things associated with coal.

We regard the animal-containing coal balls as representative of the "marine evidence" sought by Breger.

HETEROGENEOUS-MIXED COAL BALLS

The Berryville cores or marine inclusions are considered best explained by a transitory force that introduced them into the accumulating peaty plant debris. The evidence for this hypothesis is the complete embedment of the inclusions within the coal balls, apparently without interruption of coal deposition. The following possible physical setting and sequence

of events is visualized in explanation of the origin of the cores:

The coal swamp lay at or near sea level and was perhaps separated from the sea only by a low narrow strand barrier, which was sufficiently high to prevent access of marine waters to the swamp environment through normal tidal action. Offshore in shallow waters, a calcareous mud was accumulating, into which both marine animals and bits of plant material, either windblown or drifted, were being incorporated. The animal remains, as demonstrated by their consistently small size, were probably being transported from farther offshore sites of original deposition by currents, the larger representatives of the fauna being sorted out during transportation and only rarely being brought landward, or being brought in only as smaller fragments.

As previously mentioned, each insoluble residue of Berryville core material contains many spores, bits of wood, cuticles, and other plant parts. Except for the spores, many of which are complete and undistorted, the plant material is fragmentary. If the cores do represent transported samples of the sea bottom, then the plant debris included in the cores represents a part of the original organic constituents of the marine mud, and as such must be interpreted as twice-transported matter. The plant material may have been blown to sea by the wind or may have drifted out on the surface; eventually it became waterlogged and sank to the bottom to intermingle with the accumulating animal debris. As the spore contents decayed, the spore interiors were filled with minerals, so that they underwent little or no compression before final calcareous cementation. Finally, the plant material was transported back to the coal swamp, perhaps coming to rest many miles from the area in which it had originally been produced. However, it may also be that a short distance, as well as a short time lapse, for both translocations was involved, because some of the most conspicuous spores in the core material (*Triletes glabratus*, *T. auritus* var. *grandis*, and *Monoletes ovatus*) also occur abundantly in the normal coal balls from this locality.

Occasionally lumps of the semiconsolidated mud were dislodged from the sea floor by tidal currents or by other relatively minor disturbances and were worn into various shapes by wave action; some of these lumps assumed cylindroid shapes, some were more irregular.

Violent storms created unusually large waves that swept inland and inundated the swamp. The waves carried along the cylindroid wave rollers as well as less regularly shaped lumps of mud that contained both animal and plant remains. The mud lumps were deposited on the irregular surface of the peat, or fell through the upper layers. A firm consistency of the mud lumps is implied by the discrete nature of the cores and the angularity of some of the cross sections. However, parts of the mud lumps were sufficiently soft that intermixture with the adjacent peat occurred locally, and some of the firmer plant fragments penetrated the surfaces of the lumps.

The core shown in figure 45 is oriented parallel to the mass of roots that constitutes the normal matrix. The roots, preponderantly alined in the same direction, probably created a series of nearly parallel grooves on the surface of the peat, and minor agitation of the receding water could have caused the core to settle in one of the grooves. Meanwhile the turbulence also dislodged chunks of peat, redeposited them, and in some instances effected a reorientation of their original bedding planes. Evidence for this reorientation is apparent in the specimen shown in plate 30, figure 1, where the bedding of plant material in the small coal ball fragment within the coal matrix at the right is oriented nearly at right angles to that of the larger specimen containing the marine core. The same specimen shows evidence that deposition of the marine material was sudden, rather than gradual and protracted, for the plant material beneath the lump is compacted and bedded parallel to the rounded contours of the bottom of the lump, while the plant material in contact with the sides of the lump shows evidence of shearing.

Marine waters soon retreated. Upon restoration of the normal swamp environment, continued peat deposition covered the foreign marine mud-lumps and enclosed them within the plant debris.

Lithification of the mixed coal balls, just as of normal ones, preceded final compaction and coalification of the peat, as demonstrated by the direction of lamination of the coal in relation to layering in the heterogeneous-mixed coal balls and by the uncompressed condition of material within the coal balls. Concretionary action was probably responsible for calcareous preservation of plant debris and its cementation to the marine core.

While the summary above possibly represents an oversimplification of events, we believe that it best fits the evidence on hand.

In seeking to explain the slender cylindroid forms of some of the Berryville cores, let us consider an analogous modern erosional phenomenon. Along the western shore of Chesapeake Bay in Maryland are steep cliffs of the Miocene Calvert formation, including beds of blue clay. In the area south of Chesapeake Beach, large blocks of the clay occasionally slump into the water. Wave action erodes these blocks into smaller lumps, some of which eventually are thrown onto the

beach. Among these lumps some specimens are worn into long, roughly cylindroidal shapes. One, collected in 1952 by Jack E. Smedley, is a straight rodlike lump, 8 inches long, 1½ inches wide, and ½ inch thick, with an oval cross section; its width and thickness are nearly uniform, and it is abruptly rounded at either end. This rod is similar in shape to the core illustrated in plate 31, figure 1.

Occurrences of similar clay balls and boulders were reported by Grabau (1913, p. 711–712) and by Richter (1926). They reported the boulders to have been formed under water and sometimes to be encrusted with marine shells that became embedded as the balls rolled over shell-containing sands. The "schlickgerolle" observed by Richter on the coast of the North Sea are sometimes cylindroid.

Analogous modern sedimentary material has been reported in several recent papers. Armored mud balls, described from Ventura County, Calif. (Bell, 1940), provide a striking example of the effects of currents in abrading chunks of mud into symmetrical forms; many observed by Bell were nearly spherical in shape. The armor of these balls, although consisting chiefly of pebbles, illustrates the ability of rolling mud masses to accumulate foreign debris through mechanical accretion. An important observation, in regard to the content of the armor, is that "frail gastropod shells were occasionally as perfectly preserved as though they had been packed in cotton" (Bell, 1940, p. 18); this fact may in part explain the undamaged condition of the ostracodes and conodonts found in the mixed coal balls.

A paper by Kindle (1937) contains descriptions of an even more appropriate modern analog of the mixed coal balls. Kindle observed that after the Atlantic coast hurricane of mid-September 1936 "boulderlike masses of tenaceous lagoon clay bound firmly together by salt grass roots were seen widely scattered over the flat surface of a lagoon island" (Kindle, 1937, p. 433) at an inlet a few miles southwest of Atlantic City, N.J. In regard to marine shells in many of the boulders, he stated that "these recent fossils do not represent a veneer of shells attached to the surface by rolling about. They have clearly been entombed in the sediments as they were laid down near the shore of the inlet or bay. From the original bed these mud boulders have apparently been separated by undercutting of currents in lagoon channels and the lifting power of waves."

Perhaps the best documented study of effects of a severe storm on a low-lying coast is that made following hurricane "Audrey," which struck southwestern Louisiana on June 27, 1957 (Morgan, Nichols, and Wright, 1958). Two large arcuate masses of marine mud, each more than 2 miles long and 1,000 feet wide, were driven between 1,100 and 1,250 feet inland. Tidal salt water extended more than 30 miles inland, and some areas were still inundated 3 weeks after the storm struck.

An older analog was described in some detail by Croneis and Grubbs (1939). They reported subspherical calcareous nodules containing assemblages of silicified marine animal fossils in dolomitic beds of Silurian age near Chicago, Illinois; they interpreted these nodules as mechanical accretionary structures formed by the action of storm waves on clastic calcareous muds in relatively shallow sea waters.

Although other descriptions of clastic balls have been published, the foregoing selected examples illustrate the points of emphasis in our interpretation of mixed coal balls. Under certain circumstances, wave or current action does dislodge chunks of plastic sediments, wears and deforms them, and transports them to new environments; it also forms similarly shaped masses through mechanical accretion and transportation. In either instance the remains of organisms may be incorporated within the sediment. It is the shaped chunks of plastic mud that we compare with the Berryville cores.

HOMOGENEOUS-MIXED AND FAUNAL COAL BALLS

The homogeneous-mixed coal balls from Kansas, Oklahoma, and Iowa are of less obvious origin than the Berryville, Ill., specimens because of their less clearly delineated structural features. Nevertheless, we believe that they can be attributed to a series of events and a physical environment similar to that suggested above. Most of the Kansas homogeneous-mixed coal balls, and perhaps all of those from Oklahoma, may best be considered analogous to the core of a Berryville, Ill., specimen. They may represent transported marine mud lumps whose chief difference from the Berryville cores is that they usually are directly enclosed by coal rather than by a layer of petrified plant material. The presence of varied marine faunas within the coal is, of course, the primary evidence of transportation, but the texture of some mixed coal balls is also worth consideration.

The swirled texture of some of the homogeneous-mixed coal balls may be regarded as evidence of prelithification rolling of fossiliferous mud lumps. The swirls are usually irregularly ovoid; they are sometimes vaguely marked and are often accompanied by thin stringers of decomposed plant material which extend for some distance into a nodule. More important, the swirls are primarily effects of animal shell fragments oriented with their flatter surfaces more or less parallel along curved lines (pl. 27, fig. 4). This alinement may

562641 O - 62 - 5

be the result of adhesion of shell fragments to the surface of a rolling mud lump, or may be secondary orientation by pressure on the enclosing matrix. Presence in a few mixed coal balls of two or more distinct sets of swirl markings may indicate adhesion of several originally separate mud lumps that were indurated, after deposition in the swamp, by additional calcium carbonate and pyrite.

Still other homogeneous-mixed coal balls may actually be more closely comparable to the Berryville cores, although not texturally so clearly delineated. Some of these contain pockets of marine fossils, which may lie either well within the coal ball or only along its periphery and which merge vaguely with areas containing only plant material. These pockets suggest an origin similar to that of the Berryville cores: that is, marine mud lumps deposited on the surface of the peat and ultimately incorporated along with some of the peat into the same coal balls. Before lithification, however, partial solution of the calcareous mud lumps may have occurred and permitted some intermingling of the marine animals and the surrounding peat.

Several processes are considered possible for formation of the rare specimens, such as the one from Oskaloosa, Iowa, in which an ostensibly normal coal ball contains a sparse marine fauna with no physical evidence of enclosing marine sediments. A small lump of transported mud may have been dissolved chemically or dispersed by gentle current action after deposition in the coal swamp; such action would have released the enclosed animal remains, which sank into the spongy peat mass and eventually became part of an otherwise normal coal ball, formed through concretionary growth. Another possible explanation is that disintegration of mud lumps during transportation could have released the contained fossils as the waves passed over the coal swamp; again exotic animal remains would have been incorporated in coal balls. A third possibility is that the shells were introduced as clastic particles in a mud slurry. Perhaps some of the animals thus introduced into the coal swamp were actually living at the time of inundation, and were swept along as part of the foreign debris. However, the foraminiferal-incrusted inner surfaces of many of the shells in the Kansas and Illinois coal balls indicate that the animals were dead before deposition in the coal swamp.

Striking evidence of twofold transportation of plant material is found in the Kansas mixed coal balls. Some residues contain abundant tests of serpulopsid foraminifers, a generalized and simple, irregularly tubular adherent type. These tests are commonly adherent on the associated invertebrate shells (pl. 34, fig. 46) but are also found on plant debris (pl. 33, figs. 25–30). They are most common on the large megaspore species *Triletes* cf. *T. superbus*, where they occur on both the outer and inner surfaces of the spore coat (pl. 33, figs. 27–30). That these occurrences are not accidental juxtapositions is shown by the exact conformity of the foraminiferal tests with the spherical contours of the spore surfaces. The foraminiferal encrustation of the terrestrial plant material occurred in a marine habitat, and there seems no alternative to attributing this association to twofold transportation of the encrusted plant fragments.

The above concept actually strengthens rather than weakens the logic of our interpretation, because transportation of land-plant material from near-shore environments to the open sea and its subsequent deposition on the sea bottom among the remains of marine organisms is a well-known phenomenon. White (1911) summarized from the records of the *Blake*, the *Challenger*, and the *Albatross* several accounts of land-plant debris having been dredged from the sea bottom at depths of as much as 2,150 fathoms.

The Monmouth, Kans., occurrence of mixed and faunal coal balls in the Bevier coal is the most difficult phase of this overall problem to interpret, and one which warrants further and more detailed investigation. The large amount of xenoclastic marine animal debris incorporated in the coal there is obviously a reflection of proximity of coal swamp and sea waters. The plant accumulations may even have lain at the actual strand line at the time of deposition, and have thus allowed more abundant introduction of marine muds into the swamp. Possibly the peat deposit was unusually spongy with large and abundant interstices that became filled with mud lumps before the weight of overburden could compress the peat and cause collapse of the interstices. This process could explain the distribution of the faunal coal balls throughout the thickness of the seam. An alternative hypothesis that the coal itself is an allochthonous marine deposit is disproved by the presence of a well-developed stigmarian underclay. There is no obvious explanation of the scarcity of recognizable plant material in the coal balls, but it may be due to the extreme pyritization, which is several times higher in the monmouth coal balls than in those from other localities and which may have obliterated plant structures that were originally present.

Whatever the origin of the faunal coal balls, it is evident that they were brought about by a very localized set of circumstances, for their occurrence in the Bevier coal has not been sufficiently widespread to attract the attention of previous workers. Although 14 mining localities were visited during his investigations,

Hambleton (1953, p. 56) remarked that coal balls occur "only in the Mineral coal" and, furthermore, that nodular pyrite is rare in the Bevier coal.

ALTERNATIVE INTERPRETATIONS

The difficulty of arriving at an interpretation of these mixed coal balls that might be expected to meet with a consensus of approval has been emphasized to us by discussion with several colleagues. Mixed coal balls have been suggested to us to represent filled animal burrows, erratic limestone boulders, or cavities filled by normal sedimentary processes. Although none of these possibilities appeals to us, it seems fitting to discuss each briefly and to present the contradictory evidence.

The animal-burrow hypothesis was suggested chiefly by the appearance of one of the heterogeneous-mixed specimens from Berryville, Ill. This specimen, shown in plate 31, figure 1, contains the most symmetrical marine core found, the core itself being some 16 inches long and 2½ inches in diameter. Its remarkably cylindroid shape is rather atypical of the Berryville cores, but at the same time is somewhat suggestive of an animal burrow. Evidence against such an interpretation follows:

1. The orientation of this particular core is parallel with the primary axis of the containing coal ball and, accordingly, parallel with the bedding of the coal itself. Assuming that such a horizontal burrow was made at a time when marine muds and animal debris were available as a filling substance—after marine encroachment and deposition on the coal swamp surface of marine sediments—complete filling of the burrow would have necessitated horizontal infiltration through a relatively narrow pathway. Moreover, if the overlying sediments were the source of the burrow fillings, the cores and the limestone presumably should have the same texture and fossils. However, the crinoidal fragments in the cores, being relatively well sorted and smaller than those in the overlying limestone, impart a finer texture to the cores. Large spores, which are fairly abundant in the cores, are apparently absent from the overlying limestone.
2. In most of the heterogeneous-mixed coal balls it is impossible to demonstrate sufficient uniformity or symmetry to suggest the origin of the cores as filled burrows. Aside from a few Berryville cores similar to that which suggested filled burrows as a possible interpretation, most of the marine inclusions from that locality are irregularly shaped. Furthermore, animal burrows can scarcely account for the lenticular or irregular shapes of the homogeneous-mixed coal balls from Kansas, or for the unusually large size of some.

The interpretation that mixed coal balls represent indurated erratic boulders analogous to the boulders described by Dix (1942) and Price (1932) from Welsh and American coal beds seems unlikely. If the mixed coal balls represent indurated boulders of fossiliferous limestone that were swept into the coal swamps, it is difficult to explain the lenticular shapes of some specimens. Assuming that the specimens were indurated boulders at the time of introduction into the coal swamp, they would have been resistant to deformation of shape by compaction, and thus must have been lenticular in shape at the time of their deposition, in which case some other physical agency must have shaped them. It seems improbable that they were either torn loose from their source beds as small lenses, or that they were worn into such regular shapes through hydraulic erosion between the times of their derivation and deposition.

Further, in the Berryville mixed coal balls, the contacts between the cores and surrounding normal matrix commonly are sharply definable, but here and there are small areas where the contact is poorly developed and where plant material continuous with that of the normal matrix extends into the core for some distance. The material may be either woody axes that have clearly punctured the core matrix or may be partially decomposed, more or less finely comminuted, plant hash that grades almost imperceptibly into the core. These small areas suggest that at the time of its deposition in the coal swamp, part of the core was sufficiently plastic to allow for some mixture of its substance with the surrounding peat.

The view has been expressed that the mixed and faunal coal balls may be the result of normal sedimentation—that is, that the fossil animals may represent part of the first fauna that entered the drowned coal swamp. Although this view deserves serious consideration, again we regard it as untenable for several reasons:

1. The fossil associations described here and their ecological implications are not normal. Although Pennsylvanian stratigraphy and paleontology, especially of the economically important coal beds, have been studied intensively for over 100 years, to the best of our knowledge no one has previously reported marine invertebrates within the coal seams, except as contained in shale partings. In summarizing contemporary knowledge of American Pennsylvanian sedimentation, Weller (1957, p. 348) noted that "animal fossils, however, are exceedingly rare in coal seams, and those which

do occur almost invariably are preserved in cannel or canneloid layers."

2. Except for channels, "washouts," and rare sedimentary dikes, the upper surface of the coal seam is most commonly a flat surface. Had the upper surface of the coal-forming peat been notably irregular, plugs, sheets, and other irregular bodies of marine sediment should be common in coal seams. If the faunal and mixed coal balls were fillings of surface irregularities through normal sedimentation, they would likely be continuous with the overlying sediments; instead they are discrete bodies buried within the coal and have a vertical distribution throughout the thickness of the seam.
3. The coal on the upper surface of the animal-containing coal balls indicates that peat deposition continued after deposition of the marine inclusions. A permanent marine inundation that would have permitted a marine biota to flourish on the flooded peat surface would have killed the vegetation and stopped peat deposition.
4. In the West Mineral area of Kansas the fauna of the shale above the Fleming coal (Williams, 1937, p. 105) has a different aspect from that of the mixed coal ball fauna, being locally a coquinoid mass of productoid brachiopods.
5. The swirled texture of some of the homogeneous-mixed coal balls, as well as the fragmentary nature of the larger fossils, suggests transportation.

CONCLUSIONS

Studies of animal-containing coal balls suggest four conclusions, enumerated below. Some of these are long-established concepts in coal sedimentology, but they are incorporated here to complete the picture of depositional environments we are attempting to reconstruct. Whether these interpretations meet with general acceptance or not, it is hoped that this report will direct increased attention to the still preplexing problems of the physical and chemical genesis of normal coal balls.

1. Some coal swamps were close to seashores and lay at or very near sea level, separated from the sea by a bar or barrier (White and Thiessen, 1913, p. 54). The coal beds containing mixed or faunal coal balls represent seaward parts of the swamps. The barrier between the sea and the swamp was low enough to be transgressed by unusual wave action.
2. Under episodically unusual circumstances the coal swamps were briefly invaded by sea waters and were contaminated with minor amounts of clastic marine material. Such invasions, although probably of very localized nature, occurred repeatedly in time and space, as shown by the geographic and stratigraphic distributions of mixed coal balls. They also were so brief that peat accumulation was not noticeably interrupted. The presence of mixed coal balls within the seams constitutes the only physical evidence for the marine invasions.
3. The American material described here introduces the probability that not all coal balls were formed under identical circumstances. Stopes and Watson (1908) suggested that coal balls developed by concretionary growth after marine invasion and cessation of peat deposition, the dissolved carbonates in the sea water percolating downward through the uncompressed peat and forming the matrix of coal balls. Since Stopes and Watson found no evidence of transitory marine inundations, their conclusions are sound insofar as their data are concerned.

   On the other hand, transitory marine ingressions could have had various effects on the swamp environment, which in turn may have stimulated concretionary growth of normal coal balls before final marine inundation. Waves and currents powerful enough to transport chunks of marine mud into the coal swamp would also have carried significant amounts of the mud in suspension, as well as carbonates in solution. Assuming that this mud was calcareous, it may have provided chemical material for concretionary calcification of some normal coal balls. The mechanism for reprecipitation of the carbonates remains speculatory at best, but subtle localized variations in pH may explain it as well as the sporadic occurrence of coal balls.
4. Coal balls may be concretionary, clastic, or both. Exclusively plant-containing, concretionary, and most probably autochthonous (normal) coal balls preponderate, but others contain marine animal remains and are interpreted as clastic allochthonous material (homogeneous-mixed and faunal coal balls); still others (heteregeneous-mixed coal balls) combine both types of contents and modes of origin.

REFERENCES CITED

Abernathy, G. E., 1946, Strip-mined areas in the southeastern Kansas coal field: Kansas State Bull. Geol. Survey 64, pt. 4, p. 125–144.

Andrews, Henry N., Jr., 1951, American coal ball floras: The Bot. Rev., v. 17, no. 6, p. 430–468.

Andrews, Henry N., Jr., and Mamay, S. H., 1952, A brief conspectus of American coal ball studies: The Paleobotanist, v. 1, p. 66–72.

Bell, H. S., 1940, Armored mud balls, their origin, properties, and role in sedimentation: Jour. Geology, v. 48, p. 1–31.
Cady, G. H., 1936, The occurrence of coal balls in no. 6 coal bed at Nashville, Illinois: Illinois Acad. Sci. Trans., v. 29, p. 57–158.
Coal Age, 1954, Pittsburg and Midway strips two seams at once: Coal Age, v. 59, no. 11, p. 80–83.
Croneis, Carey, and Grubbs, D. M., 1939, Silurian sea balls: Jour. Geology, v. 47, p. 598–612.
Darrah, W. C., 1939, Discovery and occurrence, pt. 1 of The fossil flora of Iowa coal balls: Harvard Univ. Bot. Mus. Leaflets, v. 7, no. 8, p. 125–136.
Dix, Emily, 1942, Interesting boulders found in and associated with coal seams in the South Wales coal field: South Wales Inst. Eng. Proc., v. 58, no. 2, p. 21–56.
Douville, Henri, 1905, Les "coal balls" du Yorkshire: Soc. géol. France Bull., 4th ser., v. 5, p. 154–157.
Feliciano, Jose Marice, 1924, The relation of concretions to coal seams: Jour. Geology, v. 32, p. 230–239.
Gothan, Walther, 1911, Über ein Vorkommen von tertiären Torfdolomiten: Glückauf, v. 47, pt. 1, p. 228–230.
Grabau, A. W., Principals of stratigraphy: New York, A. G. Seiler and Co.
Hambleton, W. M., 1953, Petrographic study of southeastern Kansas coal: Geol. Survey Kansas Bull. 102, pt. 1, p. 1–76.
Henbest, Lloyd G., 1958, Ecology and life association of fossil algae and Foraminifera in a Pennsylvanian limestone, McAlester, Oklahoma; Contr. Cushman Found. Foraminiferal Research, v. 9, pt. 4, p. 104–111.
Hendricks, T. A., 1937, The McAlester District, Pittsburg, Atoka and Latimer counties: U.S. Geol. Survey Bull. 874–A, p. 1–90.
Høeg, Ove, Bose, M. N., and Manum, Svein, 1955, On double walls in fossil megaspores with description of *Duosporites congoensis* n. gen., n. sp.: Nytt Magasin for Botanikk, v. 4, p. 101–106.
Kindle, E. M., 1934, Concerning "lake balls," "cladophora balls," and "coal balls": Am. Midland Naturalist, v. 15, no. 6, p. 752–760.
——— 1937, Post hurricane sea shore observations: Am. Midland Naturalist, v. 18, no. 3, p. 426–434.
Kubart, Bruno, 1911, Corda's sphaerosiderite aus dem Steinkohlenbecken Radnitz-Braz in Bohmen nebst Bemerkungen über *Chorionopteris gleichenioides* Corda: K.-K. Akad. Wiss. Wien, Math.-phys. Kl. Sitzungsber., v. 70, pt. 1, p. 1035–1048.
Leclercq, Suzanne, 1925, Les coal balls de la couche Bouxharmont des Charbonnages de Werister: Mem. Soc. Géol. Belgique, p. 1–70.
——— 1952, Sur la présence de coal-balls dans la couche petit Buisson (Assise du Flenu) du bassin houiller de la campine: Troisième Heerieen Congress (1951), v. 2, p. 397–400.
Mamay, S. H., 1959, *Litostroma*, a new genus of problematical algae from the Pennsylvanian of Oklahoma: Am. Jour. Botany, v. 46, no. 4, p. 283–292.
Mamay, S. H., and Yochelson, E. L., 1953, Floral-faunal associations in American coal balls: Science, v. 118, no. 3061, p. 240–241.
Miser, H. D., 1954, Geologic map of Oklahoma: U.S. Geol. Survey, scale 1:500,000.
Moore, R. C. and others, 1944, Correlations of Pennsylvanian formations of North America: Geol. Soc. America Bull., v. 55, p. 657–706.
Morgan, J. P., Nichols, L. G., and Wright, Martin, 1958, Morphological effects of Hurricane Audrey on the Louisiana coast: Louisiana State Univ. Coastal Studies Inst. Tech. Rept. 10.
Price, P. H., 1932, Erratic boulders in Sewell coal of West Virginia: Jour. Geology, v. 40, p. 62–73.
Richter, Rudolph, 1926, Flachsee beobachtungen zur Palaontologie und Geologie; XVI, Die Entstehung von Tongerollen und Tongallen unter Wasser: Senckenbergiana, v. 8, p. 305–315.
Roth, E. A., 1956, The anatomy and modes of preservation of genus *Cardiocarpus spinatus* Graham: Kansas Univ. Sci. Bull., v. 37, pt. 1, p. 151–174.
Schopf, J. M., 1941 Contributions to Pennsylvanian Paleobotany. *Mazocarpon ocdipternum*, sp. nov., and Sigillarian relationships: Illinois Geol. Survey Rept. Inv. 75, p. 53.
———1949, Naturally briquetted coal from a bed in western Pennsylvania: Jour. Geology, v. 47, p. 79–82.
Shapiro, Leonard, and Brannock, W. W., 1956, Rapid analysis of silicate rocks: U.S. Geol. Survey Bull. 1036–C, p. 19–56.
Stopes, M. C. and Watson, D. M. S., 1908, On the present distribution and origin of the calcareous concretions in coal seams, known as "coal balls": Royal Soc. [London] Philos. Trans., Bull. 200, p. 167–218.
Teichmüller, M., Teichmüller, R., and Werner, H., 1953, Ein echter Torfdolomit in einem Flöz der mittleren Bochumer Schichten und die Frage nach der Herkunst der Karbonate im Ruhrkarbon: Geol. Jahrb., v. 68, p. 141–154.
Wanless, H. R., 1956, Classification of the Pennsylvanian rocks of Illinois as of 1956: Illinois Geol. Survey Circular 217, 14 p.
Weller, J. M., 1957, Paleoecology of the Pennsylvanian period in Illinois and adjacent states, *in* Harry Ladd, ed., Treatise on marine ecology and paleoecology, v. 2: Geol. Soc. America Mem. 67, p. 325–364.
White, David, 1911, Value of floral evidence in marine strata as indicative of nearness of shores: Geol. Soc. America Bull., v. 22, p. 221–227.
White, David, and Thiessen, Reinhardt, 1913, The origin of coal: U.S. Bur. Mines Bull. 38, 390 p.
Whitehead, W. A., Breger, I. A. and Schopf, J. M., 1952, Discussion *in* Second conference on the origin and constitution of coal: Nova Scotia Dept. Mines Research Found. p. 290.
Williams, James Steele, 1937, Pennsylvanian invertebrate faunas of Southeastern Kansas: Geol. Survey Bull. 24, p. 92–122 [1938].
Zalessky, M. D., and Tchirkova, H. C., 1931, Observations sur la constitution de la substance-mère Charbons du bassin de Kousnetzk: Soc. géol. France Bull., 5th ser., v. 1, p. 589–596.

DETAILS OF SAMPLES AND INSOLUBLE RESIDUES

OSKALOOSA, IOWA

One coal ball (sample E–13) from the Patik mine was available. Parts of this specimen are illustrated on plate 31, figures 2 and 4. It is one of the more significant specimens studied in this research. Casual inspection of its sawn surfaces suggests an apparently normal coal ball with no conspicuous bedding or textural features. However, close examination reveals a few small gastropod shells scattered here and there. The predominantly cordaitean plant contents are very well preserved, even though pyrite is conspicuous in the matrix. The pyrite is partly oxidized, so that its dull luster renders it inconspicuous.

Residues of this sample are high in pyrite content, but abundant organic remains, mainly plant material with many coalified wood fragments and well-preserved pieces of cuticle of several types, were also recovered. The sample also contains the most diverse large-spore assemblage recovered in this study. This includes *Triletes* cf. *T. superbus*, *T. triangulatus* (pl. 33, figs. 21, 22), *T. auritus* var. *grandis*, *Spenceriisporites* sp., *Monoletes ovatus*, and *Cystosporites* sp. Sample E-13 combines the widespread *Spenceriisporites* type of spore with forms of *Triletes* that seem to characterize samples from other distinct areas but which rarely appear together in the same sample.

The fauna consists only of a few conodonts (pl. 34, fig. 45), pyritized ostracodes, and pyritized gastropods, which establish the presence of a marine element in this otherwise normal-appearing coal ball.

McALESTER, OKLA.

Several mixed coal balls from McAlester, Okla., were studied. In a few, the animal remains appeared to be locally concentrated in hazily defined bluish-gray parts of the matrix, which were lighter in color than the remainder and showed faint swirllike markings on sawn surfaces. Otherwise, these coal balls showed no distinctive textural features, and in most there was no obvious segregation of the animal remains.

Animal assemblages from this locality are mostly dominated by well-preserved pyritized ostracodes. Pelecypods and gastropods are fairly common; conodonts, fish remains, and other animal groups are only sparsely represented. The following samples were dissolved:

E-11.—Organic contents of the residue are largely of plant origin. Most of the plant fragments are small, and their parallel ribbing and stomata arranged in rows parallel to the ribs indicates they are coalified cordaitean leaf fragments. Fusinized wood fragments and cuticular remnants are also common, but very few spores were found. Most of the spore material consists of incomplete but uncompressed fragments of the *Triletes auritus* type; one small lageniculate specimen of *Triletes* (cf. *T. rugosus*) was also found.

With the exception of conodonts and fish remains, the animal fossils are all preserved as pyritic replacements. Poorly preserved Ostracodes are most common, small pelecypods are relatively abundant, worm tubes (pl. 34, fig. 46), gastropods, and fish fragments are rare, and one bryozoan was found.

E-22.—This coal ball was similar to E-11, although slightly less pyritized. Almost the same plant material is present in the residue; several specimens of a lageniculate species of *Triletes* (cf. *T. rugosus*) were recovered (pl. 33, figs. 18, 19).

Among the animal remains, ostracodes are again the dominant element, with gastropods (pl. 34, fig. 31) and pelecypods (pl. 34, fig. 27) also common. A few bryozoans, conodonts (pl. 34, figs. 42, 43), scolecodonts (pl. 34, fig. 35), inarticulate brachiopods (pl. 34, figs. 17, 18), and fish fragments (pl. 34, figs. 52-57) were found, along with attached and free-living foraminifers. Some coprolites also occur (pl. 34, figs. 33, 34), as do worm tubes (pl. 34, figs. 38, 46).

E-30.—This small normal coal ball appeared to contain moderately well preserved plant material, but the residue yielded only a few spores, cuticles, and pyrite-filled woody fragments. The spores include a few specimens of *Triletes* cf. *T. rugosus*, two questionable fragments of *T. auritus*, and one specimen of *Monoletes ovatus*.

No animal remains are present in the residue.

E-31.—This is a large irregularly shaped homogeneous-mixed coal ball, a foot long and nearly as broad. Several stringers of coal extend inward 1 to 2 inches from the periphery of the coal ball, whose content appears on sawn surfaces, to be poorly preserved plant material. Bedding was not detected in the specimen.

Animal remains are inconspicuous on sawn surfaces and are not concentrated at any spot. The fauna in the residue is primarily molluskan, with several genera of pelecypods and gastropods, the former being the more abundant (pl. 34, figs. 22, 28). One species of cephalopod also occurs (pl. 34, fig. 29). The remainder of the fauna consists of a few fish fragments, inarticulate brachiopods, foraminifers (pl. 34, figs. 3, 8), some ostracodes, and a relatively large number of worm tubes.

Plant material is represented by many coalified wood fragments and a few cuticular scraps and spores. The latter consist of approximately equal numbers of *Triletes* cf. *T. rugosus* and *T. auritus* var. *grandis*. One specimen of *Cystosporites varius* was also found.

E-16.—Associated with the Secor coal, and presumably above it, is a fossiliferous limestone. A sample was dissolved to ascertain whether any relation exists between the fauna of the mixed coal balls and that of the limestone caprock.

Animal remains in this sample are all pyritized and too poorly preserved for generic or specific identification. The fauna shows less diversity than those of the associated mixed coal balls. It contains a few specimens of three genera of pelecypods, one genus of gastropods, some inarticulate brachiopod fragments, foraminifers, and fish parts.

Plant material consists only of small fragments of fusinized wood and a few resin rodlets.

SOUTHEASTERN KANSAS

WEST MINERAL—PITTSBURGH AND MIDWAY COAL CO. PITS

A large number of homogeneous-mixed coal balls from West Mineral, Kans., were examined. Some show rather well defined swirled textures, particularly the few that contain larger brachiopods. A few others show local concentrations of animals surrounded by fairly pure plant material.

The West Mineral specimens contain more pyrite and other insolubles than those from any other locality, with the exception of the Apex-Compton mine near Monmouth. (See table 2.) However, a few of the West Mineral coal balls approach the latter in degree of pyritization.

Biologically, the West Mineral material is the richest examined thus far, both for variety and size of fossils. It contains *Marginifera* and small specimens of *Derbyia*. Animal remains as large as these have not been found in mixed coal balls from any of the other localities.

Aside from the large brachiopods, most of the faunal contents are small unbroken individuals, either mature or preserved in younger growth stages. A few small (2 mm and less in diameter) brachiopods and pelecypods were found, with ornamentation and delicate spines undamaged.

E-9.—This large coal ball lacks any distinctive textural features and contains relatively few animals, scattered throughout the matrix. Although a few larger brachiopods and 2 cephalopods are evident on the sawn and broken surfaces, the acid residues contain a sparse fauna that consists only of 6 specimens of gastropods, one pelecypod, and several conodonts and poorly preserved ostracodes.

Recovery of plant material was poor, but a fairly large number of uncompressed spores are present in the residues. These contain *Spencerisporites* sp., *Triletes* cf. *T. superbus*, and *T. triangulatus*.

E–10.—This is a small, heavily pyritized coal ball that appears normal except for a few gastropods evident on cut surfaces. The faunal content of acid residues consisted only of four small gastropods. The plant material contains many fusinized wood slivers, a few resin rodlets, and some cuticular material. Numerous spores were recovered, chiefly large specimens that appear to represent spores of *Triletes* cf. *T. superbus* in which the large equatorial frill has been accidentally separated from the spore body; one specimen of *Spencerisporites* sp. was also found.

E–12.—Many animal fragments, including larger brachiopods, are visible on sawn surfaces of this specimen, and are scattered throughout the matrix. Although few of these were recovered in the acid residues, they embrace a variety of zoological groups. Several larger brachiopods and fragments of inarticulate brachiopods, a few pelecypods and gastropods, fish scales and teeth, ostracodes and adherent foraminiferal tests make up the fauna.

A varied spore population dominates the plant material. Most conspicuous are *Triletes* cf. *T. superbus* and *Spencerisporites* sp.; *T. triangulatus*, *Monoletes ovatus*, and *T. auritus* constitute a slightly less conspicuous fraction of the spore assemblage.

E–18.—This specimen was selected as a representative normal coal ball. Careful inspection of its sawn surfaces showed no animal fossils, and their absence was corroborated by the acid residue.

Abundant plant cuticles and spores were recovered. *Triletes* cf. *T. superbus*, so conspicuous in mixed coal ball specimens, is lacking in this sample. However, *T. triangulatus*, *Spencerisporites* sp., and *Monoletes ovatus* are present, and establish a common element with the mixed coal balls.

E–23.—This large unlayered coal ball contained numerous animals, homogeneously scattered among the plant remains throughout the matrix. Faunally, it proved to be one of our richest specimens. Acid residues yielded numerous pelecypods, gastropods, and larger brachiopods (pl. 34, figs. 19, 20), two specimens of cephalopods, rare ostracodes, fish remains, conodonts, one scolecodont, abundant worm castings, a spongelike object, and many adherent foraminiferal tests of the *Serpulopsis* type. The latter are also attached to associated fossils, both plant (pl. 33, figs. 25–30) and animal.

Plant remains in the residue contain abundant fusinized wood fragments, cuticular material, one coalified lycopodiaceous branch tip with intact leaves (pl. 33, fig. 32), intact masses of small spores, resin rodlets, and numerous large uncompressed spores. The latter are dominated by *Triletes* cf. *T. superbus*, which, with its ornate equatorial frill and trilete appendages presents a striking appearance in its fully distended, natural shape (pl. 33, figs. 5–7). Some specimens of this species have pyritic fillings (pl. 33, fig. 9), while the empty interiors of still others indicate the calcitic nature of their former fillings. Many specimens of this species were found with *Serpulopsis* tests adherent, both internally on broken fragments (pl. 33, fig. 28) and externally on intact specimens (pl. 33, figs. 27, 29, 30).

Other spores present in this sample are *T. triangulatus*, *Spencerisporites* sp., and *Monoletes ovatus*.

E–24.—This small coal ball yielded few animal remains with the exception of abundant foraminiferal tests of the *Serpulopsis* type. The few pelecypods recovered are diversified generically. A few spores of *Triletes* cf. *T. superbus* and *T. triangulatus* were recovered; these represent the total of recognizable plant material.

E–14. (*Limestone overlying Mineral Coal*).—Residues of this sample contain, in addition to pyrite, an abundance of small flakes of silty material, which is not present in significant amounts in any of the coal ball specimens.

Recovery of fossils was low. The animals consist mostly of ostracodes and broken undetermined brachiopod spines. Plant material, also scarce, consists of rare cuticle fragments, slivers of fusinized wood, compressed and poorly preserved *Triletes*-type megaspores, and two uncompressed specimens of *Spencerisporites* sp. The latter provide the single common botanical element with the coal ball residues.

MONMOUTH—APEX-COMPTON COAL CO. PITS

The area of the Bevier coal seam now being mined by the Apex-Compton Co. is unusual in that its abundant nodular impurities, which we consider to be coal balls, are extremely pyritic and composed almost exclusively of animal fragments. In the many coal ball samples examined, plant remains are nearly or completely absent, while the closest approaches to normal coal ball samples yielded only fragments of fusinized wood.

Some of the mixed coal balls show homogeneous texture and are heavily pyritized throughout. In others, however, the matrix is differentiated into a fairly distinct central nucleus of nearly pure pyrite in which all fossils have been completely obliterated, surrounded by areas of less complete pyritization in which fossils may be recognized. A few specimens contain roughly concentric zones of varying concentrations of pyrite.

Four samples were dissolved, including one that seemed to be a normal but poor quality coal ball.

E–7.—The specimen is a slightly flattened nodule with adherent coal chips on all surfaces and streaks of coal incorporated within the matrix. It contains a clearly defined, nearly central area of almost solid pyrite that is surrounded by a less heavily pyritized zone in which animal fossils are abundant. A few calcareous crinoid columnals are apparent on sawn surfaces, but most of the animal remains are pyritized brachiopods and gastropods.

The residue is estimated to contain 90 to 95 percent pyrite, most of which consists of finely comminuted animal shell fragments that apparently originated from productoid brachiopods and large bellerophontid gastropods; the pyrite is relatively lustrous and unoxidized. The residue also produced a number of complete small generically diversified gastropods (pl. 34, figs. 25, 26), some poorly preserved ostracodes, foraminiferal tests, conodonts, and fish remains.

Except for very rare and small fusinized wood particles, plant remains are absent from this sample.

E–8.—This specimen is similar to E–7, but less pyritized. The residue consists mostly of small fragments of invertebrate shells. The determinable faunal content is similar to that of E–7, except for the absence of foraminiferal remains.

No plant remains were observed in the residue.

E–20.—This specimen has adherent coal on all surfaces and coaly inclusions within the matrix. Sawn surfaces contain a definite, almost centrally located mass containing well-pre-

served baritic fossils. This area is surrounded by a zone of heavy pyritization in which the animal remains are also pyritized, and there is a clear contact between the two zones. Local areas of the outer zone are so heavily pyritized that the fossils are practically obliterated.

A part of the inner zone was dissolved, and it produced a small amount of residue. The faunal content of the residue contained abundant baritic gastropods (pl. 34, figs. 23, 30), rare baritic pelecypod fragments, a few conodonts, and fish remains.

The plant remains consisted only of small fusinized wood particles and a sparse spore assemblage, which includes *Monoletes ovatus* and *Triletes* cf. *T. auritus*.

E-21.—This is a small ellipsoidal, apparently normal coal ball, with only poorly preserved cordaitean wood fragments apparent on sawn surfaces. Acid solution produced only woody splinters, highly impregnated with pyrite. No spores or animal remains were noted.

FRANKLIN—MACKIE-CLEMENTS FUEL CO. MINE NO. 22

Normal coal balls from this locality cannot be distinguished from those of the Pittsburgh and Midway mine on the basis of plant contents or overall appearances. This fact would seem to lend weight to local miners' opinions that the same coal seam is being mined at the two sites. (See p. 201.)

The mixed coal ball specimens are variable in pyrite content, and the pyrite may be more concentrated in one part of the nodule than another. None, however, are as heavily pyritized as the Monmouth specimens.

The fauna included in the mixed specimens is fairly varied, but apparently dominated by the brachiopod *Mesolobus*, invariably replaced by pyrite. Calcareous crinoid columnals are abundant on sawn surfaces; they occur even in the most heavily pyritized parts of the nodules; these, of course, are lost in the acid treatment. Ostracodes, chonetid brachiopod spines, and worm castings are also common, and there are a few other faunal elements, as noted below.

Plant material is very rare in residues of mixed specimens from this locality.

E-1.—The sample does not appear to be heavily pyritized, nor does it show outstanding textural features. The residue is approximately 90 percent pyrite, but this includes no large masses such as characterize residues of the Monmouth specimens; the pyrite is relatively lustrous.

The larger animal fragments are apparently of *Mesolobus* (pl. 34, fig. 21) and larger productoid origin, while the finer screen sizes of the residue consist of perhaps 50 percent brachiopod spine fragments. In addition to the brachiopods, several crinoid columnals, foraminiferal tests, rare ostracodes (pl. 34, figs. 47, 51), conodonts, and fish fragments were found.

Plant material consists mostly of small fragments of fusinized wood; cuticular material is very rare, and spores were not noted.

E-2.—This sample has a swirled texture and is more pyritized than E-1; recovery of fossils was poor. Pyritization is especially localized in one eccentrically located area. The pyrite constitutes approximately 95 percent of the residue and lacks luster. The most abundant animal fossils recovered were fragments of *Mesolobus*. In addition, a few crinoid columnals, several gastropods, poorly preserved ostracodes, conodonts, and fish remains were noted.

Plant material is rare; it consists largely of small fragments of fusinized wood and a few resin rodlets. No spores or cuticular material were found.

E-17.—This is a normal coal ball, with vague horizontal layering. Parts of the specimen contain large pieces of cordaitean wood, but many well-perserved smaller plant structures are evident on sawn surfaces (principally *Cordaicarpus*, *Stigmaria*, and *Scolecopteris*). However, surprisingly few identifiable fragments survived acid solution. The residue of this sample, which contains very little pyrite, yielded only fusinized wood particles, cuticular fragments, and a few spores, which contain *Spencerisporites* sp., *Monoletes ovatus*, and one tetrad of *Triletes triangulatus*.

No animal remains were found in this sample.

BERRYVILLE, ILL.

Mixed coal balls from this locality are unique in several respects, the most striking of these being the clearly defined cores of marine sediment incorporated within the otherwise normal type of coal ball matrix (pl. 30, fig. 1–3; pl. 31, fig. 1). They are further unique in their high proportion of acid-soluble carbonates. None of the Berryville coal ball samples contained as much as 6 percent insoluble matter, whereas samples from other localities contained from 6.1 to 36 percent.

From the zoological standpoint, Berryville material is distinct in that its fauna is dominated by pyritized bryozoans, a group that is nearly absent from all other samples. Furthermore it contains pyritized trilobite fragments, which are unique in coal balls from this locality. Siliceous foraminiferal tests and crinoid columnals are also much more conspicuous here than elsewhere. The residues also contain coalified wood, cuticles, and many well-preserved spores.

The marine cores of mixed coal balls also seem to be low in pyrite content, and their sawn surfaces show many calcified crinoid remains. The residues contain 50 to 60 percent pyrite, but this is either in the form of a fine powder or animal replacements; it rarely appears in large amorphous masses like those contained in residues from other localities.

In view of the unusual nature of Berryville coal balls, a large suite of samples was dissolved. This suite includes: (a) core material from which all normal matrix had been carefully trimmed; (b) samples of normal matrix surrounding the core; (c) samples of a normal coal ball; (d) samples of limestone incorporated within the coal seam; and (e) samples of the limestone overburden.

E-3.—This specimen was taken from a long cylindroidal core containing several conspicuous calcite-filled shrinkage(?) cracks. Its cut surface showed many crinoid columnals and tubular foraminiferal tests. The residue is small (2.9 percent of the total weight), but contains a varied assemblage. Animals include conodonts, pelecypods, gastropods, rare brachiopods, fish fragments, common foraminiferal tests, a few trilobites, and abundant bryozoans.

Abundant plant material is present, including fusinized wood and cuticular fragments, in addition to a varied spore assemblage. Spores include *Triletes auritus* var. *grandis*, *T. triangulatus*, *T. glabratus*, *Spencerisporites* sp., *Monoletes ovatus* (the most abundant form—see pl. 33, figs. 1, 2), and a few specimens of *Parasporites* cf. *P. maccabei* (pl. 33, figs. 23, 24). Small trilete spores are abundant in the finest residues, but there were not identified.

E–4.—This sample resembles E–3, but its insoluble residue is smaller and contains less pyrite.

The fauna is nearly the same as that of E–3, except that foraminiferal tests are more conspicuous here. A plant assemblage similar to E–3 and differing only in the absence from E–4 of the *Parasporites* is also present.

E–19.—This is a normal coal ball with distinct layering of its abundant and well-preserved plant debris evident on sawn surfaces. It was selected for solution in order to determine (a) whether animal fossils are actually absent, as suggested by inspection of sawn surfaces, and (b) what comparisons could be made between its plant content and that of the marine cores.

Little residue was obtained (4.6 percent), and this contains almost no pyrite. The residue, all of plant origin, has the appearance of a chaffy light- to dark-brown mass of more or less finely divided fragments of cuticles and wood, complete spores, and various other reproductive parts. No animal remains were found. Spores are rare; only a few masses of small triletе spores, two specimens of *Monoletes ovatus*, and one of *Spencerisporites* sp. were found. Surprisingly enough, *Triletes auritus* was not found in this sample.

This residue is, however, of unusual interest in that it contains several uncompressed and otherwise undamaged specimens of a species of small pteridospermous seeds, and numerous scolecopterid fern fructifications. The seeds are hollow as a result of solution of their calcitic fillings, and are represented by a delicate inflated membrane that probably is the inner layer of the testa (endotesta). Cellular outlines may easily be seen with a dissecting microscope. Although the seeds cannot be identified without a knowledge of their inner structural details, overall size and shapes suggest affinity with the genus *Coronostoma* Neeley, which has been described from Berryville coal ball material; at any rate, they are unquestionably conostomalean structures (pl. 33, fig. 31).

The fern fructifications consist of uncompressed synangia that were apparently preserved after maturity and dehiscence (pl. 33, figs. 33–36). The synangia are evidently referable to *Scolecopteris minor*, and contain four or five sporangia each, the sporangia being 1 mm. or less in length. Many of the synangia have their pedicels intact, and a few specimens of fertile pecopterid pinnules have been found. Furthermore, one very delicate circinate pecopterid frond tip with several pinnules attached was found.

Although these recoveries have little bearing on the basic problem under consideration, they demonstrate that studies of coal ball plant fossils based on the peel technique might well be supplemented to great advantage by acid solution in order more accurately to understand the three-dimensional aspects of the plant fossils investigated.

E–25.—The residue of this core sample contains one of the most varied faunas found in this study. Animal remains include trilobite fragments, poorly preserved brachiopods, abundant and diversified gastropods (pl. 34, fig. 32), worm tubes and castings, some pelecypods, conodonts (pl. 34, fig. 36), abundant ostracodes, foraminiferal tests, bryozoans (pl. 34, figs. 11, 13–16), a few fish fragments, and several sponge spicules (pl. 34, figs. 9, 10).

The usual fusinized wood and cuticular fragments also occur, along with well-preserved uncompressed spores, the most abundant form being *Triletes auritus* var. *grandis*. *Monoletes ovatus*, *Spencerisporites* sp., and *Triletes glabratus* complete the spore assemblage.

E–26.—This core was physically similar to E–25. Its fauna differs from the former only in a larger representation of trilobite remains (pl. 34, figs. 39–41), and the spore assemblage contains a higher percentage of *Triletes glabratus* (pl. 34, figs. 3, 4), although *T. auritus* var. *grandis* still dominates (pl. 34, figs. 15–17). Part of this specimen is illustrated on plate 30, figure 2.

E–27.—This coal ball contains a very sharp contact delimiting its cylindroid core, and two samples, one consisting of carefully trimmed core material and the other of the surrounding normal matrix, were dissolved to compare the differences in content between the core and normal matrix surrounding it. Part of this specimen is illustrated on plate 30, figure 3.

The fauna recovered from the residue of the core is typical of the Berryville material, except that neither ostracodes nor conodonts are evident, and a few pyritized crinoid columnals were recovered. Plant material is rare in this sample, the most conspicuous elements being a few specimens each of *Triletes auritus* var. *grandis*, *T. glabratus*, and *Spencerisporites* sp.

The residue of the normal matrix surrounding the core contains no animal remains and little pyrite. It consists only of plant debris, mostly brown and peaty-appearing. The residue contains a few scolecopterid fern synangia, well-preserved cuticles, abundant fusinized wood fragments, and only a few spores, identified as *Triletes triangulatus*, *Spencerisporites* sp., and *Monoletes ovatus*.

E–28.—Two samples of this mixed coal ball were treated as in E–27. The core residue yielded a varied fauna, unusual only in the apparent absence of conodonts. Plant debris is scarce; it consists of the usual cuticles, fusinized wood fragments, and spores, the latter being represented by *Triletes auritus* var. *grandis* (the dominant form), *T. glabratus*, and *Spencerisporites* sp. (pl. 33, figs. 11–14).

Residue of the normal matrix surrounding the core contains no animal remains and almost no pyrite. Cuticles, fusinized wood fragments, and spores are abundant, but *Spencerisporites* sp. is the only spore type recovered from this residue.

E–29.—This core sample yielded a varied fauna, including trilobites, foraminiferal tests (pl. 34 figs. 4, 8), hexactinellid sponge spicules, worm tubes and castings, fish fragments, conodonts (pl. 34, fig. 44), articulate and inarticulate brachiopods, bryozoans, ostracodes (pl. 34, figs. 48–50), and diversified mollusks.

The usual type of plant debris is present in the residue, and it contains one of the most varied and richest spore assemblages found. This assemblage is dominated by *Triletes auritus* var. *grandis*, but it also contains *T. glabratus*, *T.* cf. *T. rugosus*, *T. triangulatus*, *Cystosporites varius*, *Spencerisporites* sp., and *Monoletes ovatus*.

E–6.—This sample of the limestone overlying the coal seam (unit 3 of measured section, p. 198) proved to be nearly pure carbonate, with its insoluble fraction constituting only 0.42 percent of the original weight. Sawn surfaces are similar to those of the cores, being bioclastic crinoidal limestone. However, this rock has a significantly coarser and less well sorted texture, with many of the crinoid stems two to three times as large as those in the cores.

The faunal content of the sample consists only of a few conodonts, fish remains, tubular foraminiferal tests, and one specimen each of a scolecodont, a gastropod, and pelecypod. The gastropod steinkern, though not tested, appeared to be phosphatic. No pyrite is evident in the residue; plant material is absent.

E-5.—A sample of the limestone filling of the presumed channel cut in the coal seam was more fossiliferous than the overlying limestone (E-6); its residue contains a large proportion of pyrite. In texture and faunal content this rock is very similar to the cores.

Animal remains recovered from the residue include abundant bryozoans, relatively few pelecypods, and worm castings, sparse ostracodes, rare gastropods and brachiopods, and some trilobites and conodonts; all but the worm castings and conodonts are pyritized.

Plant material is sparse, with some cuticle and woody material and a few well-preserved spores. The latter include *Triletes auritus* var. *grandis* (the dominant form), *T. glabratus*, *Spencerisporites* sp. and an unknown spore that, except for its large size, is similar to *Lycospora* in form.

E-15.—This is a sample of the impure limestone below the channel as discussed on page 198. This material is illustrated in plate 31, figures 3, 5, and 6.

The acid residues contain no animal remains. The plant debris is mostly small and unrecognizable flakes of incompletely coalified plant material. However, abundant well-preserved cuticular material and uncompressed spores were recovered. The spores include *Triletes auritus* var. *grandis* (the dominant form), *Spencerisporites* sp., *Triletes glabratus*, and one specimen of *Parasporites cf. P. maccabei*.

INDEX

A — Page

Acantbodil ... 209
Acknowledgments ... 194–195
Actinopterygii ... 209; pl. 34
Ammovertella ... 208
inclusa ... 208
labyrintha ... 208
prodigalis ... 208
sp. ... 208; pl. 34
Amphisites centronotus ... 209; pl. 34
sp. ... 209
Analyses ... 206, 207
Animal-burrow hypothesis ... 215
Annelida ... 208
Apex-Compton Coal Co. ... 194, 199, 201, 202, 218, 219
Apterrinella sp. ... 208; pl. 34
Arabellites sp. ... 208; pl. 34
Astartella sp. ... 208
auritus grandis, Triletes ... 209, 212, 218, 221, 222; pl. 33
Triletes ... 209, 218, 219, 220, 221; pl. 31
Aviculopecten sp. ... 208

B

Bairdia ... 209
garrisonensis ... 209
oklahomensis ... 209
pompilioides ... 209
rhomboidalis ... 209
texana ... 209
sp. ... 209; pl. 34
Bairdiocypris sp. ... 209; pl. 34
Ballast, coal balls used for ... 199
bassleri, Gnathodus ... 209; pl. 34
Baxter, Robert W., quoted ... 202
Belgian coal balls ... 193, 202
Bellerophontid ... 208
Berryville, Ill., coal balls ... 197–199, 206, 207, 208, 209, 220–222; pls. 26, 27, 30, 31.
cores ... 204, 205, 206, 207, 211, 212, 213, 214, 215, 220–222; pls. 30, 31
geologic section ... 198
Bevier coal ... 201, 202, 206, 207, 214, 215, 219
Boggy formation ... 197
Bohemian coal balls ... 206
Borestus sp. ... 208; pl. 34
Botryopteris ... 198
Bradydontl ... 209
Breger, I. A., quoted ... 211
Bullmorpha sp. ... 209

C

Calcitornella sp. ... 208
Calhoun coal ... 197, 206, 207
Calvert formation ... 212
Carellina sp. ... 209
Cavusgnathus fleva ... 209
centronotus, Amphisites ... 209; pl. 34
Cherokee shale ... 200, 201
Chonetid ... 208
Chordata ... 209
Cladoldachll ... 209; pl. 34

Coal, Bevier ... 201, 202, 206, 207, 214, 215, 219
Calhoun ... 197, 206, 207
Fleming seam ... 200, 201, 206, 207, 216
McAlester ... 197
Mineral seam ... 200, 201, 215
Secor ... 194, 196, 197, 206, 207, 218
Coal balls, definition ... 195–196
description of samples and insoluble residues ... 217–222
interpretation of animal-containing ... 211–216
nucellar ... 202
occurrences of animal-containing ... 199–202
physical, chemical, and biological features, fennal ... 206, 207; pls. 26, 28, 32
heterogeneous-mixed ... 204–206, 207; pls. 27–29, 31
homogeneous-mixed ... 197, 203–204, 206, 207; pls. 27, 28
normal ... 202–203, 206, 207; pls. 27, 28
Coelenterata ... 208
Compton, H. W., information provided ... 201
Conclusions ... 216
Conodonts ... 209
Corals ... 208; pl. 32
Cordaicarpus ... 220
Cordaitean plant remains ... 202, 217, 220; pls. 28, 29, 31
Cores, marine ... 204, 205, 206, 207, 211, 215, 220, 221, 222; pls. 30, 31.
Cornuspira sp. ... 208
Coronostoma ... 221; pl. 33
Crinoid stems ... 208; pl. 34
Cystosporites varius ... 209, 218, 221; pl. 33
Cystosporites sp. ... 209, 218

D

dattonensis, Kegelliites ... 209
delicatula, Ozarkodina ... 209; pl. 34
Derbyia sp. ... 208, 211, 219; pl. 34
Definition of coal balls ... 195–196
Diplomopyge sp. ... 209, pl. 34
Donaldina sp. ... 209; pl. 34
Duosporites ... 210

E

Echinodermata ... 208
Economic use of coal balls ... 199
elegantulus, Streptognathodus ... 209; pl. 34
Elmore, P. L. D., analyst ... 206
Endolobus sp. ... 209
Endothyra ... 208
Endothyranella poucrel ... 208
sp. ... 208
English coal balls ... 193, 194, 202, 206
Eucochlis sp. ... 208; pl. 34

F

Fabriocypris sp. ... 209
Fenestella sp. ... 208; pl. 34

Fish remains ... 209
Fissispongia sp. ... 208
Fleming coal seam ... 200, 201, 206, 207, 216
fleva, Cavusgnathus ... 209
Flora, in normal coal balls ... 202
Fossils, distribution ... 208–209
Fossils, preservation ... 210–211
Frank, Mona, analyst ... 206
Franklin, Kans., coal balls ... 201, 220
Fusulinids ... 208; pl. 34

G

Garrett Coal Co. ... 202
garrisonensis, Bairdia ... 209
Geologic section, Berryville, Ill. ... 198
German coal balls ... 206
Girtyspira sp. ... 209
glabratus, Triletes ... 209, 212, 221, 222; pl. 33
Glabrocingulum sp. ... 208
Globivalvulina sp. ... 208; pl. 34
Glomospira sp. ... 208
Glyptopleura sp. ... 209; pl. 34
Gnathodus bassleri ... 209; pl. 34
roundyi ... 209
sp. ... 209
grandis, Triletes auritus ... 209, 212, 218, 221, 222; pl. 33

H

Healdia sp. ... 209
Hexactinellid spicule ... 208
Hindeodella sp. ... 209; pl. 34
Hollinella sp. ... 209; pl. 34
Hurricane effects ... 213

I

Idiognathodus magnificus ... 209; pl. 34
inclusa, Ammovertella ... 208
Indurated erratic-boulder hypothesis ... 215
insita, Serpulopsis ... 208
Interpretation of animal-containing coal balls ... 211–216

K

Kansas, southeastern, animal-containing coal balls ... 197, 199–202, 218–220
Kegelliites dattonensis ... 209
Kellettina sp. ... 209
Kirkbya sp. ... 209
Knightina sp. ... 209
Knightites (Retispira) sp. ... 208; pl. 34
knoxense, Pseudorthocrras ... 209; pl. 34
Kousnetzk basin, Russia ... 206
Krebs group, Boggy formation ... 197

L

Laboratory methods ... 207–210
labyrintha, Ammovertella ... 208
Leiopteria sp. ... 208
Linguloid ... 208
Lillostroma ... 194
Lophophyllid coral ... 208
Lycospora ... 209

M — Page

McAlester, Okla., coal balls 196–197, 206, 207, 218
McAlester coal 197
McAlester shale 197
maccabei, Parasporites 209, 221, 222; pl. 33
Mackie-Clemens Mines 201, 220
McLeansboro group, Calhoun coal 197
magnificus, Idiognathodus 209; pl. 34
Marginifera sp. 208, 219; pl. 34
Marine cores 204, 205, 206, 207, 215, 220, 221, 222; pls. 30, 31.
Meekospira sp. 209
Mesolobus sp. 208, 220; pl. 34
Microdoma sp. 208
Mineral coal seam 200, 201, 215
minor, Scolecopteris 221; pl. 33
minutus, Spathognathodus 209; pl. 34
Monmouth, Kans., coal balls 201–202, 206, 207, 219–220
Monoceratina sp. 209
Monoletes ovatus 209, 212, 218, 219, 220, 221; pl. 33
Moorecerras sp. 209
Mud balls, armored, California 213
Myelid 208

N

Naticopsis sp. 209
Neilsonia sp. 208
Neopriolobus sp. 209
Normal sedimentation hypothesis 215–216
Nuculana sp. 208
Nuculoid 208

O

oklahomensis, Bairdia 209
Orbiculoid 208
Oskaloosa, Iowa, animal-containing coal balls 197, 217–218
ovatus, Monoletes 209, 212, 218, 219, 220, 221; pl. 33
Ozarkodina delicatula 209; pl. 34
sp. 209

P

Paleostylus (Pseudozygopleura) sp. 209
Paralleiodon sp. 208; pl. 34
Paraporchites sp. 209
Parasporites 209, 221, 222; pl. 33
maccabei 209, 221, 222; pl. 33
Patik mine, Iowa 196, 217
pauperata, Tetrataxis 208; pl. 34
Pectinoid 208
Pennireticpora sp. 208
Permophorus sp. 208; pl. 34
Pittsburg and Midway Coal Co. 194, 199, 200, 201, 218, 220
Pleurocantholidti 208
Pleurotomarian 208
Polypora sp. 208
pompilioides, Bairdia 209
Porifera 208
powersi, Endothyranella 208
Preservation of the fossils 210–211
Previous work 194
prodigalis, Ammovertella 208
Productoid 208
Psaronius 198, 202
Pseudorthoceras knoxense 209; pl. 34
(*Pseudozygopleura*) sp., *Paleostylus* 209

R

Ramiporalia sp. 208
rectangularis, Thurammina 208
References cited 216–217
(*Retispira*) sp., *Knightites* 208
Rhabdomeson sp. 208
Rhipidomella sp. 208
Rhombocladia sp. 209
rhomboidalis, Bairdia 209
Rhombopora sp. 208; pl. 34
Road ballast 199
Roundya 209
subacoda 209
roundyi, Gnathodus 209
rugosus, Triletes 209, 218, 221; pl. 33
Ruhr area, Germany, coal balls 206
Russian coal balls 206

S

Samples, description 217–222
Sansabella sp. 209
Schizodus sp. 208
Schliekgerolle 213
Schopf, J. M., quoted 211
Scolecopteris 220, 221; pl. 33
minor 221; pl. 33
Scott, Paul W., analyst 207
Seam coal 194, 196, 197, 206, 207, 218
Sciagincilites pl. 33
Septimyatina sp. 208; pl. 34
Septopora sp. 208
Serpulopsis 208, 214, 219
bulla 208
sp. 208; pl. 33
Shansiella, steinkern 208
sp. 208; pl. 34
Solachi 209
Spathognathodus minutus 209; pl. 34
Spectroscopic analysis 206
Spencerisporites sp. 206, 218, 219, 220, 221, 222; pl. 33
Spicule, hexactinellid 208
Spirorbis sp. 208; pl. 34
Spore, resembling *Lycospora* 209
Steinkern *Donaldina* sp. 209
Shansiella 208
Stigmaria 220; pl. 27
Stratigraphic relations, coal balls at West Mineral, Kans. 200–201
Streptognathodus elegantulus 209; pl. 34
subacoda, Roundya 209
Subulitid 209; pl. 34
superbus, Triletes 209, 210, 214, 218, 219; pl. 33

T

Tetrataxis pauperata 208; pl. 34
texana, Bairdia 209
Thurammina 208, 210
rectangularis 208
sp. 208; pl. 34
Thurammimoides sp. 208
Trepostomatous bryozoans 208
triangulatus, Triletes 209, 218, 219, 220, 221; pl. 33
Triletes 209, 210, 214, 218, 219, 220, 221, 222; pls. 31, 33.
auritus 209, 218, 219, 220, 221; pl. 31
grandis 209, 212, 218, 221, 222; pl. 33
glabratus 209, 212, 221, 222; pl. 33
rugosus 209, 218, 221; pl. 33
superbus 209, 210, 214, 218, 219; pl. 33
triangulatus 209, 218, 219, 220, 221; pl. 33
sp. 209

V

varius, Cystosporites 209, 218, 221; pl. 33

W

Welsh coal beds 215
West Mineral, Kans., coal balls 199–201, 206, 207, 218, 219; pls. 27, 28, 29.
Whitehead, W. L., quoted 211

Y

Yorkshire, England, coal balls 194

PLATES 26–34

PLATE 26

FIGURE 1. Closeup of channeling in coal bed at Berryville, Ill. Several coal balls may be seen to the right of and below the hammer.

2. A large coal ball mass overlying 4 inches of coal at Berryville, Ill. Part of this mass may be seen in the lower left corner of figure 3.

3. General view of the Berryville, Ill., locality. The channel and swelling of the overlying limestone is shown at left center of photograph, above stream level. Section was measured along trench at right of photograph.

4. A part of one of the piles of coal balls near the tipple of the Pittsburg and Midway Coal Co., West Mineral, Kans.

5. View of Bevier coal in Apex-Compton Coal Co. strip pit near Monmouth, Kans., showing two faunal coal balls in place, (at arrows), overlain by more than an inch of coal. Irregularly shaped coal ball directly above light meter, with tabular specimen to left. Flat specimen also shown in figure 6; sawn surfaces of both specimens shown in plate 32. Photograph by R. W. Baxter, University of Kansas.

6. View of Bevier coal taken a few minutes prior to figure 5, showing the flat faunal coal ball when first exposed. Arrow to left of light meter points to upper surface of coal seam; tabular coal ball below and to right of arrow. Photograph by R. W. Baxter, University of Kansas.

1

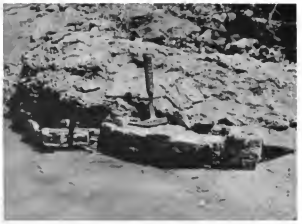

2

3

4

5

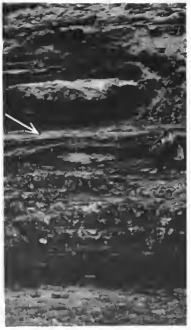

6

VIEWS AT THE BERRYVILLE, ILLINOIS, WEST MINERAL, KANSAS, AND MONMOUTH, KANSAS, COAL BALL LOCALITIES

PLATE 27

[Photographs natural size unless otherwise shown]

FIGURE 1. Sawn surface of a normal coal ball from Berryville, Ill., showing layered appearance of plant debris, primarily fern roots. Specimen 9190–31C.

2. Enlargement of part of specimen illustrated in figure 3, showing cross section of high-spired gastropod. × 3.

3. Sawn surface of small homogeneous-mixed coal ball from West Mineral, Kans., containing primarily plant debris, with gastropods scattered at random through the ball. Enlarged area indicated by arrow. Specimen 9189–123A.

4. Sawn surface of homogeneous-mixed coal ball from West Mineral, Kans., showing well-defined swirled texture and, locally, alinement of shell fragments parallel to swirls. The fossils are predominantly animal, but a large stigmarian stele is shown at left center of photograph. Specimen 9189–121C.

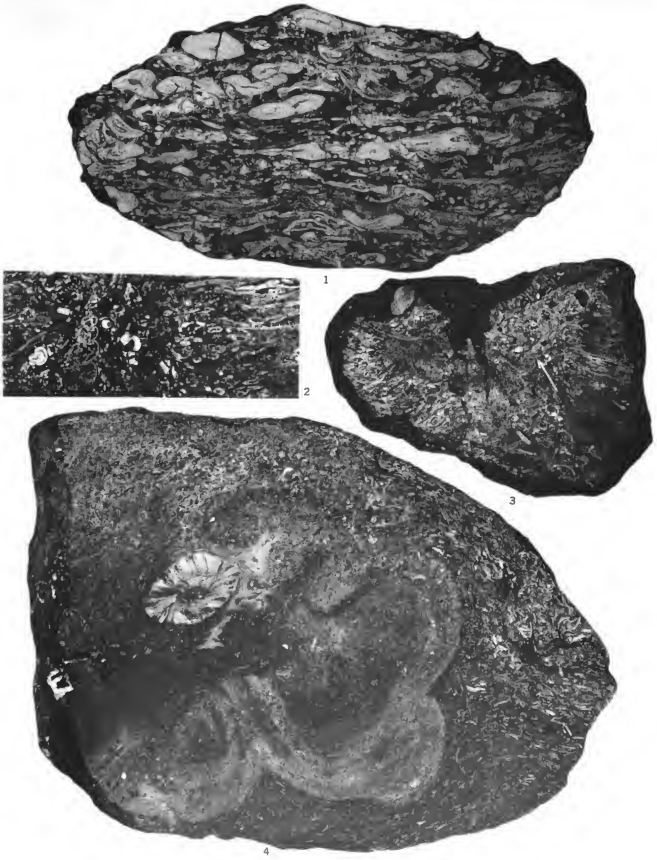

NORMAL AND MIXED COAL BALLS FROM ILLINOIS AND KANSAS

PLATE 28

[Photographs natural size]

FIGURE 1. Sawn surface of faunal coal ball from near Monmouth, Kans., showing lenticular shape and abundant pyritized animal debris. Specimen 9487-1A.

2. Sawn surface of normal coal ball from West Mineral, Kans., showing lenticular shape. Plant debris consists predominately of cordaitean leaves, stems, and fructifications. Specimen 9189-80D.

3. Sawn surface of homogeneous-mixed coal ball from West Mineral, Kans. Organic content predominately plant debris that includes well-preserved cordaitean organs. Some marine gastropod shells indicated by arrows. Specimen 9189-120C.

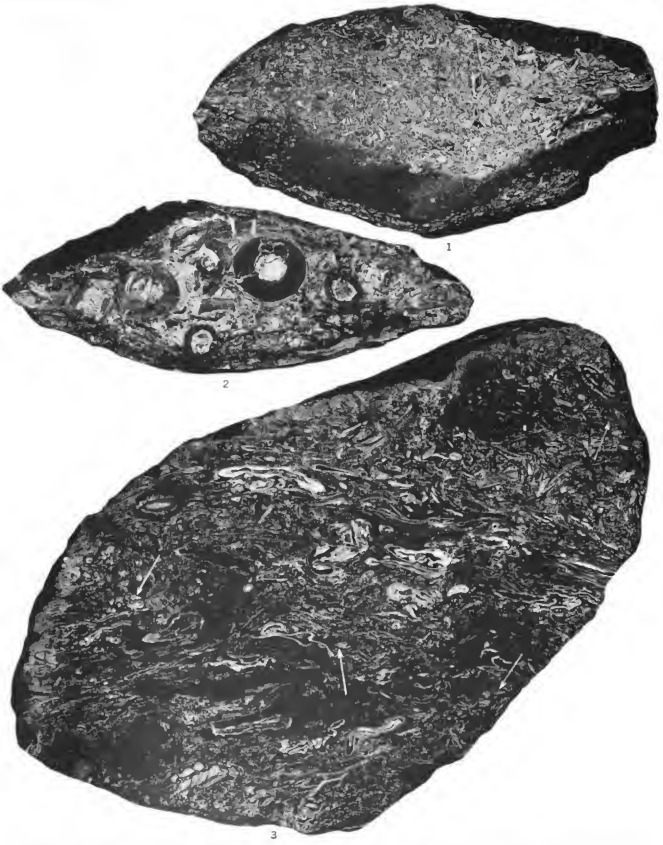

FAUNAL, MIXED, AND NORMAL COAL BALLS FROM WEST MINERAL AND MONMOUTH, KANSAS

PLATE 29

[Photographs natural size unless otherwise shown]

FIGURE 1. Sawn surface of homogeneous-mixed coal ball from West Mineral, Kans.; coal ball composed predominately of plant material that includes well-preserved cordaitean seeds. Orthoceroid cephalopod and gastropods indicated by arrows. Specimen 9189–122A.

2. Enlargement of part of specimen illustrated in figure 3, showing associated plant and animal remains. Cross section of a gastropod shell and a pteridophyllous pinnule indicated by arrows. × 4.

3. Sawn surface of a homogeneous-mixed coal ball from West Mineral, Kans., showing mixture of plants and animal remains. Specimen 9189–124C.

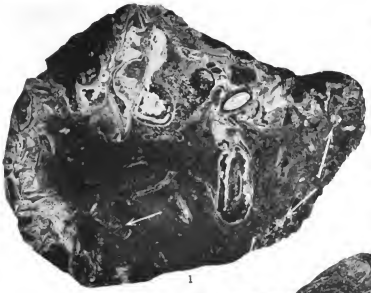

1

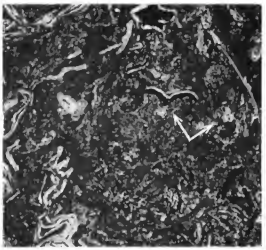

2

3

HOMOGENEOUS-MIXED COAL BALLS FROM WEST MINERAL, KANSAS

PLATE 30

[Photographs natural size]

FIGURE 1. Sawn surface of a heterogeneous-mixed coal ball from Berryville, Ill., showing stratification of marine fossil fragments within the large marine core. A small normal coal ball lies to the right of the photograph. The layering of plant debris in the normal coal ball and the normal part of the mixed coal ball are approximately at right angles to one another. Specimen 9190–1E.

2. Sawn surface of a heterogeneous-mixed coal ball from Berryville, Ill. The layering of the normal part is at right angles to the bottom of the plate. Specimen 9190–13E. Part of this specimen was dissolved as sample E–26.

3. Sawn surface of a heterogeneous-mixed coal ball from Berryville, Ill., showing an irregular marine core. The black line above the core is a coal film. Specimen 9190–17D. Part of this specimen was dissolved as sample E–27.

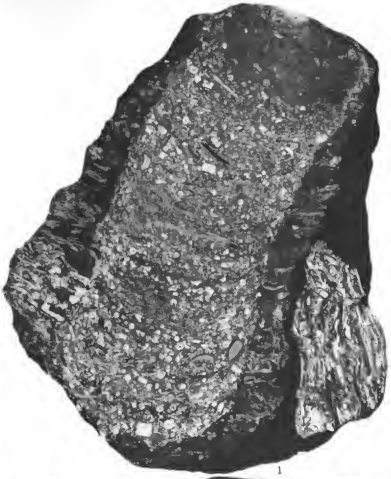

1

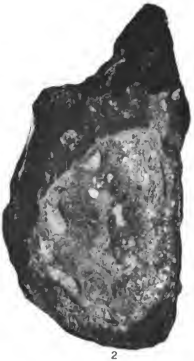

2

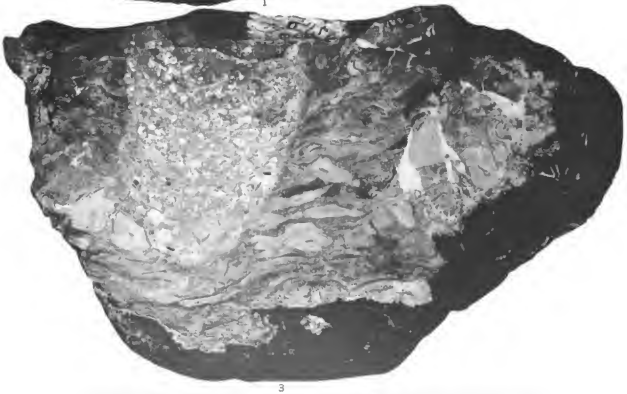

3

HETEROGENEOUS-MIXED COAL BALLS FROM BERRYVILLE, ILLINOIS

PLATE 31

[Photographs natural size unless otherwise shown]

FIGURE 1. Sawn surface of heterogeneous-mixed coal ball from Berryville, Ill., showing discrete nature of core of marine material with abundant animal debris, and complete enclosure of core within normal coal ball material. Specimen 9190–2F.

2. Broken surface of a homogeneous-mixed coal ball from Oskaloosa, Iowa, showing well-preserved plant debris. Cordaitean axis at upper left; gastropod shell indicated by arrow. Specimen 1002B. × 3. Part of this coal ball was dissolved as sample E–13.

3. Piece of limestone from Berryville, Ill., composed of coal-ball-like particles. The dark bands are streaks of coal. Specimen 9190–57. Part of this specimen was dissolved as sample E–15.

4. Part of sawn surface of homogeneous-mixed coal ball from Oskaloosa, Iowa. Several gastropods indicated by arrows. Part of this specimen illustrated in figure 2.

5. Photomicrograph of thin section cut from specimen shown in figure 3. Irregular angular and rounded particles of calcareous coal-ball-like material are tightly packed and interpenetrating. Traces of original plant tissue are still visible within the replacing calcite. Sections of two uncompressed megaspores, probably *Triletes aurilus*, are shown at right. × 10.

6. Same as figure 5, taken between crossed nicols. Calcite replacement shows up as fibrous, radially arranged crystals that superficially resemble spheralites.

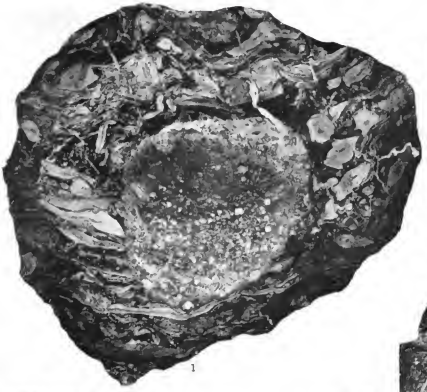

1

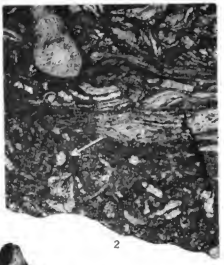

2

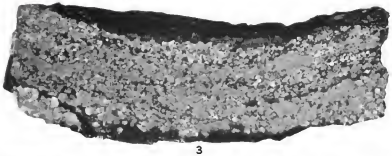

3

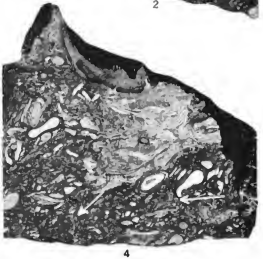

4

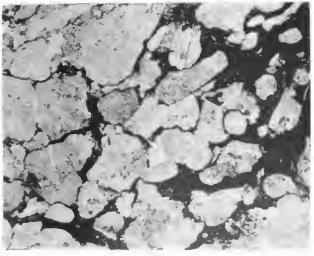

5

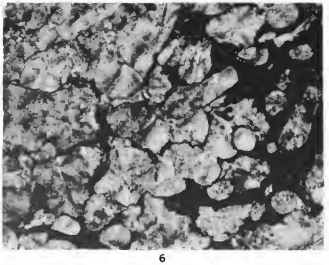

6

MIXED COAL BALLS FROM ILLINOIS AND IOWA, AND LIMESTONE FROM ILLINOIS

PLATE 32

[Photographs natural size]

FIGURE 1. Part of sawn surface of faunal coal ball from the Bevier coal, near Monmouth, Kans., shown in place in figures 5 and 6 of plate 26. Animal fossils exposed include sections of brachiopods and of gastropods and of a coral. Note adherent coal on upper and lower surfaces, and included coaly stringers. Specimen shown in original attitude. Specimen 9487–2E.

2. Remainder of same specimen shown in figure 1, the two pictures overlapping slightly. Black particles in left center are fusinized wood.

3. Sawn surface of faunal ball from the Bevier coal, near Monmouth, Kans., shown in place to right in pl. 26, fig. 5. The specimen is almost completely replaced by pyrite, but scattered shell fragments are visible. Specimen shown in original attitude. Specimen 9487–3A.

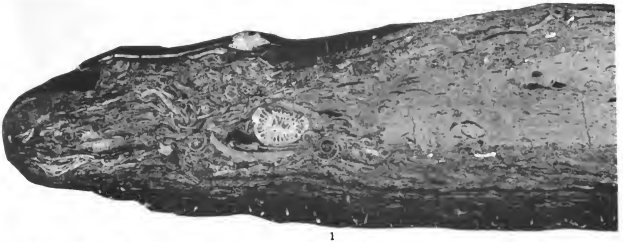

1

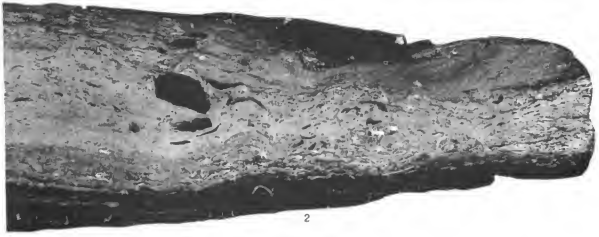

2

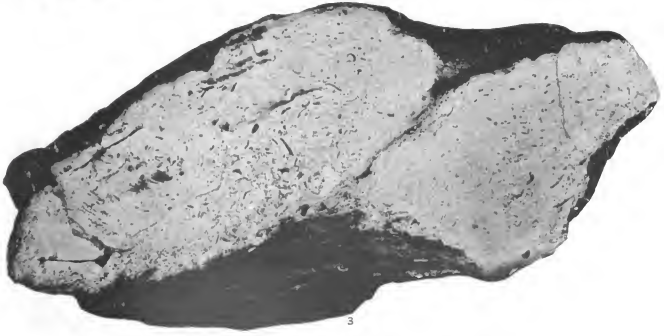

3

FAUNAL COAL BALLS FROM MONMOUTH, KANSAS

PLATE 33

[All photographs made with reflected light except as indicated]

FIGURES 1–24. Spores, mostly uncompressed, and spore contents from mixed coal ball residues.

1, 2. *Monoletes ovatus* Schopf.
Proximal and distal surfaces, × 45; from residue E–3 (marine core of heterogeneous-mixed coal ball, Berryville, Ill.); USNM 41177 (fig. 1), 41178 (fig. 2).

3, 4. *Triletes glabratus* Zerndt.
Proximal and distal surfaces, × 10; from residue E–26 (marine core of heterogeneous-mixed coal ball, Berryville, Ill.); USNM 41179 (fig. 3), 41180 (fig. 4).

5–10. *Triletes* cf. *T. superbus* Bartlett.
All specimens from residue E–23 (homogeneous-mixed coal ball, West Mineral, Kans.).
5. Proximal surface of specimen denuded of equatorial frill, × 15, USNM 41181; 6, proximal surface of nearly complete specimen, × 15, USNM 41182; 7, distal surface, × 15, USNM 41183; 8, calcareous filling of spore cavity, proximal surface, × 15, USNM 41184; 9, pyritic filling of spore cavity, proximal surface, × 15, USNM 41185; 10, fragment of proximal part of endosporal membrane dissected from spore, showing numerous round dark bodies, possibly megagametophytic remains, transmitted light, × 100; USNM 41186.

11–14. *Spencerisporites* sp.
All specimens from residue E–28 (marine core of heterogeneous-mixed coal ball, Berryville, Ill.).
11. Proximal surface, × 75, USNM 41187; 12, distal surface, × 75, USNM 41188; 13, specimen photographed with transmitted light from proximal side, × 70, USNM 41189; 14, specimen photographed with transmitted light from distal side, × 70, USNM 41190.

15–17. *Triletes auritus* var. *grandis* Zerndt.
All specimens from residue E–26 (marine core of heterogeneous-mixed coal ball, Berryville, Ill.).
15. Proximal surface, × 20, USNM 41191; 16, distal surface, × 20, USNM 41192; 17, lateral view of specimen broken along two rays of trilete suture, showing hollow nature of uncompressed spore, thick exospore, and thin endospore, somewhat separated from exospore, × 20, USNM 41193.

18–19. *Triletes* cf. *T. rugosus* (Loose) Schopf.
Both specimens from residue E–22 (homogeneous-mixed coal ball, McAlester, Okla.).
18. Lateral view of partly split but uncompressed specimen, × 30, USNM 41194; 19, lateral view of compressed specimen with segments of apical vestibule separated from each other, USNM 41195.

20. *Cystosporites varius* (Wicher) Dijkstra, × 20.
Apical view of abortive specimen showing spongy pyramidal structure at apex of spore. From residue E–31 (homogeneous-mixed coal ball, McAlester, Okla.), USNM 41196.

21–22. *Triletes triangulatus* Zerndt.
Both specimens from residue E–13 (homogeneous-mixed coal ball, Oskaloosa, Iowa).
21. Lateral-distal view, × 45, USNM 41197; 22, proximal surface, × 45, USNM 41198.

23–24. *Paraasporites* cf. *P. matabei* Schopf.
Both specimens from residue E–3 (marine core of heterogeneous-mixed coal ball, Berryville, Ill.).
23. Distal surface, × 45, USNM 41199; 24, proximal surface, × 45, USNM 41200.

25–36. Uncompressed plant parts and foraminifer-encrusted plant material from coal ball residues.

25–26. Fragments of fusinized wood, with adherent tests of *Serpulopsis* sp., × 25.
From residue E–23 (homogeneous-mixed coal ball, West Mineral, Kans.), USNM 41201 (fig. 25), 41202 (fig. 26).

27. Denuded specimen of *Triletes* cf. *T. superbus*, with adherent test of *Serpulopsis* sp., × 10.
From residue E–23 (homogeneous-mixed coal ball, West Mineral, Kans.); USNM 41203.

28. Fragment of specimen of *Triletes* cf. *T. superbus*, with test of *Serpulopsis* sp. adherent to inner surface, × 25.
From residue E–23 (homogeneous-mixed coal ball, West Mineral, Kans.); USNM 41204.

29. Oblique-lateral view of specimen of *Triletes* cf. *T. superbus*, with test of *Serpulopsis* sp. adherent to median ray of trilete appendage, × 10.
From residue E–23 (homogeneous-mixed coal ball, West Mineral, Kans.); USNM 41205.

30. Oblique-lateral view of specimen of *Triletes* cf. *T. superbus*, with two adherent tests of *Serpulopsis* sp., × 10.
From residue E–23 (homogeneous-mixed coal ball, West Mineral, Kans.); USNM 41206.

30a. Same spore, enlarged to × 25, showing conformity between *Serpulopsis* test and sinuosity of right-hand ray of trilete appendage of spore.

31. Uncompressed conostomalean seed (cf. *Coronostoma* Neeley), × 15.
From residue E–19 (normal coal ball, Berryville, Ill.); USNM 41207.

32. Uncompressed fusinized lycopod branchlet with attached leaves (cf. *Selaginellites*), × 15.
From residue E–23 (homogeneous-mixed coal ball, West Mineral, Kans.); USNM 41208.

33. Apical view of uncompressed fusinized scolecopterid fern synangium (cf. *Scolecopteris minor* Hoskins), × 30.
Tips of sporangia are broken away, showing hollow sporangial cavities. From residue E–19 (normal coal ball, Berryville, Ill.); USNM 41209.

34. Fusinized fragment of uncompressed fern pinnule, bearing scolecopterid synangium at right, × 30.
From residue E–19 (normal coal ball, Berryville, Ill.); USNM 41210.

35. Lateral view of uncompressed fusinized scolecopterid fern synangium, × 30.
From residue E–19 (normal coal ball, Berryville, Ill.); USNM 41211.

36. Apical view of uncompressed fusinized scolecopterid synangium composed of four sporangia, × 30.
From residue E–19 (normal coal ball, Berryville, Ill.); USNM 41212.

Digitized by Google

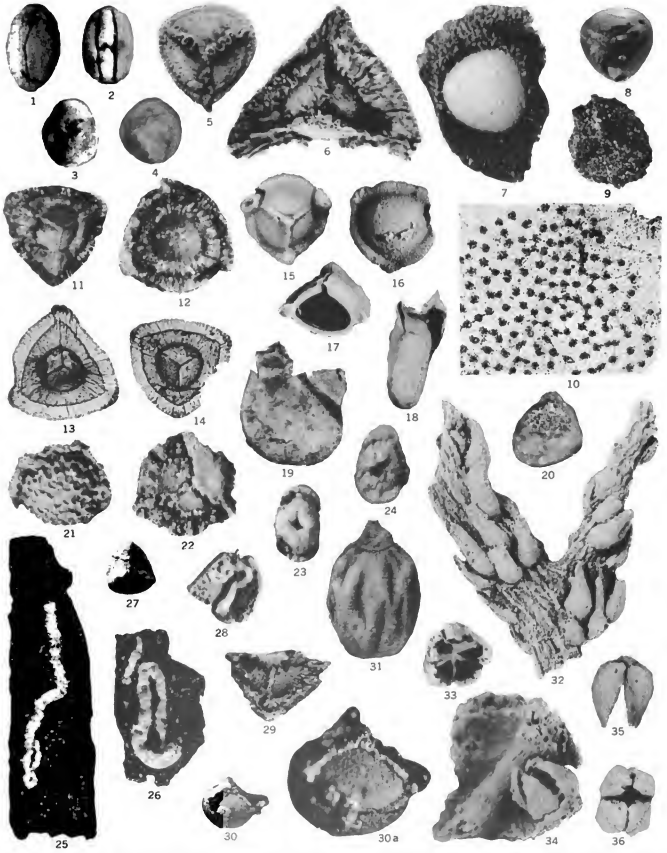

REPRESENTATIVE SPORES AND OTHER PLANT REMAINS RECOVERED FROM INSOLUBLE RESIDUES

PLATE 34

[Explanation of figures 36–57 follow plate 34]

FIGURE 1, 2. *Tetrataxis pauperata*? (Warthin), × 25.
From residue E–7, (faunal coal ball, Monmouth, Kans.); USNM 628518a,b.

3. *Globivalvulina* sp., × 25.
From residue E–31 (homogeneous-mixed coal ball, McAlester, Okla.); USNM 628519.

4. *Apterrinella* sp., pyritic cast of undivided, tubular chamber, × 25.
From residue E–29 (heterogeneous-mixed coal ball, Berryville, Ill.); USNM 628520a.

5. *Thurammina* sp., × 25.
From residue E–27 (heterogeneous-mixed coal ball, Berryville, Ill.); USNM 628521.

6. *Ammovertella* sp., × 50.
From residue E–28 (heterogeneous-mixed coal ball, Berryville, Ill.); USNM 628522.

7. Fusulinid indet., × 25.
From residue E–31 (homogeneous-mixed coal ball, McAlester, Okla.); USNM 138848.

8. *Apterrinella* sp., with adherent sponge spicule near left end of tube, × 25.
From residue E–29 (heterogeneous-mixed coal ball, Berryville, Ill.); USNM 628520b.

9, 10. Hexactinellid sponge spicules, × 30.
From residue E–25 (heterogeneous-mixed coal ball, Berryville, Ill.); USNM 138849a, 138849b.

11. *Pennriretepora* sp., × 8.
From residue E–25 (heterogeneous-mixed coal ball, Berryville, Ill.); USNM 138850.

12. Crinoid columnal incrusted by foraminifer, × 10.
From residue E–7 (faunal coal ball, Monmouth, Kans.); USNM 138851.

13. *Rhombopora* sp., × 10.
From residue E–25 (heterogeneous-mixed coal ball, Berryville, Ill.); USNM 138852.

14. *Polypora* sp., × 4.
From residue E–25 (heterogeneous-mixed coal ball, Berryville, Ill.); USNM 138853.

15, 16. *Fenestella* sp., × 10.
From residue E–25 (heterogeneous-mixed coal ball, Berryville, Ill.); USNM 138854a, b.

17. Linguloid brachiopod, × 20.
From residue E–22 (homogeneous-mixed coal ball, McAlester, Okla.); USNM 138855.

18. Orbiculoid brachiopod, × 10.
From residue E–22 (homogeneous-mixed coal ball, McAlester, Okla.); USNM 138856.

19. *Derbyia* sp., × 2.
From residue E–23 (homogeneous-mixed coal ball, West Mineral, Kans.); USNM 138857.

20. *Marginifera* sp., × 2.
From residue E–23 (homogeneous-mixed coal ball, West Mineral, Kans.); USNM 138858.

21. *Mesolobus* sp., exterior, × 8.
From residue E–1 (homogeneous-mixed coal ball, Franklin, Kans.); USNM 138859.

22. *Septimyalina* sp., interior, × 10.
From residue E–31 (homogeneous-mixed coal ball, McAlester, Okla.); USNM 138860.

23. *Knightites* (*Reticspira*) sp. × 5.
From residue E–20 (homogeneous-mixed coal ball, Monmouth, Kans.); USNM 138861.

24. *Eucoelia* sp., × 20.
From residue E–28 (heterogeneous-mixed coal ball, Berryville, Ill.); USNM 138862.

25. *Paleostylus* (*Pseudozygopleura*) sp., × 12.
From residue E–7 (faunal coal ball, Monmouth, Kans.); USNM 138863.

26. *Shansiella* sp., × 20.
From residue E–7 (faunal coal ball, Monmouth, Kans.); USNM 138864.

27. *Parallelodon* sp., × 15.
From residue E–22 (homogeneous-mixed coal ball, McAlester, Okla.); USNM 138865.

28. *Permophorus* sp., × 10.
From residue E–31 (homogeneous-mixed coal ball, McAlester, Okla.); USNM 138866.

29. *Pseudorthoceras knoxense* (McChesney), × 4.
From residue E–31 (homogeneous-mixed coal ball, McAlester, Okla.), USNM 138867.

30. *Borestus* sp., × 3.
From residue E–20 (homogeneous-mixed coal ball, Monmouth, Kans.); USNM 138868.

31. Subulitid indet., slightly oblique, apertural view. × 15.
From residue E–22 (homogeneous-mixed coal ball, McAlester, Okla.); USNM 138869.

32. *Donaldina* sp., × 8.
From residue E–25 (heterogeneous-mixed coal ball, Berryville, Ill.; USNM 138870.

33, 34. Coprolitic pellets of unknown organism, × 20.
From residue E–22 (homogeneous-mixed coal ball, McAlester, Okla.); USNM 138821a, b.

35. *Arabellites* sp., × 20.
From residue E–22 (homogeneous-mixed coal ball, McAlester, Okla.); USNM 138872.

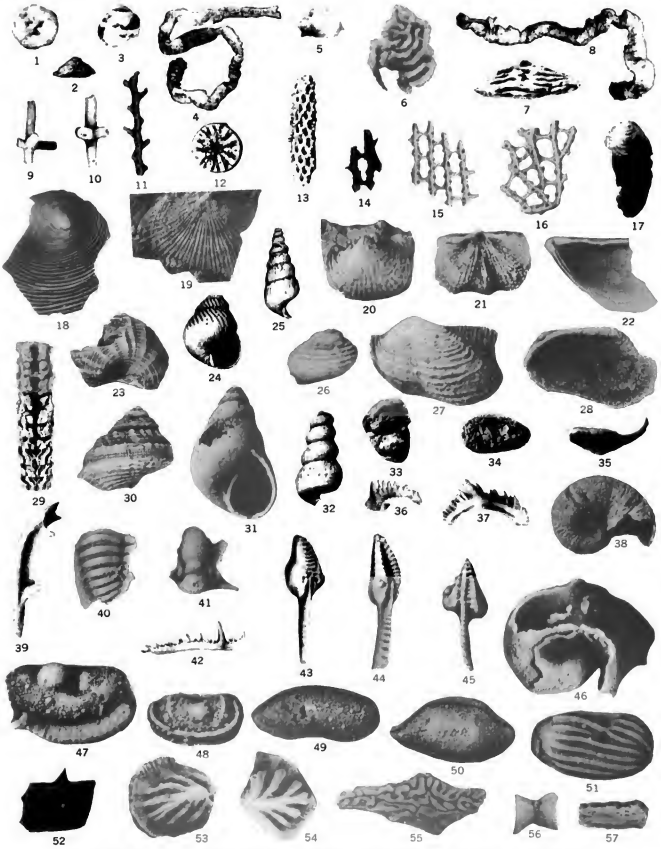

REPRESENTATIVE ANIMAL REMAINS RECOVERED FROM INSOLUBLE RESIDUES

FIGURE 36. *Spathognathodus minutus*? (Ellison), × 30.
From residue E-25 (heterogeneous-mixed coal ball, Berryville, Ill.); USNM 138873.

37. *Ozarkodina delicatula* (Stauffer and Plummer), × 30.
From residue E-4 (heterogeneous-mixed coal ball, Berryville, Ill.); USNM 138874.

38. "*Spirorbis*" sp., × 20.
From residue E-22 (homogeneous-mixed coal ball, McAlester, Okla.); USNM 138875.

39–41. Free cheek, fragment of pygidium, and cephalon, respectively of ?*Ditomopyge* sp., × 8.
From residue E-26 (heterogeneous-mixed coal ball, Berryville, Ill.); USNM 138876a, b, c.

42. *Hindeodella* sp., × 30.
From residue E-22 (homogeneous-mixed coal ball, McAlester, Okla.); USNM 138877.

43. *Idiognathodus magnificus* Stauffer and Plummer, × 30.
From residue E-22 (homogeneous-mixed coal ball, McAlester, Okla.); USNM 138878.

44. *Streptognathodus elegantulus* Stauffer and Plummer, × 30.
From residue E-29 (heterogeneous-mixed coal ball, Berryville, Ill.); USNM 138879.

45. *Gnathodus bassleri* (Harris and Hollingworth), × 30.
From residue E-13 (homogeneous-mixed coal ball, Oskaloosa, Iowa); USNM 138880.

46. "*Spirorbis*" sp. incrusted with foraminifers, × 20.
From residue E-22 (homogeneous-mixed coal ball, McAlester, Okla.); USNM 138881.

47. *Hollinella* sp., × 30.
From residue E-1 (homogeneous-mixed coal ball, Franklin, Kans.); USNM 138882.

48. *Amphisiles centronotus* (Ulrich and Bassler), × 30.
From residue E-29 (heterogeneous-mixed coal ball, Berryville, Ill.); USNM 138883.

49. *Bairdiacypris* sp., × 30.
From residue E-29 (heterogeneous-mixed coal ball, Berryville, Ill.); USNM 138884.

50. *Bairdia* sp., × 30.
From residue E-29 (heterogeneous-mixed coal ball, Berryville, Ill.); USNM 138885.

51. *Glyptopleura* sp., × 30.
From residue E-1 (homogeneous-mixed coal ball, Franklin, Kans.); USNM 138886.

52. Actinopterygii: palaeoniscoid fish scale, × 10.
From residue E-22 (homogeneous-mixed coal ball, McAlester, Okla.); USNM 138887.

53, 54. Cladoidachii: cladodont shark scales, × 10.
From residue E-22 (homogeneous-mixed coal ball, McAlester, Okla.); USNM 138888a, b.

55–57. Actinopterygii: cranial roofing element, vertebra, and lower jaw fragment, respectively, of palaeoniscoid fish, × 10.
From residue E-22 (homogeneous-mixed coal ball, McAlester, Okla.); USNM 138889a, b, c.

U.S. GOVERNMENT PRINTING OFFICE: 1962 O - 652661

Lituyapecten (New Subgenus of *Patinopecten*) From Alaska and California

AND

Stratigraphic Occurrence of *Lituyapecten* in Alaska

SHORTER CONTRIBUTIONS TO GENERAL GEOLOGY

GEOLOGICAL SURVEY PROFESSIONAL PAPER 354-J, K

UNITED STATES GOVERNMENT PRINTING OFFICE, WASHINGTON : 1961

UNITED STATES DEPARTMENT OF THE INTERIOR

STEWART L. UDALL, *Secretary*

GEOLOGICAL SURVEY

Thomas B. Nolan, *Director*

For sale by the Superintendent of Documents, U.S. Government Printing Office
Washington 25, D.C.

Lituyapecten (New Subgenus of *Patinopecten*) From Alaska and California

By F. STEARNS MacNEIL

SHORTER CONTRIBUTIONS TO GENERAL GEOLOGY

GEOLOGICAL SURVEY PROFESSIONAL PAPER 354-J

New Miocene and Pliocene species from Alaska show the relation of a known unique Miocene species from Alaska to previously known Pliocene species from California, and a new subgenus is proposed for them

CONTENTS

	Page
Abstract	225
Introduction	225
Systematic paleontology	225
Genus *Patinopecten* Dall, 1898	225
Subgenus *Lituyapecten* MacNeil, n. subgen	227
Patinopecten (*Lituyapecten*) *poulcreekensis* MacNeil, n. sp	228
Patinopecten (*Lituyapecten*) *poulcreekensis* MacNeil, subsp.?	229
Patinopecten (*Lituyapecten*) *yakatagensis* (Clark)	229
Patinopecten (*Lituyapecten*) cf. *P.* (*L.*) *yakatagensis* (Clark)	231
Patinopecten (*Lituyapecten*) *lituyaensis* MacNeil, n. sp	231
Systematic paleontology—Continued	
Subgenus *Lituyapecten* MacNeil, n. subgen—Con.	
Patinopecten (*Lituyapecten*) *purisimaensis* (Arnold)	233
Patinopecten (*Lituyapecten*) *falorensis* MacNeil, n. sp	234
Patinopecten (*Lituyapecten*) cf. *P.* (*L.*) *dilleri* (Dall)	235
Patinopecten (*Patinopecten*) *caurinus* (Gould)	236
Vertipecten sp. indet	236
References	237
Index	239

ILLUSTRATIONS

[Plates follow index]

PLATE 35. Pectinids from the Poul Creek formation and the upper part of the Katalla formation.

36. Pectinids from the Poul Creek formation, the upper part of the Katalla formation, and the uppermost Poul Creek or lowermost Yakataga formation.

37. Pectinids from the Yakataga formation.

38. Pectinids from the Poul Creek formation, the Yakataga formation, and the Falor formation of Manning and Ogle, 1950 (California).

39. Pectinids from the Yakataga formation and the upper mudstone unit of the unnamed upper Tertiary formation in the Lituya district.

40. Pectinids from the upper mudstone unit of the unnamed upper Tertiary formation in the Lituya district.

41. Pectinids from the Yakataga formation and the lower sandstone-siltstone and upper mudstone units of the unnamed upper Tertiary formation in the Lituya district.

PLATE 42. Pectinids from the Yakataga formation and the lower sandstone-siltstone and upper mudstone units of the unnamed upper Tertiary formation in the Lituya district.

43. Pectinids from the upper mudstone unit of the unnamed upper Tertiary formation in the Lituya district.

44. Pectinids from the Purisima formation (California).

45. Pectinids from the Poul Creek formation, the upper mudstone unit of the unnamed upper Tertiary formation in the Lituya district, and from the Purisima formation (California).

46. Pectinids from the Poul Creek formation, the Falor formation of Manning and Ogle, 1950 (California), and the Purisima formation (California).

SHORTER CONTRIBUTIONS TO GENERAL GEOLOGY

LITUYAPECTEN (A NEW SUBGENUS OF *PATINOPECTEN*) FROM ALASKA AND CALIFORNIA

By F. Stearns MacNeil

ABSTRACT

A new subgeneric name, *Lituyapecten*, is proposed under the genus *Patinopecten* (used as a subgenus of *Pecten* by some authors) to include a small but characteristic group of large pectinids having, usually, frill-like lamellae on the ribs of its left valve.

Of unknown origin, the subgenus appears first in early Miocene (or possibly very late Oligocene) beds of Alaska. It inhabited Alaska throughout Miocene and into Pliocene time, spreading southward into California in the Pliocene; its last survivors in the California Pliocene may be younger than its last known representatives in Alaska.

Three previously described species are included in *Lituyapecten; yakatagensis* Clark, *purisimaensis* Arnold, and *dilleri* Dall; *coosensis* Shumard may be an aberrant member. Three new species are described; *P.* (*L.*) *poulcreekensis* MacNeil, *lituyaensis* MacNeil, and *falorensis* MacNeil. An unnamed possible subspecies of *poulcreekensis* is also recognized.

The subgenus is believed to comprise two stocks, the *yakatagensis* stock (*yakatagensis, lituyaensis, falorensis,* and *purisimaensis; coosensis* may be an atypical member), and the *dilleri* stock (*poulcreekensis* and *dilleri*). The last representatives of both stocks appear to have penetrated the farthest south; *P.* (*L.*) *falorensis* is known as far south as central California where it occurs in the Purisima formation; *P.* (*L.*) *dilleri* is known in the Pliocene of northern Lower California, Mexico.

INTRODUCTION

This study was prompted by a collection made by D. J. Miller in the summer of 1958 of some exceptionally well-preserved material from Yakataga Reef in the Yakataga district, and from Cenotaph Island in Lituya Bay, Alaska. After preparing this material it was realized that some large *Patinopecten* in it were worthy not only of description in themselves, but they shed new light on the internal relation of a conspicuous but poorly known group of *Patinopecten* occurring in the late Tertiary of both Alaska and California. Accordingly, a restudy was made of similar forms in older Alaskan collections as well as of related forms in California. With one exception the specimens figured here from Alaska are from the collections of the U.S. Geological Survey; they will be deposited in the U.S. National Museum. One specimen from the collection of the California Academy of Sciences is figured. The collections of both the Academy and the University of California at Berkeley were used in listing the occurrences of species. None of the specimens from Alaska illustrated here has been figured previously. The holotype of *Pecten* (*Patinopecten*) *yakatagensis* Clark, the only Alaskan species for which an illustration was available, is a poor specimen and is not refigured.

Related species in California Pliocene formations were studied in connection with the Alaskan species. Specimens of these species in the collections of both the University of California and Stanford University are illustrated here. These include the holotype of *Patinopecten* (*Lituyapecten*) *falorensis* MacNeil, a specimen figured previously as "*Pecten oregonensis* Howe var." by Manning and Ogle (1950, pls. 6, 7), some specimens of the same species from the Purisima formation, and what is believed to be one of the best specimens known of *Patinopecten purisimaensis* Arnold.

Most of the material from Alaska occurs as soft shell in fine-grained hard rock. Complete free specimens are rare and in collecting fracture takes place most commonly through the shell material, leaving part of the shell on the internal mold and part on the external mold. Most of the rock is noncalcareous, and it was found that molds having good detail could be obtained by dissolving away the shells in acid. Casts were made from these molds with liquid latex. With the exception of one specimen (pl. 42, fig. 4) that was collected as a mold filled with decaying vegetable material, presumably dissolved naturally by humic acids, all the rubber casts were obtained in this way.

SYSTEMATIC PALEONTOLOGY

Genus PATINOPECTEN Dall, 1898

Type: *Pecten caurinus* Gould. Recent, northern California to Alaska.

The genus *Patinopecten* is known only from northern Pacific waters; its southernmost record is in Lower

California. Numerous species, ranging in age from middle Tertiary to Recent, are known from both the North American and the Asiatic sides of the Pacific. Only two species survive; *P. caurinus* (Gould) from the United States and *P. yessoensis* (Jay) from Japan. The greatest number of species occurs in the Pliocene and late Miocene. The present paper describes the oldest known American species, a species occurring in beds of early Miocene or possibly late Oligocene age in Alaska. The first American species is a large form, which, together with its abrupt appearance, suggests that it is a migrant from elsewhere. Possibly the ancestral stock of *Patinopecten* is a still unknown pectinid in the beds of early Tertiary age of east Asia.

One of the earliest known Asiatic species is *Patinopecten yamasakii ninohensis* Masuda (1954, p. 13, figs. 1–3) from the Shiratori formation (early Miocene) of Japan. It is variable enough to foreshadow several subsequent types. Its antecedents, when they are found, should shed some light on the origin of *Patinopecten*.

Patinopecten is at present the most likely genus in which to place the species under consideration. However, it is by no means certain that *Lituyapecten*, the subgenus here proposed to include the pectens of the *P. yakatagensis* group, really is a subgenus of *Patinopecten*. We still know too little about the exact lines of descent within the highly complex pectinids to make definite statements.

Grant and Gale (1931, p. 188) say, "*Vertipecten* appears to be the connecting link between *Chlamys* and *Patinopecten*." Elsewhere (p. 192) they remark

> This group of species [Patinopecten], although obviously closely related to *Chlamys* and to *Vertipecten*, is none the less, a rather distinct unit. It represents an evolutionary adaptation starting in the same direction as that taken by *Amusium;* but the external ribs did not become absolute, and hence the external lirae did not become sharp. The general shape, however, is the same. The shape of *Placopecten* is also similar. *Patinopecten* developed distinct external ribs, *Placopecten* retained but faint radial riblets on the exterior, while all that is left of the ribs of *Amusium* are the strengthened internal lirae. * * * *Amusium* is more closely related to *Janira*, and it is possible that its apparent relationship to *Patinopecten* is superficial, being a parallel adaptation to a somewhat similar environment.

There is strong reason for believing Grant and Gale are correct in assuming *Amusium* to be closely related to *Pecten* (*Pecten*) (=*Janira*). In fact, there is strong reason for believing typical *Pecten* (*Pecten*), *Amusium*, and *Pecten* (*Amussiopecten*) are coderivatives from a prototypical *Pecten* (*Pecten*). *Pecten* (*Amussiopecten*) seems to form a continuum between *Pecten* (*Pecten*) and *Amusium*.

However, the exact relation of *Patinopecten* to either *Vertipecten* or *Chlamys* is still rather obscure. *Vertipecten* seems to be closely related to some of the types included in *Chlamys*, but whether or not *Chlamys* as used by most modern authors is a monophyletic group is another matter. Certainly the left valve of the earliest known North American species of *Patinopecten* bears little resemblance to the left valve of coexisting species of *Vertipecten*. *Vertipecten* is unique in having its left valve more inflated than its right valve. It would be premature to say *Patinopecten* is not related to *Vertipecten* but it would be safe to say that if the two are related they must have diverged from each other at least as far back as early Tertiary time.

The known late Mesozoic and earliest Tertiary pectinids seem to indicate that the prototype of *Pecten* (*Pecten*) was derived from a *Camptonectes*-like ancestor. An *Amusium*-like stock was also differentiated at an early date, but it resembles true *Amusium* only in being smooth and probably was not the ancestor of *Amusium* s.s. The ontogeny of *Pecten* (*Pecten*), based on *P.* (*P.*) *jacobaeus* Lamarck, suggests that the prototypical stock may have been inequivalved but smooth. It may have been closely related to the primitive *Amusium*-like smooth forms. It developed ribs to produce *Pecten* (*Pecten*), and the ribs became secondarily obsolete but reinforced internally, along with flattening of both valves, to produce *Amusium* s.s. The more coarsely ribbed true pectens have well-developed rims along the sides of the internal projection of the interspaces between the ribs, presumably a stage in the development of the pairs of riblets on the inside of both *Pecten* (*Amussiopecten*) and *Amusium*. These paired internal ribs are probably a development independent of the single internal ribs of other externally smooth pectinids; still others are without internal ribs. *Patinopecten*, although resembling *Pecten* (*Amussiopecten*) externally, does not have paired internal ribs.

Very young shells of *Patinopecten caurinus* are nearly smooth with irregular radiating white lines in the shell, resembling some species of *Pseudamussium* and *Propeamussium*. They have a faint diagonal *Camptonectes*-like microsculpture. This, together with its lack of internal ribs, suggests a separation of the *Patinopecten* branch before the stabilization of *Pecten* (*Pecten*) and *Amusium*. Possibly *Patinopecten* came from intermediates between *Camptonectes* and *Pecten* (*Pecten*).

Left valves of most specimens of *Patinopecten caurinus* have delicate, evenly spaced raised concentric growth lines extending to the ventral margin; on some specimens there is a slight imbrication. Similar concentric growth lines are the characteristic microsculpture of the left valve of most species of *Pecten* (*Pecten*) and of *Pecten* (*Amussiopecten*). Some of the early true

Amusium may have had similar concentric growth lines, but the later species of *Amusium* have both valves smooth and polished. The group of *Patinopecten* under consideration has fine concentric growth lines on the early stages of the left valve, but the typical sculpture of the left valve of adults is characterized by lamellae or flanges which may extend entirely across the ribs or which may be divided into two series, one along each edge of the flat-topped ribs. The transition from the the juvenile to the adult sculpture may be abrupt or gradual. On some individuals the fine concentric growth lines persist in adults in the interspaces as well as on top of the ribs between the blunt spines or flanges.

No specimens of *Lituyapecten* yet observed show any suggestion of the imbricating microsculpture, resembling the surface of metal lath, that characterizes left valves of *Chlamys*, *Vertipecten*, *Fortipecten*, and some species of *Patinopecten* such as *P. yessoensis*, *P. propatulus* (Conrad), and *P. ibaragiensis* Masuda (1953), pls. 5, 6); imbricating microsculpture occurs rarely in small patches on specimens of *P. caurinus*. On the other hand, *P. coosensis* (Shumard) (see Trumbull, 1958, pls. 115–117), a species generally referred to *Patinopecten* s. s., has a concentric microsculpture, not an imbricating one.

It may be that *P. coosensis* is really a flangeless *Lituyapecten*, not a member of the *P.* (*Patinopecten*) *caurinus* group. In support of this, a flangeless variant of *P.* (*L.*) *yakatagensis* (pl. 45, fig. 3; pl. 46, fig. 5), whose left valve ribs are squared like those of *P. coosensis*, has only fine concentric growth lines all the way to the ventral margin. These two species also have a peculiar strong fold on the anterior ear of the left valve.

The origin of *Fortipecten* was discussed by Yabe and Hatai (1940, p. 153–155). Yabe and Hatai suggested that some Miocene *Patinopecten* might be the ancestor of this subgenus. Since their paper was written, a Miocene species has been described, *Patinopecten ibaragiensis* Masuda (1953, p. 44, pl. 5, figs. 1–5; pl. 6, figs. 1–5), which definitely seems to be the connecting link between *Patinopecten* and *Fortipecten*. I am inclined to regard *Fortipecten* as a subgenus of *Patinopecten* on the basis of this species. The genus *Patinopecten* would then embrace three subgenera: typical *Patinopecten*, *Fortipecten*, and *Lituyapecten*.

If an imbricating mocrosculpture is a primative character that persists in several lines of descent such as *Chlamys* (*Chlamys*), *Chlamys* (*Swiftopecten*), *Chlamys* of the *C. beringianus* group, *Vertipecten*, and *Patinopecten*), it is difficult to see why it is present in some typical *Patinopecten* and not in others. The microsculpture is developed in a layer that is readily decorticated, and it is only seen on exceptionally well-preserved specimens; sometimes only a small patch of it can be found. As far as is known, only concentric microsculpture is found in *Amusium*, *Pecten* (*Amussiopecten*, *Pecten* (*Pecten*), and *Patinopecten* (*Lituyapecten*).

It is entirely possible that *Patinopecten* inherited an imbricating microsculpture which, although persisting in *Fortipecten* and in some species of typical *Patinopecten*, was eliminated in some typical *Patinopecten* and in *Lituyapecten*. It is also possible that there was no persistence of this character in the phylogenetic lines connecting *Patinopecten* with *Vertipecten* and *Chlamys*, however short or long they might have been, and that this character was redeveloped in some branches of *Patinopecten*. At any rate, our present imperfect knowledge of pectinid phylogeny makes it impossible to settle the question.

Subgenus LITUYAPECTEN MacNeil, new subgenus

Type: *Patinopecten* (*Lituyapecten*) *lituyaensis* MacNeil, n. sp.

Diagnosis.—Shell medium large to very large; a right valve of the type species measures 8¼ inches in diameter; this size makes it one of the largest pectinids known. Outline ranges from subrounded to elliptical; long axis in some species is the height; in others, the length. Ears moderately large; byssal notch moderately strong to strong; anterior ear of right valve elongate, tends to become narrower, and curves ventrally in full grown adults; left valve ears more symmetrical, and anterior ear tends to develop a marginal fold (concave on the inside) opposite narrow ear of right valve. Ribs strong, and those of right valve moderately broad to broad; they tend to be undercut on sides, flat to rounded or irregular on top. Interspaces usually deep and round bottomed. Juvenile sculpture consisting of thin concentric raised lines.

Interstitial ribs may occur on either valve and they are usually beset by a single row of rounded frills or flanges. Right valve of *Lituyapecten* probably slightly more inflated than left valve. Crushing of known specimens makes it difficult to determine the relative inflation; certainly some known left valves more inflated now than right valves. Hinge plate relatively heavy and with a single nearly marginal groove in each of the left valve ears. Base of the hinge plate conspicuously swollen.

Discussion.—The subgenus is founded primarily on the left-valve sculpture. The ribs are moderately narrow to wide and rounded to flat topped. The juvenile sculpture consists of raised concentric growth lines that are fine and evenly spaced; they are similar to those normally covering the entire valve of *P. caurinus*.

The adult sculpture of *Lituyapecten* consists of sharply raised flanges or lamellae, which may be single or divided into two or more rows of segments.

I am indebted to Mrs. Ellen Trumbull, of the U.S. Geological Survey for a photograph of an unusually well-preserved specimen of *Patinopecten propatulus* (Conrad) from the Astoria formation (Miocene) of Oregon, a specimen which she will figure in a forthcoming paper. This specimen has several patches of imbricating microsculpture preserved. In addition, it has small frill-like flanges very close to the beak on three or four of the posterior ribs of the left valve. They are closer to the beak than I have seen them on other species having similar flanges, and they appear to have died out at the stage of growth at which they normally appear in other species. This specimen contains the only combination of imbricating microsculpture and frill-like flanges I have seen. On the basis of the frills alone, *P. propatulus* might appear to belong to *Lituyapecten*, even though the frills occur at a different growth stage than is common. I am inclined to believe that the juvenile frills on *P. propatulus* indicate that typical *Patinopecten* and *Lituyapecten* are closely related after all, something that I did not feel I could say positively from other species. Possibly *P.* (*Patinopecten*) and *P.* (*Lituyapecten*) diverged from each other in Oligocene time. *P. propatulus* certainly seems to be a typical *Patinopecten*, whereas I believe *coosensis* is an aberrent *Lituyapecten*.

Clark (1932, p. 808) in his description of *Pecten* (*Patinopecten*) *yakatagensis* said: "*Pecten yakatagensis* of all the species referable to the subgenus *Patinopecten* is unique. * * * It is very possible that *Pecten yakatagensis* should be placed in a new section." The new subgeneric name, *Lituyapecten*, is here proposed to include the species of *Patinopecten* having one to several rows of frill-like flanges on the ribs of the left valve.

Two groups of species are included under *Lituyapecten*, the *Patinopecten dilleri* group and the *Patinopecten yakatagensis* group. The *P. dilleri* group usually has subrounded ribs on the left valve and single flanges continuous across the ribs; rarely the flanges may be divided on one or two of the central ribs with the disconnected segments of the flanges alternating. In the *P. yakatagensis* group the flanges are broken up into two or more well-defined series located on ribs, which at least in full grown adults tend to be broad and flat topped. Two rows of short spinelike flanges, one along each side of flat-topped ribs, is the most common condition. However, the distinction of the flanges as single or multiple rows is sharp only in the Pliocene species, the last-known members of the group. The earliest known members are irregular in the division or nondivision of the flanges and in the distance of separation; the same specimen may have single or divided flanges on different ribs, or on different parts of the same rib. Thus, while the end members of these two groups may seem quite distinct, the earliest representatives indicate that they had a common ancestry and that the characters which distinguished their last-known representatives were characters of no more than individual variation in their earliest known representatives.

Lituyapecten commonly has large barnacles on its left valve, but none have been observed on right valves. (See pl. 37, fig. 7; pl. 42, fig. 3; pl. 43, figs. 1, 4.) Presumably it rested on its right valve. If they were active, specimens with large barnacles must have had their activity impeded; some barnacles on Alaskan specimens have bases measuring over 30 millimeters. The Geological Survey collection contains a Recent specimen of *Patinopecten* (*Patinopecten*) *caurinus* whose right valve is clean but whose left valve is covered by barnacle bases. Schools of this species are believed to move from location to location periodically.

As far as is known, *Lituyapecten* is typically North American. The known species are all from Alaska and California; apparently it never invaded Asiatic waters. It ranges from early Miocene, possibly late Oligocene, to late Miocene, possibly early Pliocene in Alaska. The California occurrences are Pliocene.

Patinopecten (Lituyapecten) poulcreekensis MacNeil, n. sp.

Plate 35, figures 1–6; plate 36, figures 1, 2(?), 3, 4, 6, 7; plate 38, figure 2

Shell moderately large, suborbicular; valves probably both moderately inflated, right valve possibly more so (inflation varies in specimens at hand, probably owing to crushing); shell of medium to above medium thickness. Dorsal margins straight to weakly concave; dorsal margins low and have a poorly defined submarginal slope. No visible denticles along margin of byssal sinus. Dorsal margin of ears straight. Ears moderately large; byssal sinus moderately deep and large; ears sculptured by strong radial riblets (about six) which are made scaly or frilled by the strongly upturned edges of closely set growth lines, the scaliness being strongest on the ribs; posterior ears of both valves have concave terminal margin with hinge line shorter than base of ear; anterior ear of left valve has convex terminal margin. Both valves with about 22 strong radial ribs and 1 or 2 additional minor ribs at both ends of valve; ribs of right valve more squared and undercut; ribs of left valve more rounded; a few ribs partly to completely bifurcating, a median cleft on 1 or 2 ribs being rather common. Ribs of right valve broad and range from

smooth and flat to irregular and bear 2 or 3 secondary radial ridges of moderate strength; central ribs smooth, but the terminal ribs at both ends may have weak frills along one or both sides or single frills extending entirely across them; interspaces have moderate to strong interstitial ribs which, when not decorticated, are strongly frilled. Left valve has regular closely set raised growth lines in early stages; growth lines change abruptly to a stage having raised frills or flanges, the earliest being single and continuous across the ribs or, at most, divided into two series by a median discontinuity; flanges on opposite sides are often staggered or alternating, especially when first appearing, but are more often at the same position in later stages. In full-grown adults, frills may range from a single row to 2 rows with very narrow separation to 4 rows formed by division of double rows. Interspaces also have a moderately strong, highly frilled midrib; a few interspaces have two such interstitial ribs. Frills fragile and easily decorticated; best examples obtained as latex impressions after acid preparation. Right-valve microsculpture not detected and presumably smooth.

Holotype, a right valve (USNM 563572), measures: diameter 113 mm, height 113 mm. Largest right valve on hand has a height of 145 mm, to which must be added a few more millimeters for wear. Paratype, USNM 563573.

This species has not been found outside of the Yakataga and Katalla districts, Alaska. It is known to occur abundantly only in the uppermost part of the Poul Creek formation at Yakataga Reef, although a few fragments of it are known from rocks of nearly the same age at a few other localities. If the supposed stratigraphic position of the youngest known specimen in the Katalla district is correct, it ranged into beds equivalent to the lowermost part of the Yakataga formation, and was presumably coexistent with the early members of *P.* (*L.*) *yakatagensis*. The specimen in question, an extreme variant, is figured on plate 35, figure 6. One specimen (pl. 36, fig. 2), while from an isolated locality in the Suckling Hills (USGS 15843) whose stratigraphic position is in some doubt (see, Miller, p. 242), is believed, nevertheless, to be the oldest specimen collected, and it may be the oldest *Patinopecten* yet collected from North America; a late Oligocene age is possible.

Patinopecten (*Lituyapecten*) *poulcreekensis* will be compared with *P.* (*L.*) *yakatagensis* under the discussion of the latter species.

The known relatives of *P.* (*L.*) *poulcreekensis* all occur in younger beds in Alaska and California. Nothing similar to it is yet known from equivalent beds elsewhere, and its ancestors and regional provenance are unknown.

Distribution.—Early Miocene, northern Gulf of Alaska region: Katalla formation (upper part), Katalla district; Poul Creek formation (uppermost part), Yakataga district, Alaska.

Type locality.—Uppermost part of the Poul Creek formation at Yakataga Reef, USGS loc. M-271.

Other occurrences.—Katalla formation, upper (?) part, USGS 15843 (float), USGS 15852. Poul Creek formation, USGS 17733, CAS 29261, 729264.

Patinopecten (Lituyapecten) poulcreekensis MacNeil, subsp†

Plate 36, figure 5; plate 38, figure 5.

Two incomplete specimens from near the Poul Creek–Yakataga formation boundary, but whose exact formational position is not known, are unique in having some sculptural details like *P.* (*L.*) *poulcreekensis*, some sculpture intermediate between *P.* (*L.*) *poulcreekensis* and *P.* (*L.*) *yakatagensis*, and narrower and more numerous ribs, agreeing in this respect more with *P.* (*L.*) *yakatagensis*. They could well represent linear intermediates between the two species, but at the same time they are typical of neither. The earliest growth stage on one fragment shows it to have concentric raised growth lines like juveniles of *poulcreekensis* and *yakatagensis*. Interstitial ribs with moderately strong flanges are present in some of the interspaces, agreeing in this respect with *poulcreekensis*.

The prevalence in this form of single strong flanges completely crossing the ribs suggests that it may be ancestral to the *P.* (*L.*) *dilleri* group, of which group a fragment obtained high in the section in the Lituya Bay district is believed to be a member (pl. 45, fig. 4; right valves on pl. 41, figs. 4, 5).

This form is not being named at present, although with better preserved material it probably would be. It seems likely that this form and typical *P.* (*L.*) *poulcreekensis* had a common ancestry but are at least subspecifically distinct. If this form and the one from the Suckling Hills (pl. 35, fig. 6) were end members of the same population it would be variable indeed.

The largest fragment figured (CAS 29285) has a diameter of 118 mm, a fraction of the whole dimension.

Distribution.—Early Miocene, uppermost part of the Poul Creek formation or the lowermost part of the Yakataga formation, Yakataga district, Alaska.

Localities.—CAS 29285; USGS D341 (T).

Patinopecten (Lituyapecten) yakatagensis (Clark)

Plate 37, figures 1–7; plate 38, figures 4, 6; plate 39, figure 2; plate 41, figures 2(?), 3; plate 42, figure 3

Pecten (*Patinopecten*) *yakatagensis* Clark, 1932, Geol. Soc. America Bull., v. 43, no. 3, p. 807, pl. 15, fig. 8, pl. 16, fig. 1.

Shell of medium size, suborbicular; valves both moderately inflated; left valve possibly less inflated than

right valve; shell moderately thin. Dorsal margins weakly concave, low with weak submarginal slope on left valve; right-valve ears swollen; this condition makes boundary between ears and disk a sharp, narrow groove. No byssal denticles. Dorsal margin of ears straight to ventrally depressed at the terminal ends. Ears moderately flat but moderately elongate; byssal sinus large and deep, wider than terminal projection of anterior ear of right valve; ears sculptured by weak to moderate radial riblets (about nine when developed all over the ear), which may be weakly beaded or nearly smooth; anterior ear of left valve tends to develop a marginal fold, and terminal edge of ear indented opposite the fold—the stronger the fold the deeper the indentation. Both valves normally have about 30 to 31 radial ribs, but some variants have no more than 26–28. Ribs of right valve moderately narrow and straight sided to slightly undercut, and top flattened, occasionally with a well-defined bifurcation of at least one rib; central ribs smooth; terminal ribs often with weak side denticles, especially on terminal sides. Ribs of left valve subrounded in juveniles but become flattened or have a median trough on top in adults, the sides developing well-defined denticles. Juvenile stage of left valve has raised concentric growth lines which continue in adults in interspaces and in concavity on top of ribs. Adult left-valve sculpture consists of frills or flanges on the ribs, most common condition being a division of frills into two rows, one on each side of the ribs; frills vary in size and in distance from each other; a less common variant has single frills completely crossing each rib, or the same specimen may have some ribs with single frills and some ribs with divided frills; a single specimen from the Poul Creek formation compared with this species has no frills, the raised concentric growth lines extending all the way to ventral margin. Interspaces rarely have an interstitial riblet, but one specimen, which has a good development of undivided flanges on main ribs, has frilled interstitial riblets in some interspaces. Right valves do not appear to have a raised concentric microsculpture.

Holotype (UC 30381) measures; diameter about 75 mm, height about 79 mm. One of the largest specimens (USNM 563590) with both dimensions complete measures 123 mm in diameter and 123 mm in height.

The typical form of this species is known only from the Yakataga formation and in an interval extending 300 to 3,700 feet above the base of the formation, although a possible variant of it was found in the uppermost part of the Poul Creek formation. The type (a poor specimen not refigured here) probably came from about 350 to 400 feet above the base of the formation. The typical form has a left valve similar to those figured on plate 37, figures 4 and 7, and plate 42, figure 3. It was characterized by a juvenile stage having fine concentric growth lines on the ribs and an adult stage having well-developed marginal flanges on the ribs separated by a median trough—the trough is sculptered by raised growth lines like those on the juvenile ribs. The ribs tend to be less raised and not as well defined in the advanced growth stages of large specimens. No specimens seen thus far from well up in the Yakataga formation have ribs with single flanges crossing them like the juvenile ribs of *P.* (*L.*) *poulcreekensis*, or the possible narrow ribbed subspecies of it illustrated on plate 38, figure 5.

Patinopecten (*Lituyapecten*) *yakatagensis* differs from *P.* (*L.*) *poulcreekensis* by having more ribs; about 28 to 31 as opposed to 22 well-defined ribs and 1 or 2 additional fine terminal radial riblets on *poulcreekensis*. The ribs of *poulcreekensis* are larger and broader. The lateral frills on the ribs of *yakatagensis* are separated from the time of their first appearance, whereas *poulcreekensis* has a long postjuvenile stage in which the frills are continuous across the ribs, and on some ribs they remain single. Furthermore, no specimens of *yakatagensis* have been observed in which the lateral frills divide again, whereas in *poulcreekensis* the frills on some of the ribs may divide secondarily to form four rows of frills.

The two species differ strikingly in the development of interstitial ribs; they are strong in *poulcreekensis* but very rare in *yakatagensis*. (See pl. 42, fig. 3.) There may be an incipient tendency towards the development of interstitial ribs on the right valve of *yakatagensis* (see pl. 37, fig. 2), but flanged interstitial ribs are always present on adults of *poulcreekensis*, and they are often as high as the primary ribs (see pl. 35, fig. 5).

In the tentative subspecies of *poulcreekensis* (pl. 38, fig. 5) weakly flanged interstitial ribs are present in some of the interspaces, but more interspaces are without them. In typical *poulcreekensis* only one or two interspaces at the terminal ends are apt to lack interstitial ribs.

The ears of *yakatagensis* are lower and longer than on *poulcreekensis;* the radial markings are finer; the suprabyssal extension of the anterior ear of the right valve is narrower and longer; and the anterior ear of the left valve tends to develop a submarginal roll or fold, a condition not apparent on any specimens of *poulcreekensis* seen. A fold is well developed in *coosensis* Shumard. (See Trumbull, 1958, pl. 117, fig. 4.)

Patinopecten (*Lituyapecten*) *yakatagensis* was probably the direct ancestor of *P.* (*L.*) *lituyaensis*, the species next described. The latter species occurs in beds believed to be equivalent to an upper part of the Yakataga formation, but so far no representatives of *Litu-*

yapecten are known from the highest part of the Yakataga formation. The beds containing *Lituyapecten* in the Lituya Bay area are believed to be late Miocene or early Pliocene in age. The subgenus is represented by still another species in beds of late Pliocene age in California. Unless the pattern of distribution known at present is merely an accident of collecting, the subgenus seems to have migrated from the northern Gulf of Alaska region in the early Miocene to California in the late Pliocene where it became extinct.

An incomplete right valve from the lower part of the sandstone-siltstone unit in the Lituya Bay district (pl. 41, fig. 2) may be *P.* (*L.*) *yakatagensis* or, at least, intermediate between *P.* (*L.*) *yakatagensis* and *P.* (*L.*) *lituyaensis*. It occurs lower in the section than typical *lituyaensis* although its position may be stratigraphically higher than the highest known occurrence of *yakatagensis* in the Yakataga formation. The ribs are narrower than on *lituyaensis*. There are 26 ribs; just under the minimum observed on *yakatagensis* in the Yakataga district and just over the maximum observed for *lituyaensis* from higher in the section in the Lituya Bay district.

Distribution.—Early to Middle Miocene, northern Gulf of Alaska region: Yakataga formation, Yakataga district, Alaska; possibly in the lower part of the sandstone-siltstone unit in the Lituya Bay district, Alaska.

Type locality.—Yakataga formation, about 350 feet above the base of the formation, Yakataga Reef, UC loc. 3859.

Other occurrences.—Yakataga formation, USGS locs. 6693, 6695, 15425, 15437(?), 17813, 17840, 17841, 17852, 17853, D256 (T); CAS locs. 29230, 29244, 29248, 29251, 29256, 29257, 29270, 29274, 29276, 29277, 29283, 29294; UC loc. 3858.

Doubtful identifications.—Sandstone-siltstone unit, Lituya Bay district, USGS D187 (T).

Patinopecten (Lituyapecten) cf. P. (L.) yakatagensis (Clark)

Plate 45, figure 3; plate 46, figure 5

The Miller collection from the upper 50 feet of the Poul Creek formation at Yakataga Reef (USGS 17733), Alaska, contains one specimen that is obviously different from other specimens from that interval, all of which appear to be referable to *poulcreekensis*. The unique specimen is more like *yakatagensis* although it is not typical. The significance of this specimen was not recognized in the field and it was not segregated, but an attempt to determine its stratigraphic position from the matrix adhering to it and Miller's very carefully described section suggests that it came from a bed stratigraphically higher than the bed containing abundant individuals of *poulcreekensis*.

This specimen has only about 24 ribs as opposed to 30 or 31 in the typical form. The ribs on its left valve have no flanges—only a weak sulcus on 1 or 2 ribs. The raised concentric microsculpture, which normally characterizes the juvenile stage, extends on this specimen all the way to the ventral margin. The specimen has a maximum height of about 90 mm; the transition from the juvenile to the adult sculpture on both *poulcreekensis* and *yakatagensis* is usually between 30 and 50 mm from the beak.

This form is the probable ancestor of typical *yakatagensis*, and since it occurs at so nearly the same stratigraphic position as *poulcreekensis*, and yet differs so much from it, the suggestion is strong that *poulcreekensis* is not the direct ancestor of *yakatagensis*. This problem is further discussed on page 232–233.

It is also possible that this form from the uppermost part of the Poul Creek formation may be ancestral to other late Tertiary pectinids besides *P.* (*L.*) *yakatagensis;* lineages which did not continue to live in the immediate area. One such possible descendent is *Patinopecten coosensis* (Shumard) from the Empire formation (Pliocene?) of Oregon which does not seem to be very closely related to the Miocene to Recent *P. propatulus*—*P. caurinus* stock, but which could very well have come from *P.* (*L.*) cf. *yakatagensis* from the Poul Creek.

Locality.—From the upper 50 feet of the Poul Creek formation at Yakataga Reef, Alaska, presumably from above the zone of *P.* (*L.*) *poulcreekensis*, USGS 17733.

Patinopecten (Lituyapecten) lituyaensis MacNeil, n. sp.

Plate 39, figures 1, 3; plate 40, figures 1–5; plate 41, figure 1; plate 42, figures 1, 2, 4; plate 43, figures 1–4

Shell large, asymmetrical; posterior extension greater than anterior extension, and greatest height posterior of median line; right valve more inflated than left valve; shell of medium thickness. Dorsal margins concave in region of ears, but become nearly straight distally; dorsal margins low; left valve may have a low steplike marginal slope, particularly along left side; left valve ears inflated and lie higher than adjacent disk; byssal fold may be greatly swollen. Dorsal margin of ears straight centrally but curves ventrally towards distal end; anterior ear of right valve curves strongly in large specimens. Ears of moderate size for a large shell; no denticles along margin; byssal sinus moderately deep; ears sculptured by scabrous or beaded radial riblets which tend to die out distally and which may be very weak or absent on some specimens; a weak dorsal fold and a corresponding terminal indentation on anterior ear of left valves. Both valves with about 23 or 24 broad radial ribs. Ribs of right valve higher centrally and low to nearly flush terminally; central ribs smooth and rounded on top; terminal ribs have weak lateral frills and concave tops; interspaces smooth or have frilled interstitial ribs in one or more of terminal interspaces. Left valve has frilled ribs, which may be single

and narrow terminally but broad centrally with a raised row of strong but narrow beadlike frills on each side, or more rarely with a middle row of frills as well; interspaces wider than ribs in adults but narrower than ribs in juveniles, sometimes with beaded or frilled interstitial riblets in one or two interspaces. Juvenile sculpture of left valve consists of raised concentric growth lines which are slightly convex towards beak and which are not raised on bottoms of interspaces, but which are raised in median trough on ribs for some distance beyond first appearance of marginal frills. Microsculpture of adults consists of growth lines convex towards margin in interspaces and concave towards margins on ribs but not raised as in juveniles. Right valve microsculpture consists of faint radial markings but otherwise smooth.

Holotype, a right valve (USNM 563598), measures: diameter 210 mm, height 220 mm. The left valve paratype is numbered USNM 563599.

The holotype of this species is one of the largest Tertiary pectinids known—if a larger specimen has ever been reported—and fragments of other specimens indicate that an even larger size was attained; possibly as much as 250 mm. It may have the distinction also of being the first pectinid observed in the rocks of western North America, the "manteau royal" mentioned in the narrative of La Pérouse's expedition of 1786.

This species is descended probably directly from *P.* (*L.*) *yakatagensis*. It is larger and asymmetrical, whereas *yakatagensis* is nearly round. Most of the known specimens appear to be deformed by rock flowage in one way or another; some are shortened, some lengthened, and others are flattened. It has fewer and broader ribs than *yakatagensis*. The ears are larger and higher, and the byssal notch and the byssal fasciole are not as broad. The terminal ribs on the right valve of *yakatagensis* usually have a row of weak frills on the outer side, but the terminal ribs of *lituyaensis* usually have frills on both sides, and the ribs tend to be broader with a concave top. However, there is considerable variation in this respect; compare figure 1 of plate 40 with the corresponding area on figure 3.

The terminal ribs of the left valve of both species tend to be narrow and to have only a single set of beads or flanges; this feature differs from specimen to specimen, and opposite ends of the same specimen may be unlike. The left valve of *lituyaensis* sometimes has a strong third beaded riblet on some of the middle ribs (pl. 43, fig. 1), possibly a function of its wider ribs. Only one specimen of *yakatagensis* seen (pl. 42, fig. 3) has any indication of a third row of beads, and on it the third row is very weak. It is interesting to note that this specimen also has a fine beaded interstitial riblet, a variation which in *lituyaensis* accompanies the presence of the third beaded riblet on the ribs. *Patinopecten* (*L.*) *lituyaensis* has its flangelike beads in well-separated rows, the variation being from well to widely separated; in *yakatagensis* the rows range from narrowly to well separated, the maximum separation in *yakatagensis* being about the minimum separation in *lituyaensis*. The minimum separation in *yakatagensis* is about equal to the maximum separation in *poulcreekensis*, the latter species ranges to specimens having no division of the flanges.

The frilled interstitial ribs seen on several right valves of this species (pl. 39, fig. 3; pl. 40, figs. 2, 5) seem to be a common occurrence, and they resemble to a lesser degree the interstitial ribs of *P.* (*L.*) *poulcreekensis*. Similar ribs have not been observed in *yakatagensis*.

The microsculpture on juvenile left valves of *lituyaensis* (pl. 42, fig. 2) is similar to that of *yakatagensis* (pl. 37, figs. 3, 5). On both species the transition to the adult stage with side frills on the ribs is less abrupt than on *poulcreekensis* (pl. 36, fig. 6).

All three species are in contrast to a specimen, identified as *P.* (*L.*) cf. *yakategensis*, collected by Miller (pl. 45, fig. 3; pl. 46, fig. 5) from above the *P.* (*Y.*) *poulcreekensis* zone but still below the base of the Yakataga formation (included in USGS 17733).

This single and only known unfrilled specimen from the upper part of the Poul Creek formation poses a problem regarding the ancestry of both *yakatagensis* and *lituyaensis*. There seems to be little doubt that *lituyaensis* is descended directly from *yakatagensis*. However, in some respects the unfrilled Poul Creek form appears to be a more likely ancestor of typical *yakatagensis* than *poulcreekensis* does; *poulcreekensis*, although related, may belong to a different lineage that is more closely related to *P. dilleri*. The strongest resemblance between *yakatagensis* and *poulcreekensis* lies in the possession by both of divided flanges. The flanges of *poulcreekensis* are more exaggerated and have a greater range of variation than those of *yakatagensis*, its possible successor. On the other hand, the unfrilled Poul Creek form is what might be expected for the ancestor of *yakatagensis*. It has narrow ribs although they are fewer than in typical *yakatagensis*. The beaks and ears are similar, even to the fold along the dorsal margin of the anterior ear of the left valve, a condition also strongly developed in *P. coosensis*. (See Arnold, 1906, pl. 6, fig. 2.) The fact that the Poul Creek form does not have frills on its ribs may be outweighted by the fact that on some specimens of

typical *yakatagensis* they are very weak and by the fact that the adult sculpture of the Poul Creek form is like the juvenile sculpture of *yakatagensis*.

It may be unsafe to draw conclusions on the few specimens known at present. It is possible, however, that *poulcreekensis* and the unfrilled form, here indentified as *P.* (*L.*) cf. *yakatagensis*, represent already divergent stocks of common ancestry and that *poulcreekensis* may be the ancestral stock of *dilleri*, whereas the unfrilled form may be the ancestral stock of the typical *yakatagensis* and *lituyaensis*, as well as of *coosensis*.

The next younger members of this group of pectinids are from the Pliocene of California; after *lituyaensis* none are known from Alaska.

Distribution.—Late Miocene(?) and (or) early Pliocene, Lituya Bay district, Alaska: Occurs in both the lower sandstone–siltstone unit and the upper mudstone unit.

Type locality.—Upper mudstone unit of unnamed upper Tertiary formation, about 300 to 340 feet above the base of the upper mudstone unit, southwest shore of Cenotaph Island, Lituya Bay, Alaska, USGS M270.

Other occurrences.—Lower sandstone(?)–siltstone unit, USGS D223 (T), D264 (T); upper mudstone unit, USGS D174 (T), M270.

Patinopecten (Lituyapecten) purisimaensis (Arnold)

Plate 44, figures 1, 3

Pecten (*Patinopecten*) *purisimaensis* Arnold, 1906, U.S. Geol. Survey Prof. Paper 47, p. 105, pl. 34, fig. 3, pl. 35, figs. 1, 1a. Grant and Gale, 1931 [in part], San Diego Soc. Nat. History Mem., v. 1, p. 194, pl. 6, fig. 3.

The type of this species, deposited at Stanford University (SU 3), is a very poor specimen; and although a better right valve was figured by Grant and Gale, it has remained inadequately illustrated. The specimen figured here, although incomplete and partly riddled by borings, is by far the best specimen of the species I have seen and illustrates most of its characters very well.

The typical form of the species has rather narrow ribs on its right valve, and most of the ribs have short marginal denticles or flares recalling those on the terminal ribs of *P.* (*L.*) *lituyaensis*. (See pl. 41, fig. 1.) The left valve has narrow ribs with wide, round-bottomed interspaces. Two or three of the central ribs are slightly wider with a weak concavity along the crest, but most of the ribs are narrowly rounded on top and bear a single row of denticles or narrow flanges along their crest. They are broken or worn on most specimens observed, and even on the fairly well preserved specimen figured here, only their base is preserved.

Patinopecten turneri Arnold from the Pliocene of the Tomales Bay region, California, was regarded by Grant and Gale (1931, p. 194) as a synonym of *purisimaensis*. If Grant and Gale were influenced by an error in Arnold's statements about his figured specimens they did not say so. Arnold figured three specimens, two of them as right valves and one as a left valve; however, all three of Arnold's specimens are left valves. This gave him an erroneous concept of his supposed new species and made it appear to be very different from *purisimaensis*. Actually *purisimaensis* and *turneri* are closely related, but some good specimens of *turneri* collected by Dr. Joseph H. Peck of the University of California show a well-defined sulcus on the right valve ribs that is not found in *purisimaensis*. These species should probably be kept separate.

Patinopecten (*L.*) *purisimaensis* is related to *P.* (*L.*) *dilleri* (Dall), a species common in the Pliocene of southern California but described from the Pliocene of Humboldt County, northern California. *P.* (*L.*) *dilleri* usually has coarse flanges on both valves, those of the right valve being either single and crossing the ribs (Arnold, 1906, pl. 5, fig. 2), or divided and along the margins of the ribs (Woodring and Bramlette, 1950, pl. 11, fig. 1). The left valve has strong single flanges (Woodring and Bramlette, 1950, pl. 11, fig. 9). It is doubtful if *dilleri* should be regarded as a variety of *coosensis* as was done by Grant and Gale (1931, p. 193). In view of the Alaskan forms now known, it seems more likely that *dilleri* and *coosensis* stem from different early Miocene forms; *dilleri* from *poulcreekensis*, and *coosensis* from an early variant of *yakatagensis*.

In spite of its apparent close relation to *dilleri*, *purisimaensis* appears to be more closely related to *falorensis*, a species here described from the Falor formation (Manning and Ogle, 1950) of northern Humboldt County, Calif., a formation equivalent to a part of the Wildeat series of Lawson (1894). In fact, it is difficult to say from the known specimens whether two species are represented in the Purisima formation, *purisimaensis* and *falorensis*, or whether all the specimens in question should be regarded as belonging to one greatly variable species. For the time being they are treated as two species although it may later be found preferable to treat *falorensis* as a subspecies of *purisimaensis*.

Distribution.—Pliocene, central California: Purisima formation, San Mateo County, Calif.

Type locality.—North of the mouth of Pescadero Creek, San Mateo County, Calif., SU 3.

Other occurrences.—UC 4417, SU 4922.

Patinopecten (Lituyapecten) falorensis MacNeil, n. sp.

Plate 38, figures 1, 3; plate 44, figures 2, 4; plate 45, figures 2, 4; plate 46, figures 1–4

Pecten oregonensis Howe var. Manning and Ogle, 1950, Calif. Div. Mines Bull. 148, p. 23–24, pls. 6, 7.

Shell moderately large; suborbicular to weakly extended posteriorly; valves moderately inflated; right valve slightly more inflated than left valve; shell moderately thin. Posterior dorsal margin moderately concave, and anterior margin nearly straight; left valve with low but sharp steplike submarginal slopes, and right valve slopes less sharp because of inflation of ears. Dorsal margin of ears straight. Ears sculptured by radial riblets with moderately strong beads, about seven riblets on posterior ear of left valve; posterior ears longer and with stronger radial riblets than anterior ears; no denticles along byssal sinus; dorsal margin of left ear of left valve with a weak swelling or fold. Ribs 21 to 23. Right valve often having a split rib, one segment having no counterpart on left valve; right valve ribs broad with undercut sides, interspaces narrow and deep; bottoms flattened; central ribs flattened or rounded on top; terminal ribs with a median sulcus which at the margin may be nearly as deep and wide as the primary interspaces. Left valve ribs moderately broad with a row of short flanges or denticles along each side; central area depressed and troughlike; three terminal ribs on each side narrow and with a single row of short flanges on their crest; interspaces round-bottomed and narrower than the ribs on some specimens, wider on others; no interstitial riblets on any specimens observed. Juvenile microsculpture unknown.

Holotype, both valves together (right valve, UC 34172, left valve UC 34171) measures; diameter 107 mm, height 99 mm. Figured specimen UC 15977 has a height of 130 mm.

The specimen figured by Manning and Ogle, refigured here and made the holotype of the species, is the only specimen of a *yakatagensis*-like *Lituyapecten* figured previously other than the type of *yakatagensis* itself. Its relationship to *yakatagensis* was not recognized and instead, it was identified tentatively as a variety of *P. oregonensis* Howe, a species described from the Empire formation of western Oregon. Possibly the association of this species with *oregonensis* came about because of the incorrect locality data given by Howe for a specimen he figured. This specimen (Howe 1922, pl. 11, fig. 2) was stated by Howe to be from the Wildcat series of Humboldt County, Calif.; but according to its number (N. P. 82 of the Arnold catalog; not 28 as stated by Howe), it comes from north of the mouth of the Raft River, Taholah, Grays Harbor County, Wash., a locality of indefinite formational assignment. There might have been some question, had the specimen figured by Howe actually come from the Wildcat series, as to whether it was *oregonensis* or *falorensis*, because it is very difficult to identify right valves, even on specimens whose left valves are very dissimilar. However, its correct locality together with the fact that it compares favorably with other right valves of *oregonensis* makes it safe to assume that it belongs to that species.

There are two specimens in the Manning and Ogle collection besides the holotype. They are smaller than the type, but they appear to have narrower ribs than the corresponding stage on the type. In this respect they approach some of the typical specimens of *P. purisimaensis*. The left valves of these two specimens have narrow but definitely flat-topped ribs with denticulate margins like the specimen from the Purisima formation illustrated on plate 45, figure 2, here referred to *P.* (*L.*) *falorensis*. Typical *P.* (*L.*) *purisimaensis*, on the other hand, has narrow rounded ribs over most of its disk with two or three of the central ribs slightly wider and having a weak concavity along the crest. (See pl. 44, figs. 1, 3.) The Purisima formation also contains a form that has wide ribs on the right valve and broad, flat-topped ribs with marginal denticles on the left valve (pl. 44, figs 2, 4), and that compares favorably with the type of *falorensis*.

Although it is difficult to say how many species are involved here and, if they are distinct, just what the varietal range of each species is, it is fairly certain that *purisimaensis* and *falorensis* are very closely related. *P.* (*L.*) *yakatagensis* is a highly variable species if all the specimens here referred to it are really conspecific. The same range of variation has not been noted in *lituyaensis*, but possibly all variants of that species have not been found. If approximately the same range of variation could be demonstrated for *lituyaensis*, a strong case for considering *falorensis* as a variety or, at most, a subspecies of *purisimaensis* could be made. To state the problem another way, it is not known whether *purisimaensis* and *falorensis* represent divergent stocks of common but not too distant ancestry or whether the three species, *yakatagensis*, *lituyaensis*, and *purisimaensis* (including *falorensis*) are linear elements of one very variable stock, no parts of it having been clearly set off by geographical isolation. If the latter were so, all the variants existing at any particular instant of time belonged to one species, whereas the mean of variation shifted sufficiently through time to make at least three distinct species recognizable.

The Stanford University collection contains another specimen from the Purisima formation (pl. 45, fig. 4;

pl. 46, fig. 1) that has wide ribs on the left valve like those of typical *falorensis*. However, the right valve has high, comparatively narrow ribs that approach those of typical *purisimaensis*. Furthermore, some of the interspaces on the right valve have strong interstitial ribs, almost as strong as those of *P.* (*L.*) *poulcreekensis*. On the basis of its left valve, and because some individuals of *falorensis* have narrower ribs than the type, I am identifying this specimen as *falorensis*. A similar specimen, except that it lacks interstitial ribs, is in the University of California collection (UC 32659).

Distribution.—Pliocene, northern and central California: Falor formation of Manning and Ogle, 1950, northern Humboldt County; Rio Dell formation of Ogle, 1953 (Wildcat series of Lawson, 1894), Humboldt County; Purisima formation, San Mateo County, Calif.

Type locality.—Falor formation, near bridge crossing Boulder Creek, adjacent to the Wiggins Rach, about 10 miles southeast of Blue Lake, Humboldt County, Calif., UC A4233.

Other occurrences.—Falor formation, SU 4837; Rio Dell formation, SU 4932, SU 4937; Purisima formation, UC 1780 (32659), UC 1788, UC A4343, SU 1095, SU 29788.

Patinopecten (Lituyapecten) cf. P. (L.) dilleri (Dall)

Plate 41, figures 4, 5; plate 45, figure 1

The following is a partial synonymy for typical *P.* (*L.*) *dilleri*:

Pecten (*Lyropecten*) *dilleri* Dall, 1901, Nautilus, v. 16, no. 10, p. 117.

Pecten (*Patinopecten*) *dilleri*. Arnold, 1906, U.S. Geol. Survey Prof. Paper 47, p. 62, pl. 5, fig. 2.
Jordan and Hertlein, 1926, California Acad. Sci. Proc., v. 15, no. 14, p. 431, pl. 30, fig. 1.

Pecten (*Palinopecten*) *coosensis* Shumard variety *dilleri* Dall. Grant and Gale, 1931, San Diego Soc. Nat. History, Mem. 1, p. 193.

Patinopecten dilleri. Woodring *in* Woodring and Bramlette, 1951, U.S. Geol. Survey Prof. Paper 222, p. 84, pl. 11, figs. 1, 9 (imprint date 1950).

Fragments of a large *Patinopecten* which may represent a new species were collected from a horizon high in the Lituya Bay section. One large fragment of a left valve and two small fragments of a right valve are represented. The left valve (pl. 45, fig. 1) has moderately broad rounded ribs with irregular flanges crossing them and broader, round-bottomed interspaces; at least one of the interspaces has a weak interstitial riblet bearing fine flanges. The right valve (pl. 41, figs. 4, 5) has broad, slightly undercut ribs and narrower deep interspaces. The fragments appear to be from the central part of the disk. No denticles or flanges are present on the right valve fragments although terminal ribs might have them.

The right- and left-valve fragments figured here are believed to be the same species, if not the same individual, but there is no assurance that this is so. If they are, the Alaskan form has much broader ribs on its right valve than does typical *dilleri* from California; the right valve also lacks the spiny lamellae commonly present on the southern form. (See Woodring, 1950, pl. 11, fig. 1.)

A nearly perfect specimen of *dilleri* with both valves together was collected by E. H. Quale in the city of San Diego. It is in the collection of the University of California at Los Angeles, (UCLA 8072, plesiotype No. 309) and is to be figured in a forthcoming paper on the fauna of the San Diego formation by L. G. Hertlein. The left valve of this specimen has the typical single-flanged ribs of the species, but the right valve has nearly smooth, moderately narrow ribs. Probably this specimen and the specimen figured by Woodring (1950, pl. 11, fig. 1) with strong lateral lamellae on the right valve ribs can be taken as nearly opposite extremes in right-valve ornamentation.

The left valve from Lituya Bay appears to be more like a specimen of *dilleri*, figured by Jordan and Hertlein (1926), from Pliocene beds near Elephant Mesa in the Scammon Lagoon quadrangle, Lower California, than any figured from farther north. The Lower California specimen has elongate flanges which are single on most ribs; on some ribs the flanges break up into two series with the opposite elements alternating, a condition found on some of the ribs of *P.* (*L.*) *poulcreekensis*. (See pl. 35, fig. 6, and pl. 36, fig. 4.) Usually, as on the specimen figured by Woodring (1950, pl. 11, fig. 9), the flanges on the left-valve ribs are shorter and more regular.

Of several good specimens, including the holotype, from the Wildcat series of Lawson (1894), all but one show only, or consists of only, the right valve. One lot from the Tomkins Hill Gas Field, Humboldt County (CAS 34391), consists of a rubber cast of a large, nearly perfect right valve (presumably made in the field) and shells of two incomplete left valves. The left valves appear to be very similar to the specimen figured from Elephant Mesa, Lower California.

There seems to be little doubt that *dilleri* is a *Lituyapecten*. It is a highly variable species if all the specimens that have been referred to it are really conspecific. Among pectens of its own age, it appears to be most closely related to *P.* (*L.*) *purisimaensis* as numerous writers have claimed. However, it has characters which link it unmistakably with both *P.* (*L.*) *poulcreekensis* and *poulcreekensis* var. (pl. 38, fig. 5), both, early Miocene forms. Its relation to *purisimaensis* may be, therefore, one of parallellism rather than of direct intergradation, *purisimaensis* merely representing the varietal extreme of the *purisimaensis-falorensis* stock that perpetuated more of the characters

that both it and the *dilleri* stock inherited from a common early Miocene ancestor.

Woodring (1950, pl. 9, figs. 6–8) figured three left valves from the Sisquoc formation of the Santa Maria district, California, as "*Patinopecten dilleri* variety." This form has well-developed interstitial riblets, concentric frills which completely bridge the interspaces between the ribs (crossing the interstitial ribs in so doing), and a well-developed imbricating microsculpture resembling the surface of metal lath. I have not seen any of these characters on other members of the *dilleri* group. In spite of its excellent preservation, this is a very puzzling shell. It will be interesting to see what its right valve looks like, if and when one is found. Dr. Leo G. Hertlein, of the California Academy of Sciences, who has had a long and special interest in west-coast pectinids, tells me that he does not believe it is a *Patinopecten* and that he knows of no other west-coast species like it. It could be the left valve of the species described by Arnold (1906, p. 117, pl. 45, figs. 3, 4) as *Pecten* (*Chlamys*) *lawsoni*. Arnold figured two fragments, one as a left valve and one as a right valve; both of them may be right valves. Grant and Gale (1931, p. 166) and Woodring (1950, p. 83) tentatively put *lawsoni* in the synonymy of *Chlamys hastatus* (Sowerby). Unfortunately, the types of *lawsoni* were lost in the San Francisco fire of 1906.

Distribution.—The Alaskan specimens identified as *Patinopecten* (*Lituyapecten*) cf. *P.* (*L.*) *dilleri* are from the upper mudstone unit of an unnamed Tertiary formation, Lituya district, Alaska, USGS 7931.

The following is the known distribution for typical *P.* (*L.*) *dilleri*: Lower California and California. Pliocene beds near Elephant Mesa, Scammon Lagoon quadrangle, Lower California, Mexico; San Diego Calif.; Puente Hills and Newport Beach Los Angeles basin, California; Hills north of Simi Valley, Ventura County, Calif.; Foxen mudstone, and Cebada fine-grained member of the Careaga sandstone, Santa Maria district, California; Rio Dell formation of Ogle, 1953 (Wildcat series of Lawson, 1894), Eel River basin, Humboldt County, Calif.

Type locality.—Bluffs opposite Rio Dell, Eel River, Humboldt County, Calif., (USNM 164846) USGS locality 3363.

Other occurrences.—Lower California: SU 4936 (CAS 2095); San Diego, UCLA 8072; Puente Hills, Pomona College collection; Newport Beach (fide J. G. Vedder); Santa Susana, SU 4828; Simi Valley, UCLA collection; Santa Maria district, USNM 560053, USGS 14649, SU 4942; Eel River, SU 4821, CAS 117; Tomkins Hill Gas Field, CAS 34391.

Patinopecten (Patinopecten) caurinus (Gould)

Pecten caurinus Gould, 1850, Boston Soc. Nat. History Proc., v. 3, p. 345.

Pecten (*Patinopecten*) *caurinus*. Dall, 1898, Wagner Free Inst. Sci. Trans., v. 3, p. 710.

Pecten (*Chlamys*) *caurinus*. Oldroyd, 1924, Stanford Univ. Pub. Geol., v. 1, p. 57, pl. 6, fig. 1, pl. 4, fig. 1.

Pecten (*Patinopecten*) *caurinus*. Grant and Gale, 1931 [in part], San Diego Soc. Nat. History Mem. 1, p. 194, pl. 6, fig. 4. (See for extended bibliography.)

Grant and Gale discuss this species at length and cite a long bibliography. Not all of their synonomy is correct, however; certainly *propatulus* Conrad and *oregonensis* Howe, although related, do not belong to this species.

This species, the type of *Patinopecten*, is here regarded as being subgenerically distinct from the other species treated in this paper. No attempt is made to list all the fossil occurrences. It is included for the purpose of recording its occurrence at two localities in the upper part of the Yakataga formation, one in the Yakataga district and one in the Malaspina district. It occurs well above the highest occurrence of *P.* (*L.*) *yakatagensis*. If the present inferred correlation is correct, its earliest occurrence in the Yakataga district falls within the age range of *P.* (*L.*) *lituyaensis* in the Lituya district. The specimens are not well preserved and are not figured.

Localities.—Yakataga formation, CAS 29280, USGS D263 (T), D336 (T).

Vertipecten sp. indet.

Another pectinid, possibly a *Vertipecten*, which so far is known only from fragments and internal molds, occurs in the Yakataga formation at about the same stratigraphic position as *P.* (*L.*) *yakatagensis*. This form has a long anterior ear on its right valve, narrower and more numerous ribs, and moderately high dorsal slopes. It may be related to *V. porterensis* (Weaver). It is still too poorly known to be described.

Patinopecten (*Lituyapecten*) *poulcreekensis* has a superficial resemblance to some species of *Vertipecten*, and it occurs in beds of the same approximate age. Both have rather smooth ribs on the right valve and scabrous ribs on the left valve. However, although the ribs of the left valve of *Vertipecten* have large frills, the frills do not show any tendency to become divided into two well-defined rows, the common condition in adults of *Lituyapecten*. The right valve of *Vertipecten* has a rather steep umbonal slope. The left valve has a strong imbricating microsculpture, and there is a tendency for the ribs to be unequal. In some species [*V. nevadanus* (Conrad)], there is a tendency for every fourth rib to be stronger, whereas in others [*V. fucanus* (Dall)] one central rib may be stronger than the others. Left valves of *Vertipecten* are more inflated than right valves.

Occurrence.—The stratigraphic occurrence of this supposed *Vertipecten* is indicated by an asterisk in figure 46; CAS 29246, 29253, 29287, 29290. Another float specimen, presumably from the lower part of the Yakataga formation, is numbered USGS 17797.

REFERENCES

Arnold, Ralph, 1906, Tertiary and Quaternary Pectens of California: U.S. Geol. Survey Prof. Paper 47, 264 p., 53 pls.

Clark, B. L., 1932, Fauna of the Poul and Yakataga formations (upper Oligocene) of southern Alaska: Geol. Soc. America Bull. 43, p. 797–846, pls. 14–21, 1 fig.

Dall, W. H., 1901, A new *Lyropecten:* Nautilus, v. 14, p. 117–118.

Grant, U. S., IV, and Gale, H. R., 1931, Catalogue of the marine Pliocene and Pleistocene mollusca of California and adjacent regions: San Diego Soc. Nat. History Mem., v. 1, 1036 p., 32 pls.

Hatai, K. M., 1938, A note on *Pecten kagamianus* Yokoyama: Japan Biogeographical Soc. Bull., v. 8, no. 6, p. 103–110.

Howe, H. V., 1922, Faunal and stratigraphic relationships of the Empire formation, Coos Bay, Oregon: California Univ. Pubs. in Geol. Sci., v. 14, no. 3, p. 85–114, pls. 7–12.

Jordan, E. K., and Hertlein, L. G., 1926, Contribution to the Geology and Paleontology of the Tertiary of Cedros Island and adjacent parts of Lower California: California Acad. Sci. Proc., 4th ser., v. 15, no. 14, p. 409–464, pls. 27–34.

La Pérouse, J. F. de G., 1797, Voyage de La Pérouse autour du monde, publié conformément au décret du 22 avril 1791, et rédigé par M. L. A. Milet-Mureau: Paris, Imprimerie de la République, v. 2, 398 p.

Lawson, A. C., 1894, The geomorphogeny of the coast of northern California: California Univ. Pubs., Dept. Geol. Bull., v. 1, p. 241–271.

Manning, G. A., and Ogle, B. A., 1950, Geology of the Blue Lake quadrangle, California: California Div. of Mines, Bull. 148, 36 p., 11 pls., 3 maps.

Masuda, K., 1953, A new species of *Patinopecten* from Ibaragi Prefecture: Tôhoku Univ., Inst. Geology and Paleontology, Short Papers no. 5, p. 41–50, pls. 5, 6.

——— 1954, Fossil Pectinidae drom Fukuoka-machi, Ninohegun, Iwate Prefecture: Saito Ho-on Kai Research Bull., no. 23, p. 11–14, figs. 1–3.

Ogle, B. A., 1953, Geology of Eel River Valley Area, Humboldt County, California: California Div. Mines Bull. 164, 128 p., 14 figs., 5 pls., 1 map.

Trumbull, E. J., 1958, Shumard's type specimens of Tertiary molluska from Oregon and other types formerly at Washington University, St. Louis: Jour. Paleontology, v. 32, no. 5, p. 893–906, pls. 115–117.

Woodring, W. P., and Bramlette, M. N., 1950, Geology and Paleontology of the Santa Maria District, California: U.S. Geol. Survey Prof. Paper 222, 179 p., 22 pls., 9 figs., 1 map [1951].

Yabe, H., and Hatai, K. M., 1940, A note on *Pecten* (*Fortipecten*, subg. nov.) *takahashii* Yokoyama and its bearing on the Neogene deposits of Japan: Tôhoku Univ. Sci. Repts., 2d ser. (Geology), v. 21, no. 2, p. 147–160, pls. 34–35.

Yokoyama, M., 1929, Pliocene shells from near Nanao, Noto: Japan Geol. Survey Rept. 104, p. 1–7, pls. 1–6.

INDEX

[Italic numbers indicate descriptions]

Page

(*Amusiopecten*), *Pecten* ... 236
Amusium ... 226, 227
Astoria formation ... 228
Barnacles ... 228
beringianus, *Chlamys* ... 227

Camptonectes ... 226
Careaga sandstone, Cebada member ... 235
caurinus, *Patinopecten* ... 226, 227, 231
Patinopecten (*Patinopecten*) ... 227, 228, 236
Pecten ... 228, 235
(*Patinopecten*) ... 236
Cebada member, Careaga sandstone, fine-grained ... 236
Chlamys ... 226, 227
beringianus ... 227
(*Chlamys*) ... 227
hastatus ... 236
(*Swiftopecten*) ... 227
(*Chlamys*) *lawsoni*, *Pecten* ... 236
Clark, B. L., quoted ... 228
coosensis, *Patinopecten* ... 227, 228, 230, 231, 232, 233
Pecten (*Patinopecten*) ... 235
dilleri group ... 236
Patinopecten ... 228, 232, 233, 235
(*Lituypecten*) ... *234*, 236, pls. 41, 45
Pecten (*Lyropecten*) ... 235
(*Patinopecten*) ... 235
var., *Patinopecten* ... 236

Empire formation ... 234

Falor formation ... 233, 235
falorensis, *Patinopecten* (*Lituypecten*) ... 225, 233, *234*, 235, pls. 38, 44, 45
Fortipecten ... 227
Foxen mudstone ... 236
fuscensis, *Vertipecten* ... 236

Grant, U. S., and Gale, H. R., quoted ... 226

hastatus, *Chlamys* ... 236

iberopiensis, *Patinopecten* ... 227

jacobaeus, *Patinopecten* (*Patinopecten*) ... 226
Janira ... 226

Kstalla formation ... 229

lawsoni, *Pecten* (*Chlamys*) ... 236
lituyensis, *Patinopecten* (*Lituypecten*) ... 227, 230, *231*, 234, 236, pls. 39–43
Lituypecten ... 226, 227, 228, 230, 231, 234, 235, 236
(*Lituypecten*) *dilleri*, *Patinopecten* ... 235, 236
falorensis, *Patinopecten* ... 225, 233, *234*, 235, pls. 38, 44, 45, 46
lituyensis, *Patinopecten* ... 227, 230, *231*, 234, 236, pls. 39, 40, 41, 42, 43
Patinopecten ... 227, 228, *231*, 233, 236 pl. 46
dilleri ... *234*, pls. 41, 45.
poulsenensis, *Patinopecten* ... *233*, 230, 231, 232, 233, 235, 236, pls. 35, 36, 38
subsp., *Patinopecten* ... *229*, 230, pls. 36, 38
var., *Patinopecten* ... 235
purisimaensis, *Patinopecten* ... *233*, 234, 235, pl. 44

yakataensis, *Patinopecten* ... 227, *229*, 230, 231, 232, 233, 234, 236, pls. 37, 38, 39, 41, 42
(*Lyropecten*) *dilleri*, *Pecten* ... 235

nerodonus, *Vertipecten* ... 236
ninohensis, *Patinopecten yamanashii* ... 226

oregonensis, *Patinopecten* ... 236

Pecten ... 225, 234
Patinopecten ... 225, 226, 227, 228, 229, 235, 236
caurinus ... 226, 227, 231
coosensis ... 227, 228, 230, 231, 232, 233
dilleri ... 228, 232, 233, 235
var. ... 236
iberopiensis ... 227

Page

Patinopecten—Continued
(*Lituypecten*) ... 227, 228, *231*, 233, 236, pl. 46
dilleri ... *235*, 236, pls. 41, 45
falorensis ... 225, 233, *234*, 235, pls. 38, 44, 45
lituyensis ... 227, *231*, 234, 236, pls. 39, 40, 41, 42, 43
poulsenensis ... *233*, 230, 231, 232, 233, 235, 236, pls. 35, 36, 38
subsp. ... *229*, 230, pls. 36, 38
var. ... 235
purisimaensis ... *233*, 234, 235, pl. 44
yakataensis ... 227, *229*, 230, 231, 232, 233, 234, 236, pls. 37, 38, 39, 41, 42
oregonensis ... 236
(*Patinopecten*) ... 228
caurinus ... 227, 228, 236
jacobaeus ... 236
propatulus ... 227, 228, 231, 236
purisimaensis ... 225, 234, 235
turneri ... 233
yakataensis ... 226, 228
yamanashii ninohensis ... 226
yessoensis ... 226, 227
(*Patinopecten*) *caurinus*, *Patinopecten* ... 227, 228, 236
caurinus, *Pecten* ... 236
coosensis, *Pecten* ... 235
dilleri, *Pecten* ... 235
jacobaeus, *Patinopecten* ... 226
Patinopecten ... 226
purisimaensis, *Pecten* ... 233
yakataensis, *Pecten* ... 225, 228
Pecten (*Amusiopecten*) ... 226, 227
caurinus ... 236
(*Chlamys*) *lawsoni* ... 236
(*Lyropecten*) *dilleri* ... 235
(*Patinopecten*) *caurinus* ... 236
coosensis ... 235
dilleri ... 235
purisimaensis ... 233
yakataensis ... 225, 228, 229
(*Pecten*) ... 236
oregonensis ... 225, 234
Pecten ... 226, 227
Placopecten ... 226
portersensis, *Vertipecten* ... 236
Poul Creek formation ... 229, 230, 231, 232
poulsenensis, *Patinopecten* (*Lituypecten*) ... *233*, 232, 233, 235, 236, pls. 35, 36, 38
subsp., *Patinopecten* (*Lituypecten*) ... *229*, 230, pls. 36, 38
var., *Patinopecten* (*Lituypecten*) ... 235
propatulus, *Patinopecten* ... 227, 228, 231, 236
Propeamusium ... 236
Pseudamusium ... 236
Purisima formation ... 225, 233, 234, 235
purisimaensis, *Patinopecten* ... 225, 234, 235
Patinopecten (*Lituypecten*) ... *233*, 234, 234, pl. 44

Pecten (*Patinopecten*) ... 233

Rio Dell formation ... 235

Shiratori formation ... 236
Sinquoc formation ... 236
(*Swiftopecten*), *Chlamys* ... 227

turneri, *Patinopecten* ... 233

Unnamed formation, upper Tertiary ... 233

Vertipecten ... 226, 227, 236
fuscensis ... 236
nerodonus ... 236
portersensis ... 236
sp. ... 236

Wildcat series ... 233, 234, 235, 236

Yakataga formation ... 229, 230, 231, 236
Yakataga Reef ... 225, 229, 231
yakataensis, *Patinopecten* ... 226, 228
Patinopecten (*Lituypecten*) ... 227, *229*, 230, 231, 232, 233, 234, 236, pls. 37, 38, 39, 41, 42
Pecten (*Patinopecten*) ... 225, 228
yamanashi ninohensis, *Patinopecten* ... 226
yessoensis, *Patinopecten* ... 226, 227

PLATES 35–46

PLATE 35

[Figs. 1-5 slightly reduced; 6, × 1. All specimens from Poul Creek formation, USGS M271, unless otherwise indicated]

FIGURE 1-6. *Patinopecten* (*Lituyapecten*) *poulcreekensis* MacNeil, n. sp. (p. 228).

1. Holotype, a right valve, USNM 563572; height 113 mm; diameter 113 mm.
2. Fragment of right valve, USNM 563574, rubber cast, showing frilled interstitial ribs.
3. Left dorsal margin of right value, USNM 563575, rubber cast, showing frilled terminal ribs.
4. Fragment of right valve, USNM 563576, rubber cast, showing a variation in the top surface of the ribs.
5. Incomplete and decorticated right valve, USNM 563577, showing strong development of interstitial ribs; diameter about 145 mm. Poul Creek formation, USGS 17733.
6. Fragment of left valve, USNM 563578, rubber cast, showing division of frills into 4 or 5 narrow rows; ribs decorticated on younger stages. Katalia formation, upper part, USGS 15852.

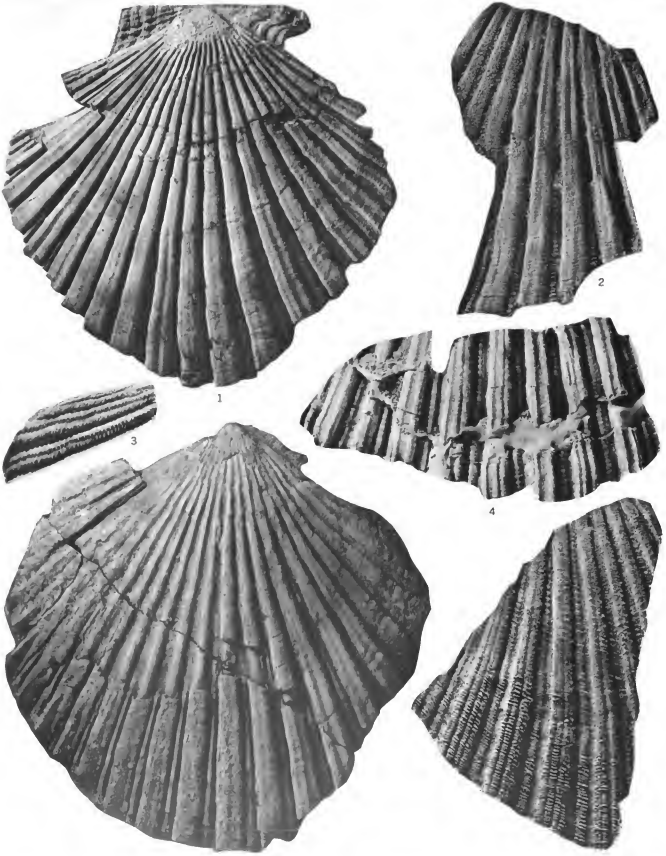

PECTINIDS FROM THE POUL CREEK FORMATION AND THE UPPER PART OF THE KATALLA FORMATION

579101 O - 61 - 3

PLATE 36

[All figures slightly reduced and from Poul Creek formation, USGS M271, unless otherwise indicated]

FIGURES 1, 3, 4, 6, 7. *Patinopecten* (*Lituyapecten*) *poulcreekensis* MacNeil, n. sp. (p. 228).

1. Left ear of left valve, USNM 563579, rubber cast.
3. Right ear of left valve, USNM 563580, rubber cast.
4. Paratype, incomplete left valve, USNM 563573, rubber cast; height of fragment 104 mm.
6. Fragment of left valve, ×2, USNM 563581, rubber cast, showing juvenile sculpture.
7. Incomplete left valve, USNM 563582, rubber cast, showing variations in sculpture.

2. *Patinopecten* (*Lituyapecten*) cf. *P.* (*L.*) *poulcreekensis* MacNeil (p. 228).
   Shell material adhering to a large specimen, USNM 563585; part not shown an internal mold; height of entire specimen 160 mm, nearly complete. Katalla formation, upper part, USGS 15843.

5. *Patinopecten* (*Lituyapecten*) *poulcreekensis* MacNeil, subsp.? (p. 229).
   Fragment of left valve, × 1, USNM 563584. Near base of Yakataga formation or top of Poul Creek formation, USGS D341 (T)

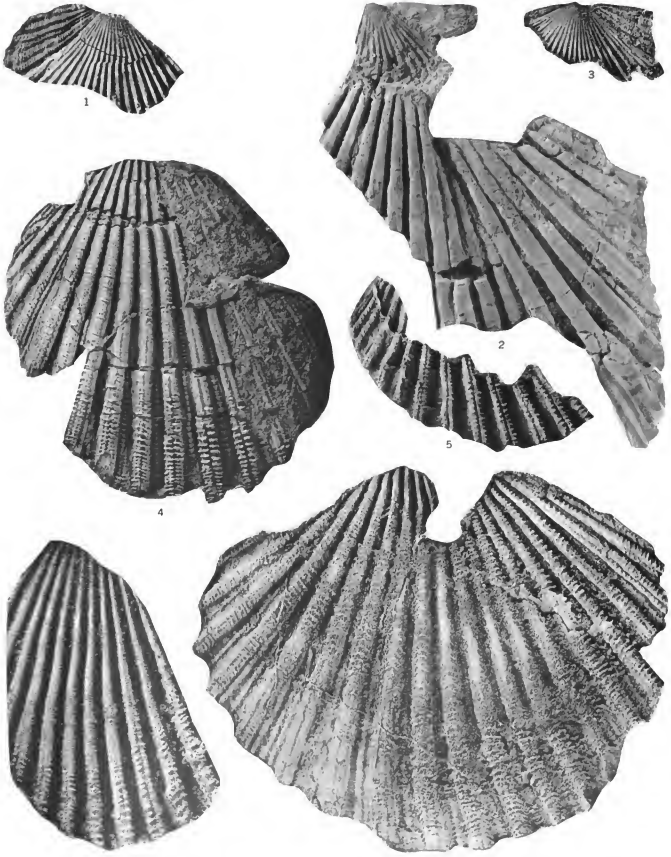

PECTINIDS FROM THE POUL CREEK FORMATION, THE UPPER PART OF THE KATALLA FORMATION, AND THE UPPERMOST POUL CREEK OR LOWERMOST YAKATAGA FORMATION

PLATE 37

FIGURES 1–7. *Patinopecten* (*Lituyapecten*) *yakataensis* (Clark) (p. 229).

1. Right valve, ×1, USNM 563586, rubber cast, incomplete and crushed, showing marginal denticles on the terminal ribs. Yakataga formation, USGS 15425.
2. Incomplete right valve, slightly reduced, USNM 563587, rubber cast; note the weakly developed interstitial ribs; height 104 mm. Yakataga formation, USGS 15425.

3, 4, 5. Fragment of left valve, USNM 563588, rubber cast, showing juvenile sculpture and adult ribs with strong well-divided flanges. 3 and 5 are ×2 enlargements of parts of 4 (×1). Yakataga formation, USGS 6693.

6. Incomplete left valve, ×1, USNM 563589, rubber cast, a juvenile, showing early appearance of single frills on terminal ribs. Yakataga formation, USGS 15425.
7. Mature left valve, slightly reduced, USNM 563590, rubber cast, showing weaker and less divided flanges than figure 4; note the strong marginal fold of left ear; height 123 mm; diameter 123 mm. Yakataga formation, USGS 17813.

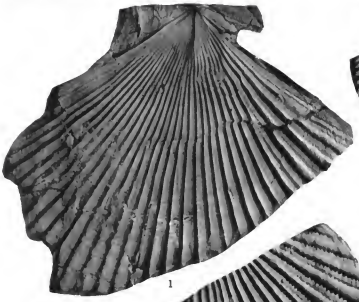
1

2

3

4

5

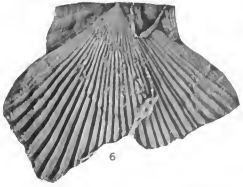
6

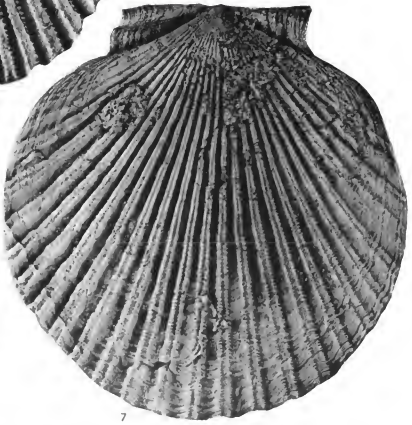
7

PECTINIDS FROM THE YAKATAGA FORMATION

PLATE 38

FIGURES 1, 3. *Patinopecten* (*Lituyapecten*) *falorensis* MacNeil, n. sp. (p. 234).

1. Holotype, right valve, slightly reduced, UC 34172; height 110 mm; diameter 115 mm. Falor formation of Manning and Ogle (1950), UC A-4233.

3. Holotype, left valve, slightly reduced, UC 34171. Falor formation of Manning and Ogle (1950), UC A-4233.

2. *Patinopecten* (*Lituyapecten*) *poulcreekensis* MacNeil, n. sp. (p. 228).

Incomplete hinge of a left valve, ×1, USNM 563583, rubber cast. Poul Creek formation, USGS M271.

4, 6. *Patinopecten* (*Lituyapecten*) *yakataganensis* (Clark) (p. 229).

4. Incomplete right valve, slightly reduced, USNM 563591, rubber cast. Yakataga formation, USGS 6695.

6. Hinge part of a decorticated right valve, slightly reduced; same specimen as plate 37, figure 7; destroyed in acid to obtain mold of left valve. Yakataga formation, USGS 17813.

5. *Patinopecten* (*Lituyapecten*) *poulcreekensis* MacNeil, subsp.? (p. 229).

Incomplete left valve, X 1, rubber cast. Float, upper part of Poul Creek formation or lower part of Yakataga formation, CAS 29285.

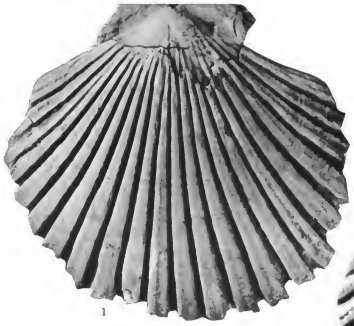

1

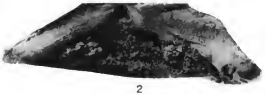

2

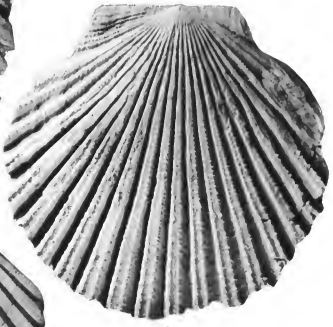

3

4

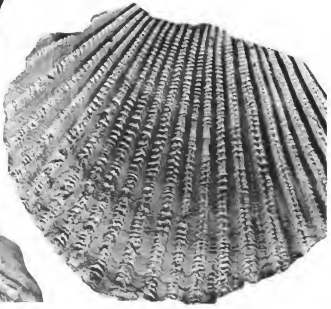

5

6

PECTINIDS FROM THE FOUL CREEK FORMATION, THE YAKATAGA FORMATION, AND THE FALOR FORMATION OF MANNING AND OGLE, 1950 (CALIFORNIA)

579101 O - 61 - 4

PLATE 39

FIGURES 1, 3. *Patinopecten* (*Lituyapecten*) *lituyaensis* MacNeil, n. sp. (p. 231).

Both from unnamed upper Tertiary formation, upper mudstone unit, USGS M270.

1. Holotype, a right valve, about ×¾, USNM 563598, rubber cast; height 220 mm; diameter 210 mm.
3. Ears and left dorsal margin of a right valve, slightly reduced, USNM 563600, rubber cast, showing a variation in sculpture of ears and ornamentation of marginal ribs.

2. *Patinopecten* (*Lituyapecten*) *yakataganesis* (Clark) (p. 229).

Incomplete right valve, ×1, USNM 563592, rubber cast. Yakataga formation, USGS 17852.

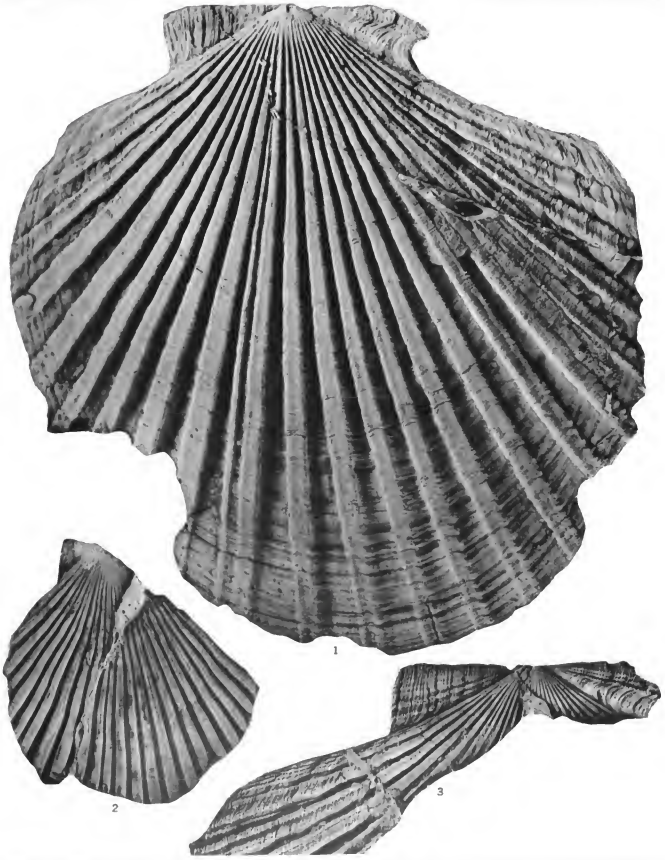

PECTINIDS FROM THE YAKATAGA FORMATION AND THE UPPER MUDSTONE UNIT OF THE UNNAMED UPPER TERTIARY FORMATION IN THE LITUYA DISTRICT

PLATE 40

[All from unnamed upper Tertiary formation, upper mudstone unit, USGS M270]

FIGURES 1-5. *Patinopecten* (*Lituyapecten*) *lituyaensis* MacNeil, n. sp. (p. 231).

1. Left dorsal margin of right valve, ×1, USNM 563601, rubber cast, showing marginal frills on terminal ribs.
2. Right dorsal part of right valve, ×1, USNM 563602, rubber cast, showing marginal frills on terminal ribs.
3. Incomplete right valve, slightly reduced, USNM 563603, rubber cast, a specimen without marginal frills on terminal ribs.
4. Hinge of left valve, slightly reduced, USNM 563604, rubber cast.
5. Fragment of right valve, slightly reduced, USNM 563605, rubber cast, showing well-developed frilled interstitial riblets.

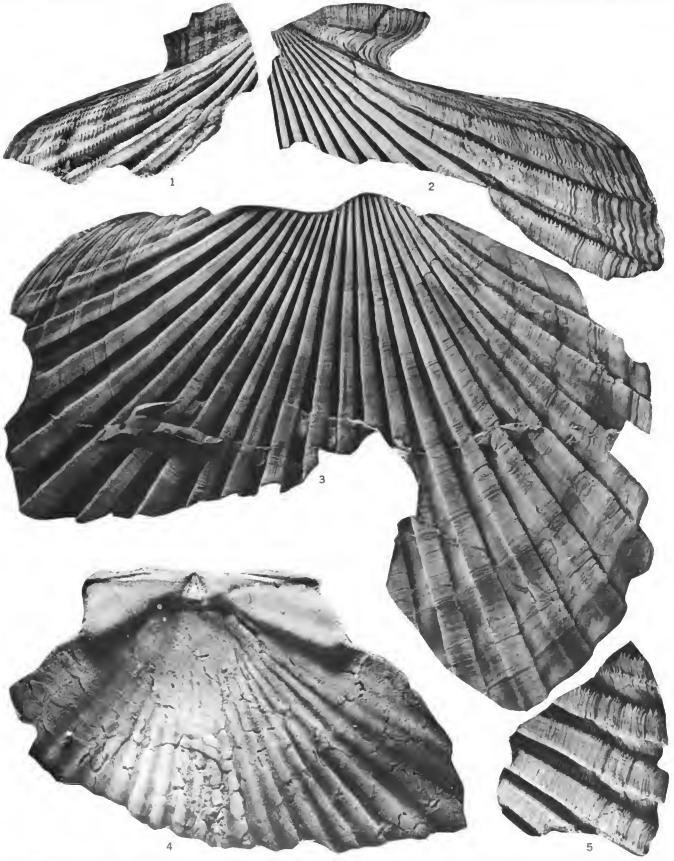

PECTINIDS FROM THE UPPER MUDSTONE UNIT OF THE UNNAMED UPPER TERTIARY FORMATION IN THE LITUYA DISTRICT

PLATE 41

FIGURE 1. *Patinopecten* (*Lituyapecten*) *lituyaensis* MacNeil, n. sp. (p. 231).
Incomplete right valve, slightly reduced, USNM 563606, rubber cast, showing ears and details of sculpture; note greater asymmetry in advanced growth stages. Unnamed upper Tertiary formation, upper mudstone unit, USGS M270.

2. *Patinopecten* (*Lituyapecten*) *yakataganesis* (?) (Clark) (p. 231).
Incomplete right valve, ×1, USNM 563595, rubber cast. Unnamed upper Tertiary formation, lower sandstone-siltstone unit, USGS D187 (T).

3. *Patinopecten* (*Lituyapecten*) *yakataganesis* (Clark) (p. 229).
Incomplete left valve, ×1, USNM 563593, rubber cast. Yakataga formation, USGS 15425.

4, 5. *Patinopecten* (*Lituyapecten*) cf. *P.* (*L.*) *dilleri* (Dall) (p. 235).
Right-valve fragments, ×1, USNM 563612, 563613, in contact with and possibly same individual as left valve on plate 45, figure 1; ribs are undercut and without marginal frills or lamellae. Unnamed upper Tertiary unit, upper mudstone unit, USGS 7931.

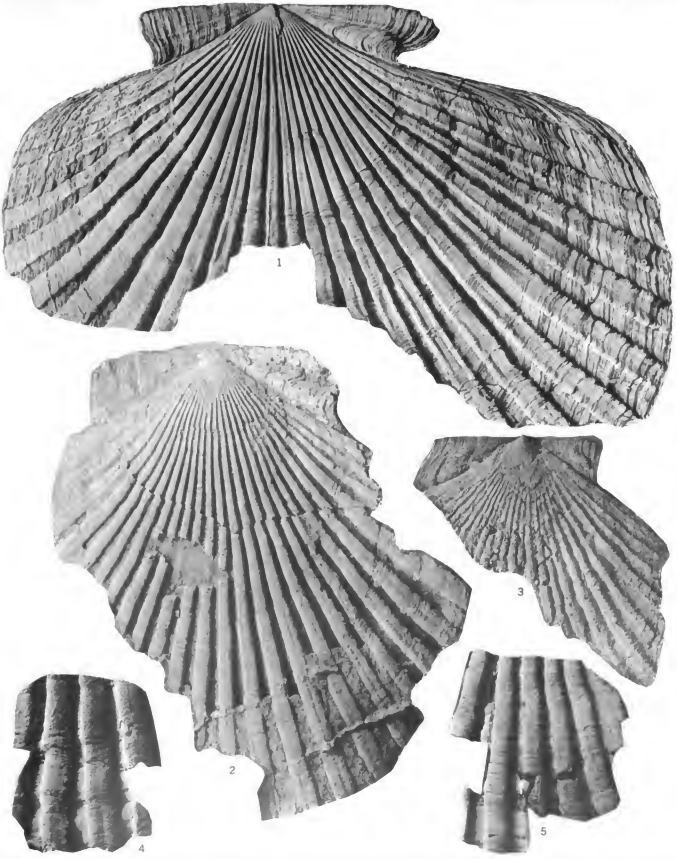

PECTINIDS FROM THE YAKATAGA FORMATION AND THE LOWER SANDSTONE-SILTSTONE AND UPPER MUDSTONE UNITS OF THE UNNAMED UPPER TERTIARY FORMATION IN THE LITUYA DISTRICT

PLATE 42

FIGURES 1, 2, 4. *Patinopecten* (*Lituyapecten*) *lituyaensis* MacNeil, n. sp. (p. 231).

1. Incomplete right valve, × 1, USNM 563607; stratigraphically the oldest known occurrence of the species. Unnamed upper Tertiary formation, lower sandstone-siltstone unit, USGS D264 (T).
2. A × 2 enlargement of a part of the paratype, figure 4.
4. Paratype, a left valve, slightly reduced, USNM 563599, rubber cast; the mold from which this cast was made was formed naturally by humic acids; specimen probably is laterally compressed. Unnamed upper Tertiary formation, upper mudstone unit, USGS M270.

3. *Patinopecten* (*Lituyapecten*) *yakatagensis* (Clark) (p. 230).

Fragment of a left valve, × 1, USNM 563594, rubber cast, with barnacles adhering, showing an interstitial riblet and a weak middle row of denticles on one rib. Yakataga formation, USGS 17853.

1

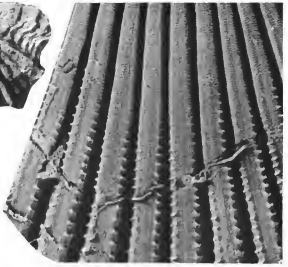

2

3

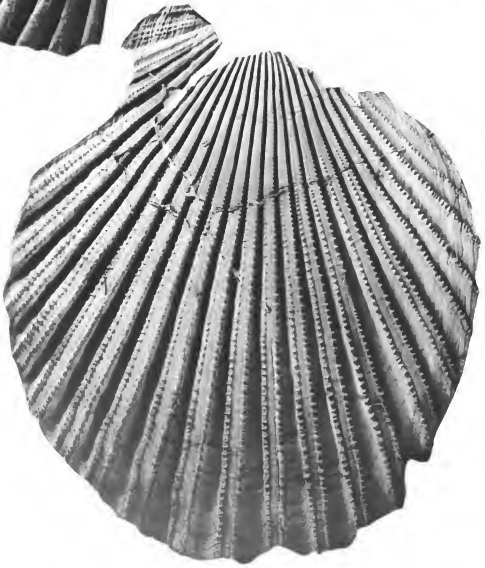

4

PECTINIDS FROM THE YAKATAGA FORMATION AND THE LOWER SANDSTONE-SILTSTONE AND UPPER MUDSTONE UNITS OF THE UNNAMED UPPER TERTIARY FORMATION IN THE LITUYA DISTRICT

PLATE 43

[All specimens from unnamed upper Tertiary formation, upper mudstone unit, USGS M270]

FIGURES 1–4. *Patinopecten* (*Lituyapecten*) *lituyaensis* MacNeil, n. sp. (p. 231).

1. Incomplete left valve, slightly reduced, USNM 563608, rubber cast, showing three rows of denticles on some ribs and several interspaces with weakly frilled interstitial riblets; note large barnacle bases.
2. Left ear and marginal sculpture of left valve, × 1, USNM 563609, rubber cast.
3. Left-valve fragment, × 1, USNM 563610, rubber cast, showing a well-preserved pair of ears.
4. Lower part of a large left valve, slightly reduced, USNM 563611, rubber cast, possibly stretched laterally; the mold of this specimen was partly destroyed to expose the right valve illustrated on plate 41, figure 1.

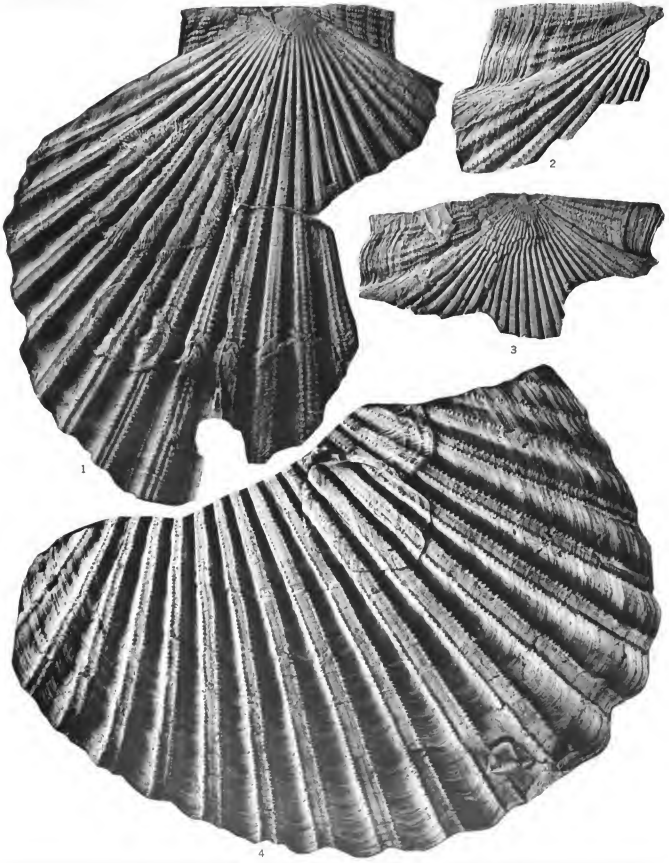

PECTINIDS FROM THE UPPER MUDSTONE UNIT OF THE UNNAMED UPPER TERTIARY FORMATION IN THE LITUYA DISTRICT

PLATE 44

FIGURES 1, 3. *Patinopecten* (*Lituyapecten*) *purisimaensis* (Arnold) (p. 233).

1. Incomplete right valve, slightly reduced, UC 15181, showing marginal denticles or lamellae on ribs; height 123 mm. Purisima formation, UC A-4417.
3. Left valve of same individual, slightly reduced, showing 2 or 3 central ribs with a median sulcus, some juvenile and adult ribs with worn single flanges on their crest.

2, 4. *Patinopecten* (*Lituyapecten*) *falorensis* MacNeil, n. sp. (p. 234).

2. Incomplete right valve, × 1, UC 15977, showing broad adult ribs; height 130 mm. Purisima formation, UC 1788.
4. Fragment of left valve of same individual, × 1, showing broad ribs and marginal denticles; remainder of left valve an internal mold.

1

2

3

4

PECTINIDS FROM THE PURISIMA FORMATION (CALIFORNIA)

PLATE 45

FIGURE 1. *Patinopecten* (*Lituyapecten*) cf. *P.* (*L.*) *dilleri* (Dall) (p. 235).

Fragment of a left valve, × 1, USNM 563614, rubber cast, believed to be from the same individual as the right-valve fragments shown on plate 41, figures 4, 5. Unnamed upper Teriary formation, upper mudstone unit, USGS 7931.

2, 4. *Patinopecten* (*Lituyapecten*) *falorensis* MacNeil, n. sp. (p. 234).

2. Left valve of a half-grown specimen, slightly reduced, SU 8690a; height 92 mm; diameter 90 mm; ribs narrower than normal. Purisima formation, Año Nuevo Point, SU 29788.

4. Partial left valve of a large specimen, slightly reduced, SU 8691; same individual as right valve on plate 46, figure 1. Purisima formation one-fourth of a mile south of San Gregorio, SU 1095.

3. *Patinopecten* (*Lituyapecten*) cf. *P.* (*L.*) *yakatagensis* (Clark) (p. 231).

Left valve of a young specimen, × 1, USNM 563596, showing the juvenile sculpture persisting to a much later stage than normal (see pl. 37, figs. 4, 6, 7); height 90 mm; possibly a subspecies. Uppermost part of Poul Creek formation, USGS 17733.

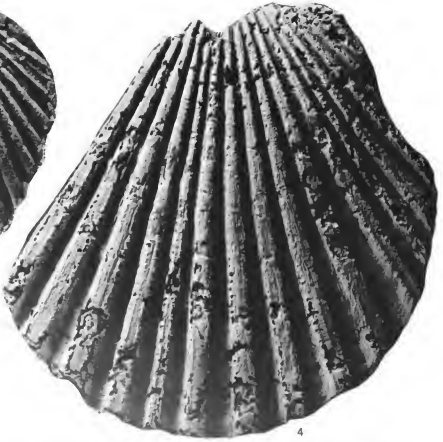

PECTINIDS FROM THE POUL CREEK FORMATION, THE UPPER MUDSTONE UNIT OF THE UNNAMED UPPER TERTIARY FORMATION IN THE LITUYA DISTRICT, AND FROM THE PURISIMA FORMATION (CALIFORNIA)

PLATE 46

FIGURES 1–4. *Patinopecten* (*Lituyapecten*) *falorensis* MacNeil, n. sp. (p. 234).

1. Right valve, slightly reduced, SU 8691, narrower ribs than normal and with strong interstitial riblets; height 135 mm; diameter 142 mm; more complete than shown; same individual as plate 45, figure 4. Purisima formation, one-fourth of a mile south of San Gregorio, SU 1095.
2. Part of right valve, × 1, UC 31333, topotype; same individual as figure 3. Falor formation of Manning and Ogle (1950), UC A-4233.
3. Part of left valve, × 1; height 78 mm; diameter 75 mm; same individual as figure 2.
4. Right valve, slightly reduced, SU 8690–b; height 118 mm; diameter 112 mm. Purisima formation, Ano Nuevo Point, SU 29788.

5. *Patinopecten* (*Lituyapecten*) cf. *P.* (*L.*) *yakatagensis* (Clark) (p. 231).
Right valve, × 1, USNM 563597, of the same individual as plate 45, figure 3. Uppermost part of the Poul Creek formation, USGS 17733.

1

2

3

4

5

PECTINIDS FROM THE POUL CREEK FORMATION, THE FALOR FORMATION OF MANNING AND OGLE, 1950 (CALIFORNIA), AND THE PURISIMA FORMATION (CALIFORNIA)

Stratigraphic Occurrence of *Lituyapecten* in Alaska

By DON J. MILLER

SHORTER CONTRIBUTIONS TO GENERAL GEOLOGY

GEOLOGICAL SURVEY PROFESSIONAL PAPER 354-K

Detailed discussion of relevant Alaskan formations containing Lituyapecten *and description of collecting localities*

CONTENTS

	Page
Abstract	241
Introduction	241
The formations	242
Katalla formation	242
Poul Creek formation	242
The formations—Continued	
Yakstaga formation	245
Unnamed formation in the Lituya district	245
Localities	245
References	248

ILLUSTRATIONS

	Page
FIGURE 46. Generalized sections and tentative correlation of middle and upper Tertiary formations in the Gulf of Alaska Tertiary province, showing approximate stratigraphic position of collections containing large pectinid pelecypods	243
FIGURE 47. Map of the Gulf of Alaska Tertiary province, showing localities at which large pectinid pelecypods have been collected	244

SHORTER CONTRIBUTIONS TO GENERAL GEOLOGY

STRATIGRAPHIC OCCURRENCE OF *LITUYAPECTEN* IN ALASKA

By Don J. Miller

ABSTRACT

The Tertiary beds in the areas where *Lituyapecten* occurs contain three gross units of deposition, the lower, middle, and upper Tertiary units. Although these units indicate a similarity in the succession of the type of sediments received in different geographic districts, they are not supposed to be strictly time divisions. The known occurrence of all types of pectinids in these deposits is stated.

Formations containing *Lituyapecten* are discussed in more detail. These include the Katalla formation in the Katalla district, the Poul Creek and Yakataga formations in the Yakataga district, and an unnamed upper Tertiary formation in the Lituya district.

A generalized correlation chart and a map of the Gulf of Alaska Tertiary province are included; fossil localities are located stratigraphically and geographically on them.

INTRODUCTION

The fossil pectinid pelecypods described in this paper are from rocks of Miocene and Pliocene age exposed in the Katalla, Yakataga, Malaspina, and Lituya districts bordering the northeast shore of the Gulf of Alaska (fig. 47). In this area there is an arcuate lowland and foothills belt that is 300 miles long and 2 to 40 miles wide. The sedimentary rocks of Tertiary age in this belt are exposed or are inferred to underlie lowland areas covered by ice or unconsolidated deposits (Gryc, Miller, and Payne, 1951, p. 159–162). It is of historical interest that the "manteau royal" found in the Lituya district in 1786 by a naturalist in the expedition commanded by the French explorer La Pérouse (1797, p. 189) is the earliest known record of a fossil pecten on the west coast of North America. In compiling the first geologic map of Alaska, Grewingk (1850, p. 99–100, map, pl. 2) cited this shell as evidence for the presence of rocks of Tertiary age on the northeast coast of the Gulf of Alaska.

The sequence of Tertiary rocks exposed in the Gulf of Alaska Tertiary province comprises deposits, mainly clastic, laid down in the Yakataga geosyncline (Payne, 1955) during each of the epochs from Eocene through Pliocene. The known thickness of the sequence at the outcrop exceeds 25,000 feet locally. Significant changes in the environment of deposition during the Tertiary period are reflected in the distinctive lithologic character and organic content in three major divisions of the Tertiary sequence.

The lower Tertiary unit consists of nonmarine, brackish, and marine strata, interbedded and intertonguing and consisting largely of siltstone, arkosic sandstone, and coal. It contains a continental flora and a marine invertebrate fauna of tropical to subtropical aspect. Only one fragmental specimen of a pectinid is known to have been collected from beds assigned to the lower Tertiary unit; it may be a *Patinopecten*.

The lower Tertiary unit includes the Stillwater and Kushtaka formations, the lower part of the Tokun formation in the Katalla district, and an unnamed siltstone and the Kulthieth formation (at the top) in the Yakataga and Malaspina districts.

The middle Tertiary unit consists mainly of marine strata deposited in water of shallow to moderate depth. This unit is characterized by massive poorly sorted or unsorted concretionary siltstone and mudstone and by widespread but generally thin beds of glauconite sandstone and water-laid volcanic breccia or tuff. The marine invertebrate fauna suggests warm, temperate to subtropical waters. Small mud pectens (*Delectopecten* have been collected at several localities from beds in the lower and middle parts of the middle Tertiary unit. At least one species of large pecten, *Patinopecten* (*Lituyapecten*) *poulcreekensis*, occurs in the uppermost part of the middle Tertiary unit, or in beds transitional between the middle and upper Tertiary units.

The middle Tertiary unit includes the upper part of the Tokun formation and lower and middle parts of the Katalla formation in the Katalla district, and the Poul Creek formation in the Yakataga district. Possibly the lowermost part of the unnamed beds constituting the Tertiary sequence in the Lituya

district belongs to the same sedimentary regimen as the middle Tertiary unit.

The upper Tertiary unit is wholly marine and consists of sandstone, siltstone and conglomerate deposited in shallow-water, and marine tillite. The tillite, a massive sandy mudstone containing marine fossils and randomly distributed coarse, ice-rafted clastic fragments is interbedded with and grades laterally into the normal marine sedimentary rocks (Miller, 1953a, p. 22–35). The lithologic evidence for supposed glaciation in the Gulf of Alaska region in late Tertiary time is supported by a marine invertebrate fauna that is generally indicative of cool, temperate to boreal water and that includes many species whose closest living relatives are found in the Gulf of Alaska or farther north. Pectinids are a conspicuous and locally abundant element of the marine invertebrate fauna in the upper Tertiary unit.

The upper Tertiary unit includes the upper part of the Katalla formation in the Katalla district, the Yakataga formation in the Yakataga and Malaspina districts, and at least the upper part of the Tertiary sequence in the Lituya district.

The pectinids described in this paper are from the following stratigraphic units: (a) The upper part of the Katalla formation in the Katalla district; (b) the uppermost part of the Poul Creek formation in the Yakataga district; (c) the Yakataga formation in the Yakataga and Malaspina districts; and (d) an unnamed formation of late Tertiary age in the Lituya district. Uncertainties regarding exact correlation of these formations (fig. 46) within the Gulf of Alaska Tertiary province and also within the Oregon and Washington Tertiary section are due mainly to discontinuity of outcrops and lack of detailed field information, to scarcity or poor preservation of fossils in some parts of the formations, to ecological differences between the dominantly cold-water fauna in the Gulf of Alaska region and the more temperate faunas of the Tertiary sections on the Pacific coast farther south, and to the difference of opinion as to the classification of the Pacific-coast Tertiary sections with reference to the international time scale.

THE FORMATIONS

KATALLA FORMATION

Martin (1905, p. 13; 1908, p. 27–37) proposed the name Katalla formation for a section of rocks of Tertiary age exposed in the hills south of Bering Lake in the Katalla district (formerly called the Controller Bay region). Martin was uncertain of the exact age of the Katalla formation and of its stratigraphic position relative to the sequence of Tertiary rocks exposed north of Bering Lake, which he divided, in ascending order, into the Stillwater, Kushtaka, and Tokun formations. More recent detailed field investigation (Miller, Rossman, and Hickcox, 1945; Miller, 1951) including a restudy of the fossils by several paleontologists, indicates that the approximately 8,600 feet of marine strata designated as the Katalla formation by Martin in the type area are Oligocene and Miocene in age, and that the basal unit of interbedded siltstone and sandstone is equivalent to the upper part of the Tokun formation.

The sequence exposed in the isolated outcrop area of the Suckling Hills, in the extreme southeast part of the Katalla district, is equivalent to the middle and upper part of the Katalla formation of Martin in the type area, and may also include some younger beds. Lot 15852, containing a fragment of a large pecten identified as *Patinopecten* (*Lituyapecten*) *poulcreekensis*, was collected from sandstone near the contact of a predominantly sandy unit with the underlying predominantly silty unit. This contact is tentatively correlated with the contact between the predominantly sandy upper part of the Katalla formation and the predominantly silty middle part in the type area, and with the contact between the Yakataga and Poul Creek formations in the Yakataga district. Another specimen of what may be the same species of pecten (USGS loc. 15843) was found in a loose concretion on the east flank of the Suckling Hills. The predominantly silty sequence exposed at this locality is thought to be equivalent to the middle or even the lower part of the middle silty unit of the Katalla formation, but the concretion may have come from higher in the section.

POUL CREEK FORMATION

The Poul Creek formation of Taliaferro (1932, p. 754–756), as redefined recently (Miller, 1957), includes about 6,100 feet of marine interbedded sandstone and siltstone of Oligocene and early Miocene age. At most localities in the Yakataga district, the contact of the Poul Creek formation with the overlying Yakataga formation is gradational through a stratigraphic interval of 50 to 200 feet in which the typical reddish-brown-weathering silty rocks of the Poul Creek are interbedded with typical gray-weathering sandstone and siltstone of the Yakataga. This change in lithology coincides with a marked change in the marine invertebrate fauna; the characteristic deeper and warmer water fauna of the middle Tertiary unit gives way to the characteristic shallower and colder water fauna of the upper Tertiary unit. The pectens from USGS localities 17733, M271, and CAS 29261 collected on Yakataga Reef, are from a 50-foot-thick transitional unit between

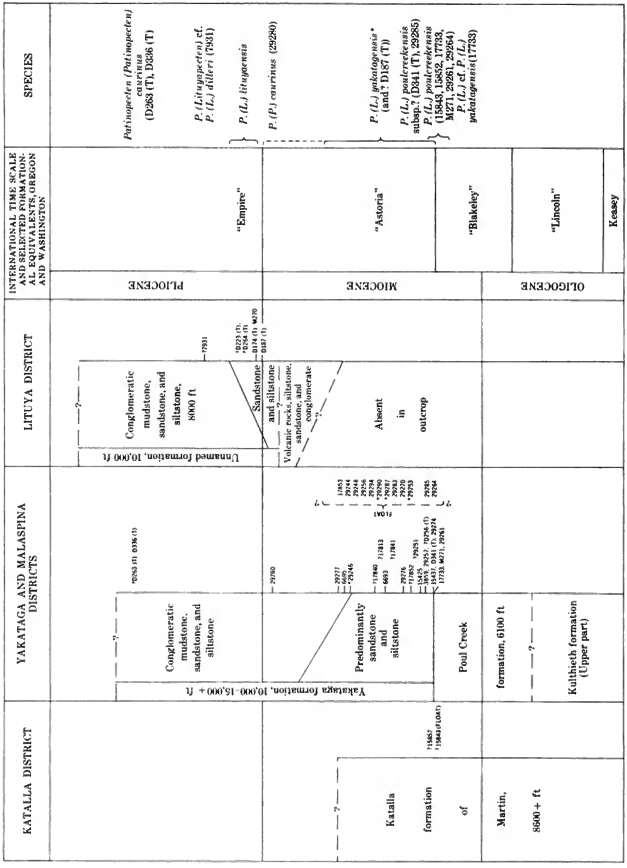

FIGURE 46. Generalized sections and tentative correlation of middle and upper Tertiary formations in the Gulf of Alaska Tertiary province, showing approximate stratigraphic position of collections containing large pectinids pectenpeds.

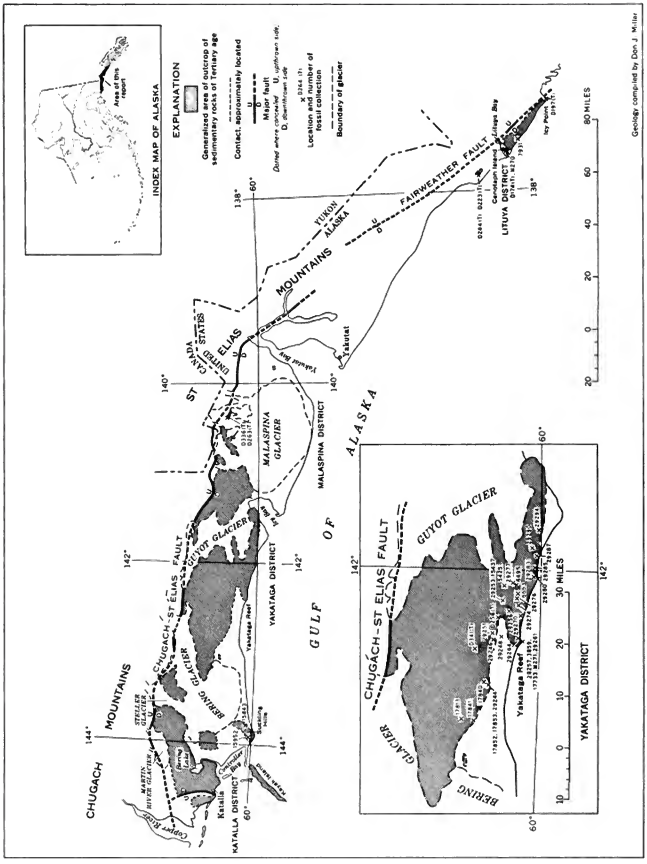

FIGURE 47.—Map of the Gulf of Alaska Tertiary province, showing localities at which large pectinid pelecypods have been collected.

the Poul Creek and Yakataga formations. The contact here was arbitrarily drawn at a more conspicuous change in lithologic character above the pecten-bearing siltstone and silty sandstone. The fragment of pecten in USGS D341 (T) came from similar muddy sandstone in the transitional zone at another locality.

YAKATAGA FORMATION

Taliaferro (1932, p. 756–762) proposed the name Yakataga formation for the younger Tertiary marine strata above the Poul Creek formation in the Yakataga district. Miller (1957) redefined the basal contact of the Yakataga formation in the Yakataga district, and Plafker and Miller (1957) extended the name to include strata in the Malaspina district that were originally named the Pinnacle system by Russel (1891, p. 170–173; 1893, p, 26). As now recognized the Yakataga formation totals a minimum of 10,000 feet, possibly 15,000 feet or even more, of marine sedimentary rocks, chiefly sandstone, siltstone, and conglomeratic sandy mudstone, of Miocene and Pliocene(?) age. In the Yakataga district, interbedded sandstone and siltstone predominate in the lower part of the formation through a section ranging in thickness from 3,500 to at least 5,500 feet; above this section, conglomeratic sandy mudstone is the predominant rock type. In the central and eastern part of the Malaspina district, only the upper part of the Yakataga formation crops out; this part rests with angular unconformity on rocks of early Tertiary age and older.

The most characteristic and abundant pectinid in the Yakataga formation, *Patinopecten* (*Lituyapecten*) *yakatagensis* (Clark), has been found mainly in sandstone beds, but also in siltstone and mudstone in the lower 3,000 to 3,700 feet. Another pectinid, probably *Patinopecten* (*Patinopecten*) *caurinus* (Gould), has been found about 7,000 feet above the base of the formation in the Yakataga district and in the uppermost part of formation in the Malaspina district.

UNNAMED FORMATION IN THE LITUYA DISTRICT

The sequence of rocks of Tertiary age exposed in the Lituya district has been provisionally divided (Miller, 1953b) into four lithologic units as follows: (a) Concretionary marine siltstone with thin interbeds of sandstone that is 1,200 feet to possibly as much as 4,400 feet thick; (b) volcanic rocks, conglomerate, sandstone, and siltstone that are nonmarine and marine and as much as 1,200 feet thick; (c) interbedded sandstone and siltstone that are marine, 600 feet to at least 2,400 feet; (d) marine conglomeratic sandy mudstone interbedded with sandstone and siltstone that is at least 8,000 feet. Units a and b are believed to be at least in part equivalent in age and to grade into each other, as both units at different places rest unconformably on pre-Tertiary rocks and are overlain with apparent conformity by unit c. The upper part of unit c grades laterally into the lower part of unit d. The two units together constitute a formation of late Miocene(?) and Pliocene age. This unnamed formation is lithologically similar to the Yakataga formation, but unit c is probably entirely or at least in large part younger than the interbedded sandstone-siltstone unit that constitutes the lower part of the Yakataga.

One species of an exceptionally large pecten, *Patinopecten* (*Lituyapecten*) *lituyaensis* MacNeil, n. sp., has been collected at two widely separated localities in the Lituya district from near the base of the unnamed Tertiary formation. A specimen doubtfully referred to *P.* (*Lituyapecten*) *yakatagensis* was found at another locality. A fragment of another species of large pecten, *Patinopecten* (*Lituyapecten*) cf. *P.* (*L.*) *dilleri* (Dall), was found higher in the formation at one locality.

LOCALITIES

The available fossils from the Tertiary rocks exposed in the Gulf of Alaska province were collected over a period of nearly 70 years, mainly by geologists engaged in areal mapping and under conditions that allowed neither time nor facilities for collecting and transporting a large number of specimens. As a consequence of these circumstances, as well as the generally poor preservation of the fossils and the hardness of the Tertiary rocks, many of the fossils, particularly the large pectinids, are fragmentary. On the other hand the conspicuous, large pectinids probably were rarely overlooked where any fossils were collected.

The following descriptions of Alaskan localities at which fossil pectinids were collected include the essential part of the original geographic description, followed, where possible or necessary, by supplementary information in parenthesis locating the collection on the most detailed published topographic map available in 1958. The stratigraphic assignments are the writer's. The California localities were compiled by MacNeil.

ALASKA LOCALITIES

Katalla district

USGS Cenozoic loc.

15843. Creek on southeast flank of Suckling Hills, 3.2 miles N. 26° E. of mouth of Kiklukh River, Bering Glacier quadrangle. Collector, D. J. Miller, 1945. Float, Katalla formation.

15852. Creek on northwest flank of Suckling Hills, 3.1 miles N. 48° W. of mouth of Kiklukh River, Bering Glacier quadrangle. Collector, D. J. Miller, 1945. Katalla formation, upper part.

Yakataga district

USGS Cenozoic loc.

6693. Bluff on south bank of White River one-half a mile below foot of [White River] glacier (2.43 miles N. 4° E. of mouth of Fulton Creek, Bering Glacier A–4 quadrangle). Collector, A. G. Maddren, 1913. Yakataga formation, about 1,800 ft above base.

6695. From sandy shale at intake tunnel of the White River Mining Co.'s flume, North Fork of White River (about 4.8 miles N. 87° W. of Munday Peak, Bering Glacier A–3 quadrangle). Collector, A. G. Maddren, 1913. Yakataga formation, about 3,500 ft above base.

15425. North flank and crest of Yakataga Ridge (5.7 miles S. 72° W. of Mount Eberly, Bering Glacier A–3 quadrangle). Collector, M. S. Walton, Jr., 1944. Yakataga formation, about 500 ft above base.

15437. Unnamed creek on north flank of and parallel to Yakataga Ridge (0.3 mile N. 16° E. of peak 2430 near west end of Yakataga Ridge, Bering Glacier A–4 quadrangle). Collector, E. M. Spieker, 1944. Poul Creek formation, near top, and possibly basal part of Yakataga formation.

17733. Yakataga Reef, about 700 ft N. 30° E. of highest rock on the reef (1.53 miles S. 56° E. of mouth of Mink Creek, Bering Glacier A–4 quadrangle; same locality as M271). Collector, D. J. Miller, 1948. Poul Creek formation, upper 50 ft.

17813. Small stream entering Kulthieth River from the east, 2.4 miles N. 53° E. of junction of Kultheith and Kaliakh Rivers, Bering Glacier quadrangle. Collector, D. J. Miller, 1947. Yakataga formation, probably lower part.

17840. South flank of Kulthieth Mountain, 0.7 mile S. 32° E. of peak 3437, Bering Glacier quadrangle. Collector, R. B. Johnson, 1947. Yakataga formation, at least 2,400 ft above base.

17841. Gulch on south face of ridge at Sunshine Point, 2.0 miles S. 53° E. of junction of Kulthieth and Kaliakh Rivers, Bering Glacier quadrangle. Collector, R. B. Johnson, 1947. Yakataga formation, lower part.

17852. Gulch on south flank of Kulthieth Mountain, 0.85 mile S. 17° E. of peak 3437, Bering Glacier quadrangle. Collector, D. J. Miller, 1947. Yakataga formation, at least 900 ft above base.

17853. Gulch on south flank of Kulthieth Mountain, between points 0.8 mile S. 34° E. and 1 mile S. 6° W. of peak 3437, Bering Glacier quadrangle. Collector, D. J. Miller, 1947. Float, lower part of Yakataga formation.

D256 (T). Small outcrop at margin of Yakataga Glacier, at head and on south side of North Channel of the Yakataga River, Bering Glacier A–4 quadrangle. Collector, D. L. Rossman, 1953. Yakataga formation.

D341 (T). Ridge at head of Cotton Creek; altitude 3,800 ft., 1.35 miles N. 30° E. of peak 4014 on Duktoth Mountain, Bering Glacier A–4 quadrangle. Collector, J. E. Heppert, Standard Oil Co. of California, 1954. Probably Yakataga formation, near base; may be at top of Poul Creek formation.

Yakataga district—Continued

USGS Cenozoic loc.—Continued

M271. Yakataga Reef, along strike of beds that intersect the shoreline at a point 700 ft N. 30° E. of the highest rock on the reef (1.53 miles S. 56° E. of mouth of Mink Creek, Bering Glacier A–4 quadrangle; same locality as 17733). Collector, D. J. Miller, 1958. Poul Creek formation, 25 to 50 ft below top.

California Univ. (Berkeley) loc.

3859. Yakataga Reef, from a sandstone about 800 ft above lowest reef exposure (about 1.36 miles S. 56° E. of mouth of Mink Creek, Bering Glacier A–4 quadrangle). Collector, N. L. Taliaferro, 1920. Yakataga formation, about 300–350 ft above base.

California Acad. Sci. loc.[1]

29244. West [south] base of Kulthieth Mountain, at mouth of small stream coming from cirquelike hanging valley, 3 to 4 miles west of Duktoth River (about 1 mile S. 6° W. of peak 3437, Kulthieth Mountain, Bearing Glacier quadrangle). Float, Yakataga formation, lower part.

29246. Gray sandy conglomerate exposed on west side of Miller Creek near mouth of small west tributary, about 1½ miles north (upstream) from first outcrop exposed along west side of creek (about 1.4 miles S. 41° W. of peak 3394 at head of Miller Creek, Bering Glacier A–4 quadrangle). Yakataga formation, probably about 3,300 ft. above base.

29248. Yakataga River (Bering Glacier A–4 quadrangle). Float, from Poul Creek formation and probably from Yakataga formation.

29251. East side of Porcupine Creek, 1½ miles upstream [north] from mouth (about 2 miles S. 31° E. of peak 3394 at head of Miller Creek, Bering Glacier A–4 quadrangle). Yakataga formation, lower part.

29253. Lower 1 mile of Opooch Creek above junction with Yakataga Glacier (along unnamed creek on the north flank of and parallel to the west end of Yakataga Ridge, Bering Glacier A–4 quadrangle). Float, from upper part of Poul Creek formation and from the Yakataga formation, probably only the lower part.

29256. Clear Creek (Bering Glacier A–3 and A–4 quadrangles). Float, from Yakataga formation.

29257. Yakataga Reef, from peeten zone just above a pebble conglomerate which projects farther into the sea than any other of the reef beds (about 1.36 miles S. 56° E. of mouth of Mink Creek, Bering Glacier A–4 quadrangle). Yakataga formation, about 350 ft. above base.

29261. Yakataga Reef, from shaly mudstone zone just above massive sandstone (along strike of beds that intersect the shoreline at a point 1.53 miles S. 56° E. of Mink Creek, Bering Glacier A–4 quadrangle. Poul Creek formation, within 30 ft. of top.

[1] All collections by field party representing The Standard Oil Co. of California, The Tidewater Associated Oil Co., and The Union Oil Co. of California, 1938.

Yakataga district—Continued

California Acad. Sci. loc.—Continued

29264. Twomile Creek, below forks (Bering Glacier A-4 quadrangle). Float, from upper part of Poul Creek formation and possibly also from lower part of Yakataga formation. The lithologic character of matrix attached to the large pecten suggests Poul Creek.

29270. Hamilton Creek (Bering Glacier A-4 quadrangle). Float, from upper part of Poul Creek formation and lower part of Yakataga formation.

29274. Outcrop of brown sandstone just above rivers edge on east side of big bend on White River, 1½ to 1¾ miles upstream from the mouth (about 1.85 miles N. 14° E. of mouth of White River, Bering Glacier A-4 quadrangle). Near base of Yakataga formation or near top of Poul Creek formation.

29276. South side of White River across from Three Cabins camp (about 2.55 miles N. 16° W. of mouth of Fulton Creek, Bering Glacier A-4 quadrangle). Yakataga formation, about 1,200 ft. above base.

29277. Nearly horizontal beds in canyon on upper part of White River, about one-quarter of a mile upstream from end of old flume (about 4.6 miles N. 84° W. of Munday Peak, Bering Glacier A-3 quadrangle). Yakataga formation, about 3,700 ft. above base.

29280. Umbrella Reef, from shore outward through an estimated stratigraphic thickness of 500 feet (about 0.3 mile west of mouth of Lawrence Creek, Bering Glacier A-3 quadrangle). Yakataga formation, about 6,000 to 6,500 ft. above base.

29283. Lawrence Creek (Bering Glacier A-3 quadrangle). Float, from lower part of Yakataga formation and upper part of Poul Creek formation.

29285. Poul Creek (Bering Glacier A-3 quadrangle). Float, from upper part of Poul Creek formation and lower part of Yakataga formation.

29287. Munday Creek (Bering Glacier A-3 quadrangle). Float, from upper part of Poul Creek formation and possibly from lower part of Yakataga formation. The lithologic character of matrix attached to the pecten suggests Poul Creek.

29290. Mouth of tributary creek entering Johnston Creek on the east side about one-quarter of a mile upstream from General Petroleum Co. drilling camp (about 3.9 miles S. 34° E. of Munday Peak, Bering Glacier A-3 quadrangle). Float, from all but the lowest part of the Poul Creek formation and probably from the lower part of the Yakataga formation. The lithologic character of matrix attached to the pecten suggests Poul Ceek formation.

29294. Little River (Bering Glacier A-3 quadrangle). Float, upper part of Poul Creek formation and lower part of Yakataga formation.

[1] All collections by field party representing The Standard Oil Co. of California, The Tidewater Associated Oil Co., and The Union Oil Co. of California, 1938.

Malaspina district

USGS Cenozoic loc.

D263 (T). Point Glorious, about 1.68 miles N. 68° W. of peak 5520, Mount St. Elias quadrangle. Collector, George Plafker, 1953. Yakataga formation, upper part.

D336 (T). Point Glorious, probably same locality as D263 (T). Collector, I. C. Russell, 1890.

Lituya district

7931. Sea cliff cut by stream 6½ miles southeast of Lituya Bay, about 500 ft from beach (about 2 miles southeast of mouth of Steelhead Creek, Mount Fairweather quadrangle). Collector, J. B. Mertie, Jr., 1917. Unnamed upper Tertiary formation about 3,200 ft above base; upper mudstone unit.

D174 (T). Southwest shore of Cenotaph Island, 3,500 ft S. 70° W. of easternmost cape of island (Lituya Bay, Mount Fairweather quadrangle). Collector, D. J. Miller, 1952. Unnamed upper Tertiary formation about 1,070 ft above base; upper mudstone unit.

D187 (T). Ocean beach reef, Icy Point measured section, 1.04 miles, S. 22° W. of mouth of Kaknau Creek (Palma Bay, Mount Fairweather quadrangle). Collector, J. F. Seitz, 1952. Unnamed upper Tertiary formation about 800 ft above base; probably lower sandstone-siltstone unit.

D223 (T). Cliff at east margin of glacier at Cape Fairweather, about 3.8 miles N. 80° W. of Mount Escures, Mount Fairweather quadrangle; same locality as D264 (T). Collector, C. E. Kirschner, Standard Oil Co. of California, 1953. Unnamed upper Tertiary formation, probably in lower sandstone-siltstone unit.

D264 (T). Cliff at east margin of glacier at Cape Fairweather, about 3.8 miles N. 80° W. of Mount Escures, Mount Fairweather quadrangle; same locality as D223 (T). Collector, D. J. Miller, 1953. Unnamed upper Tertiary formation, probably in lower sandstone-siltstone unit.

M270. Southwest shore of Cenotaph Island, along strike of beds from a point 0.83 mile N. 84° W. of easternmost cape in the island to a point 0.65 mile S. 70° W. of the same cape; Lituya Bay, Mount Fairweather quadrangle. Collector, D. J. Miller, 1958. Unnamed upper Tertiary formation 1,050 to 1,090 ft above base; upper mudstone unit.

California localities

California Univ. (Berkley) loc.

1780. In the sea cliffs and small reefs ¼ to ½ mile due west of the mouth of Ano Neuvo Creek, San Mateo County, Calif. B. Martin, collector. No date. Purisima formation, Pliocene.

1788. In the sea cliffs at the mouth of Purisima Creek, San Mateo County, Calif. B. Martin, collector. No date. Purisima formation, Pliocene.

California localities—Continued

California Univ. (Berkeley) loc.—Continued

A-4233. Bank of Boulder Creek from 100 yd south to 200 yd north of bridge near "Beckstine Ranch" (Wiggins Ranch), in about a 20 ft stratigraphic interval, about 10 miles southeast of Blue Lake, Humboldt County, Calif. B. A. Ogle, collector, 1946. Falor formation, Pliocene.

A-4343. Halfway between San Gregorio and Pescadero Lagoon on the coast, San Mateo County, Calif. M. K. Gebert, collector. No date. Purisima formation, Pliocene.

A-4417. North side of San Gregorio Lagoon, San Mateo County, Calif. J. W. Durham, collector, 1948. Purisima formation, Pliocene.

California Univ. (Los Angeles) loc.

8072 (pleistotype No. 309). India and Upas Streets, San Diego, Calif. E. H. Quale, collector, 1931. San Diego formation, Pliocene.

Stanford University catalog No.

1095. San Gregorio beach, one-quarter of a mile south of mouth of San Gregorio Creek, San Mateo County, Calif. Enos Preston, collector, 1907. Purisima formation, Pliocene.

4821. Ford across Eel River halfway between Scotia and Nanning Creek, Humboldt County, Calif. H. Hannibal, collector, 1913. "Wildcat series" of Lawson; probably from the Rio Dell formation of Ogle, Pliocene.

4828. Top of ridge between two legs of trail fork in Dry Canyon, an east branch of Tapo Canyon, 3.8 miles north of Santa Susana, north side of Simi Valley, Santa Susana quadrangle, Ventura County, Calif. George Boulware, collector, 1920. Pliocene.

4837. In Boulder Creek for one-quarter of a mile up and one-quarter of a mile down from Maple Creek post office (Boulder Creek and Maple Creek are in the Blue Lake quadrangle), Humboldt County, Calif. H. Hannibal, collector, 1913. Falor formation, Pliocene.

4922. Ano Nuevo Point, San Mateo County, Calif. R. Arnold, collector, 1903. Purisima formation, Pliocene.

4932. East branch of south fork of Eel River from mouth of Panther Creek up creek for 1 mile, Humboldt County, Calif. W. G. Cooper and H. Hannibal, collectors, 1913. "Wildcat series" of Lawson; probably from the Rio Dell formation of Ogle, Pliocene.

4936. Mouth of large arroyo northwest of Elephant Mesa, Scammon Lagoon quadrangle, Lower California. B. F. Hake, collector, 1921. Pliocene.

4937. Same as 4932.

4942. Yellow sandstone, Casmalia Hills, 2.6 miles N. 50° E. of "BM 95" (BM 95 is located in San Antonio Creek about 4.2 miles south of Casmalia—can be found on pl. 1 in U.S. Geol. Survey Bull. 322), Todos Santos y San Antonio, Santa Barbara County, Calif. C. F. Tolman, collector, 1924. "Pliocene."

29788. Ano Nuevo Point, San Mateo County, Calif. R. Arnold and W. R. Hamilton, collectors, 1903. Purisima formation, Pliocene.

California localities—Continued

California Acad. Sci. Soc.

117. "Wildcat series," Humboldt County, Calif. B. Martin, collector. 1912.

2095. Same as Stanford Univ., 4936.

34391. Tomkins Hill gasfield, secs. 23 to 24, T. 3 N., R. 1 E., Humboldt County, Calif. T. W. Cameron, collector, 1955. "Wildcat Pliocene."

USGS Cenozoic loc.

3363 (USNM 164846). Bluffs opposite Rio Del, Eel River, Humboldt County, Calif. J. S. Diller, collector, 1906. "Wildcat series" of Lawson; lower part of the Rio Dell formation of Ogle, Pliocene.

14649. Graciosa Ridge, 450 ft south-southwest of Union Oil Co. Graciosa 3 well, Orcutt field, Santa Barbara County, Calif. W. P. Woodring, collector, 1939. Cebada fine-grained member of the Careaga sand stone, Pliocene.

USNM catalog No.

560053. 1.8 miles S. 35° E. of Casmalia, Santa Barbara County, Calif. L. M. Clark, collector, no date. Foxen mudstone, Pliocene.

REFERENCES

Clark, B. L., 1932, Fauna of the Poul and Yakataga formations (upper Oligocene) of southern Alaska: Geol. Soc. America Bull. 43, p. 797–846, pls. 14–21, 1 fig.

Grewingk, Constantin, 1850, Beitrag zur Kenntniss der orographischen und geognostischen Beschaffenheit der Nord-West-Kuste Amerikas mit den anliegenden Inseln: Russ. K. min. Gesell. St. Petersburg Verh. 1848–49, p. 76–424, pls. 1–7. [1–3 are maps, 4–7 fossils.]

Grye, George, Miller, D. J., and Payne, T. G., 1951, Possible future petroleum provinces of North America; chapter on Alaska: Am. Assoc. Petroleum Geologists Bull., v. 35, p. 151–168, figs. 2–5.

La Pérouse, J. F. de G., 1797, Voyage de La Pérouse autour du monde, publié conformément au déeret du 22 avril 1791, et rédigé par M. L. A. Milet-Mureau: Paris, Imprimerie de la République, v. 2, 398 p.

Martin, G. C., 1905, The petroleum fields of the Pacific Coast of Alaska with an account of the Bering River coal deposits: U.S. Geol. Survey Bull. 250, 64 p., 7 pls., 3 figs.

——— 1908, Geology and mineral resources of the Controller Bay region, Alaska: U.S. Geol. Survey Bull. 335, 141 p., 10 pls., 2 figs.

Mertie, J. B., Jr., 1931, Notes on the geography and geology of Lituya Bay, Alaska: U.S. Geol. Survey Bull. 836–B, p. 117–135, 1 fig.

Miller, D. J., 1951, Geology and oil possibilities of the Katalla district, Alaska: U.S. Geol. Survey open-file report, 66 p., 5 figs.

——— 1953a, Late Cenozoic marine glacial sediments and marine terraces of Middleton Island, Alaska: Jour. Geol., v. 61, p. 17–40, 2 pls., 4 figs., 7 tables.

——— 1953b, Preliminary geologic map of Tertiary rocks in the southeastern part of the Lituya district, Alaska. Correlated columnar sections of Tertiary rocks in the Lituya district, Alaska: U.S. Geol. Survey open-file report.

Miller, D. J., 1957, Geology of the southeastern part of the Robinson Mountains, Yakataga district, Alaska: U.S. Geol. Survey Oil and Gas Inv. Map OM-187.

Miller, D. J., Rossman, D. L., and Hickcox, C. A., 1945, Preliminary report on petroleum possibilities in the Katalla area, Alaska. Geologic and topographic map and sections of the Katalla area, Alaska: U.S. Geol. Survey Prelim. Rept., 18 p., map.

Payne, T. G., 1955, Mesozoic and Cenozoic tectonic elements of Alaska: U.S. Geol. Survey Misc. Geol. Inv. Map I-84.

Plafker, George, and Miller, D. J., 1957, Reconnaissance geology of the Malaspina district, Alaska: U.S. Geol. Survey Oil and Gas Inv. Map OM-189.

Russell, I. C., 1891, An expedition to Mount St. Elias, Alaska: Natl. Geog. Map., v. 3, p. 53-204, pls. 2-20, 8 figs.

——— 1893, Second expedition to Mount St. Elias, in 1891, U.S. Geol. Survey Ann. Rept. 13, pt. 2, p. 1-91, map.

Taliaferro, N. L., 1932, Geology of the Yakataga, Katalla, and Nichawak districts, Alaska: Geol. Soc. America Bull., v. 43, p. 749-782, 14 figs.

Scripps Institution of Oceanography Library
University of California, San Diego

DATE DUE

JUN 09 1977
JUN 07 REC'D

SI 23 UCSD Libr.